

Biological aspects of targeted drug discovery: Development of novel targets and/or chemotherapies, and drug repurposing

Edited by

Sandeep Singh, Anjana Munshi, Jitender Bariwal
and Rajkumar S. Kalra

Published in

Frontiers in Oncology
Frontiers in Pharmacology



FRONTIERS EBOOK COPYRIGHT STATEMENT

The copyright in the text of individual articles in this ebook is the property of their respective authors or their respective institutions or funders. The copyright in graphics and images within each article may be subject to copyright of other parties. In both cases this is subject to a license granted to Frontiers.

The compilation of articles constituting this ebook is the property of Frontiers.

Each article within this ebook, and the ebook itself, are published under the most recent version of the Creative Commons CC-BY licence. The version current at the date of publication of this ebook is CC-BY 4.0. If the CC-BY licence is updated, the licence granted by Frontiers is automatically updated to the new version.

When exercising any right under the CC-BY licence, Frontiers must be attributed as the original publisher of the article or ebook, as applicable.

Authors have the responsibility of ensuring that any graphics or other materials which are the property of others may be included in the CC-BY licence, but this should be checked before relying on the CC-BY licence to reproduce those materials. Any copyright notices relating to those materials must be complied with.

Copyright and source acknowledgement notices may not be removed and must be displayed in any copy, derivative work or partial copy which includes the elements in question.

All copyright, and all rights therein, are protected by national and international copyright laws. The above represents a summary only. For further information please read Frontiers' Conditions for Website Use and Copyright Statement, and the applicable CC-BY licence.

ISSN 1664-8714
ISBN 978-2-83251-287-6
DOI 10.3389/978-2-83251-287-6

About Frontiers

Frontiers is more than just an open access publisher of scholarly articles: it is a pioneering approach to the world of academia, radically improving the way scholarly research is managed. The grand vision of Frontiers is a world where all people have an equal opportunity to seek, share and generate knowledge. Frontiers provides immediate and permanent online open access to all its publications, but this alone is not enough to realize our grand goals.

Frontiers journal series

The Frontiers journal series is a multi-tier and interdisciplinary set of open-access, online journals, promising a paradigm shift from the current review, selection and dissemination processes in academic publishing. All Frontiers journals are driven by researchers for researchers; therefore, they constitute a service to the scholarly community. At the same time, the *Frontiers journal series* operates on a revolutionary invention, the tiered publishing system, initially addressing specific communities of scholars, and gradually climbing up to broader public understanding, thus serving the interests of the lay society, too.

Dedication to quality

Each Frontiers article is a landmark of the highest quality, thanks to genuinely collaborative interactions between authors and review editors, who include some of the world's best academicians. Research must be certified by peers before entering a stream of knowledge that may eventually reach the public - and shape society; therefore, Frontiers only applies the most rigorous and unbiased reviews. Frontiers revolutionizes research publishing by freely delivering the most outstanding research, evaluated with no bias from both the academic and social point of view. By applying the most advanced information technologies, Frontiers is catapulting scholarly publishing into a new generation.

What are Frontiers Research Topics?

Frontiers Research Topics are very popular trademarks of the *Frontiers journals series*: they are collections of at least ten articles, all centered on a particular subject. With their unique mix of varied contributions from Original Research to Review Articles, Frontiers Research Topics unify the most influential researchers, the latest key findings and historical advances in a hot research area.

Find out more on how to host your own Frontiers Research Topic or contribute to one as an author by contacting the Frontiers editorial office: frontiersin.org/about/contact

Biological aspects of targeted drug discovery: Development of novel targets and/or chemotherapies, and drug repurposing

Topic editors

Sandeep Singh — Central University of Punjab, India

Anjana Munshi — Central University of Punjab, India

Jitender Bariwal — University of Nebraska Medical Center, United States

Rajkumar S. Kalra — Okinawa Institute of Science and Technology Graduate University, Japan

Citation

Singh, S., Munshi, A., Bariwal, J., Kalra, R. S., eds. (2023). *Biological aspects of targeted drug discovery: Development of novel targets and/or chemotherapies, and drug repurposing*. Lausanne: Frontiers Media SA.
doi: 10.3389/978-2-83251-287-6

Table of contents

- 05 **Editorial: Biological aspects of targeted drug discovery: Development of novel targets and/or chemotherapies, and drug repurposing**
Rajkumar Singh Kalra, Sandeep Singh, Anjana Munshi and Jitender Bariwal
- 09 **Displacement of Native FXYP Protein From Na⁺/K⁺-ATPase With Novel FXYP Peptide Derivatives: Effects on Doxorubicin Cytotoxicity**
Chia-Chi Liu, Yeon Jae Kim, Rachel Teh, Alvaro Garcia, Elisha J. Hamilton, Flemming Cornelius, Robert C. Baxter and Helge H. Rasmussen
- 20 **Chemical and Biological Evidence of the Efficacy of Shengxian Decoction for Treating Human Lung Adenocarcinoma**
Kejuan Li, Fengming You, Qin Zhang, Ruijiao Yuan, Qianghua Yuan, Xi Fu, Yifeng Ren, Qian Wang, Xiaohong Li, Zhenya Zhang, Mototada Shichiri and Yue Yu
- 30 **Ag120-Mediated Inhibition of ASCT2-Dependent Glutamine Transport has an Anti-Tumor Effect on Colorectal Cancer Cells**
Wei Yu, Jianwen Huang, Qichao Dong, Wenting Li, Lei Jiang, Qian Zhang, Li Sun, Shengtao Yuan and Xu He
- 42 **A Novel RGD-4C-Saporin Conjugate Inhibits Tumor Growth in Mouse Models of Bladder Cancer**
Stefania Zuppone, Chiara Assalini, Claudia Minici, Oronza A. Botrugno, Flavio Curnis, Massimo Degano, Angelo Corti, Francesco Montorsi, Andrea Salonia and Riccardo Vago
- 53 **Anlotinib for the Treatment of Multiple Recurrent Lumbar and Sacral Cord Hemangioblastomas: A Case Report**
Nan Jin, Chunxiao Sun, Yijia Hua, Xinyu Wu, Wei Li and Yongmei Yin
- 58 **Honokiol Induces Ferroptosis by Upregulating HMOX1 in Acute Myeloid Leukemia Cells**
Xingrong Lai, Yanhua Sun, Xuedi Zhang, Dan Wang, Jialing Wang, Haihua Wang, Yao Zhao, Xinling Liu, Xin Xu, Haoran Song, Wenjia Ping, Yanli Sun and Zhenbo Hu
- 71 **Associations of Prior Chronic Use of Non-Steroidal Anti-Inflammatory Drugs (NSAIDs) and Glucocorticoids With Cachexia Incidence and Survival**
Santiago Olaechea, Anne Gilmore, Christian Alvarez, Bhavani S. Gannavarapu, Rodney Infante and Puneeth Iyengar
- 81 **Combining Network Pharmacology and Experimental Validation to Study the Action and Mechanism of Water extract of Asparagus Against Colorectal Cancer**
Huiling Liang, Yanju Li, Feiqing Wang, Jianing Zhao, Xu Yang, Dan Wu, Chike Zhang, Yanqing Liu, Jie Huang, Min Su, Zhixu He, Yang Liu, Jishi Wang and Dongxin Tang

- 98 **The Role of Membrane-Associated E3 Ubiquitin Ligases in Cancer**
Xuankun Chen, Li Jiang, Zhesheng Zhou, Bo Yang, Qiaojun He, Chengliang Zhu and Ji Cao
- 111 **Combinatorial delivery of CPI444 and vatalanib loaded on PEGylated graphene oxide as an effective nanoformulation to target glioblastoma multiforme: *In vitro* evaluation**
Vishnu S. Mishra, Sachin Patil, Puli Chandramouli Reddy and Bimlesh Lochab
- 128 **Diallyl Disulfide: A Bioactive Garlic Compound with Anticancer Potential**
Saikat Mitra, Rajib Das, Talha Bin Emran, Rafiuddin Khan Labib, Noor-E-Tabassum, Fahadul Islam, Rohit Sharma, Islamudin Ahmad, Firzan Nainu, Kumarappan Chidambaram, Fahad A. Alhumaydhi, Deepak Chandran, Raffaele Capasso and Polrat Wilairatana
- 149 **TAIGET: A small-molecule target identification and annotation web server**
Xuxu Wei, Jiarui Yang, Simin Li, Boyuan Li, Mengzhen Chen, Yukang Lu, Xiang Wu, Zeyu Cheng, Xiaoyu Zhang, Zhao Chen, Chunxia Wang, Edwin Wang, Ruiqing Zheng, Xue Xu and Hongcai Shang
- 156 **Exploring the recent trends in perturbing the cellular signaling pathways in cancer by natural products**
Md. Mominur Rahman, Md. Taslim Sarker, Mst. Afroza Alam Tumpa, Md. Yamin, Tamanna Islam, Moon Nyeo Park, Md. Rezaul Islam, Abdur Rauf, Rohit Sharma, Simona Cavalu and Bonglee Kim
- 182 **Beta-adrenergic receptor blockade in angiosarcoma: Which beta-blocker to choose?**
Alaa Embaby, Lisanne van Merendonk, Neeltje Steeghs, Jos Beijnen and Alwin Huitema
- 187 **Effects of metformin on Sonic hedgehog subgroup medulloblastoma progression: *In vitro* and *in vivo* studies**
Huangyi Fang, Lingfei Wang, Lisheng Yu, Fang Shen, Zelin Yang, Yue Yang, Shize Li, Haipeng Dai, Feng Tan, Jian Lin and Hansong Sheng



OPEN ACCESS

EDITED AND REVIEWED BY
Olivier Feron,
Université catholique de Louvain,
Belgium

*CORRESPONDENCE

Rajkumar Singh Kalra
✉ rajkumar.singh@oist.jp
Sandeep Singh
✉ sandeepsingh82@cup.edu.in

SPECIALTY SECTION

This article was submitted to
Pharmacology of Anti-Cancer Drugs,
a section of the journal
Frontiers in Oncology

RECEIVED 23 November 2022

ACCEPTED 12 December 2022

PUBLISHED 22 December 2022

CITATION

Kalra RS, Singh S, Munshi A and
Bariwal J (2022) Editorial: Biological
aspects of targeted drug discovery:
Development of novel targets
and/or chemotherapies, and
drug repurposing.
Front. Oncol. 12:1106610.
doi: 10.3389/fonc.2022.1106610

COPYRIGHT

© 2022 Kalra, Singh, Munshi and
Bariwal. This is an open-access article
distributed under the terms of the
[Creative Commons Attribution License](#)
(CC BY). The use, distribution or
reproduction in other forums is
permitted, provided the original
author(s) and the copyright owner(s)
are credited and that the original
publication in this journal is cited, in
accordance with accepted academic
practice. No use, distribution or
reproduction is permitted which does
not comply with these terms.

Editorial: Biological aspects of targeted drug discovery: Development of novel targets and/or chemotherapies, and drug repurposing

Rajkumar Singh Kalra^{1*}, Sandeep Singh^{2,3*}, Anjana Munshi²
and Jitender Bariwal⁴

¹Okinawa Institute of Science and Technology, Graduate University, Okinawa, Japan,

²Central University of Punjab, VPO Ghudda, Bathinda, Punjab, India, ³The University of Texas MD
Anderson Cancer Center, Houston, TX, United States, ⁴University of Nebraska Medical Center,
Omaha, NE, United States

KEYWORDS

cancer, drug discovery, chemotherapy, targeted medicine, drug repurposing,
bioactive compounds, natural products, cancer therapeutics

Editorial on the Research Topic

Biological aspects of targeted drug discovery: Development of novel
targets and/or chemotherapies, and drug repurposing

Cancer drug discovery is a competitive research area in interventional cancer research. It comprises elements of biology and chemistry for developing novel drugs/small molecules demonstrating potent anti-cancer efficacy (1). Enormous efforts across laboratories and pharmaceutical industries worldwide identify thousands of such molecules annually, however, only a few reach the clinical testing stage (2). It reflects a high failure rate for several reasons that include (yet may not be limited to) drug efficacy, physiological effects, associated side effects, and drug toxicity to normal cells (3). Targeted drug discovery approaches advanced the development of refined drugs/molecules with high therapeutic potential, yet again the success rate remains limited (4). Investigation into the drugs that are approved to cure certain diseases/conditions at times were unexpectedly seen to provide benefits from unintended side effects (5). Availability of the safety, pharmacokinetic, and manufacturing data of licensed drugs/molecules enables researchers to extract/concentrate and investigate their 'unintended' beneficial effects, avoiding a longer procedure of preclinical and clinical trials for safety evaluation (6, 7). Above practice in drug designing and discovery is generally called 'drug repurposing' or 'drug repositioning' (8). Given the availability of relevant safety data that skips time and funding, drug repurposing offers opportunities for researchers to evaluate their anti-cancer and preventive efficacies against routine chemotherapeutic drugs/therapies (9).

In the present Research Topic, we gathered new knowledge on novel anticancer compounds/molecules, research strategies/approaches, and repurposing drugs.

Given the safety and accessibility, natural bioactive compounds/extracts from herbal medicinal plants attained larger interest in the field of cancer drug discovery. In an original report, [Li et al.](#) explored the anti-cancer potential of Shengxian Decoction (SXT, a traditional Chinese medicine) against lung adenocarcinoma. Extraction and analysis of crude SXT led them to reveal the abundance of mangiferin, i.e., an established anti-cancer compound. The serum pharmacological analysis exhibited growth-suppressive activity of serum SXT against A549 lung cancer cells that was further validated in the animal model. At the molecular level, their investigation revealed tumor necrosis-inducing and HIF-1 α suppressive function of SXT. Their investigation provided the first scientific evidence of the anti-cancer efficacy of SXT against lung adenocarcinoma. Another report by [Lai et al.](#) identified the anti-leukemia activity of honokiol (a natural small biphenolic phytochemical compound) on a panel of acute myeloid leukemia (AML) cell lines. To analyze honokiol's potent growth arrest (G0/G1) and anti-viability/proliferative activities at the molecular level, they discovered a noncanonical ferroptosis pathway-inducing function of honokiol that upregulates the intracellular lipid peroxide and HMOX1 levels in AML cells. This report suggested that honokiol could serve as a potential ferroptosis activator in AML. In another report, [Zuppone et al.](#) genetically modified the plant-derived single-chain ribosome-inactivating protein saporin (SAP) structure by joining its N-terminus to the ACDRCGDCFCG peptide (RGD-4C, an α v-integrin ligand), and subsequently analyzed the anti-tumor efficacy of the resulting protein *viz.* RGD-SAP *in vitro* and *in vivo* mouse model. They revealed that RGD-4C targeting domain fusion to SAP enhances the cytotoxic activity of the latter in an α v-integrin expression-dependent manner. Of note, they showed that a systemic administration of RGD-SAP with mitomycin C (a frontline chemotherapeutic drug to treat bladder cancer) extended the survival of mice with orthotopic bladder cancer, lacking any systemic toxicity. They stressed on exploiting the potent efficacy of RGD-SAP either alone or in combination with the current chemotherapy regimes to treat bladder cancer and potentially other solid tumors. In this line, another study by [Liang et al.](#) using network pharmacology and wet lab attempted to identify the potential therapeutic targets of Asparagus (ASP) in colorectal cancer (CRC). They identified 9 active components from ASP, while its 157 potential targets were predicted including the p53, FOS, AP-1, and Akt1. The obtained results from *in vitro* and *in vivo* assays affirmed the anti-cancer activities of ASP, thereby providing the first evidence of its potential role for CRC therapeutics. Consistent with the emerging significance of natural bioactive compounds in the complementary or alternative therapeutics, [Mitra et al.](#) in a review report further assessed the anti-cancer potential of Diallyl disulfide (DADS), a key bioactive organosulfur

compound from garlic. Garlic is widely regarded for its medicinal properties that have a wide range of bioactivities including antithrombotic, hypo-lipidemic, antibacterial, and anticancer, while DADS exhibited prominent anti-tumor activities against diverse cancers. The gathered information comprehensively provided insights into the anti-cancer properties of DADS, its mode of action, mechanisms, bioavailability, and pharmacokinetics from existing studies. To this end, [Rahman et al.](#) in a detailed review further explored the recent trends in natural products-led perturbed cellular signaling of a cancer cell. The report reviewed the role of natural compounds in causing cell cycle arrest, triggering intrinsic and/or extrinsic apoptosis pathways. The report highlighted the significance of several key signaling pathways and their effector proteins including MAPK, NF- κ B, Wnt, Akt, Notch, ER, and p53, which regulate apoptotic signals specifically in pre-malignant or cancer cells. They underlined the importance of non-toxic “natural drugs” for cancer prevention and therapeutics. Taken together, original research and reviews in the section enhanced our understanding of the anti-cancer activities of natural compounds at the cellular and molecular levels.

Emergence of targeted drug discovery approaches highlighted the significance of selective inhibitors, small molecules/metabolites, and novel peptides in cancer therapeutics. In this line, original research from [Yu et al.](#) elucidated the potent function of Ag120 (ivosidenib, a mutant isocitrate dehydrogenase 1 or IDH1 inhibitor) as an ASCT2 (solute carrier family 1 member 5) inhibitor in colorectal cancer. In the cancer cell metabolic reprogramming, glutamine metabolism plays an important role in tumor progression, which underlines that targeting glutamine uptake (via the transporter protein ASCT2/SLC1A5) could be an effective interventional strategy. The report showed that Ag120 blocks glutamine uptake, metabolism and restricts tumor cell growth *via* ERK and mTOR signaling pathways. These efforts identified a novel mechanism of Ag120 function as an ASCT2 inhibitor for cancer therapeutics. In another original report, [Olaechea et al.](#) studied the associations between prior long-term use of NSAIDs (non-steroidal anti-inflammatory drugs) or glucocorticoids with cachexia (i.e., an inflammatory and metabolic syndrome of unintended weight loss in muscle and adipose tissue) incidence and occurrence of post-diagnosis weight loss in a retrospective cohort of 3,180 cancer patients. Of note, they elucidated that the prior anti-inflammatory treatments, mainly NSAIDs, have protective effects against the manifestations of cachexia at the cancer diagnosis. They stressed on the requisite of detailed investigation to precisely assess the potential therapeutic benefits of NSAIDs early in cancer management. Examining the repurposing of Metformin (a first-line drug for type 2 diabetes), a report by [Fang et al.](#) further investigated inhibitory effect on the medulloblastoma (MB) and elucidated its efficacy in the Sonic hedgehog (Shh) subgroup MB cell line *in vitro* and *in vivo*. Of note, these effects were shown to cause by

AMPK-mediated inhibition of the Shh signaling pathway. In the case of hemangioblastoma (HB, a highly vascularized cystic tumor of the CNS or central nervous system), a case report by Jin et al. revealed that anlotinib, i.e., a tyrosine kinase inhibitor (targeting VEGFR) can produce the significant radiographic response. The 62-year-old woman patient with multiple recurrent lumbar and sacral cord HBs post receiving the 3 months anlotinib treatment showed marked tumor regression, hinting anlotinib could be a therapeutic approach for patients with multiple recurrent HB or multiple lesions/VHL disease. Amid increasing drug repurposing in clinical practice, a careful review of drug safety for cancer patients is important. In a perspective report, Embaby et al. underscored the need for diligence when choosing the β -adrenergic receptor blockers (β -blockers) in angiosarcoma. The β -blockers/antagonists are often prescribed in ischemic cardiac disease due to their anti-hypertensive and anti-arrhythmic activities. Given the usage of β -blockers in recent times to improve therapeutic options for angiosarcoma patients, it is crucial to determine the optimal pharmacological activities of β -blockers in the patient cohort where most patients lack cardiovascular co-morbidity. The report underlined the need to use β -blockers that have intrinsic sympathomimetic or vasodilator effects, e.g., labetalol, pindolol or carvedilol, essentially to minimize the risk of adverse cardiovascular events. To ensure efficient drug delivery, original research by Mishra et al. developed water-dispersible and biocompatible nanocargo (GO-PEG) for Glioblastoma multiforme (GBM; a primary malignant form of CNS tumor in adults). Given the utility of nanocarriers that improve a drug's water dispersibility, cellular permeability, and efficacy at a lower dose, they developed a GO-PEG nanocarrier based on modified graphene oxide with a poly(ethylene glycol) amine dendrimer (6-armed) for effectively load and carry two hydrophobic anticancer drug molecules viz. CPI444 and vatalanib targeting A2AR, VEGFR, PDGFR, and c-KIT. They validated the above regime to reduce cancer cell viability, migration/invasion, calcium levels, and expression of markers (Oct4 and Nanog) associated with GBM, and thereby affirmed the utility of the adopted strategy toward effective GBM treatment. The revised/repurposed targeting approaches against cancer are of much interest, yet tumor resistance has been an evident challenge. In this line, original research from Liu et al. attempted to overcome FXYD3 (an FXYD protein linked with Na⁺/K⁺-ATPase α/β heterodimers that protect β 1 subunit against glutathionylation that destabilizes the heterodimer and inhibits its function) -led treatment resistance in cancer cells. They developed two FXYD3 peptide derivatives viz. FXYD3-pep CKCK and -pep SKSK that allow elimination and increase of FXYD protein function, respectively. The report revealed that Cys residue is critical to counter β 1 subunit glutathionylation to promote the cytotoxicity upon siRNA-mediated FXYD3 suppression. Chen et al. in a review report, further assessed the functional significance of membrane-associated E3 ligases in

cancer and as a drug target. Authors shed light on the critical function of the ubiquitin E3 ligase in facilitating intracellular communication, while linking its dysfunction to cancer. Therefore, E3 ligase could as a novel drug target for cancer therapy, where drugs/small molecules inducing ubiquitination-mediated degradation of the cancer-cell membrane may be of prime interest. To enable the virtual and reliable identification of targets for drug discovery, Wei et al. in a method article further developed a graphical web interface viz. TAIGET, which comprises a docking, a target screen, and an annotation module respectively. TAIGET consist of a robust target annotation module (curating >14,000 cancer-related works, having 73 cancer types and 2,170 cell types), and is freely accessible at <http://www.taiget.cn/>. Also, it has a comprehensive interface to support researchers those lack technical expertise in the virtual drug discovery practice.

Taken together, the present Research Topic collects knowledge from the submitted original research article(s), reviews, case reports, method and perspective reports and comprehensively presents new findings on the anti-cancer drug (natural compounds, inhibitors/peptides, and small molecules) discovery, novel regimes, and emerging clinical significance of drug repurposing.

Author contributions

All authors made direct and intellectual contributions to the report and provided their approval for the publication.

Acknowledgments

We thank all the contributing authors and reviewers for their valuable contributions/critics to this Research Topic.

Conflict of interest

The authors declare that the research was conducted in the absence of any commercial or financial relationships that could be construed as a potential conflict of interest.

Publisher's note

All claims expressed in this article are solely those of the authors and do not necessarily represent those of their affiliated organizations, or those of the publisher, the editors and the reviewers. Any product that may be evaluated in this article, or claim that may be made by its manufacturer, is not guaranteed or endorsed by the publisher.

References

1. Moffat JG, Rudolph J, Bailey D. Phenotypic screening in cancer drug discovery - past, present and future. *Nat Rev Drug Discovery* (2014) 13:588–602. doi: 10.1038/nrd4366
2. Kamb A, Wee S, Lengauer C. Why is cancer drug discovery so difficult? *Nat Rev Drug Discovery* (2007) 6:115–20. doi: 10.1038/nrd2155
3. Hoelder S, Clarke PA, Workman P. Discovery of small molecule cancer drugs: successes, challenges and opportunities. *Mol Oncol* (2012) 6:155–76. doi: 10.1016/j.molonc.2012.02.004
4. Ramsay RR, Popovic-Nikolic MR, Nikolic K, Uliassi E, Bolognesi ML. A perspective on multi-target drug discovery and design for complex diseases. *Clin Transl Med* (2018) 7:3. doi: 10.1186/s40169-017-0181-2
5. Sleire L, Forde HE, Netland IA, Leiss L, Skeie BS, Enger PO. Drug repurposing in cancer. *Pharmacol Res* (2017) 124:74–91. doi: 10.1016/j.phrs.2017.07.013
6. Pushpakom S, Iorio F, Eyers PA, Escott KJ, Hopper S, Wells A, et al. Drug repurposing: progress, challenges and recommendations. *Nat Rev Drug Discovery* (2019) 18:41–58. doi: 10.1038/nrd.2018.168
7. Zhang Z, Zhou L, Xie N, Nice EC, Zhang T, Cui Y, et al. Overcoming cancer therapeutic bottleneck by drug repurposing. *Signal Transduct Target Ther* (2020) 5:113. doi: 10.1038/s41392-020-00213-8
8. Frantzi M, Latosinska A, Mokou M, Mischak H, Vlahou A. Drug repurposing in oncology. *Lancet Oncol* (2020) 21:e543. doi: 10.1016/S1470-2045(20)30610-0
9. Gonzalez-Fierro A, Duenas-Gonzalez A. Drug repurposing for cancer therapy, easier said than done. *Semin Cancer Biol* (2021) 68:123–31. doi: 10.1016/j.semcancer.2019.12.012



Displacement of Native FXYP Protein From Na⁺/K⁺-ATPase With Novel FXYP Peptide Derivatives: Effects on Doxorubicin Cytotoxicity

Chia-Chi Liu^{1*}, Yeon Jae Kim¹, Rachel Teh¹, Alvaro Garcia², Elisha J. Hamilton¹, Flemming Cornelius³, Robert C. Baxter⁴ and Helge H. Rasmussen^{1,5*}

¹ North Shore Heart Research Group, Kolling Medical Research Institute, University of Sydney, St Leonards, NSW, Australia, ² School of Chemistry, University of Sydney, Camperdown, NSW, Australia, ³ Department of Biomedicine, University of Aarhus, Aarhus C, Denmark, ⁴ Hormones and Cancer Laboratories, Kolling Institute, University of Sydney, St Leonards, NSW, Australia, ⁵ Department of Cardiology, Royal North Shore Hospital, St Leonards, NSW, Australia

OPEN ACCESS

Edited by:

Rajkumar S. Kalra,
Okinawa Institute of Science and
Technology Graduate University,
Japan

Reviewed by:

Devivasha Bordoloi,
Wistar Institute, United States
Aditya Sarode,
Columbia University, United States

*Correspondence:

Chia-Chi Liu
chiachi.liu@sydney.edu.au
Helge H. Rasmussen
helge.rasmussen@sydney.edu.au

Specialty section:

This article was submitted to
Pharmacology of Anti-Cancer Drugs,
a section of the journal
Frontiers in Oncology

Received: 21 January 2022

Accepted: 21 February 2022

Published: 17 March 2022

Citation:

Liu C-C, Kim YJ, Teh R, Garcia A,
Hamilton EJ, Cornelius F, Baxter RC
and Rasmussen HH (2022)
Displacement of Native FXYP Protein
From Na⁺/K⁺-ATPase With Novel
FXYP Peptide Derivatives: Effects on
Doxorubicin Cytotoxicity.
Front. Oncol. 12:859216.
doi: 10.3389/fonc.2022.859216

The seven mammalian FXYP proteins associate closely with α/β heterodimers of Na⁺/K⁺-ATPase. Most of them protect the $\beta 1$ subunit against glutathionylation, an oxidative modification that destabilizes the heterodimer and inhibits Na⁺/K⁺-ATPase activity. A specific cysteine (Cys) residue of FXYP proteins is critical for such protection. One of the FXYP proteins, FXYP3, confers treatment resistance when overexpressed in cancer cells. We developed two FXYP3 peptide derivatives. FXYP3-pep CKCK retained the Cys residue that can undergo glutathionylation and that is critical for protecting the $\beta 1$ subunit against glutathionylation. FXYP3-pep SKSK had all Cys residues mutated to Serine (Ser). The chemotherapeutic doxorubicin induces oxidative stress, and suppression of FXYP3 with siRNA in pancreatic- and breast cancer cells that strongly express FXYP3 increased doxorubicin-induced cytotoxicity. Exposing cells to FXYP3-pep SKSK decreased co-immunoprecipitation of FXYP3 with the $\alpha 1$ Na⁺/K⁺-ATPase subunit. FXYP3-pep SKSK reproduced the increase in doxorubicin-induced cytotoxicity seen after FXYP3 siRNA transfection in pancreatic- and breast cancer cells that overexpressed FXYP3, while FXYP3-pep CKCK boosted the native protein's protection against doxorubicin. Neither peptide affected doxorubicin's cytotoxicity on cells with no or low FXYP3 expression. Fluorescently labeled FXYP3-pep SKSK was detected in a perinuclear distribution in the cells overexpressing FXYP3, and plasmalemmal Na⁺/K⁺-ATPase turnover could not be implicated in the increased sensitivity to doxorubicin that FXYP3-pep SKSK caused. FXYP peptide derivatives allow rapid elimination or amplification of native FXYP protein function. Here, their effects implicate the Cys residue that is critical for countering $\beta 1$ subunit glutathionylation in the augmentation of cytotoxicity with siRNA-induced downregulation of FXYP3.

Keywords: breast cancer, pancreatic cancer, peptide therapy, membrane transport, oxidative stress, dysadherin

INTRODUCTION

The 7-member mammalian FXYD protein family is expressed in a tissue-specific manner (1). Its members associate closely with the Na^+/K^+ -ATPase, and most of them protect the Na^+/K^+ -ATPase $\beta 1$ subunit against glutathionylation, an oxidative modification in which the cytosolic tri-peptide glutathione (GSH) binds to a free SH group of a cysteine (Cys) residue in a protein. Glutathionylation of the $\beta 1$ subunit compromises the structural integrity of the $\alpha 1/\beta 1$ heterodimer of Na^+/K^+ -ATPase and inhibits its function. Countering this, FXYD proteins can stabilize Na^+/K^+ -ATPase structure and function (2).

A specific Cys residue bracketed by basic amino acids and conserved across most members of the FXYD protein family is critical for a FXYD protein's protection against $\beta 1$ subunit glutathionylation. The cellular expression of FXYD proteins that have the specific Cys residue is protective against oxidative stress-induced $\beta 1$ subunit glutathionylation and Na^+/K^+ -ATPase inhibition, while mutating the residue eliminates the protective effect of the expressed protein (2). The critical role of Cys residues is also evident from the effects of exposing cardiac myocytes to recombinant FXYD proteins with or without the Cys residue (2).

A brief (15 min) exposure of myocytes to recombinant FXYD3 protein displaces the native FXYD1 protein. Both the exogenous and the native protein have the Cys residue critical for the protective effect against $\beta 1$ subunit glutathionylation, and the additional exogenous supply of FXYD3 counters $\beta 1$ subunit glutathionylation induced by oxidative stress. In parallel, it counters sarcolemmal Na^+/K^+ -ATPase inhibition. Exogenous recombinant FXYD1 has similar effects on Na^+/K^+ -ATPase function. However, while a recombinant FXYD3 protein with Cys residues mutated to serine also displaces native FXYD1 in myocytes, it is not protective against $\beta 1$ subunit glutathionylation or Na^+/K^+ -ATPase inhibition (2).

Only the transmembrane domain and the extracellular PFXYD motif near the membrane leaflet have known bonds to α - and β Na^+/K^+ -ATPase subunits (3, 4). Other than the PFXYD motif and the motif that includes the Cys residue critical for countering $\beta 1$ subunit glutathionylation, extracellular and cytoplasmic domains are poorly conserved across the FXYD protein family (5). Since they are not expected to affect $\beta 1$ subunit glutathionylation, we designed 36 amino acid peptide analogues of the Cys-preserved FXYD3 protein and its Cys-mutated (Cys \rightarrow Ser) derivative without these domains. We refer to these peptides as FXYD3-pep CKCK and FXYD3-pep SKSK.

FXYD3 is often highly expressed in cancers, particularly in those of the pancreas (6), prostate (7), and breast (8). Suppression of FXYD3 with siRNA in cultured human breast cancer cells that overexpress FXYD3 augments cytotoxicity of doxorubicin (Dox) (9). Dox induces oxidative stress (10), and the augmentation of Dox cytotoxicity with downregulation of FXYD3 was associated with an increase in $\beta 1$ Na^+/K^+ -ATPase subunit glutathionylation (9). If augmentation of cytotoxicity with FXYD3 downregulation depends on the FXYD Cys residue that is critical for countering $\beta 1$ subunit glutathionylation, Cys-mutated FXYD3-pep SKSK but not FXYD3-pep CKCK should

reproduce the augmentation. We have examined the effects of FXYD3-pep SKSK or FXYD3-pep CKCK on Dox-induced cytotoxicity in breast and pancreatic cancer cells that do or do not overexpress FXYD3.

MATERIALS AND METHODS

Cell Cultures

Human pancreatic cancer cells BxPC-3, Panc-1, non-transformed human mammary epithelial MCF-10A cells, and human breast cancer cells MCF-7 and MDA-MB-468 were obtained from the American Type Culture Collection (ATCC, Manassas, VA, USA). The cells were then cultured as previously described (6, 9, 11). All cells were used within 20 passages of thawing and were free of mycoplasma contamination as ascertained by mycoplasma PCR detection (12).

FXYD3 siRNA Transfection

A human siRNA against FXYD3 (consisting of pools of three to five target-specific 19–25-nt siRNAs designed to knock down gene expression, sc-60665) and the non-silencing control (control siRNA-A, sc-37007) were purchased from Santa Cruz Biotechnology (Dallas, TX, USA). Cells were transfected using the siRNA Transfection Reagent/Medium (Santa Cruz Biotechnology) according to the manufacturer's instructions. The FXYD3 mRNA expression level was quantified by real-time polymerase chain reaction (RT-PCR) as described previously (9). FXYD3 protein abundance was measured by Western blotting (9).

Susceptibility to Glutathionylation of FXYD3 Peptide Derivatives

FXYD3 peptide derivatives were synthesized by Mimotopes Pty Ltd., Australia. Since an FXYD protein's susceptibility to glutathionylation is essential for the protein to counter glutathionylation of the $\beta 1$ subunit (2), we ascertained that FXYD3-pep CKCK but not FXYD3-pep SKSK is susceptible to glutathionylation. Glutathionylation was performed by disulfide exchange with oxidized glutathione (GSSG) (13). Peptides were incubated with 10 mM GSSG (30 min) or 10 mM GSH/100 mM hydrogen peroxide (H_2O_2 , 30 min). Dithiothreitol (DTT) was added for disruption of protein disulfide bonds. N-Ethylmaleimide (NEM, 5 mM for 5 min on ice) was also added to block free thiols and minimize exchange between free thiols and oxidized thiols.

Fluorescent Confocal Microscopy

The extracellular N-terminal of customized FXYD3-pep SKSK was tagged with fluorescent tetramethylrhodamine (TRITC) to visualize the distribution of FXYD peptide derivatives in cells. BxPC-3 cells grown to 70% confluence were exposed to 1 μM FXYD3-pep SKSK with or without TRITC-tag. Cells were exposed to the peptide for 2 h, the media removed, peptide-free fresh media added, and cells incubated for a further 24 h. They were then fixed in 3.7% paraformaldehyde, washed, and mounted on non-coated color frost slides in Fluoroshield

mounting medium with DAPI (ab104139, Abcam, Cambridge, MA, USA) and examined under a laser scanning confocal microscope (Leica TCS SP5, Wetzlar, Germany). The excitation wavelength was 543 nm, and the emission wavelength was 572 nm. The fluorescence images were obtained using constant settings of scanning speed, pinhole diameter, and voltage gain.

Cell Viability and Apoptosis

Cell metabolic activity was assayed as described (14) by estimating the reduction of XTT (2,3-bis(2-methoxy-4-nitro-5-sulphophenyl)-2*H*-tetrazolium-5-carboxyanilide), using a commercially available kit (Cell Signaling Technology, Danvers, MA, USA) according to the manufacturer's instructions. Metabolic activity was used as a surrogate for viability. For each set of experimental groups, we performed 5 experiments with 4 replicates. Caspase-3-like activity is increased through a protease cascade during the early stage of apoptosis (15), and we measured activities of Caspase 3/7 (DEVDase) using the caspase fluorogenic substrate (Calbiochem, San Diego, CA, USA) as described (9).

Co-Immunoprecipitation

After solubilization in RIPA lysis buffer, protein extracts (0.5–1 mg) from cells were precleared and incubated overnight at 4°C with anti- α_1 subunit Na^+ - K^+ ATPase (D4Y7E; Cell Signaling Technology, USA), anti-FXYD3 (ab205534; Abcam, UK), or anti- β_1 subunit (D6U8Q; Cell Signaling Technology, USA) Na^+ / K^+ -ATPase antibodies followed by precipitation for 2 h at 4°C with protein A/G plus agarose-coated beads (Abcam, UK). Sample buffer was added, the mixture was boiled for 5 min and sedimented, and the supernatant was used for immunoblotting.

Western Blot

Western blot analysis was performed as previously described (9). The following primary antibodies were used: Na^+ - K^+ ATPase α_1 subunit (05-369; Merck Millipore, Burlington, MA, USA), Na^+ - K^+ -ATPase β_1 subunit (A278; Merck Millipore, USA), FXYD3 (OTI1D1; Sigma-Aldrich, AUS), or GSH (recognizing GS-S-proteins purchased from Virogen, Watertown, MA, USA). For a loading control, GAPDH was detected using the anti-GAPDH monoclonal antibody (G8795; Sigma-Aldrich, Sydney, Australia). Each presented immunoblot is representative of separate experiments as indicated in text. The band densities were quantified by densitometry (Image LabTM, 6.0.1 Bio-Lab Laboratories, Inc., Hercules, CA, USA).

Measurement of Plasmalemmal Na^+ / K^+ -ATPase Activity

The whole-cell patch-clamp technique was used to measure plasmalemmal electrogenic Na^+ / K^+ -ATPase pump current (I_p , arising from the 3:2 ratio of intracellular Na^+ pumped out of cells in exchange for extracellular K^+ pumped in). Solutions and voltage-clamp protocols were designed to minimize non-pump currents. Patch pipette solutions that perfuse the intracellular compartment after the whole-cell voltage clamp configuration is established contained the following (in mM): 1 NaH_2PO_4 , 5

HEPES, 5 EGTA, 2 MgATP, 86 Na^+ -glutamate, and 70 tetramethylammonium chloride. The solution was titrated to a pH of 7.2 at 22°C using 2 M NaOH. The final concentration of Na^+ was 100 mM which causes near-maximal plasmalemmal Na^+ / K^+ -ATPase activation at intracellular sites.

Cells were initially superfused with modified Tyrode's solution containing the following (in mM): 140 NaCl, 5.6 KCl, 2.16 CaCl_2 , 0.44 NaH_2PO_4 , 10 glucose, 1.0 MgCl_2 , and 10 HEPES. The solution was titrated to a pH of 7.55 at 22°C with NaOH. After the whole-cell configuration was established, we switched the superfusate to one that was nominally Ca^{2+} -free and contained 0.2 mM CdCl_2 and 2 mM BaCl_2 . Cd^{2+} was included to block Ca^{2+} channel conductance and inhibit Na^+ - Ca^{2+} exchange (16), while Ba^{2+} was included to block K^+ channels. Cells were voltage clamped at 0 mV to inactivate voltage-sensitive Na^+ channels (17) and L-type Ca^{2+} channels (18, 19).

I_p was identified as the inward shift in holding current with exposure to K^+ -free extracellular solutions to eliminate Na^+ / K^+ -ATPase activation at extracellular sites, as described previously for measurements in cardiac myocytes (20). We switched to the K^+ -free superfusate 2–3 minutes after the whole-cell configuration had been established. Na^+ / K^+ -ATPase pump currents are small relative to other membrane currents, and it is important for their accurate measurement that holding currents are stable before and after the switch from K^+ -containing to K^+ -free solutions. As for measurement of I_p in cardiac myocytes (20), we used predetermined criteria for stability of holding currents before and after changing to K^+ -free extracellular solution. I_p was normalized for cell membrane capacitance and hence cell size.

Statistical Analysis

Results are presented as mean \pm standard deviation (SD). The IC50 values for Dox in cell viability studies were calculated by GraphPad Prism. Statistical comparisons were made with a Mann–Whitney test, ANOVA, and repeated-measure ANOVA with Geisser–Greenhouse epsilon correction. $p < 0.05$ was considered statistically significant.

RESULTS

FXYD3-siRNA Transfection Augments Dox-Induced Cytotoxicity in BxPC-3 Cells

BxPC-3 pancreatic cancer cells which have high FXYD3 expression were treated with siRNA transfection to modulate FXYD3 expression. **Figure 1A** shows that the siRNA reduced levels of endogenous FXYD3a and FXYD3b mRNA, two splice variants of FXYD3, at 24 and 48 h after treatment when compared with a control. Transfection with siRNA also decreased the protein expression of FXYD3 in BxPC-3 cells by ~60% after 48 h (**Figure 1B**).

FXYD3 siRNA transfection alone had no significant effects on viability or caspase 3/7 activation in BxPC-3 cells. When co-treated with Dox, transfection augmented a decreased viability (**Figure 1C**) and an increased caspase 3/7 activation (**Figure 1D**). The siRNA-directed suppression of FXYD3 protein sensitized BxPC-3 cells to Dox.

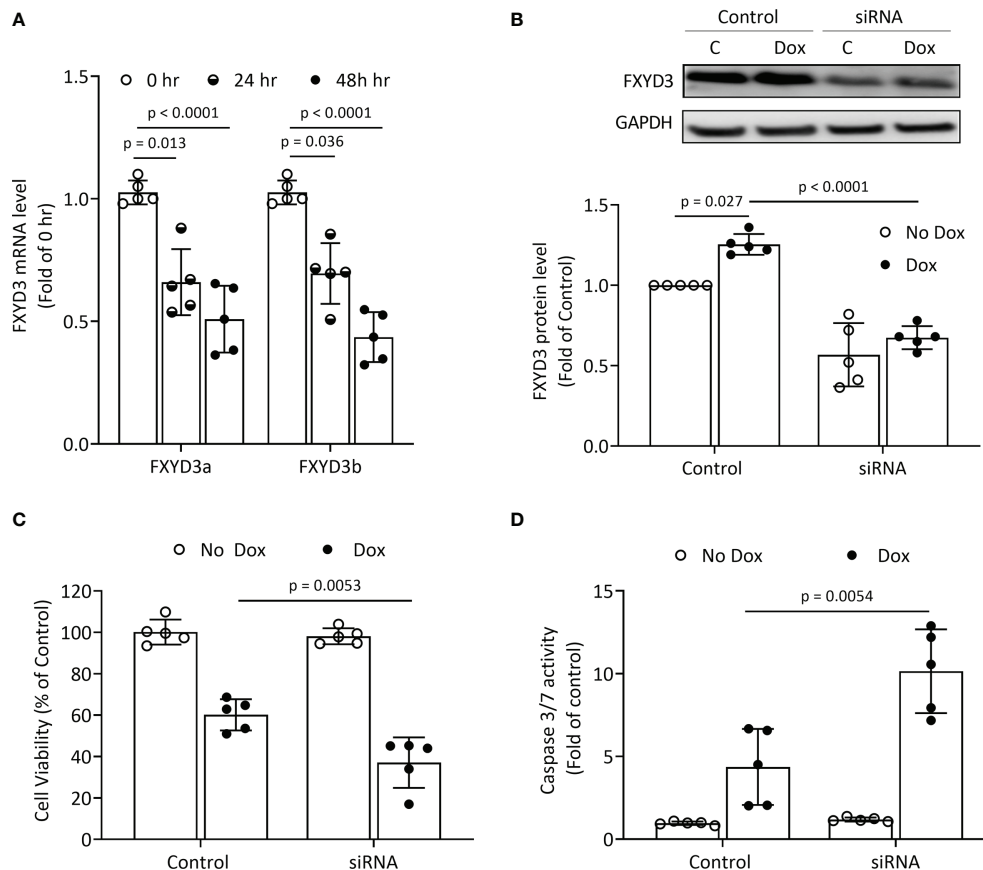


FIGURE 1 | FXYD3-siRNA transfection of BxPC-3 cells. **(A)** Expression of FXYD3a and FXYD3b mRNA after exposure of cells to FXYD3 siRNA for 24 or 48 h **(B)** Effect of siRNA and Dox on FXYD3 expression. Cells were exposed to 1 μ M Dox or Dox-free culture medium for 48 h after transfection as indicated. **(C)** FXYD3 siRNA transfection and effect of Dox on cell viability. Cells were exposed to Dox or Dox-free culture medium as for **(C)**. **(D)** FXYD3 siRNA transfection and effect of Dox on Caspase-3/7 activity.

Effects of Novel FXYD3 Derivatives on Protein Glutathionylation

The amino acid sequence of wild-type (WT) FXYD3 is shown in **Figure 2A**. The peptide analogue of the Cys-mutated FXYD3 protein with poorly conserved intracellular and extracellular domains eliminated FXYD3-pep SKSK, as shown in **Figure 2B**, and the analogue with Cys residues of the WT protein retained FXYD3-pep CKCK, as shown in **Figure 2C**. As expected, immunoblotting with a GSH antibody identified glutathionylation of FXYD3-pep CKCK but not of FXYD3-pep SKSK (**Figure 2D**, one of two similar experiments is shown). Dithiothreitol (DTT) is a reducing agent, which is expected to decrease existing glutathionylation. When incubated with DTT, the signal for glutathionylation of FXYD3-pep CKCK was eliminated (**Figure 2E**).

The effects of FXYD3-pep SKSK on glutathionylation of the $\beta 1$ Na^+/K^+ -ATPase subunit was examined in BxPC-3 cells submitted to the oxidative stress induced by Dox. BxPC-3 cells were exposed to 1 μ M FXYD3-pep SKSK for 2 h. The cells were washed and then incubated for 24 h in a solution that included only 1 μ M Dox but was free of FXYD3-pep SKSK. The levels of glutathionylation of the Na,

K-ATPase $\beta 1$ subunit was quantified in the precipitate obtained in immunoprecipitation experiments with an anti-GSH antibody. Exposure to FXYD3-pep SKSK increased the signal for $\beta 1$ Na^+/K^+ -ATPase subunit glutathionylation (**Figure 2F**).

FXYD3-pep SKSK Displaces WT FXYD3 From the $\alpha 1$ Na^+/K^+ -ATPase Subunit

Levels of FXYD3, normalized to levels in the non-transformed human breast cell line MCF-10A, were much higher in the BxPC-3 and MCF-7 cells than in the MDA-MB-468 and Panc-1 cells. Overexpression of the $\alpha 1$ Na^+/K^+ -ATPase subunit broadly followed the same pattern as FXYD3 expression (**Figure 3A**). We did not detect WT FXYD3 protein or FXYD3 mRNA for Panc-1 (not shown), as others also reported (6).

We examined the cellular distribution of FXYD3-pep SKSK. For this, we used pancreatic BxPC-3 cells because they exhibited the strongest signal for expression of $\alpha 1$ Na^+/K^+ -ATPase subunits (**Figure 3A**) that FXYD3-pep SKSK is expected to bind to. We exposed cells to TRITC-tagged FXYD3-pep SKSK for 2 h. The peptide was then washed off, and fluorescence microscopy was performed 24 h later.

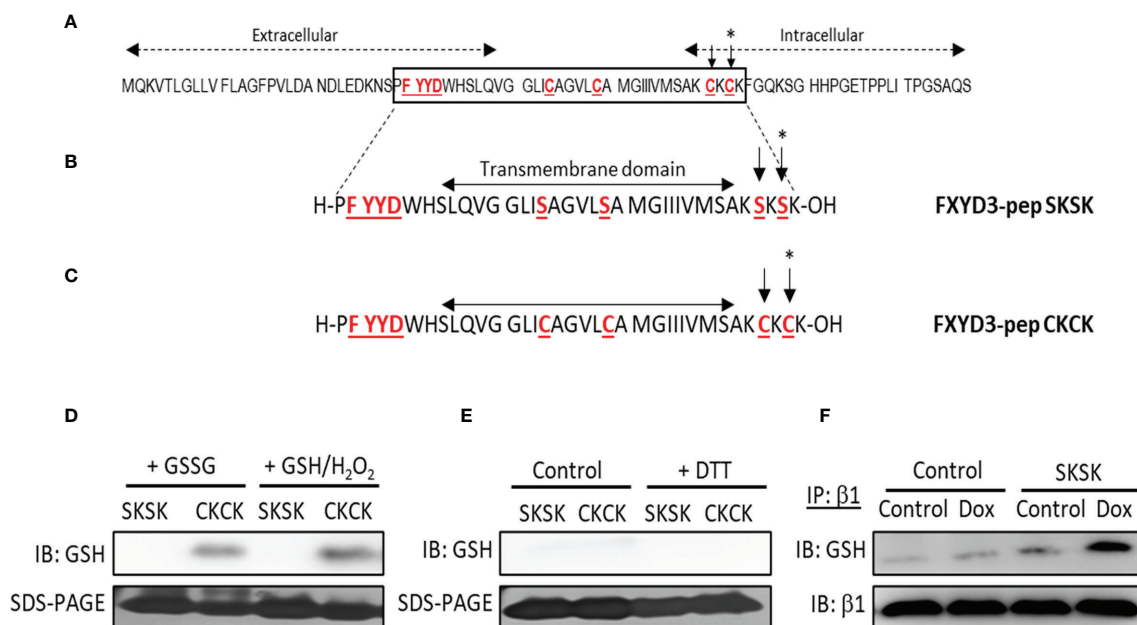


FIGURE 2 | Amino acid sequences of FXYD3 and its derivatives. **(A)** Wild-type (WT) FXYD3. Cys residues mutated to Ser in full-length recombinant protein and the FXYD motif in the extracellular domain are shown in red font and are underlined. A Cys residue (indicated by *) in the cytoplasmic domain near the inner membrane leaflet and bracketed by basic amino acids (here Lys) is obligatory for susceptibility to glutathionylation of members of the FXYD protein family. Such susceptibility is critical for a FXYD protein, including FXYD3, to counter glutathionylation of the $\beta 1$ Na⁺/K⁺-ATPase subunit. **(B)** Amino acid sequence of FXYD3-pep SKSK. Ser residues (indicated by *) that replaced Cys residues in the corresponding sites in WT FXYD3 are indicated in red font. **(C)** Amino acid sequence of FXYD3-pep CKCK that has Cys residues (indicated by *) of WT FXYD3 retained. **(D)** Immunoblots for GSH indicating glutathionylation of FXYD3-pep CKCK but not FXYD3-pep SKSK with exposure to GSSG or GSH/H₂O₂. **(E)** Reversibility of FXYD3-pep CKCK glutathionylation with exposure to DTT. **(F)** Immunoblot for GSH of cell lysate immunoprecipitated for the $\beta 1$ Na⁺/K⁺-ATPase subunit after exposure to Dox. Pre-exposure to FXYD3-pep SKSK augments Dox-induced $\beta 1$ Na⁺/K⁺-ATPase subunit glutathionylation.

TRITC-tagged FXYD3-pep SKSK was detected in the cytosol, particularly in the perinuclear region (**Figure 3B**). The fluorescent signal was not detected in cells exposed to FXYD3-pep SKSK without TRITC-tag (data not shown). A fluorescent signal that appears with a 2-h exposure to TRITC-tagged FXYD3-pep indicates that the peptide is membrane permeable, as expected for its amino acid sequence that mostly corresponds to the transmembrane domain of the FXYD3 protein (**Figure 2**). Persistence of the fluorescent signal 24 h after TRITC-tagged FXYD3-pep was washed off would not be expected unless the peptide binds intracellularly. A fluorescent signal reflecting binding to plasmalemmal Na⁺/K⁺-ATPase was not selectively detected. However, a signal from such fluorescence might be undetectable with overlapping of signals in multilayered cultured cells.

To examine if FXYD3-pep SKSK can displace WT FXYD3 from Na⁺/K⁺-ATPase, we exposed BxPC-3 cells to 1 μ M FXYD3-pep SKSK for 2 h before cell lysis. We used an antibody directed against an epitope in WT FXYD3 that is absent in the shortened FXYD3-pep SKSK to detect the FXYD3 protein and found that FXYD3-pep SKSK reduced the co-immunoprecipitation (Co-IP) of the Na⁺/K⁺-ATPase $\alpha 1$ subunit with FXYD3 by ~50% (**Figure 3C**). A similar reduction was observed in reverse Co-

IP (**Figure 3D**). The peptide displaced the native FXYD3 from the Na⁺/K⁺-ATPase $\alpha 1$ subunit.

FXYD3-pep SKSK Enhances Dox-Mediated Cytotoxicity

We examined if displacement of WT FXYD3 from Na⁺/K⁺-ATPase is reflected in viability of cells exposed to FXYD3-pep SKSK with and without co-exposure to Dox for 48 h. The culture medium that contained FXYD3-pep SKSK and Dox was replaced with fresh medium every 24 h.

FXYD3-pep SKSK alone at 1 or 2 μ M did not decrease cancer cell viability (data not shown). However, it augmented a Dox-induced decrease in viability of pancreatic BxPC-3 and breast MCF-7 cells that express high levels of FXYD3. For BxPC-3 cells, the IC₅₀ for Dox was shifted from ~1.74 to ~0.4 μ M and ~0.3 μ M with exposure to 1 and 2 μ M FXYD3-pep SKSK, respectively (**Figure 4A**). For MCF-7 cells, FXYD3-pep SKSK augmented the effects of Dox with a shift in IC₅₀ from ~4.3 to ~0.5 μ M with exposure to 2 μ M FXYD3-pep SKSK (**Figure 4B**). FXYD3-pep SKSK did not augment the effect of Dox on pancreatic Panc-1 cells that do not express FXYD3 (**Figure 4C**) or on the breast cancer cell line MDA-MB-468 that expresses FXYD3 at a low level (**Figure 4D**). The peptide derivative that retained the Cys

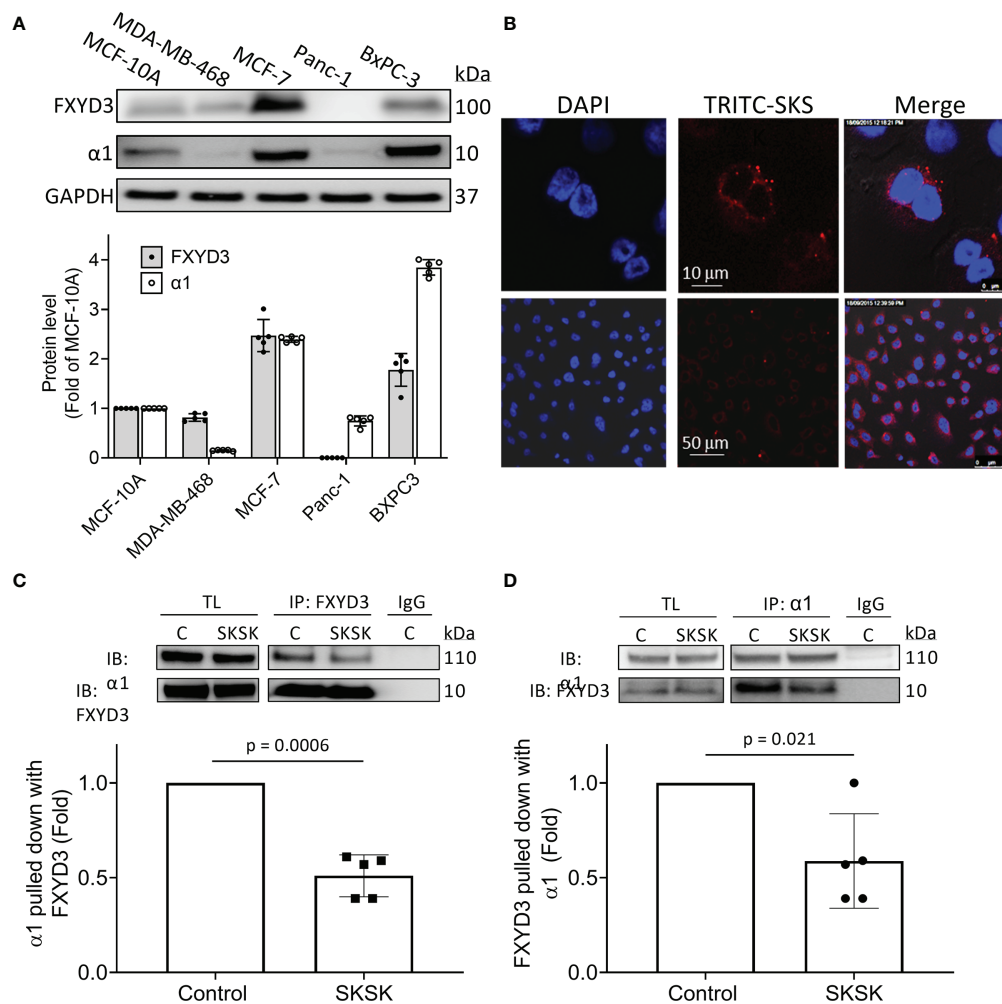


FIGURE 3 | Distribution of FXYD3-pep SKSK and its ability to displace FXYD3 from the $\alpha 1$ Na⁺/K⁺-ATPase subunit. **(A)** FXYD3 and Na⁺/K⁺-ATPase $\alpha 1$ subunit expression in MCF-7 and MDA-MB-468 breast cancer cells and in BxPC-3 and Panc-1 pancreatic cancer cells. Expression is normalized to expression in human non-cancer MCF-10A cells; GAPDH was the internal loading control. **(B)** Immunofluorescence showing distribution of TRITC-labeled FXYD3-pep SKSK in BxPC-3 cells. Cells were exposed to 1 μ M TRITC-tagged FXYD3-pep SKSK (TRITC-SKSK) (red) for 2 h and fluorescence microscopy performed 24 h after the peptide was washed off. DAPI was used to counterstain the nucleus (blue). One of 5 similar experiments is shown. Fluorescence is predominantly peri-nuclear. Scales are shown in the middle panel. **(C)** Immunoblot (IB) of $\alpha 1$ Na⁺/K⁺-ATPase subunit with WT FXYD3 immunoprecipitant in lysate of BxPC-3 with and without exposure of the cells to 1 μ M FXYD3-pep SKSK for 2 h before lysis. **(D)** Immunoblot of WT FXYD3 with the $\alpha 1$ subunit immunoprecipitant in the lysate from the cells. C, control; TL, total lysate; non-immune IgG (IgG), negative control for IP. The efficiency of the Co-IP can be estimated by the comparison of $\beta 1$ subunit expression in the initial total lysate and the unbound supernatant after IP in BxPC-3 cells (data not shown). Approximate binding efficiency was ~90%.

residues of the WT FXYD3 protein, FXYD3-pep CKCK, and reduced Dox induced cytotoxicity in BxPC-3 cells (**Figure 4E**) but had no effect on Panc-1 cells that do not express the FXYD3 protein (**Figure 4F**).

Exposure of BxPC-3 cells (**Figure 5A**) and MCF-7 cells (**Figure 5B**) to FXYD3-pep SKSK alone had no effect on caspase 3/7 activity, but exposure to the peptide augmented an effect of Dox on caspase 3/7 in both cell lines.

Plasmalemmal Na⁺/K⁺-ATPase Is an Unlikely Target for FXYD3-pep SKSK

Plasmalemmal Na⁺/K⁺-ATPase is critical for cell survival, and since WT FXYD3 protects the Na⁺/K⁺-ATPase against inhibition

induced by oxidative stress (2), we examined if direct inhibition of the Na⁺/K⁺-ATPase reproduces the effect of FXYD3-pep SKSK in augmenting Dox-induced cytotoxicity. We exposed MCF-7 breast cancer cells to ouabain that, due to its hydrophilicity, is poorly membrane-permeable and inhibits plasmalemmal Na⁺/K⁺-ATPase at extracellular sites (21). Cells were exposed to ouabain with or without co-exposure to Dox. Ouabain alone reduced cell viability in a concentration-dependent manner. However, a modest augmentation of Dox-induced cytotoxicity decreased with an increase in ouabain concentration (**Figure 6A**), in contrast to the increased augmentation of Dox cytotoxicity with an increase in the concentration of FXYD3-pep SKSK from 1 to 2 μ M (**Figure 4**).

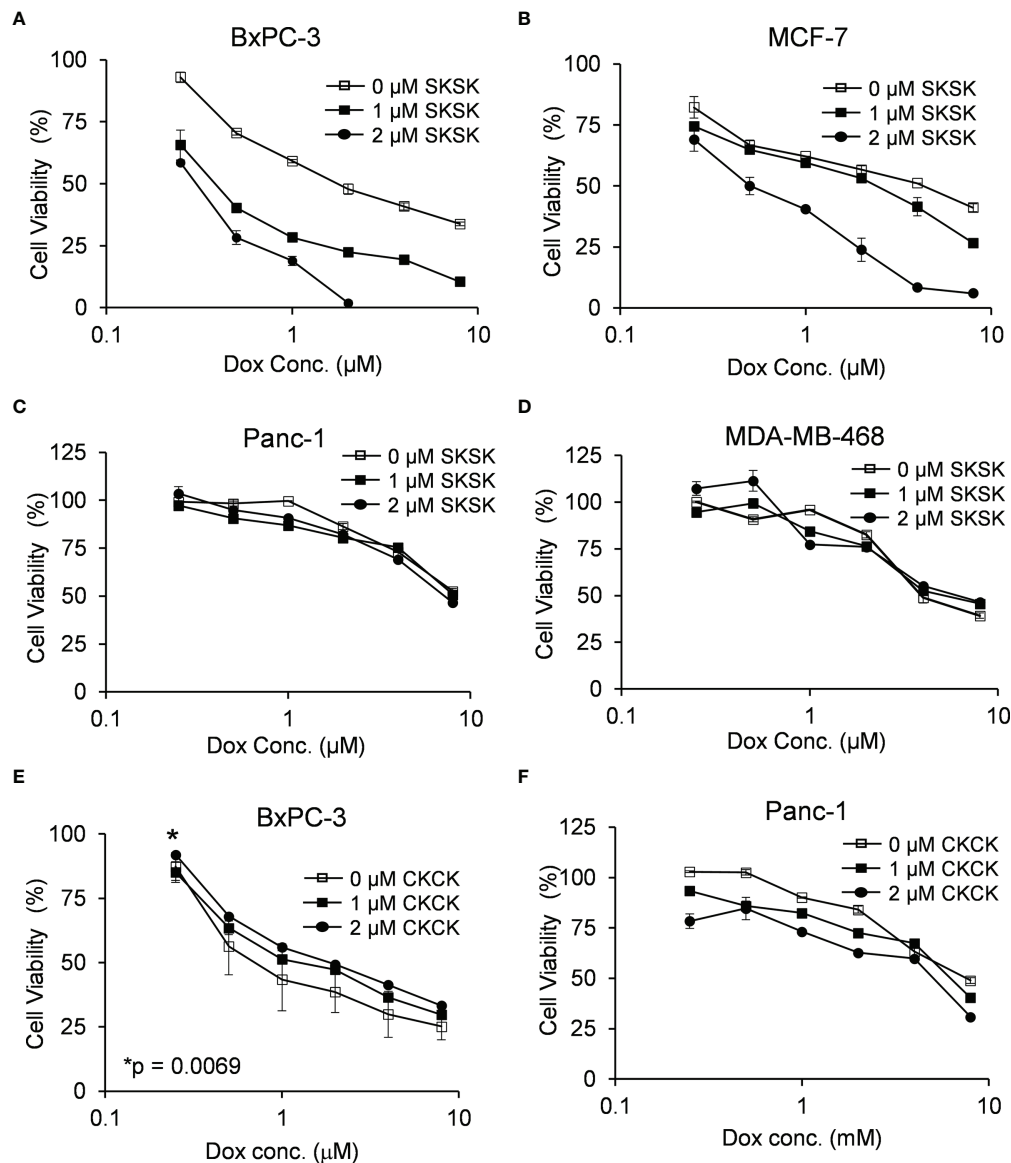


FIGURE 4 | Effect of FXYD3-pep SKSK and FXYD3-pep CKCK on cell viability with co-exposure to Dox. Viability of (A) BxPC-3 cells, (B) MCF-7 cells, (C) Panc-1 cells, and (D) MDA-MB-468 cells when treated with Dox and 0, 1, or 2 μ M FXYD3-pep SKSK for 48 h. Viability of (E) BxPC-3 cells and (F) Panc-1 cells treated with Dox and FXYD3-pep CKCK for 48 h. * in panel E refers to a significantly increased viability with exposure of cells to 2 μ M FXYD3-pep CKCK compared with exposure to solutions free of the peptide. Results are from 5 experiments for each peptide concentration.

The different levels of Na^+/K^+ -ATPase subunit expression might reflect a difference in the cells' functional plasmalemmal Na^+/K^+ -ATPase. FXYD3 and $\alpha 1$ Na^+/K^+ -ATPase subunits are markedly upregulated in MCF-7 cells that are sensitized to Dox cytotoxicity by FXYD3-pep SKSK relative to levels in the MDA-MB-468 cells that are not sensitized (Figure 3A). We measured I_p of the two cell lines. There was no difference in I_p between the cells (Figure 6B). The differences in $\alpha 1$ Na^+/K^+ -ATPase subunit expression between MCF-7 and MDA-MB-468 cells but similar plasmalemmal Na^+/K^+ -ATPase pump capacity implicate an intracellular location of overexpressed Na^+/K^+ -ATPase in the

cells that are sensitized to Dox with exposure to FXYD3-pep SKSK.

DISCUSSION

Similar to the distribution of overexpressed WT FXYD3 in resected pancreatic (6) and breast cancers (8), we detected TRITC-tagged FXYD3-pep SKSK intracellularly, predominately in a perinuclear distribution. Immunofluorescence signals for WT FXYD3 in MCF-7 cells partly overlap with signals for Na^+/K^+ -

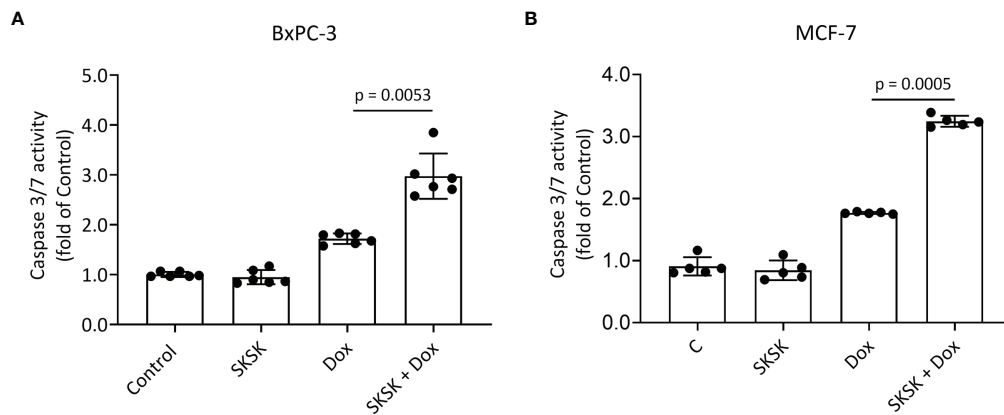


FIGURE 5 | Effect of FXYD3-pep SKSK on caspase 3/7 activity. **(A)** BxPC-3 and **(B)** MCF-7 cells were exposed to solutions that included 1 μ M FXYD3-pep SKSK or were peptide-free for 24 h and then for a further 48 h to solutions that included the peptide or were peptide-free and included Dox, 0.5 μ M for the BxPC-3 cells, and 2.5 μ M for the MCF-7 cells as indicated. Caspase 3/7 activity was used as index of apoptosis. N = 5.

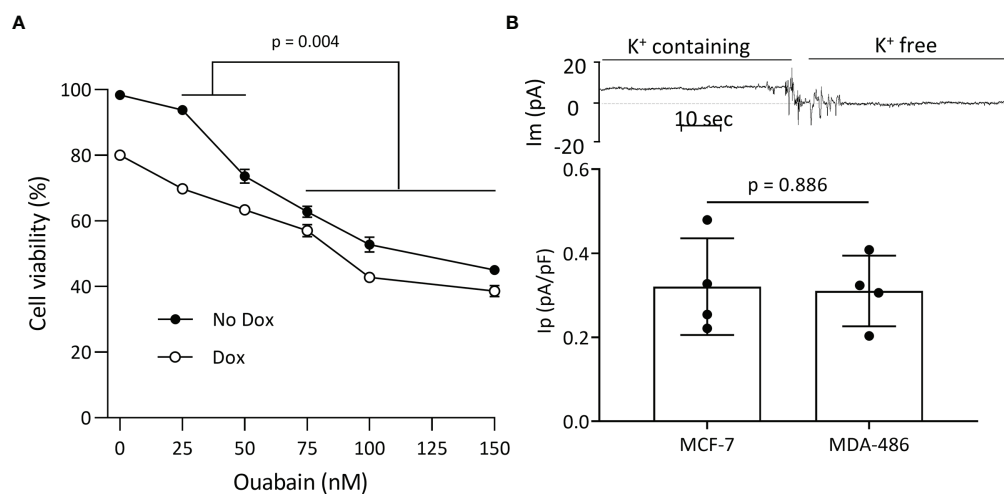


FIGURE 6 | Plasmalemmal Na⁺/K⁺-ATPase as a potential target for FXYD3-pep SKSK. **(A)** MCF-7 cell survival after a 48-h exposure to ouabain in concentrations indicated, with or without co-exposure to 1 μ M doxorubicin (Dox). * indicates difference in additive effect of ouabain and Dox at 25 or 50 nM ouabain vs. 70–150 nM ouabain. N = 5 for each ouabain concentration. **(B)** Electrogenic Na⁺/K⁺-ATPase pump currents (I_p) of MCF-7 cells that do, and MDA468 cells that do not, overexpress Na⁺/K⁺-ATPase. The trace of membrane current (I_m) was recorded in an MCF-7 cell before and after Na⁺-K⁺ pump activity was eliminated with exposure to K⁺-free extracellular solution. The inward shift to a near-zero holding current in K⁺-free solution identifies I_p. Currents were sampled with an electronic cursor after electrical noise caused by extracellular solution change had subsided.

ATPase α subunits (8), and a mostly perinuclear distribution of the β 1 Na⁺/K⁺-ATPase subunits in cancer cells is also reported with the development of some colorectal cancers (22). We are not aware of studies reporting overexpression of the intact α / β /FXYD3 Na⁺/K⁺-ATPase molecular complexes in the intracellular compartment in cancers. However, all its constituents are reported intracellularly and in a shared distribution.

FXYD3 in MCF-7 cells is expressed in the plasmalemma as well as in intracellular membrane compartments (8). The overexpressed FXYD3 is confined to the perinuclear region because the stem cell-related transcription factor SOX9

promotes FXYD3 transcription, and the synthesized FXYD3 protein in turn confines SOX9 to the nucleus in a regulatory feedback loop for FXYD3 amplification (23). With experimentally induced synthesis of FXYD3 in Chinese Hamster Ovary (CHO) cells, detectable FXYD3 becomes distributed in the nuclear envelope and the endoplasmic reticulum (ER) but not in the plasmalemma (24). Here, it is unlikely that FXYD3-pep SKSK sensitized the cells to Dox because of a dependence on a high catalytic plasmalemmal Na⁺/K⁺-ATPase activity. The high expression of WT FXYD3 in parallel with the expression of α 1 subunits in MCF-7 cells

relative to MDA-MB-468 cells was not reflected by different maximally activated I_p . Furthermore, while MDA-MB-468 cells did not overexpress WT FXYD3, they did express the protein at levels comparable to those for non-transformed human breast cells, yet FXYD3-pep SKSK did not sensitize MDA-MB-468 cells to Dox.

Facilitated by bonds from FXYD proteins to α and β subunits seen in the crystal structure (4), the primary overexpression of FXYD3 in cancer cells might lead to an intracellular accumulation of FXYD3/ α/β Na^+/K^+ -ATPase complexes. That such assembly plausibly occurs is indicated by the spontaneous formation of FXYD/ α/β Na^+/K^+ -ATPase complexes with the *in vitro* exposure of human $\alpha 1/\beta 1$ subunits to a molar excess of FXYD1, FXYD2, or FXYD3. FXYD/ α/β Na^+/K^+ -ATPase complexes also assemble when rat FXYD1, FXYD2, or FXYD4 is co-expressed with rat $\alpha 1$ subunits in HeLa cells, indicating that the effects shown for purified human proteins are biologically relevant in intact cells (25).

That an excess of FXYD proteins stabilizes the Na^+/K^+ -ATPase structure and function is supported by how recombinant full-length WT FXYD3 prevents a decrease in $\alpha 1/\beta 1$ Co-IP detected in cardiac myocyte lysate and prevents a decrease of I_p measured in intact voltage-clamped myocytes during oxidative stress (2). However, while WT- and Cys-mutated recombinant proteins in equimolar concentrations similarly displace the FXYD1 native to myocytes, only the WT FXYD3 has these preventative effects. The proteins share amino acids that have bonds to α - and β subunits, and presence of Cys residues rather than displacement of WT proteins per se accounts for their effects on integrity and function of Na^+/K^+ -ATPase.

Even with the overexpression of WT FXYD3 in BxPC-3 cells, FXYD3-pep CKCK had a protective effect against Dox-induced cytotoxicity while FXYD3-pep SKSK augmented it. The two peptides share with their full-length equivalent proteins all domains with bonds to the α/β Na^+/K^+ -ATPase complex. However, Cys residues, including the specific residue that mutational studies indicate confers susceptibility of FXYD proteins to glutathionylation, had been replaced by Ser in FXYD3-pep SKSK (**Figure 2**) and it is a FXYD protein's susceptibility to glutathionylation that counters glutathionylation of the $\beta 1$ subunit (2). Effects of the peptides here indicate that augmentation of cytotoxicity with siRNA-induced downregulation of FXYD3 (9) reflects the role of the Cys residue that is critical for countering $\beta 1$ subunit glutathionylation.

With selective inhibition of plasmalemmal Na^+/K^+ -ATPase at ouabain concentrations >50 nM, there was no dose-dependent increase in ouabain's augmentation of Dox's cytotoxicity; that is, ouabain did not reproduce the large dose-dependent augmentation of Dox's cytotoxicity that FXYD3-pep SKSK induced. Therefore, while glutathionylation of the $\beta 1$ subunit inhibits Na^+/K^+ -ATPase (26), selective inhibition of plasmalemmal Na^+/K^+ -ATPase ion transport is unlikely to account for the pattern of sensitization to Dox seen with FXYD3-pep SKSK.

In addition to mediating ion transport, Na^+/K^+ -ATPase facilitates cell adhesion *via* intercellular $\beta 1$ - $\beta 1$ subunit bridges,

and exposure to ouabain in nanomolar concentrations augments such cell adhesion in CHO fibroblasts overexpressing $\beta 1$ subunits (27). Ouabain also prevents $\beta 1$ subunit glutathionylation induced by oxidative stress, shown for intact cardiac rabbit myocytes and isolated pig kidney Na^+/K^+ -ATPase-enriched membrane fragments (28). $\beta 1$ subunit glutathionylation and $\alpha 1/\beta 1$ subunit Co-IP are inversely related (28), and molecular dynamics simulations suggest that this might reflect the structural disruption that a GSH adduct causes between transmembrane domains of the glutathionylated heterodimer, combined with a disruption of the cytosolic membrane leaflet necessary for access of the cytosolic GSH (29).

FXYD3 from intracellular α/β -FXYD3 Na^+/K^+ -ATPase complexes in cells overexpressing FXYD3 might be a source that counters glutathionylation of $\beta 1$ subunits in plasmalemmal Na^+/K^+ -ATPases. The effect such a source of FXYD proteins can have is indicated by the reversal of decreased myocyte I_p induced by oxidative stress when recombinant FXYD1 or FXYD3 proteins are included in patch pipette solutions perfusing the intracellular compartment. A decrease in the $\beta 1$ subunit's glutathionylation in parallel with an increase in its Co-IP with $\alpha 1$ subunits in lysates of myocytes supported FXYD protein-dependent protection of $\alpha 1/\beta 1$ heterodimer integrity accounting for effects on ion transport (2).

Since intercellular $\beta 1$ - $\beta 1$ subunit bridges extend to the cytoskeleton through the binding of $\beta 1$ to $\alpha 1$ subunits, that in turn have bonds to the cytoskeleton (30), disruption of the $\alpha 1/\beta 1$ heterodimer with glutathionylation is expected to disrupt cell adhesion. Conversely, overexpressed FXYD3 might counter such disruption. Consistent with this, FXYD3 knockdown impairs growth and disperses cells in MCF-7 tumors expressed in mice (23), and in human colon adenocarcinoma Caco-2 cells, FXYD3 knockdown decreases the transepithelial electrical resistance of confluent cell layers consistent with decreased intercellular adhesion (31).

In contrast to FXYD3 promoting cell adhesion, transfection of a mouse kidney cell line with FXYD5 reduces adhesion, as indicated by a decrease in transepithelial electrical resistance (32). However, this is expected if disruption of the $\alpha 1/\beta 1$ heterodimer with glutathionylation disrupts cell adhesion because FXYD5 has a Gln residue (33) at the site where a Cys residue bracketed by basic amino acids is obligatory for a FXYD protein to counter glutathionylation of the $\beta 1$ subunit. A single, selective mutation of the residue (Cys \rightarrow Ala) eliminates an FXYD protein's effect to counter $\beta 1$ subunit glutathionylation (2).

Disruption of cell adhesion with FXYD5 transfection was attributed to a decrease in glycosylation of the $\beta 1$ subunit's extracellular domain (32), and inhibiting glycosylation can augment the cytotoxicity of Dox (34). FXYD5 is functionally a WT protein equivalent of FXYD3-pep SKSK in terms of their expected effects on glutathionylation of $\beta 1$ subunits, and decreased glycosylation or increased glutathionylation of the subunits is not mutually exclusive in potential effects on subunit-dependent intercellular adhesion. The complexity of $\beta 1$ subunits Na^+/K^+ -ATPase *N*-glycans is also important for effects of the subunit on intercellular adhesion (35). However, an effect of FXYD3-pep SKSK on this cannot be invoked at present.

The FXYD peptide derivatives here augment key functions of the WT proteins they are derived from or, with a Cys-mutated modification, eliminate the function by displacing the WT protein from its only known binding partner, Na⁺/K⁺-ATPase. Exposure over minutes–hours avoids confounding cellular adjustments with transfection to overexpress FXYD proteins or silencing to reduce their abundance over days–weeks, and, in contrast to the experimental use of recombinant FXYD proteins (2), purified peptides are easy and inexpensive to make.

The FXYD3 peptide derivatives we report here are useful tools for exploring the role of overexpressed FXYD3 in cancer and its potential as a treatment target. With further modifications, FXYD3-pep SKSK might be developed into a treatment sensitizer. However, one caveat must be kept in mind. The peptide is, at least in part, expected to be a functional equivalent of FXYD5, and FXYD5 expression increases the metastatic potential in a mouse breast cancer model. This is associated with a decrease in plasmalemmal Na⁺/K⁺-ATPase β1 subunit expression and a decrease in intercellular adhesion (36). FXYD5 expression also appears to increase the metastatic potential of human cancers (37).

While the focus here is on FXYD3-pep SKSK, the protective effect of FXYD3-pep CKCK against Dox-induced cytotoxicity reflects properties that also may be useful. The peptide retains the Cys residue and, in turn, an ability to protect integrity and function of the α1/β1 Na⁺/K⁺-ATPase heterodimer (2). A potential use is exemplified by treatment of acute respiratory distress syndromes, including SARS-CoV-2 infection. Reduced Na⁺ export from alveolar cells mediated by Na⁺/K⁺-ATPase and compromised β1 subunit-dependent integrity of the alveolar epithelial barrier are implicated in the pathophysiology of pulmonary alveolar edema (38, 39). A peptide drug based on FXYD3-pep CKCK and modified to resist *in vivo* breakdown might offer an approach to treatment.

REFERENCES

1. Sweadner KJ, Rael E. The FXYD Gene Family of Small Ion Transport Regulators or Channels: cDNA Sequence, Protein Signature Sequence, and Expression. *Genomics* (2000) 68(1):41–56. doi: 10.1006/geno.2000.6274
2. Bibert S, Liu CC, Figtree GA, Garcia A, Hamilton EJ, Marassi FM, et al. FXYD Proteins Reverse Inhibition of the Na⁺-K⁺ Pump Mediated by Glutathionylation of its Beta1 Subunit. *J Biol Chem* (2011) 286(21):18562–72. doi: 10.1074/jbc.M110.184101
3. Li C, Grosdidier A, Crambert G, Horisberger JD, Michielin O, Geering K. Structural and Functional Interaction Sites Between Na,K-ATPase and FXYD Proteins. *J Biol Chem* (2004) 279(37):38895–902. doi: 10.1074/jbc.M406697200
4. Shinoda T, Ogawa H, Cornelius F, Toyoshima C. Crystal Structure of the Sodium-Potassium Pump at 2.4 Å Resolution. *Nature* (2009) 459(7245):446–50. doi: 10.1038/nature07939
5. Cornelius F, Mahmoud YA. Functional Modulation of the Sodium Pump: The Regulatory Proteins “Fixit”. *News Physiol Sci* (2003) 18:119–24. doi: 10.1152/nips.01434.2003
6. Kaye H, Kleeff J, Kolb A, Ketterer K, Keleg S, Felix K, et al. FXYD3 is Overexpressed in Pancreatic Ductal Adenocarcinoma and Influences Pancreatic Cancer Cell Growth. *Int J Cancer* (2006) 118(1):43–54. doi: 10.1002/ijc.21257
7. Grzmil M, Voigt S, Thelen P, Hemmerlein B, Helmke K, Burfeind P. Up-Regulated Expression of the MAT-8 Gene in Prostate Cancer and Its siRNA-

DATA AVAILABILITY STATEMENT

The original contributions presented in the study are included in the article/**Supplementary Material**. Further inquiries can be directed to the corresponding authors.

AUTHOR CONTRIBUTIONS

C-CL contributed to the design and implementation of the research, to the analysis of the results, and to the writing of the manuscript. YK, RT, AG, AW, and EH performed the experiments. FC, RB, and HR aided in interpreting the results and worked on the manuscript. All authors contributed to the article and approved the submitted version.

FUNDING

The work is supported by a grant from the Avner Pancreatic Cancer Foundation, Heart Research Australia, and Ramsay Research and Teaching Fund (Australia). YK was supported by Research Training Program Stipend Scholarship (Australia) and a Ramsay research top up scholarship (Australia). AG was supported by a UTS Chancellors Postdoctoral Research Fellowship (Australia). EH was supported by Heart Research Australia.

SUPPLEMENTARY MATERIAL

The Supplementary Material for this article can be found online at: <https://www.frontiersin.org/articles/10.3389/fonc.2022.859216/full#supplementary-material>

Mediated Inhibition of Expression Induces a Decrease in Proliferation of Human Prostate Carcinoma Cells. *Int J Oncol* (2004) 24(1):97–105. doi: 10.3892/ijo.24.1.97

8. Yamamoto H, Okumura K, Toshima S, Mukaisho K, Sugihara H, Hattori T, et al. FXYD3 Protein Involved in Tumor Cell Proliferation Is Overproduced in Human Breast Cancer Tissues. *Biol Pharm Bull* (2009) 32(7):1148–54. doi: 10.1248/bpb.32.1148
9. Liu CC, Teh R, Mozar CA, Baxter RC, Rasmussen HH. Silencing Overexpression of FXYD3 Protein in Breast Cancer Cells Amplifies Effects of Doxorubicin and Gamma-Radiation on Na⁺/K⁺-ATPase and Cell Survival. *Breast Cancer Res Treat* (2016) 155(2):203–13. doi: 10.1007/s10549-015-3667-x
10. Wenningmann N, Knapp M, Ande A, Vaidya TR, Ait-Oudhia S. Insights Into Doxorubicin-Induced Cardiotoxicity: Molecular Mechanisms, Preventive Strategies, and Early Monitoring. *Mol Pharmacol* (2019) 96(2):219–32. doi: 10.1124/mol.119.115725
11. Flinck M, Hagelund S, Gorbatenko A, Severin M, Pedraz-Cuesta E, Novak I, et al. The Vacuolar H(+) ATPase α3 Subunit Negatively Regulates Migration and Invasion of Human Pancreatic Ductal Adenocarcinoma Cells. *Cells* (2020) 9(2):465. doi: 10.3390/cells9020465
12. Uphoff CC, Drexler HG. Detecting Mycoplasma Contamination in Cell Cultures by Polymerase Chain Reaction. *Methods Mol Biol* (2011) 731:93–103. doi: 10.1007/978-1-61779-080-5_8
13. Letourneau M, Wang K, Mailloux RJ. Protein S-Glutathionylation Decreases Superoxide/Hydrogen Peroxide Production Xanthine Oxidoreductase. *Free Radic Biol Med* (2021) 175:184–92. doi: 10.1016/j.freeradbiomed.2021.08.243

14. Saxena NK, Vertino PM, Anania FA, Sharma D. Leptin-Induced Growth Stimulation of Breast Cancer Cells Involves Recruitment of Histone Acetyltransferases and Mediator Complex to CYCLIN D1 Promoter via Activation of Stat3. *J Biol Chem* (2007) 282(18):13316–25. doi: 10.1074/jbc.M609798200
15. Nicholson DW, Thornberry NA. Caspases: Killer Proteases. *Trends Biochem Sci* (1997) 22(8):299–306. doi: 10.1016/s0968-0004(97)01085-2
16. Gadsby DC, Nakao M. Steady-State Current-Voltage Relationship of the Na/K Pump in Guinea Pig Ventricular Myocytes. *J Gen Physiol* (1989) 94(3):511–37. doi: 10.1085/jgp.94.3.511
17. Follmer CH, ten Eick RE, Yeh JZ. Sodium Current Kinetics in Cat Atrial Myocytes. *J Physiol* (1987) 384:169–97. doi: 10.1113/jphysiol.1987.sp016449
18. Bean BP. Two Kinds of Calcium Channels in Canine Atrial Cells. Differences in Kinetics, Selectivity, and Pharmacology. *J Gen Physiol* (1985) 86(1):1–30. doi: 10.1085/jgp.86.1.1
19. Krafft DS, Kass RS. Hydrogen Ion Modulation of Ca Channel Current in Cardiac Ventricular Cells. Evidence for Multiple Mechanisms. *J Gen Physiol* (1988) 91(5):641–57. doi: 10.1085/jgp.91.5.641
20. Garcia A, Liu CC, Cornelius F, Clarke RJ, Rasmussen HH. Glutathionylation-Dependence of Na⁺-K⁺-Pump Currents Can Mimic Reduced Subsarcolemmal Na⁺ Diffusion. *Biophys J* (2016) 110(5):1099–109. doi: 10.1016/j.bpj.2016.01.014
21. Galva C, Artigas P, Gatto C. Nuclear Na⁺/K⁺-ATPase Plays an Active Role in Nucleoplasmic Ca²⁺ Homeostasis. *J Cell Sci* (2012) 125(Pt 24):6137–47. doi: 10.1242/jcs.114959
22. Baker Bechmann M, Rotoli D, Morales M, Maeso Mdel C, Garcia Mdel P, Avila J, et al. Na,K-ATPase Isozymes in Colorectal Cancer and Liver Metastases. *Front Physiol* (2016) 7:9. doi: 10.3389/fphys.2016.00009
23. Xue Y, Lai L, Lian W, Tu X, Zhou J, Dong P, et al. SOX9/FXYD3/Src Axis is Critical for ER⁺ Breast Cancer Stem Cell Function. *Mol Cancer Res* (2019) 17(1):238–49. doi: 10.1158/1541-7786.Mcr-18-0610
24. Arimochi J, Kobayashi A, Maeda M. Stable Expression and Visualization of Mat-8 (FXYD-3) Tagged With a Fluorescent Protein in Chinese Hamster Ovary (CHO)-K1 Cells. *Biotechnol Lett* (2005) 27(14):1017–24. doi: 10.1007/s10529-005-7870-4
25. Mishra NK, Peleg Y, Cirri E, Belogus T, Lifshitz Y, Voelker DR, et al. FXYD Proteins Stabilize Na,K-ATPase: Amplification of Specific Phosphatidylserine-Protein Interactions. *J Biol Chem* (2011) 286(11):9699–712. doi: 10.1074/jbc.M110.184234
26. Figtree GA, Liu CC, Bibert S, Hamilton EJ, Garcia A, White CN, et al. Reversible Oxidative Modification: A Key Mechanism of Na⁺-K⁺ Pump Regulation. *Circ Res* (2009) 105(2):185–93. doi: 10.1161/CIRCRESAHA.109.199547
27. Vilchis-Nestor CA, Roldan ML, Leonardi A, Navea JG, Padilla-Benavides T, Shoshani L. Ouabain Enhances Cell-Cell Adhesion Mediated by Beta1 Subunits of the Na⁺,K⁺-ATPase in CHO Fibroblasts. *Int J Mol Sci* (2019) 20(9):2111. doi: 10.3390/ijms20092111
28. Liu CC, Garcia A, Mahmoud YA, Hamilton EJ, Galougahi KK, Fry NA, et al. Susceptibility of Beta1 Na⁺-K⁺ Pump Subunit to Glutathionylation and Oxidative Inhibition Depends on Conformational State of Pump. *J Biol Chem* (2012) 287(15):12353–64. doi: 10.1074/jbc.M112.340893
29. Thogersen L, Nissen P. Flexible P-Type ATPases Interacting With the Membrane. *Curr Opin Struct Biol* (2012) 22(4):491–9. doi: 10.1016/j.sbi.2012.05.009
30. Vagin O, Dada LA, Tokhtaeva E, Sachs G. The Na-K-ATPase Alpha(1)Beta(1) Heterodimer as a Cell Adhesion Molecule in Epithelia. *Am J Physiol Cell Physiol* (2012) 302(9):C1271–1281. doi: 10.1152/ajpcell.00456.2011
31. Bibert S, Aebischer D, Desgranges F, Roy S, Schaer D, Kharoubi-Hess S, et al. A Link Between FXYD3 (Mat-8)-Mediated Na,K-ATPase Regulation and Differentiation of Caco-2 Intestinal Epithelial Cells. *Mol Biol Cell* (2009) 20(4):1132–40. doi: 10.1091/mbc.E08-10-0999
32. Lubarski I, Asher C, Garty H. FXYD5 (Dysadherin) Regulates the Paracellular Permeability in Cultured Kidney Collecting Duct Cells. *Am J Physiol Renal Physiol* (2011) 301(6):F1270–1280. doi: 10.1152/ajprenal.00142.2011
33. Geering K. FXYD Proteins: New Regulators of Na-K-ATPase. *Am J Physiol Renal Physiol* (2006) 290(2):F241–250. doi: 10.1152/ajprenal.00126.2005
34. Peiris D, Spector AF, Lomax-Browne H, Azimi T, Ramesh B, Loizidou M, et al. Cellular Glycosylation Affects Herceptin Binding and Sensitivity of Breast Cancer Cells to Doxorubicin and Growth Factors. *Sci Rep* (2017) 7:43006. doi: 10.1038/srep43006
35. Vagin O, Tokhtaeva E, Yakubov I, Shevchenko E, Sachs G. Inverse Correlation Between the Extent of N-Glycan Branching and Intercellular Adhesion in Epithelia. Contribution of the Na,K-ATPase Beta1 Subunit. *J Biol Chem* (2008) 283(4):2192–202. doi: 10.1074/jbc.M704713200
36. Lubarski-Gotliv I, Dey K, Kuznetsov Y, Kalchenko V, Asher C, Garty H. FXYD5 (Dysadherin) may Mediate Metastatic Progression Through Regulation of the Beta-Na⁺-K⁺-ATPase Subunit in the 4T1 Mouse Breast Cancer Model. *Am J Physiol Cell Physiol* (2017) 313(1):C108–17. doi: 10.1152/ajpcell.00206.2016
37. Tassi RA, Gambino A, Ardighieri L, Bignotti E, Todeschini P, Romani C, et al. FXYD5 (Dysadherin) Upregulation Predicts Shorter Survival and Reveals Platinum Resistance in High-Grade Serous Ovarian Cancer Patients. *Br J Cancer* (2019) 121(7):584–92. doi: 10.1038/s41416-019-0553-z
38. Dada LA, Vagin O, Sznajder JJ. Dysregulation of Ion Transport in the Lung Epithelium Infected With SARS-CoV-2. *Am J Physiol Lung Cell Mol Physiol* (2021) 320(6):L1183–5. doi: 10.1152/ajplung.00170.2021
39. Kryvenko V, Vadasz I. Molecular Mechanisms of Na,K-ATPase Dysregulation Driving Alveolar Epithelial Barrier Failure in Severe COVID-19. *Am J Physiol Lung Cell Mol Physiol* (2021) 320(6):L1186–93. doi: 10.1152/ajplung.00056.2021

Conflict of Interest: The authors declare that the research was conducted in the absence of any commercial or financial relationships that could be construed as a potential conflict of interest.

Publisher's Note: All claims expressed in this article are solely those of the authors and do not necessarily represent those of their affiliated organizations, or those of the publisher, the editors and the reviewers. Any product that may be evaluated in this article, or claim that may be made by its manufacturer, is not guaranteed or endorsed by the publisher.

Copyright © 2022 Liu, Kim, Teh, Garcia, Hamilton, Cornelius, Baxter and Rasmussen. This is an open-access article distributed under the terms of the Creative Commons Attribution License (CC BY). The use, distribution or reproduction in other forums is permitted, provided the original author(s) and the copyright owner(s) are credited and that the original publication in this journal is cited, in accordance with accepted academic practice. No use, distribution or reproduction is permitted which does not comply with these terms.



Chemical and Biological Evidence of the Efficacy of Shengxian Decoction for Treating Human Lung Adenocarcinoma

Kejuan Li^{1,4†}, Fengming You^{2†}, Qin Zhang¹, Ruijiao Yuan¹, Qianghua Yuan³, Xi Fu³, Yifeng Ren³, Qian Wang³, Xiaohong Li³, Zhenya Zhang⁴, Mototada Shichiri^{5,6} and Yue Yu^{5,6*}

¹ College of Life Science, Sichuan Normal University, Chengdu, China, ² Traditional Chinese Medicine (TCM) Regulating Metabolic Diseases Key Laboratory of Sichuan Province, Hospital of Chengdu University of Traditional Chinese Medicine, Chengdu, China, ³ Oncology Department, Hospital of Chengdu University of Traditional Chinese Medicine, Chengdu, China, ⁴ Graduate School of Life and Environmental Sciences, University of Tsukuba, Tsukuba, Japan, ⁵ Biomedical Research Institute, National Institute of Advanced Industrial Science and Technology (AIST), Ikeda, Japan, ⁶ DBT-AIST International Laboratory for Advanced Biomedicine (DAILAB), AIST, Tsukuba, Japan

OPEN ACCESS

Edited by:

Rajkumar S. Kalra,
Okinawa Institute of Science and
Technology Graduate University,
Japan

Reviewed by:

Ujjawal Sharma,
MMDU, Mullana, India
Sandeep Singh,
Hebrew University Hadassah Medical
School, Israel
Choudhary Harsha,
Indian Institute of Technology, India

*Correspondence:

Yue Yu,
yu-yue@aist.go.jp

[†]These authors have contributed
equally to this work

Specialty section:

This article was submitted to
Pharmacology of Anti-Cancer Drugs,
a section of the journal
Frontiers in Oncology

Received: 06 January 2022

Accepted: 24 February 2022

Published: 18 March 2022

Citation:

Li K, You F, Zhang Q, Yuan R, Yuan Q,
Fu X, Ren Y, Wang Q, Li X, Zhang Z,
Shichiri M and Yu Y (2022) Chemical
and Biological Evidence of the Efficacy
of Shengxian Decoction for Treating
Human Lung Adenocarcinoma.
Front. Oncol. 12:849579.
doi: 10.3389/fonc.2022.849579

Shengxian Decoction (SXT) is a traditional Chinese medicine prescription comprising several anti-cancer medicinal herbs. However, the anti-cancer effect of SXT has rarely been reported. Herein, we explored the therapeutic potential of SXT for the treatment of lung adenocarcinoma (LUAD). High-performance liquid chromatography analysis of crude SXT extract revealed the abundance of mangiferin, an established anti-cancer compound. The serum pharmacological evaluation revealed that serum SXT suppressed A549 lung cancer cell proliferation *in vitro*. The tumor-inhibitory activity of SXT was confirmed *in vivo* via tumor formation assays in nude mice. We applied biochemical, histopathological and imaging approaches to investigate the cellular targets of SXT. The results indicated that the treatment with SXT induced tumor necrosis, and downregulated hypoxia-inducible factor 1 alpha in the serum. *In vivo* biosafety assessment of SXT revealed low levels of toxicity in mouse models. Our study provides the first scientific evidence that SXT effectively represses cancer cell growth and, thus, may serve as a safe anti-cancer agent for LUAD treatment.

Keywords: Shengxian Decoction, Chinese medicine, lung cancer, anti-tumor agent, toxicity

INTRODUCTION

Lung adenocarcinoma (LUAD), a histological subtype of non-small cell lung cancer, is one of the most common malignancies in terms of morbidity and mortality, accounting for approximately 40% of lung malignancies (1). Due to the characteristics of insidious onset, rapid metastasis and high recurrence rate, LUAD is usually first diagnosed at advanced stages. The five-year overall survival rate of LUAD patients is < 25% (2). LUAD can currently be treated with surgical resection, cytotoxic drug therapy, thoracic radiotherapy, targeted therapy, immunotherapy or a combination of these techniques (3). However, recurrence remains highly likely. The complete cure rate is < 10%

(4). Although immunotherapy and targeted therapy provide new directions for improving the survival of patients with LUAD, the cost is generally exorbitant. Therefore, the search for new and cheaper drug candidates for LUAD treatment has become the focus of current research.

Shengxian Decoction (SXT), a well-known traditional Chinese formula, comprises Astragali Radix (A. radix, 18 g), Anemarrhenae Rhizoma (A. rhizoma, 9 g), Bupleuri Radix (B. radix, 4.5 g), Platycodonis Radix (P. radix, 4.5 g) and Cimicifugae Rhizoma (C. rhizoma, 3 g). (5). SXT can be used to treat experimental autoimmune myasthenia gravis (6), cardiomyocyte injuries (7), and chronic heart failure (8). The anti-cancer activity of SXT has rarely been reported; however, the individual constituents of SXT have been shown to attenuate cancer growth. For example, as the main component in SXT, A. radix inhibited LUAD development through regulation of the autophagy process (9). Meanwhile, B. radix and P. radix have been shown to have favorable anti-cancer effects in various cancer models, including human LUAD (10–13). Moreover, C. rhizoma and A. rhizoma exhibit strong cytotoxicity against human breast and colorectal cancer cells (14–16). Previous phytochemical investigations revealed three types of flavonoids (i.e. mangiferin, calycosin-7-O- β -D-glucoside and formononetin) in A. radix (17, 18), isoferulic acid in C. rhizoma (19), Timosaponin AIII in A. rhizoma (20), saikosaponins in B. radix (11), and Platycodin D in P. radix (13). These compounds are believed to be the major

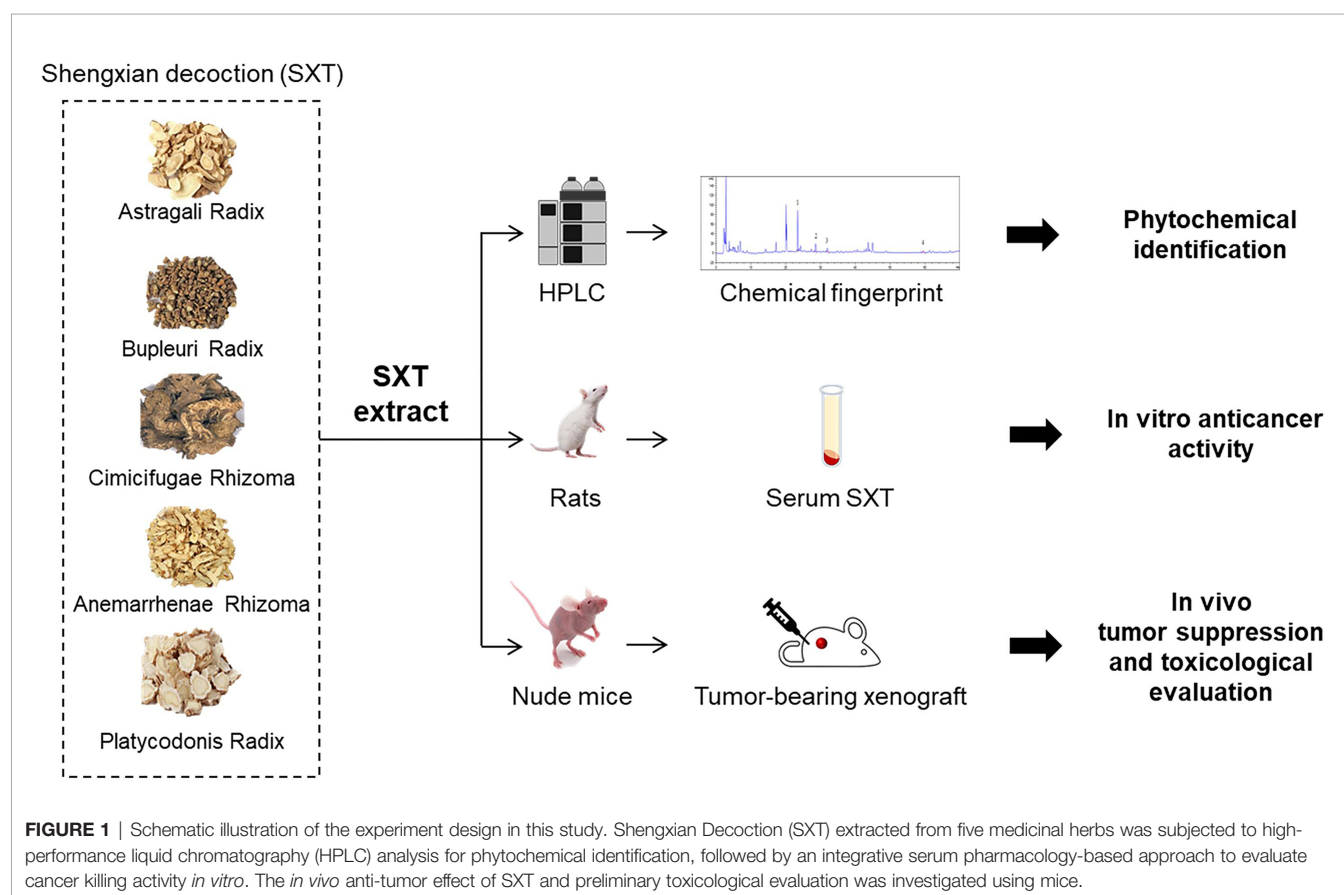
active components that account for their corresponding anti-cancer effects. Hence, we hypothesized that their integrated formulation (SXT) may have a therapeutic effect on LUAD.

Serum pharmacology is a novel method that can be used to realistically analyse pharmacological actions of drugs after their metabolization in the body. In serum pharmacology, drug or drug combinations are orally administrated to animals, and the blood from treated animals is subsequently collected after a certain period to separate the drug-containing serum for further experimental studies (21). Serum pharmacology is regarded as a reliable approach for evaluating the anti-tumor activities of traditional Chinese medicine (22). Therefore, to explore the possibility of SXT as a candidate drug for LUAD treatment, we used serum pharmacology method, together with a subcutaneous xenograft model, to study the anti-cancer effect of SXT on A549 human LUAD cells (**Figure 1**). High-performance liquid chromatography (HPLC) was also employed to identify potential phytochemicals in SXT (**Figure 1**).

MATERIALS AND METHODS

Medicines and Chemicals

A. radix (Gansu, China, batch No. 1901032), A. rhizoma (Hebei, China, batch No. 190301), B. radix (Hebei, China, batch No. 190401), P. radix (Anhui, China, batch No. 1904065), and C.



rhizoma (Liaoning, China, batch No. 1902051) were provided by the Affiliated Hospital of Chengdu University of Traditional Chinese Medicine. Mangiferin (batch No. 190822, 98.56%), calycosin-7-O- β -D-glucoside (batch No. 190817, 99.21%), formononetin (batch No. 191206, 98.61%) and isoferulic acid (batch No. 191115, 98.06%) were purchased from Chengdu Plant Standard Pure Biotechnology Co., Ltd. (Sichuan, China). Isotonic sodium chloride solution (0.9% saline) was purchased from Sichuan Kelun Pharmaceutical Co., Ltd. (Sichuan, China, batch No. A19042103-1). Cisplatin (Cis-diamminedichloroplatinum, DDP) was purchased from Jiangsu Hausen Pharmaceutical Co., Ltd. (Sichuan, China, batch No. 190602).

Cell Culture

The human LUAD cell lines A549, SK-LU-1 and NCI-H1975 were obtained from the American Type Culture Collection. A549 cells were maintained in Dulbecco Modified Eagle Medium (Life Technologies, CA, USA), supplemented with 10% fetal bovine serum (FBS) and 1% (v/v) penicillin-streptomycin. SK-LU-1 cells were maintained in Minima Essential medium (Life Technologies, CA, USA) supplemented with 10% FBS and 1% (v/v) penicillin-streptomycin. NCI-H1975 cells were maintained in Roswell Park Memorial Institute 1640 (Life Technologies, CA, USA) medium supplemented with 10% FBS and 1% (v/v) penicillin-streptomycin. The cells were incubated in a stable environment with 5% CO₂/95% air at 37°C in a humidified incubator.

Animals

Sprague-Dawley rats (male, 6-week old, 200 \pm 20 g) for the serum pharmacology experiment were purchased from Chengdu Dasuo Experimental Animal Co., Ltd. (Sichuan, China). BALB/c-nude mice (6-week old, 20 \pm 2 g) for the *in vivo* tumor suppression assay were purchased from Beijing Weitong Lihua Laboratory Animal Technology Co., Ltd. (Beijing, China). Animals were acclimated to the facilities for 5 days prior to the experiments in a specific pathogen-free environment, housed under controlled conditions (22 \pm 3°C, approximately 60% humidity, and 12 h light-dark cycle), and fed with sterilized water and standard rodent chow. All feed was provided by Chengdu Dasuo Laboratory Animal Co., Ltd. All animal experiments were conducted in accordance with strict ethical guidelines, following the recommendations of the Animal Experiments Committee of Chengdu University of Traditional Chinese Medicine.

Preparation of Crude SXT Extract

A total of 39 g (A. radix, 18 g; A. rhizoma, 9 g; B. radix, 4.5 g; P. radix, 4.5 g; C. rhizoma, 3 g) crude powders were weighed and soaked in eight times the volume of water (312 mL) for 2 h prior to the first decoction. The decoction was filtrated after boiling for 30 minutes, and the residues were collected for two additional decoctions under the same conditions. The total decoctions combined from three separate boiling instances were concentrated under reduced pressure (0.08 - 0.09 MPa) at 70°C. The resulting concentrate was subjected to freeze-drying until getting lyophilized powders (14.43 g; 37% extraction rate). SXT extract was prepared in double distilled water before use and stored at 4°C.

SXT Dose Calculation

SXT doses used in this study were estimated using the factor method, in which the conversion factor for human/rat and human/mice were determined as 6.3 and 9.1, respectively, based on the body surface area (23). In the traditional Chinese medicine system, 39 g of SXT crude powder is clinically used for preparing the decoction that is usually administrated to humans with average body weight around 70 kg. According to the extraction rate (37% of SXT extract obtained from initial crude powder), we determined the clinical dose of SXT as 0.21 g/kg/d (39 g/70 kg/d \times 37%) for human. Therefore, the equivalent dose for a 200 g Sprague-Dawley rat will be 6.3 \times 0.21 kg/d = 1.32 g/kg/d. SXT doses used in the serum pharmacological experiments for rats were set as 5 times (6.60 g/kg/d), 15 times (19.80 g/kg/d) and 20 times (26.40 g/kg/d) of the calculated equivalent doses. The SXT dose for mice (1.91 g/kg/d) was obtained in a similar manner except for the conversion factor of 6.3 was replaced with 9.1. After calculation, the low, medium and high doses of SXT used in the *in vivo* anti-tumor assay were set as 9.55 g/kg/d, 28.65 g/kg/d, and 38.20 g/kg/d, respectively. The experimental doses of DDP were 15.48 mg/kg/d and 22.36 mg/kg/d for rats and mice based on its clinical dose (2.46 mg/kg/d), respectively.

Preparation of Drug-Containing Serums

After adaptive feeding, the Sprague-Dawley rats were randomly divided into five groups (n = 6) and subjected to following treatments: normal saline (negative control, oral gavage), DDP (positive control, 15.48 mg/kg/d, intraperitoneal injection), low-dose SXT extract (6.60 g/kg/d, oral gavage), medium-dose SXT extract (19.80 g/kg/d, oral gavage), and high-dose SXT extract (26.40 g/kg/d, oral gavage). Each rat was administered twice a day with an interval of 12 hours.

On day 7, rat serum was collected as follows: the rats were anaesthetised by intraperitoneal injection of 10% chloral hydrate. Blood was then collected from the abdominal aorta and allowed to stand for 2 h. After centrifugation at 3000 rpm/min for 15 min at 4°C, the supernatant in the total blood was filtered through a 0.22 μ m filter and placed in a 56°C water bath for 30 min to remove complements. The resulting drug-containing serums corresponding to normal saline, DDP, low-dose SXT, medium-dose SXT, and high-dose SXT treatments were labeled as Normal-S, DDP-S, LSXT-S, MSXT-S and HSXT-S, respectively, and was stored at -20°C until further use.

Cell Viability Assay

A Cell Counting Kit-8 (Dojindo Laboratories, Kumamoto, Japan) was used to assess LUAD cell proliferation. Briefly, 100 μ L of cell suspension (1 \times 10⁵ cells/mL) was seeded in a 96-well plate and allowed to adhere overnight. Next, they were incubated with culture medium containing 10 μ L of Normal-S, DDP-S, LSXT-S, MSXT-S or HSXT-S. After 24 or 48 h of treatment, 10 μ L of Cell Counting Kit-8 solution was added to each well and incubated at 37°C for 4 h. Cell viability was assessed according to the change in absorbance at 450 nm using a microplate reader (Model 550; Bio-Rad, CA, USA).

In Vivo Anti-Tumor Assay

Mice bearing A549-derived tumors were generated by subcutaneously injecting A549 cells (1×10^7 cells in 0.2 mL medium) into the right axilla region. Tumor growth was monitored every second day. Successfully established tumor-bearing models were randomly divided into five groups ($n=5$) and administration was initiated as follows: saline (vehicle control, oral gavage); DDP (positive control, 22.36 mg/kg/d, intraperitoneal injection); low-dose SXT (LSXT) (9.55 g/kg/d, oral gavage), medium-dose SXT (MSXT) (28.65 g/kg/d, oral gavage), and high-dose SXT (HSXT) (38.20 g/kg/d, oral gavage). All the groups received treatment for 24 consecutive days. Body weight and tumor size were measured every two days. The tumor volume was calculated according to the formula: $V \text{ (mm}^3\text{)} = 0.5 \times L \times S^2$, where L and S are the long and short diameters of the tumor, respectively (24). Blood from each animal was collected from the eyeball at the end of the experiment for further analysis. Major organs including lung, spleen and tumor were isolated, pictured, weighed and sampled for further use. The tumor inhibitory rate was calculated using the following equation: inhibition rate (%) = $(W_c - W_e) \times 100 / W_c$, where W_c is the tumor weight of the control mice, and W_e is the mean weight of the treated mice. Lung and spleen indices were calculated according to the following equation: Organ index (mg/g) = weight of organ (mg)/body weight (g) (25).

Histopathological Evaluation

Tumors, lungs and spleens were fixed in 10% neutral buffered formalin, embedded in paraffin, and sectioned at a thickness of 4 μm . H&E staining was conducted according to routine protocols (26). Briefly, representative sections were stained with hematoxylin and eosin, and examined using a digital microphotography system (BA200, Motic China Group Co., Ltd, Xiamen, China). The lesions in each section were imaged at magnifications of 100 \times , 200 \times or 400 \times . The necrosis region was analyzed using the ImageJ software. At least three fields of view were collected to calculate the quantitative result.

Measurement of Biochemical Parameters in Blood

After collection, blood samples from each mouse were allowed to stand at room temperature for 2 h, and then centrifuged at 3000 rpm for 15 min at 4°C to obtain the serum. The levels of tumor necrosis factor- α (TNF- α) and hypoxia-inducible factor 1- α (HIF-1 α) in the serum were measured using enzyme-linked immunosorbent assay (ELISA) kits from ZCIBIO Technology Co., Ltd (Shanghai, China) according to the manufacturer's instructions. In Brief, 50 μL of serum samples were loaded into the wells, followed by the addition of 100 μL horseradish peroxidase-linked antibodies. After incubation at 37°C for 1 h, the samples were washed and then reacted with 50 μL substrates for 15 min. Absorbance of each well at 450 nm was assessed using a microplate reader (SpectraMAX Plus384, MD, USA). TNF- α and HIF-1 α levels were calculated according to the calibration curves.

HPLC Analysis

SXT extract was diluted with methanol to obtain a solution at a concentration of 72.15 mg/mL. Standard solutions of mangiferin (0.2328 mg/mL), calycosin-7-O- β -D-glucoside (0.0339 mg/mL), isoferulic acid (0.0470 mg/mL) and formononetin (0.0154 mg/mL) were carefully prepared with methanol by stepwise dilution of the stock solutions. All samples were filtered through a 0.22 μm filter prior to HPLC injection.

Measurement was performed on an HPLC equipment (Agilent 1260 equipped with DAD detector) with an Agilent SB C18 column (250 \times 4.6 mm, 5 μm ; Agilent, CA, USA), and data were collected and analyzed using Agilent ChemStation software. Column temperature was maintained at 25°C. The mobile phase was composed of a 0.2% phosphoric acid solution (solvent A) and acetonitrile (solvent B) with gradient elution for better separation. Gradient solvent system was optimized as follows: 0–20 min, 1–17% B; 20–25 min, 17–20% B; 25–33 min, 20–23% B; 33–40 min, 23–30% B; 40–50 min, 30–33% B; 50–65 min, 33–50% B; 65–70 min, 50–70% B at a flow rate of 1.0 mL/min. The detection was conducted at 220 nm with a 5 μL injection volume of each sample.

Statistical Analysis

All data were analyzed using the SPSS 26.0 software and the GraphPad Prism 8 software. Results were expressed as mean \pm standard deviation (SD), and statistical significance was evaluated using analysis of variance (ANOVA) followed by a multiple comparison test with Duncan's adjustment. Statistical significance was set at $P < 0.05$.

RESULTS

Identification of Anti-Cancer Compounds in SXT Extract

The chemical fingerprint of the SXT extract was determined using HPLC analysis. We selected four chemicals possessing anticancer properties as standard samples for comparison with the SXT extract (Figure 2A). The analysis results of SXT showed a number of peaks (Figure 2B), indicating the presence of multiple substances. Comparing with the standards (Figure 2C), compounds corresponding to peaks 1–4 were identified as mangiferin, calycosin-7-O- β -D-glucoside, isoferulic acid and formononetin, respectively. The contents of these compounds in SXT are listed in Table 1. These results indicate that the prepared SXT extract contains substantial amounts of anti-cancer compounds and may be capable of killing cancer cells.

Serum SXT Suppresses the Proliferation of LUAD Cells *in Vitro*

Next, we performed a serum pharmacology assay to investigate the anti-cancer potential of SXT. To collect SXT-containing serum, Sprague–Dawley rats were administered crude SXT extract at different concentrations (see Material and Methods). The obtained serums corresponding to high, medium, and low doses of SXT were named HSXT-S, MSXT-S and LSXT-S,

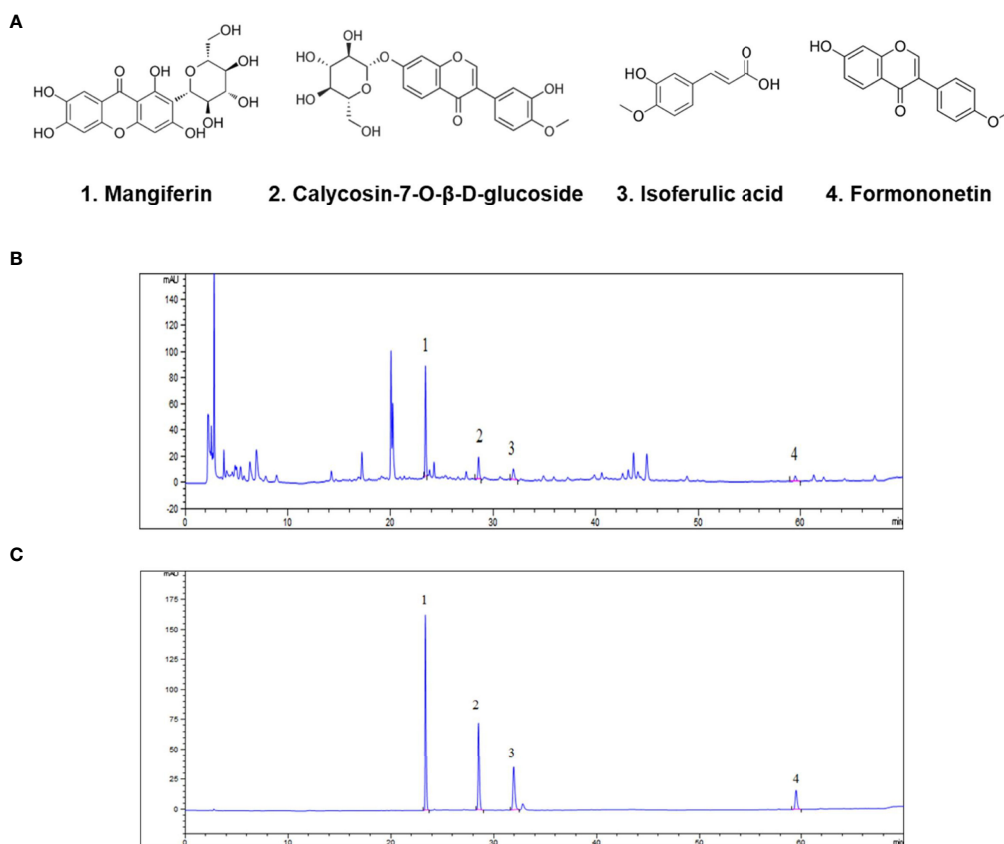


FIGURE 2 | Identification of anti-cancer phytochemicals in SXT by HPLC analysis. **(A)** Potential chemical compounds in SXT responsible for anticancer effect. HPLC chromatograms of SXT extract **(B)** and standard sample mixtures of the potential compounds **(C)**. Peak assignment as follows: 1. mangiferin; 2. calycosin-7-O-β-D-glucoside; 3. isoferulic acid; 4. formononetin.

respectively. The *in vitro* cytotoxicity of SXT-S was evaluated using Cell Counting Kit-8 kit after 24 or 48 h of incubation with LUAD cells. DDP-S was used as a positive control. As shown in **Figure 3**, compared to that of the Normal-S control group, SXT-S treatments at all doses showed cytotoxic effects against A549, SK-LU-1, and NCI-H1975 cells. Notably, the cell killing performances of MSXT-S and HSXT-S were comparable to that of the DDP-S positive control, indicating favorable anti-tumor activity. However, the viability of cells treated with HSXT-S showed no significant difference ($P > 0.05$) compared to that of MSXT-S both at 24 and 48 h, which is likely a result of the similar amount of SXT presented in MSXT-S and HSXT-S.

TABLE 1 | Amounts of bioactive compounds in SXT.

Compounds	mg/g ¹
mangiferin	2.03 ± 0.08
calycosin-7-O-β-D-glucoside	0.16 ± 0.01
isoferulic acid	0.21 ± 0.002
formononetin	0.07 ± 0.003

Results are expressed as mean \pm SD ($n=3$ independent measurements).

¹Calculated mass in the SXT extract powder.

SXT Extract Retards the Tumor Growth *in Vivo*

Considering the promising anti-proliferation results *in vitro*, we next performed *in vivo* assays to investigate the effect of SXT on tumor progression in mice. A549 subcutaneous xenograft-bearing mice were administered saline, DDP, and different doses of SXT extract for 24 days. Visible differences in tumor size were observed among the groups by the end of treatment (**Figure 4A**). We found that the mice treated with saline exhibited aggressive tumor growth, with an average volume of $482.99 \pm 13.52 \text{ mm}^3$ at the end of experiment (**Figure 4B**). In contrast, tumors in STX-treated groups grew slower over time, of which volumes on day 24 were only $402.38 \pm 12.70 \text{ mm}^3$, $278.43 \pm 23.15 \text{ mm}^3$, and $328.65 \pm 18.62 \text{ mm}^3$ for LSXT (9.55 g/kg/d), MSXT (28.65 g/kg/d) and HSXT (38.20 g/kg/d) groups, respectively (**Figure 4B**). The tumors were excised from the mice and weighed to calculate the tumor inhibition rate. Notably, the results of MSXT were comparable to DDP positive control with a tumor inhibition rate of approximately 46.85% (**Figure 4C**). These data indicate that SXT is capable of retarding tumor progression *in vivo*. The encouraging therapeutic effect was highly consistent with *in vitro* observations.

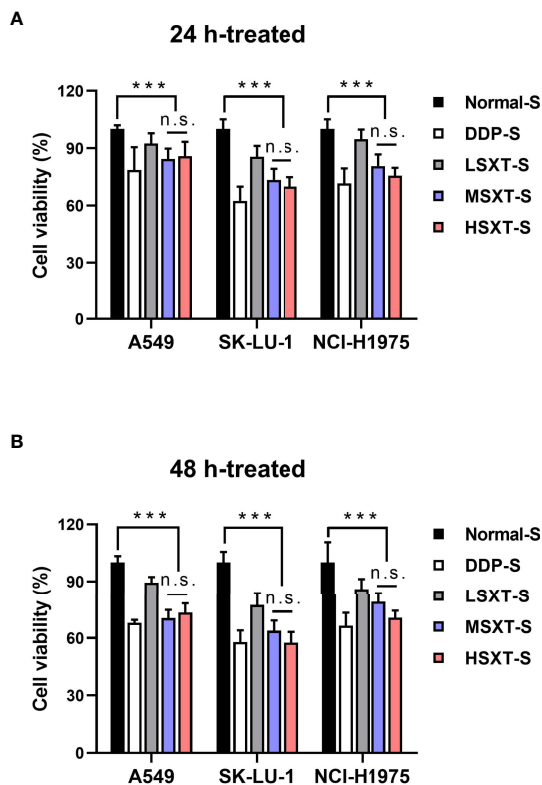


FIGURE 3 | Serum SXT suppresses the proliferation of lung adenocarcinoma cells. Incubation with serum SXT for (A) 24 h and (B) 48 h show obvious cytotoxicity to lung adenocarcinoma cell lines (mean \pm S.D., $n=10$), *** $P < 0.001$, n.s., no significance (one-way ANOVA test). Normal-S, normal serum; DDP-S, serum containing cisplatin; LSXT-S, serum containing low-dose SXT; MSXT-S, serum containing medium-dose SXT; HSXT-S, serum containing high-dose SXT.

To further investigate the anti-cancer activity of SXT, the isolated tumors were subjected to histological examination. As shown in **Figure 4D**, tumor tissues in the vehicle control group (saline) have a dense structure on a large scale, with intact nuclei and circular lipid droplets (as indicated by the red arrow). No obvious necrotic areas were observed. In contrast, tumors that received SXT treatments exhibited low cell density and irregular cell shape. Damage, such as nuclear fragmentation (green arrow), vacuolar degeneration (yellow arrow), and necrosis (black arrow), were also observed. Quantitation results (**Figure 4E**) revealed approximately 24.35%, 22.18%, 19.51% and 16.35% increases in tumor necrosis region in response to DDP, MSXT, HSXT, and LSXT treatments, respectively.

SXT Reduces the Levels of TNF- α and HIF-1 α in Mice Blood Serum

HIF-1 α plays a key role in the development of cancer. Elevated HIF-1 α levels are associated with tumor metastasis, poor patient prognosis and drug resistance (27). HIF-1 α expression is positively regulated by TNF- α (28), a major inflammatory cytokine that induces necrosis in certain tumor types (29).

Therefore, we evaluated their levels in the blood of mice following SXT treatment. As shown in **Figure 5A**, compared to the control mice injected with saline, HIF-1 α levels were significantly downregulated, after 24 days of exposure to the medium (MSXT) and high (HSXT) doses of SXT. Quantitation results revealed 20.63%, 14.67% and 16.49% reductions in the expression levels of HIF-1 α in the DDP (control drug), MSTX, and HSTX groups, respectively (**Figure 5A**). However, TNF- α levels showed no changes in all treatment groups (**Figure 5B**), indicating that SXT-mediated tumor necrosis is involved in TNF- α regulation.

Evaluation of Biosafety Potentials of SXT Using Mice

Multiple herbal medicines are pharmacologically beneficial at one dose, however, they can be toxic at another (30). The safety of traditional medicines remains a concern. Therefore, we evaluated the biosafety potential of SXT at the various therapeutic doses used in our study. Administration of SXT as high as 38.20 g/kg/d (HSXT) showed negligible changes in mice body weight over the treatment period (**Figure 6A**). Notably, we observed a noticeable reduction in body weight in the mice treated with the commercial drug, DDP. However, MSXT, whose anti-cancer effect is comparable to that of DDP (**Figure 4**), exhibited no significant loss in body weight (**Figure 6A**), demonstrating that SXT could potentially be a potent medication with low toxicity.

The effect of SXT on organ toxicity was also assessed by measuring organ indices (organ weight/body weight). We selected the spleen and lung as representative organs because their injuries frequently occur during chemotherapy (31, 32). As shown in **Figures 6B, C**, neither spleen nor lung indices exhibited significant differences ($P > 0.05$) between the control and treated groups. Saline-treated mice showed a normal splenic tissue structure, as evidenced by the intact dorsal membrane and clear boundaries between white (in blue) and red (in red) pulps (**Figure 6D**). In contrast, DDP treatment resulted in splenic atrophy, lymphocyte reduction, formation of germinal centre, sparsely arranged red marrow cells, and enhanced light reduced cell density. Compared with that of the DDP group, SXT-treated mice showed moderate pathological changes in the spleen tissue structure. Only a slight degree of this phenomenon was observed (**Figure 6D**). No obvious histological changes were observed in the lung tissue in any of the groups (**Figure 6E**), suggesting that SXT did not impair the lung. Altogether, these results demonstrated that SXT, within the concentration of 38.20 g/kg/d, caused limited organ damage in mice.

DISCUSSION

Increasing evidence suggests that traditional Chinese medicine is beneficial for improving the clinical outcomes of LUAD patients (10). SXT has been widely used for treating diseases related to immune and cardiovascular diseases in China for a long time (6–8). Although the therapeutic use of SXT for cancer treatment

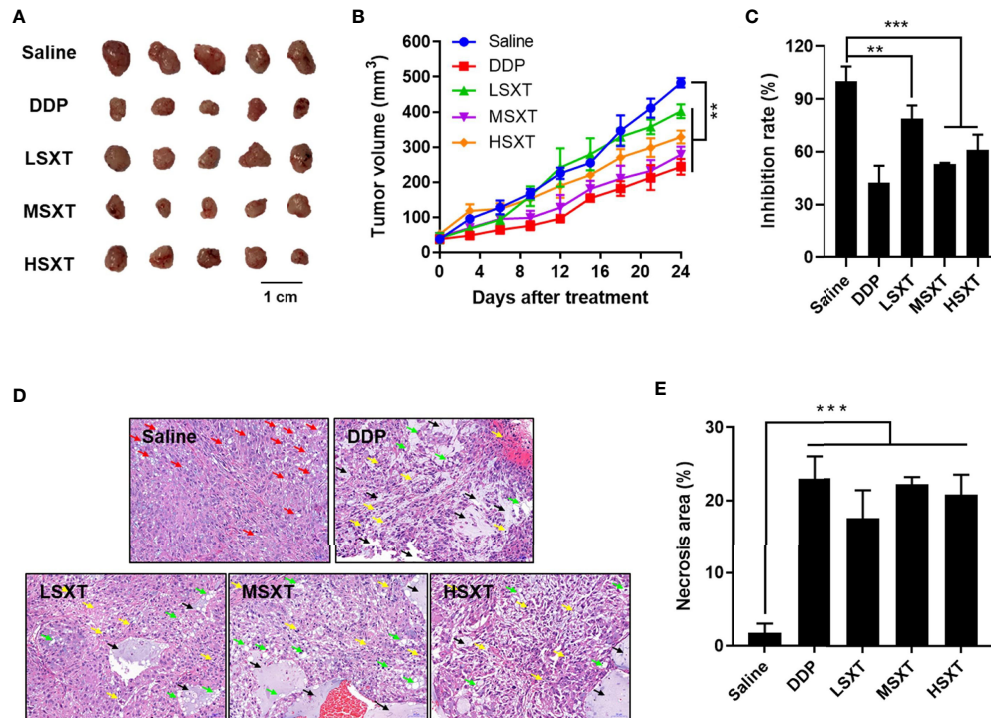


FIGURE 4 | *In vivo* anti-tumor effect of SXT. **(A)** Image of tumors isolated from mice treated with 0.9% saline (vehicle control), 22.36 mg/kg/d of cisplatin (DDP, positive control) and 9.55 g/kg/d (LSXT), 28.65 g/kg/d (MSXT) and 38.20 g/kg/d (HSXT) of SXT extract after 24 days of treatment. **(B)** Tumor volumes in different groups of mice during treatment (measured at Day 0, 4, 8, 12, 24) (mean \pm S.D., $n = 5$), $^{**}P < 0.01$ (two-way ANOVA test). Subcutaneous injection of A549 cells in SXT -treated nude mice showed low tumor forming capacity as compared to that treated with the saline control. **(C)** Inhibition rate of A549 xenograft (in weight) in mice with different treatments at the end of experiment (mean \pm S.D., $n = 5$), $^{**}P < 0.01$, $^{***}P < 0.001$ (one-way ANOVA test to saline). **(D)** Representative histological images tumor sections stained with haematoxylin and eosin showing the induction of damages and necrosis after SXT treatment at different concentrations. Objective magnification: 200 \times . Red arrow: lipid droplets; Green arrow: nucleus fragmentation; Yellow arrow: vacuolar degeneration; Black arrow: necrosis. **(E)** The quantitation result is shown on the right ($n = 3$). $^{***}P < 0.001$ (one-way ANOVA test to saline).

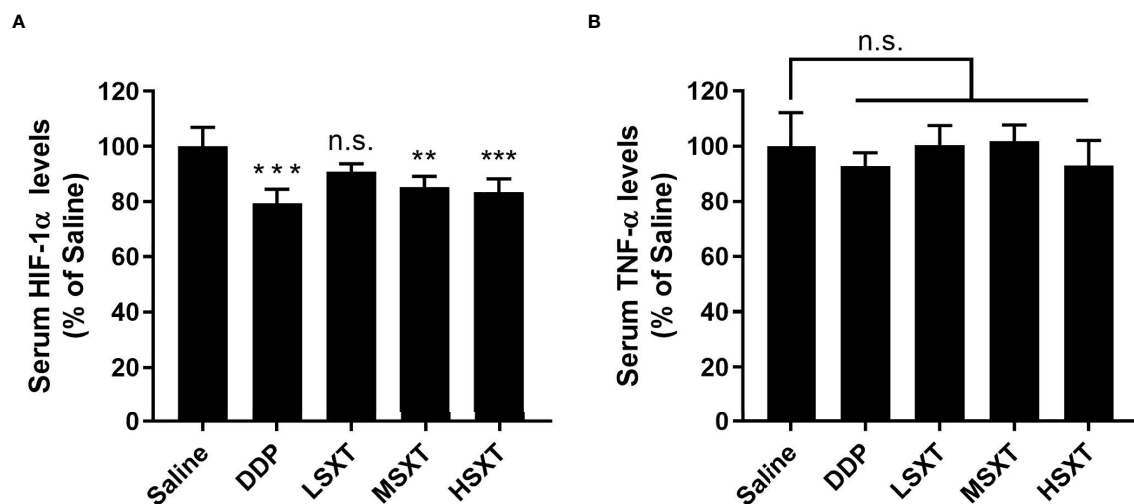


FIGURE 5 | Relative expression levels of serum HIF-1 α **(A)** and TNF- α **(B)** determined by ELISA (mean \pm S.D., $n = 5$), $^{**}P < 0.01$, $^{***}P < 0.001$, n.s., no significance (one-way ANOVA test to saline). SXT treatment at medium (MSXT; 28.65 g/kg/d) and high (HSXT; 38.20 g/kg/d) doses decreased the levels of HIF-1 α , but not TNF- α . DDP was used as a positive control.

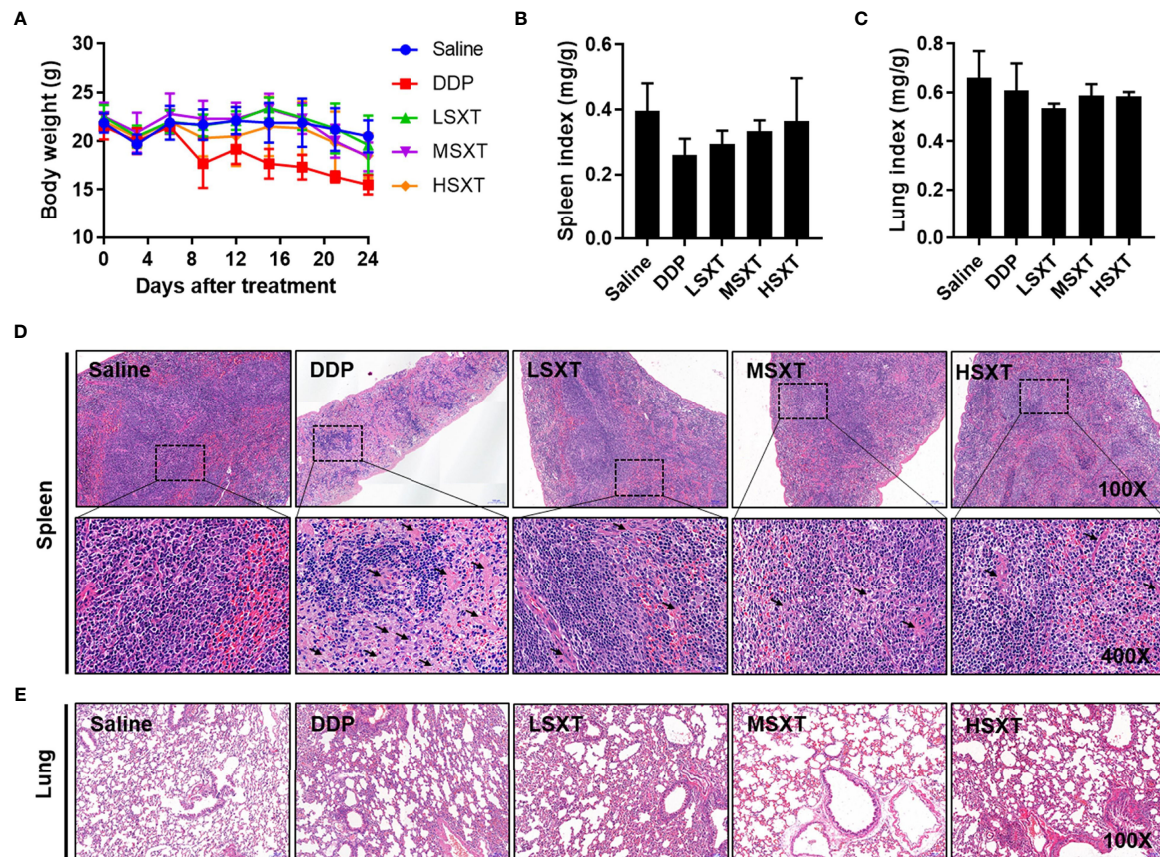


FIGURE 6 | Toxicological evaluation of SXT. **(A)** Average body weight of mice showing no loss during treatments. Spleen **(B)** and lung **(C)** indices of mice following administrations of 0.9% saline, DDP (22.36 mg/kg/d) and low (9.55 g/kg/d; LSXT), medium (28.65 g/kg/d; MSXT) and high (38.20 g/kg/d; HSXT) doses of SXT extract (mean \pm S.D., $n = 5$). The data indicates no significant difference between SXT and saline control groups. **(D)** Histological images (magnification: original 100 \times ; enlarged 400 \times) of spleen in treated mice. Treatment with commercial drug DDP induces pathological changes in the spleen tissue, whereas SXT exhibits no sign of toxicity. Black arrow indicates the germinal centre. **(E)** Observation of lung histopathology showing no abnormal changes at the tested doses of all the treatments.

has not been extensively studied, its constituent herbs have been shown to be useful for the treatment of cancers, including LUAD (10, 12, 15, 16, 33). For instance, *A. radix*, as the main component of SXT, has been recently reported to kill lung cancer cells by regulating the p53/AMPK/mTOR signaling pathway (9). *B. radix* and *P. radix*, as auxiliary prescriptions in SXT, have also been shown to induce apoptosis in cancer cells (11, 13). We verified that SXT is effective in inhibiting lung cancer growth both *in vitro* and *in vivo*.

Earlier reports revealed that mangiferin, calycosin-7-O- β -D-glucoside, and formononetin might be the major active components responsible for the anti-cancer effects of *A. radix* (17, 18). Isoferulic acid is believed to be responsible for the colorectal cancer-killing activity of *C. rhizoma*. (19). Among them, mangiferin, exhibits anti-tumor properties in A549 xenograft mice *in vivo*, and may negatively regulate the expression of miR-92a and miR-27b to influence not only cancerous growth but also the cell cycle progression and apoptosis induction of LUAD cells (34, 35). Formononetin

inhibits tumor growth by suppression of EGFR-Akt-Mcl-1 axis in non-small cell lung cancer (36). Therefore, we examined the potential anti-cancer constituents (mangiferin, calycosin-7-O- β -D-glucoside, formononetin and iso-ferulic acid) in SXT by HPLC. The results showed that SXT is abundant in mangiferin (0.203%), which may account for the favorable tumor suppression performance of SXT.

The *in vitro* anti-proliferation activity of SXT on LUAD cells (A549, SK-LU-1, and NCI-H1975) was investigated using serum pharmacology experiments. The results indicated that SXT had anticancer effect comparable to that of DDP (in the case of MSXT-S). Furthermore, an *in vivo* tumor suppression assay suggested that administration of SXT for 24 days repressed tumor progression with inhibition rates of 21.16%, 46.85% and 38.96% (**Figure 4C**) for LSXT, MSXT and HSXT, respectively. These encouraging therapeutic effects are highly consistent with *in vitro* observations.

LUAD development is a complex biological process involving numerous factors, and the activation of inflammatory cytokines is one of the most important incentives. TNF- α is a major

inflammatory cytokine, and has been reported to play decisive roles in the complex process of lung cancer onset, progression, and dissemination (37). Furthermore, the malignancy level of LUAD is closely related to the tumor microenvironment, where cancer cells use glycolysis more readily as a metabolic pathway for energy metabolism (38). HIF-1 α , which plays a regulatory role in glycolytic metabolism, is a core regulator of restoring intracellular environmental stability under hypoxia (39), and functions in the control of cell proliferation (22). Stabilization of HIF-1 α in LUAD promotes glycolysis, thereby enhances tumor metastasis (5). Using ELISA technique, we detected a significant decrease in HIF-1 α levels in the blood serum of mice receiving SXT treatment (**Figure 5**) suggesting, at least in part, that SXT may exert anti-tumor activity by modulating HIF-1 α -related signaling pathways.

Observation of mouse body weight revealed hardly any toxicity of SXT at all doses used in the present study. Since spleen is an important organ that functions in blood cell storage and filtration, its index is regarded as an acceptable indicator of immune response (40). As shown in **Figure 6B**, no significant difference in spleen index was observed, indicating that SXT hardly impaired spleen-related immune capacity in mice. In addition, treatment with SXT and DDP, had no influence on the lung tissue structure (**Figure 6C**).

In conclusion, the data presented herein demonstrate SXT is effective in LUAD treatment, with low toxicity to visceral tissues. The therapeutic performance of SXT (at a medium dose, 28.65 g/kg/d) was comparable to that of the commercial anticancer drug DDP; however, it was considerably safer. Our study provides an experimental basis for developing new anticancer agents from SXT for the treatment of LUAD.

REFERENCES

- Xu JY, Zhang C, Wang X, Zhai L, Ma Y, Mao Y, et al. Integrative Proteomic Characterization of Human Lung Adenocarcinoma. *Cell* (2020) 182:245–261. e17. doi: 10.1016/j.cell.2020.05.043
- He B, Wu C, Sun W, Qiu Y, Li J, Liu Z, et al. miR-383 Increases the Cisplatin Sensitivity of Lung Adenocarcinoma Cells Through Inhibition of the RBM24 Mediated NF- κ B Signaling Pathway. *Int J Oncol* (2021) 59:87. doi: 10.3892/ijo.2021.5267
- Herbst R, Morgensztern D, Boshoff C. The Biology and Management of Non-Small Cell Lung Cancer. *Nature* (2018) 553:446–54. doi: 10.1038/nature25183
- Zhang H, Guo L, Chen J. Rationale for Lung Adenocarcinoma Prevention and Drug Development Based on Molecular Biology During Carcinogenesis. *Onco Targets Ther* (2020) 13:3085–91. doi: 10.2147/OTT.S248436
- Huang C, Qiu S, Fan X, Jiao G, Zhou X, Sun M, et al. Evaluation of the Effect of Shengxian Decoction on Doxorubicin-Induced Chronic Heart Failure Model Rats and a Multicomponent Comparative Pharmacokinetic Study After Oral Administration in Normal and Model Rats. *Biomed Pharmacother* (2021) 144:112354. doi: 10.1016/j.biopha.2021.112354
- Xu JY, Zhu J, Cheng Y, Wu ZY, Chen YD, Xia BM, et al. Research on Immune Mechanism of Shengxian Decoction in Experimental Autoimmune Myasthenia Gravis Rats. *Chin J Immunol* (2016) 32:1462–6. (Chinese journal with English abstract). doi: 10.3969/j.issn.1000-484X.2016.10.012
- Yao L, Gui M, Li J, Lu B, Fu D. Shengxian Decoction Decreases Doxorubicin Induced Cardiac Apoptosis by Regulating the TREM1/NF κ B Signaling Pathway. *Mol Med Rep* (2021) 23:1–1(1). doi: 10.3892/mmr.2021.11858
- Ma Y, Wang BL, Wang L, Huang CY, Chen WS. Effective Components of Shengxian Decoction and Its Mechanism of Action in Treating Chronic Heart Failure Based on UHPLC-Q-TOF-MS Integrated With Network Pharmacology. *China J Chin Mater Med* (2021) 46:2489–500. doi: 10.19540/j.cnki.cjcmm.20200915.201
- Yang B, Yang N, Chen Y, Zhu M, Jia X. An Integrated Strategy for Effective-Component Discovery of *Astragali Radix* in the Treatment of Lung Cancer. *Front Pharmacol* (2021) 11:580978. doi: 10.3389/fphar.2020.580978
- Yang F, Dong X, Yin X, Wang W, You L, Jian N. Radix Bupleuri: A Review of Traditional Uses, Botany, Phytochemistry, Pharmacology, and Toxicology. *BioMed Res Int* (2017) 2017:7597596. doi: 10.1155/2017/7597596
- Hsu Y-L, Kuo P-L, Weng T-C, Yen MH, Chiang LC, Lin CC. The Antiproliferative Activity of Saponin-Enriched Fraction From Bupleurum Kaoh Is Through Fas-Dependent Apoptotic Pathway in Human Non-Small Cell Lung Cancer A549 Cells. *Biol Pharm Bull* (2004) 27:1112–5. doi: 10.1248/bpb.27.1112
- Khan M, Maryam A, Zhang H, Mehmood T, Ma T. Killing Cancer With Platycodin D Through Multiple Mechanisms. *J Cell Mol Med* (2016) 20:389–402. doi: 10.1111/jcmm.12749
- Zhao R, Chen M, Jiang Z, Zhao F, Xi B, Zhang X, et al. Platycodin-D Induced Autophagy in Non-Small Cell Lung Cancer Cells via PI3K/Akt/mTOR and MAPK Signaling Pathways. *J Cancer* (2015) 6:623–31. doi: 10.7150/jca.11291
- Hostanska K, Nisslein T, Freudenstein J, Reichling J, Saller R. Evaluation of Cell Death Caused by Triterpene Glycosides and Phenolic Substances From *Cimicifuga Racemosa* Extract in Human MCF-7 Breast Cancer Cells. *Biol Pharm Bull* (2004) 27:1970–5. doi: 10.1248/bpb.27.1970

DATA AVAILABILITY STATEMENT

The original contributions presented in the study are included in the article/supplementary material. Further inquiries can be directed to the corresponding author.

ETHICS STATEMENT

The animal study was reviewed and approved by Animal Experiments Committee of Chengdu University of Traditional Chinese Medicine.

AUTHOR CONTRIBUTIONS

KL, FY and YY conceived and designed the experiments. KL, QZ, RY, QY, XF, YR, QW and XL performed the experiments. KL, ZZ, MS and YY analyzed the data. KL, FY and YY prepared the draft. All authors discussed the results and contributed in writing the manuscript.

FUNDING

KL thanks for the financial support from the National Natural Science Fund of China (81904081). YY is grateful to the Japan Society for the Promotion of Science (JSPS) KAKENHI Grant-in-Aid for Early-Career Scientists (21K14508). DAILAB is funded by DBT (Government of India) and AIST (Japan).

15. Guo Y, Yin T, Wang X, Zhang F, Pan G, Lv H, et al. Traditional Uses, Phytochemistry, Pharmacology and Toxicology of the Genus *Cimicifuga*: A Review. *J Ethnopharmacol* (2017) 209:264–82. doi: 10.1016/j.jep.2017.07.040
16. Ji KY, Kim KM, Kim YH, Shim KS, Lee JY, Kim T, et al. Serum Starvation Sensitizes Anticancer Effect of *Anemarrhena Asphodeloides* via P38/JNK-Induced Cell Cycle Arrest and Apoptosis in Colorectal Cancer Cells. *Am J Chin Med* (2021) 49:1001–16. doi: 10.1142/S0192415X21500488
17. Chen Y, Bi L, Luo H, Jiang Y, Chen F, Wang Y, et al. Water Extract of Ginseng and Astragalus Regulates Macrophage Polarization and Synergistically Enhances DDP's Anticancer Effect. *J Ethnopharmacol* (2019) 232:11–20. doi: 10.1016/j.jep.2018.12.003
18. Mei S, Ma H, Chen X. Anticancer and Anti-Inflammatory Properties of Mangiferin: A Review of Its Molecular Mechanisms. *Food Chem Toxicol* (2021) 149:111997. doi: 10.1016/j.fct.2021.111997
19. Long Z, Feng G, Zhao N, Wu L, Zhu H. Isoferulic Acid Inhibits Human Leukemia Cell Growth Through Induction of G2/M Phase Arrest and Inhibition of Akt/mTOR Signaling. *Mol Med Rep* (2020) 21:1035–42. doi: 10.3892/mmr.2020.10926
20. King FW, Fong S, Griffin C, Shoemaker M, Staub R, Zhang Y-L, et al. Timosaponin AIII Is Preferentially Cytotoxic to Tumor Cells Through Inhibition of mTOR and Induction of ER Stress. *PLoS One* (2009) 4(9):e7283. doi: 10.1371/journal.pone.0007283
21. Wang B, Zhu L, Qi C. Primary Study on the Application of Serum Pharmacology in Chinese Traditional Medicine. *Colloids Surf B Biointerfaces* (2005) 43:194–7. doi: 10.1016/j.colsurfb.2005.04.013
22. Huang CH, Lu Y, Gao XJ, Sun ZG, Yan LG. Advances of Serum Pharmacology of Chinese Medicine. *Chin J Exp Tradit Med Form* (2011) 17:266–71. (Chinese journal with English abstract). doi: 10.13422/j.cnki.syfx.2011.10.078
23. Nair AB, Jacob S. A Simple Practice Guide for Dose Conversion Between Animals and Human. *J Basic Clin Pharm* (2016) 7:27–31. doi: 10.4103/0976-0105.177703
24. Yu Y, Yang X, Reghu S, Kaul SC, Wadhwa R, Miyako E. Photothermogenetic Inhibition of Cancer Stemness by Near-Infrared-Light-Activatable Nanocomplexes. *Nat Commun* (2020) 11:4117. doi: 10.1038/s41467-020-17768-3
25. Huang F, Zhang R, Liu Y, Xiao J, Wei Z, Yi Y, et al. Dietary Litchi Pulp Polysaccharides Could Enhance Immunomodulatory and Antioxidant Effects in Mice. *Int J Biol Macromol* (2016) 92:1067–73. doi: 10.1016/j.ijbiomac.2016.08.021
26. Wang C, Yue F, Kuang S. Muscle Histology Characterization Using H&E Staining and Muscle Fiber Type Classification Using Immunofluorescence Staining. *Bio Protoc* (2017) 7:e2279. doi: 10.21769/BioProtoc.2279
27. Semenza GL. Defining the Role of Hypoxia-Inducible Factor 1 in Cancer Biology and Therapeutics. *Oncogene* (2010) 29:625–34. doi: 10.1038/onc.2009.441
28. Zhou J, Schmid T, Brüne B. Tumor Necrosis Factor-Alpha Causes Accumulation of a Ubiquitinated Form of Hypoxia Inducible Factor-1alpha Through a Nuclear factor-kappaB-Dependent Pathway. *Mol Biol Cell* (2003) 14:2216–25. doi: 10.1091/mbc.e02-09-0598
29. Balkwill F. Tumour Necrosis Factor and Cancer. *Nat Rev Cancer* (2009) 9:361–71. doi: 10.1038/nrc2628
30. Ekor M. The Growing Use of Herbal Medicines: Issues Relating to Adverse Reactions and Challenges in Monitoring Safety. *Front Pharmacol* (2013) 4:177. doi: 10.3389/fphar.2013.00177
31. Koyama N, Tomoda K, Matsuda M, Fujita Y, Yamamoto Y, Hontsu S, et al. Acute Bilateral Renal and Splenic Infarctions Occurring During Chemotherapy for Lung Cancer. *Intern Med* (2016) 55:3635–9. doi: 10.2169/internalmedicine.55.6891
32. Otani T, Yamaguchi K, Nakao S, Sakamoto S, Horimasu Y, Masuda T, et al. Association Between Glucose Intolerance and Chemotherapy-Induced Lung Injury in Patients With Lung Cancer and Interstitial Lung Disease. *Cancer Chemother Pharmacol* (2021) 88:857–65. doi: 10.1007/s00280-021-04341-y
33. Lin J, Dong HF, Oppenheim JJ, Howard OM. Effects of Astragali Radix on the Growth of Different Cancer Cell Lines. *World J Gastroenterol* (2003) 9:670–3. doi: 10.1080/00365520310000753
34. Shi W, Deng J, Tong R, Yang Y, He X, Lv J, et al. Molecular Mechanisms Underlying Mangiferin-Induced Apoptosis and Cell Cycle Arrest in A549 Human Lung Carcinoma Cells. *Mol Med Rep* (2016) 13:3423–32. doi: 10.3892/mmr.2016.4947
35. Chi XJ, Meng JJ, Lin CY, Su QS, Qin YY, Wei RH, et al. Mangiferin Inhibits Human Lung Adenocarcinoma by Suppressing MiR-27b and MiR-92a. *Evid Based Complement Alternat Med* (2021) 2021:2822950. doi: 10.1155/2021/2822950
36. Yu X, Gao F, Li W, Zhou L, Liu W, Li M. Formononetin Inhibits Tumor Growth by Suppression of EGFR-Akt-Mcl-1 Axis in Non-Small Cell Lung Cancer. *J Exp Clin Cancer Res* (2020) 39:62. doi: 10.1186/s13046-020-01566-2
37. Benoot T, Piccioni E, De Ridder K, Goyvaerts C. TNF α and Immune Checkpoint Inhibition: Friend or Foe for Lung Cancer? *Int J Mol Sci* (2021) 22:8691. doi: 10.3390/ijms22168691
38. Hensley CT, Faubert B, Yuan Q, Lev-Cohain N, Jin E, Kim J, et al. Metabolic Heterogeneity in Human Lung Tumors. *Cell* (2016) 164(4):681–94. doi: 10.1016/j.cell.2015.12.034
39. Del Rey MJ, Valín Á, Usategui A, García-Herrero CM, Sánchez-Aragó M, Cuezva JM, et al. Hif-1 α Knockdown Reduces Glycolytic Metabolism and Induces Cell Death of Human Synovial Fibroblasts Under Normoxic Conditions. *Sci Rep* (2017) 7:3644. doi: 10.1038/s41598-017-03921-4
40. Sun S, Li K, Lei Z, Xiao L, Gao R, Zhang Z. Immunomodulatory Activity of Polysaccharide From *Helicteres Angustifolia* L. on 4T1 Tumor-Bearing Mice. *BioMed Pharmacother* (2018) 101:881–8. doi: 10.1016/j.biopha.2018.03.029

Conflict of Interest: The authors declare that the research was conducted in the absence of any commercial or financial relationships that could be construed as a potential conflict of interest.

Publisher's Note: All claims expressed in this article are solely those of the authors and do not necessarily represent those of their affiliated organizations, or those of the publisher, the editors and the reviewers. Any product that may be evaluated in this article, or claim that may be made by its manufacturer, is not guaranteed or endorsed by the publisher.

Copyright © 2022 Li, You, Zhang, Yuan, Yuan, Fu, Ren, Wang, Li, Zhang, Shichiri and Yu. This is an open-access article distributed under the terms of the Creative Commons Attribution License (CC BY). The use, distribution or reproduction in other forums is permitted, provided the original author(s) and the copyright owner(s) are credited and that the original publication in this journal is cited, in accordance with accepted academic practice. No use, distribution or reproduction is permitted which does not comply with these terms.



Ag120-Mediated Inhibition of ASCT2-Dependent Glutamine Transport has an Anti-Tumor Effect on Colorectal Cancer Cells

Wei Yu^{1,2†}, Jianwen Huang^{1†}, Qichao Dong^{3†}, Wenting Li¹, Lei Jiang², Qian Zhang², Li Sun^{2*}, Shengtao Yuan^{2*} and Xu He^{1*}

¹Zhuhai Interventional Medical Center, Zhuhai Precision Medical Center, Zhuhai People's Hospital, Zhuhai Hospital Affiliated with Jinan University, Jinan University, Zhuhai, China, ²Jiangsu Key Laboratory of Drug Screening, China Pharmaceutical University, Nanjing, China, ³Department of General Surgery, Zhuhai People's Hospital (Zhuhai Hospital Affiliated with Jinan University), Zhuhai, China

OPEN ACCESS

Edited by:

Rajkumar S. Kalra,
Okinawa Institute of Science and
Technology Graduate University,
Japan

Reviewed by:

Aftab Alam,
Roswell Park Comprehensive Cancer
Center, United States
Aditya Sarode,
Columbia University, United States

*Correspondence:

Li Sun
sunli@cpu.edu.cn
Shengtao Yuan
yuanst@cpu.edu.cn
Xu He
hexu220@163.com

[†]These authors have contributed
equally to this work

Specialty section:

This article was submitted to
Pharmacology of Anti-Cancer Drugs,
a section of the journal
Frontiers in Pharmacology

Received: 08 February 2022

Accepted: 11 March 2022

Published: 28 March 2022

Citation:

Yu W, Huang J, Dong Q, Li W, Jiang L,
Zhang Q, Sun L, Yuan S and He X
(2022) Ag120-Mediated Inhibition of
ASCT2-Dependent Glutamine
Transport has an Anti-Tumor Effect on
Colorectal Cancer Cells.
Front. Pharmacol. 13:871392.
doi: 10.3389/fphar.2022.871392

Metabolic reprogramming is considered to be a hallmark of cancer, and increased glutamine metabolism plays an important role in the progression of many tumors, including colorectal cancer (CRC). Targeting of glutamine uptake via the transporter protein ASCT2/SLC1A5 (solute carrier family 1 member 5) is considered to be an effective strategy for the treatment of malignant tumors. Here, we demonstrate that Ag120 (ivosidenib), a mutant isocitrate dehydrogenase 1 (IDH1) inhibitor approved for the treatment of certain cancers, acts as an ASCT2 inhibitor in CRC cells. Ag120 blocked glutamine uptake and metabolism, leading to reduced cell proliferation, elevated autophagy, and increased oxidative stress in CRC cells *in vitro* and *in vivo*, potentially via the ERK and mTOR signaling pathways. These effects occurred independently of mutant IDH1 activity and were supported by experiments with ASCT2-depleted or -overexpressing cells. These data identify a novel mechanism of Ag120 anti-tumor activity and support further exploration of ASCT2 inhibitors for cancer therapy.

Keywords: ASCT2, AG120, CRC, glutamine metabolism, tumor proliferation

INTRODUCTION

Deregulation of cell metabolism, also known as metabolic rewiring, is a hallmark of cancer and is a response to the increased demands for energy and materials needed to support the growth phenotypes of cancer cells (Hanahan and Weinberg, 2000; San-Millán and Brooks, 2017). L-glutamine is a crucial amino acid for protein synthesis and energy generation by many tumors, including colorectal cancer (CRC) (Deberardinis and Cheng, 2010; Noel et al., 2010). Typically, transportation of glutamine into cells is mediated by amino acid carrier proteins, particularly solute carrier family 1 member 5 (SLC1A5), also known as alanine, serine, cysteine-preferring transporter 2 (ASCT2) (Wang et al., 2015). SLC1A5 is highly expressed in many cancers,

Abbreviations: ASCT2, alanine, serine, cysteine-preferring transporter 2; SLC1A5, solute carrier family 1, member 5; CRC, colorectal cancer; ATP, adenosine triphosphate; ROS, reactive oxygen species; NADH, nicotinamide adenine dinucleotide (reduced); Ag120, ivosidenib; TCA, tricarboxylic acid; α-KG, 2-ketoglutaric acid; Glc, glucose; Gln, glutamine

including CRC (Deberardinis and Cheng, 2010), and plays an important role in supplying glutamine for energy production, autophagy, redox homeostasis, and activation of mTOR signaling, thereby promoting tumor growth (Hassanein et al., 2013; Willems et al., 2013; Huang et al., 2014; Marzi et al., 2016; van Geldermalsen et al., 2016). Inhibition of ASCT2 protein and glutamine starvation represents a promising strategy for cancer therapy. Consistent with this, many studies have investigated the effects on cancer growth of ASCT2 inhibition with small molecule compounds such as V9302 (Schulte et al., 2018), L-γ-glutamyl-p-nitroanilide (GPNA) (Esslinger et al., 2005), and benzylserine (Grewer and Grabsch, 2004), and with ASCT2-specific monoclonal antibodies (Hara et al., 2020). However, each of these approaches has some limitations such as high toxicity and poor solubility (Grewer and Grabsch, 2004; Esslinger et al., 2005; Schulte et al., 2018; Hara et al., 2020). And there is an urgent need to continue the search for new ASCT2 inhibitors for the treatment of cancer.

Ag120, also known as ivosidenib, is a small molecule inhibitor of mutant isocitrate dehydrogenase (IDH1mt). The driver mutations in IDH1 abolish its normal function in the conversion of isocitrate to α-ketoglutarate (α-KG) and instead confer gain-of-function activity that results in the production of the oncometabolite 2-hydroxyglutarate (2-HG) (Lucia et al., 2017; Marina et al., 2021). In the United States, ivosidenib was approved for the treatment of IDH1mt acute myeloid leukemia in 2018 and for IDH1mt cholangiocarcinoma in 2021, and it is currently in clinical trials for other cancers such as advanced hematological malignancies (NCT02074839) and advanced solid tumors (NCT02073994) harboring IDH1mt (Lucia et al., 2017; Marina et al., 2021). Ag120 mainly targets tumor cells by inhibiting IDH1mt-mediated production of 2-HG, thereby blocking of tumor progression (Pollyea et al., 2014; Fan et al., 2015). Interestingly, Ag120 inhibits the proliferation of a subcutaneous grade 3 IDH1mt glioma by 52% through an unknown mechanism (Brandon et al., 2017). Therefore, it seems likely that the anti-tumor effects and mechanisms of action of Ag120 are incompletely understood, and continued study of this compound is warranted. To date, the anti-CRC effects of Ag120 have not been investigated and its mechanisms of action other than *via* IDH1 mt are also unknown.

In the present study, we report for the first time that Ag120 is an ASCT2 inhibitor in CRC cells and suppresses tumor growth *via* inhibition of glutamine uptake and metabolism. This work not only has important implications for broadening the potential indications for Ag120 but also identifies ASCT2 as a potential anti-cancer therapeutic target of Ag120.

MATERIALS AND METHODS

Cell Culture and Reagents

The human CRC cell lines HCT116 and HT29 were obtained from NEWGAINBIO (Wuxi, China) and were authenticated using short tandem repeat analysis (Genetic Testing Biotechnology Corporation, Suzhou) to exclude possible contamination. CRC cells were maintained in McCoy's 5A medium containing 10% fetal bovine serum at 37°C in a 5%

CO₂ humidified atmosphere. Ag120 and the ASCT2 inhibitor V9302 were obtained from Selleck and were resuspended in phosphate-buffered saline (PBS) for experiments.

Computational Screening

The datafile for the structure of the human ASCT2 protein [Protein Data Bank (PDB): 5LLM] was downloaded from PDB (<http://www.rcsb.org/>). All heterogeneous atoms were removed for subsequent molecular docking. The PDB file (5LLM) was converted to the PDBQT format for macromolecules before virtual screening. The grid (ligand docking search space) was located and maximized. Autodock Vina 1.1.2 was used for molecular docking. Protein–ligand interactions were visualized using PyMOL version 1.7.4.5.

Surface Plasmon Resonance

Binding of Ag120 to purified human ASCT2 protein (ACROBiosystems, Beijing, China) was measured by SPR using a Biacore T200 system (General Electric, Sweden). Binding was tested in the presence of two-fold serial dilutions of Ag120 from 0.15625 to 10 μM. Each sample was analyzed in triplicate.

Construction of CRC Cell Lines With Stable ASCT2 Knockdown or Overexpression

HCT116 and HT29 cells were seeded in tissue culture dishes and grown for approximately 24 h to reach 50–60% confluence. The medium was then changed to McCoy's 5A containing 30 μg/ml polybrene and the appropriate lentiviruses encoding control or ASCT2 shRNAs (sh *SLC1A5*#1: 5'-GCTTGGTAGTGTGGTCCATCG-3'; sh *SLC1A5*#2: 5'-GGATGTGGGTTTACTCTTTGC-3'; sh NC: 5'-TTCTCCGAA CGTGTACAGT-3'; Public Protein/Plasmid Library, Nanjing, China) or overexpression vectors (pLenti-CMV-GFP-Puro-*SLC1A5*; Public Protein/Plasmid Library, Nanjing, China) were added and incubated at 37°C for 24 h. The medium was exchanged for fresh McCoy's 5A medium and the cells were further cultured for an additional 24 h. Stable ASCT2 knockdown (ASCT2-KD) or ASCT2-overexpressing (ASCT2-OE) cell lines were selected by growth in medium containing 10 μM puromycin. Efficient knockdown or overexpression was verified by RT-qPCR and immunoblotting.

Colony-forming Assay

CRC cells were seeded in 6-well culture plates at 10³ cells/well and treated with Ag120 or V9302 for 10 days (wild-type cells) or 14 days (ASCT2-KD or ASCT2-OE cells). At the end of the incubation, the cells were stained with crystal violet solution (Beyotime, Jiangsu, China) and the number of colonies was counted manually.

Colorimetric Cell Proliferation Assay

Cells were seeded in 96-well plates at 2 × 10⁴ cells/well and incubated for 72 h. Every 24 h, cell numbers were determined using a Cell Counting Kit-8 (CCK-8; Beyotime, Jiangsu, China) according to the manufacturer's instructions.

EdU Incorporation

To assess proliferation by incorporation of the fluorescent nucleoside analog 5-ethynyl-2'-deoxyuridine (EdU), CRC cells

TABLE 1 | Primer sequences for quantitative RT-PCR.

Gene	Sequences
SLC1A5	Forward Sequence: TCCTCTTCACCCGCAAAACCC
—	Reverse Sequence: CCACGCCATTATTCTCTCCAC

were seeded in 96-well plates at 3×10^4 cells/well and incubated for 72 h. EdU incorporation was assessed using an EdU Staining Proliferation kit (RuiBo, Suzhou, China) according to the manufacturer's instructions.

Immunoblotting

CRC cells were incubated with Ag120 or V9302 for 48 h and processed for immunoblotting as previously described (Schulte et al., 2018). Primary antibodies against β -actin, ASCT2, mTOR, phosphorylated (p)-mTOR, P70S6K, p-P70S6K, ERK1, p-ERK1, IDH1wt, LC3, LAMP1, ATG7, ATG5, and beclin-1 and a secondary FITC-conjugated goat anti-rabbit IgG (H + L) antibody were purchased from ABclonal Biotechnology (Wuhan, China). Horseradish peroxidase (HRP)-conjugated anti-mouse IgG was purchased from ABclonal Biotechnology (Wuhan, China) and anti-rabbit IgG secondary antibodies were purchased from Cell Signaling Technology (Beverly, MA, United States). Protein bands were visualized using enhanced chemiluminescence reagents (Millipore).

Quantitative Reverse-Transcription PCR (RT-qPCR)

Total cellular RNA was isolated from cells or tissues using TRIzol reagent (Vazyme, Jiangsu, China) and RNA was reverse transcribed using a Revert Aid First Strand cDNA Synthesis Kit (Vazyme). qPCR was performed using SYBR GREEN master mix (Vazyme) on a Bio-Rad CFX-96 fluorescence quantitative PCR instrument. mRNA levels of the genes of interest were standardized with an internal control (18s rRNA). Primer sequences are provided in Table 1.

Mouse Xenograft Experiments

Groups ($n = 5$) of female athymic BALB/c nude mice (5–6 weeks of age, body weight 18–22 g) were obtained from Charles River (Zhejiang, China). Subconfluent HCT116 cells were collected, resuspended in serum-free medium at 10^6 cells/100 μ l, and injected subcutaneously into one flank. After 7 days, the animals were injected intraperitoneally with the indicated doses of Ag120, V9302, or vehicle (PBS) in 100 μ l/injection. Animal care and experimental protocols were approved by the Animal Care Committee of JINAN University. Animals were treated appropriately and used in a scientifically valid and ethical manner.

BrEdU Incorporation Assay

Four hours after the final injection of vehicle, Ag120 or V9302, the mice were injected intraperitoneally with 100 μ l of 1 mg/ml bromodeoxyuridine (BrEdU) labeling reagent (RuiBO) and

sacrificed 4 h later. The tumors were excised, frozen, and cryosectioned. Sections were incubated with 10 μ g of mouse anti-BrEdU primary antibody (ABclonal Biotechnology, Wuhan, China) for 12 h at 4°C and then with a rhodamine red-labeled goat anti-mouse IgG secondary antibody (Invitrogen Molecular Probes, Carlsbad, CA) for 2 h at 20°C. Sections were counterstained with the DNA-binding dye 4',6-diamidino-2-phenylindole (DAPI). Cells were imaged on an inverted fluorescence microscope and photographs were obtained and scanned into ImageJ software. BrEdU-incorporating and proliferating cells were quantified using high-magnification photographs.

Glutamine Uptake

Cells were cultured overnight in 3.5-ml culture dishes at 2×10^6 /dish. Cells were transferred to PBS containing 1 mg/mL D-glucose and 0.11 mg/ml sodium pyruvate and incubated with Ag120 or V9302 for 2 h. L-glutamine (2 mM) was then added to the cells for an additional 10 min and the cells were collected, washed, and lysed. Intracellular glutamine concentrations were measured using a glutamine assay kit (Abnova, United States) according to the manufacturer's instructions. Luminescence was measured using a FilterMax F3 microplate reader. The data were normalized to total protein levels.

Glucose Uptake

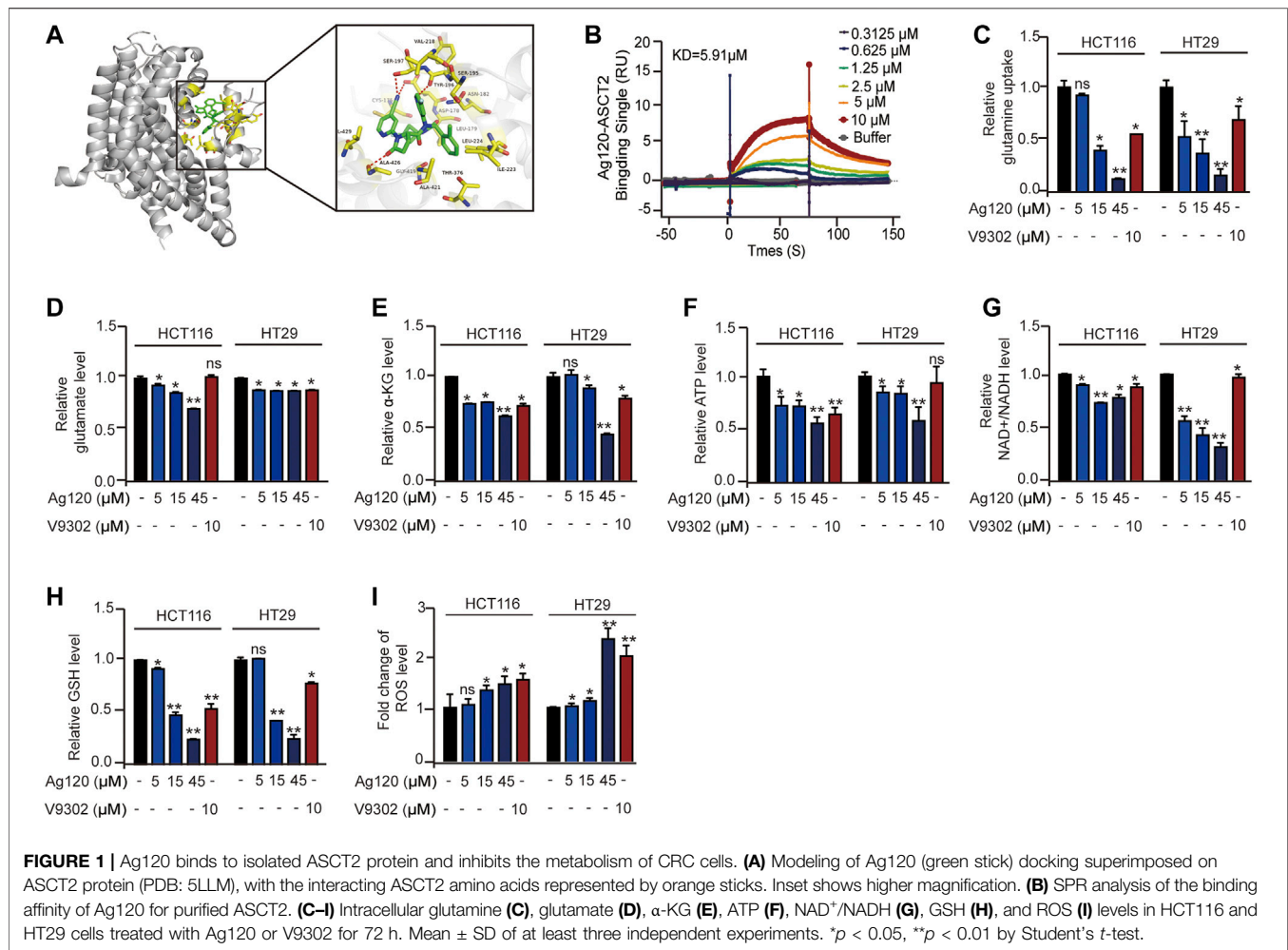
Cells were seeded in a 6-well plate at 5×10^5 cells/well. The cells were glucose-starved by preincubation in 1 ml Krebs-Ringer-Phosphate-HEPES buffer containing 2% bovine serum albumin and Ag120 or V9302 for 40 min, and 10 μ l of 10 mM 2-deoxyglucose (Sigma Aldrich, St. Louis, MO, United States) was then added for an additional 20 min. At the end of the incubation, the cells were collected, washed, and lysed, and glucose concentrations in the supernatants were measured with a Glucose Uptake kit (Abcam, Cambridge, United Kingdom) according to the manufacturer's instructions.

Intracellular Metabolite Assays

CRC cells were treated for 48 h with Ag120 and then processed for measurement of intracellular levels and analyzed for intracellular levels of NAD⁺/NADH, GSH, and ATP using kits from Beyotime; for glutamate, glucose, and α -KG using kits from Abcam (Cambridge, United Kingdom); and for D-2-hydroxyglutarate (2-HG) levels using a colorimetric assay kit from BioVision (Bioptics, Tucson, AZ, USA).

Immunohistochemistry

Tumors were excised from the mice within 4 h of the final vehicle, Ag120, or V9302 administration, and then fixed in 10% formalin for 24 h and stored in 70% ethanol in PBS at 4°C. Tissues were sectioned (5 μ m thickness) and stained with primary antibodies against ASCT2 (Cell Signaling Technology, #8057S), Ki67 (Abclonal #A2094), or LC3 (Cell Signaling Technology, #12741S) followed by anti-rabbit IgG secondary antibodies (Cell Signaling Technology, Beverly, MA, United States). Tissues were imaged using an inverted fluorescence microscope at $\times 20$ magnification.



Transmission Electron Microscopy

TEM was used to visualize autophagic vesicles and mitochondrial morphology. CRC cells were treated with Ag120 and V9302 for 72 h and fixed in glutaraldehyde (Sigma). Ultrathin sections were prepared using a Sorvall MT5000 microtome and stained with lead citrate and/or 1% uranyl acetate. Sections were visualized using a Philips EM420 electron microscopy.

Detection of Lysosomes and Autophagosomes

Lysosomes and autophagosomes were visualized using the fluorescent probes LysoTracker and monodansylcadaverine (MDC), respectively. Cells were seeded in 6-well plates at 5×10^5 /well and grown overnight. Ag120 or V9302 was added and the cells were incubated for 72 h. The culture medium was then removed and the cells were processed using a LysoTracker staining kit (Beyotime), or an MDC staining kit (Solarbio, Beijing, China) according to the manufacturers' instructions. Cells were visualized using an inverted fluorescence microscope.

Statistical Analysis

Data are presented as the mean \pm standard deviation (SD). Multiple group means were compared using two-way analysis of variance followed by the Student–Newman–Keuls multiple comparison test, and two group means were compared using Student's *t*-test. A *p* value < 0.05 was considered to be statistically significant.

RESULTS

Ag120 Binds to Purified Human ASCT2 Protein and Modulates Energy Metabolism in CRC Cells

By employing the crystal structure of ASCT2 to perform molecular docking modeling, we find the potential interaction between Ag120 and ASCT2 protein (Canul-tec et al., 2017). As shown in **Figure 1A**, Ag120 binds to ASCT2 through amino acids CYS175, LEU179, ASN182, SER195, SER197, VAL218, ILE223, LEU224, THR376, GLY419, ALA421, ALA426, and VAL429 (**Figure 1A**). Consistent with this, SPR experiments

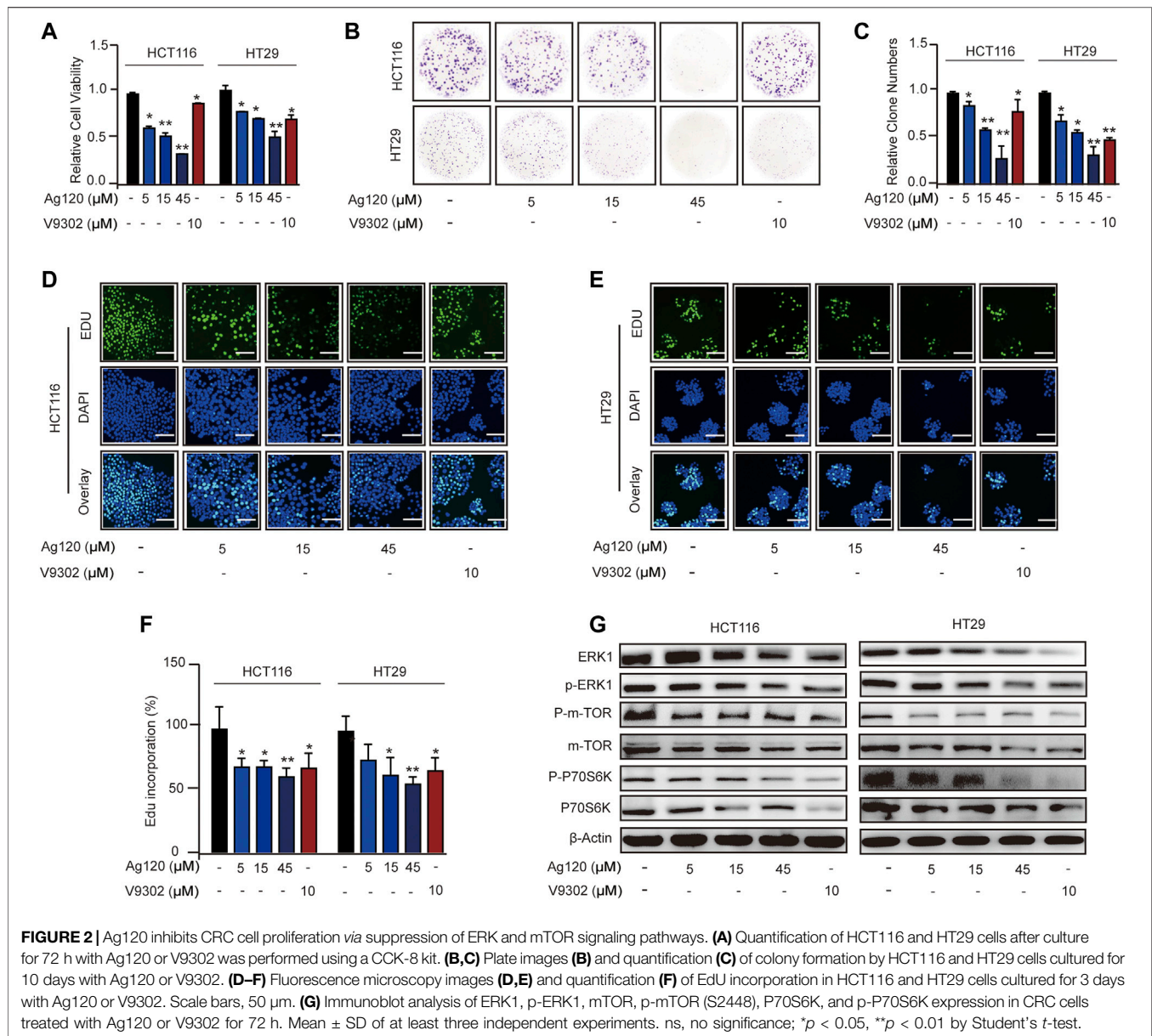


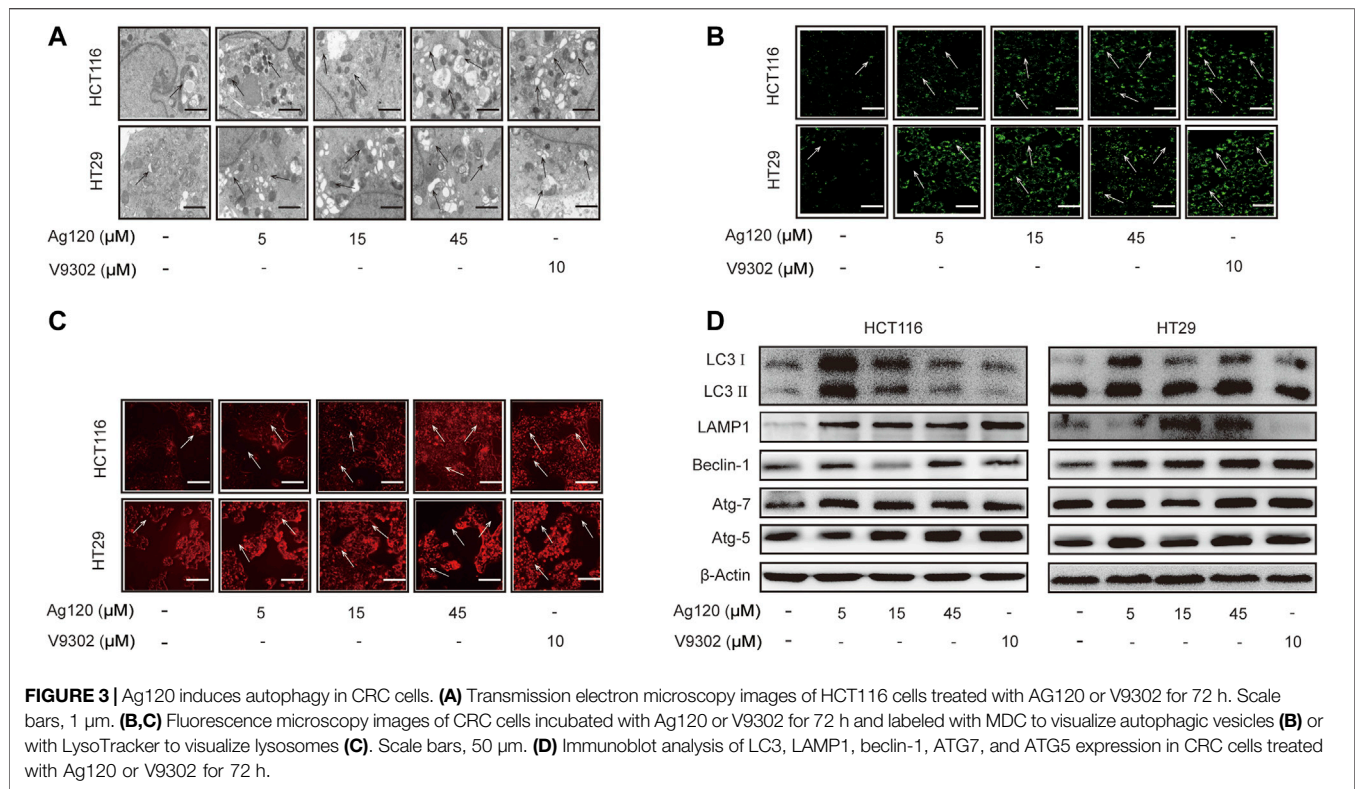
FIGURE 2 | Ag120 inhibits CRC cell proliferation *via* suppression of ERK and mTOR signaling pathways. **(A)** Quantification of HCT116 and HT29 cells after culture for 72 h with Ag120 or V9302 was performed using a CCK-8 kit. **(B,C)** Plate images **(B)** and quantification **(C)** of colony formation by HCT116 and HT29 cells cultured for 10 days with Ag120 or V9302. **(D–F)** Fluorescence microscopy images **(D,E)** and quantification **(F)** of EdU incorporation in HCT116 and HT29 cells cultured for 3 days with Ag120 or V9302. Scale bars, 50 μm. **(G)** Immunoblot analysis of ERK1, p-ERK1, mTOR, p-mTOR (S2448), P70S6K, and p-P70S6K expression in CRC cells treated with Ag120 or V9302 for 72 h. Mean ± SD of at least three independent experiments. ns, no significance; * $p < 0.05$, ** $p < 0.01$ by Student's *t*-test.

demonstrated a binding affinity of 5.91 μM between purified human ASCT2 protein and Ag120 (Figure 1B) and V9302 is regarded as the positive control (Supplementary Figure S1A) (Schulte et al., 2018). To examine the pharmacological effects of Ag120, we incubated two human CRC cell lines, HCT116 and HT29, with various concentrations of Ag120 or with 10 μM of V9302, a previously described ASCT2 inhibitor (Schulte et al., 2018) for 72 h and then analyzed the intracellular concentrations of glutamine, α-KG, ATP, NAD⁺/NADH, glutathione (GSH), and reactive oxygen species (ROS). Ag120 was found to significantly decrease intracellular levels of glutamate, α-KG, ATP, and NAD⁺/NADH in both cell types (Figures 1D–G), whereas glucose concentrations were significantly elevated (Supplementary Figure S1B), possibly as a compensation mechanism. Moreover, the block of glutamine uptake could cause the

reduce of GSH and increase of ROS thereby inducing oxidative stress (Schulte et al., 2018; Hara et al., 2020). Ag120 altered the redox balance in CRC cells, as reflected by the significant depletion of GSH levels and elevation of ROS levels compared with untreated cells (Figures 1H,I). These changes were also observed with the known ASCT2 inhibitor V9302, although V9302 appeared to be the more effective inhibitor of the two (Figures 1D–I). Collectively, these results demonstrated that Ag120 binds to ASCT2, inhibits glutamine metabolism and energy production, and induces oxidative stress in CRC cells.

Ag120 Inhibits Proliferation in CRC Cells

To determine whether Ag120 exhibited an anti-tumor effect on CRC cells, we analyzed cell proliferation, colony formation, and DNA synthesis. Incubation of CRC cells with Ag120 significantly



and dose-dependently decreased the number of viable cells present after 72 h (**Figure 2A**) and the number of colonies formed after 10 days (**Figures 2B,C**). These effects were confirmed by demonstrating a significant reduction in incorporation of the fluorescent nucleoside EdU into CRC cell DNA after 72 h treatment with Ag120 (**Figures 2D–F**). To identify the potential mechanism of action of Ag120, we performed immunoblot analysis of key components of the ERK and mTOR signaling pathways in HCT116 and HT29 cells. Ag120 treatment for 72 h resulted in decreased expression of ERK1, phosphorylated (p)-ERK1, mTOR, p-mTOR (S2448), P70S6K, and p-P70S6K (**Figure 2G**; **Supplementary Figure S2**) which is related to tumor proliferation (van Geldermalsen et al., 2016; Schulte et al., 2018). Collectively, these results suggest that Ag120 exhibits a significant anti-tumor effect in CRC that may be mediated by inhibition of the mTOR and ERK1 signaling pathways.

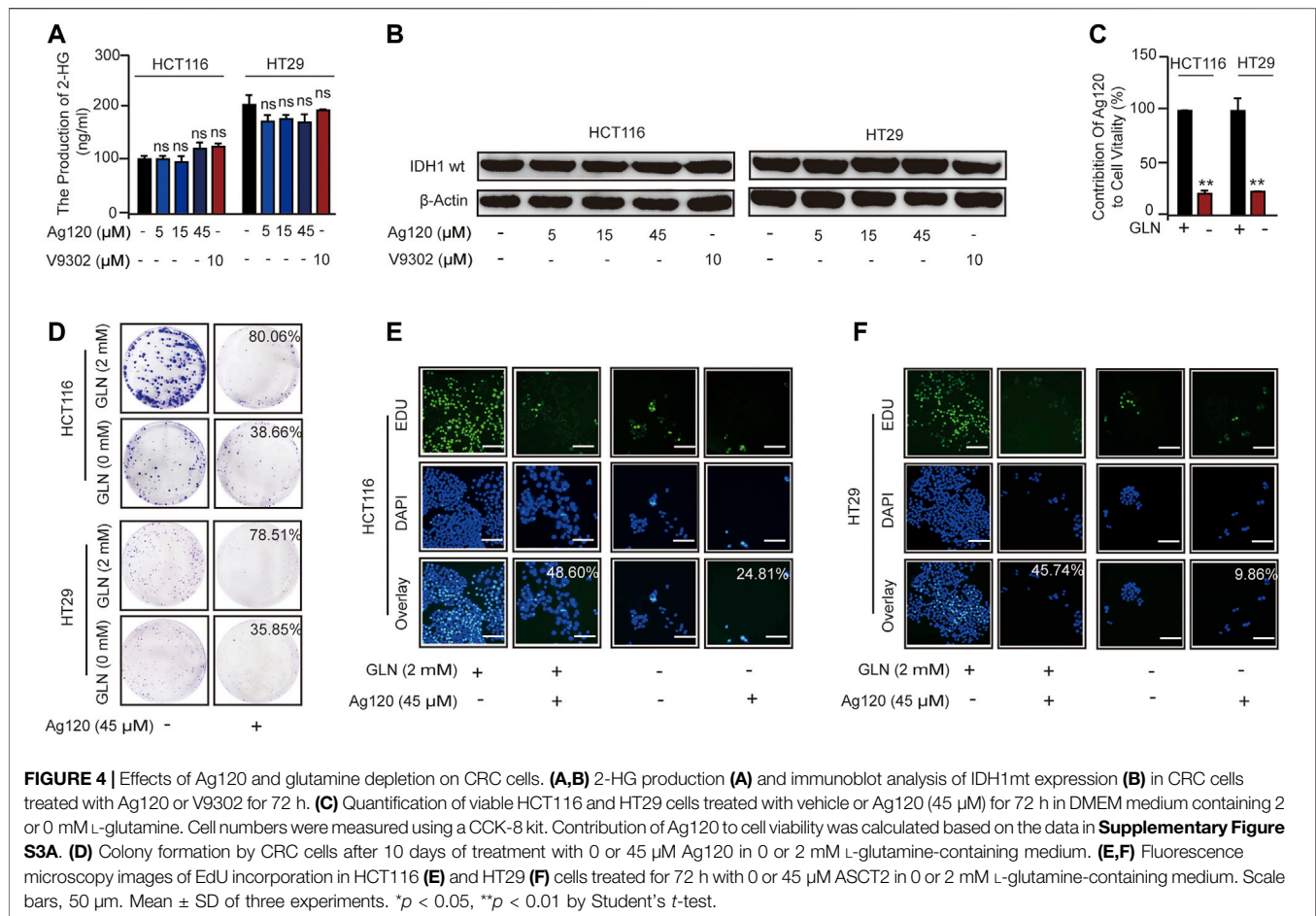
Ag120 Induces Autophagy in CRC Cells

Autophagy has been shown to be elevated upon ASCT2 depletion and glutamine starvation *in vitro* and *in vivo* (Schulte et al., 2018). Therefore, we next investigated whether Ag120 might affect autophagy in CRC. To this end, we performed TEM as well as fluorescence microscopy of cells stained with the fluorescent probes MDC or LysoTracker Red, which preferentially accumulate in autophagosomes and lysosomes, respectively. Ag120 treatment of HCT116 cells for 72 h resulted in the presence of a large number of vacuoles of varying sizes and clear punctate structures in the cytoplasm or perinucleus

(**Figure 3A**), suggesting that Ag120 treatment induced the formation of autophagic vesicles. Ag120 treatment also increased the number of MDC- and LysoTracker Red-stained foci in the cytoplasm of Ag120-treated cells, indicative of autophagosome and lysosome accumulation (**Figures 3B,C**; **Supplementary Figures S2A,B**). To probe this further, we examined expression of a number of autophagy-related proteins by immunoblot analysis and found that Ag120 treatment increased the expression of the autophagy markers LC3, beclin-1, ATG7, and ATG5, and of the lysosomal marker LAMP-1 (**Figure 3D**; **Supplementary Figures S3C–H**). Taken together, these results demonstrate that Ag120 induces autophagy in CRC cells.

Ag120 Suppresses the Proliferation of CRC Cells by Inhibiting Glutamine Metabolism

We next asked whether the anti-tumor effects of Ag120 in CRC cells were mediated *via* inhibition of glutamine metabolism alone or whether IDH1mt inhibition might also contribute. Ag120 might also have an effect on the IDH1wt in tumor cells (Pollyea et al., 2014; Fan et al., 2015). In addition, IDH-mutated tumor cells could also cause abnormalities in the glutamine metabolic pathway (Lucia et al., 2017; Marina et al., 2021). However, we examined the effects of Ag120 treatment for 72 h on intracellular 2-HG levels and found that the production of 2-HG in CRC cells is about 100–300 ng/ml (**Figure 4A**), which means CRC cells do not exist IDH1 mutation (Pollyea et al., 2014; Marina et al., 2021). Moreover, we examined the effects of Ag120



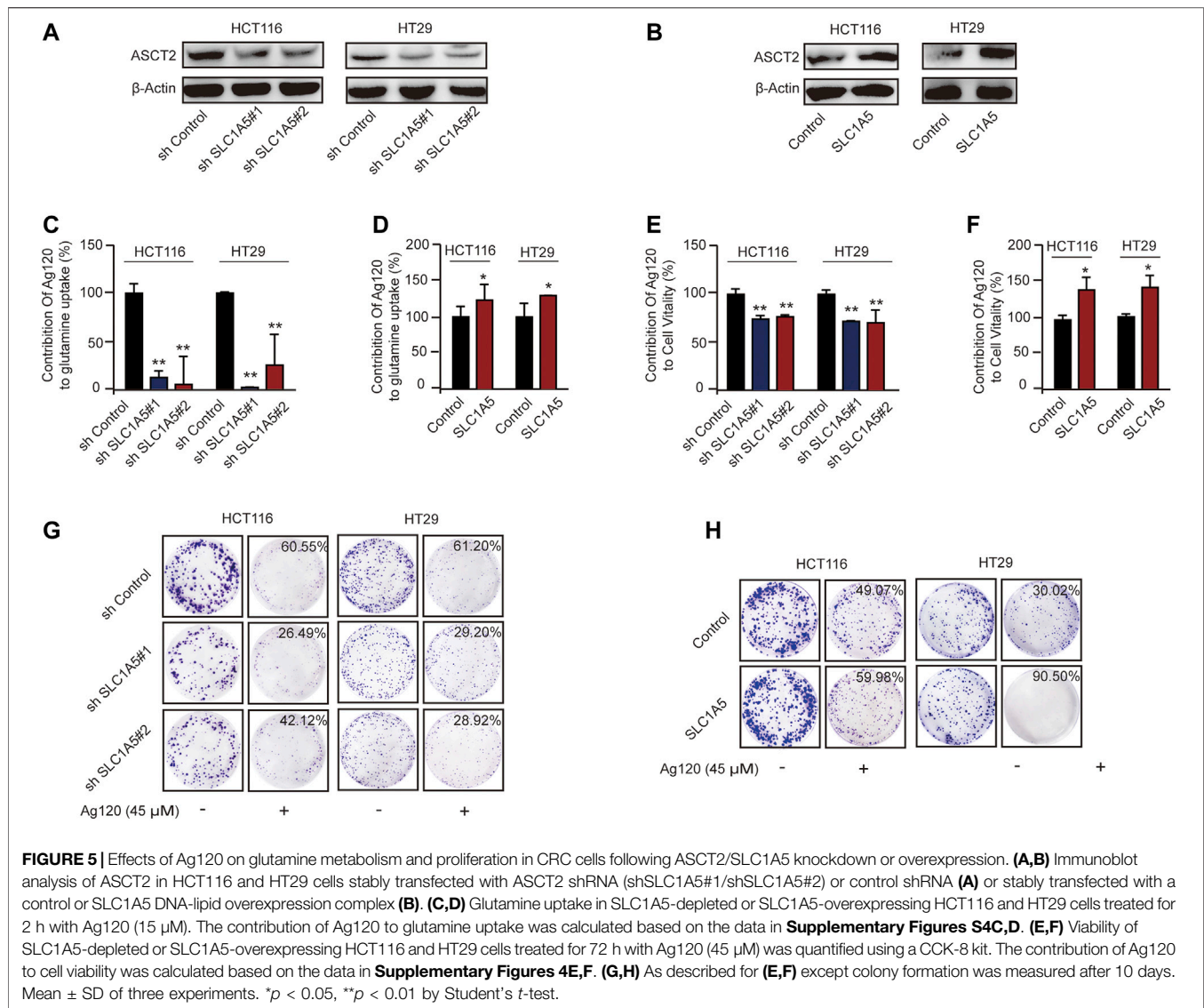
treatment for 72 h on intracellular 2-HG levels and on IDH1wt expression and found that concentrations of Ag120 that could inhibit CRC proliferation and promote autophagy had no significant effects on either 2-HG production (**Figure 4A**) or IDH1wt expression (**Figure 4B**; **Supplementary Figure S4A**), suggesting that Ag120 effects were independent of IDH1mt and IDH1wt in these CRC cells. We next examined the effects of Ag120 in cells grown in glutamine-depleted medium. As expected, depletion of extracellular glutamine significantly reduced the growth of CRC cells over 72 h (**Figure 4C**; **Supplementary Figure S4B**). However, Ag120 exhibited a more significant anti-tumor effect in 2 mM glutamine-containing compared with glutamine-depleted medium, as shown by colony formation and EdU incorporation assays (**Figures 4D–F**; **Supplementary Figures S4C–F**). These results suggested that Ag120 inhibition of CRC cell proliferation most likely occurs independently of IDH1mt and instead is mediated *via* its effects on glutamine metabolism.

Ag120 Anti-Tumor Effect is Predominantly Mediated by ASCT2 Inhibition in CRC Cells

To test this hypothesis further, we constructed HCT116 and HT29 cell lines with stable ASCT2 knockdown (ASCT2-KD)

induced by lentivirus-mediated expression of *SLC1A5* shRNA (sh*SLC1A5*#1/sh*SLC1A5*#2) or with stable overexpression of ASCT2 (ASCT2-OE) mediated by transfection of DNA-lipid complexes. We performed immunoblot analysis and RT-qPCR to verify effective ASCT2 silencing or overexpression (**Figures 5A,B**; **Supplementary Figures S5A–D**) and then analyzed the tumor cell phenotypes. In keeping with the proposed mechanism of action of Ag120, we found that the inhibitor had different effects in ASCT2-KD and ASCT2-OE CRC cells (**Supplementary Figures S5E,F**). ASCT2 KD and OE resulted in decreased and increased glutamine uptake, respectively (**Supplementary Figures S5E,F**). Compared with cells expressing control shRNA, the relative glutamine inhibition rate of ASCT2-KD cells which is calculated based on the data in **Supplementary Figure S5E** decreased significantly (**Figure 5C**; **Supplementary Figure S5E**), and conversely, ASCT2-OE cells exhibited a high rate of glutamine inhibition rate compared with the control cells (**Figure 5D**; **Supplementary Figure S5F**).

We next compared the effect of Ag120 on ASCT2-KD and ASCT2-OE cells. CRC cell viability decreased in ASCT2-KD cells (**Supplementary Figure S5G**) and increased in ASCT2-OE cells (**Supplementary Figure S5H**). Additionally, compared with the control cells, the relative inhibition rate of Ag120 which is calculated based on the data in **Supplementary Figures**



S5G,H) was decreased in the ASCT-KD cells (Figure 5G; Supplementary Figure S5G) and increased in the ASCT-OE cells (Figure 5F; Supplementary Figure S5H). The effects of Ag120 on colony formation were consistent with these observations (Figures 5G,H; Supplementary Figures S5I–L). These results suggested that Ag120 might exert its anti-tumor effects in CRC cells *via* ASCT2.

Ag120 Exhibits an Anti-CRC Effect *in Vivo*

Finally, we determined whether the effects of Ag120 on CRC cell phenotypes observed *in vitro* also translate *in vivo* using a mouse xenograft model. Groups of nude mice were injected subcutaneously with HCT116 cells. Beginning on day 7, the mice were injected with Ag120 once daily or with V9302 every 3 days until day 28, at which time the tumors were excised and analyzed (Figure 6A). Ag120 treatment was found to have no significant effect on body weight (Figure 6B) but significantly inhibited tumor volumes and weights (Figures 6C–E). V9302

also potentially inhibited *in vivo* tumor growth, but it also affected the general health and body weight of the mice (Figure 6B). Analysis of blood and tumor samples on day 28 showed that Ag120 treatment significantly reduced serum glutamine levels (Figure 6F) and reduced EdU incorporation into tumor cells (Figure 6G; Supplementary Figure S6A). Finally, by quantifying the staining intensities obtained in immunohistochemical and fluorescent labeling experiments, we found that Ag120 decreased the expression of ASCT2, significantly inhibited expression of Ki67, and significantly increased expression of the autophagy protein LC3 in the tumors (Figure 6H; Supplementary Figures S6B–D). Taken together, these data demonstrate that treatment of CRC tumor-bearing mice with Ag120 effectively inhibited glutamine metabolism and augmented autophagy, thereby suppressing tumor progression *in vivo*. A model of the potential glutamine-mediated anti-tumor effects of Ag120 is shown in Figure 6I.

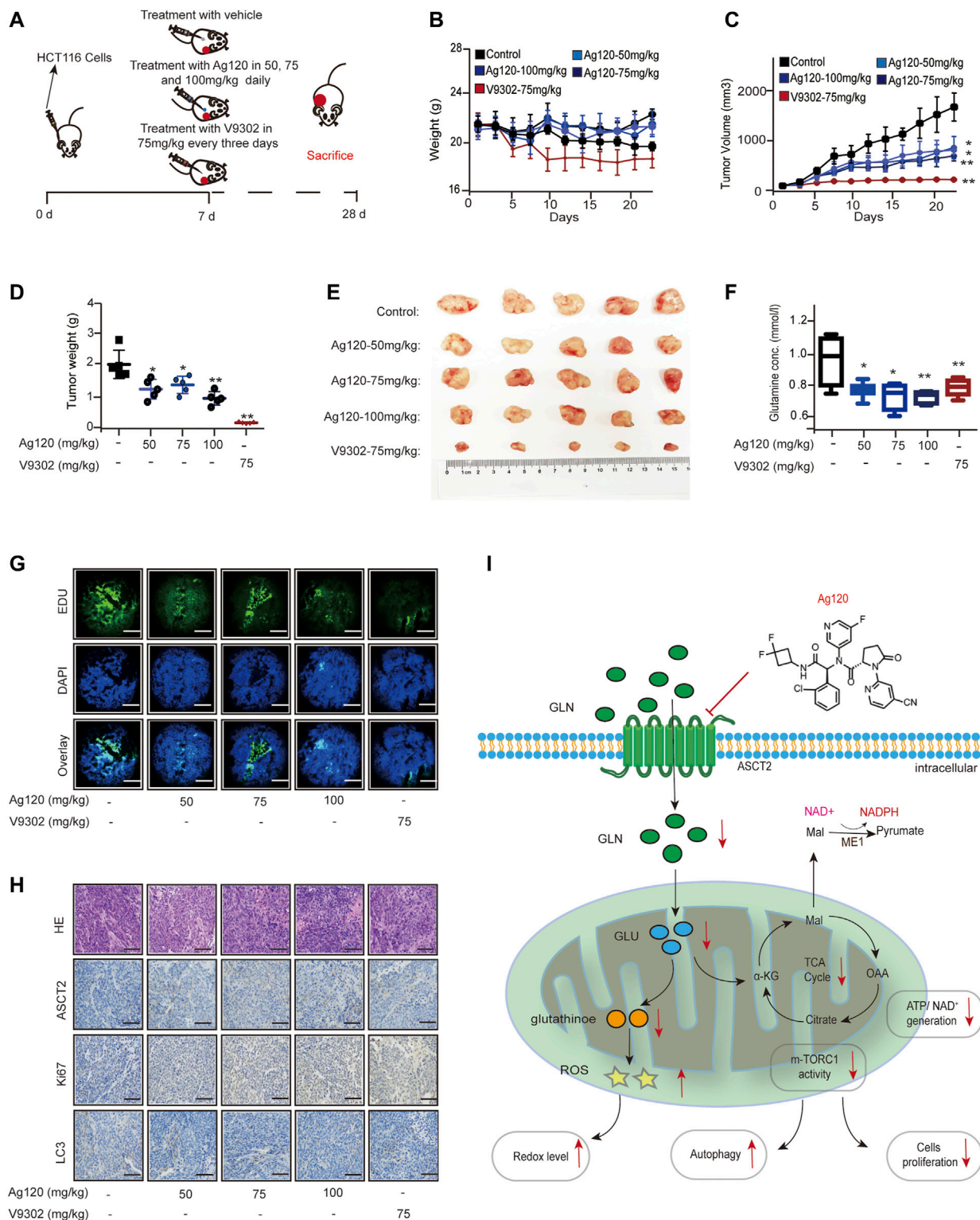


FIGURE 6 | Effect of Ag120 on HCT116 xenograft growth in mice. **(A)** Experimental protocol. Groups of athymic BALB/c nude mice were injected subcutaneously with 10^6 HCT116 cells and treatments were initiated 7 days later. Ag120 was injected once daily and V9302 was injected every 3 days via the intraperitoneal route. On day 28, animals were sacrificed and tumors and blood samples were collected for analysis. **(B)** Body weight change. **(C)** Tumor volumes. **(D,E)** Weights **(D)** and photographs **(E)** of tumor xenografts excised on day 28. **(F)** Blood glutamine levels on day 28. **(G)** Fluorescence microscopy images of EdU incorporation in sections of excised tumors. Scale bars, 50 μ m. **(H)** Representative images of ASCT2, Ki67, and LC3 immunostaining in sections of excised tumors. Scale bars, 50 μ m. **(I)** Schematic diagram of the proposed anti-tumor mechanism of action of Ag120 via regulation of glutamine metabolism in CRC cells. Mean \pm SD of five mice per group. Symbols represent individual mice. * $p < 0.05$, ** $p < 0.01$ by Student's *t*-test.

DISCUSSION

Metabolic reprogramming in cancer cells provides many opportunities for therapeutic drug development and precision medicine (Hanahan and Weinberg, 2011; Koppenol et al., 2011). Cancer cells exhibit an increased demand for glutamine compared with normal cells because of their rapid metabolism and proliferation (Deberardinis and Cheng, 2010; Noel et al., 2010; Mohamed et al., 2014; Manabu et al., 2020). In this context, glutamine is a conditional essential amino acid (Liu et al., 2018). Previous studies have revealed that ASCT2 is a major glutamine transporter and is upregulated in multiple cancer cell types such as breast, gastric, prostate, and colorectal cancers (Fuchs and Bode, 2005; Miyo et al., 2016). Consequently, a large number of ASCT2-targeting small molecule drugs have been developed or discovered; however, none of them have entered clinical trials as ASCT2 inhibitors to date (Grewer and Grabsch, 2004; Esslinger et al., 2005; Canul-tec et al., 2017; Schulte et al., 2018). In the present study, we identified Ag120 as a novel ASCT2 inhibitor that had anti-tumor effects in CRC cells mediated by blockade of ASCT2-dependent glutamine transport. Most importantly, Ag120 has been approved in the United States for the treatment of several cancers and is undergoing clinical testing for other indications (Alan et al., 2014; Emadi et al., 2014; Kelly et al., 2019), which provides a wealth of information regarding the safety profile of Ag120 in healthy volunteers and cancer patients. Our study increases the spectrum of cancers that may be treatable with Ag120 and provides proof of concept for the development of ASCT2 inhibitors for cancer therapy.

Previous work has identified several ASCT2-targeting small molecule inhibitors and antibodies that block glutamine uptake and inhibit the proliferation of CRC cells (Schulte et al., 2018; Hara et al., 2020). Here, we report that the effects of Ag120 were equivalent to or exceeded those of the known ASCT2 inhibitor V9302, including inhibition of growth and survival caused by a reduction in mTOR and ERK signaling (Papa et al., 2019; Hara et al., 2020), induction of autophagy, and increased oxidative stress caused by a decrease in GSH levels (Hara et al., 2020). Importantly, the anti-tumor effect of Ag120 was also observed in a nude mouse xenograft model of CRC. The anti-ASCT2 monoclonal antibody Ab3-8 has been shown to have a weak inhibitory effect on CRC cells (Hara et al., 2020); however, this appears to be less potent than Ag120. Similarly, Ag120 fares well when compared with another glutamine uptake inhibitor, GPNA (Esslinger et al., 2005). This compound is a known ASCT2 inhibitor but exhibits poor potency and selectivity for human cells (Esslinger et al., 2005; Chiu et al., 2017). Thus, Ag120 appears to have equal or better anti-tumor effects in CRC compared with several known ASCT2 inhibitors.

ASCT2 is expressed in normal large intestinal tissue, suggesting that targeting ASCT2 as a cancer therapy might cause some side effects (Utsunomiya-Tate et al., 1996). However, recent studies showed that ASCT2/*SLC1A5*-deficient mice exhibit normal growth and survival (Nakaya et al., 2014; Masle-Farquhar et al., 2017), indicating that targeting of ASCT2 for cancer therapy is likely to be well tolerated and elicit few

adverse effects. Moreover, Ag120 had little effect on the body weights of tumor-bearing mice compared with V9302 in the present study. In support of this, data from clinical trials of Ag120 in healthy volunteers and cancer patients have shown mild liver damage and other moderate adverse effects (Kelly et al., 2019). Other studies with Ag120 also indicate that the compound is well tolerated and that most adverse events are of mild to moderate severity (Alan et al., 2014; Emadi et al., 2014; Fan et al., 2015; Brandon et al., 2017).

In the present study, we observed that the Ag120-induced inhibition of glutamine metabolism was accompanied by a concomitant increase in glucose uptake, suggesting that the latter is a compensatory mechanism of energy production. Similarly, a previous study showed that V9302 induced a compensatory increase in glucose uptake in CRC cells (Hara et al., 2020). These results suggest that the anti-tumor efficacy of Ag120 could be diminished or subverted by an increase in glucose uptake and metabolism. Since the metabolic heterogeneity of tumor cells suggests that some cells are dependent on both glucose and glutamine for energy production and proliferation (Vander Heiden et al., 2009; Deberardinis and Cheng, 2010; Li and Zhang, 2016). Therefore, it may be more effective to combine the therapeutic use of Ag120 with inhibitors of glucose metabolism. For example, co-treatment of breast cancer and CRC cells with V9302 and the glucose analog 2-deoxyglucose is known to increase the efficacy of V9302 (Luo et al., 2020). The results of our study suggest that combination therapy with Ag120 and glucose inhibitors might be a potential new strategy for the treatment of cancer.

Our study suggests that Ag120 is a new ASCT2 inhibitor and exerts an anti-tumor effect in CRC. However, there are no specific biomarkers for the anti-tumor efficacy of Ag120 and other ASCT2 inhibitors. It is reported that the anti-tumor activity of ASCT2 inhibitors does not necessarily correlate with the expression of transporter proteins (Schulte et al., 2018), and tumor cells that are sensitive to ASCT2 inhibitors are mainly susceptible to glutamine withdrawal (Schulte et al., 2018; Hara et al., 2020). Clinically, the anti-tumor efficacy of ASCT2 inhibitors could be quantitatively assessed by using non-invasive PET imaging of glutamine uptake (Schulte et al., 2018). However, this technology cannot measure the anti-tumor activity of ASCT2 inhibitors. Therefore, larger studies will be needed to evaluate correlations between the efficacy of Ag120 and other ASCT2 inhibitors and oncogene status and metabolic heterogeneity, and to identify biomarkers of their activity.

CONCLUSION

In the past several years, interest has increased in the use of ASCT2 inhibitors as a treatment for cancer. In our study, we report for the first time that inhibition of ASCT2 function and glutamine metabolism may be a second mechanism to explain the anti-cancer effects of the IDH1mt inhibitor Ag120. We anticipate that our findings will shed light on the mechanism of Ag120 activity, extend the potential cancers that may be treatable with

Ag120, and provide new insight into the potential utility of other ASCT2 inhibitors as anti-cancer agents.

DATA AVAILABILITY STATEMENT

The original contributions presented in the study are included in the article/Supplementary Material, further inquiries can be directed to the corresponding authors.

ETHICS STATEMENT

The animal study was reviewed and approved by the Protocols for the mouse experiments were approved by the Animal Ethics Committee of JiNan University.

AUTHOR CONTRIBUTIONS

LS, XH, and SY conceived and designed the study. WY, LJ, and QZ performed the experiments. WY analyzed the data. XH, JH, QD, and WL provided assistance. WY wrote the manuscript. All authors read and approved the final manuscript.

ACKNOWLEDGMENTS

We thank Anne M. O'Rourke, from Liwen Bianji, Edanz Group China (www.liwenbianji.cn/ac), for editing the English text of a draft of this manuscript.

SUPPLEMENTARY MATERIAL

The Supplementary Material for this article can be found online at: <https://www.frontiersin.org/articles/10.3389/fphar.2022.871392/full#supplementary-material>

REFERENCES

- Alan, A., Gary, D., and Johnson, S. (2014). IDH1 Inhibitor Shows Promising Early Results. *Cancer Discov.* 4, 5.
- Brandon, N., Rohini, N., Elia, A., Nagaraja, R., Murtie, J., Liu, G., et al. (2017). The IDH1 Mutant Inhibitor AG-120 Shows strong Inhibition of 2-HG Production in an Orthotopic IDH1 Mutant Glioma Model *In Vivo*. Presented 22nd Annu. Scientific Meet. Educ. Day Soc. Neurooncol. 9, 16–19.
- Canul-tec, J. C., Assal, R., Cirri, E., Legrand, P., Brier, S., Chamot-Rooke, J., et al. (2017). Structure and Allosteric Inhibition of Excitatory Amino Acid Transporter 1. *Nature* 544, 446–451. doi:10.1038/nature22064
- Chiu, M., Sabino, C., Taurino, G., Bianchi, M. G., Andreoli, R., Giuliani, N., et al. (2017). GPNA Inhibits the Sodium-independent Transport System L for Neutral Amino Acids. *Amino Acids* 49, 1365–1372. doi:10.1007/s00726-017-2436-z
- Deberardinis, R. J., and Cheng, T. (2010). Q's Next: the Diverse Functions of Glutamine in Metabolism, Cell Biology and Cancer. *Oncogene* 29, 313–324. doi:10.1038/onc.2009.358
- Emadi, A., Jun, S. A., Tsukamoto, T., Fathi, A. T., Minden, M. D., and Dang, C. V. (2014). Inhibition of Glutaminase Selectively Suppresses the Growth of Primary

Supplementary Figure 1 | The combination of V9302 with ASCT2 and Effect of Ag120 on glucose uptake in CRC cells. (A) SPR analysis of the binding affinity of V9302 for purified ASCT2. (B) Glucose uptake was measured after incubation with Ag120 or V9302 for 40 min.

Supplementary Figure 2 | Quantifications of the indicated protein levels. The relative protein levels of ERK1 (A), p-ERK1 (B), p-mTOR1 b, m-TOR (D), p-P70S6K (E) and P70S6K (F) in Figure 2G were quantified by Image-Pro Plus 6 software. Mean \pm SD of 3 experiments. * $P < 0.05$, ** $P < 0.01$ by Student's *t*-test.

Supplementary Figure 3 | Quantification of autophagy induction by Ag120. (A,B) Autophagosome density (A) and lysosome density (B) were assessed by counting of cells labeled with MDC and LysoTracker dyes, respectively, after incubation with Ag120 or V9302 for 72 h. The relative protein levels of LC3 II (C), LC3 II (D), LAMP1 (E), Beclin-1 (F), ATG7 (G) and ATG5 (H) in Figure 3D were quantified by Image-Pro Plus 6 software. Mean \pm SD of 3 experiments. * $P < 0.05$, ** $P < 0.01$ by Student's *t*-test.

Supplementary Figure 4 | Effects of Ag120 on CRC proliferation in glutamine-free medium. (A) The relative protein levels of IDH1 in Figure 4 (B) were quantified by Image-Pro Plus 6 software. (B–F) HCT116 and HT29 cells were treated with Ag120 (45 μ M) for 72 h in DMEM medium containing 0 or 2 mM L-glutamine and then analyzed. (B) Cell numbers detected using a CCK-8 kit. (C) Colony formation quantified by light microscopy. (D) Relative contribution of Ag120 after glutamine depletion to inhibition of colony formation. (E) Quantification of EdU incorporation by fluorescence microscopy. (F) Relative contribution of Ag120 to inhibition of EdU incorporation after glutamine depletion. Mean \pm SD of three experiments. * $P < 0.05$, ** $P < 0.01$ by Student's *t*-test.

Supplementary Figure 5 | Effects of Ag120 on glutamine metabolism and proliferation of CRC cells after ASCT2/SLC1A5 knockdown or overexpression. (A,B) RT-qPCR analysis of SLC1A5 mRNA levels in ASCT2-knockdown (A) and ASCT2-overexpressing (B) HCT116 and HT29 cells. (C,D) The relative protein levels of ASCT2 in Figure 5 (A,B) were quantified by Image-Pro Plus six6 software. (E,F) Glutamine uptake in ASCT2-knockdown (E) and ASCT2-overexpressing (F) HCT116 and HT29 cells treated with Ag120 (15 μ M) for 2 h. (G,H) As described for (E,F) except cell numbers were quantified using a CCK-8 kit. (I,K) Colony formation by ASCT2-knockdown (I) and ASCT2-overexpressing (K) HCT116 and HT29 cells after Ag120 (45 μ M) treatment for 10 days. (J,L) Relative contribution of Ag120 treatment to inhibition of colony formation in ASCT2-knockdown (J) and ASCT2-overexpressing (L) cells. Mean \pm SD of 3 experiments. * $P < 0.05$, ** $P < 0.01$ by Student's *t*-test.

Supplementary Figure 6 | Quantification of Ag120-mediated inhibition of ASCT2 expression, proliferation, and autophagy in HCT116 xenografts *in vivo*. (A–D) Figure 6A for experimental protocol. Tumors were excised on day 28 and positively stained cells were quantified. (A) EdU-incorporating cells measured by fluorescence microscopy. (B–D) Intensity of immunohistochemical staining of ASCT2 (B), Ki67 (C), and LC3 (D) expression. Mean \pm SD of 3 experiments. * $P < 0.05$, ** $P < 0.01$ by Student's *t*-test.

- Acute Myeloid Leukemia Cells with IDH Mutations. *Exp. Hematol.* 42, 247–251. doi:10.1016/j.exphem.2013.12.001
- Esslinger, C. S., Cybulski, K. A., and Rhoderick, J. F. (2005). Ngamma-aryl Glutamine Analogues as Probes of the ASCT2 Neutral Amino Acid Transporter Binding Site. *Bioorg. Med. Chem.* 13, 1111–1118. doi:10.1016/j.bmc.2004.11.028
- Fan, B., Le, K., Manyak, E., Liu, H., Prah, M., Bowden, C.J., et al. (2015). Longitudinal Pharmacokinetic/Pharmacodynamic Profile of AG-120, a Potent Inhibitor of the IDH1 Mutant Protein, in a Phase 1 Study of IDH1-Mutant Advanced Hematologic Malignancies. *Blood* 126, 1310.
- Fuchs, B. C., and Bode, B. P. (2005). Amino Acid Transporters ASCT2 and LAT1 in Cancer: Partners in Crime? *Semin. Cancer Biol.* 15, 254–266. doi:10.1016/j.semcancer.2005.04.005
- Grewer, C., and Grabsch, E. (2004). New Inhibitors for the Neutral Amino Acid Transporter ASCT2 Reveal its Na⁺-dependent Anion Leak. *J. Physiol.* 557, 747–759. doi:10.1113/jphysiol.2004.062521
- Hanahan, D., and Weinberg, R. A. (2011). Hallmarks of Cancer: the Next Generation. *Cell* 144, 646–674. doi:10.1016/j.cell.2011.02.013
- Hanahan, D., and Weinberg, R. A. (2000). The Hallmarks of Cancer. *Cell* 100, 57–70. doi:10.1016/s0092-8674(00)81683-9

- Hara, Y., Minami, Y., Yoshimoto, S., Hayashi, N., Yamasaki, A., Ueda, S., et al. (2020). Anti-tumor Effects of an Antagonistic mAb against the ASCT2 Amino Acid Transporter on KRAS-Mutated Human Colorectal Cancer Cells. *Cancer Med.* 9, 302–312. doi:10.1002/cam4.2689
- Hassanein, M., Hoeksema, M. D., Shiota, M., Qian, J., Harris, B. K., Chen, H., et al. (2013). SLC1A5 Mediates Glutamine Transport Required for Lung Cancer Cell Growth and Survival. *Clin. Cancer Res.* 19, 560–570. doi:10.1158/1078-0432.CCR-12-2334
- Huang, F., Zhao, Y., Zhao, J., Wu, S., Jiang, Y., Ma, H., et al. (2014). Upregulated SLC1A5 Promotes Cell Growth and Survival in Colorectal Cancer. *Int. J. Clin. Exp. Pathol.* 7, 6006–6014.
- Kelly, J., Lola, L., and Vicky, H. (2019). FDA Approval Summary: Ivosidenib for Relapsed or Refractory Acute Myeloid Leukemia with an Isocitrate Dehydrogenase-1 Mutation. *Clin. Cancer Res.* 25, 3205–3029.
- Koppenol, W. H., Bounds, P. L., and Dang, C. V. (2011). Otto Warburg's Contributions to Current Concepts of Cancer Metabolism. *Nat. Rev. Cancer* 11, 325–337. doi:10.1038/nrc3038
- Li, Z., and Zhang, H. (2016). Reprogramming of Glucose, Fatty Acid and Amino Acid Metabolism for Cancer Progression. *Cell Mol Life Sci* 73, 377–392. doi:10.1007/s00018-015-2070-4
- Liu, Y., Zhao, T., Li, Z., Wang, L., Yuan, S., and Sun, L. (2018). The Role of ASCT2 in Cancer: a Review. *Eur. J. Pharmacol.* 837, 81–87. doi:10.1016/j.ejphar.2018.07.007
- Lucia, S. C., Hardik, S., Alex, J. P., Correa, F. M., Di Galleonardo, V., Lui, H., et al. (2017). In Vivo Imaging of Glutamine Metabolism to the Oncometabolite 2-Hydroxyglutarate in IDH1/2 Mutant Tumors. *Cel Metabolism*. 26, 830–841. doi:10.1016/j.cmet.2017.10.001
- Luo, Z., Xu, J., Sun, J., Huang, H., Zhang, Z., Ma, W., et al. (2020). Co-delivery of 2-Deoxyglucose and a Glutamine Metabolism Inhibitor V9302 via a Prodrug Micellar Formulation for Synergistic Targeting of Metabolism in Cancer. *Acta Biomater.* 105, 239–252. doi:10.1016/j.actbio.2020.01.019
- Manabu, K., Kiyotaka, O., Hideyuki, S., Yoshioka, S., Takahashi, M., Bamba, T., et al. (2020). A Shift in Glutamine Nitrogen Metabolism Contributes to the Malignant Progression of Cancer. *Nat. Communication*. 11, 1320. doi:10.1038/s41467-020-15136-9
- Marina, R., Donghyun, H., Anne, M. G., Najac, C., Viswanath, P., Pieper, R. O., et al. (2021). Early Noninvasive Metabolic Biomarkers of Mutant IDH Inhibition in Glioma. *Metabolites* 11, 109. doi:10.3390/metabo11020109
- Marzi, L., Combes, E., Vié, N., Ayrolles-Torro, A., Tosi, D., Desigaud, D., et al. (2016). FOXO3a and the MAPK P38 Are Activated by Cetuximab to Induce Cell Death and Inhibit Cell Proliferation and Their Expression Predicts Cetuximab Efficacy in Colorectal Cancer. *Br. J. Cancer* 115, 1223–1233. doi:10.1038/bjc.2016.313
- Masle-Farquhar, E., Bröer, A., Yabas, M., Enders, A., and Bröer, S. (2017). ASCT2 (SLC1A5)-Deficient Mice Have normal B-Cell Development, Proliferation, and Antibody Production. *Front. Immunol.* 8, 549. doi:10.3389/fimmu.2017.00549
- Miyo, M., Konno, M., Nishida, N., Sueda, T., Noguchi, K., Matsui, H., et al. (2016). Metabolic Adaptation to Nutritional Stress in Human Colorectal Cancer. *Sci. Rep.* 6, 38415. doi:10.1038/srep38415
- Mohamed, A., Deng, X., Khuri, F. R., and Owonikoko, T. K. (2014). Altered Glutamine Metabolism and Therapeutic Opportunities for Lung Cancer. *Clin. Lung Cancer* 15, 7–15. doi:10.1016/j.clc.2013.09.001
- Nakaya, M., Xiao, Y., Zhou, X., Chang, J. H., Chang, M., Cheng, X., et al. (2014). Inflammatory T Cell Responses Rely on Amino Acid Transporter ASCT2 Facilitation of Glutamine Uptake and mTORC1 Kinase Activation. *Immunity* 40, 692–705. doi:10.1016/j.immuni.2014.04.007
- Noel, R., Kevin, P., Ravinder, T., Borrok, J., Coats, S., Herbst, R., et al. (2010). MEDI7247, a Novel Pyrrolbenzo diazepine ADC Targeting ASCT2 with Potent In Vivo Activity across a Spectrum of Hematological Malignancies. *Oncogene* 29, 313–324. doi:10.1158/1538-7445.AM2018-LB-295
- Papa, S., Choy, P. M., and Bubici, C. (2019). The ERK and JNK Pathways in the Regulation of Metabolic Reprogramming. *Oncogene* 38, 2223–2240. doi:10.1038/s41388-018-0582-8
- Pollyea, D., Botton, S. D. A. T., Stein, E. M., Tallman, M. S., Agresta, S., Bowden, C., et al. (2014). "Clinical Safety and Activity of AG-120, a First-In-Class, Potent Inhibitor of the IDH1 Mutant Protein," in *A Phase 1 Study of Patients with Advanced IDH1-Mutant Hematologic Malignancies* (Vienna: 20th Annual Meeting of European Hematology Association). Abstract P563.
- San-Millán, I., and Brooks, G. A. (2017). Reexamining Cancer Metabolism: Lactate Production for Carcinogenesis Could Be the Purpose and Explanation of the Warburg Effect. *Carcinogenesis* 38, 119–133. doi:10.1093/carcin/bgw127
- Schulte, M. L., Fu, A., Zhao, P., Li, J., Geng, L., Smith, S. T., et al. (2018). Pharmacological Blockade of ASCT2-dependent Glutamine Transport Leads to Antitumor Efficacy in Preclinical Models. *Nat. Med.* 24, 194–202. doi:10.1038/nm.4464
- Utsunomiya-Tate, N., Endou, H., and Kanai, Y. (1996). Cloning and Functional Characterization of a System ASC-like Na⁺-dependent Neutral Amino Acid Transporter. *J. Biol. Chem.* 271, 14883–14890. doi:10.1074/jbc.271.25.14883
- van Geldermalsen, M., Wang, Q., Nagarajah, R., Marshall, A. D., Thoeng, A., Gao, D., et al. (2016). ASCT2/SLC1A5 Controls Glutamine Uptake and Tumour Growth in Triple-Negative Basal-like Breast Cancer. *Oncogene* 35, 3201–3208. doi:10.1038/onc.2015.381
- Vander Heiden, M. G., Cantley, L. C., and Thompson, C. B. (2009). Understanding the Warburg Effect: the Metabolic Requirements of Cell Proliferation. *Science* 324, 1029–1033. doi:10.1126/science.1160809
- Wang, Q., Hardie, R. A., Hoy, A. J., van Geldermalsen, M., Gao, D., Fazli, L., et al. (2015). Targeting ASCT2-Mediated Glutamine Uptake Blocks Prostate Cancer Growth and Tumour Development. *J. Pathol.* 236, 278–289. doi:10.1002/path.4518
- Willems, L., Jacque, N., Jacquel, A., Neveux, N., Maciel, T. T., Lambert, M., et al. (2013). Inhibiting Glutamine Uptake Represents an Attractive New Strategy for Treating Acute Myeloid Leukemia. *Blood* 122, 3521–3532. doi:10.1182/blood-2013-03-493163

Conflict of Interest: The authors declare that the research was conducted in the absence of any commercial or financial relationships that could be construed as a potential conflict of interest.

Publisher's Note: All claims expressed in this article are solely those of the authors and do not necessarily represent those of their affiliated organizations, or those of the publisher, the editors and the reviewers. Any product that may be evaluated in this article, or claim that may be made by its manufacturer, is not guaranteed or endorsed by the publisher.

Copyright © 2022 Yu, Huang, Dong, Li, Jiang, Zhang, Sun, Yuan and He. This is an open-access article distributed under the terms of the Creative Commons Attribution License (CC BY). The use, distribution or reproduction in other forums is permitted, provided the original author(s) and the copyright owner(s) are credited and that the original publication in this journal is cited, in accordance with accepted academic practice. No use, distribution or reproduction is permitted which does not comply with these terms.



A Novel RGD-4C-Saporin Conjugate Inhibits Tumor Growth in Mouse Models of Bladder Cancer

Stefania Zuppone¹, Chiara Assalini¹, Claudia Minici², Oronza A. Botrugno³, Flavio Curnis⁴, Massimo Degano², Angelo Corti^{4,5}, Francesco Montorsi^{1,5}, Andrea Salonia^{1,5} and Riccardo Vago^{1,5*}

¹ Urological Research Institute, Division of Experimental Oncology, IRCCS San Raffaele Scientific Institute, Milano, Italy, ² Biocrystallography Unit, Division of Immunology, Transplantation, and Infectious Diseases, IRCCS San Raffaele Scientific Institute, Milano, Italy, ³ Functional Genomics of Cancer Unit, Division of Experimental Oncology, IRCCS San Raffaele Scientific Institute, Milano, Italy, ⁴ Tumor Biology and Vascular Targeting Unit, Division of Experimental Oncology, IRCCS San Raffaele Scientific Institute, Milano, Italy, ⁵ Faculty of Medicine and Surgery, Università Vita-Salute San Raffaele, Milano, Italy

OPEN ACCESS

Edited by:

Anjana Munshi,
Central University of Punjab, India

Reviewed by:

Francesco Saverio Di Leva,
University of Naples Federico II, Italy
Massimo Bortolotti,
University of Bologna, Italy

*Correspondence:

Riccardo Vago
vago.riccardo@hsr.it

Specialty section:

This article was submitted to
Pharmacology of Anti-Cancer Drugs,
a section of the journal
Frontiers in Oncology

Received: 31 December 2021

Accepted: 18 March 2022

Published: 11 April 2022

Citation:

Zuppone S, Assalini C,
Minici C, Botrugno OA, Curnis F,
Degano M, Corti A, Montorsi F,
Salonia A and Vago R (2022)
A Novel RGD-4C-Saporin
Inhibits Tumor Growth in Mouse
Models of Bladder Cancer.
Front. Oncol. 12:846958.
doi: 10.3389/fonc.2022.846958

Although toxin may have some advantages compared to chemotherapeutic drugs in cancer therapy, e.g. a potent cytotoxic activity and a reduced risk of resistance, their successful application in the treatments to solid tumors still remains to be fully demonstrated. In this study, we genetically modified the structure of the plant-derived single-chain ribosome inactivating protein saporin (SAP) by fusing its N-terminus to the ACDRCGDCFCG peptide (RGD-4C), an α v-integrin ligand, and explored the anti-tumor activity of the resulting protein (called RGD-SAP) *in vitro* and *in vivo*, using a model of muscle invasive bladder cancer. We found that the RGD-4C targeting domain enhances the cytotoxic activity of SAP against various tumor cell lines, in a manner dependent on α v-integrin expression levels. In a subcutaneous syngeneic model of bladder cancer, RGD-SAP significantly reduced tumor growth in a dose-dependent manner. Furthermore, systemic administration of RGD-SAP in combination with mitomycin C, a chemotherapeutic drug currently used to treat patients with bladder cancer, increased the survival of mice bearing orthotopic bladder cancer with no evidence of systemic toxicity. Overall, the results suggest that RGD-SAP represents an efficient drug that could be exploited, either alone or in combination with the state-of-the-art therapies, for the treatment of bladder cancer and, potentially, of other solid tumors.

Keywords: saporin, recombinant protein, bladder cancer, RGD peptide, targeted therapy, ribosome inactivating proteins, RGD-integrins

INTRODUCTION

Toxic molecules produced by plants have been assumed to be part of their defense weapons, even if in some cases a few of them are present in edible plants, including species that are eaten raw. From an evolutionary point of view, the selective pressure by the environment on plants has led to the development and optimization of highly efficient toxin molecules, which may represent potent and efficient cytotoxic agents that can be potentially exploited in cancer therapy. Their small size, high

molecular stability, easy of production, high potency and direct cell-killing property make this class of cytotoxic agents very attractive for the development of new anti-cancer therapies (1–4). Among the various toxins so far studied for this purpose, the plant-derived type I ribosome inactivating proteins (RIPs) represent ideal candidates, owing to their high efficiency in irreversibly inhibiting protein translation and causing prompt cell death (2, 5). Furthermore, type I RIPs consist only of an N-glycosidase domain, lacking the lectin domain, typical of type II RIP, which bind galactose residues on the cell surface and facilitates the catalytic portion to enter the cell. This feature offers the opportunity to couple type I RIPs with a tumor-targeting ligand that enable specific and selective delivery of the toxins to cancer cells, thereby improving their therapeutic index. According to this view, type I RIPs have been coupled to growth factors or other polypeptides capable of recognizing receptors over-expressed on the surface of cancer cells or on tumor endothelial cells (2, 6–8).

Saporin (SAP), a type I RIP characterized by unusual resistance to high temperature, denaturation and proteolysis and by a strong intrinsic cytotoxic activity, may represent a suitable candidate for the design and development of new anti-cancer drugs. Recent studies have shown that coupling SAP with tumor targeting ligands, such as monoclonal antibodies, peptides and aptamers, improves its cytotoxic effects on different cancer types, both *vitro* and *in vivo* (9–14). In particular, SAP-based, chimeric recombinant proteins formed by the toxin fused to the amino-terminal fragment of urokinase (11, 13), the epidermal growth factor (12, 15), the anti-CD22 ScFv (9) have been produced and successfully tested. Thus, the development of new strategies for targeted delivery of SAP to tumors is of great experimental and pharmacological interest. At this regard, a growing body of evidence suggests that integrins may represent important molecular targets on cancer cells. In fact, the expression of certain integrins is increased on various types of cancer cells and tumor vasculature, to regulate many steps of tumor progression, such as angiogenesis and tumor cell growth, survival, migration and invasion (16–19). For example, certain α v-integrins, such as α v β 3, α v β 6, α 5 β 1 and α v β 5, are upregulated in various solid cancers, tumor microenvironment and upon anti-cancer therapy, while they are expressed at lower or undetectable levels in normal tissues (20). In particular, α v β 3 and α v β 5 are known to be overexpressed in the tumor vasculature and to be involved in tumor angiogenesis (21, 22). Integrin over-expression is associated with pathological outcomes including disease stage, metastasis formation, treatment resistance, and patient survival (20). Thus, ligands of specific integrin subclasses may be exploited, in principle, for the development of new tumor-homing derivatives of SAP.

In the last years, many investigators have explored the potential of peptides as integrin ligands, a promising class of molecules that, owing to their small size, low immunogenicity, ease of manufacture at reasonable costs, can overcome many of the limitations related to the use of monoclonal antibodies as targeting moieties. For instance, RGD-based peptides have been widely investigated as ligands for targeted delivery of drugs and nanoparticles to tumors. In particular,

ACDCRGDCFCG (RGD-4C), a peptide capable of recognizing with high affinity α v β 3, and, although with a lower affinity, also α v β 5, α 5 β 1 and α v β 6 (26) has proven useful to enhance the selective delivery of various types of compounds to tumors, including cytokines and toxins (23–26).

Based on these notions, we tested the hypothesis that fusing RGD-4C to SAP, by recombinant DNA technology, can increase its tumor selectivity and therapeutic activity. We show that the RGD-SAP conjugate can be easily produced in *E.coli* with no need of renaturation, and that this product can kill integrin-expressing cells more efficiently than a SAP variant lacking the RGD domain. Moreover, we show that RGD-SAP can inhibit the tumor growth in mouse models of bladder cancer.

MATERIALS AND METHODS

Cell Cultures

Human bladder RT4, RT112, 5637 were maintained in RPMI 1640 supplemented with 10% fetal calf serum (FCS), 2 mM L-glutamine and antibiotics (100 U/mL penicillin and 100 μ g/mL streptomycin-sulphate); breast MDA-MB 468 and glioblastoma U87 cancer cell lines as well as skin fibroblast cells were maintained in DMEM supplemented with 10% FCS, 2 mM L-glutamine and antibiotics (100 U/mL penicillin and 100 μ g/mL streptomycin-sulphate). Murine MB49 bladder cancer cells were cultured in DMEM, supplemented with 10% FCS, 2 mM L-glutamine, antibiotics (100 U/mL penicillin and 100 μ g/mL streptomycin-sulphate) and 1 mM sodium pyruvate.

MB49 Luc cells stably expressing luciferase were generated by transduction with a 3rd generation lentiviral vector carrying the luciferase gene. pLenti PGK V5-LUC Neo (w623-2) was a gift from Eric Campeau, University of Massachusetts Medical School, Worcester, Massachusetts, US (Addgene plasmid # 21471). For lentivirus production, a monolayer of HEK293T cells, cultured in 10 cm² dish, were incubated with the following mixture: transfer vector (10 μ g), packaging vector Δ r 8.74 (6.5 μ g), Env VSV-G vector (3.5 μ g), REV vector (2.5 μ g) in 450 μ l double distilled water, 50 μ l calcium chloride (2.5 M) and 500 μ l Hank's buffered saline (2-fold). Sixteen hours later, the medium was replaced with culture medium and 24 hours later the medium was collected and 0.22 μ m-filtered to recover virus particles. Virus particles were then used to transduce MB49 cells. Infected cells were then cultured in presence of G418 antibiotic (0.5 mg/ml) for fifteen days.

Cloning of RGD-SAP and CYS-SAP in pET22b Vector

SAP fused with ACDCRGDCFCG or CGGSGG at its N-terminus were prepared by GenScript (New Jersey, USA). The nucleotide sequences were obtained from the corresponding amino acid sequences of saporin S and optimized for the expression in *E.coli*. A GGSSRSS sequence was interposed between ACDCRGDCFCG and SAP as a spacer and a 6xHis tag was added at the C-terminus to allow the purification by affinity chromatography. The whole encoding sequences were inserted

into the pET22b(+) vector (Novagen), forming the pET22b(+)–RGD-SAP (5′-NdeI-ACDCRGDCFCG-GGSSRSS-SAP-HHHHHH-EcoRI-3′) and the pET22b(+)–CYS-SAP (5′-NdeI-CGGSGG-SAP-HHHHHH-EcoRI-3′) expression vectors. Ligation products were used to transform the *E. coli* strain DH5alpha (Invitrogen).

Expression and Purification of RGD-SAP and CYS-SAP

The expression of RGD-SAP and CYS-SAP in transformed BL21 (DE3) *E. coli* cells (Novagen) was induced for 3 hours at 37°C with 0.1 mM IPTG. Bacterial pellet from 1 L culture was resuspended in 15 ml of 50 mM Tris-HCl, pH 7.5, supplemented with a cocktail of protease inhibitor (Sigma-Aldrich). Soon after, 10 mM of imidazole, lysozyme (250 µg/ml) and DNase (20 µg/ml) were added. The bacterial solution was then incubated on ice for 45 min, subjected to 3 cycles of sonication (using a UW3100 Bandelin sonicator operating at 60% power; 2 min cycle duration with 1 sec pulse and 1 sec pause), and centrifuged at 4°C for 25 min at 10000 × g. Soluble RGD-SAP and CYS-SAP contained in the supernatant were then purified by metal chelate affinity chromatography using a HisTrap HP 5 ml column (GE Healthcare Life Sciences) equilibrated in Tris-HCl 50 mM pH 7.5, 300 mM NaCl supplemented with 10 mM imidazole (and 5 mM DTT for CYS-SAP) operated with the AktaPurifier10 FPLC system. To elute proteins, imidazole concentration was increased step by step up to 500 mM in 20 column volumes (CV). The fractions containing the target proteins were dialyzed against 50 mM Tris-HCl, pH 7.5 (CYS-SAP) or 50 mM bicine, pH 8.2 (RGD-SAP) at 4°C for 16 hours. A cation exchange chromatography on HiTrap SP Sepharose FF column (GE Healthcare Life Sciences) was then performed for further purification, using a 20 CV gradient up to 1 M NaCl for protein elution. The proteins were then concentrated using 10 KDa cutoff Amicon centrifugal filters (Millipore-Sigma) and dialyzed against PBS with slide A lyzer dialysis cassette (Thermo Fisher). All solutions used in purification steps were prepared with sterile and endotoxin-free water (S.A.L.F. Laboratorio Farmacologico SpA, Bergamo, Italy). Protein concentration was measured using the BCA Protein Assay DC™ Kit (BioRad). Protein purity and identity was checked by SDS-PAGE and Western blotting. Both CYS-SAP and RGD-SAP showed comparable yields ranging from 0.6 to 1.2 mg/l of bacterial culture.

Western Blot Analysis

Cells were washed twice with cold PBS, collected by scraping and centrifuged 5 min at 300 g. Cells were lysed for 30 min on ice in ice-cold buffer (50 mM Tris-HCl, pH 7.5, containing 150 mM NaCl, 2 mM NaF, 1 mM EDTA, 1 mM EGTA, 1 mM Na₃VO₄, 1 mM PMSF, 75 µg/ml aprotinin (Sigma-Aldrich), 1% TritonX-100 and a proteinase inhibitor cocktail® (Sigma-Aldrich). Cell lysates were centrifuged at 10000 × g at 4°C for 10 min and the supernatants were recovered and quantified for total protein content. Equal amounts of cell protein extracts were separated by SDS-PAGE under reducing conditions unless stated otherwise. For western blot analysis, proteins were transferred

onto a nitrocellulose membrane, incubated with 5% non-fat powdered milk in TBS-T (0.5% Tween-20) for 1 hour and then with the following antibodies: anti-saporin anti-serum (rabbit, 1:5000), anti-caspase 3 (rabbit, 1:2000, clone E87, Abcam), anti-beta actin (mouse, 1:10000, clone AC-15, Sigma-Aldrich). The antibody binding was detected using a secondary horseradish peroxidase conjugated antibodies (donkey anti-mouse/rabbit IgG HRP-linked, GE Healthcare) and an enhanced chemiluminescent (ECL, Merck Millipore).

Seed SAP used as positive control for Western blot analysis was purchased from Advanced Targeting Systems, which had purified it from the seeds of the Soapwort plant (*Saponaria officinalis*).

Flow Cytometry Analysis

Cultured cell lines were detached by TripLE Express (Gibco) to preserve receptor integrity, washed with PBS containing 1% FCS and incubated with PE-conjugated Ab specific for human αvβ3 and αvβ5 (R&D System) and FITC-conjugated Ab specific for human αvβ6 integrins (NovusBio). For receptor detection, cells were incubated with the fluorescently labelled Ab at 4°C for 30 min. Stained cells were resuspended in 100 µL of PBS containing 1% FCS. Samples were run through an Accuri™ flow cytometer (BD Biosciences). All data were analysed by FCS Express and expressed as relative fluorescence intensity (RFI), calculated as follows: mean fluorescence intensity after mAb staining/mean fluorescence intensity after isotype-negative control staining. Analysis was done on 20,000 gated events acquired per sample.

Cell Viability Assay (MTT)

Cultured cell lines (5 × 10³ cells/well) were seeded in 96 wells plates and incubated for 72 h with various amounts of RGD-SAP or CYS-SAP at 37°C, 5% CO₂. Cell viability was then quantified by 3-(4,5-dimethylthiazol-2-yl)-2,5-diphenyltetrazolium bromide staining (MTT) (working solution 0.5 µg/ml). After 1 h of incubation, the supernatants were removed, the formazan crystals were dissolved with dimethyl sulfoxide and the absorbance at 570 nm was measured using a microtiter plate reader. Competitive experiments were performed as described above using 100 nM of RGD-SAP or 1000 nM of CYS-SAP in the presence of 5000 nM of ACDCRGDCFCG peptide for 48 and 72 hours.

To induce caspase 3 activation, cells were treated with 30 nM RGD-SAP or 2 mM DTT for 48 and 72 hours.

In Vivo Studies

Studies on animal models were approved by the Institutional Animal Care and Use Committee (Institutional Animal Care and Use Committee, IACUC) and performed according to the prescribed guidelines. C57BL/6 female mice (7 weeks old, Charles River, Calco, Italy) were challenged with subcutaneous injection in the left flank of 3–5 × 10⁵ MB49 living cells; 5 days later, 4–6 mice/group were intravenously administered with various doses of RGD-SAP or CYS-SAP diluted in sodium chloride (0.9%, i.v., 200 µl). Tumor growth was estimated by calculating the volume using the formula $r_1 \times r_2 \times r_3 \times 4/3 \pi$, where r_1 and r_2 are the longitudinal and lateral radii, and r_3 is the thickness of tumors protruding from

the surface of normal skin. Animals were euthanized when tumors reached 10 mm in diameter, became ulcerated or a 15% animal body weight loss was measured.

Orthotopic syngeneic tumor were developed according to the procedure described by Loskog et al. (27). Briefly, C57BL/6 female mice were anesthetized with ketamine/xylazine (80/10 mg/kg) and catheterized (PE50 catheter, BD Biosciences) using lubricated catheters with 2.5% lidocaine-containing gel (Luan). To enhance tumor engraftment, 100 μ l of poly-L-lysine (0.1 mg/ml, mw 70000–150000, Sigma Aldrich), was injected transurethrally into the bladder and left in place for 30 min, then bladder was washed with PBS and instilled with 5x10⁴ MB49 Luc diluted in serum-free medium (100 μ l/mice), 30 min later the catheters were removed. On day 7, mice were treated with mitomycin C (MMC) alone (n=10), administered transurethrally and kept in the bladder for 1 hour (50 μ g in 100 μ l of PBS, every 4 days for 2 times), or combined with RGD-SAP (n=5) or RGD-SAP alone (i.v., 200 μ l, every 5 days, for 3 times) (n=10), starting at day 9. Control group of mice was treated with vehicle (sodium chloride, 0.9%, i.v., 200 μ l) (n=10). Orthotopic tumor engraftment and growth was monitored once a week by *in vivo* bioluminescence imaging (IVIS). Tumor growth was estimated by acquiring the bioluminescence signal (BLI) and it expressed in total photon flux. Mice were euthanized when the BLI intensity suddenly drop, due to irreversible necrosis and accompanied with hematuria or animal lethargy.

Blood Sample Collection and Biochemical Parameters Analysis

Blood samples were collected from the retroorbital plexus of anesthetized mice using 4% isoflurane at the end of each experiment or before animal sacrifice. Blood samples were left at room temperature for at least 30 min before being processed and then centrifuged (800 x g, 10 min) for serum separation. Serum albumin, aspartate transaminase, alanine transaminase, creatinine and urea were determined by using an automated analyzer (SciVet ABC plus and Idexx Procyte analyzers) according to the manufacturers' instructions. Standard controls were run before each determination.

Statistical Analysis

All *in vitro* experiments were performed at least in triplicate. Mouse experiments were performed using at least 4 mice per group. When appropriate, statistical significance was determined using a 2-tailed Student's *t* test. For tumor growth analyses, we performed one-way ANOVA statistical analysis. Survival curves were compared using the log rank test. Tests symbols mean: **p* < 0.05; ***p* < 0.01; ****p* < 0.001; ns, not significant.

RESULTS

Production and Characterization of RGD-SAP and CYS-SAP

RGD-SAP, consisting of RGD-4C fused to the N-terminus of SAP was produced in *E.coli* cells by recombinant DNA

technology. In parallel we have also produced a SAP variant with a Cys residue in place of the RGD-4C domain (CYS-SAP) (Figures 1A, B).

To facilitate their purification and to promote endosomal escape of the toxin into recipient cells, both products were genetically engineered to express a histidine tag at the C-terminus (28). Since SAP can inactivate prokaryotic ribosomes, their production in *E.coli* was induced with IPTG for only 3 h. Western blot analysis of the purified RGD-SAP, performed under reducing and non-reducing conditions, showed a single band of 30 kDa as expected for monomers (Figure 1C), suggesting that inter-chain disulfide bonds between the ACDCRGDCFCG domains of different molecules were not formed. In contrast, two bands corresponding to monomers and dimers were detected in CYS-SAP, suggesting that an inter-chain disulfide bond was formed between the N-terminal cysteines of this protein (Figure 1C).

RGD-SAP Can Kill Integrin-Expressing Cells More Efficiently Than CYS-SAP

RGD-4C can recognize α v-integrins with different affinities (29). Integrins, such as α v β 3, α v β 5 and α v β 6, are present on a variety of tumor cells (24–26, 30). Therefore, to identify tumor cells that could be exploited as targets to validate the targeting properties of RGD-SAP *in vitro*, we characterized the surface expression of integrins by various cancer cell lines, including U87 glioblastoma cells, RT4, RT112 and 5637 bladder cancer cells, MDA-MB-468 breast cancer cells and normal fibroblasts, by flow cytometry. The results showed that U87 cells express high levels of α v β 3, but not of α v β 5 and α v β 6, whereas RT4, RT112 and 5637 and MDA-MB-468 cells showed a moderate-high positivity for α v β 5 and α v β 6, but not of α v β 3. Normal fibroblasts expressed none of these integrins (Figure 2A).

To assess whether the RGD domain can increase the cytotoxic effects of saporin against cancer cells, we then tested the cytotoxic effects of RGD-SAP and CYS-SAP on these cell lines. A stronger cytotoxic effect of RGD-SAP, compared to CYS-SAP, was observed with all cancer cells, but not with normal fibroblasts (Figure 2B). Considering that fibroblasts do not express α v β 3 and α v β 5, i.e. integrins known to be recognized by RGD-4C, these data suggest that the stronger cytotoxic effects of RGD-SAP against cancer cells was mediated by an RGD-dependent targeting mechanism.

To verify this hypothesis, we performed competition experiments with the free RGD-4C peptide on 5637 cell line, selectively sensitive to RGD-SAP and representative of a human muscle-invasive model of bladder cancer. To this end, cells were treated with 0.1 μ M RGD-SAP or 1 μ M CYS-SAP, concentrations reflecting the different sensitivity of cells towards the two toxins, in the presence or absence of an excess of free RGD-4C. As expected, RGD-4C significantly decreased the activity of RGD-SAP, but not that of CYS-SAP (Figure 3A). This result lends support to the hypothesis that indeed the RGD domain of RGD-SAP contribute to the cytotoxic activity of this conjugate by a receptor-mediated targeting mechanism, likely involving integrins.

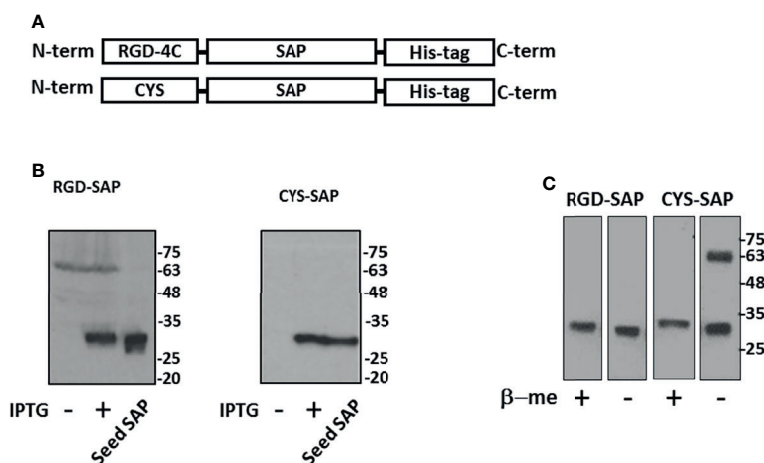


FIGURE 1 | Design, expression and purification of RGD-SAP and CYS-SAP recombinant proteins. **(A)** Schematic representation of RGD-SAP and CYS-SAP recombinant proteins. The RGD (ACDCRGDCFCG) targeting and CYS (CGGSGG) non-targeting peptides were inserted by genetic recombination at the N-terminus of SAP. A histidine (His)-tag was added at the C-terminus of the two constructs to aid in the purification of the recombinant proteins. **(B)** Effect of IPTG on RGD-SAP and CYS-SAP expression in BL21DE3 *E. coli* cells as determined by western blot using an anti-SAP antibody. IPTG (+) and (-), induced and not induced cells, respectively. Seed-derived SAP (200 ng) was used as positive control for WB analysis. **(C)** WB analysis of purified RGD-SAP and CYS-SAP under reducing (β -mercaptoethanol (β -me) +) or non-reducing (β -me -) conditions.

It is well known that SAP induces cell apoptosis. Thus, we then investigated the activation of programmed cell death by analyzing caspase 3 in cells treated with RGD-SAP. To this aim, 5637 and MDA-MB-468 epithelial cells were incubated with RGD-SAP or DTT, a

positive control, for 48 and 72 h. As shown in **Figure 3B**, caspase 3 activation was detectable as cleaved form in all samples treated with the toxin. These and the above results indicate that fusing the RGD moiety to SAP enhances the delivery and uptake of the toxin.

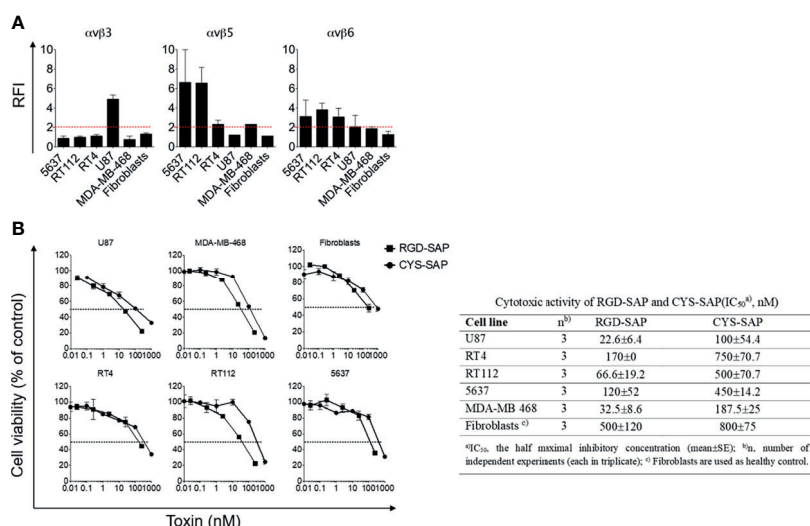


FIGURE 2 | Integrins expression on cancer cell lines and *in vitro* biological activity evaluation of RGD-SAP and CYS-SAP recombinant proteins. **(A)** 5637, RT112, RT4, U87, MDA-MB-468 cancer cell lines and fibroblasts were analyzed by flow cytometry for $\alpha v \beta 3$, $\alpha v \beta 5$ and $\alpha v \beta 6$ integrins expression. Relative Fluorescence Intensity (RFI) are shown as mean±SD. The dashed red line represents the threshold arbitrarily defining positive expression (RFI=2). **(B)** Effect of various amounts of RGD-SAP or CYS-SAP on the indicated cells as determined by MTT assay after 72 h treatment. One representative experiment out of three performed is shown. Cell viability is expressed as percentage to untreated cells (mean ± SD). The IC₅₀ from three different experiments is reported as mean ± SE.

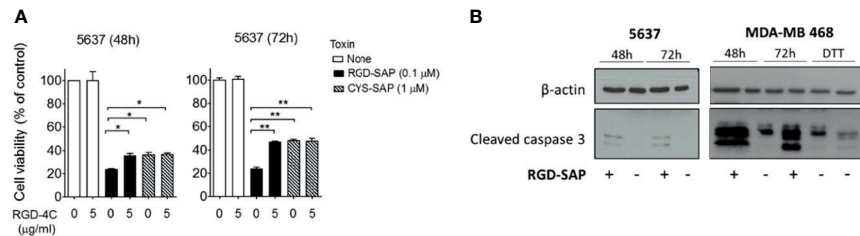


FIGURE 3 | RGD-SAP target specificity and caspase 3 activation. **(A)** 5637 bladder cancer cells were incubated with RGD-SAP (0.1 μM) or CYS-SAP (1 μM) in the presence or absence of ACDCRGDCFC peptide (5 μM). The cell viability was evaluated after 48 and 72 h by MTT assay. Results are shown as mean ± SE. * $p < 0.05$, ** $p < 0.01$ by non-parametric unpaired t test. **(B)** The activation of apoptosis via caspase 3 cleavage upon RGD-SAP (30 nM) treatment was evaluated in 5637 and MDA-MB-468 cells by analyzing the intracellular levels of caspase-3. Cells were incubated with RGD-SAP for 48 and 72 h and cell lysates were analyzed by western blot with anti-caspase-3 or an anti-β-actin antibodies for protein normalization. DTT (2 mM) was included as positive control for caspase-3 activation.

RGD-SAP Is Endowed With Antitumor Activity on a Subcutaneous Model of Bladder Cancer

The anti-tumor activity of RGD-SAP and CYS-SAP were then investigated using C57BL/6 mice bearing subcutaneous murine MB49 urothelial carcinoma cells. A preliminary experiment,

performed *in vitro*, showed that RGD-SAP could kill these cells (**Figure 4A**).

Thus, mice were treated, systemically, with 1 mg/kg of RGD-SAP or CYS-SAP at day 5. The treatment was repeated three times every five days (**Figure 4B**). RGD-SAP could reduce tumor growth after the second administration, leading to marked

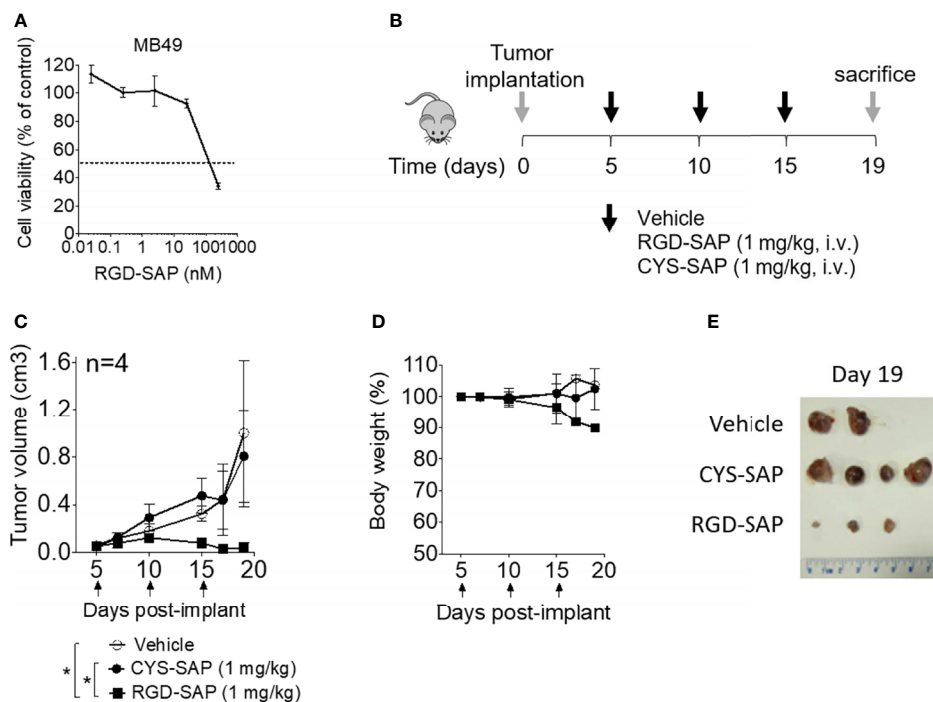


FIGURE 4 | Effects of RGD-SAP and CYS-SAP on tumor growth in a subcutaneous syngeneic bladder cancer mouse model. **(A)** Effect of RGD-SAP on MB49 murine bladder cancer cell line viability as measured by MTT assay. **(B)** Schematic representation of the experimental design and treatment schedule. MB49 cells were subcutaneously implanted in 7-week-old C57BL/6 WT female mice. Tumor bearing-mice were treated i.v. with the indicated doses of CYS-SAP or RGD-SAP or vehicle every 5 days after tumor implantation (arrows). **(C)** Effect of 1 mg/kg dose of CYS-SAP or RGD-SAP on MB49 bladder cancer growth. Tumor volumes (mean ± SD, $n=4$ mice/group) are shown. * $p < 0.05$, by one-way ANOVA test. **(D)** Effect of treatments on the animal body weight change. Animal weights are reported as percent of starting body weight (mean ± SD of 4 animals per group). **(E)** A representative image of MB49 subcutaneous tumors explanted from mice that survived to the end of the experiment (day 19): (vehicle ($n=2$), 2 mice were sacrificed at day 16 due to tumor ulceration; RGD-SAP ($n=4$), 1 tumor undetectable).

reduction of the tumor volume in all mice and complete eradication in one mouse (**Figures 4C–E** and **Supplementary Figure 1A**). On the contrary, CYS-SAP did not show any effect on tumor growth, suggesting that the therapeutic effect of RGD-SAP crucially involved the RGD domain. However, the dose of RGD-SAP used in this experiment also caused loss of body weight at day 19 (**Figure 4D**) and severe necrosis in the tails where the drug was injected.

To determine the minimal effective, non-toxic dose of RGD-SAP tumor-bearing mice were treated with 0.75, 0.5, 0.25 mg/kg of RGD-SAP at days 5, 10, 15 after tumor implantation, as described above. The doses of 0.75 and 0.5, but not 0.25 mg/kg, caused a significant delay of tumor growth, pointing to a dose-dependent effect (**Figure 5A** and **Supplementary Figure 1B**), without causing loss of body weight (**Figures 5B–D**).

The toxicological effects RGD-SAP was further investigated. To this aim, we collected blood samples at the end of each experiment or before animal sacrifice and analyzed biochemical parameters of liver and kidney toxicity (albumin, alanine transaminase, aspartate transaminase for liver toxicity, and creatinine and urea for kidney toxicity). As shown in **Figure 6**, RGD-SAP systemic toxicity was dose dependent and apparent only with the highest dose used (1 mg/kg). In fact, significantly higher values of AST and CHE were measured in mice treated with 1 mg/kg RGD-SAP, but not with the lower doses.

RGD-SAP Can Delay Tumor Growth in an Orthotopic Mouse Model of Syngeneic Bladder Cancer

The anti-tumor efficacy of RGD-SAP was then investigated in an orthotopic model of urothelial carcinoma. To this aim, we genetically engineered MB49 cells to express luciferase (MB49-luc). MB49-luc cells were then orthotopically implanted into immunocompetent C57BL/6 mice. Tumor engraftment and growth, as monitored by *in vivo* bioluminescence imaging, occurred in 100% of mice in 5–7 days after cells inoculation. This tumor model resembles advanced bladder cancer and is

characterized by high proliferation rate accompanied by protrusion of the mass into the bladder lumen, obstruction of urethra, hematuria and necrosis in the tumor core a few days upon engraftment (27). These features can lead to an inadequate drug delivery to the tumor mass (27). To overcome this limitation, we decided to use mitomycin C (MMC) as a tool to slow down the tumor growth and delay necrosis formation, thereby allowing the toxin to reach tumor cells and exert its specific effect. MMC is one of the most widely used agents for preventing recurrence of superficial bladder cancer in clinics, usually administered intravesically after transurethral resection of cancer lesions (31–33). Of note, MB49 bladder cancer cells were extremely sensitive to MMC (IC₅₀ ~2 µg/ml) (**Figure 7A**).

At the time of tumor detection (day 7 after cells infusion into the bladder) two experimental groups were treated with MMC through transurethral administration. A second dose of MMC was given after four days. In between, mice received a first dose of RGD-SAP (systemically, 0.5 mg/kg) or vehicle, which was repeated for three times (**Figure 7B**). One group of mice was treated with RGD-SAP alone, as control. As previously demonstrated (34), in this model, after an initial increase, the bioluminescent signal drops in a time dependent manner, due to the reduced light emission from extended necrotic and hemorrhagic areas compared with vital tumor areas. In the control group the bioluminescent signal increased, reaching the maximum value after 11 days, and then started decreasing. Although a similar behavior was observed after treatment with MMC or RGD-SAP alone, the combination of these drugs greatly limited the increase of the signal (**Figure 7C**), which implies a relevant anti-tumor effect. Accordingly, a significant effect on mice survival was observed in the group of mice treated with RGD-SAP/MMC combination (**Figures 7E, F**), as 80% of mice were still alive when the experiment ended after 23 days. Histochemical analysis of the tumors, explanted after mouse scarification, showed that only one mouse treated with the combined therapy had a necrotic tumor, while all the others did not display any necrotic area, suggesting that this treatment

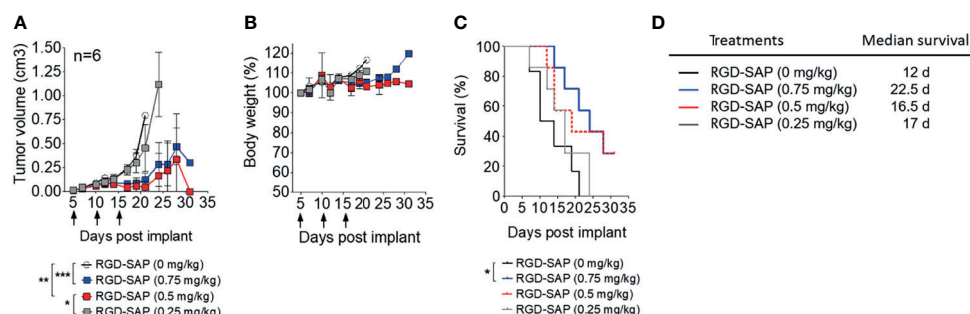


FIGURE 5 | Dose dependent effects of RGD-SAP on tumor growth in a subcutaneous syngeneic bladder cancer mouse model. **(A)** MB49 cells were subcutaneously implanted in 7-week-old C57BL/6 WT female mice (n=6/group) were treated i.v. with the indicated doses of RGD-SAP every 5 days after tumor implantation for three times (arrows). Tumor volumes (mean ± SD) are shown. *p < 0.05; **p < 0.01; ***p < 0.001 by using one-way ANOVA test. **(B)** Animal weights are reported as percent of starting body weight (mean ± SD of 6 animals per group). **(C)** Kaplan–Meyer plot of animal survival and **(D)** the associated median survival time. Results from a Mantel–Cox two-sided log-rank test are shown when statistically significant (*p < 0.05) for RGD-SAP 0.75 mg/kg (blue line, hazard ratio 5.25; 95% CI, 1.19–23.10) versus vehicle (black line).

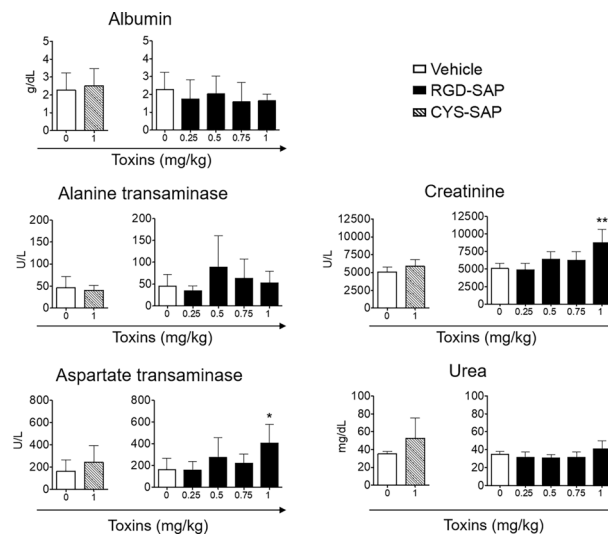


FIGURE 6 | Comparison of clinical biochemistry parameters in mice treated with CYS-SAP or different RGD-SAP concentrations. Blood samples were collected from treated mice and the concentration of albumin, alanine transaminase, aspartate transaminase, creatinine and urea in the serum were measured. Data are shown as mean ± SD from $n = 4/6$ mice per condition. Results from unpaired Student t test are shown. All treatments were compared to vehicle (* $p < 0.05$; ** $p < 0.01$).

consistently reduced the tumor growth. Furthermore, no evidence of toxicity was observed, judging from the lack of significant changes of body weight (**Figure 7D**), as well as of albumin, alanine transaminase or urea levels in the bloodstream (**Figure 8**).

DISCUSSION

The results show that the fusion of RGD-4C with SAP enables selective delivery of this toxin to tumors, thereby enhancing its antitumor activity. In particular, the results show that RGD-SAP can kill cells expressing the integrins $\alpha v\beta 3$, $\alpha v\beta 5$ and $\alpha v\beta 6$ more efficiently than CYS-SAP, a control conjugate lacking the RGD-4C domain. As expected, the improved cytotoxic activity of RGD-SAP was inhibited, *in vitro*, by an excess of free RGD-4C peptide. Considering the known ability of RGD-4C to bind $\alpha v\beta 3$ (affinity value: 8.3 nM), $\alpha v\beta 5$ (46 nM), $\alpha 5\beta 1$ (244 nM) and $\alpha v\beta 6$ (380 nM) integrins (26), although with different affinities, and the known overexpression of these integrins in tumors, these findings suggest that integrin targeting was an important mechanism that contribute to the improved activity of RGD-SAP. We tested the expression of $\alpha v\beta 3$, $\alpha v\beta 5$ and $\alpha v\beta 6$, to associate the RGD-SAP cytotoxicity to the integrin expression on target tumor cells. U87, which expresses the highest amount of $\alpha v\beta 3$, are the most sensitive to RGD-SAP, but also other cell lines, expressing $\alpha v\beta 5$ and $\alpha v\beta 6$ are enough sensitive to RGD-SAP, considerably more than the untargeted CYS-SAP. It is likely that not only $\alpha v\beta 3$, but also the other abovementioned integrins can contribute to the RGD-SAP cytotoxicity. In addition, we cannot exclude contribution of other RGD-interacting integrins to RGD-SAP cytotoxicity. To lower the risk that RGD-4C fusion

with saporin could reduce or abolish the binding of the peptide to integrins, e.g. by steric hindrance, we have introduced a seven amino acids flexible linker. The higher activity of RGD-SAP with respect to untargeted SAP and the reduction of its cytotoxicity upon competition with RGD-4C peptide, suggests that with this linker RGD-4C preserved, at least partially if not at all, its functional properties after coupling to saporin. The results of *in vivo* studies in different mouse models of bladder cancer show that RGD-SAP can reduce tumor growth and significantly prolong animal survival without inducing detectable side effects. These results and the notion that RGD-4C is a compound with a proven utility as ligand for the targeted delivery of therapeutic molecules to αv integrins (16, 24, 26, 29), and that αv integrins are significantly over-expressed in bladder tumors in a stage and grade-dependent manner (35, 36), lend support to the hypothesis that this class of receptors may represent important molecular targets for toxin delivery to bladder cancer.

The approved clinical practice for the management of bladder cancer consists in transurethral resection of cancer lesions or by the removal of the entire organ (radical cystectomy), depending on the tumor grade and stage. Most of the times, a chemoprophylaxis regimen based on chemotherapeutics like platinum complexes or mitomycin C (MMC) is given either before surgery (neoadjuvant chemotherapy) or after surgery (adjuvant chemotherapy) to reduce the risk of cancer recurrence (33). In case of advanced or metastatic bladder tumor, immune checkpoint inhibitors (anti-PDL1 antibodies) and tyrosine kinase inhibitors (specific for FGFR) represent the most effective targeted options, showing promising results in the treatment of specific subtypes. However, the clinical outcome of these treatments strictly relies on the presence of an elevated

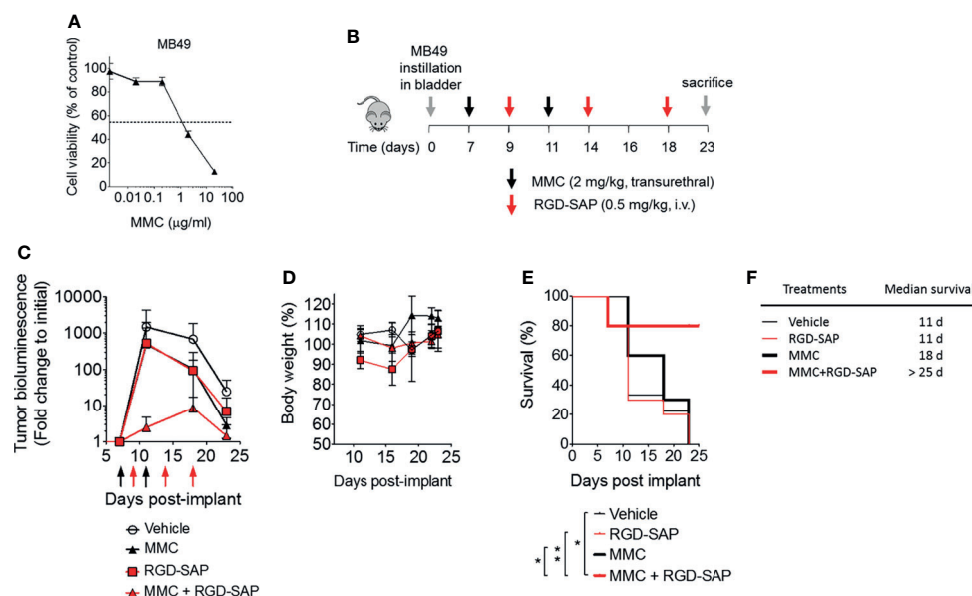


FIGURE 7 | Effects of MMC and RGD-SAP on tumor growth in an orthotopic syngeneic bladder cancer mouse model. **(A)** Effect of mitomycin C (MMC) on MB49 murine bladder cancer cell line viability as measured by MTT assay. **(B)** Schematic representation of the *in vivo* experimental design and treatment schedule. Luciferase-expressing MB49 cells were transurethrally injected into the bladder of 7-week-old C57BL/6 female mice. Tumor engraftment was monitored by *in vivo* bioluminescence imaging. Tumor bearing mice were randomized into 4 experimental groups and treated with the indicated dose of MMC (transurethral, black arrows, $n=10$ mice), RGD-SAP (i.v., red arrows, $n=10$ mice), MMC + RGD-SAP ($n=5$ mice) or vehicle ($n=10$ mice). The results of two experiments with 5 animals/group were considered and cumulated **(C)** Tumor growth (mean \pm SD) as determined over time by fold change to the initial detectable bioluminescence. **(D)** Effect of treatments on the animal body weight change. Animal weights are reported as percent of starting body weight (mean \pm SD of 5–10 animals per group). **(E)** Kaplan–Meyer plot of animal survival and **(F)** median survival time. Results from a Mantel–Cox two-sided log-rank test are shown when statistically significant (* $p < 0.05$, ** $p < 0.01$) for MMC+RGD-SAP (bold red line) versus vehicle (thick black line, hazard ratio 7.19; 95% CI, 1.51–34.26) or MMC (bold black line, hazard ratio 5.96, 95% CI, 1.44–24.69) or RGD-SAP (bold red line, hazard ratio 0.15, 95% CI, 0.03–0.62).

immune signature or FGFR2/3 specific mutation (typical of patients with a luminal I bladder cancer subtype) (37, 38).

To recapitulate advanced bladder cancer features, we have tested the pharmacological efficacy of our recombinant protein, systemically administered, using syngeneic bladder cancer mouse models. At first we used a subcutaneous cancer model to determine the optimal dosage and found that RGD-SAP can inhibit the tumor growth in a dose-dependent manner. In this model, RGD-SAP was significantly more active than the CYS-SAP control, the latter being almost completely inactive. This suggest that RGD-SAP can actively target the tumor environment

and exclude a “passive targeting” mechanism potentially related to the enhanced permeability of tumor tissues. Then, we used an orthotopically implanted tumor model (MB49) to assess the therapeutic effect of RGD-SAP alone and in combination with MMC. The MB49 orthotopic model of advanced bladder cancer is characterized by a logarithmic proliferation rate of the tumor mass, leading in several days to the formation of an inner necrotic area, causing a sudden drop of luminescence signal (27, 39). It is expected that the uptake of drugs in solid tumors is heterogeneous and the general distribution decreases with increasing tumor weight, since cells that are progressively distant to blood vessels

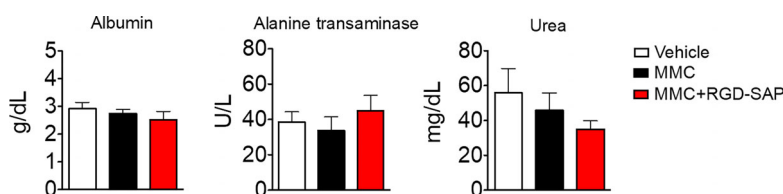


FIGURE 8 | Comparison of clinical biochemistry parameters in mice treated with mitomycin C (MMC) alone or in combination with RGD-SAP. Blood samples were collected from treated mice and the concentration of albumin, alanine transaminase and urea in the serum were measured. Values are shown as mean \pm SD from $n = 10$ for vehicle and MMC; $n=5$ for MMC + RGD-SAP.

and located in high-pressure regions constitute large areas of hypoxic, necrotic, or semi-necrotic tissue. Thus, this condition can limit an adequate penetration of drug administrated systemically, such as RGD-SAP, into the tumor mass. Interestingly, upon MMC pre-treatment, RGD-SAP reduced tumor growth compared to MMC alone, significantly increasing overall survival (80% of mice) and improving animal welfare. Notably, RGD-SAP has shown a low cytotoxic activity on MB49 cells *in vitro*, suggesting that its activity *in vivo* could be related to the targeting of microenvironment components as well. Indeed, $\alpha v \beta 3$ is expressed by the endothelium in the neo-angiogenic blood vessels (16–19) and it represent a potential target of RGD-SAP.

Intra-tumoral heterogeneity represents a major obstacle to cancer therapeutics, including conventional chemotherapy, immunotherapy, and targeted therapies. Due to its potential effects on tumor cells and microenvironment, RGD-SAP may represent a good therapeutic tool for bladder cancer. In addition, by inhibiting proteins synthesis, SAP acts in a cell cycle independent manner, thus targeting both quiescent and rapidly dividing tumor cells. This feature makes it suitable to contrast both aggressively growing cancers and tumors with slower progression. RGD-SAP can be employed also in combination with other therapeutic options based on different mechanisms of action, e.g. inhibition of DNA synthesis, cell division, and signal transduction.

CONCLUSIONS

Our study demonstrates that the fusion of RGD-4C to SAP enables specific delivery of the toxin to the tumor mass and enhances its anti-tumor activity in bladder cancer models without showing detectable side effects. The RGD-SAP may be potentially applicable to other solid tumors, especially in combination with other therapeutic agents to tackle tumor heterogeneity.

REFERENCES

1. Vago R, Ippoliti R, Fabbrini MS. Current Status & Biomedical Applications of Ribosome-Inactivating Proteins. In: *Antitumor Potential and Other Emerging Medicinal Properties of Natural Compounds*. Springer (2013). p. 145–79.
2. Fabbrini MS, Katayama M, Nakase I, Vago R. Plant Ribosome-Inactivating Proteins: Progresses, Challenges and Biotechnological Applications (and a Few Digressions). *Toxins (Basel)* (2017) 9(10):314. doi: 10.3390/toxins9100314
3. Musidlak O, Nawrot R, Gozdicka-Jozefiak A. Which Plant Proteins Are Involved in Antiviral Defense? Review on *In Vivo* and *In Vitro* Activities of Selected Plant Proteins Against Viruses. *Int J Mol Sci* (2017) 18(11):2300. doi: 10.3390/ijms18112300
4. Lapadula WJ, Ayub MJ. Ribosome Inactivating Proteins From an Evolutionary Perspective. *Toxicon* (2017) 136:6–14. doi: 10.1016/j.toxicon.2017.06.012
5. Rust A, Partridge LJ, Davletov B, Hautbergue GM. The Use of Plant-Derived Ribosome Inactivating Proteins in Immunotoxin Development: Past, Present and Future Generations. *Toxins (Basel)* (2017) 9(11):344. doi: 10.3390/toxins9110344

DATA AVAILABILITY STATEMENT

The raw data supporting the conclusions of this article will be made available by the authors, without undue reservation.

ETHICS STATEMENT

The animal study was reviewed and approved by Institutional Animal Care and Use Committee, IACUC.

AUTHOR CONTRIBUTIONS

RV designed the project and supervised the work. SZ, CA, CM, OAB, and FC performed the experiments, acquired data, provide methods and reagents. RV, SZ, FC, MD, and AC discussed the results. SZ drafted the manuscript. RV, MD, FC, and AC revised the manuscript. All the authors approved the manuscript.

FUNDING

This work was supported by the Italian Ministry of Health (GR-2011-02351220 to RV).

SUPPLEMENTARY MATERIAL

The Supplementary Material for this article can be found online at: <https://www.frontiersin.org/articles/10.3389/fonc.2022.846958/full#supplementary-material>

Supplementary Figure 1 | (A) Quantitative analysis of growing tumor volume for each individual mouse treated with vehicle, RGD-SAP or CYS-SAP. **(B)** Quantitative analysis of growing tumor volume for each individual mouse treated with vehicle (0 mg/kg) or RGD-SAP 0.25, 0.5 and 0.75 mg/kg).

6. Giansanti F, Flavell DJ, Angelucci F, Fabbrini MS, Ippoliti R. Strategies to Improve the Clinical Utility of Saporin-Based Targeted Toxins. *Toxins (Basel)* (2018) 10(2):82. doi: 10.3390/toxins10020082
7. Fuchs H. Dianthin and Its Potential in Targeted Tumor Therapies. *Toxins (Basel)* (2019) 11(10):592. doi: 10.3390/toxins11100592
8. Zuppone S, Fabbrini MS, Vago R. Hosts for Hostile Protein Production: The Challenge of Recombinant Immunotoxin Expression. *Biomedicines* (2019) 7(2):38. doi: 10.3390/biomedicines7020038
9. Della Cristina P, Castagna M, Lombardi A, Barison E, Tagliabue G, Ceriotti A, et al. Systematic Comparison of Single-Chain Fv Antibody-Fusion Toxin Constructs Containing Pseudomonas Exotoxin A or Saporin Produced in Different Microbial Expression Systems. *Microb Cell Fact* (2015) 14:19. doi: 10.1186/s12934-015-0202-z
10. Dhez AC, Benedetti E, Antonosante A, Panella G, Ranieri B, Florio TM, et al. Targeted Therapy of Human Glioblastoma *via* Delivery of a Toxin Through a Peptide Directed to Cell Surface Nucleolin. *J Cell Physiol* (2018) 233(5):4091–105. doi: 10.1002/jcp.26205
11. Errico Provenzano A, Posterl R, Giansanti F, Angelucci F, Flavell SU, Flavell DJ, et al. Optimization of Construct Design and Fermentation Strategy for the Production of Bioactive ATF-SAP, a Saporin Based Anti-Tumoral uPAR-

- Targeted Chimera. *Microb Cell Fact* (2016) 15(1):194. doi: 10.1186/s12934-016-0589-1
12. Thakur M, Mergel K, Weng A, von Mallinckrodt B, Gilabert-Oriol R, Durkop H, et al. Targeted Tumor Therapy by Epidermal Growth Factor Appended Toxin and Purified Saponin: An Evaluation of Toxicity and Therapeutic Potential in Syngeneic Tumor Bearing Mice. *Mol Oncol* (2013) 7(3):475–83. doi: 10.1016/j.molonc.2012.12.004
 13. Zuppone S, Assalini C, Minici C, Bertagnoli S, Branduardi P, Degano M, et al. The Anti-Tumoral Potential of the Saporin-Based uPAR-Targeting Chimera ATF-SAP. *Sci Rep* (2020) 10(1):2521. doi: 10.1038/s41598-020-59313-8
 14. di Leandro L, Giansanti F, Mei S, Ponziani S, Colasante M, Ardini M, et al. Aptamer-Driven Toxin Gene Delivery in U87 Model Glioblastoma Cells. *Front Pharmacol* (2021) 12:588306. doi: 10.3389/fphar.2021.588306
 15. Fuchs H, Bachran C, Li T, Heisler I, Durkop H, Sutherland M. A Cleavable Molecular Adapter Reduces Side Effects and Concomitantly Enhances Efficacy in Tumor Treatment by Targeted Toxins in Mice. *J Control Release* (2007) 117(3):342–50. doi: 10.1016/j.jconrel.2006.11.019
 16. Wang H, Chen K, Cai W, Li Z, He L, Kashefi A, et al. Integrin-Targeted Imaging and Therapy With RGD4C-TNF Fusion Protein. *Mol Cancer Ther* (2008) 7(5):1044–53. doi: 10.1158/1535-7163.MCT-07-2084
 17. Bianconi D, Unseld M, Prager GW. Integrins in the Spotlight of Cancer. *Int J Mol Sci* (2016) 17(12):2037. doi: 10.3390/ijms17122037
 18. Blandin AF, Renner G, Lehmann M, Lelong-Rebel I, Martin S, Dontenwill M. Beta1 Integrins as Therapeutic Targets to Disrupt Hallmarks of Cancer. *Front Pharmacol* (2015) 6:279. doi: 10.3389/fphar.2015.00279
 19. Hynes RO. Integrins: Bidirectional, Allosteric Signaling Machines. *Cell* (2002) 110(6):673–87. doi: 10.1016/S0092-8674(02)00971-6
 20. Li M, Wang W, Li M, Wu X, Setterrahmane S, Xu H. Integrins as Attractive Targets for Cancer Therapeutics. *Acta Pharm Sin B* (2021) 11(9):2726–37. doi: 10.1016/j.apsb.2021.01.004
 21. Brooks PC, Stromblad S, Klemke R, Visscher D, Sarkar FH, Cheresh DA. Antiintegrin Alpha V Beta 3 Blocks Human Breast Cancer Growth and Angiogenesis in Human Skin. *J Clin Invest* (1995) 96(4):1815–22. doi: 10.1172/JCI118227
 22. Friedlander M, Brooks PC, Shaffer RW, Kincaid CM, Varner JA, Cheresh DA. Definition of Two Angiogenic Pathways by Distinct Alpha V Integrins. *Science* (1995) 270(5241):1500–2. doi: 10.1126/science.270.5241.1500
 23. Boderio L, Lopez Rivas P, Korsak B, Hechler T, Pahl A, Muller C, et al. Synthesis and Biological Evaluation of RGD and isoDGR Peptidomimetic-Alpha-Amanitin Conjugates for Tumor-Targeting. *Beilstein J Org Chem* (2018) 14:407–15. doi: 10.3762/bjoc.14.29
 24. Curnis F, Gasparri A, Sacchi A, Longhi R, Corti A. Coupling Tumor Necrosis Factor-Alpha With alphaV Integrin Ligands Improves Its Antineoplastic Activity. *Cancer Res* (2004) 64(2):565–71. doi: 10.1158/0008-5472.CAN-03-1753
 25. Danhier F, Le Breton A, Preat V. RGD-Based Strategies to Target Alpha(V) Beta(3) Integrin in Cancer Therapy and Diagnosis. *Mol Pharm* (2012) 9(11):2961–73. doi: 10.1021/mp3002733
 26. Temming K, Schiffelers RM, Molema G, Kok RJ. RGD-Based Strategies for Selective Delivery of Therapeutics and Imaging Agents to the Tumour Vasculature. *Drug Resist Update* (2005) 8(6):381–402. doi: 10.1016/j.drug.2005.10.002
 27. Loskog A, Ninalga C, Hedlund T, Alimohammadi M, Malmstrom PU, Totterman TH. Optimization of the MB49 Mouse Bladder Cancer Model for Adenoviral Gene Therapy. *Lab Anim* (2005) 39(4):384–93. doi: 10.1258/002367705774286475
 28. Ferrer-Miralles N, Corchero JL, Kumar P, Cedano JA, Gupta KC, Villaverde A, et al. Biological Activities of Histidine-Rich Peptides; Merging Biotechnology and Nanomedicine. *Microb Cell Fact* (2011) 10:101. doi: 10.1186/1475-2859-10-101
 29. Kapp TG, Rechenmacher F, Neubauer S, Maltsev OV, Cavalcanti-Adam EA, Zarka R, et al. A Comprehensive Evaluation of the Activity and Selectivity Profile of Ligands for RGD-Binding Integrins. *Sci Rep* (2017) 7:39805. doi: 10.1038/srep39805
 30. Curnis F, Sacchi A, Longhi R, Colombo B, Gasparri A, Corti A. IsoDGR-Tagged Albumin: A New AlphaV Selective Carrier for Nanodrug Delivery to Tumors. *Small* (2013) 9(5):673–8. doi: 10.1002/smll.201202310
 31. Bosschiet J, Nieuwenhuijzen JA, van Ginkel T, Vis AN, Witte B, Newling D, et al. Value of an Immediate Intravesical Instillation of Mitomycin C in Patients With Non-Muscle-Invasive Bladder Cancer: A Prospective Multicentre Randomised Study in 2243 Patients. *Eur Urol* (2018) 73(2):226–32. doi: 10.1016/j.eururo.2017.06.038
 32. Racioppi M, Di Gianfrancesco L, Ragonese M, Palermo G, Sacco E, Bassi P. Chemoablation With Intensive Intravesical Instillation of Mitomycin C Treatment: A New Approach for Non-Muscle-Invasive Bladder Cancer. *Eur Urol Oncol* (2019) 2(5):576–83. doi: 10.1016/j.euo.2018.08.032
 33. Soloway MS. Expectant Treatment of Small, Recurrent, Low-Grade, Noninvasive Tumors of the Urinary Bladder. *Urol Oncol* (2006) 24(1):58–61. doi: 10.1016/j.urolonc.2005.07.005
 34. Jurczok A, Fornara P, Soling A. Bioluminescence Imaging to Monitor Bladder Cancer Cell Adhesion *In Vivo*: A New Approach to Optimize a Syngeneic, Orthotopic, Murine Bladder Cancer Model. *BJU Int* (2008) 101(1):120–4. doi: 10.1111/j.1464-410X.2007.07193.x
 35. Sachs MD, Rauen KA, Ramamurthy M, Dodson JL, De Marzo AM, Putzi MJ, et al. Integrin Alpha(V) and Coxsackie Adenovirus Receptor Expression in Clinical Bladder Cancer. *Urology* (2002) 60(3):531–6. doi: 10.1016/S0090-4295(02)01748-X
 36. van der Horst G, Bos L, van der Mark M, Cheung H, Heckmann B, Clement-Lacroix P, et al. Targeting of Alpha-V Integrins Reduces Malignancy of Bladder Carcinoma. *PloS One* (2014) 9(9):e108464. doi: 10.1371/journal.pone.0108464
 37. Li H, Zhang Q, Shuman L, Kaag M, Raman JD, Merrill S, et al. Evaluation of PD-L1 and Other Immune Markers in Bladder Urothelial Carcinoma Stratified by Histologic Variants and Molecular Subtypes. *Sci Rep* (2020) 10(1):1439. doi: 10.1038/s41598-020-58351-6
 38. Loriot Y, Necchi A, Park SH, Garcia-Donas J, Huddart R, Burgess E, et al. Ertufitinib in Locally Advanced or Metastatic Urothelial Carcinoma. *N Engl J Med* (2019) 381(4):338–48. doi: 10.1056/NEJMoa1817323
 39. Mangsbo SM, Ninalga C, Essand M, Loskog A, Totterman TH. CpG Therapy Is Superior to BCG in an Orthotopic Bladder Cancer Model and Generates CD4+ T-Cell Immunity. *J Immunother* (2008) 31(1):34–42. doi: 10.1097/CJI.0b013e3181587d29

Conflict of Interest: The authors declare that the research was conducted in the absence of any commercial or financial relationships that could be construed as a potential conflict of interest.

Publisher's Note: All claims expressed in this article are solely those of the authors and do not necessarily represent those of their affiliated organizations, or those of the publisher, the editors and the reviewers. Any product that may be evaluated in this article, or claim that may be made by its manufacturer, is not guaranteed or endorsed by the publisher.

Copyright © 2022 Zuppone, Assalini, Minici, Botrugno, Curnis, Degano, Corti, Montorsi, Salonia and Vago. This is an open-access article distributed under the terms of the Creative Commons Attribution License (CC BY). The use, distribution or reproduction in other forums is permitted, provided the original author(s) and the copyright owner(s) are credited and that the original publication in this journal is cited, in accordance with accepted academic practice. No use, distribution or reproduction is permitted which does not comply with these terms.



Anlotinib for the Treatment of Multiple Recurrent Lumbar and Sacral Cord Hemangioblastomas: A Case Report

Nan Jin^{1,2†}, Chunxiao Sun^{1†}, Yijia Hua¹, Xinyu Wu¹, Wei Li^{1*} and Yongmei Yin^{1,3*}

¹ Department of Oncology, The First Affiliated Hospital of Nanjing Medical University, Nanjing, China, ² The First Clinical College of Nanjing Medical University, Nanjing, China, ³ Jiangsu Key Lab of Cancer Biomarkers, Prevention and Treatment, Collaborative Innovation Center for Personalized Cancer Medicine, Nanjing Medical University, Nanjing, China

OPEN ACCESS

Edited by:

Rajkumar S. Kalra,
Okinawa Institute of Science and
Technology Graduate University,
Japan

Reviewed by:

Ujjawal Sharma,
Maharishi Markandeshwar University,
Mullana, India
Alok Kumar,
Kyoto University, Japan

*Correspondence:

Yongmei Yin
ymyin@njmu.edu.cn
Wei Li
real.lw@163.com

[†]These authors have contributed
equally to this work

Specialty section:

This article was submitted to
Pharmacology of Anti-Cancer Drugs,
a section of the journal
Frontiers in Oncology

Received: 21 January 2022

Accepted: 30 March 2022

Published: 27 April 2022

Citation:

Jin N, Sun C, Hua Y,
Wu X, Li W and Yin Y (2022)
Anlotinib for the Treatment of
Multiple Recurrent Lumbar and
Sacral Cord Hemangioblastomas:
A Case Report.
Front. Oncol. 12:859157.
doi: 10.3389/fonc.2022.859157

Background: Hemangioblastoma (HB) is a rare and highly vascularized tumor that originates from the central nervous system as well as other part of the body. They can appear sporadically or as part of von Hippel–Lindau (VHL) disease, a rare hereditary cancer syndrome. Although surgery can cure the majority of HBs, the disease shows a treatment-refractory challenge upon recurrence. HBs express a high amount of vascular endothelial growth factor (VEGF) which is responsible for angiogenesis and subsequently tumor progression. Anti-angiogenic treatment like bevacizumab has showed effect on HB, so we hypothesized that anlotinib could trigger HB regression via its inhibitory effect on VEGF.

Case Presentation: We will share our experience in treating a 62-year-old woman with multiple recurrent lumbar and sacral cord HBs. She was treated with anlotinib (8mg qd d1-14, q3w) for three months and her follow up radiological examination demonstrated marked tumor regression which was evaluated as having partial response pursuant to RECIST 1.1 system. She is currently still receiving treatment of anlotinib orally and the lesions continuously reduced.

Conclusion: We have reported that anlotinib can cause significant radiographic response in a patient with multiple recurrent lumbar and sacral cord HBs for the first time. This might enable a novel therapeutic approach for patients with multiple recurrent HB or those with multiple lesions such as in VHL disease which are difficult to resect surgically.

Keywords: anlotinib, hemangioblastoma, anti-angiogenesis, case report, tyrosine kinase inhibitor (TKI)

INTRODUCTION

Hemangioblastoma (HB) is a rare and highly vascularized tumor that originates from the central nervous system (CNS) as well as other part of the body. HBs located in the CNS commonly arise in the brain and less commonly in the spinal cord. Most of HB lesions are sporadic and approximately account for 75% of cases, whereas in 25% of patients, they are manifestations of von Hippel–Lindau

(VHL) disease and are often multifocal (1). HBs can result in significant neurological dysfunction by mass effect or hemorrhage in spite of their slow-growing benign nature. These tumors express a high amount of vascular endothelial growth factor (VEGF) which drives angiogenesis, a process that explains their highly vascular nature (2). The traditional treatment for HBs within accessible locations is surgical resection (3), leading to a cure typically. Nonetheless, up to 25% of HB patients have recurrence after surgical extirpation on the basis of past statistics (4, 5). For patients with recurrent HB, repeated surgical procedures are less recommended and surgery should be reserved as a salvage modality. Radiation therapy (RT) is performed following surgery for incompletely resected or recurrent lesions. However, it increases risks of radiation necrosis owing to overlapped irradiation zones (6). To date, targeted treatments and chemotherapy play a limited role in recurrent HB (7).

Given that HBs express high levels of VEGF, it appeals to be a promising target to block angiogenesis for controlling tumor proliferation conceptually. Anti-angiogenic agents like bevacizumab have showed significant clinical benefit on a 51-year-old man with a surgically unresectable cervical cord HB (8). Anlotinib, a novel orally administered tyrosine kinase inhibitor (TKI), is characterized as a potent and highly selectively vascular endothelial growth factor receptor (VEGFR)-2 inhibitor (9). Therefore, recurrent HB patients could derive benefit from anlotinib logically. Anlotinib has been reported to inhibit pathological ocular neovascularization (10), improve the life quality of patients with advanced non-small cell lung cancer (NSCLC) (11) and so on. Furthermore, previous literatures have demonstrated that anlotinib possesses additional advantages, including well bioavailability and tolerable safety profiles (12). But as far as we know, there are no published reports regarding the administration of this agent in HB. In this report, we will show tumor regression and meaningful clinical improvement

responding to anlotinib in a patient with multiple recurrent lumbar and sacral cord HB.

CASE PRESENTATION

A 62-year-old woman came to our department for a consultation due to multiple recurrent HBs. In May 2016, she presented to our neurosurgery with a half-year history of persistent lower back pain that was radiating to left leg. She was initially diagnosed with lumbar disk herniation and received symptomatic treatment, but the clinical condition continued to deteriorate. The magnetic resonance imaging (MRI) showed a space-occupying lesion at L1-L2 (**Figure 1A**). Then she underwent a complete surgical resection under general anesthesia and symptoms were significantly alleviated after the operation. Histology confirmed the diagnosis of HB and immunohistochemical results showed EMA (-), S-100 (-), GFAP (-), Vimentin (++) and Ki-67 (10-15%). The patient has no similar family history and no other lesions characteristic of VHL disease were found, so she was diagnosed as a sporadic HB case. A MRI was done every six months postoperatively to follow up.

In July 2019, the patient was admitted to our clinic again due to a one-year history of left leg pain which progressively worsened over the last three months with difficulty in urination and defecation. She underwent a MRI of the lumbar spine which showed a space-occupying lesion at S1 (**Figure 1B**), thus the tumor resection was performed again. Immunohistochemical results showed EMA (-), S-100 (-), GFAP (-) and Ki-67 (sporadic +). Recurrent HB was diagnosed according to pathological results and medical history. Postoperatively, her pain significantly relieved. In June 2020, MRI indicated tumor recurrence at L2 and S1-S2 (**Figure 1C**). The patient did not receive any treatment due to free of symptoms in the next one year.

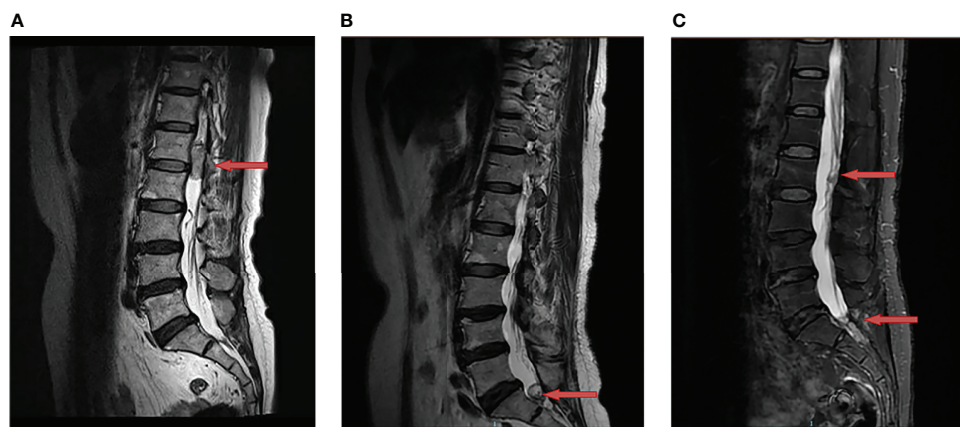


FIGURE 1 | Changes of hemangioblastoma of the magnetic resonance imaging (MRI). **(A)** A space-occupying lesion at L1-L2 was detected (red arrow) in May 2016; **(B)** A recurrent site at S1 was observed (red arrow) after the first surgery in July 2019; **(C)** Two recurrent sites at L2 and S1-S2 were discovered (red arrow) after the second surgery in June 2020.

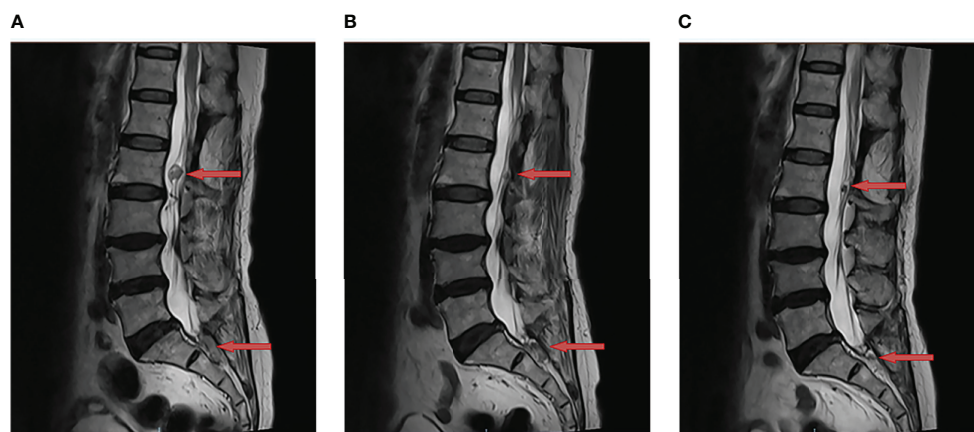


FIGURE 2 | Anlotinib resulted in tumor regression of multiple recurrent lumbar and sacral cord hemangioblastoma. This is a sagittal magnetic resonance imaging (MRI) view of lumbar and sacral spine; **(A)** The two lesions at L2 and S1-S2 were observed to have increased in size (red arrow) in June 2021; **(B)** The MRI demonstrated tumor regression (red arrow) following one month of anlotinib in July 2021; **(C)** The MRI showed further regression in the enhancing tumor (red arrow) following three months of anlotinib in Sep 2021.

In June 2021, tumor progression was observed. the MRI showed that the diameter of two lesions at L2 and S1-S2 increased to 1.8cm and 2.3cm respectively (**Figure 2A**). Despite the fact that the patient was symptom-free, she came to our department for further treatment. Anlotinib was begun after obtaining informed consent. Then, anlotinib (8mg qd d1-14, q3w) was orally administrated. There was a considerable improvement in the T2 signal change around the enhancing component, as well as a decrease in the size on the MRI from 1.8cm to 1.0cm at L2 and from 2.3cm to 2.0cm at S1-S2 after use of one month (**Figure 2B**). To date of Sep 22, 2021, the MRI demonstrated further decrease in the dimensions of residual lesions (**Figure 2C**). The patient was in good condition, evaluated as having partial response in accordance with the RECIST 1.1 system. In addition, apart from hypertension (grade I), no other adverse side effects of anlotinib such as hemorrhage, thrombopenia, fatigue and hypertriglyceridemia were observed in the patient. All of these adverse effects were evaluated pursuant to the Common Terminology Criteria for Adverse Events (CTCAE) Version 5.0. The treatment timeline of

the patient is depicted in **Figure 3**. The patient has given her consent for the case report to be published.

DISCUSSION

HBs are benign and exceedingly vascular CNS tumors. They account for approximately 1.5% to 2.5% of all intracranial tumors, the majority of which are encountered in the cerebellar hemispheres (13). They occur both as sporadic disease and in association with VHL disease particularly in spinal manifestations (14). Sporadic HB in the absence of VHL disease is often curable with surgical resection, whereas there are still many patients suffering from recurrent or multifocal disease that is incompletely resected, normally treated with adjuvant RT (15). Despite their benign nature, repeated surgeries caused by a high recurrence rate are often of limited value and increase the clinical risk especially for patients with multiple recurrent lesions. There is no standard treatment beyond surgery for these types of HB particularly outside of CNS. Furthermore,

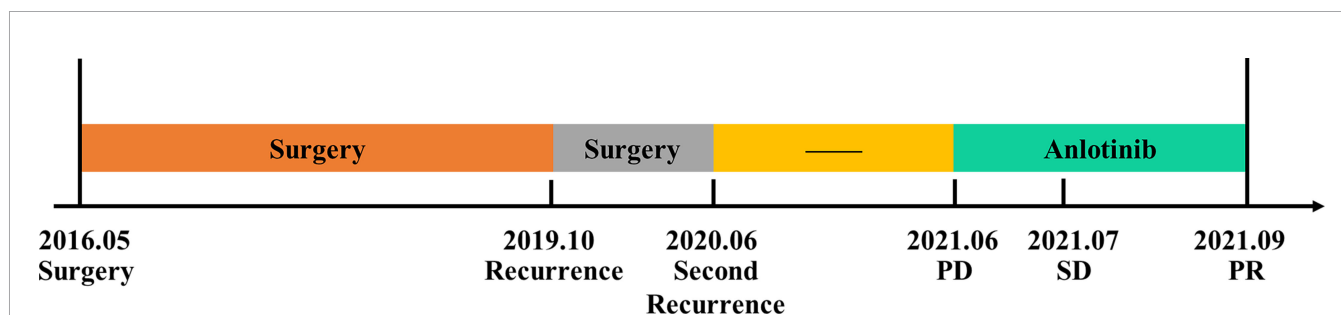


FIGURE 3 | The treatment timeline of the patient with multiple recurrent hemangioblastoma.

the effectiveness of RT diminishes over time. Swelling after RT could also lead to neurologic decline and significant morbidity. Additionally, it has been reported that radiation necrosis, a complication following RT, can lead to poor outcomes for patients (6, 16). Therefore, developing new therapeutic options or drugs is of great significance for treatment of multiple recurrent HB.

The biological pathogenesis of HB is not completely elucidated; however, it has been reported that VHL disease is linked to a mutation of the VHL gene on chromosome 3p25-26 (17), leading to a stabilization of the hypoxia-inducible factor 1 α protein and thereby to an up-regulation of target genes, which coding for VEGF, erythropoietin, platelet-derived growth factor, and so on (18). Considering that VEGF and its receptors seem to play a momentous part in HB tumor cell proliferation, we anticipated that using a high-selective and potent VEGFR inhibitor to block the VEGF signaling would alter the growth pattern of HB and consequently cause tumor regression. So far, progressive HBs successfully treated with VEGF-based anti-angiogenic therapy, such as monoclonal antibody bevacizumab, have been published (8, 19). In a single arm, phase II study with the VEGFR inhibitor sunitinib in patients with VHL disease, 9/11 patients with HB were evaluated as stable disease, whereas partial response was observed in 6/18 individuals with other lesions associated with VHL syndrome (20). Meanwhile, 1 open-label phase II study with sunitinib malate in patients who have VHL disease has reported partial response in 6/18 lesions (ClinicalTrials.gov Identifier: NCT00330564). Hence Anti-angiogenic therapy seems to be an attractive alternative for patients with multiple recurrent HB.

Anlotinib is a small molecular TKI inhibiting tumor angiogenesis and proliferation signaling. In clinical applications, it has exhibited satisfactory efficacy against diverse solid tumors, containing NSCLC, breast cancer, soft-tissue sarcoma, renal cell cancer and so on. Anlotinib has been approved by the Chinese Food and Drug Administration for third-line treatment for advanced NSCLC patients. Also, anlotinib has exhibited inspiring efficacy as well as low toxicity in heavily pre-treated HER2-negative metastatic breast cancer (21).

In this case report, we first delineate the significant effectiveness of anlotinib in the patient with multiple recurrent HB. Moreover, anlotinib showed few adverse effects, ensuring their life quality while increasing the treatment efficacy. The clinical benefit is hard to explain but it could be attributed to a reduction in perfusion and edema, as well as improved perfusion of adjacent brain parenchyma. Possible mechanisms are the known decreases in capillary density, microvascular flow, and blood vessel permeability in response to anlotinib. We believe that anlotinib merits further investigation in order to better define its role in patients with this challenging disease. In addition, more clinical trials are still needed to determine whether the effect of anlotinib on multiple recurrent HB will translate into improvements in disease control, including prolonged progression-free survival (PFS) and overall survival (OS).

CONCLUSION

No reports were found in a Medline search (keywords: anlotinib; hemangioblastoma) that showed HB may be in response to anlotinib favorably. As far as we are aware, our case is the first report that demonstrates anlotinib induces a positive radiographic response when used to treat multiple recurrent lumbar and sacral cord HBs. The mechanism underlying this remains scanty. Additionally, the effect of anlotinib in treating multiple recurrent HB is yet to be determined, including whether it will improve PFS and OS, but we believe this case report will provide indication for future research.

DATA AVAILABILITY STATEMENT

The original contributions presented in the study are included in the article/supplementary material. Further inquiries can be directed to the corresponding authors.

ETHICS STATEMENT

Ethical review and approval was not required for the study on human participants in accordance with the local legislation and institutional requirements. The patients/participants provided their written informed consent to participate in this study. Written informed consent was obtained from the individual(s) for the publication of any potentially identifiable images or data included in this article.

AUTHOR CONTRIBUTIONS

NJ and CS performed the data acquisition and manuscript drafting. YH and XW completed the radiological images analysis. YY and WL reviewed the manuscript. All authors contributed to the article and approved the submitted version.

FUNDING

This case report was financially supported by the National Key Research and Development Program of China (ZDZX2017ZL-01), High-level Innovation Team of Nanjing Medical University (JX102GSP201727), Wu Jieping Foundation (320.6750.17006), Key Medical Talents (ZDRCA2016023), 333 Project of Jiangsu Province (BRA2017534 and BRA2015470), The Collaborative Innovation Center for Tumor Individualization Focuses on Open Topics (JX21817902/008) and Project of China Key Research and Development Program Precision Medicine Research (2016YFC0905901).

REFERENCES

- Joseph J, Behari S, Gupta S, Bhaisora K, Gandhi A, Srivastava A, et al. Brain-Stem Hemangioblastomas: The Seemingly Innocuous Lesion in a Perilous Location. *Neurol India* (2018) 66(3):779–96. doi: 10.4103/0028-3886.232294
- Morii K, Tanaka R, Washiyama K, Kumanishi T, Kuwano R. Expression of Vascular Endothelial Growth Factor in Capillary Hemangioblastoma. *Biochem Biophys Res Commun* (1993) 194(2):749–55. doi: 10.1006/bbrc.1993.1885
- Koh ES, Nichol A, Millar BA, Menard C, Pond G, Laperriere NJ. Role of Fractionated External Beam Radiotherapy in Hemangioblastoma of the Central Nervous System. *Int J Radiat Oncol Biol Phys* (2007) 69(5):1521–6. doi: 10.1016/j.ijrobp.2007.05.025
- de la Monte S, Horowitz S. Hemangioblastomas: Clinical and Histopathological Factors Correlated With Recurrence. *Neurosurgery* (1989) 25(5):695–08.
- Sakamoto N, Ishikawa E, Nakai Y, Akutsu H, Yamamoto T, Nakai K, et al. Preoperative Endovascular Embolization for Hemangioblastoma in the Posterior Fossa. *Neurologia Med Chir* (2012) 52(12):878–84. doi: 10.2176/nmc.52.878
- Moss JM, Choi CY, Adler JR Jr., Soltys SG, Gibbs IC, Chang SD. Stereotactic Radiosurgical Treatment of Cranial and Spinal Hemangioblastomas. *Neurosurgery* (2009) 65(1):79–85; discussion. doi: 10.1227/01.NEU.0000348015.51685.D2
- Dowell JE, Shen Y, Harford WV, Lai WS. Case 1. Melanoma in African Americans. *J Clin Oncol* (2005) 23(15):3622–4. doi: 10.1200/JCO.2005.04.132
- Omar AI. Bevacizumab for the Treatment of Surgically Unresectable Cervical Cord Hemangioblastoma: A Case Report. *J Med Case Rep* (2012) 6:238. doi: 10.1186/1752-1947-6-238
- Shen G, Zheng F, Ren D, Du F, Dong Q, Wang Z, et al. Anlotinib: A Novel Multi-Targeting Tyrosine Kinase Inhibitor in Clinical Development. *J Hematol Oncol* (2018) 11(1):120. doi: 10.1186/s13045-018-0664-7
- Lu C, Zhang Q, Zhang H, Li X, Jiang Q, Yao J. A Small Molecular Multi-Targeting Tyrosine Kinase Inhibitor, Anlotinib, Inhibits Pathological Ocular Neovascularization. *BioMed Pharmacother* (2021) 138:111493. doi: 10.1016/j.biopha.2021.111493
- Wu D, Nie J, Dai L, Hu W, Zhang J, Chen X, et al. Salvage Treatment With Anlotinib for Advanced Non-Small Cell Lung Cancer. *Thorac Cancer* (2019) 10(7):1590–6. doi: 10.1111/1759-7714.13120
- Sun Y, Niu W, Du F, Du C, Li S, Wang J, et al. Safety, Pharmacokinetics, and Antitumor Properties of Anlotinib, an Oral Multi-Target Tyrosine Kinase Inhibitor, in Patients With Advanced Refractory Solid Tumors. *J Hematol Oncol* (2016) 9(1):105. doi: 10.1186/s13045-016-0332-8
- Hussein MR. Central Nervous System Capillary Haemangioblastoma: The Pathologist's Viewpoint. *Int J Exp Pathol* (2007) 88(5):311–24. doi: 10.1111/j.1365-2613.2007.00535.x
- Takai K, Taniguchi M, Takahashi H, Usui M, Saito N. Comparative Analysis of Spinal Hemangioblastomas in Sporadic Disease and Von Hippel-Lindau Syndrome. *Neurol Med Chir (Tokyo)* (2010) 50(7):560–7. doi: 10.2176/nmc.50.560
- Na J, Kim H, Eoh W, Kim J, Kim J, Kim E. Spinal Cord Hemangioblastoma: Diagnosis and Clinical Outcome After Surgical Treatment. *J Korean Neurosurg Soc* (2007) 42(6):436–40. doi: 10.3340/jkns.2007.42.6.436
- Asthagiri AR, Mehta GU, Zach L, Li X, Butman JA, Camphausen KA, et al. Prospective Evaluation of Radiosurgery for Hemangioblastomas in Von Hippel-Lindau Disease. *Neuro Oncol* (2010) 12(1): 80–6. doi: 10.1093/neuonc/nop018
- Latif F, Tory K, Gnarr J, Yao M, Duh FM, Orcutt ML, et al. Identification of the Von Hippel-Lindau Disease Tumor Suppressor Gene. *Science* (1993) 260(5112):1317–20. doi: 10.1126/science.8493574
- Ghosh G, Subramanian IV, Adhikari N, Zhang X, Joshi HP, Basi D, et al. Hypoxia-Induced microRNA-424 Expression in Human Endothelial Cells Regulates HIF-Alpha Isoforms and Promotes Angiogenesis. *J Clin Invest* (2010) 120(11):4141–54. doi: 10.1172/JCI42980
- Riklin C, Seystahl K, Hofer S, Happold C, Winterhalder R, Weller M. Antiangiogenic Treatment for Multiple CNS Hemangioblastomas. *Onkologie* (2012) 35(7-8):443–5. doi: 10.1159/000341075
- Jonasch E, McCutcheon IE, Waguespack SG, Wen S, Davis DW, Smith LA, et al. Pilot Trial of Sunitinib Therapy in Patients With Von Hippel-Lindau Disease. *Ann Oncol* (2011) 22(12):2661–6. doi: 10.1093/annonc/mdr011
- Hu N, Si Y, Yue J, Sun T, Wang X, Jia Z, et al. Anlotinib has Good Efficacy and Low Toxicity: A Phase II Study of Anlotinib in Pre-Treated HER-2 Negative Metastatic Breast Cancer. *Cancer Biol Med* (2021) 18(3):849–59. doi: 10.20892/j.issn.2095-3941.2020.0463

Conflict of Interest: The authors declare that the research was conducted in the absence of any commercial or financial relationships that could be construed as a potential conflict of interest.

Publisher's Note: All claims expressed in this article are solely those of the authors and do not necessarily represent those of their affiliated organizations, or those of the publisher, the editors and the reviewers. Any product that may be evaluated in this article, or claim that may be made by its manufacturer, is not guaranteed or endorsed by the publisher.

Copyright © 2022 Jin, Sun, Hua, Wu, Li and Yin. This is an open-access article distributed under the terms of the Creative Commons Attribution License (CC BY). The use, distribution or reproduction in other forums is permitted, provided the original author(s) and the copyright owner(s) are credited and that the original publication in this journal is cited, in accordance with accepted academic practice. No use, distribution or reproduction is permitted which does not comply with these terms.



Honokiol Induces Ferroptosis by Upregulating HMOX1 in Acute Myeloid Leukemia Cells

Xingrong Lai^{1,2†}, Yanhua Sun^{3†}, Xuedi Zhang^{1,2}, Dan Wang², Jialing Wang^{1,2}, Haihua Wang^{1,4}, Yao Zhao^{1,4}, Xinling Liu^{1,4}, Xin Xu^{1,5}, Haoran Song⁶, Wenjia Ping⁶, Yanli Sun^{1,6*} and Zhenbo Hu^{1,4*}

¹Laboratory for Stem Cell and Regenerative Medicine, Affiliated Hospital of Weifang Medical University, Weifang, China, ²Weifang Medical University, Weifang, China, ³Department of Hematology, Weifang People's Hospital, Weifang, China, ⁴Department of Hematology, Affiliated Hospital of Weifang Medical University, Weifang, China, ⁵School of Life Science and Technology, Weifang Medical University, Weifang, China, ⁶Department of Laboratory Medicine, Weifang Medical University, Weifang, China

OPEN ACCESS

Edited by:

Sandeep Singh,
Central University of Punjab, India

Reviewed by:

Saeed Mohammadi,
Golestan University of Medical
Sciences, Iran
Nilambra Dogra,
Panjab University, India

*Correspondence:

Zhenbo Hu
huzhenbo@wfmuc.edu.cn
Yanli Sun
sunyzbx@163.com

[†]These authors share first authorship

Specialty section:

This article was submitted to
Pharmacology of Anti-Cancer Drugs,
a section of the journal
Frontiers in Pharmacology

Received: 16 March 2022

Accepted: 26 April 2022

Published: 11 May 2022

Citation:

Lai X, Sun Y, Zhang X, Wang D,
Wang J, Wang H, Zhao Y, Liu X, Xu X,
Song H, Ping W, Sun Y and Hu Z
(2022) Honokiol Induces Ferroptosis
by Upregulating HMOX1 in Acute
Myeloid Leukemia Cells.
Front. Pharmacol. 13:897791.
doi: 10.3389/fphar.2022.897791

Acute myeloid leukemia (AML) is one of the malignant hematological cancers with high mortality. Finding a more effective and readily available treatment is of the utmost importance. Here, we aimed to identify the anti-leukemia effect of a natural small molecule compound honokiol on a panel of AML cell lines, including THP-1, U-937, and SKM-1, and explored honokiol's potential biological pathways and mechanisms. The results showed that honokiol decreased the viability of the targeted AML cells, induced their cell cycle arrest at G0/G1 phase, and inhibited their colony-formation capacity. Honokiol also triggers a noncanonical ferroptosis pathway in THP-1 and U-937 cells by upregulating the level of intracellular lipid peroxide and HMOX1 significantly. Subsequent studies verified that HMOX1 was a critical target in honokiol-induced ferroptosis. These results reveal that honokiol is an effective anti-leukemia agent in AML cell lines and may be a potential ferroptosis activator in AML.

Keywords: honokiol, AML, ferroptosis, heme oxygenase (HO)-1, lipid peroxidation

INTRODUCTION

Acute myeloid leukemia (AML) with complex karyotypes accounts for 10–14% of all AML patients, and the overall survival rate is less than 20% (Daneshbod et al., 2019; Mrózek et al., 2019). Until now, most AML patients have been treated by chemotherapeutic regimens. While chemotherapy kills leukemia cells, it often results in serious side effects to the patients and drug resistance of the leukemia cells. Although hematopoietic stem cell transplantation can alleviate or even cure AML with complex karyotype, its limited source restricts its wide application in clinical settings (Fenwarth et al., 2021). Therefore, finding a more effective and readily available treatment for AML is of the utmost importance.

Several components with a deep history in traditional Chinese medicine have been proven effective in treating AML. For example, arsenic trioxide combined with all-trans retinoic acid can achieve a complete response in 90–100% of acute promyelocytic leukemia (APL) patients, with an overall survival rate of 86–97% (Lo-Coco et al., 2013; Ni et al., 2019). In addition, Homoharringtonine (HHT) can be a reliable choice for patients with AML, especially for newly diagnosed or patients younger than 60. Additionally, the use of HHT can reduce relapse in elderly intolerant patients (Mi et al., 2021).

Several previous studies proved that lipid metabolism was reprogrammed and lipid synthesis was significantly up-regulated in hematological malignancy (Stuani et al., 2018; Humbert et al., 2021; Ito

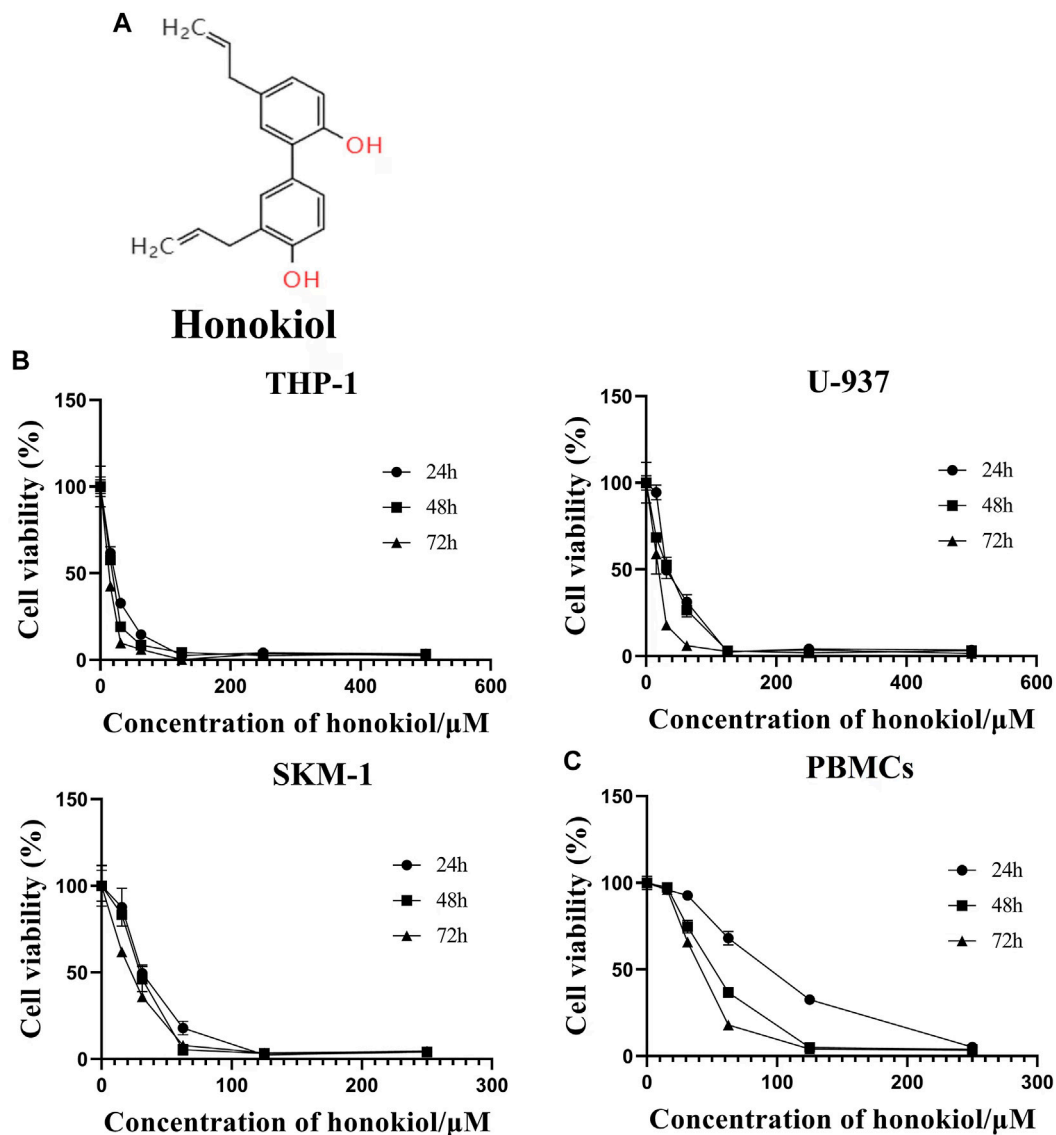


FIGURE 1 | Effects of honokiol on the viability and apoptosis of THP-1, U-937, and SKM-1 cells. **(A)** Chemical structure of honokiol. **(B)** Effects of honokiol on the viability of THP-1, U-937, and SKM-1 cells. Cells were incubated with different concentrations of honokiol for 24, 48, 72 h, then CCK-8 was added, and the absorbance at 450 nm was determined. The points represent mean \pm SEM from three independent experiments. **(C)** Cytotoxic effect of honokiol on human PBMCs. PBMCs were incubated with different concentrations of honokiol for 24, 48, 72 h, then CCK-8 reagent was added, and the absorbance at 450 nm was determined. The points represent mean \pm SEM from three independent experiments.

et al., 2021; Tcheng et al., 2021). Therefore, it may be an effective strategy to treat AML through interfering fatty acid and lipid metabolism.

Honokiol (**Figure 1A**), from the bark of the magnolia (Fang et al., 2015), is a biphenolic phytochemical that possesses potent antioxidant, anti-inflammatory, antiangiogenic, antimicrobial, and anti-cancer activities (Banik et al., 2019). In addition, it displayed diverse anti-cancer efficacy in different tumors, including but not limited to prostate cancer, gastric cancer, oral cancer, glioblastoma, skin cancer, ovarian cancer, osteosarcoma, lung cancer, leukemia, liver cancer, and colon cancer (Arora et al., 2012).

Till now, a variety of signaling pathways have been studied to elucidate the anti-cancer effect of honokiol, including apoptosis (Li et al., 2015), EGFR signaling pathway (Leeman-Neill et al., 2010), STAT3 activation cascade pathway (Rajendran et al., 2012), mTOR pathway (Liu et al., 2008), NF- κ B signaling pathway (Dikalov et al., 2008), and autophagy pathway (Muniraj et al., 2020). Moreover, honokiol has been proven to play a vital role in modulating fatty acid oxidation in normal cells (Zhu et al., 2018; Li et al., 2020a), whether this mechanism is involved in its anti-leukemia effect has not been determined yet. Furthermore, no study has yet to determine if honokiol can induce ferroptosis in leukemia cells.

Ferroptosis, discovered in 2012 (Dixon et al., 2012), is a ROS-dependent form of lipid peroxidation-induced cell death, accompanied by iron accumulation (Tang et al., 2021a). Generally, there are canonical and noncanonical mechanisms in ferroptosis: the former is induced by dropping the protein level and activity of glutathione peroxidase 4 (GPX4), while the latter is induced by increasing the expression and activation of heme oxygenase 1 (HMOX1) (Tang et al., 2021a).

This study aimed to evaluate the anti-leukemia effect and mechanism of honokiol in the AML cell lines with complex karyotypes. We found that honokiol can induce ferroptosis of AML cells with complex karyotypes by upregulating the expression of HMOX1.

MATERIALS AND METHODS

Chemicals and Equipment

Honokiol purchased from MedChemExpress was dissolved in DMSO and stored at -20°C . RPMI-1640 medium, FBS, penicillin 5,000 U/ml, streptomycin 5,000 mg/ml were purchased from GIBCO (GIBCO, United States). The Propidium iodide (PI)/RNase buffer and the Fluorescein Isothiocyanate (FITC) Annexin V apoptosis detection kit were purchased from BD Biosciences (San Jose, CA, United States). HMOX1 inhibitor ZnPP (Zinc Protoporphyrin Zn(II)-protoporphyrin IX) and ferroptosis inhibitor Ferrostatin -1 were purchased from Sigma-Aldrich LLC (Shanghai, China). SLC7A11/xCT (AB175186), HO-1 (AB189491), and GPX4 were purchased from Abcam (Cambridge, MA, United States). PrimerScript RT kit and SYBR Premix Ex Taq Kit were purchased from TAKARA Bio (Otsu, Japan). Flow cytometry analysis was performed using the CytoFLEX V0-B3-R2 Flow Cytometer (Beckman Coulter, United States). PCR amplification was performed using the Applied Bio 7,500 Fast Real-Time PCR System (Thermo Fisher Scientific, Waltham, MA, United States).

Cell Lines and Cell Culture

AML cell lines THP-1, U-937, and SKM-1, all monocytes origin with complex karyotypes, obtained from DSMZ (DSMZ, Brunswick, Germany, <https://www.dsmz.de/>) were cultured in RPMI 1640 medium containing 10% or 20% FBS and 1% penicillin/streptomycin at 37°C and 5% CO_2 .

Cell Viability Assay

CCK-8 assay was used to detect cell viability. THP-1, U-937, and SKM-1 cells were seeded into 96-well plates with 6×10^3 cells per well. Simultaneously, the cytotoxicity of honokiol for the peripheral blood mononuclear cells (PBMCs) was also evaluated. Six hours later, the specified compounds were added and cultured for 24, 48, 72 h. Four hours before ending the incubation, 10 μl of CCK-8 was added to each well and incubated for 4 h. The total volume in each well was 100 μl . The absorbance was measured at 450 nm using a microplate reader (Thermo Fisher Scientific, United States).

Cell-Cycle Analysis

THP-1, U-937, and SKM-1 cells in their logarithmic growth phases were added to a 24-well plate with 2×10^5 /well and incubated with different concentrations of honokiol for 24 h before cells were collected. The cells were fixed using 70% pre-cold ethanol overnight and then stained with 400 μl PI (50 $\mu\text{g}/\text{ml}$) and 100 μl RNase A (100 $\mu\text{g}/\text{ml}$) at room temperature for 15 min in the dark. Flow cytometry analysis was performed using CytoFLEX V0-B3-R2 Flow Cytometer (Beckman Coulter, United States) to determine the percentage of cells at every phase of the cell cycle.

Cell Apoptosis Assay

THP-1, U-937, and SKM-1 cells were incubated with different concentrations of honokiol, respectively. After 24 h, the cells were collected, washed twice using the binding buffer, and incubated with FITC-labeled Annexin-V and PI (BD Biosciences) at room temperature in the dark for 30 min. Cell apoptosis was determined by flow cytometry.

Colony Formation Assay

5×10^3 THP-1, U-937, and SKM-1 cells were mixed with the indicated concentration of honokiol in 500 μL methylcellulose medium (MethoCultTM H4100, Stemcell Technologies) containing 10% fetal bovine serum, 10% 5,637 cell cultural supernatant, and 1% penicillin/streptomycin, then added to 24-well plates, 500 $\mu\text{l}/\text{well}$. After 14 days of incubation, the total number of cell colonies consisting of at least 50 cells was counted using an inverted microscope. To determine any toxicity of honokiol towards normal cells, normal hematopoietic stem/progenitor cells were isolated and enhanced from cord blood of health donors with informed consent by gradient centrifugation. 1×10^3 enhanced hematopoietic stem/progenitor cells were incubated with specified concentration of honokiol (25, 35 and 45 μM) in 100 μl of methyl-cellulose medium per well of 96-well plate (MethoCult H4434, STEMCELL Technologies, Victoria, Canada) containing cytokines and 10% FBS. The groups without honokiol treatment and with DMSO were used as controls. After about 14 days, the total colony formation numbers of containing all the BFU-E-, CFU-GM-, and CFU-GEMM- derived colonies in different groups were counted under an inverted microscope.

Detection of Lipid Peroxidation

The liperfluo (Dojindo) was used to detect lipid peroxidation per the manufacturer's protocol. THP-1, U-937, and SKM-1 cells (5×10^5 cells/well) were seeded in 24-well plates. Six hours later, different concentrations of honokiol were added to these cells. After 12 h incubation, cells were washed with HBSS twice and incubated with 1 μM liperfluo reagent at 37°C , 5% CO_2 for 30 min. Following that, the cells were washed with HBSS twice. The content of intracellular lipid peroxide was detected by flow cytometry (Beckman Coulter, United States).

mRNA Sequencing

mRNA sequencing was performed on THP-1 and U-937 cell lines (Hangzhou Lianchuan Biotechnology Co., LTD., Zhejiang,

China). After incubation with honokiol for 24 h, the cells were collected, and RNA was extracted from the cell samples. The quality of extracted RNA was evaluated. Total 2 µg RNA was purified and used to construct the cDNA libraries. Sequencing was performed using Illumina HiSeq 4,000 platform. The gene expressions were calculated using fragments per kilobase of exon per million fragments mapped (FPKM) values. False discovery rate (FDR) was used to identify the *p*-value threshold and analyze the differences' significance. Significantly differentially expressed genes (DEGs) were set with a standard [the adjusted *p*-value < 0.05 and the absolute value of log2 FC.

(fold change) > 1]. Enrichment analysis of the KEGG pathway of DEGs was performed using R language. The enriched KEGG pathway was statistically significant, with the adjusted *p*-value < 0.05.

Real-Time Quantitative PCR

THP-1, U-937, and SKM-1 cells were incubated with a specific concentration of honokiol. After a certain interval (6 and 12 h), the cells were collected, and total RNA was extracted from the TRIzol samples. The cDNA was reversely transcribed from 1 µg total RNA. Based on the SYBR Green method, HMOX1, SLC7A11, and GPX4 were quantified by RT-qPCR using Applied Biosystems 7,500 Fast Real-Time PCR system. The relative quantification results of gene expression were calculated using the $2^{-\Delta\Delta C_t}$ method. The primers used are as follows: GAPDH-Forward: 5'-TGGGTGTGAACCATGAGA AGT-3' and GAPDH-Reverse: 5'-TGAGTCCTTCCACGATAC CAA-3'; HMOX1-Forward: 5'-AGTTCAAGCAGCTCTACC GC-3' and HMOX1-Reverse: 5'-GCAACTCCTCAAAGAGCT GGAT-3'; SLC7A11-Forward: 5'-TCTCCAAAGGAGGTTACC TGC-3' and SLC7A11-Reverse: 5'-AGACTCCCCTCAGTAAAG TGAC-3'; GPX4-Forward: 5'-GAGGCAAGACCGAAGTAA ACTAC-3' and GPX4-Reverse: 5'-CCGAAGTGGTTACAC GGGAA-3'.

Western Blotting

Equal amounts (about 40 µg) of cell lysates from samples were loaded to the SDS-PAGE gel, and electrophoresis was performed. After electrophoresis, the proteins were transferred from 12% SDS-PAGE gels onto 0.45 µm PVDF (polyvinylidene fluoride) membranes. First, they were blocked by 5% skim milk in TBST (Tris-buffered saline with 0.1% Tween-20). Then, they were incubated with GAPDH, HMOX1, SLC7A11, or GPX4 antibodies overnight. After that, the membranes were immersed in the HRP-labeled goat anti-rabbit antibody solution at 37°C for 1 h, followed by enhanced chemiluminescence reagent added. The specific protein bands were visualized using the Amersham Imager 600 (GE Healthcare Biosciences, Pittsburgh, PA, United States).

Statistical Analysis

All experiments were repeated at least three times, and the data were presented as the mean ± SEM. ANOVA analysis or *t*-test was used to determine the control and experimental groups' statistical significance. Data were considered statistically significant when *p* < 0.05.

TABLE 1 | IC50 Values of Honokiol on AML cell lines.

Cell lines	IC50 (µM) ± SD		
	24 h	48 h	72 h
THP-1	20.64 ± 2.94	17.64 ± 2.51	13.78 ± 0.86
U-937	36.49 ± 2.36	29.72 ± 2.05	17.85 ± 3.23
SKM-1	32.05 ± 1.3	28.71 ± 1.87	21.07 ± 2.86

IC50 values are calculated from cell proliferation assays. IC50 (µM) ± SD: the compound concentration at which cell survival was inhibited by 50% (means ± SD). Values are representative of three independent experiments, and each experiment was performed in triplicate.

RESULTS

Honokiol can Effectively Inhibit the Proliferation of Acute Myeloid Leukemia Cells

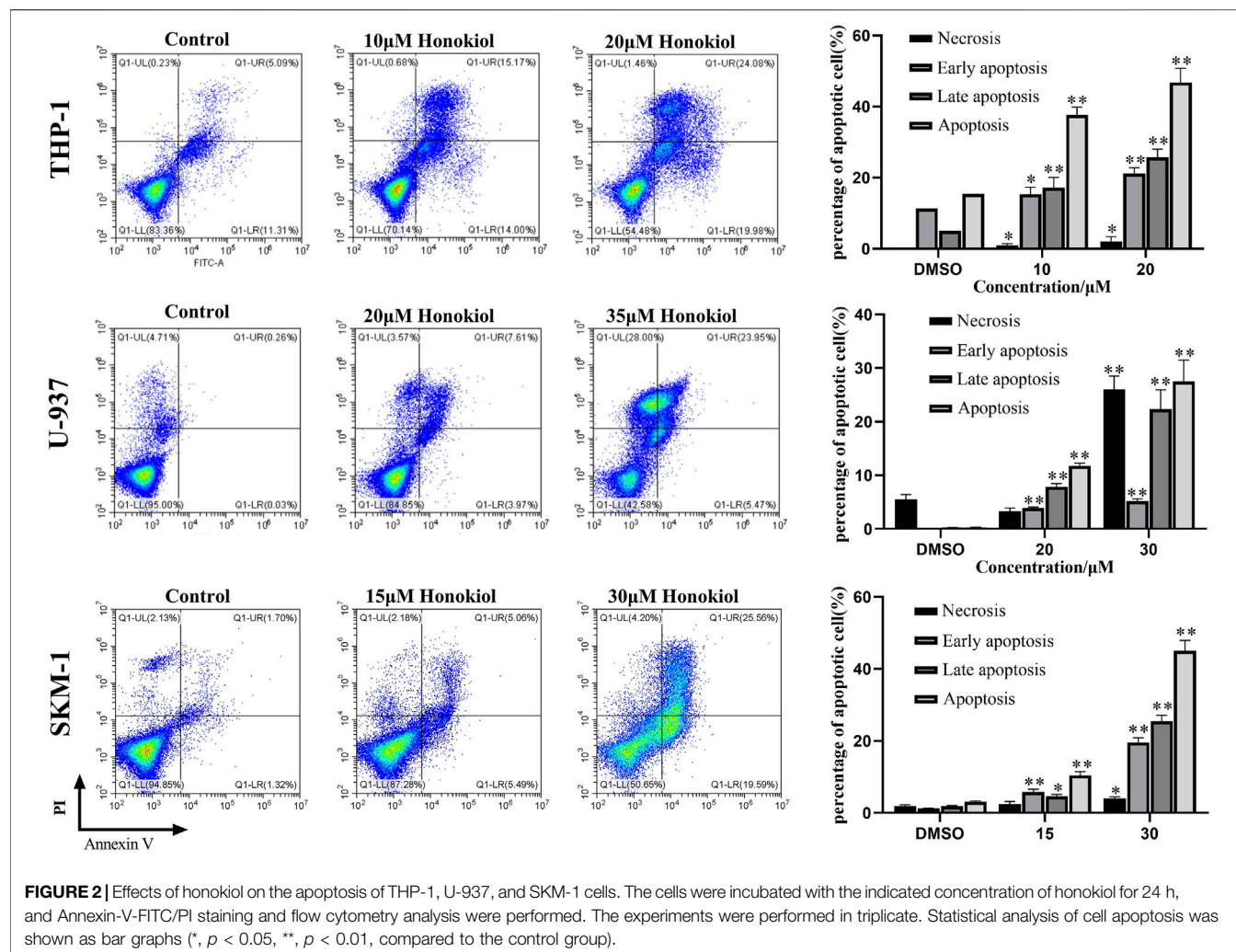
In order to evaluate if Honokiol can effectively inhibit the proliferation of acute myeloid leukemia cell, we used CCK-8 to detect the effects of honokiol on the viability of AML cells. As shown in **Figure 1B**, honokiol significantly reduced the cell viability of the three cell lines THP-1, U-937 and SKM-1. According to IC50 shown in **Table 1**, THP-1 cells were more sensitive than U-937 and SKM-1 cells to honokiol. As the incubation dose and time increased, IC50 of honokiol decreased, indicating the inhibition effect of honokiol on leukemia cells is dependent on dose and time in each cell line. However, no obvious cytotoxic effect was observed for the PBMCs treated with the dose of less than 50 µM of honokiol as shown in **Figure 1C**.

Honokiol Induced the Apoptosis of THP-1, U-937, and SKM-1 Cells

To explore whether the proliferation inhibition of honokiol is related to apoptosis, we incubated THP-1, U-937, and SKM-1 cells with different concentrations of honokiol for 24 h. As shown in **Figure 2**, the apoptosis rate of THP-1, U-937, and SKM-1 cells rose significantly as the concentration of honokiol increased. Moreover, THP-1 was more sensitive to honokiol compared to U-937 and SKM-1. For U-937 cells, the apoptotic cells occurred mainly at the late phase. In contrast, the apoptotic cells occurred mainly at the early and late phases in THP-1 and SKM-1 cells. The results reveal that the cell death mechanism induced by honokiol varies per cell line.

Honokiol Induced G0/G1 Phase Arrest of THP-1, U-937, and SKM-1 Cells

To evaluate the influence of honokiol on the cell cycle in THP-1, U-937, and SKM-1 cells, we treated these cell lines, each with a specific concentration of honokiol established by ID50 values for 24 h (THP-1: 20 µM; U-937: 35 µM; SKM-1: 30 µM). The results demonstrated that the percentage of AML cells in G0/G1 phase was significantly increased after honokiol treatment (**Figure 3**).



These findings suggest that honokiol suppresses the proliferation of AML cells by inducing AML cell-cycle arrest at G0/G1.

Honokiol inhibited the Leukemia Colony Formation of THP-1 and SKM-1 Cells

Next, we analyzed the effect of honokiol on the colony formation of THP-1, U-937, and SKM-1 cells. As seen from **Figure 4**, the number of THP-1 and SKM-1 cell colonies decreased significantly as honokiol concentration increased. Eventually, neither cell line could form colonies at a high enough honokiol concentration (THP-1: 25 μM; SKM-1: 35 μM). Furthermore, the U-937 cell line, whether treated with honokiol or not, could not form colonies in MethoCult™ H4100 with or without 10% 5,637 cell conditioning medium. From the results above, we conclude that honokiol can effectively inhibit the colony-formation ability of AML cells. To determine any toxicity of honokiol towards normal cells, normal hematopoietic stem/progenitor cells isolated from cord blood of healthy donors were used for colony formation assay. The result showed there were no significant differences in colony

formation numbers among these groups treated with or without honokiol, indicating honokiol had no obvious toxicity for normal hematopoietic stem/progenitor cells at the concentration of less than 45 μM (**Supplementary Figure S1**).

Honokiol Activated Ferroptosis Pathway in AML Cells

We performed transcriptome sequencing (mRNA sequencing) in THP-1 and U-937 cells treated with honokiol in order to explore the regulation mechanism of honokiol killing leukemia cells (**Supplementary Table S1**). As shown in **Figure 5A**, there were 2,447 and 1,991 differentially expressed genes in THP-1 and U-937 cells treated with honokiol, respectively. In addition, we further screened 685 genes that are common to both cell lines within this pool. These data revealed that the genes regulated by honokiol varied per cell line. The Kyoto Encyclopedia of Genes and Genomes (KEGG) analysis was performed for these differentially expressed genes in both cell lines. The top 20 signaling pathways were shown in **Figure 5B**, and there were four statistically significant common pathways: ferroptosis, regulation of lipolysis in adipocytes, PPAR

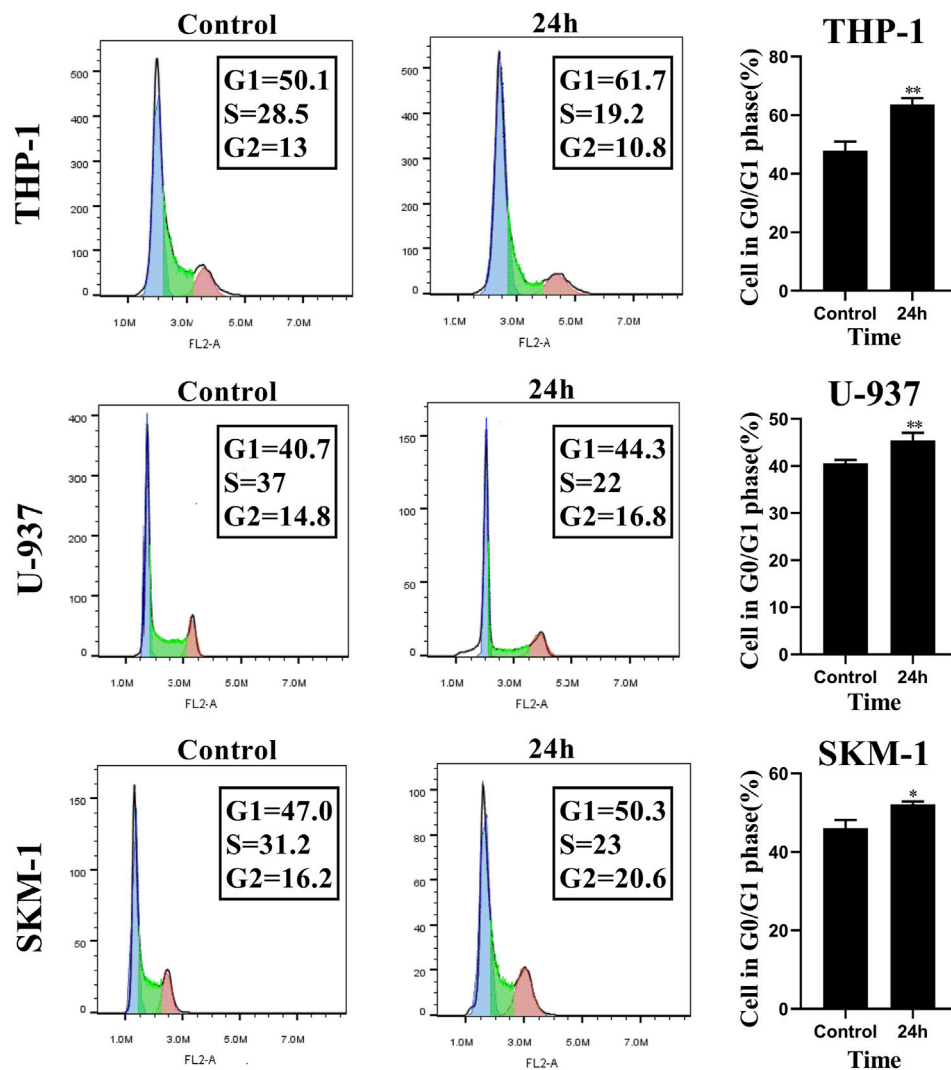


FIGURE 3 | Honokiol arrests cell cycle of THP-1, U-937 and SKM-1 cells at G0/G1 Phases. The cells were incubated with the specified concentration of honokiol (THP-1: 20 μ M; U-937: 35 μ M; SKM-1: 30 μ M) and then analyzed using flow cytometry with PI staining. Statistical analysis of G0/G1 phase cells was shown as a bar graph (*, $p < 0.05$, **, $p < 0.01$, compared to the control group). These data are from three separate replicates.

signaling pathway, and bile secretion. Among them, ferroptosis is closely correlated with cell death induced by honokiol.

Additionally, we generated a heat map portraying the expression of the relevant genes in these pathways (**Figure 5C**). In the ferroptosis pathway, HMOX1 (Heme Oxygenase 1, HO-1) and SAT1 (Spermidine/Spermine N1-Acetyltransferase 1) were upregulated significantly in the group treated with honokiol, as was SLC7A11 (Solute Carrier Family seven Member 1, XCT), compared to the control group treated with DMSO only. Also, the expression of CEBPB (CCAAT Enhancer Binding Protein Beta), a gene closely related to the cell differentiation of AML (Guerzoni et al., 2006; Novikova et al., 2021), increased significantly after honokiol treatment.

In order to determine the relationships and interactions amongst these common genes in both cell lines, we performed

PPI (protein-protein interaction network) analysis using STRING software. As shown in **Figure 5D**, HMOX1, the key member of the noncanonical ferroptosis mechanism, interacted with seven genes: SLC7A11, TFRC, HAMP, TNF, TLR4, SERPINE1, and TXNIP. Two of which, SLC7A11 and TFRC, were involved in ferroptosis.

We further detected more ferroptosis-related markers including TFR1 (TFRC), ACSL4, PTGS2, CHAC1 and SAT1 using qPCR. Three cell lines THP-1, U-937 and SKM-1 were treated with honokiol at the concentration of 20, 35, 30 μ M respectively for 12h, and mRNA expression of the ferroptosis-related genes was detected by qPCR. The results showed there was no identical change for TFR1 (TFRC), ACSL4, PTGS2 and CHAC1 in these 3 cell lines, however, the mRNA expression of SAT1 increased in all the 3 cell lines treated with honokiol, which was consistent with the results of mRNA sequencing. Thus,

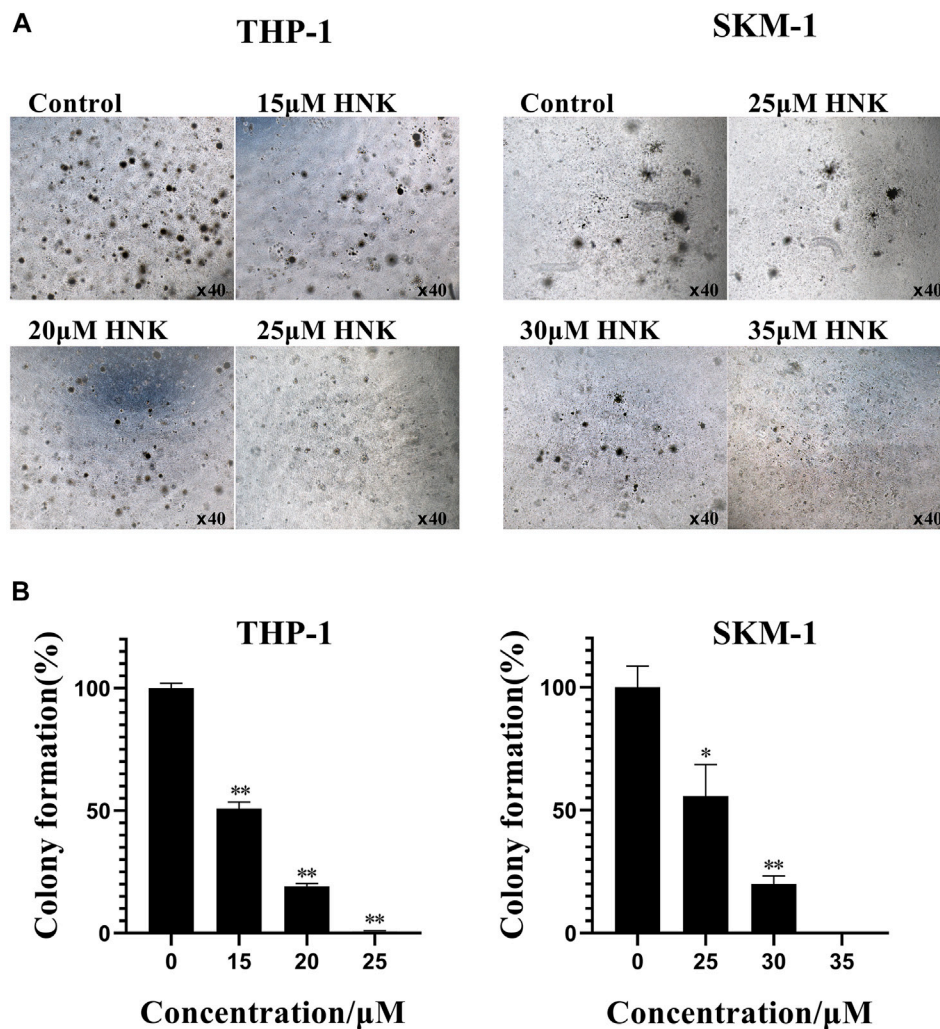


FIGURE 4 | Honokiol inhibits colony formation of THP-1 and SKM-1 cells. **(A)** Cell colony results of THP-1 and SKM-1 cells. Cells were incubated with different concentrations of honokiol for 14 days and then observed under a light microscope. **(B)** Bar graphs show the statistical analysis of colony formation, presented as (*, $p < 0.01$; **, $p < 0.001$). These results represent three separate experiments.

our result suggested that SAT1 may play an important role in ferroptosis induced by honokiol (Supplementary Figure S2).

Honokiol Enhanced Lipid Peroxidation in THP-1, U-937, and SKM-1 Cells

As the existence of lipid peroxide serves as one of the most reliable pieces of evidence of ferroptosis, we opted to investigate the level of lipid peroxide in THP-1, U-937, and SKM-1 cells after being treated with honokiol for 12 h. It was shown in **Figure 6** that honokiol elevated the expression of lipid peroxide in these cell lines. Moreover, the lipid peroxide level positively correlated with the concentration of honokiol within a specific concentration range. These data provide strong evidence for ferroptosis being induced by honokiol.

Honokiol Induced Ferroptosis by Upregulating HMOX-1, Not by Downregulating SLC7A11

To verify the expression of ferroptosis-related genes, qPCR and WB were used. The qPCR results (**Figure 7A**) indicated that the mRNA level of HMOX1 and SLC7A11 in THP-1, U-937, and SKM-1 cells treated with honokiol were upregulated significantly compared to the control group at 6 and 12 h. WB results further revealed that honokiol enhanced the protein expression level of both genes (**Figure 7B**). As both upregulation of HMOX1 and downregulation of SLC7A11 promoted ferroptosis, we postulate that the ferroptosis induced by honokiol in these cells mediated by the overexpression of the HMOX1 protein. The effect of SLC7A11 on ferroptosis induced by honokiol needs to be clarified in future studies.

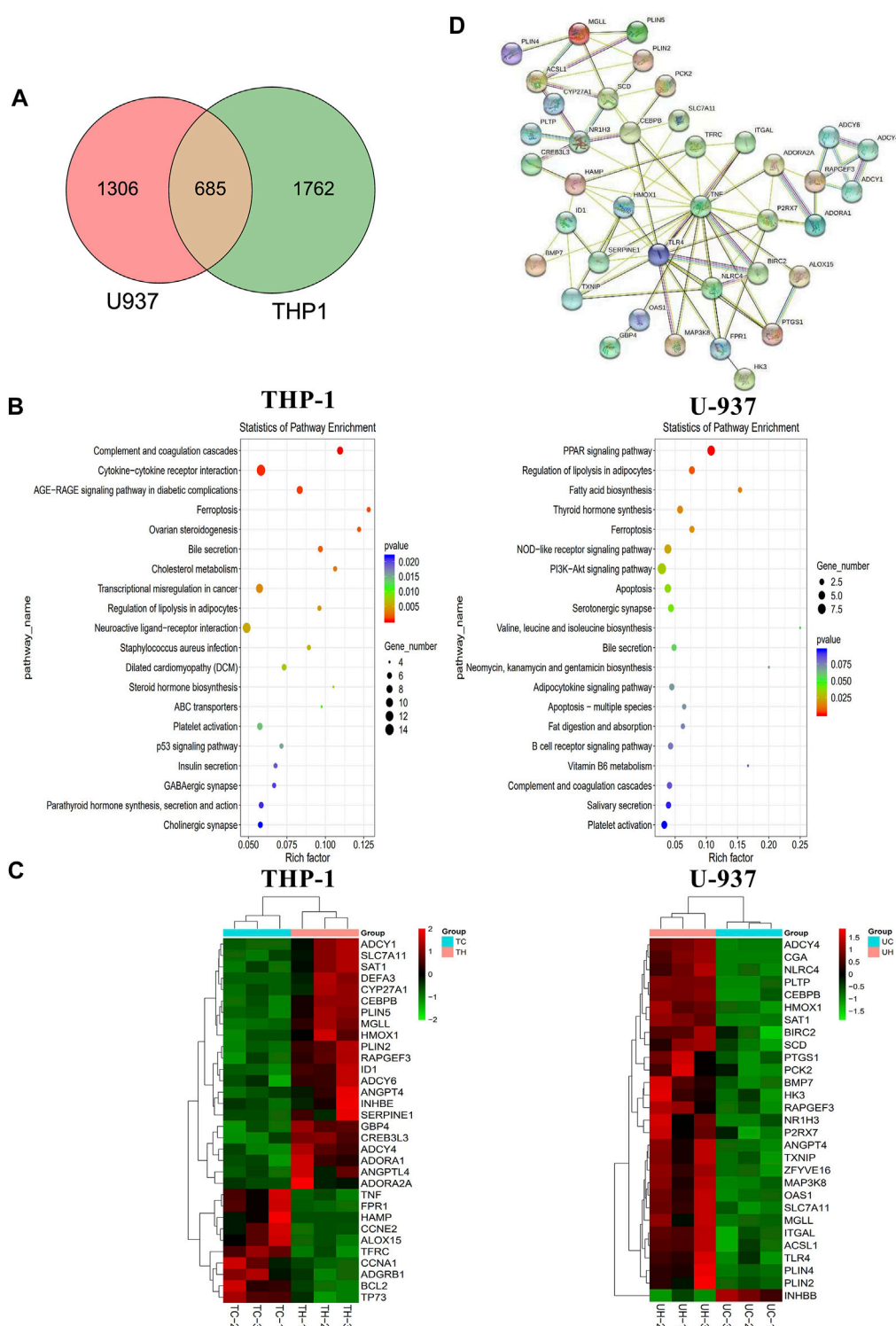


FIGURE 5 | The mechanism of the inhibitory effect of honokiol on THP-1 and U-937 cells. **(A)** Venn diagram. **(B)** KEGG pathway analyses of all differentially expressed genes. **(C)** Heatmap of the partial differentially expressed genes. **(D)** Protein-Protein interaction (PPI) Network diagram.

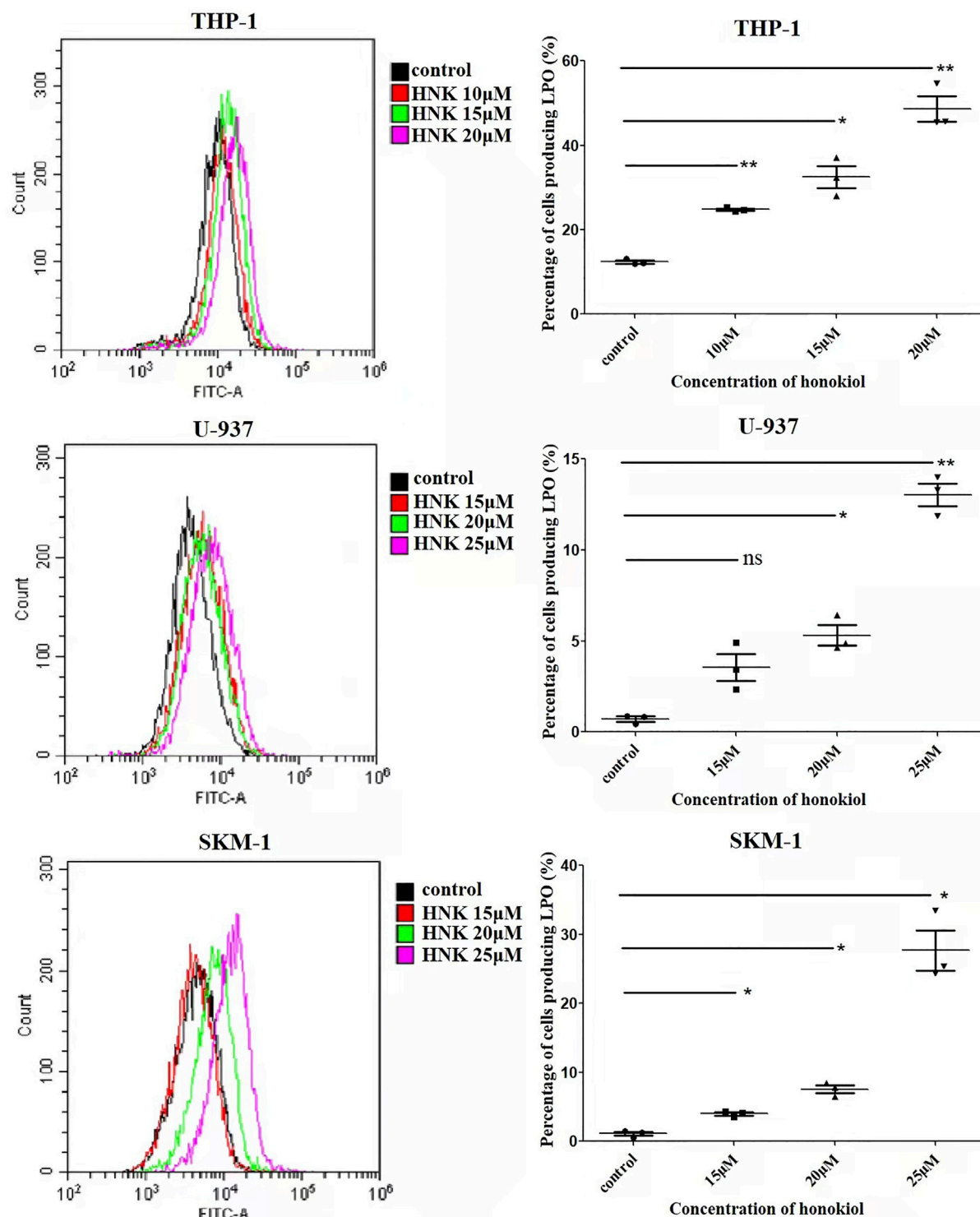
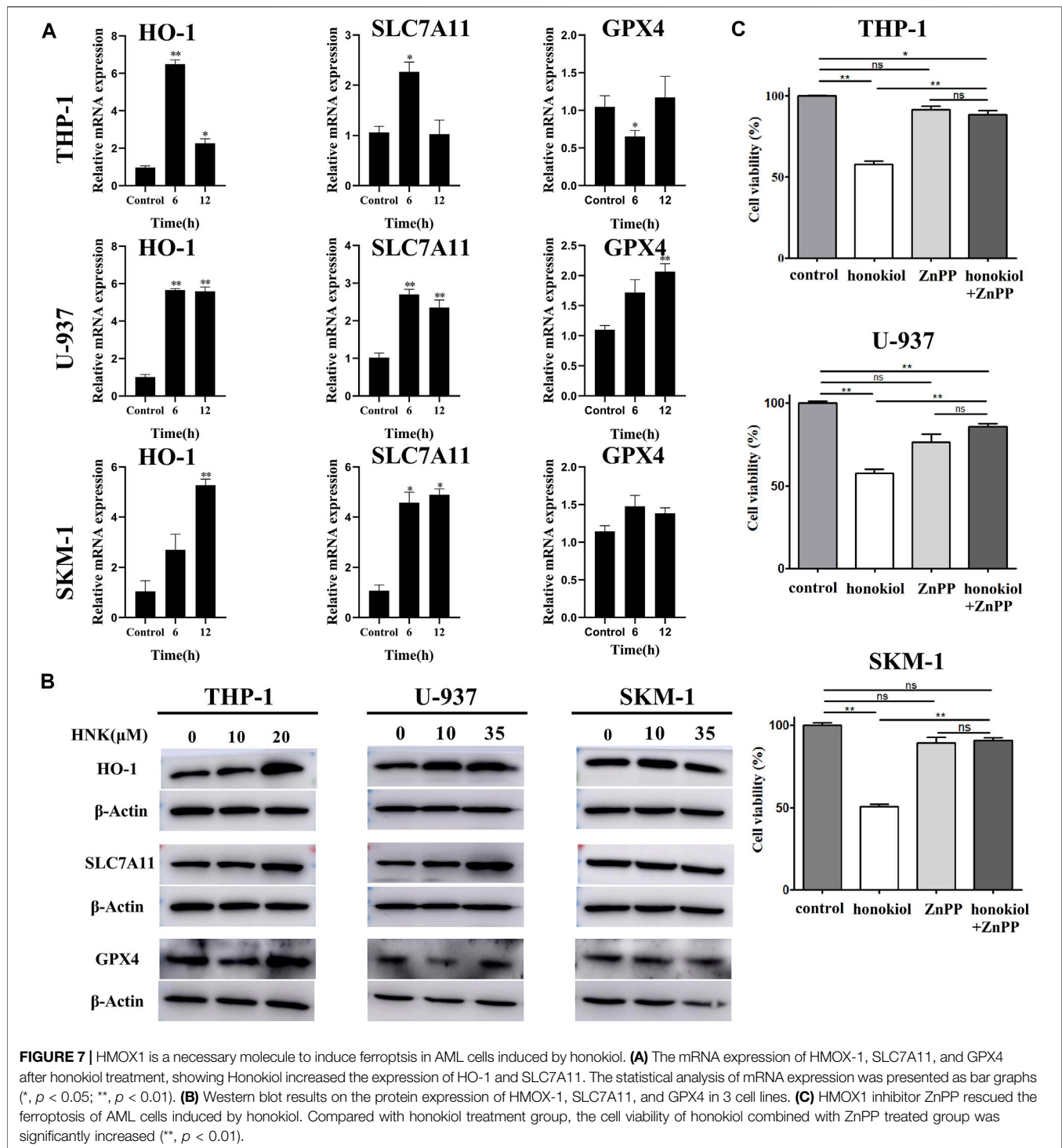


FIGURE 6 | Effects of honokiol on lipid peroxidation in THP-1, U-937, and SKM-1 cells. The cells were incubated with different concentrations of honokiol for 24h, then liperfluor was added for flow cytometry analysis. Statistical analysis of lipid peroxide was presented as scatter plots (*, $p < 0.05$; **, $p < 0.01$).



HMOX1 Inhibitor ZnPP Rescued the Ferroptosis of AML Cells Induced by Honokiol

To learn if HMOX1 is a necessary molecule to induce ferroptosis in AML cells induced by honokiol, three AML cell lines U-937, THP-1 and SKM-1 were treated with DMSO as control, honokiol

and honokiol combined with HMOX1 inhibitor ZnPP respectively. CCK-8 assay was used to measure cell viability after treatment of the cells for 24 h and the concentrations of honokiol used were for THP-1: 20 μ M, U-937: 35 μ M and SKM-1: 30 μ M. As shown in **Figure 7C**, compared with honokiol treated group, the cell viability of honokiol combined with ZnPP treated

group was significantly increased (**, $p < 0.01$), suggesting that HMOX1 inhibitor ZnPP can rescue the ferroptosis of AML cells and HMOX1 is a necessary molecule to induce ferroptosis in AML cells induced by honokiol.

To confirm ferroptosis as the major cause of cell death in AML induced by honokiol, we used Ferrostatin-1 as a ferroptosis inhibitor that has proven to inhibit ferroptosis by preventing the accumulation of ROS from lipid peroxidation. THP-1, U-937 and SKM-1 cells were pretreated with Ferrostatin-1 (5 μ M) for 2 h, then honokiol was added to the cell culture at specified concentration and incubated for 24 h. Cell viability of the three cell lines was measured by CCK-8 assay. The result indicated that the ferroptosis inhibitor Ferrostatin-1 partially rescued honokiol-induced cell death in THP-1, U-937 and SKM-1 cells, suggesting that these cells underwent ferroptosis after honokiol treatment (Supplementary Figure S3).

DISCUSSION

AML is characterized by high chemoresistance, high recurrence risk, and poor prognosis (Siegel et al., 2021). Although several recently approved pharmacologic agents expanded AML treatment options, the outcomes of chemoresistant patients, accounting for 35–45% of new cases, are still unsatisfactory with less than 30% of long-term survival rate (Song et al., 2018; Shallis et al., 2019). Till now, practitioners have resorted to using a few Chinese herb extracts, including arsenic trioxide and HHT, to treat AML (Stahl and Tallman, 2019; Zhang et al., 2019; Zhou et al., 2020) effectively. Notwithstanding the above, new effective therapeutic strategies or drugs for AML are still in urgent need.

Honokiol has recently attracted more attention due to its potent anti-cancer activity and low cytotoxicity (Ong et al., 2019). In this study, we evaluated the anti-leukemia effect of honokiol from one Chinese herb in AML-M5 subtype cell lines THP-1, U-937, and SKM-1 with complex karyotypes, which are closely associated with poor prognosis of AML patients (Daneshbod et al., 2019; Mrózek et al., 2019). Firstly, HNK inhibited the viability of THP-1, U-937, and SKM-1 cells, but showed almost no cytotoxicity for the normal PBMCs. Further experimental results demonstrated that HNK could induce cell cycle arrest at the G0/G1 phase and inhibit the leukemic colony formation of THP-1 and SKM-1 cells. Additionally, the dead cells mainly accumulated in the upper right quadrant with the late apoptotic cells regardless of the concentration of honokiol used. These results suggest that HNK inhibits AML cells' proliferation by nonapoptotic programmed death manner. Our transcriptome sequencing results showed that the only cell death mode induced by honokiol in THP-1 cells was ferroptosis, whereas that in U-937 cells was ferroptosis and apoptosis (Figure 5B). Moreover, ferroptosis is statistically the primary cell death mode in U-937 cells compared to apoptosis (Figure 5B). Different from many known cell death modes, Ferroptosis is a ROS-dependent type of cell death accompanied by iron accumulation and lipid peroxidation (Tang et al., 2021a). The accumulation of lipid peroxide is considered the

primary feature of ferroptosis (Li et al., 2020b). It was found that increased lipid peroxide occurred in THP-1, U-937, and SKM-1 cells, suggesting that honokiol may induce ferroptosis-like cell death.

Based on the existing data, ferroptosis is mainly divided into downregulated GPX4-induced and upregulated HMOX1-induced (Chang et al., 2018; Hassannia et al., 2018; Li et al., 2020a). Honokiol elevated the expression of HMOX1 but did not inhibit the expression of GPX4. Therefore, HMOX1 is considered directly responsible for the ferroptosis induced by honokiol.

An increasing number of studies have shown that HMOX1 plays a dual role in ferroptosis. A proper cellular level of HMOX1 plays an antioxidative function to protect cells from ROS toxicity (Ryter and Tyrrell, 2000). However, its overexpression has pro-oxidant effects to induce ferroptosis of cells, which is dependent on intracellular iron accumulation and increased ROS content upon excessive activation of HMOX1 (Chang et al., 2018). Several HO-1 inhibitors have been discovered and are widely used. ZnPP (Zinc Protoporphyrin Zn(II)-protoporphyrin IX), a heme analog, has been widely used in studying HO-1 in ferroptosis (Tang et al., 2021b). It may competitively inhibit enzymatic activity by occupying the heme-binding site of HMOX-1. In AML cell lines THP-1, U-937, and SKM-1, ZnPP inhibited honokiol-induced cell ferroptosis significantly. Here, it was concluded that honokiol materially enhanced the expression of HMOX1, which led to the ferroptosis of THP-1, U-937, and SKM-1 cells. However, our study found that after honokiol treatment, the expression of SLC7A11 was also upregulated. This detected change is different from that in previously published data. SLC7A11 serves as one of the essential regulatory factors of ferroptosis. It protects cells from ferroptosis by importing cystine for the biosynthesis of glutathione (Stockwell et al., 2017). However, there is evidence that drugs, radiation, and other stimuli can induce cancer cells to adapt to these stress conditions by increasing the expression of SLC7A11, which is often unrelated to ferroptosis (Lin et al., 2020; Koppula et al., 2021). In tumors, SLC7A11 regulates nonferroptotic cell death, cell proliferation, drug-/radio-resistance, and tumor immunity, all of which are dependent on cystine import and/or glutamate export mediated by SLC7A11 (Zhou et al., 2020). Based on these data, we conjectured that there might be two functions of overexpressed SLC7A11 induced by honokiol. First, the overexpression of SLC7A11 due to negative feedback on lipid peroxide induced by HMOX-1 could regulate redox homeostasis by importing cystine in AML cells. Secondly, SLC7A11 may also induce cell death by excessive cysteine intake, which is likely toxic to cells (Koppula et al., 2021).

In short, honokiol has a significant inhibitory effect on THP-1, U-937, and SKM-1 cells, which is achieved by honokiol through ferroptosis, a novel cell death mechanism confirmed by mRNA sequencing technology and typical marker detection. The results of our present study suggest that honokiol triggers phenotype features of ferroptosis in AML cells by increasing the expression of HMOX1. Moreover, the HMOX1 inhibitor ZnPP rescued the ferroptosis of AML cells induced by honokiol. Therefore, these data highlight that honokiol plays a vital anti-cancer role in AML through activating the ferroptosis pathway and that HO-1 is the

crucial regulating molecule in this pathway. However, it is critical to note that the results of this study also suggest that the level of SLC7A11 expression detected is contradictory to that in other published studies of ferroptosis, so the function of SLC7A11 in honokiol treatment remains to be clarified. Additionally, the anti-cancer effects of honokiol were only examined on three AML cell lines. Therefore, whether honokiol can be used as a broad-spectrum anti-leukemia drug remains uncertain. Nevertheless, our study explains the potential molecular mechanism of the anti-cancer activity of honokiol and paves the ground for further studies on the topic.

DATA AVAILABILITY STATEMENT

The datasets presented in this study can be found in online repositories. The names of the repository/repositories and accession number(s) can be found below: <https://www.ncbi.nlm.nih.gov/geo/>; GSE200099.

ETHICS STATEMENT

The studies involving human participants were reviewed and approved by the Affiliated Hospital of Weifang Medical University. The patients/participants provided their written informed consent to participate in this study.

REFERENCES

- Arora, S., Singh, S., Piazza, G. A., Contreras, C. M., Panyam, J., and Singh, A. P. (2012). Honokiol: a Novel Natural Agent for Cancer Prevention and Therapy. *Curr. Mol. Med.* 12 (10), 1244–1252. doi:10.2174/156652412803833508
- Banik, K., Ranaware, A. M., Deshpande, V., Nalawade, S. P., Padmavathi, G., Bordoloi, D., et al. (2019). Honokiol for Cancer Therapeutics: A Traditional Medicine that Can Modulate Multiple Oncogenic Targets. *Pharmacol. Res.* 144, 192–209. doi:10.1016/j.phrs.2019.04.004
- Chang, L. C., Chiang, S. K., Chen, S. E., Yu, Y. L., Chou, R. H., and Chang, W. C. (2018). Heme Oxygenase-1 Mediates BAY 11-7085 Induced Ferroptosis. *Cancer Lett.* 416, 124–137. doi:10.1016/j.canlet.2017.12.025
- Daneshbod, Y., Kohan, L., Taghadosi, V., Weinberg, O. K., and Arber, D. A. (2019). Prognostic Significance of Complex Karyotypes in Acute Myeloid Leukemia. *Curr. Treat. Options Oncol.* 20 (2), 15. doi:10.1007/s11864-019-0612-y
- Dikalov, S., Losik, T., and Arbisser, J. L. (2008). Honokiol Is a Potent Scavenger of Superoxide and Peroxyl Radicals. *Biochem. Pharmacol.* 76 (5), 589–596. doi:10.1016/j.bcp.2008.06.012
- Dixon, S. J., Lemberg, K. M., Lamprecht, M. R., Skouta, R., Zaitsev, E. M., Gleason, C. E., et al. (2012). Ferroptosis: an Iron-dependent Form of Nonapoptotic Cell Death. *Cell* 149 (5), 1060–1072. doi:10.1016/j.cell.2012.03.042
- Fang, C. Y., Chen, S. J., Wu, H. N., Ping, Y. H., Lin, C. Y., Shiu, D., et al. (2015). Honokiol, a Lignan Biphenol Derived from the Magnolia Tree, Inhibits Dengue Virus Type 2 Infection. *Viruses* 7 (9), 4894–4910. doi:10.3390/v7092852
- Fenwarth, L., Thomas, X., de Botton, S., Duployez, N., Bourhis, J. H., Lesieur, A., et al. (2021). A Personalized Approach to Guide Allogeneic Stem Cell Transplantation in Younger Adults with Acute Myeloid Leukemia. *Blood* 137 (4), 524–532. doi:10.1182/blood.2020005524
- Guerzoni, C., Bardini, M., Mariani, S. A., Ferrari-Amorotti, G., Neviani, P., Panno, M. L., et al. (2006). Inducible Activation of CEBPB, a Gene Negatively Regulated by BCR/ABL, Inhibits Proliferation and Promotes Differentiation of BCR/ABL-expressing Cells. *Blood* 107 (10), 4080–4089. doi:10.1182/blood-2005-08-3181

AUTHOR CONTRIBUTIONS

XRL and YHS performed the majority of experiments; XZ performed cell culture, qPCR and WB; DW performed the collection and statistical analysis of data; JW performed cell culture and WB; HW and YZ provided technical support for all experiments; XLL and XX performed cell cultures and flow cytometry analysis; HS and WP helped in mRNA sequencing; YLS supervised the project, performed mRNA sequencing and drafted the manuscript; ZH supervised the project and finalized the manuscript.

FUNDING

The research was supported by the grants of Shandong Provincial Natural Science Foundation of China (ZR2020MH379, ZR2020KC016, and ZR2020QH096); the Special Project of Shandong Province Social Science Planning and Research of China (21CLYJ53); the Weifang Science and Technology Bureau (Grant No. 2020YQFK013).

SUPPLEMENTARY MATERIAL

The Supplementary Material for this article can be found online at: <https://www.frontiersin.org/articles/10.3389/fphar.2022.897791/full#supplementary-material>

- Hassannia, B., Wiernicki, B., Ingold, I., Qu, F., Van Herck, S., Tyurina, Y. Y., et al. (2018). Nano-targeted Induction of Dual Ferroptotic Mechanisms Eradicates High-Risk Neuroblastoma. *J. Clin. Invest.* 128 (8), 3341–3355. doi:10.1172/JCI99032
- Humbert, M., Seiler, K., Mosimann, S., Rentsch, V., Sharma, K., Pandey, A. V., et al. (2021). Reducing FASN Expression Sensitizes Acute Myeloid Leukemia Cells to Differentiation Therapy. *Cell Death Differ.* 28 (8), 2465–2481. doi:10.1038/s41418-021-00768-1
- Ito, H., Nakamae, I., Kato, J. Y., and Yoneda-Kato, N. (2021). Stabilization of Fatty Acid Synthesis Enzyme Acetyl-CoA Carboxylase 1 Suppresses Acute Myeloid Leukemia Development. *J. Clin. Invest.* 131 (12), e141529. doi:10.1172/JCI141529
- Koppula, P., Zhuang, L., and Gan, B. (2021). Cystine Transporter SLC7A11/xCT in Cancer: Ferroptosis, Nutrient Dependency, and Cancer Therapy. *Protein Cell* 12 (8), 599–620. doi:10.1007/s13238-020-00789-5
- Leeman-Neill, R. J., Cai, Q., Joyce, S. C., Thomas, S. M., Bhola, N. E., Neill, D. B., et al. (2010). Honokiol Inhibits Epidermal Growth Factor Receptor Signaling and Enhances the Antitumor Effects of Epidermal Growth Factor Receptor Inhibitors. *Clin. Cancer Res.* 16 (9), 2571–2579. doi:10.1158/1078-0432.CCR-10-0333
- Li, H. Y., Ye, H. G., Chen, C. Q., Yin, L. H., Wu, J. B., He, L. C., et al. (2015). Honokiol Induces Cell Cycle Arrest and Apoptosis via Inhibiting Class I Histone Deacetylases in Acute Myeloid Leukemia. *J. Cell Biochem.* 116 (2), 287–298. doi:10.1002/jcb.24967
- Li, M., Li, C. M., Ye, Z. C., Huang, J., Li, Y., Lai, W., et al. (2020a). Sirt3 Modulates Fatty Acid Oxidation and Attenuates Cisplatin-Induced AKI in Mice. *J. Cell Mol. Med.* 24 (9), 5109–5121. doi:10.1111/jcmm.15148
- Li, R., Zhang, J., Zhou, Y., Gao, Q., Wang, R., Fu, Y., et al. (2020b). Transcriptome Investigation and *In Vitro* Verification of Curcumin-Induced HO-1 as a Feature of Ferroptosis in Breast Cancer Cells. *Oxid. Med. Cell Longev.* 2020, 3469840. doi:10.1155/2020/3469840
- Lin, W., Wang, C., Liu, G., Bi, C., Wang, X., Zhou, Q., et al. (2020). SLC7A11/xCT in Cancer: Biological Functions and Therapeutic Implications. *Am. J. Cancer Res.* 10 (10), 3106–3126.

- Liu, H., Zang, C., Emde, A., Planas-Silva, M. D., Rosche, M., Kühnl, A., et al. (2008). Anti-tumor Effect of Honokiol Alone and in Combination with Other Anticancer Agents in Breast Cancer. *Eur. J. Pharmacol.* 591 (1–3), 43–51. doi:10.1016/j.ejphar.2008.06.026
- Lo-Coco, F., Avvisati, G., Vignetti, M., Thiede, C., Orlando, S. M., Iacobelli, S., et al. (2013). Retinoic Acid and Arsenic Trioxide for Acute Promyelocytic Leukemia. *N. Engl. J. Med.* 369 (2), 111–121. doi:10.1056/NEJMoa1300874
- Mi, R., Zhao, J., Chen, L., Wei, X., Liu, J., and Wei, X. (2021). Efficacy and Safety of Homoharringtonine for the Treatment of Acute Myeloid Leukemia: A Meta-Analysis. *Clin. Lymphoma Myeloma Leuk.* 21 (10), e752–e767. doi:10.1016/j.clml.2021.06.002
- Mrózek, K., Eisfeld, A. K., Kohlschmidt, J., Carroll, A. J., Walker, C. J., Nicolet, D., et al. (2019). Complex Karyotype in De Novo Acute Myeloid Leukemia: Typical and Atypical Subtypes Differ Molecularly and Clinically. *Leukemia* 33 (7), 1620–1634. doi:10.1038/s41375-019-0390-3
- Muniraj, N., Siddharth, S., Shriver, M., Nagalingam, A., Parida, S., Woo, J., et al. (2020). Induction of STK11-dependent Cytoprotective Autophagy in Breast Cancer Cells upon Honokiol Treatment. *Cell Death Discov.* 6, 81. doi:10.1038/s41420-020-00315-w
- Ni, X., Hu, G., and Cai, X. (2019). The Success and the Challenge of All-Trans Retinoic Acid in the Treatment of Cancer. *Crit. Rev. Food Sci. Nutr.* 59 (Suppl. 1), S71–S80. doi:10.1080/10408398.2018.1509201
- Novikova, S., Tikhonova, O., Kurbatov, L., Farafonova, T., Vakhrushev, I., Lupatov, A., et al. (2021). Omics Technologies to Decipher Regulatory Networks in Granulocytic Cell Differentiation. *Biomolecules* 11 (6), 907. doi:10.3390/biom11060907
- Ong, C. P., Lee, W. L., Tang, Y. Q., and Yap, W. H. (2019). Honokiol: A Review of its Anticancer Potential and Mechanisms. *Cancers (Basel)* 12 (1), 48. doi:10.3390/cancers12010048
- Rajendran, P., Li, F., Shanmugam, M. K., Vali, S., Abbasi, T., Kapoor, S., et al. (2012). Honokiol Inhibits Signal Transducer and Activator of Transcription-3 Signaling, Proliferation, and Survival of Hepatocellular Carcinoma Cells via the Protein Tyrosine Phosphatase SHP-1. *J. Cell Physiol.* 227 (5), 2184–2195. doi:10.1002/jcp.22954
- Ryter, S. W., and Tyrrell, R. M. (2000). The Heme Synthesis and Degradation Pathways: Role in Oxidant Sensitivity. Heme Oxygenase Has Both Pro- and Antioxidant Properties. *Free Radic. Biol. Med.* 28 (2), 289–309. doi:10.1016/s0891-5849(99)00223-3
- Shallis, R. M., Wang, R., Davidoff, A., Ma, X., and Zeidan, A. M. (2019). Epidemiology of Acute Myeloid Leukemia: Recent Progress and Enduring Challenges. *Blood Rev.* 36, 70–87. doi:10.1016/j.blre.2019.04.005
- Siegel, R. L., Miller, K. D., Fuchs, H. E., and Jemal, A. (2021). Cancer Statistics, 2021 [published Correction Appears in CA Cancer J Clin. *CA Cancer J. Clin.* 71 (1), 3597–3633. doi:10.3322/caac.21654
- Song, X., Peng, Y., Wang, X., Chen, Y., Jin, L., Yang, T., et al. (2018). Incidence, Survival, and Risk Factors for Adults with Acute Myeloid Leukemia Not Otherwise Specified and Acute Myeloid Leukemia with Recurrent Genetic Abnormalities: Analysis of the Surveillance, Epidemiology, and End Results (SEER) Database, 2001–2013. *Acta Haematol.* 139 (2), 115–127. doi:10.1159/000486228
- Stahl, M., and Tallman, M. S. (2019). Acute Promyelocytic Leukemia (APL): Remaining Challenges towards a Cure for All. *Leuk. Lymphoma* 60 (13), 3107–3115. doi:10.1080/10428194.2019.1613540
- Stockwell, B. R., Friedmann Angeli, J. P., Bayir, H., Bush, A. I., Conrad, M., Dixon, S. J., et al. (2017). Ferroptosis: A Regulated Cell Death Nexus Linking Metabolism, Redox Biology, and Disease. *Cell* 171 (2), 273–285. doi:10.1016/j.cell.2017.09.021
- Stuani, L., Riols, F., Millard, P., Sabatier, M., Batut, A., Saland, E., et al. (2018). Stable Isotope Labeling Highlights Enhanced Fatty Acid and Lipid Metabolism in Human Acute Myeloid Leukemia. *Int. J. Mol. Sci.* 19 (11), 3325. doi:10.3390/ijms19113325
- Tang, D., Chen, X., Kang, R., and Kroemer, G. (2021). Ferroptosis: Molecular Mechanisms and Health Implications. *Cell Res.* 31 (2), 107–125. doi:10.1038/s41422-020-00441-1
- Tang, Z., Ju, Y., Dai, X., Ni, N., Liu, Y., Zhang, D., et al. (2021). HO-1-mediated Ferroptosis as a Target for Protection against Retinal Pigment Epithelium Degeneration. *Redox Biol.* 43, 101971. doi:10.1016/j.redox.2021.101971
- Tcheng, M., Roma, A., Ahmed, N., Smith, R. W., Jayanth, P., Minden, M. D., et al. (2021). Very Long Chain Fatty Acid Metabolism Is Required in Acute Myeloid Leukemia. *Blood* 137 (25), 3518–3532. doi:10.1182/blood.2020008551
- Zhang, J., Geng, H., Liu, L., and Zhang, H. (2019). Synergistic Cytotoxicity of Homoharringtonine and Etoposide in Acute Myeloid Leukemia Cells Involves Disrupted Antioxidant Defense. *Cancer Manag. Res.* 11, 1023–1032. doi:10.2147/CMAR.S187597
- Zhou, H., Xu, R. Z., Gu, Y., Shi, P. F., and Qian, S. (2020). Targeting of Phospho-eIF4E by Homoharringtonine Eradicates a Distinct Subset of Human Acute Myeloid Leukemia. *Leuk. Lymphoma* 61 (5), 1084–1096. doi:10.1080/10428194.2017.1390229
- Zhu, X., Cai, J., Zhou, F., Wu, Z., Li, D., Li, Y., et al. (2018). Genome-wide Screening of Budding Yeast with Honokiol to Associate Mitochondrial Function with Lipid Metabolism. *Traffic* 19 (11), 867–878. doi:10.1111/tra.12611

Conflict of Interest: The authors declare that the research was conducted in the absence of any commercial or financial relationships that could be construed as a potential conflict of interest.

Publisher's Note: All claims expressed in this article are solely those of the authors and do not necessarily represent those of their affiliated organizations, or those of the publisher, the editors and the reviewers. Any product that may be evaluated in this article, or claim that may be made by its manufacturer, is not guaranteed or endorsed by the publisher.

Copyright © 2022 Lai, Sun, Zhang, Wang, Wang, Wang, Zhao, Liu, Xu, Song, Ping, Sun and Hu. This is an open-access article distributed under the terms of the Creative Commons Attribution License (CC BY). The use, distribution or reproduction in other forums is permitted, provided the original author(s) and the copyright owner(s) are credited and that the original publication in this journal is cited, in accordance with accepted academic practice. No use, distribution or reproduction is permitted which does not comply with these terms.



Associations of Prior Chronic Use of Non-Steroidal Anti-Inflammatory Drugs (NSAIDs) and Glucocorticoids With Cachexia Incidence and Survival

Santiago Olaechea¹, Anne Gilmore², Christian Alvarez¹, Bhavani S. Gannavarapu³, Rodney Infante^{1*} and Puneeth Iyengar^{1,3*}

¹ Center for Human Nutrition, University of Texas (UT) Southwestern Medical Center, Dallas, TX, United States, ² Department of Clinical Nutrition, University of Texas (UT) Southwestern Medical Center, Dallas, TX, United States, ³ Department of Radiation Oncology, University of Texas (UT) Southwestern Medical Center, Dallas, TX, United States

OPEN ACCESS

Edited by:

Rajkumar S. Kalra,
Okinawa Institute of Science and
Technology Graduate University,
Japan

Reviewed by:

Prashanth Thevkar Nagesh,
Harvard Medical School, United States
Andrea Sbrana,
University of Pisa, Italy

*Correspondence:

Rodney Infante
rodney.infante@utsouthwestern.edu
Puneeth Iyengar
puneeth.iyengar@utsouthwestern.edu

Specialty section:

This article was submitted to
Pharmacology of Anti-Cancer Drugs,
a section of the journal
Frontiers in Oncology

Received: 17 April 2022

Accepted: 17 May 2022

Published: 07 June 2022

Citation:

Olaechea S, Gilmore A, Alvarez C,
Gannavarapu BS, Infante R and
Iyengar P (2022) Associations of Prior
Chronic Use of Non-Steroidal Anti-
Inflammatory Drugs (NSAIDs) and
Glucocorticoids With Cachexia
Incidence and Survival.
Front. Oncol. 12:922418.
doi: 10.3389/fonc.2022.922418

Background: Cachexia is an inflammatory and metabolic syndrome of unintentional weight loss through depletion of muscle and adipose tissue. There is limited knowledge of how chronic use of non-steroidal anti-inflammatory drugs (NSAIDs) and glucocorticoids affect cachexia development. The purpose of this study was to investigate associations between prior long-term use of NSAIDs or glucocorticoids with cachexia incidence and post-diagnosis weight loss progression in a retrospective cancer patient cohort.

Methods: Of 3,802 lung or gastrointestinal cancer patient records, 3,180 comprised our final cohort. Patient demographic information, tumor qualities, medication histories, and comorbidities were assessed. Cachexia was defined as having developed prior to oncologic treatment. Statistical evaluations included categorical, multivariate logistic regression, and log-rank survival analyses. Development of substantial post-diagnosis weight loss was calculated and interpreted for patients without cachexia at diagnosis.

Results: Chronic prior use of any NSAID or glucocorticoid medication was associated with approximate absolute and relative reductions in cachexia incidence at diagnosis of 10 and 25 percent ($P < 0.0001$). In multivariate analyses, NSAID medications demonstrated a 23 percent reduction in cachexia incidence likelihood ($OR = 0.770$; 95% $CI = 0.594, 0.998$; $P = 0.0481$). Patients without cachexia at diagnosis were significantly more likely to develop substantial post-diagnosis weight loss from pre-diagnosis use groups of glucocorticoids ($OR = 1.452$; 95% $CI = 1.065, 1.979$; $P = 0.0183$) or NSAIDs ($OR = 1.411$; 95% $CI = 1.082, 1.840$; $P = 0.011$).

Conclusions: Our findings suggest a protective effect of prior anti-inflammatory medications, primarily NSAIDs, against manifestations of the cachexia phenotype at cancer diagnosis. These observations support further exploration of potential therapeutic benefits from anti-inflammatory medications early in cancer management.

Keywords: cachexia, NSAIDs (non-steroidal anti-inflammatory drugs), glucocorticoids, weight loss, palliative care, drug repurposing and discovery

INTRODUCTION

Cancer-associated wasting, known as cancer cachexia, poses a significant challenge in the management of patients across many primary malignancies. While weight loss is the hallmark of this syndrome, cachexia is further characterized by maladaptive inflammatory signaling through modulation of pathways including JAK/STAT (often through IL-6 cytokines) and both NF- κ B and MAP kinase (through TNF- α induction) (1–4). These tumor-directed, cytokine-dependent mechanisms help set apart cachectic weight loss from weight loss attributable to alternative processes such as treatment induced anorexia and dysphagia. Developments within the field have further implicated cancer cachexia with reduced physical function, loss of appetite, sarcopenia, fatigue, lower self-reported quality of life scores, increased treatment-related toxicity, and worse survival outcomes (5, 6). Currently, physicians have few pharmacological interventions available for cachexia-specific management. Available therapies primarily address nutritional consequences without targeting the maladaptive systemic changes underpinning cachectic pathophysiology (7).

Multiple pre-clinical and clinical trials have suggested potential benefits in application of non-steroidal anti-inflammatory drugs (NSAIDs) and glucocorticoid medications in the treatment of cachexia-associated weight loss (5, 8–11). The mechanistic premise for NSAID use is their COX inhibition, which impairs the production of prostaglandins known to contribute to inflammation and tumor progression. In addition to appetite stimulation, corticosteroids alter gene expression with significant downstream anti-inflammatory effects, such as interference with NF- κ B activation (12). Cohort characteristics, treatment groups, and outcomes of notable studies are summarized in **Supplementary Table 1**.

The aforementioned trials have been insufficient to validate the inclusion of NSAIDs or glucocorticoids in cachexia treatment guidelines (7, 13, 14). Of note, these trials have almost exclusively included patients with advanced cancer, where the degree of cachexia might be exceedingly difficult to overcome with treatment. In these cohorts, patients have already undergone surgical, chemotherapeutic, hormonal, immunologic, or radiation treatments, most of which are known to introduce various alternative mechanisms for weight loss outside the metabolic paraneoplastic effects of cachexia. In contrast, our current effort in this study focuses on patient use of daily medications with anti-inflammatory properties prior to their cancer diagnosis. The novel emphasis on cachexia and use of these medications use prior to a cancer diagnosis and tumor-directed treatment allows for a better understanding of the effects of these medications on the development of cachectic weight loss specifically attributable to the metabolic and inflammatory alterations induced by the tumor itself on host tissues. Fundamentally, the purpose of this study was to determine the association between prior long-term use of NSAIDs or glucocorticoids with cachexia incidence at the time of cancer diagnosis and their effects on cachexia and non-cachexia associated survival.

MATERIALS AND METHODS

Patient Cohort

Figure 1 demonstrates our cohort selection and stratification process. Using the clinical research data warehouse at UT Southwestern Medical Center and supplemental chart review for validation and data collection, we identified 3,802 patients with lung or gastrointestinal cancer diagnosed between 1/1/2006 and 12/31/2013 for evaluation. Patients were excluded if records were incomplete or if the classification of tumor histology was carcinoma in situ, sarcoma, or melanoma. After applying exclusion criteria, 3,180 patients were eligible for the study database. Demographic and tumor characteristics from the time of cancer diagnosis were recorded, and a calculation of each patient's Charlson Comorbidity Index (15) was carried out to demonstrate their comorbidity risk. The UT Southwestern Medical Center Institutional Review Board approved this study.

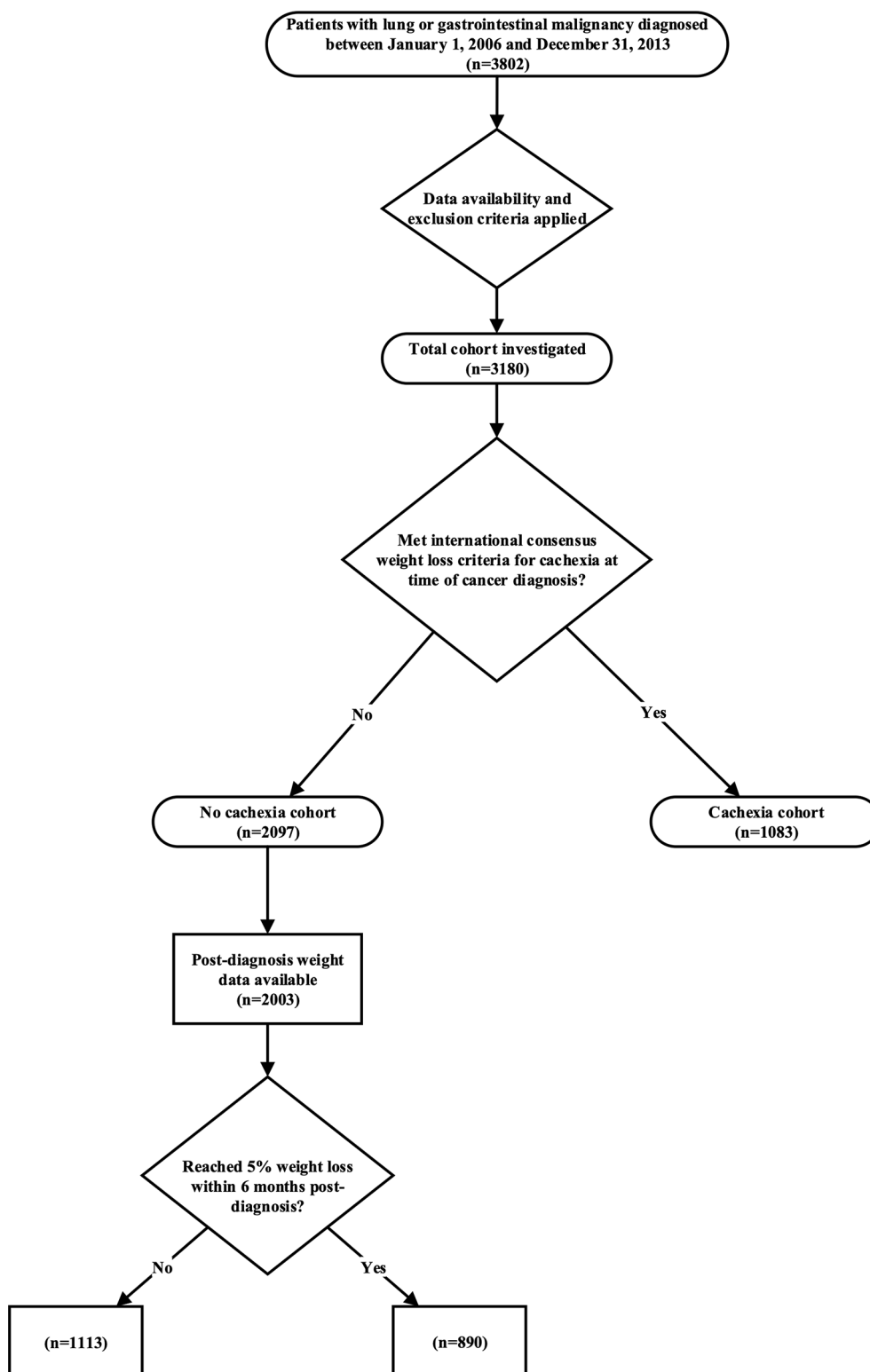
Determination of Cachectic Weight Loss at Diagnosis and Significant Post-Diagnosis Weight Loss

Cachexia was retrospectively evaluated for the total cohort through review of patient medical records in which weight measurements were routinely documented at each office visit. The assessment of cachexia for each patient was supplemented by vital signs, physician notes, and dietitian notes specifically at the time of cancer diagnosis but before any treatment had been administered. The international consensus definition of cancer cachexia served as the basis for our classification of cachexia at diagnosis (16). In patients with a BMI ≥ 20 kg/m², unintentional weight loss greater than 5% of total weight within 6 months prior to cancer diagnosis led to a classification of demonstrating cachectic pre-treatment weight loss. In patients with a BMI < 20 kg/m², unintentional weight loss greater than 2% within 6 months prior to cancer diagnosis led to the same classification. Patients with stable weight, purposeful weight loss, or weight gain were not categorized as having cachectic weight loss.

To define significant weight loss in patients who did not present with cachexia at diagnosis, we applied criterion of reaching 5% weight loss within any 6-month period that ended within 6 months post-diagnosis.

Defining Prior Anti-Inflammatory Medication Use

Medication prescription and administration logs were obtained through extraction of health system medical records. Patients were placed into prior medication use groups if they were prescribed or administered the selected medications for chronic use prior to cancer diagnosis. We defined chronic use medications as daily medications started at least 3 months before the cancer diagnosis date. Stringent criteria were applied in the selection of medication dosage and formulation type, and any acute or subacute intervention was excluded. Median time from initial medication use per patient to their cancer diagnosis was calculated.

**FIGURE 1** | Cohort selection and stratification diagram.

Statistical Analysis

Chi square testing determined categorical associations between prior medication use groups and cachexia at diagnosis, as both were recorded as binary variables for each patient. The primary control group consisted of patients without chronic use of anti-inflammatory medications (specifically NSAIDs and glucocorticoids in this study) prior to their cancer diagnosis. An additional control group, patients positive for chronic metformin use and negative for chronic anti-inflammatory medication use, was included in categorical testing. Metformin was selected due to its classification as an unrelated medication class and prevalent chronic use.

Multivariate logistic regressions were conducted to consider potentially interfering patient and tumor factors in our evaluation of relationships between anti-inflammatory medication use and cachexia incidence at diagnosis. Cachexia incidence at diagnosis functioned as the binary dependent variable. Patient factors included as covariates were age at diagnosis, sex, race, alcohol history, tobacco history, and Charlson Comorbidity Index. Tumor factors included were primary site and stage. Prior chronic medication use was included as a binary covariate, with null use denoting patients without prior use of any anti-inflammatory medications. Investigated. Overall survival differences between each medication use group versus the medication null group were estimated using the Kaplan-Meier method and evaluated statistically using log-rank testing for the total, cachectic, and noncachectic cohorts.

Associations between prior medication use and significant post-diagnosis weight loss in the non-cachectic cohort were evaluated through chi square testing and multivariate analyses. Multivariate analyses included all covariates from the previous multivariate analyses (age at diagnosis, sex, race, alcohol history, tobacco history, and Charlson Comorbidity Index), with the addition of systemic, surgical, radiation interventions as binary covariates. To visually represent weight loss progression in patients non-cachectic at diagnosis, Kaplan-Meier curves were created with significant post-diagnosis weight loss within as the event investigated and days from diagnosis to this event as the time variable.

All statistics were conducted with the alpha level of 0.05 defining statistical significance on SPSS Statistics for Mac Version 28.0.1.1 (International Business Machines, Armonk, NY).

RESULTS

Patient Cohort and Cachexia at Diagnosis

After applying exclusion criteria, the database was composed of 3,180 consecutive cancer patients seen at the UT Southwestern Medical Center diagnosed between 1/1/2006 and 12/31/2013. Patient and tumor characteristics for the total cohort, as well as sub-cohorts defined by cachexia status at diagnosis, are presented in **Table 1**.

Prior Medication Use and Cachexia Incidence at Diagnosis

The median time from the start of medication use to cancer diagnosis was 17 months. Patients with prior glucocorticoid use

demonstrated an absolute decrease of 7.93% and a 21.94% relative decrease of cachexia incidence compared to patients who did not take anti-inflammatory medications prior to diagnosis ($P=0.0052$). Prior chronic use of any NSAID had 10.25% absolute and 28.36% relative decreases in cachexia incidence compared to patients who did not take anti-inflammatory medications prior to diagnosis ($P<0.0001$). Patients with prior chronic metformin use did not have significant reductions in cachexia incidence ($P=0.4685$; **Table 2; Figure 2A**).

Specific NSAID medications included: patients with chronic use of low-dose aspirin; other nonselective COX-1 and COX-2 inhibitors such as indomethacin, diclofenac, and meloxicam; and selective COX-2 inhibitors such as celecoxib. Independently, all NSAID classifications demonstrated significantly decreased cachexia incidence at cancer diagnosis, with 8.94-10.56% absolute and 24.74-29.22% relative reductions, compared to patients without prior anti-inflammatory medication use (aspirin: $P=0.0003$; other nonselective: $P=0.0172$; selective: $P=0.0418$; **Table 2; Figure 2B**).

Multivariate analyses considering patient and tumor factors as covariates did not determine statistically significant changes in likelihood of cachexia incidence associated with glucocorticoid medication use (Odds ratio=1.046; 95% CI=0.778, 1.406; $P=0.7665$). Use of any NSAID prior to diagnosis was associated with decreased likelihood of cachexia incidence by 23.0% (Odds ratio=0.770; 95% CI=0.594, 0.998; $P=0.0481$; **Table 3**).

Survival

Prior to the review of the effect of anti-inflammatory medications on non-cachectic- and cachectic-specific survival, median survival time was determined to be 23 months (95% CI=21.161, 24.839) in the total patient cohort, 14 months (95% CI=12.659, 15.341) in patients with cachexia at diagnosis, and 31 months (95% CI=26.797, 35.203) for patients without cachexia at diagnosis. Patients with prior use of glucocorticoid medications had median survival times significantly lower than their medication-null counterparts in the non-cachexia group (20 vs 34 months; $P=0.0018$) and did not reach a significant difference within the cachexia cohort (16 vs 13 months; $P=0.8961$). Patients with prior NSAID use had median survival times significantly lower than their medication-null counterparts in the non-cachexia group (26 vs 34 months; $P=0.0149$) and did not reach a significant difference for the cohort of patients with cachexia at diagnosis (13 vs 13 months; $P=0.1554$). Similar findings were observed across specific NSAID groups and are further demonstrated in **Table 4**.

Prior Anti-Inflammatory Use and Incidence of Significant Post-Diagnosis Weight Loss

Of the 2003 patients that did not meet criteria for cachexia at cancer diagnosis, 44.43% met the cutoff of 5% weight decrease within 6 months post-diagnosis. When evaluated based on prior medication use, 42.06% of non-cachectic patients who did not take any anti-inflammatory medication prior to diagnosis met

TABLE 1 | Study population characteristics in total, cachectic, and non-cachectic cohorts.

Characteristic	Total cohort	No cachexia	Cachexia	Percent with cachexia
N	3180	2097	1083	34.06%
Median age at diagnosis (IQR)	62 (55-71)	63 (55-71)	62 (54-71)	
Female (%)	1355 (42.61%)	929 (44.30%)	426 (39.33%)	31.44% [‡]
Race (%)				
Asian or Pacific Islander	127 (3.99%)	82 (3.91%)	45 (4.16%)	35.43%
Black	758 (23.84%)	426 (20.31%)	332 (30.66%)	43.80% [†]
Non-Hispanic White	1854 (58.30%)	1332 (63.52%)	522 (48.20%)	28.16% [‡]
Hispanic	363 (11.42%)	206 (9.82%)	157 (14.50%)	43.25% [†]
Other/unknown	78 (2.45%)	51 (2.43%)	27 (2.49%)	34.62%
Primary tumor site (%)				
Anal	92 (2.89%)	68 (3.24%)	24 (2.22%)	26.09%
Colorectal	623 (19.59%)	451 (21.51%)	172 (15.88%)	27.61% [‡]
Gastroesophageal	329 (10.35%)	143 (6.82%)	186 (17.17%)	56.53% [†]
Hepatobiliary	342 (10.75%)	259 (12.35%)	83 (7.66%)	24.27% [‡]
Pancreatic	267 (8.40%)	125 (5.96%)	142 (13.11%)	53.18% [†]
NSCLC	1369 (43.05%)	953 (45.45%)	416 (38.41%)	30.39% [‡]
Small cell lung cancer	158 (4.97%)	98 (4.67%)	60 (5.54%)	37.97%
Tobacco (%)	2267 (71.29%)	1477 (70.43%)	790 (72.95%)	34.85%
Alcohol (%)	1502 (47.23%)	1005 (47.93%)	497 (45.89%)	33.09%
Charlson comorbidity index (%)				
0	1034 (32.52%)	642 (30.62%)	392 (36.20%)	37.91% [†]
1	1049 (32.99%)	679 (32.38%)	370 (34.16%)	35.27%
2	541 (17.01%)	366 (17.45%)	175 (16.16%)	32.35%
3+	556 (17.48%)	410 (19.55%)	146 (13.48%)	26.26% [‡]
Tumor grade (%)				
1	142 (7.28%)	111 (8.42%)	31 (4.91%)	21.83% [‡]
2	1034 (53.03%)	731 (55.42%)	303 (48.02%)	29.30% [‡]
3	739 (37.90%)	459 (34.80%)	280 (44.37%)	37.89% [†]
4	35 (1.79%)	18 (1.36%)	17 (2.69%)	48.57% [†]
Tumor stage (%)				
1	541 (17.54%)	446 (21.86%)	95 (9.09%)	17.56% [‡]
2	531 (17.21%)	394 (19.31%)	137 (13.11%)	25.80% [‡]
3	879 (28.49%)	557 (27.30%)	322 (30.81%)	36.63% [†]
4	1134 (36.76%)	643 (31.52%)	491 (46.99%)	43.30% [†]

Significantly increased (†) or decreased (‡) cachexia incidence within row category relative to total cohort indicated ($P < 0.05$).

Significant (*) or non-significant (n.s.) differences of cachexia incidence between medication use groups indicated ($P < 0.05$).

criteria for weight loss within 6 months post-diagnosis. This was significantly lower than the 52.11% ($P = 0.0006$) and 51.75% ($P = 0.0059$) of non-cachectic patients with prior NSAID or glucocorticoid use, respectively, that met the post-diagnosis weight loss cutoff. Similar findings were observed across specific NSAID groups (Table 5).

Within the same cohort of 2003 patients who did not meet cachexia criteria at diagnosis, multivariate analyses considering

patient, tumor, and treatment factors, prior use of any glucocorticoid medication associated with a 45.2% (Odds ratio=1.452; 95% CI=1.065, 1.979; $P = 0.0183$) increased likelihood of meeting criterion for significant post-diagnosis weight loss by 6 months. Prior use of any NSAID medication similarly predicted for 41.1% (Odds ratio=1.411; 95% CI=1.082, 1.840; $P = 0.0110$) increased likelihood of reaching the same criterion (Supplementary Table 2).

TABLE 2 | Categorical comparison of cachexia incidence in prior medication use cohorts and patients without prior anti-inflammatory medication use.

Prior medication use (n)	Patients with cachexia at diagnosis	P-value
Total cohort (3180)	1083 (34.06%)	
No anti-inflammatory medication (2521)	911 (36.14%)	
Medication groups		
Any glucocorticoid (319)	90 (28.21%)	0.0053
Any NSAID (479)	124 (25.89%)	<0.0001
Low-dose aspirin (301)	77 (25.58%)	0.0003
Other nonselective NSAIDs (157)	42 (26.75%)	0.0172
Selective COX-2 inhibitors (125)	34 (27.20%)	0.0418
Metformin only (95)	31 (32.63%)	0.4685

P values bolded if < 0.05 .

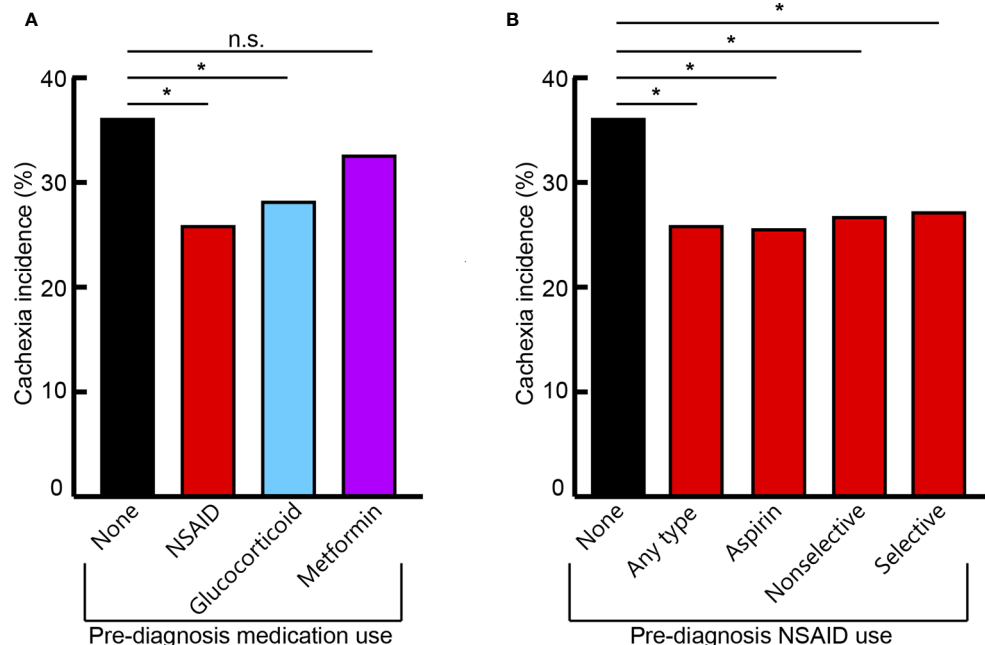


FIGURE 2 | Cachexia incidence across cohorts of different prior medication use with overall anti-inflammatory medication class **(A)** and specific NSAID medication groups **(B)**. Nonselective NSAID medications include combined COX-1 and COX-2 inhibitors. Selective NSAID medications include specific COX-2 inhibitors. Significant (*) or non-significant (n.s.) differences of cachexia incidence between medication use groups indicated ($P < 0.05$).

Figures 3A, B demonstrate Kaplan-Meier curves for time-to-cachexia for patients with prior chronic use of any glucocorticoid or NSAID medication compared to patients without prior anti-inflammatory medication use.

DISCUSSION

Overall Findings

In this study, we investigated relationships between prior chronic use of NSAID and glucocorticoid medications with cachexia at cancer diagnosis. Multivariate analyses demonstrated a particularly relevant 25% reduction in likelihood of cachexia presentation associated with the NSAID medication class that was independent of potentially confounding patient and tumor characteristics, including comorbidities. Furthermore, our survival and post-diagnosis cachexia analyses are consistent with a delay in cachexia progression attributable to these medications. Although retrospective studies cannot establish causality and are vulnerable to sampling bias, we applied statistical rigor to our dataset through the application of multiple analytical methods and subdivided our cohort to decrease bias and reduce error in our investigation. The novel focus of this study on use of NSAIDs and glucocorticoids prior to cancer treatment intervention primarily highlights NSAIDs for further investigation of therapeutic potential early in cachexia-specific cancer management.

Bridging Cachexia Pathophysiology and Therapeutic Strategy

Our decision to further investigate the therapeutic potential of NSAID and glucocorticoid medications stemmed from the mechanistic link between these medications and cachexia, as well as further evidence from animal models (17) and clinical trials supporting the use of these medications to attenuate weight loss in the setting of advanced malignancy (**Supplementary Table 1**) (18–22). In our comprehensive literature review, we were unable to identify any prior attempts at evaluating potential benefits of these medications in early or even sub-clinical stages of cachexia progression.

The central mechanism of NSAIDs is inhibition of COX-1 and COX-2 enzymes, which are expressed in almost every human tissue (23). Although COX-1 function is largely stable as a mediator of various housekeeping functions, COX-2 function can vary widely due to upregulation in states of inflammation. COX-2 upregulation has been demonstrated to contribute to tumor growth and metastatic spread by promoting angiogenesis and immune evasion (24–28). Many of the pathologic manifestations of cancer cachexia are understood to arise from inflammatory signaling dependent on upregulated COX production of prostaglandins.

Pivotal to progression of cachexia is the combination of hypophagia and excessive energy expenditure that promote a debilitating state of catabolism. Although multifactorial in nature, hypophagia observed in cancer cachexia is understood to be primarily generated through the dysregulation of hypothalamic-

TABLE 3 | Multivariate logistic regressions evaluating covariate associations with cachexia incidence at diagnosis including glucocorticoid and NSAID medication use groups.

Variable	Odds ratio (95% CI)	P-value
Age at diagnosis	1.012 (1.004, 1.020)	0.0026
Female sex	0.810 (0.678, 0.968)	0.0206
Race		
Asian or Pacific Islander	–	<0.0001
Black	1.602 (1.034, 2.482)	0.0350
Non-Hispanic White	0.719 (0.471, 1.098)	0.1262
Hispanic	1.508 (0.947, 2.401)	0.0838
Other/unknown	1.042 (0.528, 2.06)	0.9049
Alcohol history	0.924 (0.777, 1.099)	0.3719
Tobacco history	1.363 (1.100, 1.688)	0.0046
Charlson Comorbidity Index		
0	–	0.0400
1	0.979 (0.797, 1.201)	0.8362
2	0.848 (0.655, 1.098)	0.2117
3+	0.690 (0.524, 0.909)	0.0084
Primary Tumor Site		
Anal	–	<0.0001
Colorectal	0.762 (0.435, 1.335)	0.3420
Gastroesophageal	2.491 (1.400, 4.430)	0.0019
Hepatobiliary	0.735 (0.406, 1.332)	0.3108
Pancreatic	2.814 (1.547, 5.118)	0.0007
NSCLC	0.725 (0.420, 1.252)	0.2483
Small-cell lung cancer	0.824 (0.431, 1.575)	0.5590
Tumor stage		
I	–	<0.0001
II	1.232 (0.882, 1.719)	0.2208
III	2.309 (1.728, 3.086)	<0.0001
IV	3.290 (2.477, 4.369)	<0.0001
Prior glucocorticoid use	1.046 (0.778, 1.406)	0.7665
Prior NSAID use	0.770 (0.594, 0.998)	0.0481

P values bolded if <0.05.

pituitary axis function by characteristic inflammatory cytokines including TNF- α , IL-1 β , and IL-6 (29, 30). Prostaglandins propagate the generation of these cytokines in the periphery and modulate the integration of signaling centrally within the hypothalamus and brainstem (31–34). Additionally, this inflammatory signaling disturbs thermoregulatory control, contributing to maladaptive energy expenditure. Prostaglandins have also been implicated in the metabolically inefficient sympathetic overactivation observed in cachexia (35–37). At sites

of adipose stores, prostaglandins mediate the induction and recruitment of thermogenic brown adipose tissue, further contributing to energy wasting in cachexia in a mechanism attenuated by COX-2 inhibition in murine models (38).

In addition to negative overall metabolic flux, functional decline in cachexia is largely attributable to skeletal muscle wasting from systemic catabolic and inflammatory signaling (39). In multiple murine tumor models, COX inhibition has demonstrated efficacy at preventing cachectic skeletal muscle

TABLE 4 | Log-rank analysis comparing overall survival in medication groups to no anti-inflammatory medication groups across all, cachectic, and non-cachectic cohorts.

Prior medication use	All patients (n=3180)		Cachectic patients (n=1083)		Non-cachectic patients (n=2097)	
	Median time (95% CI) (months)	P-value log-rank	Median time (95% CI) (months)	P-value log-rank	Median time (95% CI) (months)	P-value log-rank
All patients	23 (21.161, 24.839)		14 (12.659, 15.341)		31 (26.797, 35.203)	
No anti-inflammatory medication	23 (20.780, 25.220)		13 (11.564, 14.436)		34 (28.401, 39.599)	
Medication groups						
Any glucocorticoid	19 (14.030, 23.970)	0.0252	16 (8.588, 23.412)	0.8961	20 (13.708, 26.292)	0.0018
Any NSAID	21 (16.922, 25.078)	0.0449	13 (8.646, 17.354)	0.1554	26 (18.86, 33.14)	0.0149
Low-dose aspirin	21 (16.048, 25.952)	0.0610	10 (6.946, 13.054)	0.0285	25 (15.084, 34.916)	0.0781
Other nonselective NSAIDs	19 (11.379, 26.621)	0.0606	13 (6.991, 19.009)	0.3157	26 (14.818, 37.182)	0.0337
Selective COX-2 inhibitors	22 (14.415, 29.585)	0.5529	10 (2.857, 17.143)	0.6695	26 (15.873, 36.127)	0.3469

P values bolded if <0.05.

TABLE 5 | Categorical comparison of significant post-diagnosis weight loss incidence (in patients without cachexia at diagnosis) between prior medication use groups and anti-inflammatory medication null patients.

Prior medication use category (N)	Patients that reached significant weight loss within 6 months of cancer diagnosis (%)	P-value
No anti-inflammatory medication (1517)	638 (42.06%)	
Medication groups		
Any glucocorticoid (228)	118 (51.75%)	0.0059
Any NSAID (355)	185 (52.11%)	0.0006
Low-dose aspirin (224)	113 (50.45%)	0.0180
Other nonselective NSAIDs (115)	58 (50.43%)	0.0799
Selective COX-2 inhibitors (91)	53 (58.24%)	0.0025

P values bolded if <0.05.

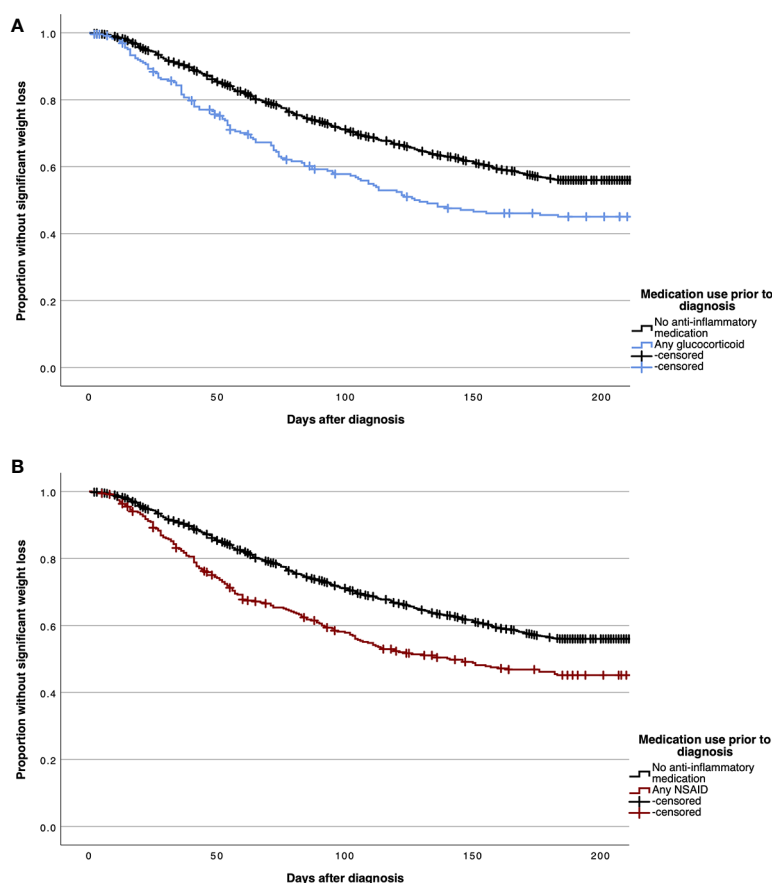
degradation, furthering the relevance of NSAID function in this syndrome (40, 41).

Clinical Relevance

Cancer cachexia remains a critically undertreated component of disease burden across almost every cancer type. Factors contributing to this deficiency include limited options available for management and identification. Although cancer patients are well known to undergo weight loss from treatment-induced

anorexia, cachexia uniquely intensifies energy expenditure through malignant metabolic and inflammatory mechanisms.

The evaluation of relationships between retrospective medication was carefully considered, as chronic use of any anti-inflammatory medication implies a comorbid condition. This implication prompted our application of multivariate analyses to simultaneously control for comorbidity, as represented by Charlson Comorbidity Index in our cohort, in addition to a multitude of patient and tumor factors. The

**FIGURE 3** | Kaplan Meier curves demonstrating time to significant post-diagnosis weight loss in patients without cachexia at diagnosis for patients with prior chronic use of any glucocorticoid (A) and any non-steroidal anti-inflammatory drug (NSAID) (B) medications.

significant 23% decreased likelihood of cachexia incidence attributable to prior NSAID use interpreted through this method suggests these medications might currently be underutilized in cachexia management and prevention.

On initial evaluation, our results demonstrated a survival detriment observed across medication use groups primarily in patients without cachexia at diagnosis. Further evaluation of non-cachectic patients revealed an approximate increase of 10% in the incidence of significant weight loss within 6 months post-diagnosis in patients with prior use of NSAIDs or glucocorticoids. In this cohort of patients without cachexia at diagnosis, multivariate analyses considering interfering patient, tumor, and treatment factors found significant increases in likelihood of post-diagnosis weight loss of more than 40% in NSAID and glucocorticoid use groups. If these medications indeed suppressed the inflammatory ramifications of cachexia-inducing tumor phenotypes prior to diagnosis, it is possible that the reduction of non-cachectic survival represents a progression of cancers which would have classified patients as having cachexia at diagnosis in the absence of prior NSAID or glucocorticoid use. Ultimately, the observed reduction in overall survival within non-cachectic patients with prior NSAID or glucocorticoid use in combination with their increased burden of post-diagnosis weight change potentially represents a delay in cachexia progression by these medications.

Conclusion

The findings of this study substantiate further investigation into cachexia-specific intervention with these medications, primarily NSAIDs, early in cancer development. The clinical outcomes we observed are consistent with the biomolecular reasoning that cachexia progression would possess vulnerability to this medication type, which specifically mitigates inflammatory mechanisms of the syndrome not attributable to the body tissue wasting observed consequently to oncologic therapies. Individuals with elevated cancer risk or unexplained weight loss may benefit from these medications prophylactically, as they could potentially blunt cachexia development before patients are burdened by sequelae from cancer progression and treatment. Deciphering the clinical merit contributed by medications with anti-inflammatory properties in this context can alter their prioritization in treatment protocols and physician judgement for managing patients with chronic conditions simultaneously at risk for developing cachexia-inducing tumors.

REFERENCES

1. Fearon KC, Glass DJ, Guttridge DC. Cancer Cachexia: Mediators, Signaling, and Metabolic Pathways. *Cell Metab* (2012) 16(2):153–66. doi: 10.1016/j.cmet.2012.06.011
2. Arora GK, Gupta A, Guo T, Gandhi AY, Laine A, Williams DL, et al. Janus Kinase Inhibitors Suppress Cancer Cachexia-Associated Anorexia and Adipose Wasting in Mice. *JCSM Rapid Commun* (2020) 3(2):115–28. doi: 10.1002/rco.2.24
3. Arora GK, Gupta A, Narayanan S, Guo T, Iyengar P, Infante RE. Cachexia-Associated Adipose Loss Induced by Tumor-Secreted Leukemia Inhibitory Factor is Counterbalanced by Decreased Leptin. *JCI Insight* (2018) 3(14):e121221. doi: 10.1172/jci.insight.121221

DATA AVAILABILITY STATEMENT

The patient data supporting the conclusions of this article is deidentified through statistical interpretation. The raw data can be made available, without undue reservation, upon reasonable request to the corresponding authors.

AUTHOR CONTRIBUTIONS

SO, PI, and RI designed and conceptualized study. SO, BG, and AG participated in data curation. SO conducted formal analyses. PI RI contributed to funding, project administration, and supervision. SO wrote the original draft. All authors participated in review and editing of this project for final publication. All authors contributed to the article and approved the submitted version.

FUNDING

This work was supported by National Institutes of Health [P30 CA142543]; Burroughs Wellcome Fund Career Awards for Medical Scientists [1019692]; American Cancer Society grant [133889-RSG-19-195-01-TBE]; Cancer Prevention and Research Institute of Texas [RP200170]; V Foundation Scholar Award [V2019-014]; and American Gastroenterological Association Scholar Award [2019AGARSA3].

ACKNOWLEDGMENTS

Data acquisition was facilitated by Xie, Donglu through UT Southwestern's Clinical Data Exchange Network and tumor registry. We thank the UTSW Department of Radiation Oncology Clinical Research Team for their support of our study.

SUPPLEMENTARY MATERIAL

The Supplementary Material for this article can be found online at: <https://www.frontiersin.org/articles/10.3389/fonc.2022.922418/full#supplementary-material>

4. Kant S, Swat W, Zhang S, Zhang ZY, Neel BG, Flavell RA, et al. TNF-Stimulated MAP Kinase Activation Mediated by a Rho Family GTPase Signaling Pathway. *Genes Dev* (2011) 25(19):2069–78. doi: 10.1101/gad.17224711
5. Tuca A, Jimenez-Fonseca P, Gascon P. Clinical Evaluation and Optimal Management of Cancer Cachexia. *Crit Rev Oncol Hematol* (2013) 88(3):625–36. doi: 10.1016/j.critrevonc.2013.07.015
6. Olaechea S, Gannavarapu BS, Gilmore A, Alvarez C, Iyengar P, Infante R. The Influence of Tumour Fluorodeoxyglucose Avidity and Cachexia Development on Patient Survival in Oesophageal or Gastroesophageal Junction Cancer. *JCSM Clin Rep* (2021) 6(4):128–36. doi: 10.1002/crt.2.42
7. Roeland EJ, Bohlke K, Baracos VE, Bruera E, Del Fabbro E, Dixon S, et al. Management of Cancer Cachexia: ASCO Guideline. *J Clin Oncol* (2020) 38(21):2438–53. doi: 10.1200/JCO.20.00611

8. Reid J, Hughes CM, Murray LJ, Parsons C, Cantwell MM. Non-Steroidal Anti-Inflammatory Drugs for the Treatment of Cancer Cachexia: A Systematic Review. *Palliat Med* (2013) 27(4):295–303. doi: 10.1177/0269216312441382
9. Solheim TS, Fearon KC, Blum D, Kaasa S. Non-Steroidal Anti-Inflammatory Treatment in Cancer Cachexia: A Systematic Literature Review. *Acta Oncol* (2013) 52(1):6–17. doi: 10.3109/0284186X.2012.724536
10. Del Fabbro E. Combination Therapy in Cachexia. *Ann Palliat Med* (2019) 8(1):59–66. doi: 10.21037/apm.2018.08.05
11. Yavuzsen T, Davis MP, Walsh D, LeGrand S, Lagman R. Systematic Review of the Treatment of Cancer-Associated Anorexia and Weight Loss. *J Clin Oncol* (2005) 23(33):8500–11. doi: 10.1200/JCO.2005.01.8010
12. Barnes PJ. How Corticosteroids Control Inflammation: Quintiles Prize Lecture 2005. *Br J Pharmacol* (2006) 148(3):245–54. doi: 10.1038/sj.bjp.0706736
13. Arends J, Strasser F, Gonella S, Solheim TS, Madeddu C, Ravasco P, et al. Cancer Cachexia in Adult Patients: ESMO Clinical Practice Guidelines(). *ESMO Open* (2021) 6(3):100092. doi: 10.1016/j.esmoop.2021.100092
14. Aoyagi T, Terracina KP, Raza A, Matsubara H, Takabe K. Cancer Cachexia, Mechanism and Treatment. *World J Gastrointest Oncol* (2015) 7(4):17–29. doi: 10.4251/wjgo.v7.i4.17
15. Charlson ME, Pompei P, Ales KL, MacKenzie CR. A New Method of Classifying Prognostic Comorbidity in Longitudinal Studies: Development and Validation. *J Chronic Dis* (1987) 40(5):373–83. doi: 10.1016/0021-9681(87)90171-8
16. Fearon K, Strasser F, Anker SD, Bosaeus I, Bruera E, Fainsinger RL, et al. Definition and Classification of Cancer Cachexia: An International Consensus. *Lancet Oncol* (2011) 12(5):489–95. doi: 10.1016/S1470-2045(10)70218-7
17. Cahlin C, Korner A, Axelsson H, Wang W, Lundholm K, Svanberg E. Experimental Cancer Cachexia: The Role of Host-Derived Cytokines Interleukin (IL)-6, IL-12, Interferon-Gamma, and Tumor Necrosis Factor Alpha Evaluated in Gene Knockout, Tumor-Bearing Mice on C57 Bl Background and Eicosanoid-Dependent Cachexia. *Cancer Res* (2000) 60(19):5488–93.
18. Maccio A, Madeddu C, Gramignano G, Mulas C, Floris C, Sanna E, et al. A Randomized Phase III Clinical Trial of a Combined Treatment for Cachexia in Patients With Gynecological Cancers: Evaluating the Impact on Metabolic and Inflammatory Profiles and Quality of Life. *Gynecol Oncol* (2012) 124(3):417–25. doi: 10.1016/j.ygyno.2011.12.435
19. Mantovani G, Maccio A, Madeddu C, Serpe R, Antoni G, Massa E, et al. Phase II Nonrandomized Study of the Efficacy and Safety of COX-2 Inhibitor Celecoxib on Patients With Cancer Cachexia. *J Mol Med (Berl)* (2010) 88(1):85–92. doi: 10.1007/s00109-009-0547-z
20. Lundholm K, Daneryd P, Korner U, Hyltander A, Bosaeus I. Evidence That Long-Term COX-Treatment Improves Energy Homeostasis and Body Composition in Cancer Patients With Progressive Cachexia. *Int J Oncol* (2004) 24(3):505–12. doi: 10.3892/ijo.24.3.505
21. McMillan DC, O'Gorman P, Fearon KC, McArdle CS. A Pilot Study of Megestrol Acetate and Ibuprofen in the Treatment of Cachexia in Gastrointestinal Cancer Patients. *Br J Cancer* (1997) 76(6):788–90. doi: 10.1038/bjc.1997.463
22. Lundholm K, Gelin J, Hyltander A, Lonnroth C, Sandstrom R, Svaninger G, et al. Anti-Inflammatory Treatment may Prolong Survival in Undernourished Patients With Metastatic Solid Tumors. *Cancer Res* (1994) 54(21):5602–6.
23. Zidar N, Odar K, Glavac D, Jerse M, Zupanc T, Stajer D. Cyclooxygenase in Normal Human Tissues—is COX-1 Really a Constitutive Isoform, and COX-2 an Inducible Isoform? *J Cell Mol Med* (2009) 13(9B):3753–63. doi: 10.1111/j.1582-4934.2008.00430.x
24. Liu B, Qu L, Yan S. Cyclooxygenase-2 Promotes Tumor Growth and Suppresses Tumor Immunity. *Cancer Cell Int* (2015) 15:106. doi: 10.1186/s12935-015-0260-7
25. Stolina M, Sharma S, Lin Y, Dohadwala M, Gardner B, Luo J, et al. Specific Inhibition of Cyclooxygenase 2 Restores Antitumor Reactivity by Altering the Balance of IL-10 and IL-12 Synthesis. *J Immunol* (2000) 164(1):361–70. doi: 10.4049/jimmunol.164.1.361
26. Axelsson H, Lonnroth C, Andersson M, Lundholm K. Mechanisms Behind COX-1 and COX-2 Inhibition of Tumor Growth. *Vivo Int J Oncol* (2010) 37(5):1143–52. doi: 10.3892/ijo_00000766
27. Ghosh N, Chaki R, Mandal V, Mandal SC. COX-2 as a Target for Cancer Chemotherapy. *Pharmacol Rep* (2010) 62(2):233–44. doi: 10.1016/s1734-1140(10)70262-0
28. Huang M, Stolina M, Sharma S, Mao JT, Zhu L, Miller PW, et al. Non-Small Cell Lung Cancer Cyclooxygenase-2-Dependent Regulation of Cytokine Balance in Lymphocytes and Macrophages: Up-Regulation of Interleukin 10 and Down-Regulation of Interleukin 12 Production. *Cancer Res* (1998) 58(6):1208–16.
29. Moldawer LL, Rogy MA, Lowry SF. The Role of Cytokines in Cancer Cachexia. *JPN J Parenter Enteral Nutr* (1992) 16(6 Suppl):43S–9S. doi: 10.1177/014860719201600602
30. Noguchi Y, Yoshikawa T, Matsumoto A, Svaninger G, Gelin J. Are Cytokines Possible Mediators of Cancer Cachexia? *Surg Today* (1996) 26(7):467–75. doi: 10.1007/BF00311551
31. Nakamura K, Li YQ, Kaneko T, Katoh H, Negishi M. Prostaglandin EP3 Receptor Protein in Serotonin and Catecholamine Cell Groups: A Double Immunofluorescence Study in the Rat Brain. *Neuroscience* (2001) 103(3):763–75. doi: 10.1016/s0306-4522(01)00027-6
32. Saper CB, Romanovsky AA, Scammell TE. Neural Circuitry Engaged by Prostaglandins During the Sickness Syndrome. *Nat Neurosci* (2012) 15(8):1088–95. doi: 10.1038/nn.3159
33. Turnbull AV, Lee S, Rivier C. Mechanisms of Hypothalamic-Pituitary-Adrenal Axis Stimulation by Immune Signals in the Adult Rat. *Ann N Y Acad Sci* (1998) 840:434–43. doi: 10.1111/j.1749-6632.1998.tb09582.x
34. Ohinata K, Suetsugu K, Fujiwara Y, Yoshikawa M. Activation of Prostaglandin E Receptor EP4 Subtype Suppresses Food Intake in Mice. *Prostaglandins Other Lipid Mediat* (2006) 81(1-2):31–6. doi: 10.1016/j.prostaglandins.2006.06.008
35. Gullner HG. The Interactions of Prostaglandins With the Sympathetic Nervous System—a Review. *J Auton Nerv Syst* (1983) 8(1):1–12. doi: 10.1016/0165-1838(83)90017-6
36. Molderings GJ, Colling E, Likungu J, Jakschik J, Gothert M. Modulation of Noradrenaline Release From the Sympathetic Nerves of the Human Saphenous Vein and Pulmonary Artery by Presynaptic EP3- and DP-Receptors. *Br J Pharmacol* (1994) 111(3):733–8. doi: 10.1111/j.1476-5381.1994.tb14799.x
37. Olson B, Diba P, Korzun T, Marks DL. Neural Mechanisms of Cancer Cachexia. *Cancers (Basel)* (2021) 13(16):3990. doi: 10.3390/cancers13163990
38. Vegiopoulos A, Muller-Decker K, Strzoda D, Schmitt I, Chichelnitskiy E, Ostertag A, et al. Cyclooxygenase-2 Controls Energy Homeostasis in Mice by De Novo Recruitment of Brown Adipocytes. *Science* (2010) 328(5982):1158–61. doi: 10.1126/science.1186034
39. Argiles JM, Busquets S, Stemmler B, Lopez-Soriano FJ. Cachexia and Sarcopenia: Mechanisms and Potential Targets for Intervention. *Curr Opin Pharmacol* (2015) 22:100–6. doi: 10.1016/j.coph.2015.04.003
40. Smith KL, Tisdale MJ. Mechanism of Muscle Protein Degradation in Cancer Cachexia. *Br J Cancer* (1993) 68(2):314–8. doi: 10.1038/bjc.1993.334
41. Zhou W, Jiang ZW, Tian J, Jiang J, Li N, Li JS. Role of NF-kappaB and Cytokine in Experimental Cancer Cachexia. *World J Gastroenterol* (2003) 9(7):1567–70. doi: 10.3748/wjg.v9.i7.1567

Conflict of Interest: The authors declare that the research was conducted in the absence of any commercial or financial relationships that could be construed as a potential conflict of interest.

Publisher's Note: All claims expressed in this article are solely those of the authors and do not necessarily represent those of their affiliated organizations, or those of the publisher, the editors and the reviewers. Any product that may be evaluated in this article, or claim that may be made by its manufacturer, is not guaranteed or endorsed by the publisher.

Copyright © 2022 Olaechea, Gilmore, Alvarez, Gannavarapu, Infante and Iyengar. This is an open-access article distributed under the terms of the Creative Commons Attribution License (CC BY). The use, distribution or reproduction in other forums is permitted, provided the original author(s) and the copyright owner(s) are credited and that the original publication in this journal is cited, in accordance with accepted academic practice. No use, distribution or reproduction is permitted which does not comply with these terms.



Combining Network Pharmacology and Experimental Validation to Study the Action and Mechanism of Water extract of Asparagus Against Colorectal Cancer

Huiling Liang^{1†}, Yanju Li^{2†}, Feiqing Wang^{1,3†}, Jianing Zhao¹, Xu Yang¹, Dan Wu¹, Chike Zhang², Yanqing Liu¹, Jie Huang², Min Su⁴, Zhixu He⁴, Yang Liu^{1,2,4*}, Jishi Wang^{2*} and Dongxin Tang^{1*}

OPEN ACCESS

Edited by:

Anjana Munshi,
Central University of Punjab, India

Reviewed by:

Shujie Cheng,
China Pharmaceutical University,
China
Mansi Wu,
Jinan University, China

*Correspondence:

Yang Liu
ly7878@163.com
Jishi Wang
wjszhp@163.com
Dongxin Tang
tangdongxintcm@163.com

[†]These authors have contributed
equally to this work

Specialty section:

This article was submitted to
Pharmacology of Anti-Cancer Drugs,
a section of the journal
Frontiers in Pharmacology

Received: 26 January 2022

Accepted: 30 March 2022

Published: 14 June 2022

Citation:

Liang H, Li Y, Wang F, Zhao J, Yang X,
Wu D, Zhang C, Liu Y, Huang J, Su M,
He Z, Liu Y, Wang J and Tang D (2022)
Combining Network Pharmacology
and Experimental Validation to Study
the Action and Mechanism of Water
extract of Asparagus Against
Colorectal Cancer.
Front. Pharmacol. 13:862966.
doi: 10.3389/fphar.2022.862966

¹Department of Scientific Research, The First Affiliated Hospital of Guizhou University of Traditional Chinese Medicine, Guiyang, China, ²Department of Hematology, Affiliated Hospital of Guizhou Medical University, Guiyang, China, ³Academy of Medical Engineering and Translational Medicine, Medical College of Tianjin University, Tianjin, China, ⁴National and Guizhou Joint Engineering Laboratory for Cell Engineering and Biomedicine Technique, Guizhou Province Key Laboratory of Regenerative Medicine, Key Laboratory of Adult Stem Cell Translational Research, Chinese Academy of Medical Sciences, Guizhou Medical University, Guiyang, China

Asparagus (ASP) is a well-known traditional Chinese medicine with nourishing, moistening, fire-clearing, cough-suppressing, and intestinal effects. In addition, it exerts anti-inflammatory, antioxidant, anti-aging, immunity-enhancing, and anti-tumor pharmacological effect. The anti-tumor effect of ASP has been studied in hepatocellular carcinoma. However, its action and pharmacological mechanism in colorectal cancer (CRC) are unclear. The present study aimed to identify the potential targets of ASP for CRC treatment using network pharmacology and explore its possible therapeutic mechanisms using *in vitro* and *in vivo* experiments. The active compounds and potential targets of ASP were obtained from the TCMSP database, followed by CRC-related target genes identification using GeneCards and OMIM databases, which were matched with the potential targets of ASP. Based on the matching results, potential targets and signaling pathways were identified by protein-protein interaction (PPI), gene ontology (GO) functions, and Kyoto Encyclopedia of Genes and Genomes (KEGG) pathway enrichment analyses. Finally, *in vitro* and *in vivo* experiments were performed to further validate the anti-cancer effects of ASP on CRC. Network pharmacology analysis identified nine active components from ASP from the database based on oral bioavailability and drug similarity index, and 157 potential targets related to ASP were predicted. The PPI network identified tumor protein 53 (TP53), Fos proto-oncogene, AP-1 transcription factor subunit (FOS), and AKT serine/threonine kinase 1 (AKT1) as key targets. GO analysis showed that ASP might act through response to wounding, membrane raft, and transcription factor binding. KEGG enrichment analysis revealed that ASP may affect CRC through the phosphatidylinositol-4,5-bisphosphate 3-kinase PI3K/AKT/mechanistic target of rapamycin kinase (mTOR) signaling pathway. *In vitro*, ASP inhibited cell proliferation, migration, and invasion of HCT116 and LOVO cells, and caused G0/G1 phase arrest and

apoptosis in CRC cells. *In vivo*, ASP significantly inhibited the growth of CRC transplanted tumors in nude mice. Furthermore, pathway analysis confirmed that ASP could exert its therapeutic effects on CRC by regulating cell proliferation and survival through the PI3K/AKT/mTOR signaling pathway. This study is the first to report the potential role of ASP in the treatment of colorectal cancer.

Keywords: colorectal cancer, Chinese medicine, network pharmacology, asparagus, PI3K/AKT/mTOR signaling pathway

1 INTRODUCTION

Colorectal cancer (CRC) is a highly prevalent malignancy of the digestive system and is the second leading cause of cancer-related deaths worldwide, with a higher incidence in men than in women, and has the third highest rate of malignant lethality (Zhu et al., 2017). Approximately 20%–25% of patients with CRC already have metastases at the time of initial diagnosis because of the insidious onset of colorectal cancer and the lack of effective clinical screening biomarkers (Xu et al., 2020). One study predicted that by 2030, there will be more than 2.2 million new cases and 1.1 million cancer deaths worldwide. The burden will increase by 60%, with low- and middle-income countries facing greater challenges (Arnold et al., 2017). In recent years, good progress has been made in surgical techniques and systemic drug therapy; however, side effects, such as nausea, vomiting, pain, and leukopenia, can be particularly distressing for patients with CRC (Hattori et al., 2019; Vodenkova et al., 2020). Encouragingly, traditional Chinese medicine (TCM) has played an increasingly important role in the treatment of CRC as a major source of natural medicines and herbal products, with advantages of reliable efficacy and low rates of adverse effects.

In recent years, several studies have described the extensive use of TCM in cancer treatment, which has received increasing international attention (Chen et al., 2018; Wang et al., 2018). In a cohort study including 1,988 patients with lung adenocarcinoma treated with tyrosine kinase inhibitors (TKI), TCM treatment was associated with better progression-free survival and overall survival compared with those of the untreated group (Li C. L. et al., 2019). Similarly, in CRC, a multicenter prospective cohort study including 312 patients with stage II and III CRC reached similar conclusions (Xu et al., 2017). In a retrospective cohort study including 817 patients with CRC, TCM improved disease-free survival in patients with stage II and III disease (Shi et al., 2017). With the development of herbal injections, the intravenous delivery of antitumor herbs has been used widely in clinical practice. A study containing 366 randomized controlled trials and 48 systematic evaluations and meta-analyses reported more consistent benefits of herbal injections in terms of tumor response, quality of life, bone marrow suppression, and improvement in immune function (Yang et al., 2021). It was found that the active ingredients of herbal medicines usually exert their anti-cancer effects by inhibiting cell proliferation, inducing apoptosis, suppressing metastasis, inhibiting angiogenesis, reversing multidrug resistance, and modulating

immune function (Yan et al., 2017; Li X. et al., 2019; Liu et al., 2020).

Chinese asparagus (*Asparagus cochinchinensis* (Lour) Merr., hereafter referred to as ASP) is a tuberous root vegetable in the lily family, which is widely distributed in Asia and is one of the common Chinese herbs with a long history in China (Lee et al., 2017). ASP has nourishing, moistening, fire-clearing, cough-suppressing, and intestinal effects and exerts anti-inflammatory, antioxidant, anti-aging, immunity-enhancing, and anti-tumor pharmacological effect (Samad et al., 2014; Lei et al., 2017; Cheng et al., 2019; Sun et al., 2020). Recent studies have reported that ASP polysaccharides can inhibit hypoxia-induced hepatocellular carcinoma cell migration, invasion, and angiogenesis by regulating hypoxia inducible factor alpha (HIF-1 α) and vascular endothelial growth factor (VEGF) expression through mitogen activated protein kinase (MAPK) and phosphatidylinositol-4,5-bisphosphate 3-kinase (PI3K) signaling pathways (Cheng et al., 2021). In addition, ASP-derived exosome-like nanovesicles could inhibit hepatocellular carcinoma cell proliferation, induce apoptosis, and inhibit tumor growth without significant side effects in mice (Zhang et al., 2021).

Network pharmacology is a strategy that combines network science, bioinformatics, and computer science methods into the pharmacological study of TCMs to determine their mechanism of action in the context molecular network regulation. It is holistic and systematic in nature, similar to the holistic view of TCM, and uses the principle of discriminative treatment, providing a more scientific and effective strategy for modern TCM research (Zhang et al., 2019). The aim of the present study was to identify the natural compounds of ASP through network pharmacology, explore the key targets of ASP for the treatment of CRC, understand their potential mechanism of action, and provide a basis for the development and application of ASP. The flow chart of the study is shown in **Figure 1**.

2 METHODS AND MATERIALS

2.1 Network Pharmacology

The systematic Pharmacology Database of Traditional Chinese Medicine (TCMSP, <http://tcmbspw.com/tcmbsp.php>) (Zhang et al., 2019) was used to screen active ASP compounds. Oral bioavailability and drug similarity were set to $\geq 30\%$ and ≥ 0.18 using a pharmacokinetic information retrieval filter based on the TCMSP platform to obtain qualified herbal compounds. The chemical structures of the corresponding compounds were

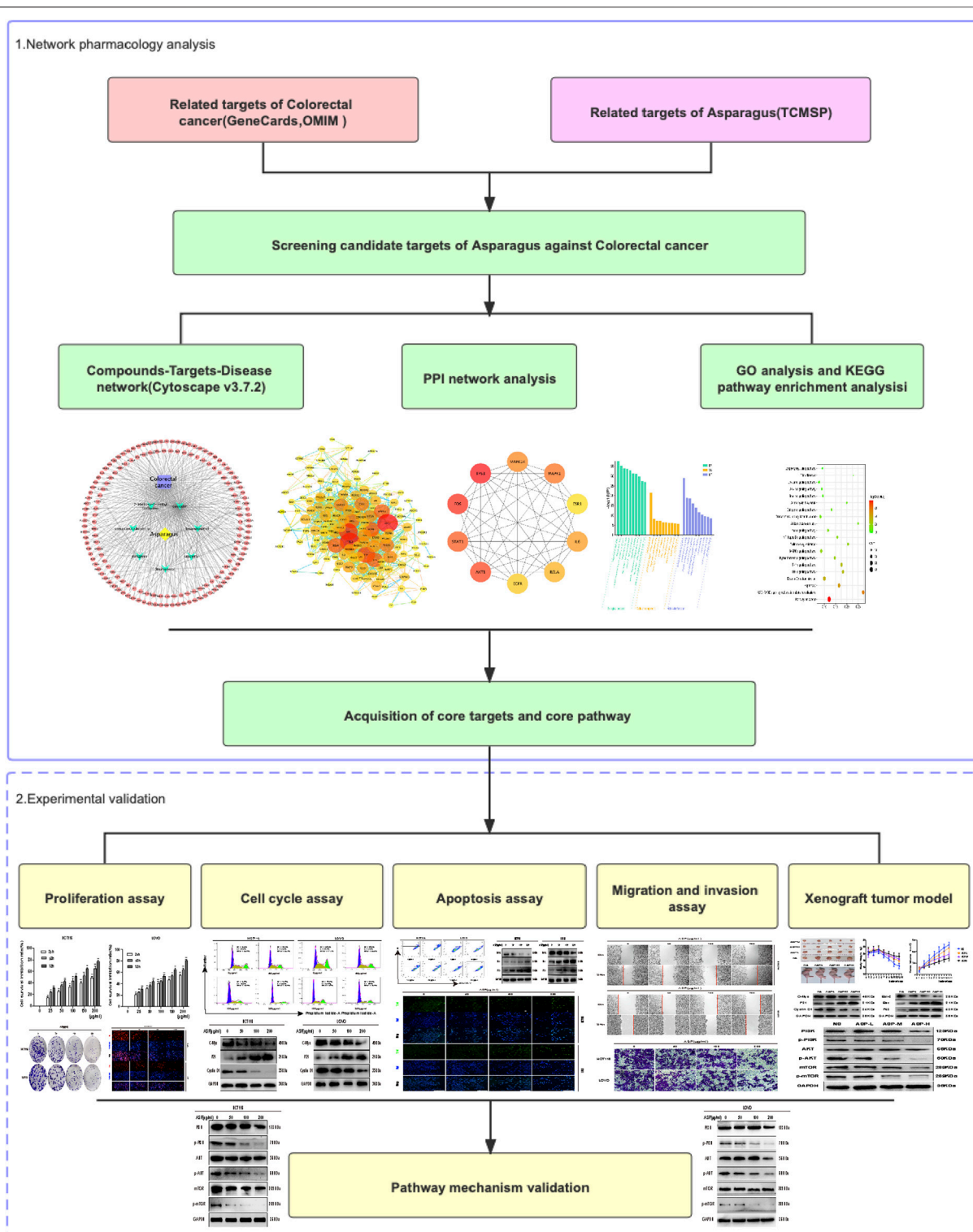
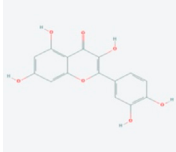
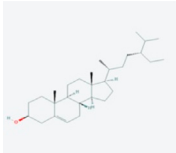
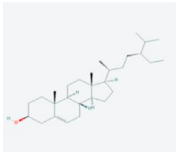
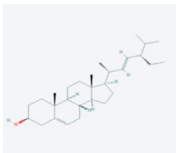
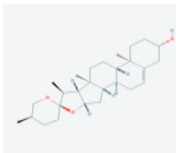
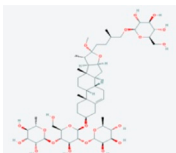
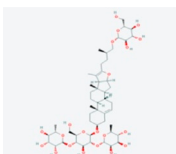
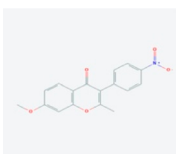
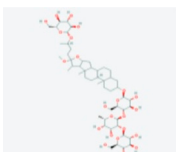


FIGURE 1 | The workflow of the network pharmacology analysis and validation of ASP against CRC.

TABLE 1 | Active ingredients and absorbed, distributed, metabolized and excreted (ADME) parameters of ASP.

Mol ID	Molecule name	Structure	OB (%)	DL
MOL000098	quercetin		46.43	0.28
MOL000358	beta-sitosterol		36.91	0.75
MOL000359	sitosterol		36.91	0.75
MOL000449	Stigmasterol		43.83	0.76
MOL000546	diosgenin		80.88	0.81
MOL003889	methylprotodioscin_qt		35.12	0.86
MOL003891	pseudoprotodioscin_qt		37.93	0.87
MOL003896	7-Methoxy-2-methyl isoflavone		42.56	0.20
MOL003901	Asparaside A_qt		30.60	0.86

downloaded using the PubChem database (<https://pubchem.ncbi.nlm.nih.gov/>). The GeneCard database (<https://www.genecards.org/>) and OMIM database (<http://www.omim.org/> updated in 2020) were used to predict and screen of CRC targets. Oliveros, J. C. Venny 2.1 was used to screen for common targets between ASP and CRC-related targets (<https://bioinfogp.cnb.csic.es/tools/venny/index.html>).

Cytoscape V 3.7.2 (<http://www.cytoscape.org/>) software was used to construct drug compound-disease-target networks and to analyze core compounds using the merge function. The STRING database platform was used to construct protein-protein (PPI) interaction networks for common ASP and CRC-related targets with a medium confidence level (0.7) and to reject target proteins independent of the network. Metascape (<http://metascape.org/>) was used for gene ontology (GO) analysis and Kyoto Encyclopedia of Genes and Genomes (KEGG) pathway analysis (Zhou et al., 2019).

2.2 Experimental Validation

2.2.1 Preparation of ASP

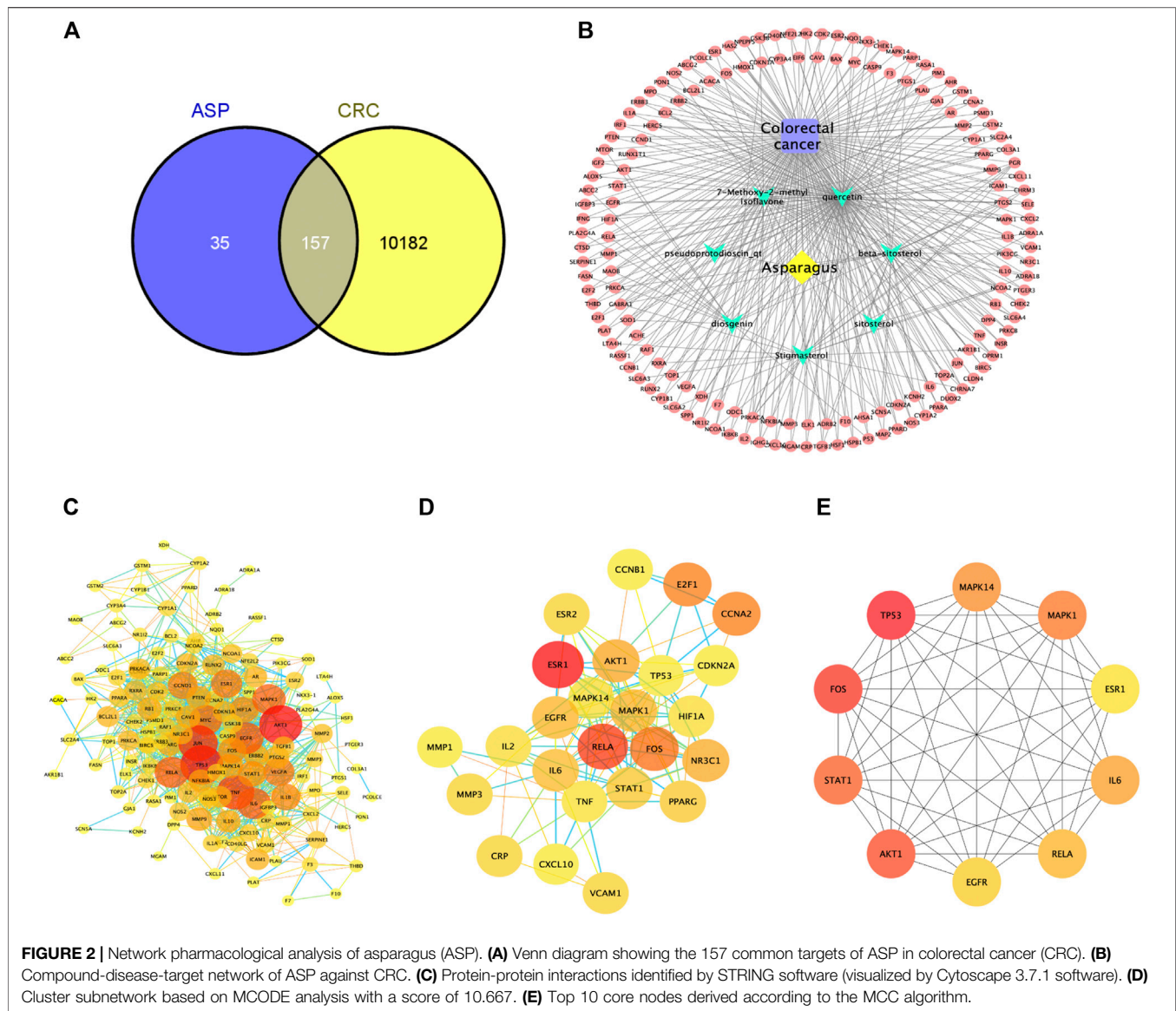
Pieces of ASP were purchased from GuizhouRen Ji Tang Company Limited (Guiyang, China). Fifty grams of raw drug were crushed, placed in 10 times the volume of purified water, soaked for 2 h, extracted twice at reflux, 1 h/time, filtered, combined filtrate, made up the reduced weight with water, concentrated at 70°C under reduced pressure, and concentrated to 1 g/ml of raw drug. Two ml of the concentrated solution was diluted to 10 ml using purified water, filtered through a 0.22 µm pore size filter, divided into sterile centrifuge tubes, and stored at -20°C.

2.2.2 Cell Culture

Human CRC cell lines (HCT116, LOVO, and LO2) were provided by the Shanghai Institute of Cell Biology, Chinese Academy of Sciences. Cells were cultured in high-sugar Dulbecco's modified Eagle medium (DMEM, GIBCO, Grand Island, NY, United States) supplemented with 10% fetal bovine serum (FBS, BI, Kibbutz, Israel) and 1% penicillin-streptomycin (Solarbio, Beijing, China). Cells were cultured at 37°C in a 5% CO₂ atmosphere.

2.2.3 Cell Viability Assay

CRC and LO2 cells 100 µl/well (6×10^3 cells/ml) were inoculated into 96-well plates and incubated overnight in a humidified incubator at 37°C and 5% CO₂. Cells were then pretreated with ASP (0, 25, 50, 100, 150, and 200 µg/ml) for 24, 48, and 72 h. Then, 10 µl of Cell Counting Kit-8 (CCK-8) (Dojindo, Kumamoto, Japan) was added to each well, and the cells were incubated at 37°C, 5% CO₂ for 4 h. Finally, the absorbance was measured at 450 nm using a Microplate Reader (Thermo Fisher Scientific, Waltham, MA, United States) and the cell proliferation inhibition rate was calculated. Cell proliferation inhibition rate = $(1 - \text{absorbance value of experimental group} / \text{absorbance value of control group}) \times 100\%$.



2.2.4 Crystalline Violet Staining

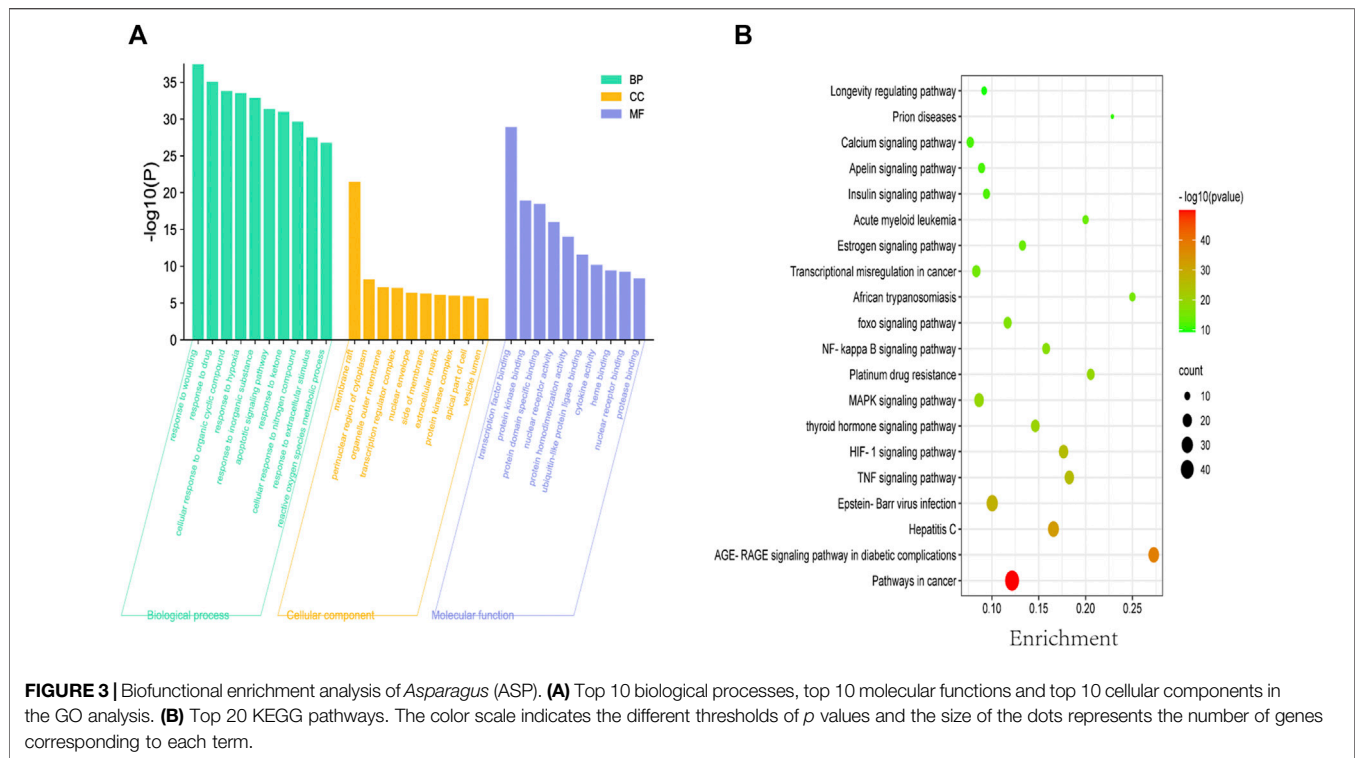
When cell growth reached 70%–90% confluence, cells were digested (Trypsin-EDTA solution, 0.25% with phenol red, Solarbio, Beijing, China) and collected in 6-well cell culture plates at a cell density of 1×10^5 cells/ml. Cells were incubated in a 5% CO₂ cell culture incubator at 37°C for 24 h. When cells reached 50% confluence, they were exposed to ASP (0, 50, 100, and 200 µg/ml) for 24 h. Cells were fixed with 4% paraformaldehyde, washed twice with phosphate buffered saline (PBS, Solarbio, Beijing, China), and stained with 1% crystalline violet solution (Solarbio). Excess crystal violet dye was washed away using tap water. After natural drying at room temperature, the morphological changes of the cells were observed, analyzed, and photographed under an inverted microscope (Leica DM2500, Heidelberg, Germany).

2.2.5 Colony Formation Assay

Cells were inoculated into 6-well plates at 700 cells per well and treated with different concentrations of ASP for 24 h. Cells were washed with PBS and culture was continued in complete growth medium, which was replaced with fresh medium every 3 days for a total of 14 days. Colonies were fixed with 4% paraformaldehyde and stained with 1% crystalline violet solution for 15 min. The colonies were observed under a light microscope and manually counted in three randomly selected fields to measure the cell colony number (>50 cells/colony).

2.2.6 5-Ethynyl-2'-deoxyuridine (EdU) Assay

CRC cells in logarithmic phase of growth (5,000 cells per well) were inoculated into 96-well plates and incubated for 24 h. Cells were exposed to 0, 50, 100, and 200 µg/ml of ASP and incubation was continued for 24 h. EdU (RiboBio, Guangzhou, China) labeling solution at a dilution of 1,000:1 was added and



incubated for 2 h. The remaining operations were completed according to the manufacturer's instructions, taking care to avoid light. Cells were then imaged under an inverted fluorescence microscope (Nikon, Tokyo, Japan, three random positions in each well were photographed, and the fluorescence of EdU-positive cells was measured using ImageJ 1.8.0 software (NIH, Bethesda, MD, United States). EdU-positive cells (%) = red EdU count/blue Hoechst count $33,342 \times 100$.

2.2.7 Flow Cytometry to Assay the Cell Cycle

HCT116 and LOVO cells were treated with 0, 50, 100, and 200 $\mu\text{g}/\text{ml}$ of ASP for 24 h. The collected cells (1×10^6) were fixed in cold ethanol and stored overnight at 4°C . The next day, cells were washed twice with cold PBS; then 100 μl of RNase A (25 $\mu\text{g}/\text{ml}$) and 400 μl of propidium iodide (PI, 50 $\mu\text{g}/\text{ml}$) were added to each sample according to the instructions of the cell cycle kit (KeyGEN, Nanjing, China) and incubated for 40 min in the dark. The cells were analyzed using a flow cytometer (BD Biosciences, San Jose, CA, United States) and FlowJo 10.0 software (FlowJo, Ashland, OR, United States).

2.2.8 Flow Cytometry to Assay Cell Apoptosis

Cells (1×10^5 cells/ml) were inoculated in 6-well plates and incubated for 24 h and then reacted with the indicated concentrations of ASP for 24 h. Cells were collected according to the instructions of the Fluorescein isothiocyanate (FITC) Annexin V/PI Apoptosis Detection Kit (KeyGEN), and 500 μl of Binding Buffer was added to each sample tube to prepare a cell suspension, the Annexin V-FITC/PI fluorescent dye was added, and incubated for 15 min in the dark. The cells were then

measured using flow cytometry (BD Biosciences) and the data were analyzed using FlowJo 10.0 software.

2.2.9 Terminal Deoxynucleotidyl Transferase Nick-End-Labeling (TUNEL) Assay

CRC cells were inoculated at 4,000 cells per well into 96-well plates and incubated for 24 h. The cells were then treated with the indicated concentrations of ASP for 24 h. Cells were fixed in 4% paraformaldehyde for 20 min at room temperature. Apoptosis was detected using the TUNEL Apoptosis Assay Kit (Beyotime, Shanghai, China). TUNEL assay solution (50 μl) was added to each well according to the manufacturer's protocol and incubated for 60 min at 37°C in the dark. The cell nuclei were counterstained using 4',6-diamidino-2-phenylindole (DAPI). TUNEL-positive cells were imaged under a fluorescence microscope and measured using the ImageJ 1.8.0 software. TUNEL-positive cells (%) = Green TUNEL count/blue DAPI count $\times 100$.

2.2.10 Wound Healing Assay

Cells (2×10^5 cells/well) were inoculated onto 6-well plates and incubated for 24 h in a 37°C incubator. A sterile pipette tip was used to make a scratch in the cell monolayer, the cells were washed three times with PBS to dislodge the cells debris, photographed under an inverted microscope, and the culture was continued with fresh medium without FBS in the presence of the indicated concentrations of ASP for 24 h. Six different locations were photographed randomly under an inverted microscope, and the wound area was analyzed using ImageJ 1.8.0 software. Wound healing was assessed according to the size of the wound at 0 h and 24 h.

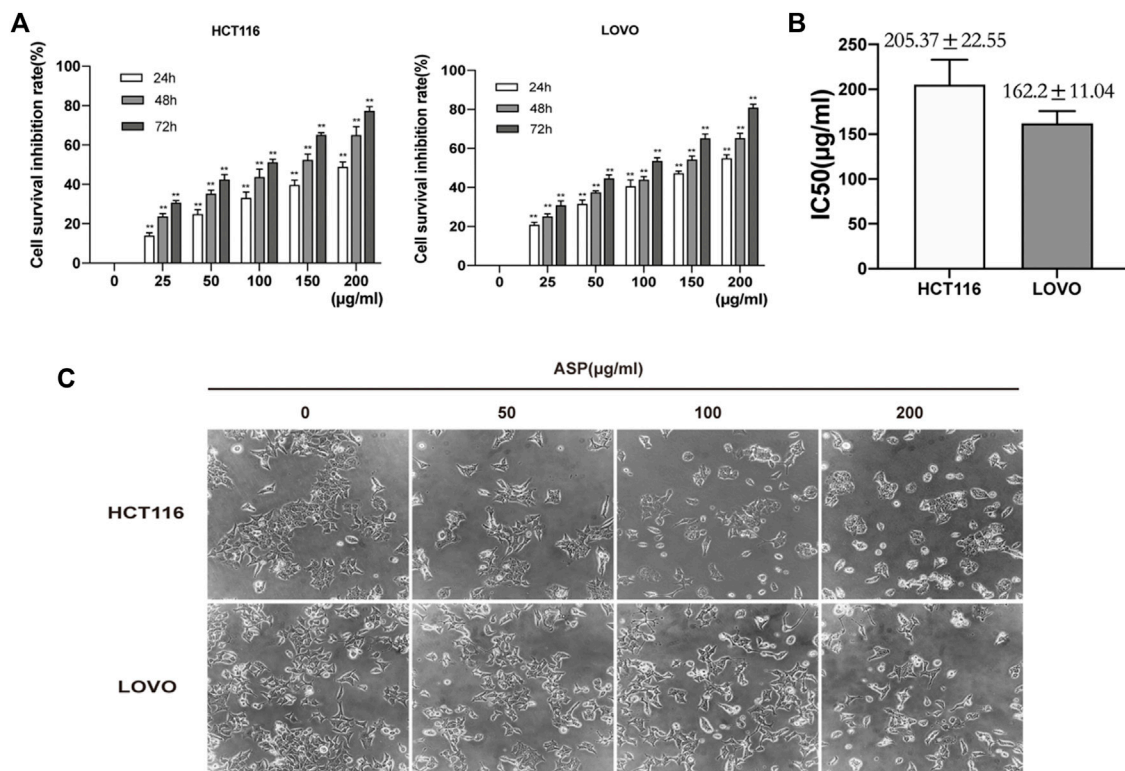


FIGURE 4 | *Asparagus* aqueous extract (ASP) inhibits the proliferation of HCT116 and LOVO cells. **(A)** Cell Counting Kit-8 (CCK-8) analysis of human colorectal cancer (CRC) cell lines (HCT116 and LOVO cells) after treatment with the indicated doses of ASP for 24, 48, and 72 h. **(B)** Median inhibitory concentrations (IC₅₀) of ASP acting against HCT116 and LOVO cells for 24 h. **(C)** Morphological changes of cells observed by light microscopy after 24 h of ASP application at the indicated concentrations. **p* < 0.05, ***p* < 0.01 vs. control.

2.2.11 Transwell Invasion Assay

Transwell invasion assays were performed using an 8 µm well Transwell chamber system (Corning Inc. Corning, NY, United States). The upper chamber was coated with Matrigel matrix gel (BD Biosciences). Cells (5×10^4 cells/well) after 24 h of treatment were resuspended in 200 µl of FBS-free medium, inoculated into the upper chamber, and 600 µl of complete medium containing 10% FBS was added to the lower chamber. After 24 h of incubation, uninvaded cells were removed from the upper surface of the membrane using a cotton swab, and the invaded cells were fixed and stained with 1% crystal violet solution. Finally, light microscopy was performed to photograph and count six random fields of view in each group.

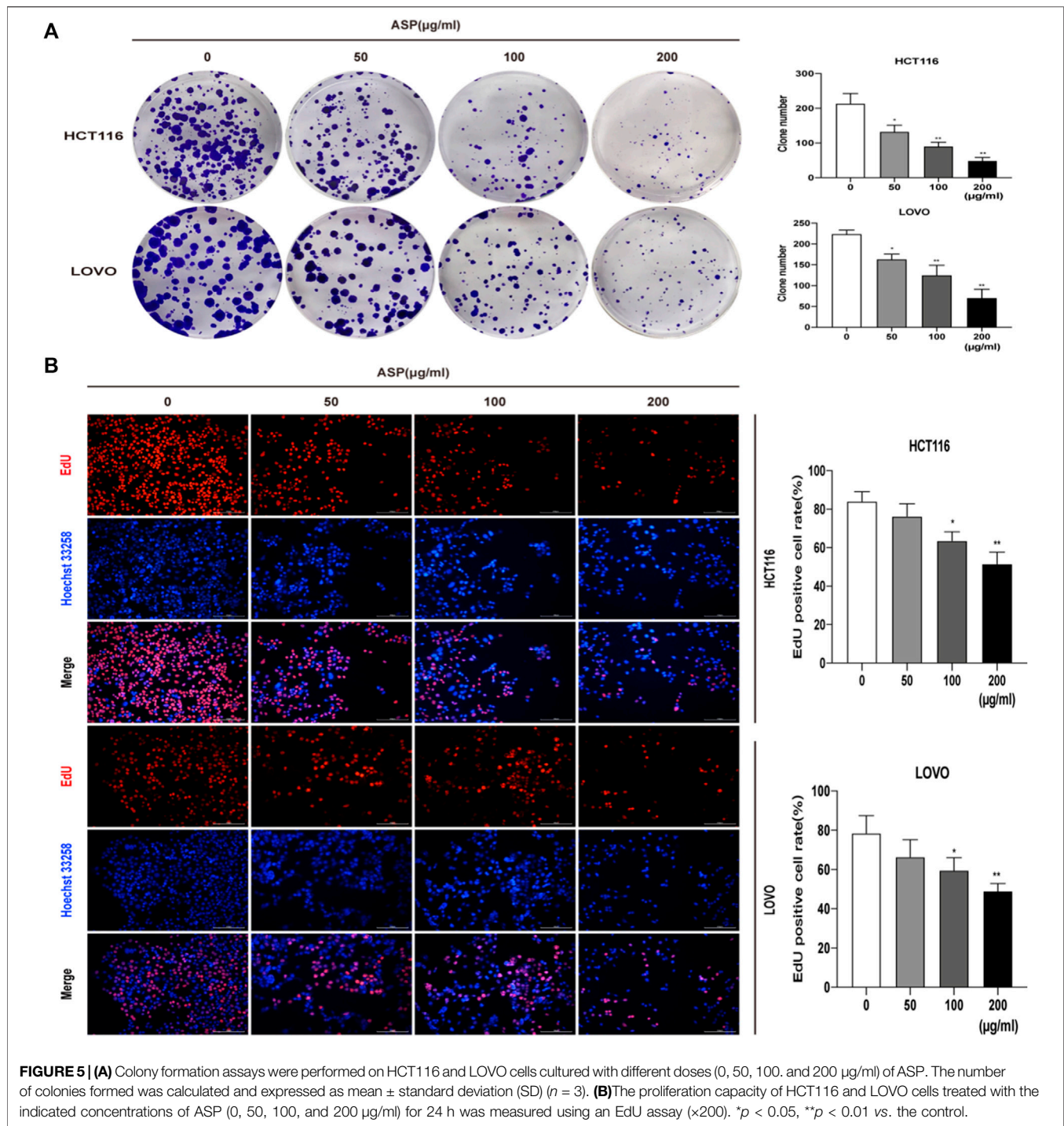
2.2.12 Western Blotting Analysis

Total cellular or tissue proteins were extracted using Radioimmunoprecipitation assay (RIPA) lysis buffer containing protease inhibitor, phosphatase inhibitor, and PMSF (Solarbio, Beijing, China). Equal amounts of proteins were subjected to 10% sodium dodecyl sulfate polyacrylamide gel electrophoresis (SDS-PAGE) (Solarbio) for separation and then transferred to polyvinylidene difluoride (PVDF) membranes (0.45 µm, Millipore, United States). The membranes were blocked using with 5% skim milk for 1 h at room temperature, and then

incubated with primary antibodies overnight at 4°C. The next day, the membranes were washed three times with Tris-buffered saline-Tween 20 (TBST, Solarbio) and incubated with goat anti-rabbit or goat anti-mouse horseradish peroxidase (HRP)-coupled secondary antibodies for 2 h at room temperature. Finally, immunoreactive protein bands were visualized using ultrasensitive ECL chemiluminescent ready-to-use substrate (BOSTER, Wuhan, China). The grayscale values of the protein bands were quantified using ImageJ software and the relative level of the proteins was normalized by the level of glyceraldehyde-3-phosphate (GAPDH). The antibodies used were as follows: anti-tumor protein 53 (TP53), anti-BCL2 associated X (Bax), anti-BCL2 apoptosis regulator (Bcl-2), anti-Cyclin D1, anti-P21, anti-C-Myc, anti-PI3K, anti-phospho (p)-PI3K, anti-protein kinase B (AKT), anti-p-AKT, anti-mechanistic target of rapamycin kinase (mTOR), anti-p-mTOR, and anti-GAPDH 1:1,000 (Beyotime), goat anti-rabbit and goat anti-mouse HRP-coupled secondary antibodies 1:5,000 (BOSTER).

2.3 Nude Mice Tumor Xenografts

Twenty male BALB/c nude mice (4 weeks old, 20 ± 2 g) were purchased from Spelford Biotechnology Ltd. (Beijing, China). All animal experiments were performed in the pathogen-free medical animal laboratory of the First Affiliated Hospital of Guizhou University of Traditional Chinese and were approved by the



Animal Ethics Committee of the First Affiliated Hospital of Guizhou University of Traditional Chinese (approval number: AHQU20180310A). After 3 days of acclimatization in a specific pathogen free (SPF)-grade animal room, 200 μl (5×10^7 cells/ml) of HCT116 cells were implanted subcutaneously into the right axilla of each nude mouse. At 7 days after cell inoculation, non-tumor-forming and tumor-oversized mice were excluded, and then the mice were randomly divided into four groups: control

($n = 5$, 0.9% saline, 0.1 ml/10 g) and ASP-L, ASP-M, and ASP-H groups ($n = 5$, ASP at 100, 200, and 300 mg/kg, 0.1 ml/10 g, respectively). The drug concentration in the ASP-treated group was derived from a previous study (Agrawal et al., 2008). The drug was administered via gavage, once daily for 2 weeks. The body weight and tumor size of nude mice were measured every other day. The tumor volume was determined by measuring the length (L) and width (W) and calculated according to the

following formula: tumor volume (mm³) = 0.5 × L × W²). At the end of the experiment, the neck of nude mice was dislocated, and the tumors were excised, weighed, and photographed.

2.4 Statistical Analysis

Data analysis was performed using GraphPad Prism 8.3.1 software (San Diego, CA, United States). All experimental data are expressed as the mean ± SD. The statistical significance of the results was analyzed using one-way analysis of variance (ANOVA) for multiple group comparisons and by Student's t-test for two group comparisons. A *p* value < 0.05 indicates a significant difference. All experiments were performed in triplicate.

3 RESULTS

3.1 Network Pharmacological Analysis of ASP Targeting CRC

In this study, using the TCMSP database (Table 1), we retrieved a total of nine compounds (among which methylprotodioscin_{qt} and Asparaside A_{qt} had no relevant targets) from ASP using Oral Bioavailability (OB) ≥30% and Drug-like (DL) ≥0.18 as screening conditions.

From these 7 compounds, 192 relevant genes were screened. 10,339 genes associated with CRC were screened in GeneCard and OMIM databases (duplicates were removed). A total of 157 common targets were obtained using Venny 2.1.0 (Figure 2A), and these intersections were considered as potential candidate targets for ASP against CRC. Seven active ingredients and 157 “drug-disease” key target genes were introduced into Cytoscape 3.7.1 software. A visualized active ingredient-cancer target network was constructed (Figure 2B). The active ingredients with the most target genes in ASP were quercetin, beta-sitosterol, and 7-Methoxy-2-methyl isoflavone.

The target PPI network was constructed using the STRING database platform, and 157 target genes were introduced. The selected species was *Homo sapiens*, and the PPI network with confidence level >0.7 and potential targets of ASP against CRC is shown in Figure 2C. The PPI network consists of 141 hub nodes and 972 edges (after removing the free nodes). The results show that there were five cluster subnetworks based on MCODE analysis, where the highest scoring cluster subnetwork made up of 25 hub nodes and 128 edges. The clusters included: RELA, STAT1, ESR1, AKT1, MAPK1, IL2, MAPK14, CCNB1, CRP, TP53, CCNA2, PPARG, VCAM1, CXCL10, FOS, ESR2, E2F1, MMP3, IL6, TNF, EGFR, CDKN2A, MMP1, HIF1A, and NR3C1, with a score of 10.667 (Figure 2D). Moreover, the top 10 core nodes were obtained in the order of the MCC algorithm score from highest to lowest, namely TP53, FOS, AKT1, STAT1, MAPK1, MAPK14, IL6, RELA, EGFR, and ESR1 (Figure 2E). These results suggest that these core targets may contribute to the fundamental therapeutic role of ASP in CRC.

To explore the therapeutic mechanisms of putative ASP targets for CRC, GO and KEGG pathway enrichment analysis was performed using Metascape (updated 2021-02-01). A total of 2068 biological processes (BP), 89 cellular components (CC) and 165 molecular functions (MF),

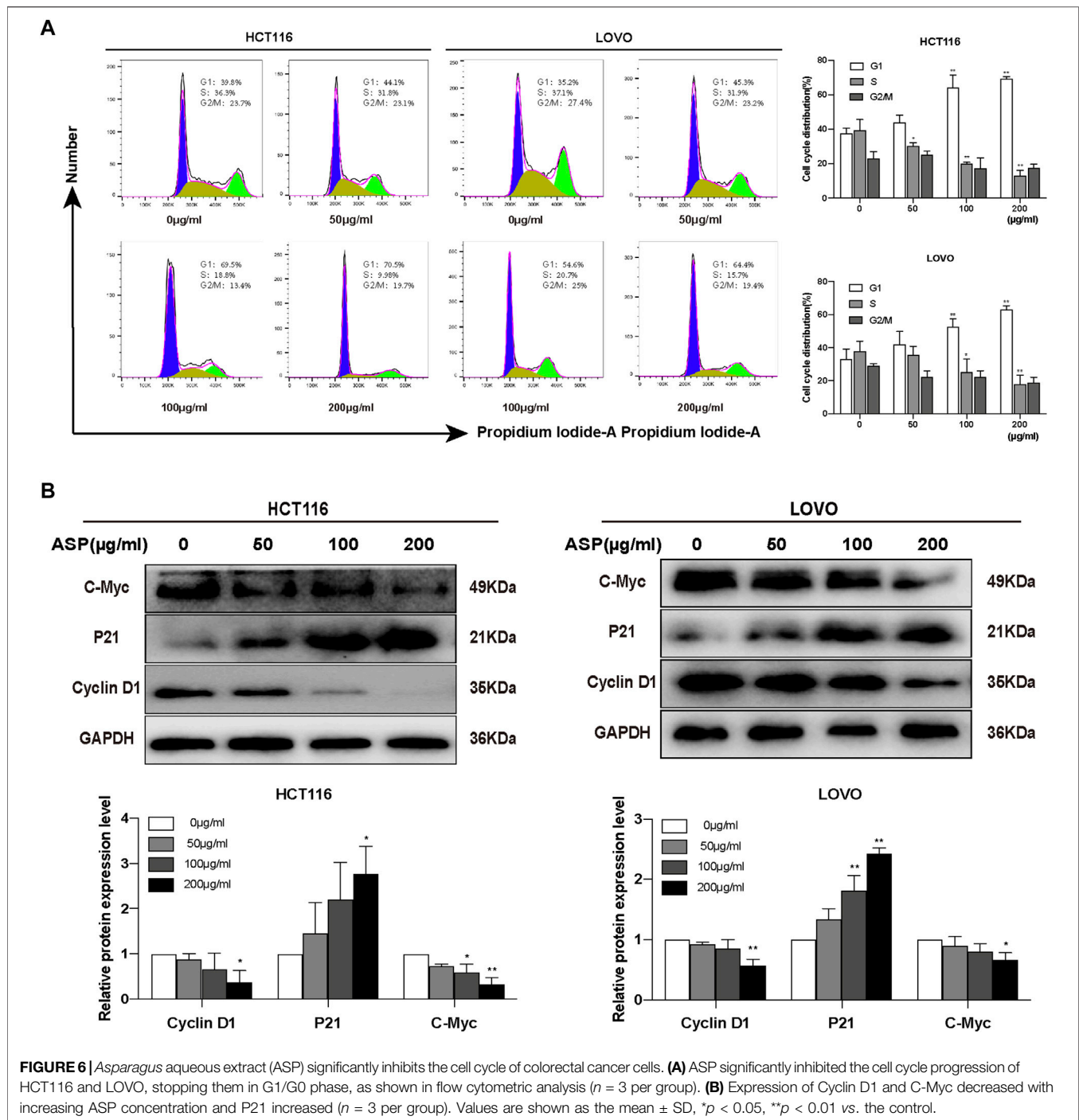
respectively, satisfied the requirements of gene count ≥3 and *p*-value ≤ 0.01. The top 10 significantly enriched GO terms in BP, CC and MF are plotted in Figure 3A, and the results showed that ASP's effects might be mediated through response to wounding, response to drug, membrane raft, perinuclear region of cytoplasm, organelle outer membrane, transcription factor binding, protein kinase binding, and protein domain specific binding, to regulate the proliferation and apoptosis of CRC cancer cells, thus exerting its anti-cancer effects on CRC. A total of 329 related signaling pathways were obtained by KEGG enrichment analysis. The top 20 signaling pathways with high confidence and *p*-values ≤ 0.01 were selected for analysis, as shown in Figure 3B. From Figure 3B, it can be seen that most of the target genes affect substances or signaling pathways, including Pathways in cancer, AGE-RAGE signaling pathway in diabetic complications, Hepatitis C, Epstein-Barr virus infection, and TNF signaling pathway. We found that Pathways in cancer play an important role in ASP against CRC. This pathway is large and complex, including ERK signaling, PI3K Signaling, WNT Signaling, NOTCH Signaling, Other RAS Signaling, etc.

3.2 ASP Inhibited the Proliferation of CRC Cells *in vitro*

CRC cells (HCT116, LOVO, and LO2) were pretreated with different concentrations of ASP (0–200 µg/ml) for 24, 48, and 72 h. CCK-8 analysis showed that ASP significantly inhibited the viability of CRC cells in a dose- and time-dependent manner (Figure 4A). However, the cytotoxicity of ASP to normal LO2 cells was significantly lower than that of CRC cells (Supplementary Figures S1A,B). The median inhibitory concentration (IC₅₀) values for HCT116 and LOVO cells were 205.37 ± 22.55 µg/ml and 162.2 ± 11.04 µg/ml for 24 h (Figure 4B). Light microscopy images showed a gradual decrease in the number of cells with increasing ASP concentration, poor cell wall adhesion, cell wrinkling, varying degrees of nuclear consolidation, and nuclear vacuolization (Figure 4C). These data suggest that ASP has cytotoxic effects.

We used colony formation and EdU assays to investigate the effect of ASP on the proliferation of CRC cells (HCT116 and LOVO). As shown in Figure 5A, ASP inhibited the colony formation of HCT116 and LOVO cells at the indicated concentrations. The EdU assay further showed that ASP reduced the percentage of EdU-positive cells in a dose-dependent manner (Figure 5B). These findings clearly indicate that ASP has an anti-proliferative effect on HCT116 and LOVO cells.

Cell cycle analysis showed that the percentage of HCT116 cells in the S phase decreased significantly with increasing ASP concentrations compared with controls, whereas the number of cells in the G0/G1 phase increased significantly (Figure 6A). Similar results were obtained in LOVO cells (Figure 6A). ASP inhibited the expression of Cyclin D1 (200 µg/ml *p* < 0.05) and C-Myc (100 and 200 µg/ml *p* < 0.05) proteins, and promoted the expression of P21 in HCT116 cells (200 µg/ml *p* < 0.05, Figure 6B); in LOVO cells, similar results



were observed. These data further suggested that ASP has an inhibitory effect on cell proliferation.

3.3 ASP Promoted CRC Cell Apoptosis *in vitro*

Flow cytometry was used to detect the effect of different concentrations of ASP on the apoptosis of CRC cells. The results showed that when treated with 0, 50, 100, and 200 µg/

ml of ASP, the total apoptosis rate of HCT116 cells increased with increasing ASP concentrations, with early (100 and 200 µg/ml $p < 0.01$) and late (50, 100, and 200 µg/ml $p < 0.05$) apoptosis being significantly promoted; similar results were obtained for LOVO cells (Figure 7A). Similarly, TUNEL staining showed an increase in the percentage of apoptosis after ASP treatment (Figure 7B). In HCT116 cells, ASP inhibited the expression of Bcl-2 (100 and 200 µg/ml $p < 0.05$) and promoted the expression of TP53 (200 µg/ml $p < 0.05$) and Bax (200 µg/ml $p < 0.05$) proteins;

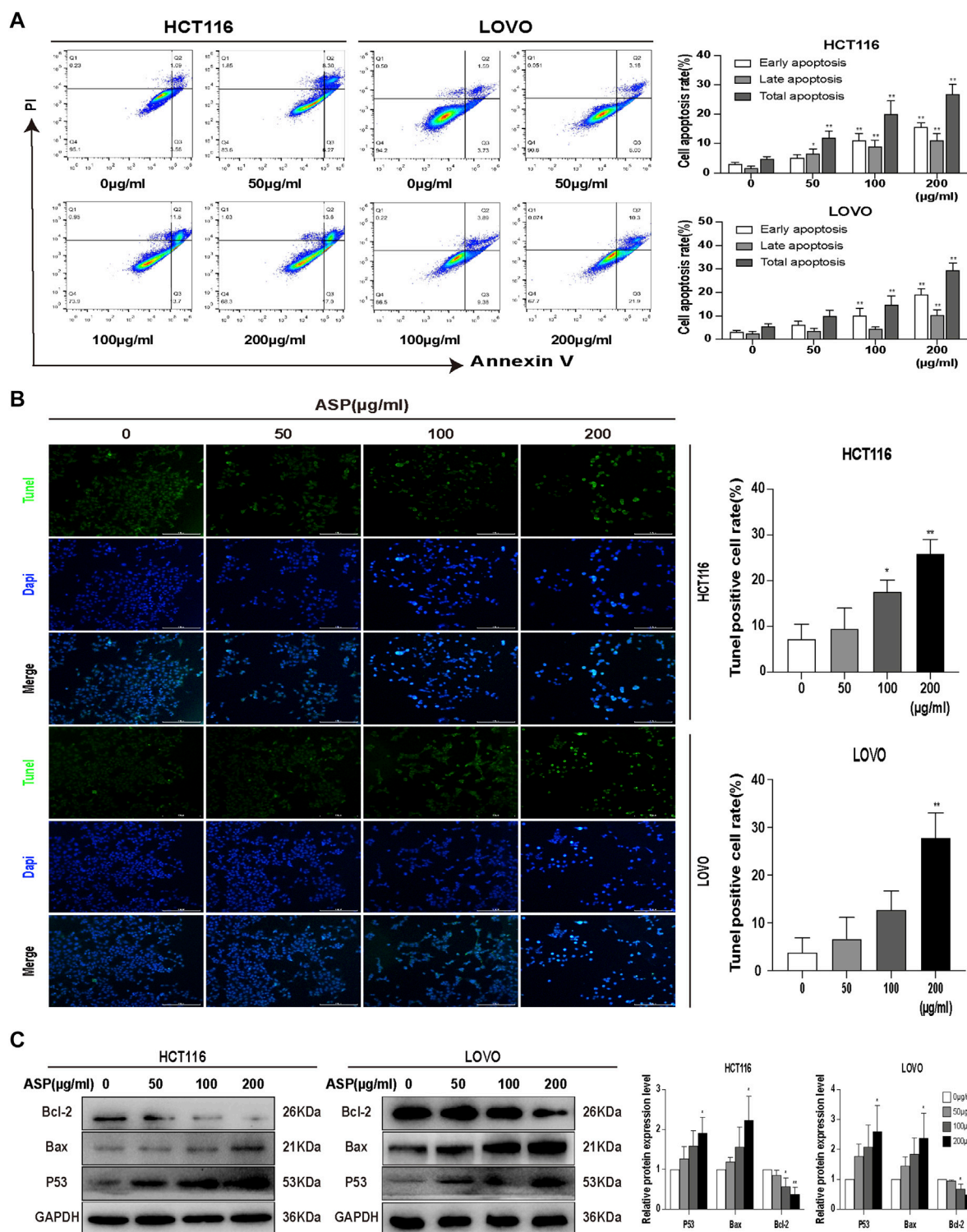
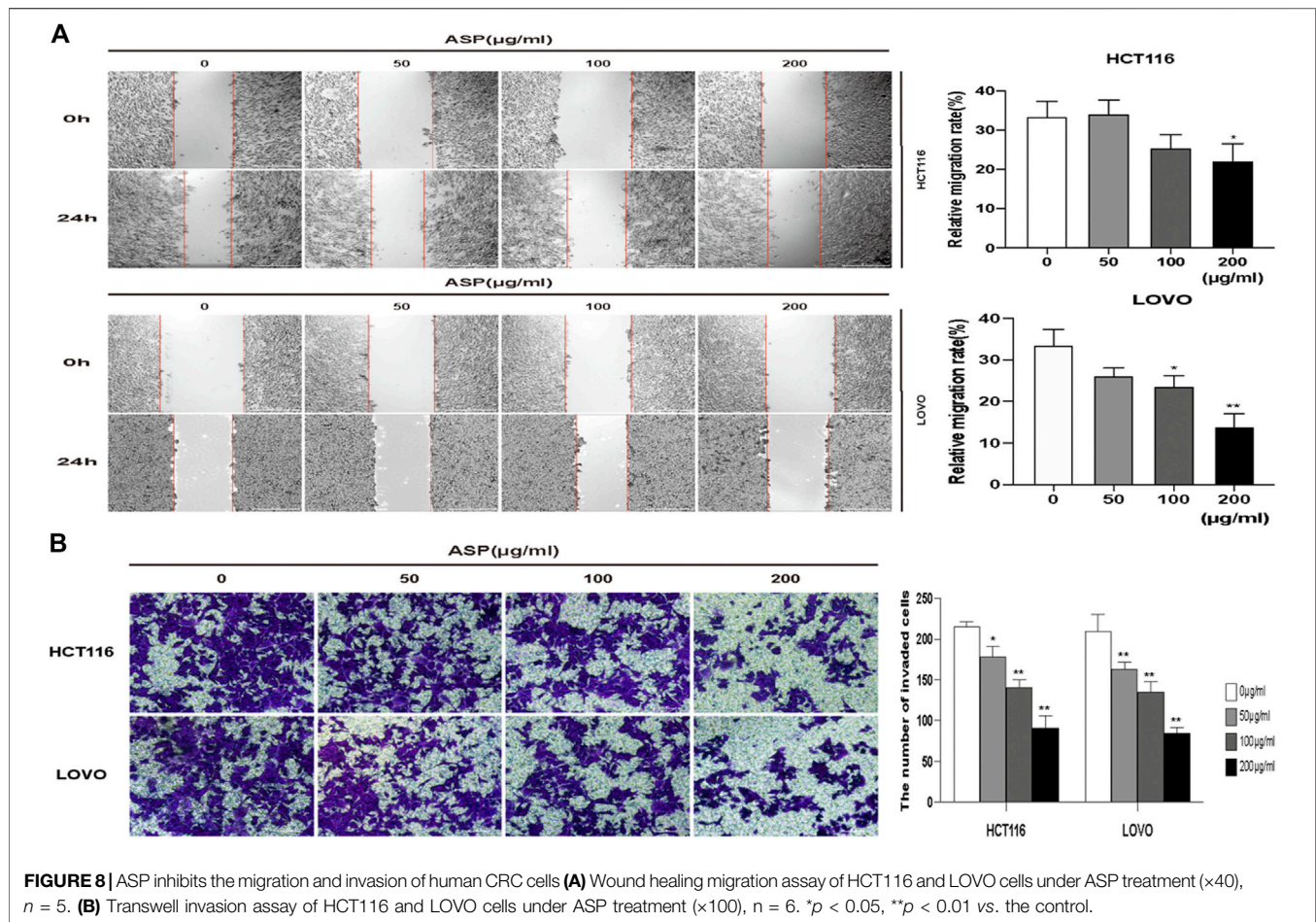


FIGURE 7 | *Asparagus* aqueous extract (ASP) significantly promoted apoptosis in colorectal cancer cells. **(A)** Flow cytometry analysis showed that ASP promoted early and late apoptosis in HCT116 and LOVO cells ($n = 3$ in each group). **(B)** TUNEL staining analysis showed that ASP promoted apoptosis ($\times 200$). **(C)** Expression of Bcl-2 decreased and expression of TP53 and Bax increased with increasing ASP concentration ($n = 3$ per group) Values are shown as the mean \pm SD, * $p < 0.05$, ** $p < 0.01$ vs. the control.



similar results were observed in LOVO cells (Figure 7C). These results suggested that ASP has a pro-apoptotic effect on CRC cells.

3.4 ASP Inhibited the Migration and Invasion of CRC Cells *in vitro*

We performed wound healing and Transwell invasion assays to explore the effect of ASP on the migration and invasive ability of human CRC cells. As shown in Figure 8A, the migration of HCT116 and LOVO cells was significantly inhibited in the ASP treated group compared with that in the control group. As shown in Figure 8B, in the Transwell invasion assay, invasion of HCT116 and LOVO cells was inhibited in a dose-dependent manner in the ASP-treated group. These results confirmed that ASP inhibits the migration and invasion of CRC cells.

3.5 ASP Induced Apoptosis in CRC Cells via the PI3K-Akt-mTOR Pathway

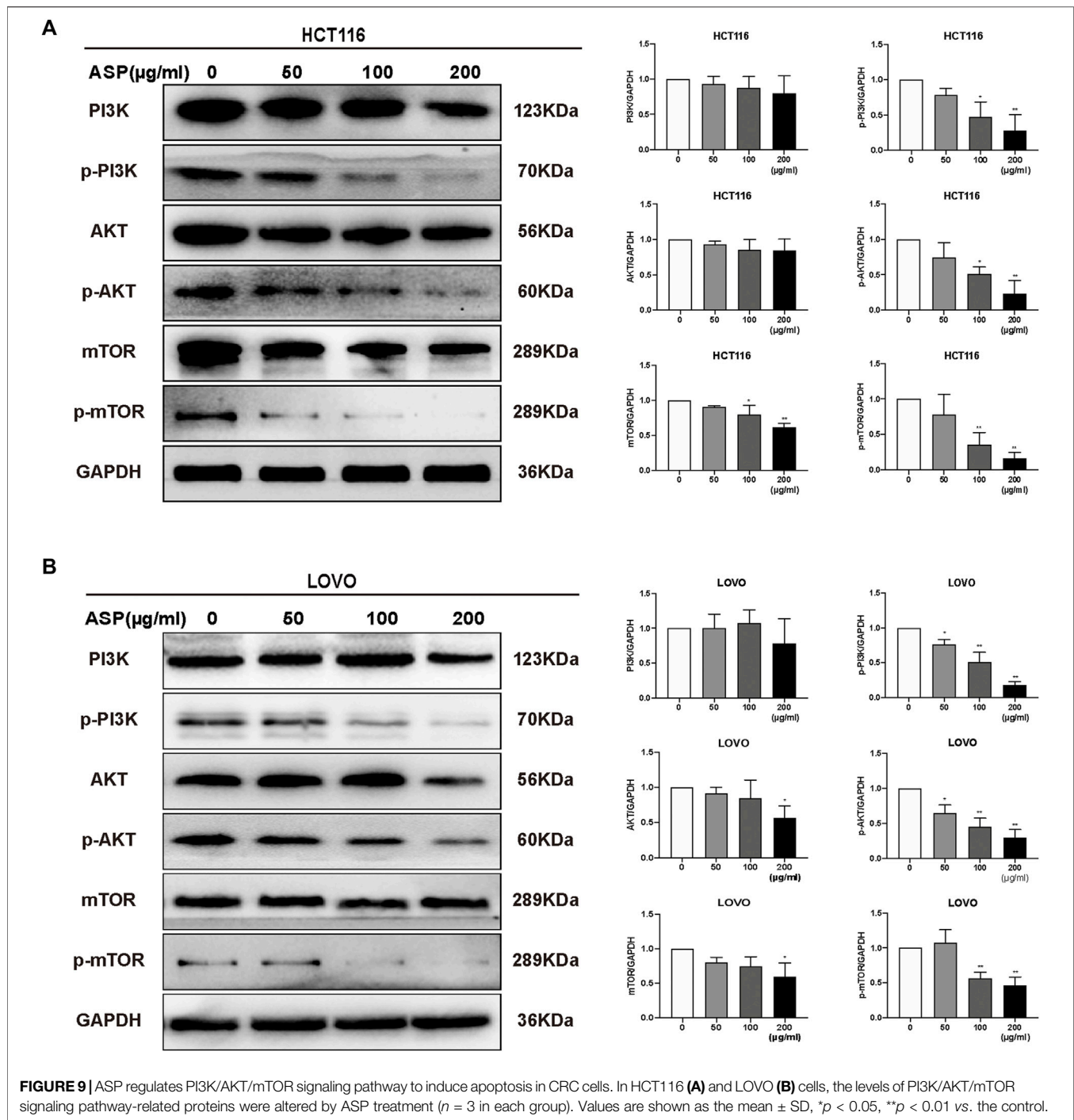
Based on previous informatics data, as shown in Figures 2E, 3B, *AKT1* was one of the key targets in the top 10 bioenrichments, and Pathways in cancer was the most enriched signaling pathway;

therefore, we decided to test whether mTOR/PI3K/AKT pathway involved in the anti-tumor effect of ASP.

We further investigated the mechanism of how ASP promotes apoptosis using western blotting of HCT116 and LOVO cells. As shown in Figure 9, ASP downregulated the levels of p-PI3K, p-AKT, and p-mTOR (100 and 200 µg/ml $p < 0.05$) proteins in HCT116 and LOVO cells compared with those in the controls. In conclusion, these data support the hypothesis that ASP induces apoptosis in CRC cells by regulating the PI3K/AKT/mTOR pathway.

3.6 ASP Inhibited the Growth of HCT116 Cell Xenografts in Nude Mice

The HCT116 cell xenograft tumor model was used to study the antitumor effects of ASP. The results showed that ASP significantly inhibited tumor growth compared to the NS control group (Figures 10A,B). In addition, the rate of weight loss of mice in the ASP-treated group slowed down with increasing drug concentration in the middle and late stages compared with that in the NS group (Figure 10C). At the same time, the rate of tumor volume increase slowed down in the ASP group, although not significantly (Figure 10D). Meanwhile, western blotting analysis of tumor tissues was



performed (Figure 10E). Compared with the control group, the levels of p-PI3K, p-AKT, and p-mTOR in mice treated with ASP decreased. Levels of apoptosis markers, including P53 and Bax, were increased and those of Bcl-2 decreased in tumor cells. The levels of cycle-related proteins was consistent with the results of *in vitro* studies. These data suggested that ASP inhibits tumor growth, induces cell cycle arrest and apoptosis in HCT116 cells, and inhibits the PI3K/AKT/mTOR signaling pathway *in vivo*.

4 DISCUSSION

Chinese medicine is a great repository of knowledge related to disease prevention and treatment; however, because of the complexity and diversity of chemical components in Chinese medicine, it is difficult to explore the active ingredients and the corresponding mechanism of efficacy after entering the human body, which is the main challenge to research on Chinese medicine. In recent years, network pharmacology technology

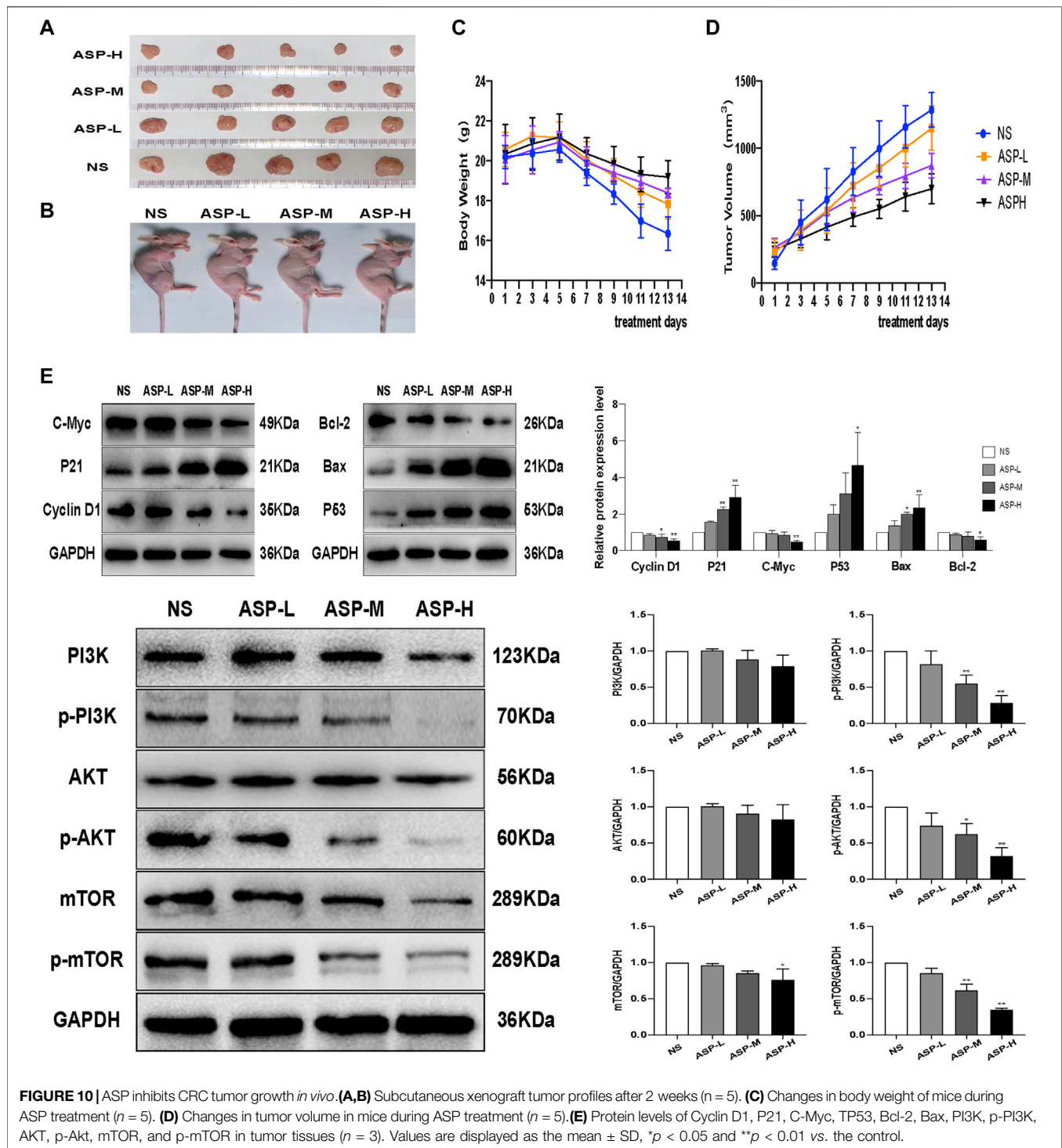


FIGURE 10 | ASP inhibits CRC tumor growth *in vivo*. **(A,B)** Subcutaneous xenograft tumor profiles after 2 weeks ($n = 5$). **(C)** Changes in body weight of mice during ASP treatment ($n = 5$). **(D)** Changes in tumor volume in mice during ASP treatment ($n = 5$). **(E)** Protein levels of Cyclin D1, P21, C-Myc, TP53, Bcl-2, Bax, PI3K, p-PI3K, AKT, p-Akt, mTOR, and p-mTOR in tumor tissues ($n = 3$). Values are displayed as the mean \pm SD, * $p < 0.05$ and ** $p < 0.01$ vs. the control.

has been rapidly developed. Its theoretical ideas are similar to the multi-component, multi-target, and multi-pathway action characteristics of TCM, providing new ideas for studying complex TCM systems (Li, 2016).

The anticancer activity of polysaccharide, saponin, and flavonoid extracts from ASP has been reported in various cancers, such as lung and bladder cancer (Bilušić et al., 2019),

liver cancer (Cheng et al., 2021), and ovarian cancer (Xu et al., 2021). Some studies have found that asparagus saponin extracts have significant cytotoxic effects on colorectal cancer cells (Jaramillo-Carmona et al., 2018), and the results of Bousserouel (Bousserouel et al., 2013) and others have shown in more detail that methanolic extracts of ASP can induce apoptosis by activating the TRAIL death receptor pathway in

SW480 and SW620 human colon adenocarcinoma cells. However, the anticancer effects and mechanisms of ASP on colorectal cancer have not been determined systematically. Therefore, we used a network pharmacology approach to construct a relational network of asparagus active ingredients targeting disease pathways. By analyzing the importance of each node in the topological network, we initially screened the key active ingredients of asparagus against colorectal cancer, including quercetin, β -sitosterol, and 7-methoxy-2-methylisoflavone. Quercetin has been shown to inhibit a variety of cancers, such as nasopharyngeal, colorectal, and breast cancers, by affecting different cancer pathways (Almatroodi et al., 2021). β -sitosterol is known to have a wide range of antitumor effects, and Wang et al. (Wang Z. et al., 2020) found that β -sitosterol can mediate the p53/NF- κ B/BCRP signaling axis to modulate the response of CRC to chemotherapy. Jiang et al. (2016) showed a negative correlation between isoflavone intake and colorectal cancer risk in a case-control study. All these studies and our experimental studies support the theory of “different treatment for the same disease” and “different treatment for different diseases” in TCM and demonstrate the good practice of the network pharmacology approach in identifying the mechanism of action of TCM.

We identified 157 potential drug targets, and through PPI network analysis, we identified the core targets among them as TP53, FOS, AKT1, STAT1, MAPK1, MAPK14, IL6, RELA, EGFR, and ESR1. In addition, analysis at the Metascape database (Zhou et al., 2019) showed that multiple signaling pathways are closely related to ASP treatment of CRC, with the highest correlation being “Pathways in cancer,” and combined with the core targets, we speculated that ASP might act therapeutically through the PI3K/AKT/mTOR signaling pathway.

The results of previous studies confirmed that a saponin extract and methanol extract of asparagus have some toxic effects on CRC cells (Bousserouel et al., 2013; Jaramillo-Carmona et al., 2018). Similarly, the results of the present study showed that an aqueous extract of asparagus significantly decreased the proliferation of HCT116 and LOVO human colorectal cancer cells. The same results were observed in xenograft tumor models. The tumor growth rate was reduced in the ASP-treated group compared with that in the NS group. A previous study showed that methanolic extract of asparagus increased the percentage of G2/M phase and apoptosis in MCF-7 cells (Mfengwana et al., 2019). In comparison, our results showed that ASP induced cell cycle arrest in the G0/G1 phase of CRC cells and similarly, promoted apoptosis in HCT116 and LOVO cells.

Phosphorylation of PI3K activates phosphorylation of AKT and mTOR, which play key roles in regulating cell proliferation, growth, angiogenesis, migration, and nutrient metabolism (Manning and Toker, 2017). Previous studies have shown that numerous natural substances have the ability to inhibit the PI3K/AKT/mTOR signaling pathway in a variety of cancer cells, which is considered to be an key effective strategy for cancer inhibition (Narayanankutty, 2019) and has become a

popular target for new cancer drugs (Janku et al., 2018). We detected the phosphorylation level of PI3K/AKT/mTOR pathway members using western blotting and found that ASP inhibited phosphorylation of related proteins in a dose-dependent manner.

Activation of the PI3K/AKT pathway increases the expression of mTOR, which enters the nucleus and initiates the expression of CyclinD1, facilitating the rapid entry of cells into mitosis (Xie et al., 2021). C-Myc stimulates cell cycle progression by regulating many genes related to cell cycle control (Elbadawy et al., 2019; García-Gutiérrez et al., 2019). Claassen et al. (Claassen and Hann, 2000) found that upregulation of p21^{CIP1} correlated with the downregulation of c-Myc levels after transforming growth factor β treatment in HaCaT cells. In the present study, the analysis of the above-mentioned cell cycle proteins revealed that different concentrations of ASP extracts decreased the levels of CyclinD1 and c-Myc proteins and increased the levels of p21 in cells in a concentration-dependent manner. This result indicates that ASP negatively regulates cell cycle proteins in CRC cells.

The role of p53 proteins in apoptosis, senescence, and DNA damage repair is well understood (Lacroix et al., 2020). Bcl-2 family proteins are involved in apoptosis through various mechanisms, and elevated Bax expression is usually associated with apoptosis, while decreased Bcl-2 expression levels indicate a reduced ability to inhibit apoptosis (Ramesh and Medema, 2020), which is closely related to the PI3K pathway (Wang Y. et al., 2020). Cheng et al. (2020) found that naringin effectively promoted Bax expression and inhibited Bcl-2 expression in a concentration-dependent manner. Similarly, our results showed that the pro-apoptotic regulators TP53 and Bax were upregulated and the anti-apoptotic regulator Bcl-2 was downregulated by ASP. The expression of these regulators confirms the pro-apoptotic effect of ASP on CRC. Flow-cytometry apoptosis analysis and cellular TUNEL assays also showed that ASP induced apoptosis in HCT116 and LOVO cells. In addition, it has been suggested that mTOR pathway inhibition might abrogate tumor cell invasion and migration (Duan et al., 2018). The results of our scratch healing and Transwell invasion assays showed that ASP inhibited the migration and invasion of CRC cells.

Based on these results, we found that ASP inhibited cell proliferation, migration and invasion, promoted cell G0/G1 phase block and apoptosis, and inhibited the PI3K/Akt/mTOR pathway to achieve therapeutic effects on colorectal cancer. Although we demonstrated the anticancer effect of ASP and its mechanism, further study is required to determine the mechanism of the antimetastatic effect of ASP on CRC and further *in vivo* experiments are needed to better validate the predicted results of network pharmacology.

5 CONCLUSION

In conclusion, the pharmacological mechanism of ASP's effect on CRC was explored through a combination of network

pharmacological analysis and *in vivo* and *in vitro* experimental validation. We demonstrated that ASP inhibited the proliferation of HCT116 and LOVO cells through PI3K/AKT/mTOR-mediated pathway and induced cell cycle arrest and apoptosis. In addition, ASP reduced the migration and invasion of CRC cells. This study provides a theoretical and experimental basis for the use of traditional Chinese medicines as antitumor agents.

DATA AVAILABILITY STATEMENT

The original contributions presented in the study are included in the article/**Supplementary Material**, further inquiries can be directed to the corresponding authors.

ETHICS STATEMENT

The animal study was reviewed and approved by The Ethics Committee of the First Affiliated Hospital of Guizhou University of Traditional Chinese.

AUTHOR CONTRIBUTIONS

HL, YL, FW, DT, and YL designed the study. HL, FW, JZ, XY, and YL generated the data. HL, FW, DW, CZ, JH, MS, YL, JW, ZH, and YL analyzed the data. HL, YL, FW, DT, and YL prepared the manuscript draft. All authors approved the final manuscript.

REFERENCES

- Agrawal, A., Sharma, M., Rai, S. K., Singh, B., Tiwari, M., and Chandra, R. (2008). The Effect of the Aqueous Extract of the Roots of *Asparagus racemosus* on Hepatocarcinogenesis Initiated by Diethylnitrosamine. *Phytother. Res.* 22 (9), 1175–1182. doi:10.1002/ptr.2391
- Almatroodi, S. A., Alsahli, M. A., Almatroodi, A., Verma, A. K., Aloliki, A., Allemailem, K. S., et al. (2021). Potential Therapeutic Targets of Quercetin, a Plant Flavonol, and its Role in the Therapy of Various Types of Cancer through the Modulation of Various Cell Signaling Pathways. *Molecules* 26 (5), 1315. doi:10.3390/molecules26051315
- Arnold, M., Sierra, M. S., Laversanne, M., Soerjomataram, I., Jemal, A., and Bray, F. (2017). Global Patterns and Trends in Colorectal Cancer Incidence and Mortality. *Gut* 66 (4), 683–691. doi:10.1136/gutjnl-2015-310912
- Bilušić, T., Šola, I., Rusak, G., Poljuha, D., and Čikeš Čulić, V. (2019). Antiproliferative and Pro-apoptotic Activities of Wild asparagus (*Asparagus acutifolius*L.), Black Bryony (*Tamus communis*L.) and Butcher's Broom (*Ruscus aculeatus*L.) Aqueous Extracts against T24 and A549 Cancer Cell Lines. *J. Food Biochem.* 43 (4), e12781. doi:10.1111/jfbc.12781
- Bousserouel, S., Le Grandois, J., Gossé, F., Werner, D., Barth, S. W., Marchioni, E., et al. (2013). Methanolic Extract of white asparagus Shoots Activates TRAIL Apoptotic Death Pathway in Human Cancer Cells and Inhibits colon Carcinogenesis in a Preclinical Model. *Int. J. Oncol.* 43 (2), 394–404. doi:10.3892/ijo.2013.1976
- Chen, Q., Shu, C., Laurence, A. D., Chen, Y., Peng, B. G., Zhen, Z. J., et al. (2018). Effect of Huaier Granule on Recurrence after Curative Resection of HCC: a Multicentre, Randomised Clinical Trial. *Gut* 67 (11), 2006–2016. doi:10.1136/gutjnl-2018-315983
- Cheng, H., Jiang, X., Zhang, Q., Ma, J., Cheng, R., Yong, H., et al. (2020). Naringin Inhibits Colorectal Cancer Cell Growth by Repressing the PI3K/AKT/mTOR Signaling Pathway. *Exp. Ther. Med.* 19 (6), 3798–3804. doi:10.3892/etm.2020.8649

FUNDING

This study was supported by the National Natural Science Foundation of China (No. 82160519, No. 31660326, No. 81760814, and No. 81960818), the Research on the Modernization of Traditional Chinese Medicine in the National Key Research and Development Program of the Ministry of Science and Technology (No. 2019YFC1712504), the Natural Science Foundation of Guizhou Province (No.(2018)2759, No. QianKeHe Support (2022)181), the China Postdoctoral Science Foundation (No. 2018M640938 and 43XB3794XB), the Natural Science Foundation of Guiyang City (No. (2019)9-2-2, (2019)9-2-22), and the Doctoral Foundation of the First Affiliated Hospital of Guizhou University of Traditional Chinese Medicine (No.GYZYFY-BS-2018 (12)). The funders of the study played no role in the study design, data collection, data analysis, data interpretation, or writing of the report.

SUPPLEMENTARY MATERIAL

The Supplementary Material for this article can be found online at: <https://www.frontiersin.org/articles/10.3389/fphar.2022.862966/full#supplementary-material>

Supplementary Figure S1 | (A) LO2 cells were treated with asparagus water extract (ASP) at the specified concentration for 24 h. **(B)** Cytotoxicity of ASP to LO2 cells in vitro. **P* < 0.05, ***P* < 0.01 vs. control.

- Cheng, W., Cheng, Z., Weng, L., Xing, D., and Zhang, M. (2021). Asparagus Polysaccharide Inhibits the Hypoxia-Induced Migration, Invasion and Angiogenesis of Hepatocellular Carcinoma Cells Partly through Regulating HIF1α/VEGF Expression via MAPK and PI3K Signaling Pathway. *J. Cancer* 12 (13), 3920–3929. doi:10.7150/jca.51407
- Cheng, W., Cheng, Z., Xing, D., and Zhang, M. (2019). Asparagus Polysaccharide Suppresses the Migration, Invasion, and Angiogenesis of Hepatocellular Carcinoma Cells Partly by Targeting the HIF-1α/VEGF Signalling Pathway *In Vitro*. *Evid Based. Complement. Altern. Med.* 2019, 3769879. eCAM. doi:10.1155/2019/3769879
- Claassen, G. F., and Hann, S. R. (2000). A Role for Transcriptional Repression of p21CIP1 by C-Myc in Overcoming Transforming Growth Factor Beta -induced Cell-Cycle Arrest. *Proc. Natl. Acad. Sci. U S A.* 97 (17), 9498–9503. doi:10.1073/pnas.150006697
- Duan, S., Huang, W., Liu, X., Liu, X., Chen, N., Xu, Q., et al. (2018). IMPDH2 Promotes Colorectal Cancer Progression through Activation of the PI3K/AKT/mTOR and PI3K/AKT/FOXO1 Signaling Pathways. *J. Exp. Clin. Cancer Res.* 37 (1), 304. doi:10.1186/s13046-018-0980-3
- Elbadawy, M., Usui, T., Yamawaki, H., and Sasaki, K. (2019). Emerging Roles of C-Myc in Cancer Stem Cell-Related Signaling and Resistance to Cancer Chemotherapy: A Potential Therapeutic Target against Colorectal Cancer. *Int. J. Mol. Sci.* 20 (9), 2340. doi:10.3390/ijms20092340
- García-Gutiérrez, L., Delgado, M. D., and León, J. (2019). MYC Oncogene Contributions to Release of Cell Cycle Brakes. *Genes (Basel)* 10 (3), 244. doi:10.3390/genes10030244
- Hattori, T., Imaoka, A., Akiyoshi, T., and Ohtani, H. (2019). Irinotecan-induced Gastrointestinal Damage Impairs the Absorption of Dabigatran Etexilate. *Biopharm. Drug Dispos* 40 (9), 315–324. doi:10.1002/bdd.2205
- Janku, F., Yap, T. A., and Meric-Bernstam, F. (2018). Targeting the PI3K Pathway in Cancer: Are We Making Headway? *Nat. Rev. Clin. Oncol.* 15 (5), 273–291. doi:10.1038/nrclinonc.2018.28

- Jaramillo-Carmona, S., Guillén-Bejarano, R., Jiménez-Araujo, A., Rodríguez-Arcos, R., and López, S. (2018). *In Vitro* Toxicity of Asparagus Saponins in Distinct Multidrug-Resistant Colon Cancer Cells. *Chem. Biodivers.* 15 (11), e1800282. doi:10.1002/cbdv.201800282
- Jiang, R., Botma, A., Rudolph, A., Hüsing, A., and Chang-Claude, J. (2016). Phytoestrogens and Colorectal Cancer Risk: a Systematic Review and Dose-Response Meta-Analysis of Observational Studies. *Br. J. Nutr.* 116 (12), 2115–2128. doi:10.1017/S0007114516004360
- Lacroix, M., Riscal, R., Arena, G., Linares, L. K., and Le Cam, L. (2020). Metabolic Functions of the Tumor Suppressor P53: Implications in normal Physiology, Metabolic Disorders, and Cancer. *Mol. Metab.* 33, 2–22. doi:10.1016/j.molmet.2019.10.002
- Lee, H. A., Koh, E. K., Sung, J. E., Kim, J. E., Song, S. H., Kim, D. S., et al. (2017). Ethyl Acetate Extract from Asparagus cochinchinensis Exerts Anti-inflammatory E-effects in LPS-stimulated RAW264.7 Macrophage Cells by Regulating COX-2/iNOS, Inflammatory Cytokine Expression, MAPK Kinase Pathways, the Cell Cycle and Anti-oxidant Activity. *Mol. Med. Rep.* 15 (4), 1613–1623. doi:10.3892/mmr.2017.6166
- Lei, L., Chen, Y., Ou, L., Xu, Y., and Yu, X. (2017). Aqueous Root Extract of Asparagus Cochinchinensis (Lour.) Merr. Has Antioxidant Activity in D-Galactose-Induced Aging Mice. *BMC Complement. Altern. Med.* 17 (1), 469. doi:10.1186/s12906-017-1975-x
- Li, C. L., Hsia, T. C., Li, C. H., Chen, K. J., Yang, Y. H., and Yang, S. T. (2019). Adjunctive Traditional Chinese Medicine Improves Survival in Patients with Advanced Lung Adenocarcinoma Treated with First-Line Epidermal Growth Factor Receptor (EGFR) Tyrosine Kinase Inhibitors (TKIs): A Nationwide, Population-Based Cohort Study. *Integr. Cancer Ther.* 18, 1534735419827079. doi:10.1177/1534735419827079
- Li, S. (2016). Exploring Traditional Chinese Medicine by a Novel Therapeutic Concept of Network Target. *Chin. J. Integr. Med.* 22 (9), 647–652. doi:10.1007/s11655-016-2499-9
- Li, X., Chen, C., Dai, Y., Huang, C., Han, Q., Jing, L., et al. (2019). Cinobufagin Suppresses Colorectal Cancer Angiogenesis by Disrupting the Endothelial Mammalian Target of Rapamycin/hypoxia-Inducible Factor 1 α axis. *Cancer Sci.* 110 (5), 1724–1734. doi:10.1111/cas.13988
- Liu, J., Guo, Y., and Cao, J. (2020). Matrine Triggers colon Cancer Cell Apoptosis and G0/G1 Cell Cycle Arrest via Mediation of microRNA-22. *Phytother. Res.* 34 (7), 1619–1628. doi:10.1002/ptr.6626
- Manning, B. D., and Toker, A. (2017). AKT/PKB Signaling: Navigating the Network. *Cell* 169 (3), 381–405. doi:10.1016/j.cell.2017.04.001
- Mfengwana, P. H., Mashele, S. S., and Manduna, I. T. (2019). Cytotoxicity and Cell Cycle Analysis of Asparagus Laricinus Burch. And Senecio Asperulus DC. on Breast and Prostate Cancer Cell Lines. *Heliyon* 5 (5), e01666. doi:10.1016/j.heliyon.2019.e01666
- Narayanankutty, A. (2019). PI3K/Akt/mTOR Pathway as a Therapeutic Target for Colorectal Cancer: A Review of Preclinical and Clinical Evidence. *Curr. Drug Targets* 20 (12), 1217–1226. doi:10.2174/1389450120666190618123846
- Ramesh, P., and Medema, J. P. (2020). BCL-2 Family Deregulation in Colorectal Cancer: Potential for BH3 Mimetics in Therapy. *Apoptosis* 25 (5–6), 305–320. doi:10.1007/s10495-020-01601-9
- Samad, N. B., Debnath, T., Abul Hasnat, M., Pervin, M., Kim, D. H., Jo, J. E., et al. (2014). Phenolic Contents, Antioxidant and Anti-inflammatory Activities of Asparagus Cochinchinensis (Loureiro) Merrill. *J. Food Biochem.* 38, 83–91. doi:10.1111/jfbc.12028
- Shi, Q., Liu, S., Li, W., Zong, S., Han, S., Yang, W., et al. (2017). Exploring the Medication Duration Based on the Effect of Traditional Chinese Medicine on Postoperative Stage I–III Colorectal Patients: a Retrospective Cohort Study. *Oncotarget* 8 (8), 13488–13495. doi:10.18632/oncotarget.14567
- Sun, Q., Zhu, L., Li, Y., Cui, Y., Jiang, S., Tao, N., et al. (2020). A Novel Inulin-type Fructan from Asparagus Cochinchinensis and its Beneficial Impact on Human Intestinal Microbiota. *Carbohydr. Polym.* 247, 116761. doi:10.1016/j.carbpol.2020.116761
- Vodenkova, S., Buchler, T., Cervena, K., Veskrnova, V., and Vodicka, P. (2020). 5-fluorouracil and Other Fluoropyrimidines in Colorectal Cancer: Past, Present and Future. *Pharmacol. Ther.* 206, 107447. doi:10.1016/j.pharmthera.2019.107447
- Wang, Y., Gu, J., Hu, L., Kong, L., Wang, T., Di, M., et al. (2020). miR-130a Alleviates Neuronal Apoptosis and Changes in Expression of Bcl-2/Bax and Caspase-3 in Cerebral Infarction Rats through PTEN/PI3K/Akt Signaling Pathway. *Exp. Ther. Med.* 19 (3), 2119–2126. doi:10.3892/etm.2020.8415
- Wang, Z., Qi, F., Cui, Y., Zhao, L., Sun, X., Tang, W., et al. (2018). An Update on Chinese Herbal Medicines as Adjuvant Treatment of Anticancer Therapeutics. *Biosci. Trends* 12 (3), 220–239. doi:10.5582/bst.2018.01144
- Wang, Z., Zhan, Y., Xu, J., Wang, Y., Sun, M., Chen, J., et al. (2020). β -Sitosterol Reverses Multidrug Resistance via BCRP Suppression by Inhibiting the P53-MDM2 Interaction in Colorectal Cancer. *J. Agric. Food Chem.* 68 (12), 3850–3858. doi:10.1021/acs.jafc.0c00107
- Xie, Y., Liu, C., Zhang, Y., Li, A., Sun, C., Li, R., et al. (2021). PKI-587 Enhances Radiosensitization of Hepatocellular Carcinoma by Inhibiting the PI3K/AKT/mTOR Pathways and DNA Damage Repair. *PLoS one* 16 (10), e0258817. doi:10.1371/journal.pone.0258817
- Xu, G., Kong, W., Fang, Z., Fan, Y., Yin, Y., Sullivan, S. A., et al. (2021). Asparagus Officialis Exhibits Anti-tumorigenic and Anti-metastatic Effects in Ovarian Cancer. *Front. Oncol.* 11, 688461. doi:10.3389/fonc.2021.688461
- Xu, W., He, Y., Wang, Y., Li, X., Young, J., Ioannidis, J. P. A., et al. (2020). Risk Factors and Risk Prediction Models for Colorectal Cancer Metastasis and Recurrence: an Umbrella Review of Systematic Reviews and Meta-Analyses of Observational Studies. *BMC Med.* 18 (1), 172. doi:10.1186/s12916-020-01618-6
- Xu, Y., Mao, J. J., Sun, L., Yang, L., Li, J., Hao, Y., et al. (2017). Association between Use of Traditional Chinese Medicine Herbal Therapy and Survival Outcomes in Patients with Stage II and III Colorectal Cancer: A Multicenter Prospective Cohort Study. *J. Natl. Cancer Inst. Monogr.* 2017 (52), lgx015. doi:10.1093/jncimonographs/lgx015
- Yan, Z., Lai, Z., and Lin, J. (2017). Anticancer Properties of Traditional Chinese Medicine. *Comb. Chem. High Throughput Screen.* 20 (5), 423–429. doi:10.2174/1386207320666170116141818
- Yang, M., Zhu, S. J., Shen, C., Zhai, R., Li, D. D., Fang, M., et al. (2021). Clinical Application of Chinese Herbal Injection for Cancer Care: Evidence-Mapping of the Systematic Reviews, Meta-Analyses, and Randomized Controlled Trials. *Front. Pharmacol.* 12, 666368. doi:10.3389/fphar.2021.666368
- Zhang, L., He, F., Gao, L., Cong, M., Sun, J., Xu, J., et al. (2021). Engineering Exosome-like Nanovesicles Derived from Asparagus Cochinchinensis Can Inhibit the Proliferation of Hepatocellular Carcinoma Cells with Better Safety Profile. *Int. J. Nanomedicine* 16, 1575–1586. doi:10.2147/IJN.S293067
- Zhang, R., Zhu, X., Bai, H., and Ning, K. (2019). Network Pharmacology Databases for Traditional Chinese Medicine: Review and Assessment. *Front. Pharmacol.* 10, 123. doi:10.3389/fphar.2019.00123
- Zhou, Y., Zhou, B., Pache, L., Chang, M., Khodabakhshi, A. H., Tanaseichuk, O., et al. (2019). Metascape Provides a Biologist-Oriented Resource for the Analysis of Systems-Level Datasets. *Nat. Commun.* 10 (1), 1523. doi:10.1038/s41467-019-09234-6
- Zhu, J., Tan, Z., Hollis-Hansen, K., Zhang, Y., Yu, C., and Li, Y. (2017). Epidemiological Trends in Colorectal Cancer in China: An Ecological Study. *Dig. Dis. Sci.* 62 (1), 235–243. doi:10.1007/s10620-016-4362-4

Conflict of Interest: The authors declare that the research was conducted in the absence of any commercial or financial relationships that could be construed as a potential conflict of interest.

Publisher's Note: All claims expressed in this article are solely those of the authors and do not necessarily represent those of their affiliated organizations, or those of the publisher, the editors and the reviewers. Any product that may be evaluated in this article, or claim that may be made by its manufacturer, is not guaranteed or endorsed by the publisher.

Copyright © 2022 Liang, Li, Wang, Zhao, Yang, Wu, Zhang, Liu, Huang, Su, He, Liu, Wang and Tang. This is an open-access article distributed under the terms of the Creative Commons Attribution License (CC BY). The use, distribution or reproduction in other forums is permitted, provided the original author(s) and the copyright owner(s) are credited and that the original publication in this journal is cited, in accordance with accepted academic practice. No use, distribution or reproduction is permitted which does not comply with these terms.



The Role of Membrane-Associated E3 Ubiquitin Ligases in Cancer

Xuankun Chen¹, Li Jiang¹, Zhesheng Zhou¹, Bo Yang^{1,2}, Qiaojun He^{1,3,2,4},
Chengliang Zhu^{1,3,2*} and Ji Cao^{1,2,4*}

¹Zhejiang Province Key Laboratory of Anti-Cancer Drug Research, College of Pharmaceutical Sciences, Institute of Pharmacology and Toxicology, Zhejiang University, Hangzhou, China, ²The Innovation Institute for Artificial Intelligence in Medicine, Zhejiang University, Hangzhou, China, ³Center for Drug Safety Evaluation and Research of Zhejiang University, Zhejiang University, Hangzhou, China, ⁴Cancer Center of Zhejiang University, Hangzhou, China

OPEN ACCESS

Edited by:

Sandeep Singh,
Central University of Punjab, India

Reviewed by:

Ting Zhuang,
Xinxiang Medical University, China
Zhang Naijin,
The First Affiliated Hospital of China
Medical University, China

*Correspondence:

Chengliang Zhu
chengliangzhu@zju.edu.cn
Ji Cao
caoji88@zju.edu.cn

Specialty section:

This article was submitted to
Pharmacology of Anti-Cancer Drugs,
a section of the journal
Frontiers in Pharmacology

Received: 26 April 2022

Accepted: 10 June 2022

Published: 01 July 2022

Citation:

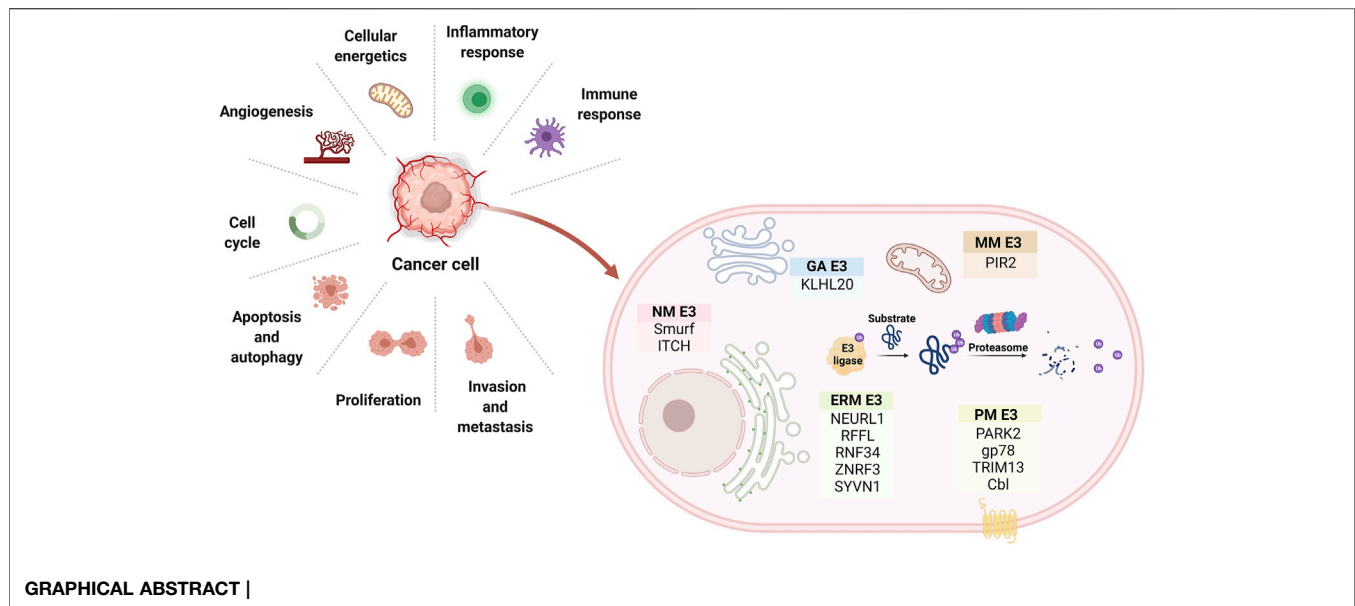
Chen X, Jiang L, Zhou Z, Yang B, He Q,
Zhu C and Cao J (2022) The Role of
Membrane-Associated E3 Ubiquitin
Ligases in Cancer.
Front. Pharmacol. 13:928794.
doi: 10.3389/fphar.2022.928794

The cell membrane system comprises the plasma membrane, endoplasmic reticulum, Golgi apparatus, lysosome, mitochondria, and nuclear membrane, which are essential for maintaining normal physiological functions of cells. The proteins associated with these membrane-organelles are frequently modified to regulate their functions, the most common of which is ubiquitin modification. So far, many ubiquitin E3 ligases anchored in the membrane system have been identified as critical players facilitating intracellular biofunctions whose dysfunction is highly related to cancer. In this review, we summarized membrane-associated E3 ligases and revealed their relationship with cancer, which is of great significance for discovering novel drug targets of cancer and may open up new avenues for inducing ubiquitination-mediated degradation of cancer-associated membrane proteins via small chemicals such as PROTAC and molecular glue.

Keywords: cell membrane system, cancer, E3 ligases, drug targets, PROTAC (proteolysis-targeting chimeric molecule)

INTRODUCTION

The cell membrane system comprises the plasma membrane, endoplasmic reticulum (ER), Golgi apparatus, mitochondria, and nuclear membrane, which is essential for maintaining cell morphology and functions. By way of illustration, plasma membrane control the substances' entrance and exit of cells and protect the integrity of cells and maintain the shape of cells. Other membrane structures provide for the manufacture and packaging of substances within cells. Similarly, other subcellular membranes surround organelles resembling the cell membrane but with different protein and phospholipids compositions. Membrane-bound organelles provide many benefits to eukaryotic cells. Firstly, the membrane system divides the cell into multiple compartments, enabling enzymes to be concentrated in specific compartments, thereby improving the efficiency of biochemical reactions therein. Secondly, Membrane structures can protect the rest of the cell from damage by confining harmful substances to specific compartments. Thirdly, membrane-composed organelles usually rely on vesicles to transport substances and proteins (Dacks and Field, 2018). Remarkably, different



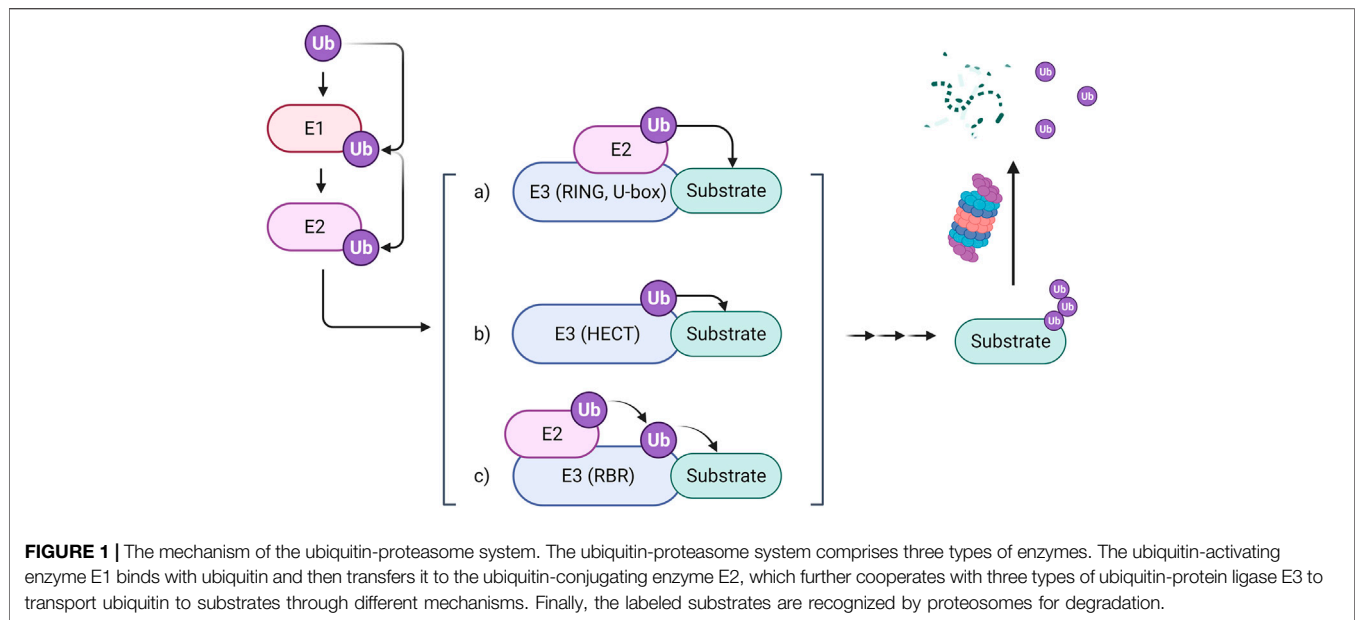
membranes are well suited for their functions, primarily thanks to their various molecular composition, especially some anchor proteins. However, the dysfunction of these anchor proteins is closely associated to some human diseases like cancer (Martin and List, 2019), etc.

Ubiquitylation regulates protein breakdown and signaling cascades, and hence plays a crucial role in cellular physiology. Three kinds of enzymes are required for the ubiquitylation process: E1, E2, and E3. E3 ligases, in particular, endow ubiquitination with selectivity by promoting ubiquitin transfer from an E2 enzyme to the substrate (Zheng and Shabek, 2017). So far, more than six hundred E3 ubiquitin ligases have been identified in the human proteome, which can be classified into three main types: Really Interesting New Gene (RING) E3s, Homologous to the E6-AP Carboxyl Terminus (HECT) E3s, and RING-between-RING (RBR) E3s. RING E3s are the most abundant ubiquitin ligases. They especially contain RING domains that can bind with an E2-ubiquitin thioester and promote ubiquitin cargo release. RING E3s can also stimulate the transfer of ubiquitin from E2s to the substrate directly (Deshaies and Joazeiro, 2009). The HECT E3s, containing a conserved enzymatic cysteine (Cys), accept ubiquitin from E2s and then transfer it to the substrate by a specific Lys residue (Rotin and Kumar, 2009). Another type of E3 ligases, RBR, play a role in ubiquitination through a HECT-RING hybrid mechanism. Ubiquitin is recruited to RBR *via* forming a disulfide bond with the crucial cysteine residue on RING2 and then transported to the substrate, forming an isopeptide bond with it (Figure 1). Based on the ubiquitination degradation process, E3 ubiquitin ligases have potential application value in relative researches of some proteins' structures, functions and distribution. For instance, E3 ligases have been involved in PROteolysis-TArgeting Chimeras (PROTACs) related research to target substrate proteins for degradation. In

addition, some E3 ligases were reported as novel biomarkers for some diseases like COVID-19 (Novelli et al., 2021). Furthermore, some preceding works of our group revealed that E3 ligases may participate in regulating carcinogenesis including WD repeat and SOCS box containing 1 (WSB1) and Murine double minute-2 (MDM2) (Cao et al., 2015; Ying et al., 2016). These researches inspire us to shine a spotlight on the relationship between E3 ligases and cancer.

According to the statistics, E3 ligases distribute in a great many organs, cells and subcellular compartments. Compared with other subcellular localized E3 ligases, membrane-associated E3 ligases are much more crucial for the membrane-organelles, which play vital roles in maintaining their morphology and functions. For instance, mainly distributed in the mitochondrion and endoplasmic reticulum, the membrane-associated RING-CH-type finger (MARCH) proteins of E3 ubiquitin ligases positively regulate mitochondrial fission (Xu et al., 2016) and play a crucial role in controlling mitochondrial mass. It can degrade itself in dysfunctional mutants to maintain mitochondrial homeostasis and prevent cellular senescence (Bauer et al., 2017). Another E3 ligase Synoviolin (SYVN1), located in ER, stimulates the degradation of IRE1 α through interaction with p53 and maintains ER function by regulating activation of the IRE1 α /XBP1 pathway (Namba et al., 2015). However, the membrane-associated E3 ligases remain poorly summarized.

In this review, we summarized the 84 membrane-associated E3 ligases from the following aspects: UniProt ID, gene name, subcellular localization, E3 type and the number of transmembrane segments (Table 1). Moreover, we also described the relationship of some important E3 ligases with carcinogenesis in detail, which is significant for uncovering novel targets of cancer and may provide a new perspective of understanding the ubiquitination process,



especially providing inspiration for inducing membrane protein degradation *via* ubiquitination and proteasome pathway.

ER-LOCALIZED E3

The endoplasmic reticulum functions as the transportation system of the eukaryotic cell and manufactures lipids and proteins. What's more, the studies presented thus far provide evidence that endoplasmic reticulum stress is closely related to cancer (Yadav et al., 2014). Due to the critical role that E3 ligases play in metabolism occurred in the endoplasmic reticulum, ER-localized E3 ligases are essential for cancer development (Figure 2).

TRIM13

TRIM13 is a tumor suppressor gene whose deletion is common in various malignant tumors. It is a tumor suppressor in non-small-cell lung carcinoma (NSCLC) and its mRNA and protein expression was reduced in NSCLC tissues and cell lines (Xu et al., 2019). It has been reported that it is mainly located in the endoplasmic reticulum membrane, mediates the degradation of endoplasmic reticulum-related proteins, and regulates autophagy caused by endoplasmic stress (Tomar et al., 2012). So far, caspase-8, MDM2, Akt, and Nur77 have all been identified as TRIM13 substrates. Furthermore, several studies have suggested that these substrates are all related to tumor cell apoptosis and proliferation.

As for caspase-8, its ubiquitination is critical to proceed downstream caspase cascade, which results in cell apoptosis. TRIM13-induced caspase-8 ubiquitination may lead to its transportation to autophagosomes. Autophagosomes anchor caspase-8 and fusion with lysosomes, providing an environment for cleavage and activation of caspase-8. When the endoplasmic reticulum is stressed, the cell will amplify the

downstream caspase cascade and cause cell death (Tomar et al., 2013).

Besides caspase-8, TRIM13 can also form complexes with MDM2, which negatively regulates the tumor suppressor p53 and AKT to provoke cell apoptosis. As a result of their interaction, MDM2 and AKT are ubiquitinated and degraded by proteasomes, thereby increasing the stability of p53, reducing the AKT kinase activity, and inducing cell apoptosis consequently (Joo et al., 2011).

This study suggests that TRIM13 can promote tumor cell apoptosis, which indicates that TRIM13 may be deleted or inactivated in some cancer tissues and cell lines. In 2019, the hypothesis was confirmed by Xu et al. (2019) experimentally. They found that compared with non-cancerous tissues and normal bronchial epithelial cell lines, non-small cell lung cancer tissues and cell lines have reduced TRIM13 mRNA and protein expression. And it is also been found that TRIM13 partly induces the apoptosis of NSCLC cells under the mediation of caspase-3 and exerts an antitumor effect.

TRIM13 can not only promote tumor cell apoptosis but also regulate cell proliferation. In 2014, Tomar and Singh (2014) investigated the influence of TRIM13 on cell growth and proliferation. According to their research, NEMO, a substrate of TRIM13, plays a notable role in the NF- κ B signaling pathway, which regulates the expression of several inflammatory cytokines and is associated with cancer. TRIM13 initially interacts with NEMO to induce its ubiquitination and degradation, which may suppress the activity of the IKK complex and thus hinder NF- κ B signaling. Ultimately, TRIM13 inhibits the proliferation of cancer cells.

Gp78

Gp78, commonly known as autocrine motility factor receptor (AMFR), was initially found in the B16-F1 melanoma cell line (Nabi and Raz, 1987) and has been discovered to be an AMFR

TABLE 1 | 84 membrane-associated E3 ligases.

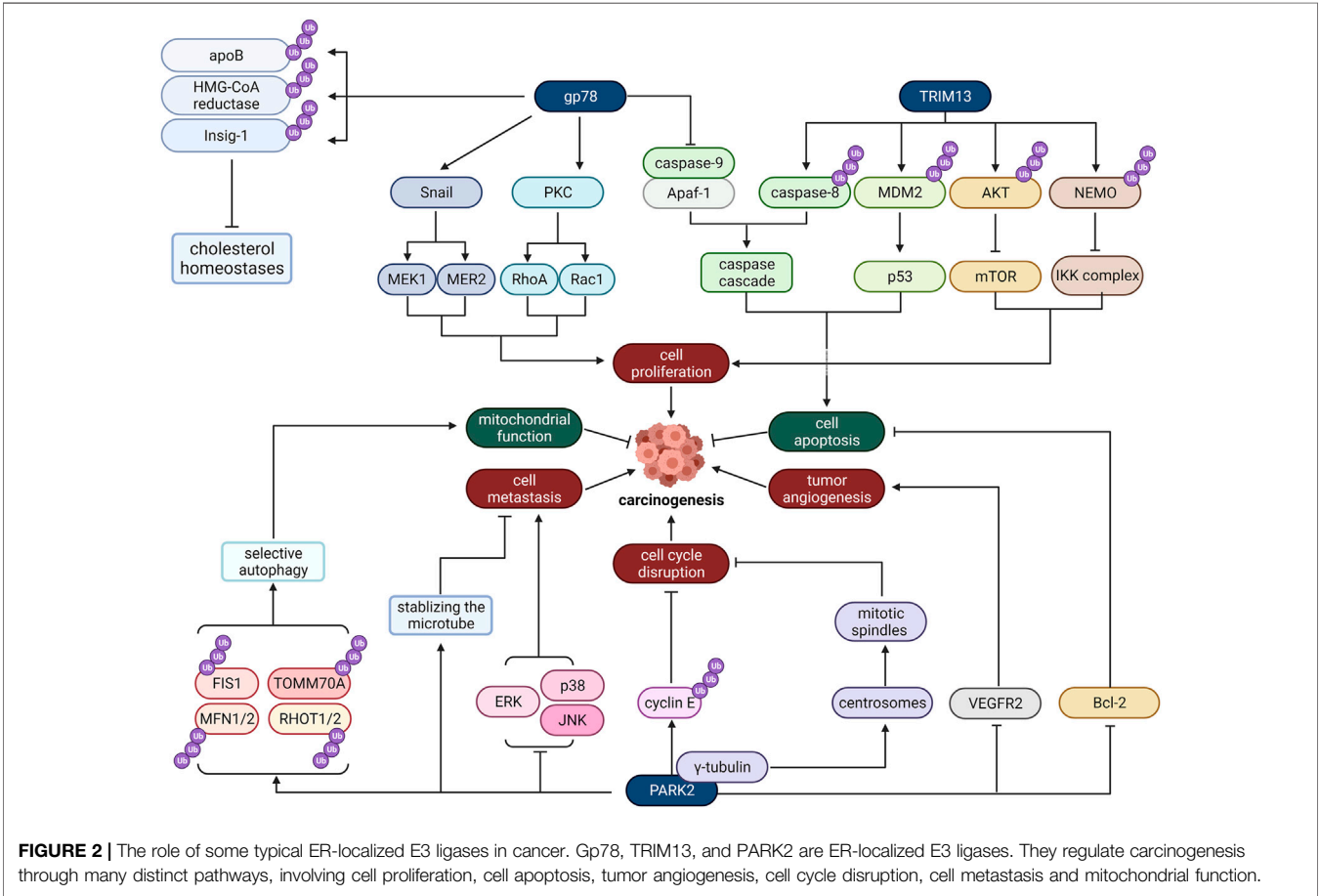
Uniprot ID	Name	Subcellular location	Type	Transmembrane regions
Q9NZS9	BFAR	ERM	RING	4
Q9UKV5	AMFR	ERM	RING	7
Q5T197	DCST1	PM	RING	6
Q9Y4D8	HECTD4	Membrane	HECTc	1
Q96J02	ITCH	PM, cytoplasm, nucleus, EM	HECTc	NA
Q8TDB6	DTX3L	Cytoplasm, nucleus, EM, LM	RING	NA
A6NNE9	MARCHF11	VM	RING	2
Q86UD3	MARCHF3	VM, EM	RING	2
Q9P2E8	MARCHF4	GAM	RING	2
Q9NX47	MARCHF5	MM, ERM	RING	4
Q8TCQ1	MARCHF1	GAM, LM, VM, EM, PM	RING	2
Q86YJ5	MARCHF9	GAM, LM	RING	2
Q9P0N8	MARCHF2	ERM, LM, EM	RING	2
Q5T0T0	MARCHF8	VM, LM, EM	RING	2
Q86YT6	MIB1	Cytoplasm, SK, CK, PM	RING	NA
Q7L5Y9	MAEA	Cytoplasm, nucleus, PM, SK	RING	NA
O60337	MARCHF6	ERM	RING	14
Q00987	MDM2	Cytoplasm, nucleus	RING	NA
Q969V5	MUL1	MM	RING	2
Q8WY64	MYLIP	Cytoplasm, PM	RING	NA
P46934	NEDD4	Cytoplasm, PM	HECTc	NA
O76050	NEURL1	Cytoplasm, PM	RING	NA
Q6ZNB6	NFXL1	Membrane	RING	1
Q60683	PEX10	Peroxisome membrane	RING	NA
O00623	PEX12	Peroxisome membrane	RING	2
O43164	PJA2	Cytoplasm, PM, ERM, GAM	RING	NA
Q8WZ73	RFFL	EM	RING	NA
O00237	RNF103	ERM	RING	4
Q9H920	RNF121	Membrane	RING	6
O60260	PRKN	Cytoplasm, nucleus, ERM, MM, PM	RING	NA
Q9H9V4	RNF122	GAM, ERM	RING	1
Q9ULX5	RNF112	Cytoplasm, nucleus, VM, PM	RING	2
Q96EQ8	RNF125	GAM	RING	NA
P29590	PML	Cytoplasm, nucleus, ERM	RING	NA
Q8WVZ7	RNF133	ERM	RING	1
Q8WU17	RNF139	ERM	RING	12
Q86XS8	RNF130	Membrane, cytoplasm	RING	1
P50876	RNF144A	PM, VM	RING	1
Q7Z419	RNF144B	MM, cytoplasm	RING	1
Q8WVD5	RNF141	Membrane	RING	NA
Q8N8N0	RNF152	LM	RING	1
Q8TEB7	RNF128	M, cytoplasm, SK, perinuclear region	RING	1
Q9H6Y7	RNF167	M	RING	1
Q8NC42	RNF149	Membrane	RING	1
Q96MT1	RNF145	ERM	RING	14
Q8N7C7	RNF148	Membrane	RING	1
Q9ULK6	RNF150	Membrane	RING	1
Q96K19	RNF170	ERM	RING	3
Q8N4F7	RNF175	Membrane	RING	5
Q96D59	RNF183	ERM, GAM, LM	RING	1
Q9NXI6	RNF186	ERM	RING	2
Q8N6D2	RNF182	Membrane, cytoplasm	RING	2
Q9Y6U7	RNF215	Membrane	RING	2
Q9NV58	RNF19A	Membrane, cytoplasm, SK	RING	2
Q6ZMZ0	RNF19B	Cytoplasmic granule membrane, ERM	RING	2
A6NCQ9	RNF222	Membrane	RING	1
E7ERA6	RNF223	Membrane	RING	1
Q96GF1	RNF185	MM, ERM	RING	2
M0QZC1	RNF225	Membrane	RING	1
Q9BY78	RNF26	ERM	RING	5
Q969K3	RNF34	PM, nucleus, cytoplasm, cytosol	RING	NA
Q9Y225	RNF24	GAM	RING	1
Q8TC41	RNF217	Membrane, cytoplasm	RING	1
Q5M7Z0	RNFT1	ERM	RING	6

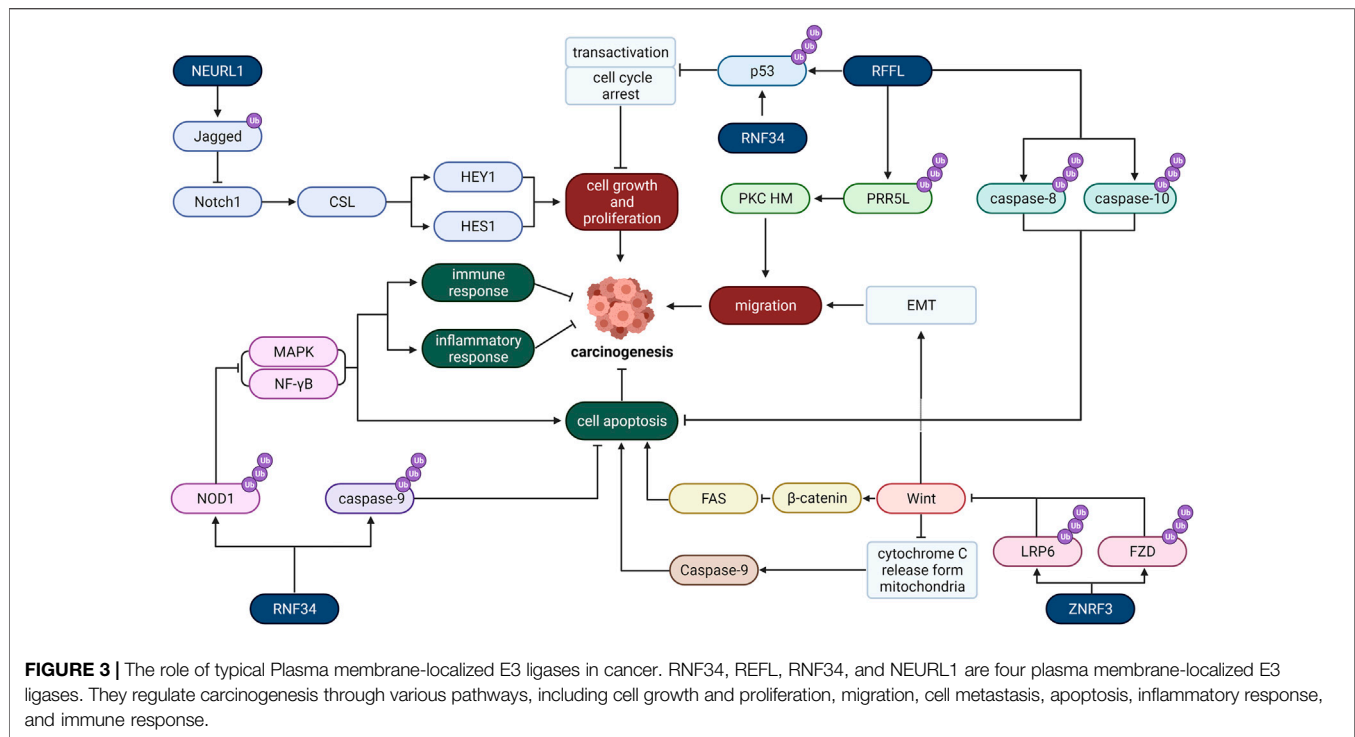
(Continued on following page)

TABLE 1 | (Continued) 84 membrane-associated E3 ligases.

Uniprot ID	Name	Subcellular location	Type	Transmembrane regions
Q96EX2	RNFT2	Membrane	RING	4
Q9HCE7	SMURF1	Cytoplasm, PM	HECTc	NA
A0AVI4	TMEM129	ERM	RING	3
Q9HAU4	SMURF2	Nucleus, cytoplasm, PM, membrane raft	HECTc	NA
Q60858	TRIM13	ERM	RING	1
P36406	TRIM23	Cytoplasm, GAM, LM	RING	NA
Q86TM6	SYVN1	ERM	RING	6
Q8IWR1	TRIM59	ERM	RING	1
Q6ZMU5	TRIM72	PM, sarcolemma, VM	RING	NA
Q6ZT12	UBR3	Membrane	UBR	3
Q5T4S7	UBR4	Membrane	UBR	2
Q9H270	VPS11	EM, LM, VM, autophagosome	RING	NA
P49754	VPS41	EM, LM, GAM, VM, clathrin-coated vesicle	RING	NA
Q6PJ19	WDR59	LM	RING	NA
Q95159	ZFPL1	GAM	RING	1
Q9H0M0	WWP1	Cytoplasm, PM, nucleus	HECTc	NA
Q8ND25	ZNRF1	VM	RING	NA
Q9ULT6	ZNRF3	PM	RING	1
Q8NHG8	ZNRF2	EM, LM, PM	RING	NA
Q8WWF5	ZNRF4	ERM	RING	1
Q9P253	VPS18	EM, LM, VM, autophagosome	RING	NA

ERM, endoplasmic reticulum membrane; GAM, golgi apparatus membrane; PM, plasma membrane; VM, vesicle membrane; EM, endosome membrane; LM, lysosome membrane; MM, mitochondrion membrane; SK, cytoskeleton and microtubule.





essential for tumor metastasis and migration (Watanabe et al., 1991). The ligand for gp78 is AMF (Nabi et al., 1990), an extracellular tumor cytokine. In response to AMF stimulation, gp78 is activated and then changes cell adhesion, proliferation, movement, and apoptosis activities by activating the downstream signaling pathway. Specifically, the activation of gp78 triggers a protein kinase C-dependent signal cascade and then activates and upregulates RhoA and Rac1 (Kanbe et al., 1994; Tsutsumi et al., 2002), which induce the reorganization of the lesion contact and the formation of stress fibers, resulting in enhanced cell motility and proliferation. The activated gp78 also upregulates the transcription factor SNAIL, leading to loss of cell adhesion (Silletti et al., 1996; Tsutsumi et al., 2004), and phosphorylates MEK1 and MEK2 to activate the MAPK pathway and increases cell proliferation (Torimura et al., 2001). Besides, the expression level of Apaf-1 and caspase-9 is reduced when gp78 is activated, which may inhibit tumor cell apoptosis (Haga et al., 2003).

Other than the function mentioned above of gp78 as a receptor, it can ubiquitinate and degrade some proteins as an E3 ligase, which is associated with its locations. Gp78 is internalized through the endocytosis pathway and directly enters the smooth ER when combined with AMF. Therefore, gp78 is located on the plasma membrane, smooth ER closely connected with mitochondria, and a small amount of rough ER. In ER, gp78 is crucial in proteasomal degradation of ERAD-targeted proteins, and some substrates identified so far contain cholesterol homeostases, such as apolipoprotein B (Liang et al., 2003), HMG coenzyme A reductase (Song et al., 2005) and Insig-1 (Lee et al., 2006). Other gp78 substrates like KAI1, a metastasis inhibitor, are closely correlated with sarcoma metastasis (Tsai et al., 2007).

PARK2

PARK2 is a tumor suppressor gene that plays an essential part in cancer progression. It is related to microtubule stability, cell cycle disruption, mitochondrial homeostasis, cell apoptosis, and metabolism that regulates cell state (Manzanillo et al., 2013). Current studies have confirmed loss of function of PARK2 in various human cancers, including breast (Rodriguez et al., 2000), ovarian (Saito et al., 1996), lung (Kong et al., 2000), and renal cancers (Morita et al., 1991), implying that its inactivation may promote tumor transformation and progression. What's more, PARK2 protein is negatively regulated in many primary tumors, which may contribute to cancer development. For instance, Parkin deficiency may promote pancreatic tumors through dysregulation of microtubule-dependent mitotic kinesin Eg5 expression and subsequent spindle behavior defects (Sun et al., 2013).

Microtubule stability is critical for cell proliferation, and PARK2 may inhibit tumor migration by stabilizing microtubules through an E3-independent way when paclitaxel is administered as an anticancer drug. This effect is triggered by the binding of three microtubule-binding domains of Parkin (MAPKs), which are mitogen-activated protein kinases, to microtubules. By binding to the external layer of microtubules, Parkin enhances microtubule-paclitaxel interaction as well as the activity of paclitaxel, thereby promoting microtubule stability and assembly, which are two hallmarks of paclitaxel cytotoxicity. Therefore, PARK2 levels may predict paclitaxel treatment outcomes in breast cancer (Wang et al., 2009). In addition, the following activation of protein kinases associated with microtubules such as p38, ERK, and JNK is also blocked, thereby antagonizing the effects of microtubule depolymerization drugs like colchicine (Ren et al., 2009).

Carcinogenesis may be incited by cell cycle disruption induced by Parkin dysfunction. A seminal study of PARK2 by Kyoko Ikeuchi (2009) reports that Parkin help with the ubiquitination and proteasome degradation of cyclin E in human colon cells (Ikeuchi et al., 2009). Furthermore, Shiam-Peng (2010) demonstrated that PARK2 contributes to cell cycle arrest and growth inhibition by specifically upregulating CDK6 mRNA levels in MCF7 breast cancer cells (Tay et al., 2010). Multiple shreds of evidence suggest that PARK2 also modulates centrosomes and mitotic spindles *via* interacting with γ -Tubulin (Chen et al., 2012). Since centrosomes contribute to mitotic spindles formation, their inactivation may contribute to cell division dysregulation.

Mitochondrial function is usually impaired in cancer, and PARK2 is implicated in mitochondrial functional regulation and turnover. PARK2 combines with mtDNA to enhance mitochondrial transcription mediated by TFAM and restore the expression of PGC-1 α , thus promoting mitochondrial production (Kuroda et al., 2006). In addition, it protects mitochondrial genomes from reactive oxygen species-induced damage, and it is also involved in mtDNA repair (Rothfuss et al., 2009). What's more, activated PARK2 acts as a catalyst for rapid ubiquitination of various mitochondrial proteins, such as FIS1, MFN1/2, TOMM70A, RHOT1/2, etc. (Chan et al., 2011; Narendra et al., 2012; Sarraf et al., 2013), which then recruits adaptor proteins to initiate selective autophagy. Ultimately, PARK2-reliant mitochondrial autophagy maintains healthy mitochondrial populations by selectively degrading damaged mitochondria. Therefore, PARK2 is vital for promoting mitochondrial function and maintaining mitochondrial genome integrity and popularity. As a result, changes in PARK2 can be associated with tumorigenesis.

PARK2 also regulates the activity of several apoptosis-related proteins of the Bcl-2 family, including Bax, Bcl-2, and Mcl1 (Chen et al., 2010; Johnson et al., 2012; Ekholm-Reed et al., 2013), promoting apoptosis of tumor cells. In addition, PARK2 boosts cell apoptosis produced by Microtubule stabilizers and HDAC inhibitors in liver and breast tumor cells, according to studies (Wang et al., 2004; Wang et al., 2009). Furthermore, PARK2 makes HeLa cells susceptible to apoptosis induced by TNF- α (Lee et al., 2012).

PARK2 may influence cancer cell metabolism to some extent. For example, PARK2 is the target gene of p53, which regulates energy metabolism. PARK2 deficiency enhances glycolysis while decreasing mitochondrial respiration, leading to the Warburg effect (Zhang et al., 2011). Moreover, in gliomas, the EGFR-Akt pathway is negatively regulated by PARK2, and PARK2 overexpression can inhibit signal transduction through Akt/mTOR. And the loss of parkin function will enhance the expression of cyclin D1 and Akt-related growth promotion signals and, at the same time, promote the proliferation of glioma cells. Besides, in gliomas PARK2 downregulates VEGFR2, a high-affinity tyrosine kinase receptor involved in tumor angiogenesis. Therefore, it may have the effect of inhibiting tumor angiogenesis (Yeo et al., 2012).

SYVN1

SYVN1 inhibits breast cancer growth and metastasis through the miR-96-5p/SYVN1 axis (Gao et al., 2018). It interacts with IGF-1R

and promotes its ubiquitination and degradation through the proteasome. This, in turn, leads to inhibition of the growth, migration and invasion of breast cancer cells (Xu et al., 2015). Tumor metastasis is closely associated with the poor prognosis of hepatocellular carcinoma (HCC). Some studies have found that E3 ubiquitin has been analyzed by proteomics and ubiquitinomics of HCC. Furthermore, there is a correlation between SYVN1 and tumor metastasis. Moreover, SYVN1 interacts with heat shock protein 90 and contributes to the ubiquitination of eukaryotic elongation factor 2 kinase. (Ji et al., 2021).

Tumor cell metabolic abnormalities may cause ER lesion and unfolded protein response (UPR), which maintains ER homeostasis by inducing degradation of unfolded proteins. Typically, proteins not properly folded are perceived by adaptor proteins such as chaperones, ubiquitinated by E3 ubiquitin ligases and degraded by proteasomes. However, ER stress would induce cell apoptosis to exclude them from normal cells. Therefore, ER function is critical for the survival of cancer cells.

PLASMA MEMBRANE-LOCALIZED E3

Plasma membrane not only regulates the flow of substances into and out of cells but also protects the integrity of cells and keeps their form. Multitudes of researches have proved that frequent mutations of plasma membrane-associated E3 ligases are engaged in carcinogenesis (Figure 3).

ZNRF3

Zinc and ring finger 3 (ZNRF3) is located in the plasma membrane, which is usually correlated to cancer development. In 2014, Assié et al. (2014) reported frequent mutations of ZNRF3 in adrenocortical carcinoma (ACC). Compared to normal surrounding tissues, the ZnRF3 level in gastric tumor tissues has been lower (Zhou et al., 2013), and ZnRF3 mutations are prevalent in pancreatic cancer (Wolpin et al., 2014). Numerous literature has investigated how ZNRF3 regulates the Wnt/ β -Catenin signal, which is correlated with cancer (Clevers and Nusse, 2012) because Wnt helps the stabilization and nuclear localization of β -Catenin, which contributes to the formation of TCF/ β -Catenin complex and recreation of other co-activators to promote gene activation like c-MYC and cyclin D1 (Ma et al., 2012).

Ubiquitination-mediated Wnt receptor turnover has become a key regulating factor of the Wnt pathway because it affects the sensibility of cells to Wnt ligands. And ZNRF3 precisely regulates Wnt pathway activity by promoting the degradation of Wnt receptors. ZNRF3 inhibits Wnt/PCP and Wnt/ β -Catenin signaling pathway by promoting the ubiquitination and degradation of Wnt protein core receptor FZD (Jiang et al., 2015) and Wnt protein co-receptor LRP6 (Hao et al., 2012; Koo et al., 2012). Therefore, ZNRF3 negatively regulates the Wnt pathway and may inhibit cancer cell growth.

It has also been found that ZNRF3 hinders the growth of cancer cells and promotes cell apoptosis by regulating the Wnt/ β -Catenin/TCF signaling pathway (Zhou et al., 2013) for the reason that Wnt-1 inhibits apoptosis by blocking mitochondrial

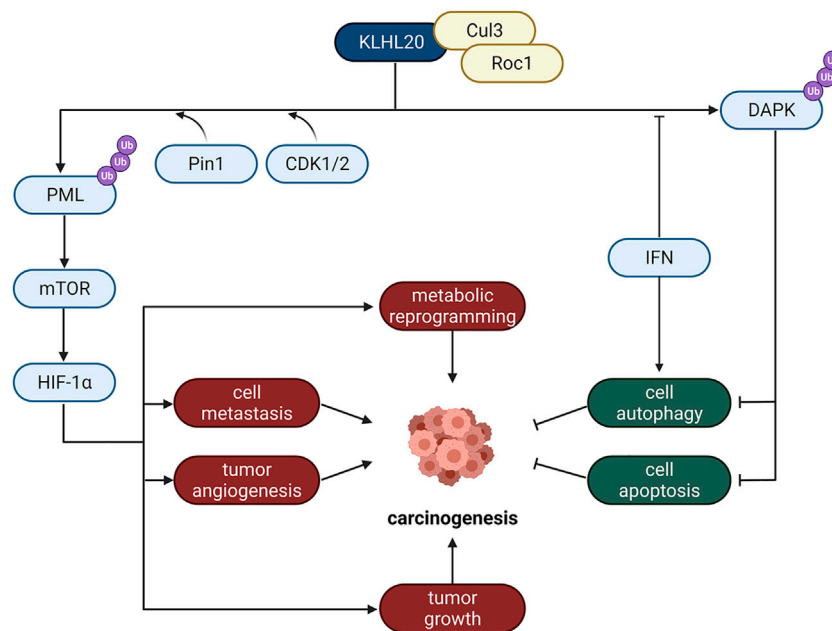


FIGURE 4 | The role of Golgi localized E3 ligases in cancer. KLHL20 is an important Golgi E3 protein, which regulates carcinogenesis through many different pathways, including metabolic reprogramming, cell metastasis, tumor angiogenesis and tumor growth.

cytochrome C release, thereby inhibiting the activity of caspase-9 (Li et al., 2006; Brocardo and Henderson, 2008). And other studies have shown that Wnt signaling inhibits cancer cell apoptosis by impelling NF- κ B. Activated β -Catenin may decrease the expression level of FAS, targeted by NF- κ B, whence possibly suppressing Fas-mediated apoptosis, leading to tumorigenesis (Ma and Hottiger, 2016).

Furthermore, ZNRF3 may also restrain the migration and invasiveness of some cancer cells like papillary thyroid carcinoma cells by this pathway (Deng et al., 2015). Previous research has established that epithelial-mesenchymal transition (EMT) is a critical step in the migration of cancer cells from the original cancer lesions to nearby organs (Christofori, 2006). The Wnt/ β -Catenin pathway is one mechanism for cells to undergo EMT (Thiery et al., 2009). Consequently, ZNRF3 peradventure inhibits cancer cell invasion.

RFFL (CARP-2)

The ring finger and FYVE-like (RFFL) domain-containing E3 ligase is a member of caspase 8/10-associated RING proteins (CARPs), so it is also named CARP-2. Studies have found that RFFL inhibits p53, which is an effective tumor suppressor that tends to be mutated in tumor cells (Bode and Dong, 2004; Olivier et al., 2004) and promotes the growth of cancer cells. RFFL has been reported to have strong functions in colorectal cancer cells (Dong et al., 2013). In contrast, CARP's silencing upregulates p53 expression and facilitates transcriptional activation and tumor suppression. CARPs negatively regulate p53 through ubiquitination and proteasome degradation of p53 and inhibit transactivation and cell cycle arrest. CARPs can target not only non-phosphorylated p53 but also phospho-p53^{ser20} and possibly

phospho-p53^{ser15} 74, both of which are accumulated after DNA damage and cannot be ubiquitinated by other p53 associated E3s like MDM2. Consequently, CARPs are critical to regulating cancer cell growth through the p53 pathway.

Apart from promoting cancer cell proliferation, CARPs also inhibit cancer cell apoptosis. It helps the ubiquitin-mediated proteolysis of death effector domain (DED) caspase, which induces the damage of cell target during apoptosis and is challenging to be inhibited by regular inhibitors of apoptosis proteins (IAP). It has been found that CARPs interact specifically with caspase-8 and caspase-10 (McDonald and El-Deiry, 2004) and induce their ubiquitination and degradation *via* the proteasome pathway, thereby impeding cancer cell apoptosis.

And RFFL plays a pivotal part in cell migration. RFFL induces ubiquitination and degradation of PRR5L, which leads to mTORC2-mediated phosphorylation and activation of PKC HM. Continuous activation of PKC is indispensable for maintaining tumor cell migration. Therefore, RFFL may be a potential target to promote tumor migration and metastasis (Gan et al., 2013). Hence, the regulation of RFFL is essential for tumors. Studies have reported that miR-133a can straight bind to RFFL mRNA and inhibit its translation, thereby reducing the level of RFFL protein, enhancing cell apoptosis and inhibiting cell proliferation (Dong et al., 2013).

RNF34 (CARP-1)

Belonging to the CARP family, RNF34 induces the ubiquitination and degradation of death effector domain (DED) caspase to suppress cancer cell apoptosis (McDonald and El-Deiry, 2004). And RNF34 can also inhibit cancer cell apoptosis by regulating

the NOD1 pathway. NOD1 can not only induce cell apoptosis but also control cell proliferation, and NOD1 activation can lead to caspase-8 and caspase-9-induced apoptosis (da Silva Correia et al., 2007). Recently there have been reports of missing NOD1 and breast tumor growth (da Silva Correia et al., 2006). RNF34 mainly affects the NOD1 pathway negatively. It interacts directly with NOD1 to induce its ubiquitination and subsequent degradation, therefore reducing the expression level of NOD1 in the cell. As a result, RNF34 hinders NOD1-mediated apoptosis. And it inhibits the activation of NOD1-dependent nuclear factor- κ B (NF- γ B) along with mitogen-activated protein kinase (MAPK), which results in cytokine, chemokine, antimicrobial peptide production and apoptosis when activated (da Silva Correia et al., 2007; Hasegawa et al., 2008; Park et al., 2007). Therefore, it may inhibit the cellular immune response, inflammatory response and apoptosis in this way.

In addition, RNF34 also stimulates the degradation of p53 and then hinders transactivation, and cell cycle arrests like other CARP members, such as RFFL mentioned above (Yang et al., 2007), which means it also regulates cancer cell cycles and may accelerate cell growth and proliferation.

NEURL1

Neuralized-like protein 1 (NEURL1) is a conserved E3 ligase investigated as a candidate tumor suppressor. The subcellular localization of NEURL1 has not been definitively determined, while some studies demonstrated that overexpressed NEURL1 is localized in the plasma membrane in an N-myristylation-dependent manner (Koutelou et al., 2008). According to studies, NEURL1 is significantly down-regulated in medulloblastoma cells through histone modification and exhibits various tumor suppressor properties, including promotion of cell apoptosis and suppression of tumor growth, angiogenesis, and invasion (Koutelou et al., 2008). These effects are mainly produced through the regulation of the Notch signaling cascade.

NEURL1 can function as an E3 ubiquitin ligase to monoubiquitinate the extracellular domain of a membrane-tethered protein Jagged1 and trigger the endocytosis and degradation of Jagged1 (Koutelou et al., 2008). Decreased Jagged1 level weakens signaling between Jagged1 and its receptor, Notch1, on the surfaces of neighboring cells. This results in less cleavage and detaching of Notch intracellular region (icN1) from the membrane and binding with CSL transcription factor in the nucleus (Sjölund et al., 2005). Consequently, inhibition of the Notch1 signaling pathway downregulates the transcriptional initiation of a variety of cell cycle-related proteins, including HES1 and HEY1 (Teider et al., 2010), suppressing the growth and division of tumor cells.

Other upstream proteins may regulate this effect of NEURL1. Fe65 facilitates the recruitment of NEURL1 to form a stable ternary complex with Jagged1 and is considered a factor negatively regulating the Jagged1/Notch1 pathway (Lee et al., 2015). Neuritin interacted with NEURL1 and down-regulates NEURL1 expression. Therefore, it is considered a positive regulator of the Jagged1/Notch1 pathway (Zhang et al., 2017).

Cbl

Cbl proteins mainly exist on the cell membrane surface and play a significant role in tumorigenesis and antitumor immunity (Liyasova et al., 2015). And it is been reported that Cbl expression correlates with human colorectal cancer (Kumaradevan et al., 2018) and it may inhibit lung cancer and glioblastoma cells' migration (Lee et al., 2018). First, its activity as an E3 ligase negatively regulates signalings by activated RTKs: this family of proteins attenuates receptor tyrosine kinases by ubiquitinating RTKs, targeting them to lysosomes for degradation (RTK)-related signaling (Ma et al., 2013). Nevertheless, Cbl's E3 function is lost due to cancer mutations. Furthermore, Cbl-mediated ubiquitination can alter the cellular localization of the protein to modulate its function. In addition, Cbl also act as adaptors to active RTKs by recruiting signaling molecules. For example, it has been shown that Cbl act as adaptors to recruit PI3K to activate RTKs, which subsequently activate the PI3K/AKT pathway (Dombrosky-Ferlan and Corey, 1997; Ueno et al., 1998).

Cbl-b negatively regulates the antitumor function of T cells and natural killer (NK) cells through its E3 ligase activity. Therefore, deletion of Cbl-b will potentiate the NK cell activity. For example, Cbl-b deficient NK cells can suppress oncogene-driven breast cancer. The tyrosine kinase receptor TAM family is the molecular substrate of Cbl-b, including Tyro3, Axl, and Mer. And TAM receptors also negatively regulate NK cells. Therefore, the Cbl-b/TAM receptors inhibit NK cell activation (Paolino et al., 2014), and the consequences of Cbl protein deficiency can lead to malignant tumors or immune dysfunction.

GOLGI LOCALIZED E3 LIGASES

The Golgi apparatus is of particular importance for secretory proteins. Its significant function of regulating metabolism mainly depends on membrane fluidity and abundant important anchored proteins. And Golgi localized E3 ligases are closely related to tumor hypoxia responses and cell apoptosis, such as KLHL20 (Figure 4).

KLHL20, a Cullin3 (Cul3) substrate adaptor, belongs to Broad-Complex, Tramtrack, and Bric-a-brac (BTB) family (Pintard et al., 2004). Only if it forms an E3 ligase complex with Cul3 and Roc1 can it induce the ubiquitination of its substrates like PML and DAPK. It promotes tumor growth, migration, angiogenesis and metabolic reprogramming as well as inhibits the processes of autophagy and apoptosis of cancer cells by promoting substrate ubiquitination and degradation, thus promoting prostate cancer progression (Yuan et al., 2011).

KLHL20 mediates hypoxia-induced PML ubiquitination and proteasome-induced degradation. CDK1/2 and Pin1 are also implicated in the regulation of this pathway. CDK1 and CDK2 promote KLHL20-mediated degranulation of PML, and Pin1-mediated proline isomerization promotes the recruitment of PML to KLHL20. Because PML negatively regulates hypoxia-inducible 1 α (HIF-1 α) protein synthesis by inhibiting mTOR activity (Bernardi et al., 2006). Therefore, degradation of PML

would increase HIF-1 α content, thereby promoting a variety of HIF-1 α -regulated metabolic reprogramming, migration, tumor growth and angiogenesis, etc. (Brahimi-Horn et al., 2007; Finger and Giaccia, 2010; Semenza, 2010).

Studies have shown that KLHL20 also enhances DAPK ubiquitination and proteasome degradation to inhibit cell apoptosis. Death-associated protein kinase (DAPK) is a tumor suppressor. Moreover, interferon (IFN) can suppress tumor cell proliferation and trigger apoptosis, and it has been used in cancer therapy. Because DAPK is a pivotal factor of IFN-induced autophagy (Inbal et al., 2002), KLHL20 impairs its proapoptotic function. It was also found that IFN could reduce the efficiency of KLHL20-DAPK complex formation by sequestering KLHL20, thus reducing DAPK ubiquitination by KLHL20 and stabilizing DAPK protein content; as a result, aiding IFN-induced autophagy (Inbal et al., 2002).

MITOCHONDRIA LOCALIZED E3

PIR2/RNF144B is a potential targeted biomarker in endometrial cancer to promote proliferation and is mainly localized on the mitochondrion membrane. Experiments in human osteosarcoma cells Saos-2 revealed that the expression of apoptin issues in the activation of proapoptotic TAp73, ending in the upregulation of PUMA and cell death. Thus, PIR2 degrades anti-apoptotic Δ Np73 to increase TAp73 stability to induce apoptosis. In brief, it induces ubiquitination of Δ Np73 for degradation and activates the TAp73-mediated apoptosis pathway. And it was previously shown to regulate the stability of p21WAF1 or p63, which mediate cell growth arrest and epithelial homeostasis (Conforti et al., 2013).

NUCLEAR MEMBRANE-LOCALIZED E3

ITCH

ITCH is localized on the cell and nuclear membranes. It plays a fundamental role in different cellular contexts depending on its different substrates. Its substrates are mainly divided into two categories: transcription factors and cell growth factors, like ErbB-4, a member of the EGFR/ERbB family. These substrates' ubiquitination and proteasomal degradation affects cell growth, differentiation and apoptosis, and is associated with tumors malignant transformation and chemoresistance (Melino et al., 2008). And it is been found that ITCH is a downstream target of miR-10b which promoted melanoma progression by repressing ITCH (Wang et al., 2019).

Smurf1 and Smurf2

Smad ubiquitin regulatory factor 1 (Smurf1) and Smurf2 are E3 ligases that inhibit the TGF- β pathway through ubiquitination-induced receptors for degrading smads and transforming growth factor- β (TGF- β). Smurf1 may promote ovarian cancer invasion and epithelial-to-mesenchymal transition (EMT) (Fan et al., 2019) and Smurf2 may motivate colon cancer cell proliferation (Yu et al., 2019). However, their substrates are different. Smurf1

binds to Smad1 and Smad5, while Smurf2 binds to Smad1, Smad2, Smad3, Smad6, and Smad7. Smurf2 enhanced the repressive activity of Smad7 while decreasing the transcriptional activity of Smad2. Smurf2 can bind to the transcriptional co-repressor SnoN and degrade it through Smad2 (Bonni et al., 2001). Therefore, Smurf2 may enhance TGF- β signaling beneath certain circumstances. In addition, due to differences in post-translational regulation, the functions of smurf2 and smurf1 also differ to some extent. At the same time, Smurf1 can regulate cell motility by promoting the ubiquitination and degradation of RhoA (Wang et al., 2003), which plays a certain role in the development of cancer. On MDA-MB 231 cells, Smurf2 can ubiquitinate and subsequently degrade Smurf1, but not vice versa. The knockdown of Smurf2 leads to an increase in the protein level of Smurf1, which promotes cell migration *in vitro* and bone metastasis *in vivo* (Fukunaga et al., 2008).

CONCLUSION AND PROSPECTS

In summary, membrane-associated E3 ligases are of great significance to the therapeutic improvement of cancer. Lipid alterations in membrane and other cancer syndromes in cancer cells are closely related to E3 ligases (Zalba and ten Hagen, 2017). Thus, the membrane system regulates the proliferation, migration and differentiation of cancer cells partly *via* E3 ligases. Increasing evidence indicates that specific E3 ligases play a key role in carcinogenesis. What's more, some membrane-associated E3 ubiquitin ligases are observed to be frequently mutated in many human cancer cell lines, which may induce chemoresistance and cause poor clinic prognosis. These research findings would eventually shed light on a new class of antitumor drugs targeting E3 ubiquitin ligases and the research and development of sensitive biomarkers for cancer diagnosis, treatment, and prognosis, which requires further constant exploration. What's more, several studies have demonstrated that some E3 ubiquitin ligases are related to the regulation of innate immune response, which provides a solid theoretical basis for expanding the application of E3 ligases to promote tumor immunotherapy.

In the future, the rapid development and breakthrough of PROTAC may largely depend on some research on membrane-associated E3 ligases. Some membrane-anchored proteins, for example, are difficult to target using targeted degradation techniques, but a new strategy utilizing membrane-associated E3 ligases may help the ubiquitination and degradation of these proteins. In addition, the cellular trafficking system may deliver some proteins from the plasma membrane to the trans-Golgi network, thereby chewing up these proteins.

Consequently, the membrane-associated E3 ligases have crucial functions and potential application values in developing new therapeutic strategies for cancer. It is anticipated that membrane E3 ligases will soon be of great significance in tackling medical and biological research problems with more in-depth research and understanding of membrane-associated E3 ubiquitin ligases.

AUTHOR CONTRIBUTIONS

Concept design: JC, CZ, and XC; XC, LJ, ZZ, and JC wrote the manuscript; JC, QH, and BY directed the study.

FUNDING

This work was supported by grants from the Zhejiang Provincial Natural Science Foundation of China (No.

REFERENCES

- Assié, G., Letouze, E., Fassnacht, M., Jouinot, A., Luscip, W., Barreau, O., et al. (2014). Integrated Genomic Characterization of Adrenocortical Carcinoma. *Nat. Genet.* 46 (6), 607–612. doi:10.1038/ng.2953
- Bauer, J., Bakke, O., and Morth, J. P. (2017). Overview of the Membrane-Associated RING-CH (MARCH) E3 Ligase Family. *N. Biotechnol.* 38, 7–15. doi:10.1016/j.nbt.2016.12.002
- Bernardi, R., Guernah, I., Jin, D., Grisendi, S., Alimonti, A., Teruya-Feldstein, J., et al. (2006). PML Inhibits HIF-1 α Translation and Neoangiogenesis through Repression of mTOR. *Nature* 442 (7104), 779–785. doi:10.1038/nature05029
- Bode, A. M., and Dong, Z. (2004). Post-translational Modification of P53 in Tumorigenesis. *Nat. Rev. Cancer* 4 (10), 793–805. doi:10.1038/nrc1455
- Bonni, S., Wang, H. R., Causing, C. G., Kavsak, P., Stroschein, S. L., Luo, K., et al. (2001). TGF- β Induces Assembly of a Smad2-Smurf2 Ubiquitin Ligase Complex that Targets SnO for Degradation. *Nat. Cell Biol.* 3 (6), 587–595. doi:10.1038/35078562
- Brahimi-Horn, M. C., Chiche, J., and Pouyssegur, J. (2007). Hypoxia and Cancer. *J. Mol. Med. Berl.* 85 (12), 1301–1307. doi:10.1007/s00109-007-0281-3
- Brocardo, M., and Henderson, B. R. (2008). APC Shuttling to the Membrane, Nucleus and beyond. *Trends Cell Biol.* 18 (12), 587–596. doi:10.1016/j.tcb.2008.09.002
- Cao, J., Wang, Y., Dong, R., Lin, G., Zhang, N., Wang, J., et al. (2015). Hypoxia-Induced WSB1 Promotes the Metastatic Potential of Osteosarcoma Cells. *Cancer Res.* 75 (22), 4839–4851. doi:10.1158/0008-5472.CAN-15-0711
- Chan, N. C., Salazar, A. M., Pham, A. H., Sweredoski, M. J., Kolawa, N. J., Graham, R. L., et al. (2011). Broad Activation of the Ubiquitin-Proteasome System by Parkin Is Critical for Mitophagy. *Hum. Mol. Genet.* 20 (9), 1726–1737. doi:10.1093/hmg/ddr048
- Chen, D., Gao, F., Li, B., Wang, H., Xu, Y., Zhu, C., et al. (2010). Parkin Mono-Ubiquitinates Bcl-2 and Regulates Autophagy. *J. Biol. Chem.* 285 (49), 38214–38223. doi:10.1074/jbc.M110.101469
- Chen, Y., Fang, S. T., Yeh, P. C., Yang, H. H., Chen, S. Y., Chang, C. J., et al. (2012). The C-Terminus of PARK2 Is Required for its Self-Interaction, Solubility and Role in the Spindle Assembly Checkpoint. *Biochim. Biophys. Acta* 1822 (4), 573–580. doi:10.1016/j.bbdis.2011.12.007
- Christofori, G. (2006). New Signals from the Invasive Front. *Nature* 441 (7092), 444–450. doi:10.1038/nature04872
- Clevers, H., and Nusse, R. (2012). Wnt/ β -catenin Signaling and Disease. *Cell* 149 (6), 1192–1205. doi:10.1016/j.cell.2012.05.012
- Conforti, F., Yang, A. L., Piro, M. C., Mellone, M., Terrinoni, A., Candi, E., et al. (2013). PIR2/Rnf144B Regulates Epithelial Homeostasis by Mediating Degradation of p21WAF1 and P63. *Oncogene* 32 (40), 4758–4765. doi:10.1038/ncr.2012.497
- da Silva Correia, J., Miranda, Y., Austin-Brown, N., Hsu, J., Mathison, J., Xiang, R., et al. (2006). Nod1-dependent Control of Tumor Growth. *Proc. Natl. Acad. Sci. U. S. A.* 103 (6), 1840–1845. doi:10.1073/pnas.0509228103
- da Silva Correia, J., Miranda, Y., Leonard, N., and Ulevitch, R. J. (2007). The Subunit CSN6 of the COP9 Signalosome Is Cleaved during Apoptosis. *J. Biol. Chem.* 282 (17), 12557–12565. doi:10.1074/jbc.M609587200
- Dacks, J. B., and Field, M. C. (2018). Evolutionary Origins and Specialisation of Membrane Transport. *Curr. Opin. Cell Biol.* 53, 70–76. doi:10.1016/j.ccb.2018.06.001
- Deng, X., Wu, B., Xiao, K., Kang, J., Xie, J., Zhang, X., et al. (2015). MiR-146b-5p Promotes Metastasis and Induces Epithelial-Mesenchymal Transition in

LR22H310002 to JC and No. LGF21B020001 to CZ), the National Natural Science Foundation of China (No. 81930102 to BY and No. 81872885 to JC), and Zhejiang University K. P. Chao's High Technology Development Foundation.

ACKNOWLEDGMENTS

The figures were created with BioRender.com

- Thyroid Cancer by Targeting ZNRF3. *Cell Physiol. Biochem.* 35 (1), 71–82. doi:10.1159/000369676
- Deshaies, R. J., and Joazeiro, C. A. (2009). RING Domain E3 Ubiquitin Ligases. *Annu. Rev. Biochem.* 78, 399–434. doi:10.1146/annurev.biochem.78.101807.093809
- Dombrosky-Ferlan, P. M., and Corey, S. J. (1997). Yeast Two-Hybrid *In Vivo* Association of the Src Kinase Lyn with the Proto-Oncogene Product Cbl but Not with the P85 Subunit of PI 3-kinase. *Oncogene* 14 (17), 2019–2024. doi:10.1038/sj.onc.1201031
- Dong, Y., Zhao, J., Wu, C. W., Zhang, L., Liu, X., Kang, W., et al. (2013). Tumor Suppressor Functions of miR-133a in Colorectal Cancer. *Mol. Cancer Res.* 11 (9), 1051–1060. doi:10.1158/1541-7786.MCR-13-0061
- Eklholm-Reed, S., Goldberg, M. S., Schlossmacher, M. G., and Reed, S. I. (2013). Parkin-dependent Degradation of the F-Box Protein Fbw7 β Promotes Neuronal Survival in Response to Oxidative Stress by Stabilizing Mcl-1. *Mol. Cell Biol.* 33 (18), 3627–3643. doi:10.1128/MCB.00535-13
- Fan, X., Wang, Y., Fan, J., and Chen, R. (2019). Deletion of SMURF 1 Represses Ovarian Cancer Invasion and EMT by Modulating the DAB2IP/AKT/Skp2 Feedback Loop. *J. Cell Biochem.* 120 (6), 10643–10651. doi:10.1002/jcb.28354
- Finger, E. C., and Giaccia, A. J. (2010). Hypoxia, Inflammation, and the Tumor Microenvironment in Metastatic Disease. *Cancer Metastasis Rev.* 29 (2), 285–293. doi:10.1007/s10555-010-9224-5
- Fukunaga, E., Inoue, Y., Komiya, S., Horiguchi, K., Goto, K., Saitoh, M., et al. (2008). Smurf2 Induces Ubiquitin-dependent Degradation of Smurf1 to Prevent Migration of Breast Cancer Cells. *J. Biol. Chem.* 283 (51), 35660–35667. doi:10.1074/jbc.M710496200
- Gan, X., Wang, C., Patel, M., Kreutz, B., Zhou, M., Kozasa, T., et al. (2013). Different Raf Protein Kinases Mediate Different Signaling Pathways to Stimulate E3 Ligase RFL Gene Expression in Cell Migration Regulation. *J. Biol. Chem.* 288 (47), 33978–33984. doi:10.1074/jbc.M113.477406
- Gao, Z., Wang, H., Li, H., Li, M., Wang, J., Zhang, W., et al. (2018). Long Non-coding RNA CASC2 Inhibits Breast Cancer Cell Growth and Metastasis through the Regulation of the miR-96-5p/SYVN1 Pathway. *Int. J. Oncol.* 53 (5), 2081–2090. doi:10.3892/ijo.2018.4522
- Haga, A., Funasaka, T., Niinaka, Y., Raz, A., and Nagase, H. (2003). Autocrine Motility Factor Signaling Induces Tumor Apoptotic Resistance by Regulations Apaf-1 and Caspase-9 Apoptosome Expression. *Int. J. Cancer* 107 (5), 707–714. doi:10.1002/ijc.11449
- Hao, H. X., Xie, Y., Zhang, Y., Charlat, O., Oster, E., Avello, M., et al. (2012). ZNRF3 Promotes Wnt Receptor Turnover in an R-Spondin-Sensitive Manner. *Nature* 485 (7397), 195–200. doi:10.1038/nature11019
- Hasegawa, M., Fujimoto, Y., Lucas, P. C., Nakano, H., Fukase, K., Núñez, G., et al. (2008). A Critical Role of RICK/RIP2 Polyubiquitination in Nod-Induced NF- κ B Activation. *EMBO J.* 27 (2), 373–383. doi:10.1038/sj.emboj.7601962
- Ikeuchi, K., Marusawa, H., Fujiwara, M., Matsumoto, Y., Endo, Y., Watanabe, T., et al. (2009). Attenuation of Proteolysis-Mediated Cyclin E Regulation by Alternatively Spliced Parkin in Human Colorectal Cancers. *Int. J. Cancer* 125 (9), 2029–2035. doi:10.1002/ijc.24565
- Inbal, B., Bialik, S., Sabanay, I., Shani, G., and Kimchi, A. (2002). DAP Kinase and DRP-1 Mediate Membrane Blebbing and the Formation of Autophagic Vesicles during Programmed Cell Death. *J. Cell Biol.* 157 (3), 455–468. doi:10.1083/jcb.200109094
- Ji, F., Zhou, M., Sun, Z., Jiang, Z., Zhu, H., Xie, Z., et al. (2021). Integrative Proteomics Reveals the Role of E3 Ubiquitin Ligase SYVN1 in Hepatocellular Carcinoma Metastasis. *Cancer Commun.* 41 (10), 1007–1023. doi:10.1002/cac2.12192

- Jiang, X., Charlat, O., Zamponi, R., Yang, Y., and Cong, F. (2015). Dishevelled Promotes Wnt Receptor Degradation through Recruitment of ZNRF3/RNF43 E3 Ubiquitin Ligases. *Mol. Cell* 58 (3), 522–533. doi:10.1016/j.molcel.2015.03.015
- Johnson, B. N., Berger, A. K., Cortese, G. P., and LaVoie, M. J. (2012). The Ubiquitin E3 Ligase Parkin Regulates the Proapoptotic Function of Bax. *Proc. Natl. Acad. Sci. U. S. A.* 109 (16), 6283–6288. doi:10.1073/pnas.1113248109
- Joo, H. M., Kim, J. Y., Jeong, J. B., Seong, K. M., Nam, S. Y., Yang, K. H., et al. (2011). Ret Finger Protein 2 Enhances Ionizing Radiation-Induced Apoptosis via Degradation of AKT and MDM2. *Eur. J. Cell Biol.* 90 (5), 420–431. doi:10.1016/j.ejcb.2010.12.001
- Kambe, K., Chigira, M., and Watanabe, H. (1994). Effects of Protein Kinase Inhibitors on the Cell Motility Stimulated by Autocrine Motility Factor. *Biochim. Biophys. Acta* 1222 (3), 395–399. doi:10.1016/0167-4889(94)90046-9
- Kong, F. M., Anscher, M. S., Washington, M. K., Killian, J. K., and Jirtle, R. L. (2000). M6P/IGF2R Is Mutated in Squamous Cell Carcinoma of the Lung. *Oncogene* 19 (12), 1572–1578. doi:10.1038/sj.onc.1203437
- Koo, B. K., Spit, M., Jordens, L., Low, T. Y., Stange, D. E., Van De Wetering, M., et al. (2012). Tumour Suppressor RNF43 Is a Stem-Cell E3 Ligase that Induces Endocytosis of Wnt Receptors. *Nature* 488 (7413), 665–669. doi:10.1038/nature11308
- Koutelou, E., Sato, S., Tomomori-Sato, C., Florens, L., Swanson, S. K., Washburn, M. P., et al. (2008). Neuralized-like 1 (Neurl1) Targeted to the Plasma Membrane by N-Myristoylation Regulates the Notch Ligand Jagged1. *J. Biol. Chem.* 283 (7), 3846–3853. doi:10.1074/jbc.M706974200
- Kumaradevan, S., Lee, S. Y., Richards, S., Lyle, C., Zhao, Q., Tapan, U., et al. (2018). c-Cbl Expression Correlates with Human Colorectal Cancer Survival and its Wnt/ β -Catenin Suppressor Function Is Regulated by Tyr371 Phosphorylation. *Am. J. Pathol.* 188 (8), 1921–1933. doi:10.1016/j.ajpath.2018.05.007
- Kuroda, Y., Mitsui, T., Kunishige, M., Shono, M., Akaike, M., Azuma, H., et al. (2006). Parkin Enhances Mitochondrial Biogenesis in Proliferating Cells. *Hum. Mol. Genet.* 15 (6), 883–895. doi:10.1093/hmg/ddl006
- Lee, G. W., Park, J. B., Park, S. Y., Seo, J., Shin, S. H., Park, J. W., et al. (2018). The E3 Ligase C-CBL Inhibits Cancer Cell Migration by Neddylation of the Proto-Oncogene C-Src. *Oncogene* 37 (41), 5552–5568. doi:10.1038/s41388-018-0354-5
- Lee, H. J., Yoon, J. H., Ahn, J. S., Jo, E. H., Kim, M. Y., Lee, Y. C., et al. (2015). Fe65 Negatively Regulates Jagged1 Signaling by Decreasing Jagged1 Protein Stability through the E3 Ligase Neuralized-like 1. *Biochim. Biophys. Acta* 1853 (11), 2918–2928. Part A):2918–28. doi:10.1016/j.bbamcr.2015.08.009
- Lee, J. N., Song, B., DeBose-Boyd, R. A., and Ye, J. (2006). Sterol-regulated Degradation of Insig-1 Mediated by the Membrane-Bound Ubiquitin Ligase Gp78. *J. Biol. Chem.* 281 (51), 39308–39315. doi:10.1074/jbc.M608999200
- Lee, K., Lee, M. H., Kang, Y. W., Rhee, K. J., Kim, T. U., and Kim, Y. S. (2012). Parkin Induces Apoptotic Cell Death in TNF- α -Treated Cervical Cancer Cells. *BMB Rep.* 45 (9), 526–531. doi:10.5483/bmbrep.2012.45.9.104
- Li, F., Chong, Z. Z., and Maiese, K. (2006). Winding through the WNT Pathway during Cellular Development and Demise. *Histol. Histopathol.* 21 (1), 103–124. doi:10.14670/HH-21.103
- Liang, J. S., Kim, T., Fang, S., Yamaguchi, J., Weissman, A. M., Fisher, E. A., et al. (2003). Overexpression of the Tumor Autocrine Motility Factor Receptor Gp78, a Ubiquitin Protein Ligase, Results in Increased Ubiquitinylation and Decreased Secretion of Apolipoprotein B100 in HepG2 Cells. *J. Biol. Chem.* 278 (26), 23984–23988. doi:10.1074/jbc.M302683200
- Liyasova, M. S., Ma, K., and Lipkowitz, S. (2015). Molecular Pathways: Cbl Proteins in Tumorigenesis and Antitumor Immunity-Opportunities for Cancer Treatment. *Clin. Cancer Res.* 21 (8), 1789–1794. doi:10.1158/1078-0432.CCR-13-2490
- Ma, B., and Hottiger, M. O. (2016). Crosstalk between Wnt/ β -Catenin and NF-Kb Signaling Pathway during Inflammation. *Front. Immunol.* 7, 378. doi:10.3389/fimmu.2016.00378
- Ma, J., Wang, R., Fang, X., and Sun, Z. (2012). β -catenin/TCF-1 Pathway in T Cell Development and Differentiation. *J. Neuroimmune Pharmacol.* 7 (4), 750–762. doi:10.1007/s11481-012-9367-y
- Ma, K., Kales, S. C., Nau, M. M., and Lipkowitz, S. (2013). “Cbl as a Master Regulator of Receptor Tyrosine Kinase Trafficking,” in *Vesicle Trafficking in Cancer*. Editors Y. Yarden and G. Tarcic (New York, NY: Springer), 219–244. doi:10.1007/978-1-4614-6528-7_11
- Manzanillo, P. S., Ayres, J. S., Watson, R. O., Collins, A. C., Souza, G., Rae, C. S., et al. (2013). The Ubiquitin Ligase Parkin Mediates Resistance to Intracellular Pathogens. *Nature* 501 (7468), 512–516. doi:10.1038/nature12566
- Martin, C. E., and List, K. (2019). Cell Surface-Anchored Serine Proteases in Cancer Progression and Metastasis. *Cancer Metastasis Rev.* 38 (3), 357–387. doi:10.1007/s10555-019-09811-7
- McDonald, E. R., and El-Deiry, W. S. (2004). Suppression of Caspase-8- and -10-associated RING Proteins Results in Sensitization to Death Ligands and Inhibition of Tumor Cell Growth. *Proc. Natl. Acad. Sci. U. S. A.* 101 (16), 6170–6175. doi:10.1073/pnas.0307459101
- Melino, G., Gallagher, E., Aqeilan, R. I., Knight, R., Peschiaroli, A., Rossi, M., et al. (2008). Itch: a HECT-type E3 Ligase Regulating Immunity, Skin and Cancer. *Cell Death Differ.* 15 (7), 1103–1112. doi:10.1038/cdd.2008.60
- Morita, R., Saito, S., Ishikawa, J., Ogawa, O., Yoshida, O., Yamakawa, K., et al. (1991). Common Regions of Deletion on Chromosomes 5q, 6q, and 10q in Renal Cell Carcinoma. *Cancer Res.* 51 (21), 5817–5820.
- Nabi, I. R., and Raz, A. (1987). Cell Shape Modulation Alters Glycosylation of a Metastatic Melanoma Cell-Surface Antigen. *Int. J. Cancer* 40 (3), 396–402. doi:10.1002/ijc.2910400319
- Nabi, I. R., Watanabe, H., and Raz, A. (1990). Identification of B16-F1 Melanoma Autocrine Motility-like Factor Receptor. *Cancer Res.* 50 (2), 409–414.
- Namba, T., Chu, K., Kodama, R., Byun, S., Yoon, K. W., Hiraki, M., et al. (2015). Loss of P53 Enhances the Function of the Endoplasmic Reticulum through Activation of the IRE1 α /XBP1 Pathway. *Oncotarget* 6 (24), 19990–20001. doi:10.18632/oncotarget.4598
- Narendra, D., Walker, J. E., and Youle, R. (2012). Mitochondrial Quality Control Mediated by PINK1 and Parkin: Links to Parkinsonism. *Cold Spring Harb. Perspect. Biol.* 4 (11), a011338. doi:10.1101/cshperspect.a011338
- Novelli, G., Liu, J., Biancolella, M., Alonzi, T., Novelli, A., Patten, J. J., et al. (2021). Inhibition of HECT E3 Ligases as Potential Therapy for COVID-19. *Cell Death Dis.* 12 (4), 1–18. doi:10.1038/s41419-021-03513-1
- Olivier, M., Hussain, S. P., Caron de Fromental, C., Hainaut, P., and Harris, C. C. (2004). TP53 Mutation Spectra and Load: a Tool for Generating Hypotheses on the Etiology of Cancer. *IARC Sci. Publ.* 157, 247–270.
- Paolino, M., Choidas, A., Wallner, S., Pranjic, B., Uribealago, I., Loeser, S., et al. (2014). The E3 Ligase Cbl-B and TAM Receptors Regulate Cancer Metastasis via Natural Killer Cells. *Nature* 507 (7493), 508–512. doi:10.1038/nature12998
- Park, J. H., Kim, Y. G., McDonald, C., Kanneganti, T. D., Hasegawa, M., Body-Malapel, M., et al. (2007). RICK/RIP2 Mediates Innate Immune Responses Induced through Nod1 and Nod2 but Not TLRs. *J. Immunol.* 178 (4), 2380–2386. doi:10.4049/jimmunol.178.4.2380
- Pintard, L., Willems, A., and Peter, M. (2004). Cullin-based Ubiquitin Ligases: Cul3-BTB Complexes Join the Family. *EMBO J.* 23 (8), 1681–1687. doi:10.1038/sj.emboj.7600186
- Ren, Y., Jiang, H., Yang, F., Nakaso, K., and Feng, J. (2009). Parkin Protects Dopaminergic Neurons against Microtubule-Depolymerizing Toxins by Attenuating Microtubule-Associated Protein Kinase Activation. *J. Biol. Chem.* 284 (6), 4009–4017. doi:10.1074/jbc.M806245200
- Rodriguez, C., Causse, A., Ursule, E., and Theillet, C. (2000). At Least Five Regions of Imbalance on 6q in Breast Tumors, Combining Losses and Gains. *Genes Chromosom. Cancer* 27 (1), 76–84. doi:10.1002/(sici)1098-2264(200001)27:1<76::aid-gcc10>3.0.co;2-e
- Rothfuss, O., Fischer, H., Hasegawa, T., Maisel, M., Leitner, P., Miesel, F., et al. (2009). Parkin Protects Mitochondrial Genome Integrity and Supports Mitochondrial DNA Repair. *Hum. Mol. Genet.* 18 (20), 3832–3850. doi:10.1093/hmg/ddp327
- Rotin, D., and Kumar, S. (2009). Physiological Functions of the HECT Family of Ubiquitin Ligases. *Nat. Rev. Mol. Cell Biol.* 10 (6), 398–409. doi:10.1038/nrm2690
- Saito, S., Sirahama, S., Matsushima, M., Suzuki, M., Sagae, S., Kudo, R., et al. (1996). Definition of a Commonly Deleted Region in Ovarian Cancers to a 300-kb Segment of Chromosome 6q27. *Cancer Res.* 56 (24), 5586–5589.
- Sarraf, S. A., Raman, M., Guarani-Pereira, V., Sowa, M. E., Huttlin, E. L., Gygi, S. P., et al. (2013). Landscape of the PARKIN-dependent Ubiquitylome in Response to Mitochondrial Depolarization. *Nature* 496 (7445), 372–376. doi:10.1038/nature12043
- Semenza, G. L. (2010). Defining the Role of Hypoxia-Inducible Factor 1 in Cancer Biology and Therapeutics. *Oncogene* 29 (5), 625–634. doi:10.1038/onc.2009.441
- Silletti, S., Paku, S., and Raz, A. (1996). Tumor Autocrine Motility Factor Responses Are Mediated through Cell Contact and Focal Adhesion Rearrangement in the Absence of New Tyrosine Phosphorylation in Metastatic Cells. *Am. J. Pathol.* 148 (5), 1649–1660.

- Sjölund, J., Manetopoulos, C., Stockhausen, M. T., and Axelson, H. (2005). The Notch Pathway in Cancer: Differentiation Gone Awry. *Eur. J. Cancer* 41 (17), 2620–2629. doi:10.1016/j.ejca.2005.06.025
- Song, B. L., Sever, N., and DeBose-Boyd, R. A. (2005). Gp78, a Membrane-Anchored Ubiquitin Ligase, Associates with Insig-1 and Couples Sterol-Regulated Ubiquitination to Degradation of HMG CoA Reductase. *Mol. Cell* 19 (6), 829–840. doi:10.1016/j.molcel.2005.08.009
- Sun, X., Liu, M., Hao, J., Li, D., Luo, Y., Wang, X., et al. (2013). Parkin Deficiency Contributes to Pancreatic Tumorigenesis by Inducing Spindle Multipolarity and Misorientation. *Cell Cycle* 12 (7), 1133–1141. doi:10.4161/cc.24215
- Tay, S. P., Yeo, C. W., Chai, C., Chua, P. J., Tan, H. M., Ang, A. X., et al. (2010). Parkin Enhances the Expression of Cyclin-dependent Kinase 6 and Negatively Regulates the Proliferation of Breast Cancer Cells. *J. Biol. Chem.* 285 (38), 29231–29238. doi:10.1074/jbc.M110.108241
- Teider, N., Scott, D. K., Neiss, A., Weeraratne, S. D., Amani, V. M., Wang, Y., et al. (2010). Neuralized1 Causes Apoptosis and Downregulates Notch Target Genes in Medulloblastoma. *Neuro Oncol.* 12 (12), 1244–1256. doi:10.1093/neuonc/ono091
- Thiery, J. P., Acloque, H., Huang, R. Y., and Nieto, M. A. (2009). Epithelial-Mesenchymal Transitions in Development and Disease. *Cell* 139 (5), 871–890. doi:10.1016/j.cell.2009.11.007
- Tomar, D., Prajapati, P., Sripada, L., Singh, K., Singh, R., Singh, A. K., et al. (2013). TRIM13 Regulates Caspase-8 Ubiquitination, Translocation to Autophagosomes and Activation during ER Stress Induced Cell Death. *Biochim. Biophys. Acta* 1833 (12), 3134–3144. doi:10.1016/j.bbamer.2013.08.021
- Tomar, D., Singh, R., Singh, A. K., Pandya, C. D., and Singh, R. (2012). TRIM13 Regulates ER Stress Induced Autophagy and Clonogenic Ability of the Cells. *Biochim. Biophys. Acta* 1823 (2), 316–326. doi:10.1016/j.bbamer.2011.11.015
- Tomar, D., and Singh, R. (2014). TRIM13 Regulates Ubiquitination and Turnover of NEMO to Suppress TNF Induced NF-Kb Activation. *Cell Signal* 26 (12), 2606–2613. doi:10.1016/j.cellsig.2014.08.008
- Torimura, T., Ueno, T., Kin, M., Harada, R., Nakamura, T., Kawaguchi, T., et al. (2001). Autocrine Motility Factor Enhances Hepatoma Cell Invasion across the Basement Membrane through Activation of Beta1 Integrins. *Hepatology* 34 (1), 62–71. doi:10.1053/jhep.2001.25546
- Tsai, Y. C., Mendoza, A., Mariano, J. M., Zhou, M., Kostova, Z., Chen, B., et al. (2007). The Ubiquitin Ligase Gp78 Promotes Sarcoma Metastasis by Targeting KAI1 for Degradation. *Nat. Med.* 13 (12), 1504–1509. doi:10.1038/nm1686
- Tsutsumi, S., Gupta, S. K., Hogan, V., Collard, J. G., and Raz, A. (2002). Activation of Small GTPase Rho Is Required for Autocrine Motility Factor Signaling. *Cancer Res.* 62 (15), 4484–4490.
- Tsutsumi, S., Yanagawa, T., Shimura, T., Kuwano, H., and Raz, A. (2004). Autocrine Motility Factor Signaling Enhances Pancreatic Cancer Metastasis. *Clin. Cancer Res.* 10 (22), 7775–7784. doi:10.1158/1078-0432.CCR-04-1015
- Ueno, H., Sasaki, K., Honda, H., Nakamoto, T., Yamagata, T., Miyagawa, K., et al. (1998). c-Cbl Is Tyrosine-Phosphorylated by Interleukin-4 and Enhances Mitogenic and Survival Signals of Interleukin-4 Receptor by Linking with the Phosphatidylinositol 3'-kinase Pathway. *Blood* 91 (1), 46–53. doi:10.1182/blood.v91.1.46.46_46_53
- Wang, F., Denison, S., Lai, J. P., Philips, L. A., Montoya, D., Kock, N., et al. (2004). Parkin Gene Alterations in Hepatocellular Carcinoma. *Genes Chromosom. Cancer* 40 (2), 85–96. doi:10.1002/gcc.20020
- Wang, H., Liu, B., Zhang, C., Peng, G., Liu, M., Li, D., et al. (2009). Parkin Regulates Paclitaxel Sensitivity in Breast Cancer via a Microtubule-dependent Mechanism. *J. Pathol.* 218 (1), 76–85. doi:10.1002/path.2512
- Wang, H. R., Zhang, Y., Ozdamar, B., Ogunjimi, A. A., Alexandrova, E., Thomsen, G. H., et al. (2003). Regulation of Cell Polarity and Protrusion Formation by Targeting RhoA for Degradation. *Science* 302 (5651), 1775–1779. doi:10.1126/science.1090772
- Wang, S., Wu, Y., Xu, Y., and Tang, X. (2019). miR-10b Promoted Melanoma Progression through Wnt/ β -Catenin Pathway by Repressing ITC Expression. *Gene* 710, 39–47. doi:10.1016/j.gene.2019.05.043
- Watanabe, H., Carmi, P., Hogan, V., Raz, T., Silletti, S., Nabi, I. R., et al. (1991). Purification of Human Tumor Cell Autocrine Motility Factor and Molecular Cloning of its Receptor. *J. Biol. Chem.* 266 (20), 13442–13448. doi:10.1016/s0021-9258(18)98859-9
- Wolpin, B. M., Rizzato, C., Kraft, P., Kooperberg, C., Petersen, G. M., Wang, Z., et al. (2014). Genome-wide Association Study Identifies Multiple Susceptibility Loci for Pancreatic Cancer. *Nat. Genet.* 46 (9), 994–1000. doi:10.1038/ng.3052
- Xu, L., Wu, Q., Zhou, X., Wu, Q., and Fang, M. (2019). TRIM13 Inhibited Cell Proliferation and Induced Cell Apoptosis by Regulating NF-Kb Pathway in Non-small-cell Lung Carcinoma Cells. *Gene* 715, 144015. doi:10.1016/j.gene.2019.144015
- Xu, S., Cherok, E., Das, S., Li, S., Roelofs, B. A., Ge, S. X., et al. (2016). Mitochondrial E3 Ubiquitin Ligase MARCH5 Controls Mitochondrial Fission and Cell Sensitivity to Stress-Induced Apoptosis through Regulation of MiD49 Protein. *Mol. Biol. Cell* 27 (2), 349–359. doi:10.1091/mbc.E15-09-0678
- Xu, Y. M., Wang, H. J., Chen, F., Guo, W. H., Wang, Y. Y., Li, H. Y., et al. (2015). HRD1 Suppresses the Growth and Metastasis of Breast Cancer Cells by Promoting IGF-1R Degradation. *Oncotarget* 6 (40), 42854–42867. doi:10.18632/oncotarget.5733
- Yadav, R. K., Chae, S. W., Kim, H. R., and Chae, H. J. (2014). Endoplasmic Reticulum Stress and Cancer. *J. Cancer Prev.* 19 (2), 75–88. doi:10.15430/JCP.2014.19.2.75
- Yang, W., Rozan, L. M., McDonald, E. R., Navaraj, A., Liu, J. J., Matthew, E. M., et al. (2007). CARPs Are Ubiquitin Ligases that Promote MDM2-independent P53 and Phospho-P53ser20 Degradation. *J. Biol. Chem.* 282 (5), 3273–3281. doi:10.1074/jbc.M610793200
- Yeo, C. W., Ng, F. S., Chai, C., Tan, J. M., Koh, G. R., Chong, Y. K., et al. (2012). Parkin Pathway Activation Mitigates Glioma Cell Proliferation and Predicts Patient Survival. *Cancer Res.* 72 (10), 2543–2553. doi:10.1158/0008-5472.CAN-11-3060
- Ying, M., Zhang, L., Zhou, Q., Shao, X., Cao, J., Zhang, N., et al. (2016). The E3 Ubiquitin Protein Ligase MDM2 Dictates All-Trans Retinoic Acid-Induced Osteoblastic Differentiation of Osteosarcoma Cells by Modulating the Degradation of RAR α . *Oncogene* 35 (33), 4358–4367. doi:10.1038/onc.2015.503
- Yu, L., Dong, L., Wang, Y., Liu, L., Long, H., Li, H., et al. (2019). Reversible Regulation of SATB1 Ubiquitination by USP47 and SMURF2 Mediates Colon Cancer Cell Proliferation and Tumor Progression. *Cancer Lett.* 448, 40–51. doi:10.1016/j.canlet.2019.01.039
- Yuan, W. C., Lee, Y. R., Huang, S. F., Lin, Y. M., Chen, T. Y., Chung, H. C., et al. (2011). A Cullin3-KLHL20 Ubiquitin Ligase-dependent Pathway Targets PML to Potentiate HIF-1 Signaling and Prostate Cancer Progression. *Cancer Cell* 20 (2), 214–228. doi:10.1016/j.ccr.2011.07.008
- Zalba, S., and ten Hagen, T. L. (2017). Cell Membrane Modulation as Adjuvant in Cancer Therapy. *Cancer Treat. Rev.* 52, 48–57. doi:10.1016/j.ctrv.2016.10.008
- Zhang, C., Lin, M., Wu, R., Wang, X., Yang, B., Levine, A. J., et al. (2011). Parkin, a P53 Target Gene, Mediates the Role of P53 in Glucose Metabolism and the Warburg Effect. *Proc. Natl. Acad. Sci. U. S. A.* 108 (39), 16259–16264. doi:10.1073/pnas.1113884108
- Zhang, P., Luo, X., Guo, Z., Xiong, A., Dong, H., Zhang, Q., et al. (2017). Neuritin Inhibits Notch Signaling through Interacted with Neuralized to Promote the Neurite Growth. *Front. Mol. Neurosci.* 10, 179. doi:10.3389/fnmol.2017.00179
- Zheng, N., and Shabek, N. (2017). Ubiquitin Ligases: Structure, Function, and Regulation. *Annu. Rev. Biochem.* 86, 129–157. doi:10.1146/annurev-biochem-060815-014922
- Zhou, Y., Lan, J., Wang, W., Shi, Q., Lan, Y., Cheng, Z., et al. (2013). ZNRF3 Acts as a Tumour Suppressor by the Wnt Signalling Pathway in Human Gastric Adenocarcinoma. *J. Mol. Histol.* 44 (5), 555–563. doi:10.1007/s10735-013-9504-9

Conflict of Interest: The authors declare that the research was conducted in the absence of any commercial or financial relationships that could be construed as a potential conflict of interest.

Publisher's Note: All claims expressed in this article are solely those of the authors and do not necessarily represent those of their affiliated organizations, or those of the publisher, the editors and the reviewers. Any product that may be evaluated in this article, or claim that may be made by its manufacturer, is not guaranteed or endorsed by the publisher.

Copyright © 2022 Chen, Jiang, Zhou, Yang, He, Zhu and Cao. This is an open-access article distributed under the terms of the Creative Commons Attribution License (CC BY). The use, distribution or reproduction in other forums is permitted, provided the original author(s) and the copyright owner(s) are credited and that the original publication in this journal is cited, in accordance with accepted academic practice. No use, distribution or reproduction is permitted which does not comply with these terms.



OPEN ACCESS

EDITED BY
Sandeep Singh,
Central University of Punjab, India

REVIEWED BY
Sandeep Kumar Yadav,
University of Texas MD Anderson
Cancer Center, United States
Alvaro Otero Rodríguez,
University Hospital of Salamanca,
Spain

*CORRESPONDENCE
Puli Chandramouli Reddy
pc.reddy@snu.edu.in
Bimlesh Lochab
bimlesh.lochab@snu.edu.in

[†]These authors have contributed
equally to this work

SPECIALTY SECTION
This article was submitted to
Pharmacology of Anti-Cancer Drugs,
a section of the journal
Frontiers in Oncology

RECEIVED 25 May 2022
ACCEPTED 20 July 2022
PUBLISHED 16 August 2022

CITATION
Mishra VS, Patil S, Reddy PC and
Lochab B (2022) Combinatorial
delivery of CPI444 and vatalanib
loaded on PEGylated graphene oxide
as an effective nanoformulation to
target glioblastoma multiforme:
In vitro evaluation.
Front. Oncol. 12:953098.
doi: 10.3389/fonc.2022.953098

COPYRIGHT
© 2022 Mishra, Patil, Reddy and Lochab.
This is an open-access article
distributed under the terms of the
Creative Commons Attribution License
(CC BY). The use, distribution or
reproduction in other forums is
permitted, provided the original
author(s) and the copyright owner(s)
are credited and that the original
publication in this journal is cited, in
accordance with accepted academic
practice. No use, distribution or
reproduction is permitted which does
not comply with these terms.

Combinatorial delivery of CPI444 and vatalanib loaded on PEGylated graphene oxide as an effective nanoformulation to target glioblastoma multiforme: *In vitro* evaluation

Vishnu S. Mishra^{1†}, Sachin Patil^{2†},
Puli Chandramouli Reddy^{1*} and Bimlesh Lochab^{2*}

¹Department of Life Sciences, School of Natural Sciences, Shiv Nadar University, Delhi, India,

²Materials Chemistry Laboratory, Department of Chemistry, School of Natural Sciences, Shiv Nadar University, Delhi, India

Glioblastoma multiforme (GBM) is known as the primary malignant and most devastating form of tumor found in the central nervous system of the adult population. The active pharmaceutical component in current chemotherapy regimens is mostly hydrophobic and poorly water-soluble, which hampers clinical implications. Nanodrug formulations using nanocarriers loaded with such drugs assisted in water dispersibility, improved cellular permeability, and drug efficacy at a low dose, thus adding to the overall practical value. Here, we successfully developed a water-dispersible and biocompatible nanocargo (GO-PEG) based on covalently modified graphene oxide (GO) with a 6-armed poly(ethylene glycol) amine dendrimer for effective loading of the two hydrophobic anticancer drug molecules, CPI444 and vatalanib. These drug molecules target adenosine receptor (A2AR), vascular endothelial growth factor receptor (VEGFR), platelet-derived growth factor receptor (PDGFR), and type III stem cell receptor tyrosine kinase (c-KIT), which plays a crucial role in cancers. The effective cellular delivery of the drugs when loaded on GO-PEG is attributed to the increased permeability of the drug-nanoconjugate formulation. We observed that this combinatorial drug treatment with nanocargo resulted in a significant reduction in the overall cell survival as supported by reduced calcium levels and stem cell markers such as Oct4 and Nanog, which are two of the prime factors for GBM stem cell proliferation. Furthermore, reduced expression of CD24 upon treatment with nanoformulation impeded cellular migration. Cellular assays confirmed inhibition of cell proliferation, migration, and angiogenic potential of GBM treated with GO-PEG-Drug conjugates. Ultimately, GBM U87 cells assumed programmed cell death at a very low concentration due to nanocarrier-mediated drug delivery along with the chosen combination of drugs.

Together, this study demonstrated the advantage of GO-PEG mediated combined delivery of CPI444 and vatalanib drugs with increased permeability, a three-pronged combinatorial strategy toward effective GBM treatment.

KEYWORDS

glioblastoma multiforme, A2A receptor, drug delivery, graphene oxide, PEGylation, CPI444, vatalanib, combination therapy

1 Introduction

Neuro-oncology is a challenging area dealing with malignancies of the brain and spinal cord. Among all the central nervous system (CNS) cancers, glioblastoma multiforme (GBM) is a rare-grade 4 glioma (1) that emerges from glial cells and is one of the most malignant and aggressive forms of brain tumor. The incidence rate of GBM is about 2–3 per 100,000 individuals every year, with a survival rate of around 15 months (2). The major challenge in treating GBM is their physical isolation by the blood–brain barrier (BBB), which restricts their accessibility to many drugs. Another important feature is the multilevel molecular and cellular heterogeneity (3). In particular, due to stem cell heterogeneity, GBM can overcome the loss of a cell type upon chemotherapy by other cell types and quickly evolve. Owing to the complex nature of GBM, a multifaceted approach by which divergent properties of GBM can be targeted with a better drug delivery system is the need of the hour.

Glioblastoma tumors exhibit abnormal vasculature that promotes tumor hypoxia, eventually leading to treatment resistance. One of the major players, vascular endothelial growth factor (VEGF), contributes to the abnormal vasculature and could be a prime target to treat GBM (4). VEGF and its signaling pathway have been most extensively explored in context with angiogenesis in tumors, including GBM (5), and have been targeted by various chemotherapeutic drugs like tivozanib, sorafenib, and others. Bevacizumab, a humanized mAb (mono clonal antibody) against VEGF, is the first and only FDA (U.S. Food and Drug Administration) approved immunotherapy for GBM. However, it has been suggested that bevacizumab increases progression-free survival but does not significantly increase the overall survival of the patients (6). Another anti-angiogenic drug, vatalanib (PTK787), is a tyrosine kinase inhibitor of all VEGF (VEGFR-1, -2, and -3) receptors, platelet-derived growth factor receptor- β (PDGFR- β), and proto-oncogene, c-kit (4, 7). This drug has been shown to be well tolerated by cancer patients (8, 9). A recent study using vatalanib in a mouse model for Alzheimer's disease (AD) has

demonstrated its capability to cross the BBB and cause reduced AD pathology (10). A previous report also indicated that vatalanib can be effective in treating gliomas (11). These studies suggest that vatalanib could be effective in targeting the characteristic angiogenic properties of GBM along with a suitable partner to tackle heterogeneous nature of GBM.

Another emerging target of various cancers is the A2A adenosine receptor (A2AR). It is a guanine nucleotide-binding protein, and a G-protein coupled adenosine receptor and acts through mitogen-activated protein kinase (MAPK) and protein kinase A (PKA), signaling converging at the cyclic adenosine monophosphate (cAMP) response element (CREB) (12). This signaling axis regulates various cellular processes such as neuronal plasticity, neuroprotection, vasodilation, and immunosuppression (13). In glial cells, purinergic signaling has been shown to be modulated by various stress factors such as hypoxia, pro-inflammatory cytokines such as tumor necrosis factor- α (TNF- α), interleukin-1 β (IL-1 β) by elevated A2A receptor (13). These dynamics in A2A receptor mediated signaling affect various cellular processes of glial cells such as proliferation, differentiation, and apoptosis (14). Among these, targeting the immunosuppressive properties of purinergic signaling has been explored as a potential cancer therapy by using various antagonists to this pathway (15–17). Moreover, due to the neuronal origin of GBM, targeting A2A receptor mediated signaling may also affect different cellular functions. Therefore, choosing the A2A receptor antagonist might prove a double-edged sword.

CPI444, an antagonist of the human A2A receptor (18), is one of the earliest drugs evaluated in cancer therapies (19, 20). This drug has shown promising antitumor activity by increasing the CD8+ (cluster of differentiation 8 positive) T-cell infiltration due to blockage of adenosine activity (20). CPI444 also exhibited 66-fold higher inhibition specificity in A2A receptor over the A1 receptor (18). A recent report indicates the promising tolerance of this drug by renal cancer patients (19). Moreover, a recent study by Corvus Pharmaceuticals, Inc. has shown a minimum of 15% of CPI444 crossing BBB (21). Therefore, CPI444 is a viable choice to targeting divergent cellular mechanisms associated with GBM.

Nanoparticles have been widely explored as a carrier in the past few decades to improve the efficacy and reduce the side effects of anticancer drugs. Graphene and functionalized graphene derivatives offer unique physico-chemical properties and are the most widely explored nanocargos to deliver payloads such as drugs, nucleotides, proteins, etc. (22, 23). Graphene assists in excellent loading of hydrophobic cancer drugs by either non-covalent or covalent interactions due to its two-dimensional planar nanoarchitecture and a very high specific area. The ease of its preparation *via* chemical oxidation of graphite, followed by exfoliation to form graphene oxide (GO) nanoflakes, resulted in well-exposed oxygen-enriched functionalities such as hydroxyl, carbonyl, carboxyl, and epoxide. These multiple surface functionalities on GO provide excellent aqueous dispersion stability and scope of derivatization to impart biocompatibility and tuning capabilities to modulate charge, size, etc., essential for the delivery of anticancer drugs. In the past, several efforts have been made to amplify biocompatibility, aqueous stability and opsonization with a prolonged blood circulation time of GO, by functionalization with poly(ethylene glycol) (PEG), FDA approved polymer (24, 25). There are several reports on using GO-PEG to deliver several cancer drug molecules such as doxorubicin, cis-platin, camptothecin, etc. However, single drug-based conventional therapeutic approaches are not successful due to the complexity of the tumors and may cause drug resistance. Usage of multiple drugs is an attractive option where each component has a specific role to play and mitigates heterogeneity associated with the tumors. Various physical properties of drugs, such as molecular size, solubility, stability, and cellular delivery, are an important aspect of combinatorial drug treatment. However, their optimal dosage reaching the tumor site is essentially important for effective cancer treatment. This demands exploration of rational design of nanocarriers which can efficiently load multiple drugs and assist cellular delivery in the desired ratio to enable synergistic interactions, if any, with improved chemotherapeutic potential. Additionally, independent studies have demonstrated that GO-based nanostructures, including GO-PEG, can cross the BBB (26, 27) and are used in drug delivery for targeting glioma (28). This property proves invaluable, especially in the treatment of GBMs where crossing the BBB is a major hurdle for many chemotherapeutic agents.

In this work, a GO-PEG nanodrug delivery system is designed, synthesized, and characterized for the combinatorial therapy of two drug molecules, CPI444 and vatalanib. The drug molecules are separately loaded on GO-PEG and then combined in an optimal ratio to form a nanoformulation. The effective ratio of the two drugs was predetermined using a carrier-free *in vitro* experiment in the GBM U87 cell line. The current combinatorial therapeutic approach may provide new avenues and directions to the forefront of several therapeutic and developmental chemotherapy regimens.

2 Materials and methods

2.1 Materials

Graphite flakes (Alfa Aesar, 99.8%, natural graphite 325 mesh), 6-arm PEG-amine (JenKem Technology, 15 kDa), sulfuric acid (H_2SO_4 , Rankem, 95%–98%), potassium permanganate (KMnO_4 , Aldrich, 99%), phosphoric acid (H_3PO_4), hydrogen peroxide (30% w/v) and potassium hydroxide (KOH, powder) from Finar Scientific, Vatalanib (cat#A3969, APExBIO), CPI444 (cat#1202402-40-1, MedChemExpress), and GBM U87 cell lines were obtained from the National Centre for Cell Sciences (NCCS) Pune. The origin of GBM U87 (or U-87 MG) is a malignant glioma from a human male patient with epithelial morphology. It is from the primary brain tumor and grade IV glioma according to the WHO classification (29). MEM (Minimum Essential Medium Eagle, Cat#AL080A) media, trypsin-EDTA solution $1 \times 0.25\%$ (Cat#TCL007), FBS (Fetal Bovine Serum, Cat#RM10681), antibiotic solution (penicillin and streptomycin), and PBS (Dulbecco's Phosphate Buffered Saline, powder pH 7.4) were purchased from HiMEDIA, India. Fluorescein isothiocyanate (FITC, Invitrogen) and CCK-8 (Cell Counting Kit-8/ Cytotoxicity assay kit) were purchased from Dojindo Molecular Technologies, USA.

2.2 Characterization

A Thermo Scientific Evolution 201 UV–visible spectrophotometer was used to measure the absorbance in a 1 cm quartz cuvette over the range of 200–800 nm. A Nicolet iS20 mid-infrared FTIR spectrometer equipped with an interferometer with KBr/Ge coated beam splitter, deuterated triglycine sulfide (DTGS) detector, and attenuated total reflectance diamond (iD5-ATR) accessory was used to measure the Fourier transform infrared (FTIR) in the range of 4,000 to 450 cm^{-1} with a resolution of 0.25 cm^{-1} . A Jobin Yvon HR800 Raman microscope was used for Raman analysis of nanomaterials at a wavelength (λ) of 514 nm. Disorder and defects in graphitic materials were measured by the ratio of the intensity of D and G bands, i.e., (I_D/I_G). Structure disorder in the graphite network raises the intensity ratio and is inversely proportional to the average sp^2 cluster size. The distance between defect points (L_D) in the GO samples was calculated from the intensities of the D (sp^2 -hybridized carbon breathing mode) and G (graphitic sp^2 -hybridized carbon) bands in the Raman spectra using the Tuinstra–Koenig relation, ($C \times \lambda = 102 \text{ nm}^2$), using Equation (1) (30).

$$L_D = \sqrt{(C \times \lambda)(I_G/I_D)} \quad (\text{Equation 1})$$

The average crystallite size (L_a) of the sp^2 domains in the synthesized GOs was determined by Equation (2),

$$L_a = (2.4 \times 10^{-10}) \lambda^4 \left(\frac{I_D}{I_G} \right)^{-1} \quad (\text{Equation 2})$$

A Rigaku Smart Lab X-ray diffractometer was used to study the powder X-ray diffraction (PXRD) of nanoparticles using $\text{Cu-K}\alpha$ radiation ($\lambda = 0.154 \text{ nm}$) over a 2θ scan range of 4° to 60° , where θ is the Bragg angle. A Mettler Toledo thermogravimetric analyzer (TGA) with a built-in gas controller (TGA2 SF/1100) and fitted with an XP1U TGA balance (ultra-micro balance) was used to study the thermodynamic properties of nanoparticles in a temperature range from 50 to 700°C in a nitrogen atmosphere at a flow rate of 50 ml min^{-1} and a heating rate of $10^\circ\text{C min}^{-1}$. The surface chemistry of nanomaterials was analyzed by X-ray photoelectron spectroscopy (XPS) (Omicron multiprobe surface analysis system) using a monochromatized $\text{AlK}\alpha$ ($1,486.7 \text{ eV}$) radiation source. A dynamic light scattering (DLS) instrument (Nanosizer, Malvern, UK) was used to measure hydrodynamic particle size and zeta potential (ζ) using an argon laser at a $\lambda = 633 \text{ nm}$, with a detector angle of 90° , at room temperature.

2.3 Preparation of graphene oxide (GO)

GO was prepared from graphite powder using a previously reported method (23). Graphite powder (1.0 g) was oxidized by a mixture of concentrated sulfuric acid and phosphoric acid ($134:15 \text{ ml, v/v}$) followed by the addition of potassium permanganate (6.0 g) at room temperature. The reaction mixture was stirred at 50°C for 12 h , and after that allowed to cool to room temperature before the slow addition of a mixture of ice-cold water: H_2O_2 ($250:3 \text{ ml}$) with vigorous stirring. A color change from dark brown to yellow is noticed. Upon gravity settling, GO particles settled down and the supernatant was decanted. The so-obtained residue was washed multiple times with water and GO as the residue was separated by centrifugation (Eppendorf 5425 R) at $11,000 \text{ rpm}$. This process was repeated until the pH of the supernatant became neutral. Finally, the brown slurry obtained was dried under vacuum on a rotary evaporator at 50°C and GO was obtained as a black powder (2.3 g).

2.4 Preparation of PEGgylated graphene oxide (GO-PEG)

An aqueous dispersion of GO (0.5 mg/ml , 20 ml) was prepared in deionized water by probe sonication for 2 min (Sonics USA, 500 W , 20 kHz) at 40% maximum amplitude and a

pulse rate of 10 s (on and off) followed by bath sonication for 2 h . To this GO dispersion, 6-armed PEG amine (60 mg) and KOH (80 mg) were added. The reaction mixture was stirred vigorously at 80°C for 24 h . Finally, GO-PEG was obtained by purifying the reaction mixture by dialysis membrane (mol. weight cut-off = 10 kDa) against deionized water for 24 h to remove the excess or unbound 6-armed PEG amine. The GO-PEG dispersion was stored at 4°C .

2.5 Preparation of CPI444@GO-PEG and vatalanib@GO-PEG

A stock solution of CPI444 (1.1 mg) was prepared in a cosolvent mixture of water and tetrahydrofuran ($1:1 \text{ v/v}$, 2 ml) and mixed with the prepared dispersion of GO-PEG (0.5 mg/ml , 2 ml). The resultant mixture was stirred vigorously at room temperature for 24 h . Excess or unbound CPI444 was removed by dialysis membrane (mol. weight cut-off = 10 kDa) against deionized water ($50 \text{ ml} \times 4$) for 24 h . Removal of excessive unbound amounts of CPI444 on GO-PEG was monitored and calculated using UV-visible spectroscopy at a maximum absorption wavelength (λ_{max}) of CPI444 at 356 nm . The so-formed CPI444@GO-PEG nanoconjugate was stored at 4°C for further study. Similarly, vatalanib@GO-PEG was also prepared following the same method. In brief, a stock solution of vatalanib (1.01 mg) was prepared in a cosolvent mixture of water and tetrahydrofuran ($1:1 \text{ v/v}$, 2 ml) and mixed with the prepared dispersion of GO-PEG (0.5 mg/ml , 2 ml) and dialyzed. For CPI444 + vatalanib@GO-PEG, optimal amounts of CPI444@GO-PEG and vatalanib@GO-PEG (with the same drug combination, $1:1$ molar ratio, as without GO-PEG) were premixed and probe sonicated for 2 min to homogenize, just prior to study.

2.6 Drug loading capacity on GO-PEG nanocarrier

To determine the loading of CPI444 on GO-PEG, UV-vis spectroscopy measurements were carried out. A standard curve of CPI444 (linear fitting with $R^2 = 0.99505$) at different concentrations was plotted at a λ_{max} of 356 nm . After the reaction completion of the CPI444@GO-PEG preparation, an unbound or excess amount of leached out CPI44 drug, during dialysis, was calculated using a standard curve and subtracted from the added amount of drug. The percentage loading and encapsulation efficacy were calculated using Equation (3) and Equation (4), respectively.

$$\text{Drug loading (\%)} = \frac{\text{Drug adsorbed on GO-PEG } (\mu\text{g})}{\text{GO-PEG added } (\mu\text{g})} \times 100 \quad (\text{Equation 3})$$

$$\text{Drug encapsulation efficacy (\%)} = \frac{\text{Drug adsorbed on GO-PEG } (\mu\text{g})}{\text{Drug added } (\mu\text{g})} \times 100$$

(Equation 4)

Similarly, the percentage loading and encapsulation efficacy of vatalanib on GO-PEG were determined using the same protocol as in the case of CPI444 on GO-PEG, by UV-vis spectroscopy. The standard curve of vatalanib (linear fitting with $R^2 = 0.99665$) at different concentrations was plotted at a λ_{max} of 335 nm.

2.7 Cell culture conditions

Glioblastoma multiforme (Human) cancer cell line GBM U87 was cultured in Minimum Essential Media (MEM) containing 10% FBS and 1% antibiotic (penicillin/streptomycin) solution in a humidified cell culture incubator (Galaxy 170R, Eppendorf) containing 5% CO₂ at 37°C.

2.8 Cell viability study

The cell viability study of pristine drugs (CPI444, vatalanib, and CPI444 + vatalanib), GO-PEG, and respective drug-GO-PEG nanoconjugates (CPI444@GO-PEG, vatalanib@GO-PEG, and CPI444 + vatalanib@GO-PEG) were assessed using the CCK-8 kit (Cat#CK04, Dojindo). The GBM U87 cells were seeded into a fresh 96-well flat-bottom plate at a density of 5,000 cells/well. After cells were attached for 18–24 h, they were treated separately with pristine drugs (2–60 μM), GO-PEG (2–20 $\mu\text{g/ml}$), and nanoconjugates (with a drug loading of 1–30 μM) at different concentrations for 48 h. After the treatment, 10 μl of CCK-8 solution was added to each well. Optical density (OD) at a λ of 450 nm was recorded on a microplate reader (BioRad). All the experiments were repeated three times independently. The relative percentage of absorbance was calculated, considering control as cent percent.

2.9 Cellular uptake of GO-PEG

GBM U87 cells were seeded in a 60 mm culture dish and treated with FITC-tagged GO-PEG with a concentration of 0 $\mu\text{g/ml}$ (untreated negative control), 5 $\mu\text{g/ml}$, 10 $\mu\text{g/ml}$, and 15 $\mu\text{g/ml}$. After 24 h, cells were harvested using trypsin. Cells were washed with 1 \times PBS twice and then resuspended in 500 μl of 1 \times PBS + 0.1% FBS solution. The cells were analyzed using a CytoFLEX flow cytometer and 10,000 events were acquired for each sample.

2.10 Fluorescent activated cell sorting (FACS) analysis

GBM U87 cells were seeded in a 60 mm dish and, after 18 h, cells were subjected to target drug formulations with appropriate controls. After 48 h of treatment, the cells were harvested and processed for FACS analysis.

2.10.1 Cellular calcium level quantitation by Fuo-4AM fluorophore

Harvested cells were incubated in 3 μM concentration of Fluo-4AM dye (cat#F14201, Life technologies) in dark at room temperature for 20 min. After incubation, cells were washed twice with 1 \times PBS and resuspended in 500 μl of 1 \times PBS solution with 0.1% FBS solution.

2.10.2 CD24 marker staining

Here, cells were washed twice with 1 \times PBS and then resuspended in a 1 \times PBS solution with 0.1% FBS. Cells were stained with CD24 mAb-FITC (cat#MHCD2401) at a concentration of 1:100 for 45 min in the dark at room temperature. Cells were collected and resuspended in 500 μl of 1 \times PBS solution with 0.1% FBS solution.

The cell suspensions were analyzed using a CytoFLEX flow cytometer and 10,000 events were acquired for each sample.

2.11 Transwell-chamber migration assay

Transwell inserts (24 well, 8 μm pore size; HiMEDIA) were used to assess the migratory abilities of cells. Pre-treated GBM U87 cells with GO-PEG, CPI444 + vatalanib, and CPI444 + vatalanib@GO-PEG along with untreated control for 48 h were used for this assay. The treated cells were suspended at a final density of 3.5×10^4 cell/ml in a serum-free medium and seeded in the upper-well of the chamber. The lower-well of the chamber contained media supplemented with 10% FBS. After 24 h, cells on the surface of the upper-well were removed by a cotton swab. Cells that had migrated through the filter to the lower chamber were fixed in 4% paraformaldehyde and stained with 1% crystal violet. Cells were counted from three randomly selected fields per each chamber under a microscope (ECLIPSE Ti, Nikon).

2.12 Cell adhesion assay

Cells were seeded in a 60 mm dish and treated with drugs as mentioned above for 48 h. Cells were harvested and re-suspended in media. Meanwhile 12-well plate coated with 50 μM poly-L-lysine (cat#P3513, Sigma) for 1 h at room temperature. Treated/untreated GBM U87 cells were harvested and suspended at a final density of 3×10^5 cells/ml and plated on poly-L-lysine-coated

plates for 30 min. After that, unattached cells were removed by inverting the 12-well plate and gently washing twice with 1× PBS. The attached cells were fixed in ice-cold methanol for 10 min at room temperature. After a wash with 1× PBS, cells were stained with 1% crystal violet stain for 5 min with gentle shaking. The plate was washed with water and kept for drying. After that, images were captured by a color camera. Later, stain was solubilized into 1 ml of 1% sodium dodecyl sulfate (SDS) for 1 h and collected in fresh 1.5 ml centrifuge tubes. Absorbance was recorded at 595 nm (Bio-Rad microplate reader) in a 96-well plate in four replicates. The absorbance value of the control sample was converted to 100% and relative percentage changes in other treatment conditions were calculated.

2.13 Invadopodia assay

GBM U87 cells were harvested and seeded in a 60 mm dish for the invadopodia experiment. The cells were treated with specific drugs and GO-PEG–drug conjugates for 48 h following the procedure mentioned above. Prepared fluorescent gelatin-coated coverslips according to the protocol (31). Briefly, GBM U87 cells were harvested and plated on coverslip in 60%–70% confluency which was already coated with gelatin labeled with oregon green 488 (cat#G13186, Life technologies). After that, the coverslip with the cells was transferred to a CO₂ incubator for 15 h for the initiation of the gelatin degradation. After 15 h of incubation, the coverslip was taken out of the plate and quickly fixed with 4% formaldehyde for 10–15 min at room temperature. The fixation solution was removed and washed with 1× PBS twice. Blocking and permeabilization were performed with a solution (3% BSA in 1× PBS containing 0.1% Triton X-100) for 15–20 min at room temperature in the dark. The blocking solution was removed and washed with 1× PBS twice. This was probed with Alexa Fluor 555 Actin-Phalloidin (1:500 dilution) for 30–40 min in the dark. Actin-Phalloidin was removed and washed with 1× PBS twice, and after that, the coverslip was mounted by inverting it over a glass slide containing a drop of mounting medium ProLongTM Gold antifade reagent with Hoechst (Invitrogen). The slides were dried and sealed with colorless nail paint. Images were taken under a Nikon Fluorescent Microscope (at ×60) for visual comparison.

2.14 Colony forming assay

To perform a 2D colony forming assay, cells were seeded in 6-well plates and then treated with various combinations of test drugs for 48 h. After 48 h, treated/untreated cells were placed in fresh 6-well plates at a cell density of 1,000 cells/well. Every third day, the media was replenished until control well-achieved confluency. The experiment was observed for up to 12 days and images were captured under a microscope (DIC imaging,

ECLIPSE Ti, Nikon). Then, cells were fixed in 4% paraformaldehyde for 10 min and stained with crystal violet stain for 10 min. After washing the plates with water slowly, cells were collected in 1% SDS and absorbance was measured at 595 nm. The relative absorbance was compared to control sample in percentages (control was treated as cent percent).

2.15 Tube formation assay and proteome array

The tube formation assay and cytokine array analysis were conducted as described previously (32). Briefly, primary endothelial cells were cultured and incubated with conditioned media of treated and untreated cells. Tube formation was analyzed after 4 h and images were captured. The number of branches and nodes was calculated manually and the same was shown as bar plots. For proteome array analysis, total cell lysate of all treated cells was collected and quantified by Bradford reagent. An equal amount of protein was loaded on each membrane for 24 h and developed as per the protocol of the manufacturer (cat#ARY010, R&D systems).

2.16 Western blot analysis

The effect of treatment of CPI444 and vatalanib@GO-PEG on apoptotic markers (proteins) was tested. Here, after 48 h of treatment with test drug formulations and appropriate controls, total cell lysate was prepared and quantified using Bradford reagent. Proteins were separated by 10% sodium dodecyl sulfate–polyacrylamide gel electrophoresis (SDS-PAGE) for 3 h. The proteins were transferred onto the polyvinylidene fluoride (PVDF) membrane after blocking blots were incubated with primary antibodies overnight at 4°C. The blots were washed and developed using appropriate horseradish peroxidase (HRP)-conjugated secondary antibodies following a standard protocol using chemiluminescent substrate (SuperSignalTM West Pico PLUS, cat#34580, ThermoFischer). The images were acquired by the FluorChem E system and densitometry was carried out by ImageJ software.

Primary antibodies: anti-PARP in Rabbit, cat#ITM3132; Anti-Bcl2 in Mouse, cat#ITT5756 and anti-β-actin in Rabbit from G-biosciences

Secondary antibodies: HRP-Goat-anti-Rabbit, cat#SE134 from G-biosciences and HRP-Goat-anti-Mouse, 554002 from BD biosciences.

2.17 Statistical analyses

The statistical analyses were performed using the GraphPad Prism Version 7.04 software. Here, the Student's two-tailed *t*-test

was performed using the mean from the minimum of three independent observed values, and respective *p*-values are reported.

3 Result and discussion

3.1 Synthesis and characterization of nanoparticles

The preparation of GO-PEG from graphite proceeds in two steps, as illustrated in Figure 1. In the first step, graphene oxide (GO) was prepared from graphite using the modified Hummer's method. This involved chemical oxidation of graphite by acidified potassium permanganate. This method provides the benefit of keeping the graphitic planes relatively intact, and oxidation occurs mainly on the edges to introduce oxo-functionalities. The fewer defect in the basal plane ensures swift binding and efficient loading of the highly aromatic drug molecules *via* π - π stacking. The oxygen-rich functionalities such as carboxyl and hydroxyl groups are necessary to improve the aqueous dispersion stability of the GO nanoparticles, while epoxide and carbonyl groups on the basal plane are desired for the covalent modification of the GO (24). In the second step, the epoxide and carbonyl groups on GO were reacted with the 6-armed PEG-amine to form PEGylated graphene oxide, GO-PEG. The reaction is favored in alkaline medium and proceeded by base mediated nucleophilic ring-opening and addition reaction. This led to the enrichment of the surface of nanoparticles with an enormous number of covalently-linked free amine groups, in addition to the existing carboxyl and hydroxyl functionalities. As a result, the subsequent increase in polar functionalities in GO-PEG occurs to offer hydrophilic properties to the prepared nanocarrier. Following the purification, both GO

and GO-PEG were characterized by various techniques. Figure 2A shows the FTIR spectra of GO and GO-PEG. The successful synthesis of GO from graphite was confirmed by the presence of oxygen-rich functionalities. The characteristic peaks at $3,400\text{ cm}^{-1}$, $1,740\text{ cm}^{-1}$, $1,590\text{ cm}^{-1}$, $1,412\text{ cm}^{-1}$ and $1,050\text{ cm}^{-1}$ are assigned to the O-H (of carboxylic group), $>\text{C}=\text{O}$ (carbonyl), C=C (aromatic, sp^2 hybridized carbon), O-H (adsorbed water) and C-O-C (epoxide ring) vibrations, respectively. The FTIR spectrum of GO-PEG is grossly dissimilar to GO, and clearly the carbonyl-related stretch is relatively vanished. Additionally, several new IR vibrations at $3,390\text{ cm}^{-1}$, $2,868\text{ cm}^{-1}$, and $1,250\text{ cm}^{-1}$ for the N-H stretching, C-H stretching, and C-H deformation vibrations, respectively, are observed. It is evident that the intensity of C-O-C stretching vibration at $1,050\text{ cm}^{-1}$ substantially increased in GO-PEG, which is due to the large number of ether linkages in the PEG structure. This demonstrated the presence of PEG-amine bound to GO in the synthesized nanocarrier.

To determine the amount of PEG-amine coating on GO, thermogravimetric analysis (TGA) was performed. From Figure 2B, GO showed mass loss in the range of 80 to 220°C associated with the evaporation of adsorbed water and thermodynamic decomposition of highly labile oxygen functionalities (33). GO revealed a residual char yield of 0% at 650°C . Unlike GO, GO-PEG is relatively more thermodynamically stable and showed an initial mass at a high temperature of $\sim 315^\circ\text{C}$, which clearly demonstrated the existence of a polymer coating on GO sheets (34). Comparison of residual char yield obtained at 650°C in GO and GO-PEG revealed a $\sim 12\%$ loading of PEG-amine on GO.

The powder X-ray diffractogram (PXRD) spectrum (Figure 2C) of GO showed the absence of graphite (002) peak at $2\theta = 26.28^\circ$ (35), but a new (001) peak at low $2\theta = 9.7^\circ$ clearly supports the successful oxidation of graphite to GO and the

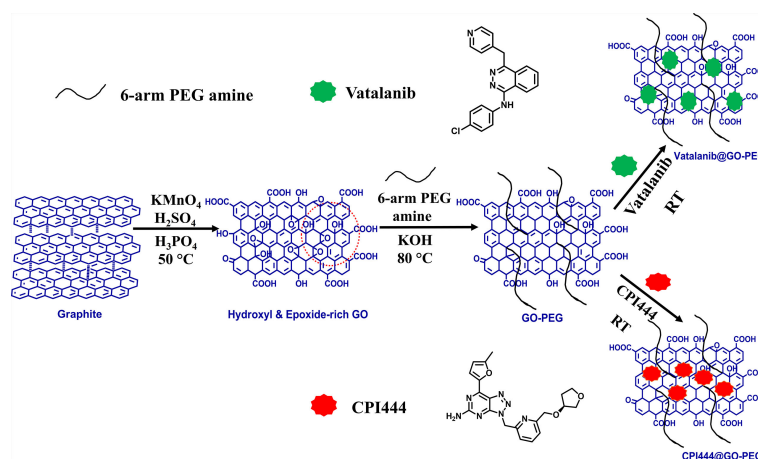


FIGURE 1

Schematic diagram for the synthesis of GO, GO-PEG, and drug loaded GO-PEG nanocarriers (CPI444@GO-PEG and vatalanib@GO-PEG).

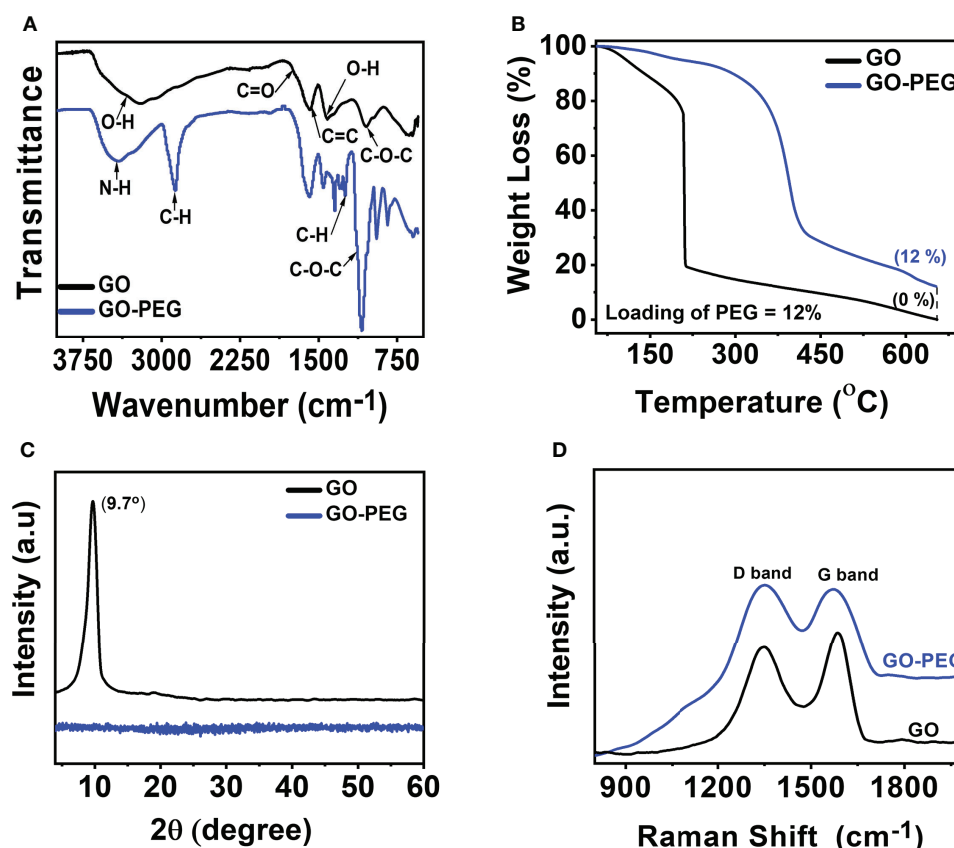


FIGURE 2
Characterization of GO and GO-PEG nanoparticles. (A) FTIR, (B) TGA, (C) PXRD, and (D) Raman spectra.

absence of graphite impurity in it. Surprisingly, no diffraction peaks are observed in GO-PEG, including the disappearance of diffraction peaks related to GO, which suggests PEG coating resulted in the formation of amorphous GO-PEG nanoparticles. The interlayer spacing of the materials is proportional to the degree of functionalization and inversely related to the observed 2θ . GO showed an interlayer spacing of 9.1 Å (>3.4 Å in graphite), calculated using Bragg's equation (36) suggesting significant oxidation occurred in graphite to form GO. GO-PEG diffractogram remained featureless, suggesting the interlayer spacing may be further enhanced due to the introduction of extra PEG-amine coating on the GO-PEG nanostructure.

The Raman spectra as shown in Figure 2D show D and G bands centered at $\sim 1,350\text{ cm}^{-1}$ and $\sim 1,590\text{ cm}^{-1}$, respectively, confirming the typical lattice distortions (37) in GO. Defects in graphitic materials can be assessed by evaluating the ratio of intensities in the D and G bands, i.e., the I_D/I_G ratio. A higher I_D/I_G (1.04) in GO-PEG than that observed in GO (0.907), along with a subsequent broadening of bands, signifies an increased defect ratio of GO upon functionalization with the dendrimer.

Interestingly, since PEGylation occurred on the pre-existing epoxide and carbonyl defects in GO, both the nanoparticles demonstrated an identical distance between defects (L_D , ~ 10 nm). GO-PEG revealed a reduced in-plane crystallite size (L_a) from 18.5 nm to 16.1 nm, supporting PEGylation induced shrinking and disruption of stacked GO domains, consistent with the PXRD studies.

The UV-vis spectra of the aqueous dispersion of the synthesized nanomaterials are shown in Figure 3A. GO revealed two distinct absorption peaks at 230 nm and 300 nm, which originated from $\pi-\pi^*$ transition of the conjugated C=C bond and the $n-\pi^*$ transition of the $>\text{C}=\text{O}$ bond, respectively (38). GO-PEG showed a red shift in the $\pi-\pi^*$ transition from 230 nm to 240 nm with an undetectable shoulder at 300 nm, confirming that PEGylation of GO led to greater retention of conjugation in its basal plane. Additionally, optical images of the aqueous dispersions (Figure 3A, inset) clearly showed an alteration in color from red-brown in GO to dark-black in GO-PEG, which further supports the formation of a more conjugated structure in the latter.

XPS analysis was performed to determine chemical functionality and confirm successful functionalization of GO

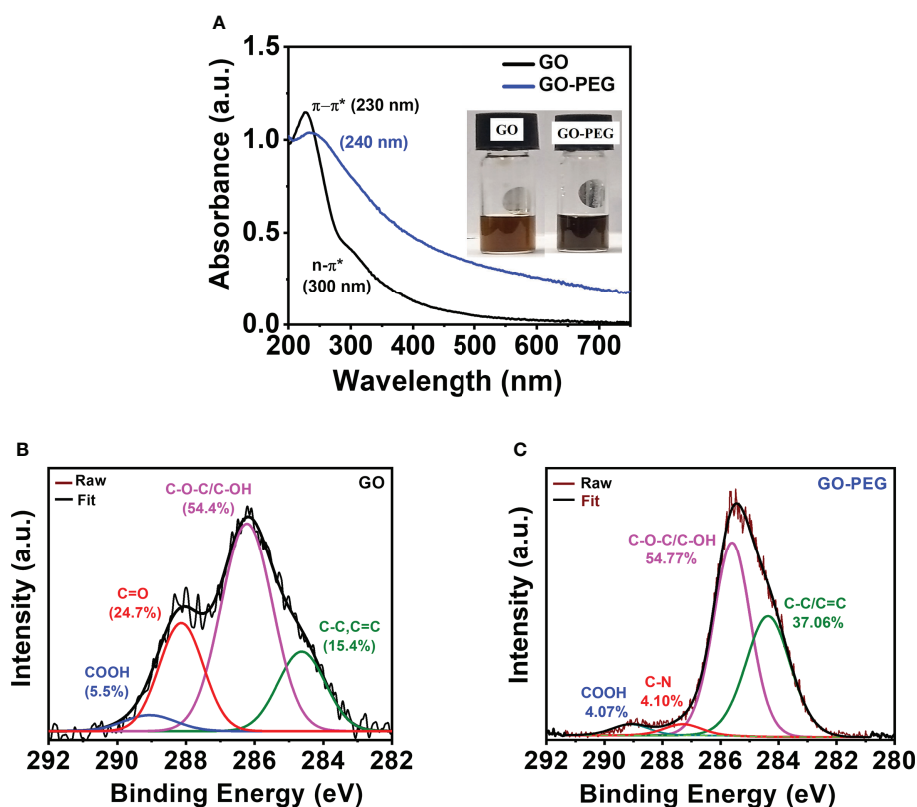


FIGURE 3
PEGylation of GO. (A, B) UV-visible spectra (inset shows digital images of the nanoparticle aqueous dispersions at a concentration of 0.5 mg/ml). XPS high-resolution deconvoluted spectra of C1s of (B) GO and (C) GO-PEG.

nanoparticles with PEG-amine. Deconvolution of the C1s XPS spectrum (Figure 3B) in GO revealed the existence of four main types of carbon bonds (binding energy) as C-C/C=C (284.5 eV), C-O/C-O-C (286.3 eV), C=O (288.1 eV) and COOH (289.0 eV) with relative percentages of 15.4%, 54.4%, 24.7%, and 5.5%, respectively. Similarly, the C1s spectra of GO-PEG were deconvoluted into four peaks (Figure 3C) as C-C/C=C (284.4 eV), C-O/C-O-C (285.7 eV), C-N (288.3 eV) and COOH (289.1 eV). Successful attachment of PEG to GO was confirmed by a simultaneous increase in the percentage of C-C/C=C to 37.06% and vanishing of $>\text{C}=\text{O}$ XPS peak, and appearance of a new peak which is attributed to the C-N (of bound PEG-amine) with a relative percentage of 4.10%. This clearly demonstrated the base-mediated nucleophilic addition reaction of PEG-NH₂ on the carbonyl groups in GO, consistent with the FTIR results.

The particle size and surface charge (zeta potential, ζ) of nanoparticles are critical parameters that dictate the interaction with the payload and may guide their cellular uptake. As can be seen in Figures 4A, C, the average hydrodynamic sizes (ζ) of GO and GP were determined as 450 nm (−49 mV) and 80 nm (−12 mV), respectively. PEG binding to GO substantially reduced the

hydrodynamic size and reduction in negative charge (ζ) due to the positively charged amino groups of PEG, which counteracted the negatively charged carboxylate group (COO[−]) in GO. This may enable GO-PEG as an attractive nanocargo for intracellular delivery. The CPI444@GO-PEG and vatalanib@GO-PEG showed a hydrodynamic sizes of 275 nm and 220 nm, respectively (Figure 4B). Drug loading on GO-PEG led to an increment in hydrodynamic size, clearly supporting the loading of hydrophobic drug molecules on GO-PEG nanoflakes. Further, a change in ζ value of GO-PEG in CPI444@GO-PEG and Vatalanib@GO-PEG showed (Figure 4D) a −21 mV and −16 mV, respectively, is noticed. Both zeta potential (ζ) and average hydrodynamic values of drug-nanoconjugates confirmed the successful loading of drug molecules on the GO-PEG nanocarrier.

3.2 Drug loading efficiency

The amount of drug loading on GO-PEG as in CPI444@GO-PEG and vatalanib@GO-PEG was determined spectrophotometrically. A standard curve was plotted by recording absorbance at a respective wavelength maximum

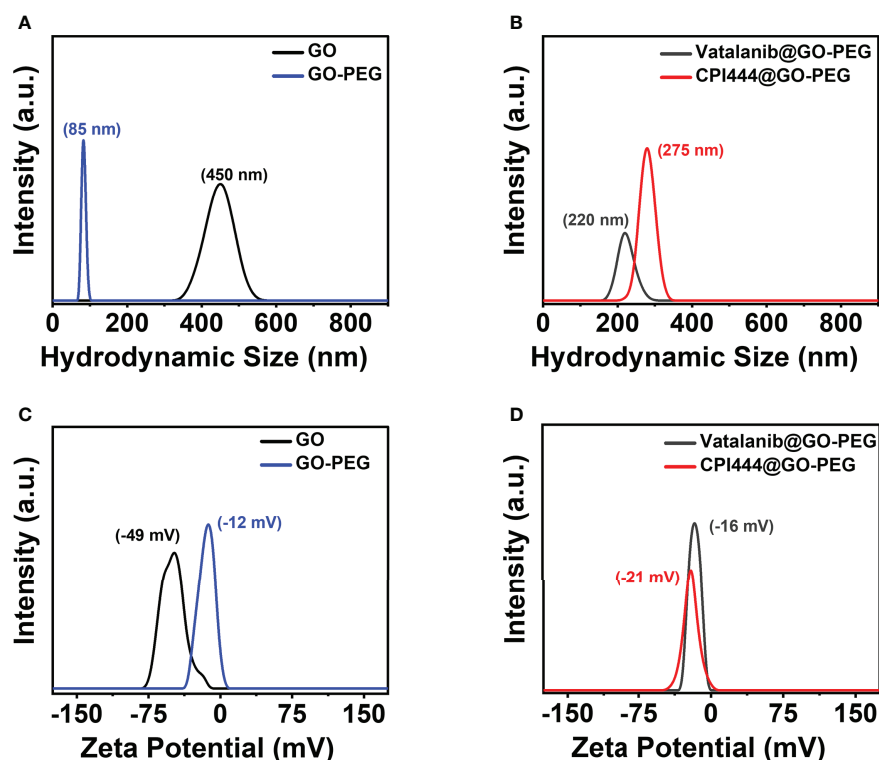


FIGURE 4
Dynamic Light Scattering measurements. (A, B) Hydrodynamic size, and (C, D) Zeta potential of GO, GO-PEG, vatalanib@GO-PEG and CPI444@GO-PEG, respectively.

using variable drug (CPI444, $\lambda_{\text{max}} = 356$ nm and vatalanib, $\lambda_{\text{max}} = 335$ nm) concentrations, and a linear good fit (Figures 5A, B, Figures S1A, B) was obtained. The unbound drug was removed by dialysis on the carrier and purification was monitored by UV-vis spectroscopy. As can be seen from Figure 5C, a subsequent decrease in absorbance at 356 nm in the dialysate is noticed to support leaching out of the loosely bound CPI444 on GO-PEG. The fourth washing showed the absence of any released CPI444, confirming the successful formation of a stable CPI444@GO-PEG conjugate. The CPI444 loading capacity and encapsulation efficacy were calculated as 55 wt% and 50 wt%, respectively. Figure 5D shows UV-vis spectra for GO and CPI444@GO-PEG, qualitatively confirming the loading of CPI444 onto the GO-PEG nanocarrier as it revealed the shoulder at 356 nm associated with bound CPI444 on GO-PEG. Likewise, the amount and existence of vatalanib on the GO-PEG nanocarrier was also determined. As can be seen in Figure S1, for vatalanib, the dialysate revealed almost no release of the unbound drug, supporting its excellent adsorption on the GO-PEG nanocarrier. Structurally, vatalanib has a highly rigid aromatic framework compared to CPI444, which ensures relatively strong van der Waals interactions of the former with the carrier.

3.3 Improved cellular uptake of CPI444 and vatalanib via PEGylated graphene oxide nanocarrier resulting in enhanced cell death

The highly evasive nature of glioblastoma (GBM) is mainly due to the heterogeneity of the cellular and molecular players (3). This demands exploration of combinatorial nanotherapeutic approaches, i.e., utility of two or more drug molecules on a carrier to enhance high cellular uptake of drug and to induce pronounced effects in their specific roles to target different cellular mechanisms.

CPI444 is an adenosine A_{2A} receptor antagonist emerging as a potential antitumor drug (20, 39, 40). Vatalanib is another potential drug that targets VEGFR tyrosine kinase and other class III kinases (41) and plays a significant role in targeting angiogenesis in GBMs (4). CPI444 and vatalanib have different molecular targets, enabling them to be suitable for GBM treatment. A nanocarrier, GO-PEG, was used to deliver both CPI444 and vatalanib drug molecules for better outcomes. Initially, a cell viability study was performed to assess the cytotoxic effects of CPI444, vatalanib, CPI444 + vatalanib, GO-PEG, and CPI444 + vatalanib@GO-PEG at different concentrations than individual drug molecules (Figures 6A–C).

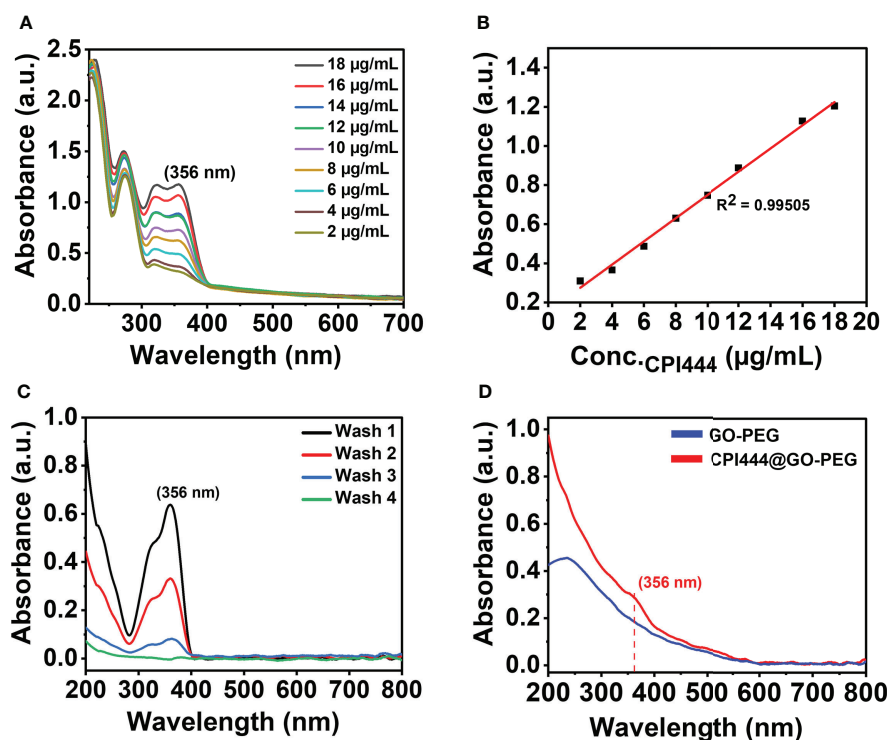


FIGURE 5

Quantitative and qualitative analysis for the formation of CPI44@GO-PEG using UV-vis spectroscopy: (A) UV-vis spectra of CPI444 solution recorded at different concentrations in (water: THF) solvent mixture, (B) Linear equation obtained from the standard curve at a wavelength maximum of 356 nm, (C) UV-vis spectra recorded for unbound CPI444, (D) UV-vis spectra for GO-PEG and purified CPI444@GO-PEG.

The inhibitory concentration (IC_{50}) values of CPI444, vatalanib, and in combination were determined as 48, 33, and 26 μM , respectively (Figure 6A). The combination of CPI444 and vatalanib exhibited a drastic effect on cell survival at a relatively lower concentration than individual drug molecules. Further, the biocompatibility of the designed GO-PEG over GO was evaluated. It clearly revealed PEGylation substantially improved the cell viability up to 20 $\mu g/ml$, supporting it as a safe carrier (Figure 6B). Finally, an IC_{50} value for the drug loaded GO-PEG (CPI444 + vatalanib@GO-PEG) was determined as 14 μM (Figure 6C). Drug molecules loaded with GO-PEG induced an elevated cytotoxic effect compared to the individual drug molecules or their combination. This assay suggests that the GO-PEG nanocarrier improves therapeutic efficacy without raising dosage. Additionally, the cellular uptake of GO-PEG nanoparticles in GBM U87 cells was calculated through flow cytometry (Figure 6D, Figure S2). To perform this experiment, GO-PEG was tagged with FITC and incubated with the cells for 24 h in different concentrations (5 $\mu g/ml$, 10 $\mu g/ml$, and 15 $\mu g/ml$). Here, a concentration-dependent cellular uptake of GO-PEG-FITC was observed. Previously, GO-PEG has been shown to exhibit a minimal effect on cell viability in the range of $\sim 50 \mu g/ml$ (42). This novel formulation of nanocarrier (GO-PEG) with CPI444 and vatalanib facilitated increased cellular

uptake, thus allowing the effective reduction of inhibitory concentrations affecting cell viability. This will reduce significant side effects due to overdosage.

3.4 CPI444 and vatalanib loaded GO-PEG affect the proliferation and stemness properties of GBM U87 cells

Glioblastoma multiforme (GBM) is a type of high-grade primary brain cancer that comprises a subpopulation called glioblastoma stem cells (GSC), which are responsible for tumor initiation, development, and recurrence following treatment (3). Calcium (Ca^{2+}) is a secondary messenger that plays a vital role in cell proliferation, cell death, differentiation, migration, metabolism, neural plasticity, and gene transcription, among other processes (43, 44). Calcium signaling is reported to have a significant impact on neuronal cell development and function (45). Glioblastoma is of neuronal origin, and therefore, calcium pathways are active in controlling and promoting various cellular functions (46). Therefore, intracellular calcium (Ca^{2+}) levels were assessed in GBM U87 cells upon treatment with CPI444 and vatalanib-loaded PEGylated graphene oxide nanoparticles. Here, a

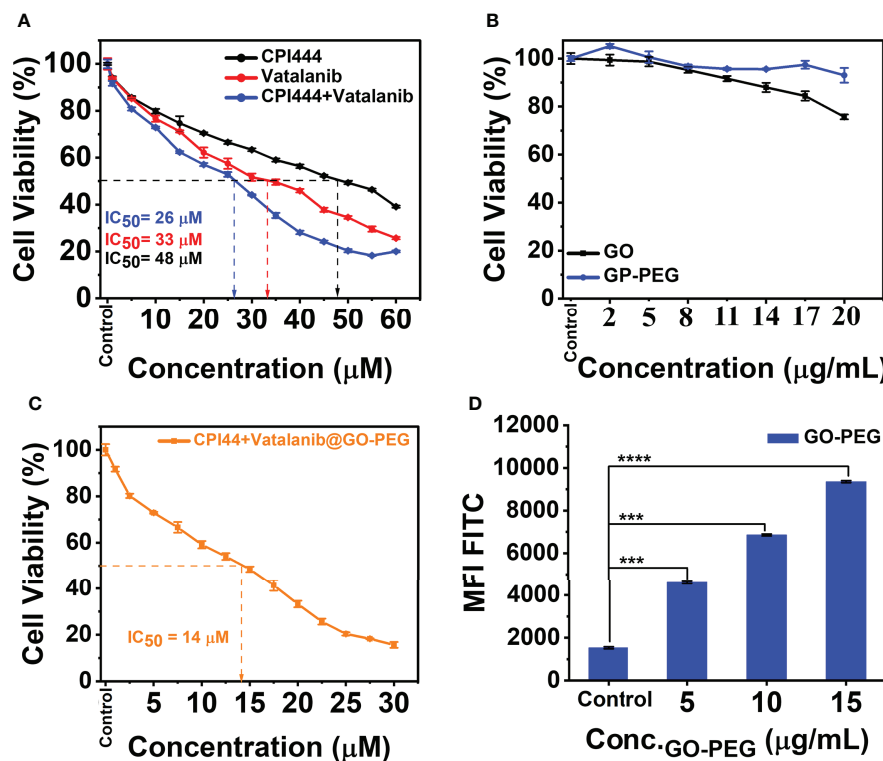


FIGURE 6

Cell viability studies and cellular uptake of PEGylated graphene oxide. (A) CPI444 and vatalanib cell cytotoxicity were calculated in GBM U87 cells. Cells were treated with drugs individually along with different concentrations for 48 h. After 48 h, IC_{50} values were calculated. (B) Cytotoxicity analyses of GO and GO-PEG were performed in GBM U87 cells. The PEGylated graphene oxide carrier did not show significant cytotoxicity in the GBM cell line up to 20 $\mu\text{g}/\text{mL}$. (C) In the GBM U87 cell line IC_{50} value of CPI444 + vatalanib@GO-PEG is $\sim 14 \mu\text{M}$. (D) To confirm the cellular internalization of PEGylated GO nanoparticles in the GBM cells, we conducted a FACS study after 24 h of incubation with different concentrations of PEGylated graphene oxide nanoparticles; MFI (Mean Fluorescence Intensity) in arbitrary units (AU); **** $p < 0.0001$ and *** $p < 0.001$.

significant reduction in Ca^{2+} levels was observed in CPI444 + vatalanib and CPI444 + vatalanib@GO-PEG treated cells compared to untreated or cells treated with either of the drugs individually (Figure 7A, Figure S3). A 2D colony forming assay was performed to identify the role of reduced intracellular calcium (Ca^{2+}) in the inhibition of GBM stem cell properties. A combination of nanoconjugated CPI444 and vatalanib reduced the colony formation in GBM U87 cells (Figures 7B, C). This indicates that reduced cellular calcium levels affect the proliferation ability of glioblastoma stem cells (GSCs). A human pluripotent stem cell array analysis was performed under similar treatment conditions to further investigate the molecular targets that are affected. Here, markers for pluripotency such as Oct3/4, Nanog, and Sox2 exhibit significant downregulation upon treatment with CPI444 and vatalanib loaded on GO-PEG (Figure 7D). Additionally, markers associated with the epithelial to mesenchymal transition (EMT), such as Snail and Goosecoid (Gsc), as well as other markers for differentiation to other cell lineages exhibited downregulation (Figure 7D). This suggests that the GSCs are not undergoing differentiation into assume other cell fates.

These observations suggest that combinatorial treatment of CPI444 with vatalanib with the aid of GO-PEG is effective in reducing the cellular calcium pool of GBM U87 cells. This is a very promising observation as Ca^{2+} levels play a critical role not only in GSC proliferation and in glial cell function that helps in the survival and fate determination process (44, 47).

3.5 GBM U87 cells migration and invasive potential is compromised by combinatorial treatment of CPI444 and vatalanib loaded on GO-PEG

Glioblastoma multiforme is an aggressive tumor that has an aggressive migratory property and invades the microenvironment and adjacent brain tissue. CD24, a motility and invasion marker, was overexpressed in gliomas, particularly in GBM (48–50). Therefore, to assess the effect of CPI444 and vatalanib loaded GO-PEG on CD24 expression in GBM U87 by

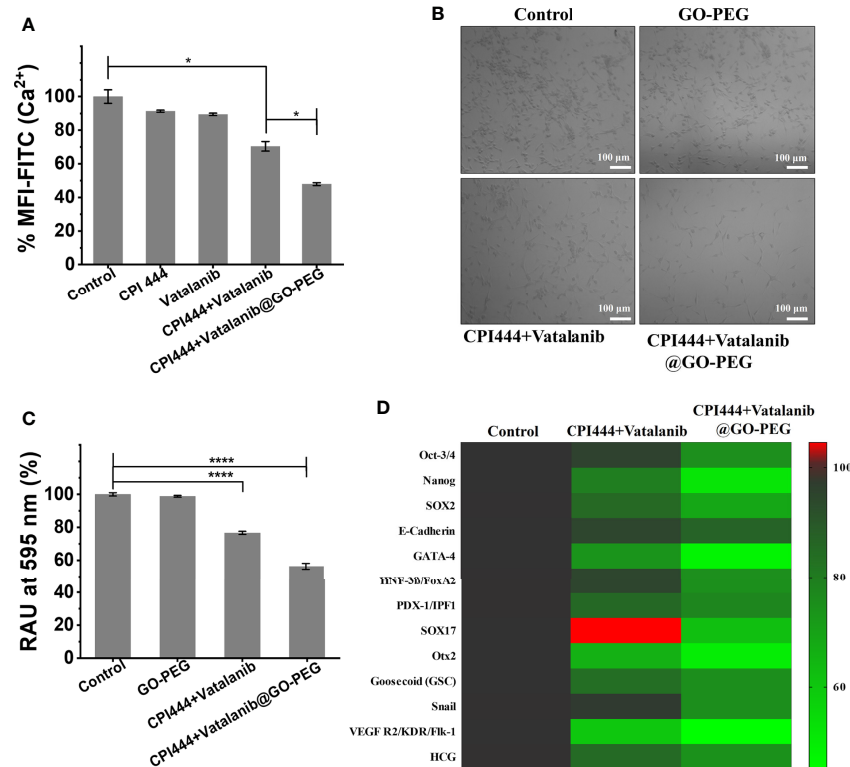


FIGURE 7

CPI444 and vatalanib-loaded GO-PEG affect the proliferation and stemness properties of GBM U87 cells. (A) Cellular calcium levels were estimated by FACS analysis using Fluo-4AM dye under different drug treatment conditions. (B) Colony forming assay of GBM U87 treated with untreated control, GO-PEG, CPI444 + vatalanib and CPI444 and vatalanib conjugated with GO-PEG. (C) Quantitation of colony forming assay, %RAU, relative absorbance units in percentage. (D) Heatmap depicting the expression levels of human pluripotent stem cell protein array for pluripotency and differentiation markers upon treatment with CPI444 and vatalanib loaded on GO-PEG with appropriate controls. MFI (Mean Fluorescence Intensity) in arbitrary units (AU); **** $p < 0.0001$ and * $p < 0.05$.

FACS analysis is therefore necessary. A significant reduction in the CD24 expression was observed (Figure 8A, Figure S4). Further, the migration abilities of GBM U87 cells under similar treatment conditions were estimated by the Boyden chamber assay. Here, a drastic reduction in the cell numbers that have migrated to the Boyden chamber was observed (Figures 8B, C). Cell motility is linked to adhesive properties; an important reason for the decreased migration is the attenuation of adhesion. Therefore, we assessed the adhesive property of GBM U87 cells upon treatment with the CPI444 + vatalanib@GO-PEG along with the comparable controls and observed reduced cellular adhesion compared to the control conditions (Figure 8D). Finally, gelatin degradation assay was performed after treatment with CPI444 + vatalanib@GO-PEG, CPI444 + vatalanib, and compared with the untreated cells as a control. A visible reduction in the dark patches formed by invadopodia during cell migration in nanoparticles mediated drug-treated cells was evident (Figure 8E). This clearly demonstrates a profound impairment in the cellular migration of GBM U87 cells.

In the previous section, a drastic reduction in the cellular Ca^{2+} levels was observed upon treatment with CPI444 + vatalanib@GO-PEG. There are ever-growing studies suggesting the role of calcium-mediated signaling in cell migration during development and in cancer metastasis (51, 52). Previous reports have also shown that CD24 plays a critical role in the invasive properties of cancer/tumor cells (48, 50). Therefore, we hypothesize that the observed reduction in expression of CD24, along with the non-invasive phenotype of GBM U87, upon treatment with CPI444 and vatalanib *via* GO-PEG, could be due to reduced Ca^{2+} levels.

3.6 Treatment with CPI444, vatalanib, and CPI444 +vatalanib@GO-PEG caused reduced secretion of angiogenic factors and apoptosis of GBM U87 cells

The glioblastoma tumor microenvironment exhibits characteristic vascularization mediated by various growth

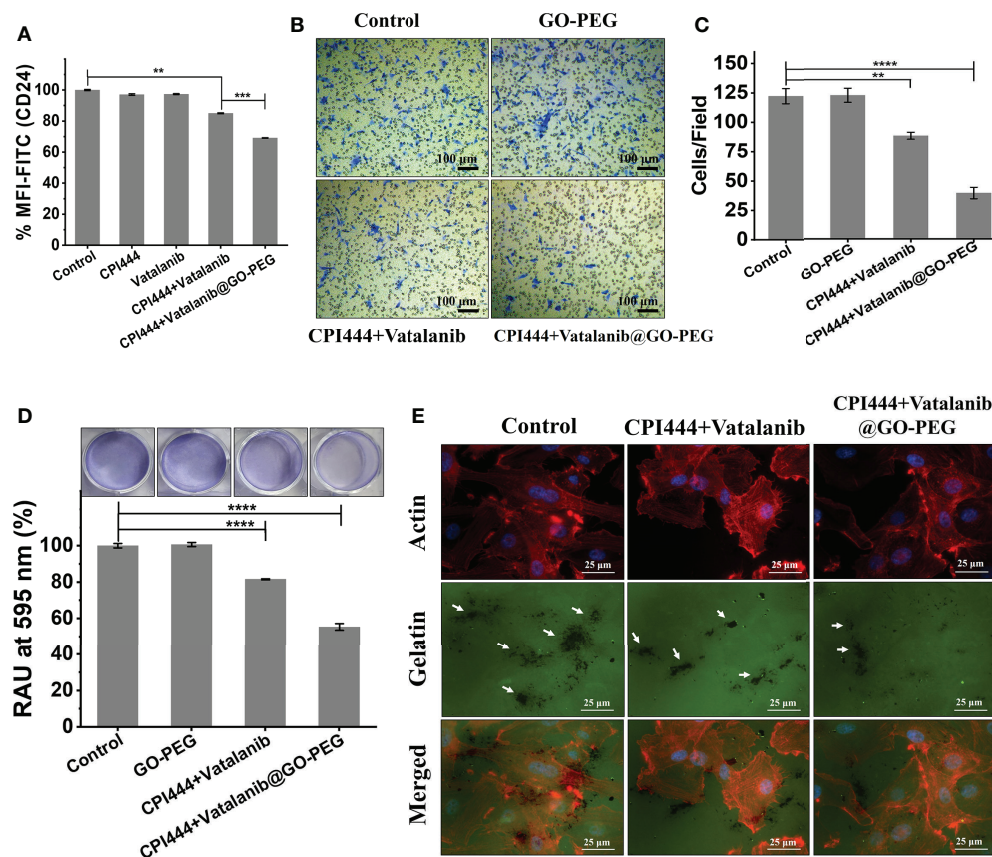


FIGURE 8

CPI444 and vatalanib@GO-PEG hindered the cellular migration and invasive behavior of GBM U87 cells. (A) CD24 expression levels in GBM U87, quantitated by FACS analysis after treatment with CPI444 and vatalanib-loaded GO-PEG and other combinations. (B, C) Boyden chamber analysis (Transwell migration assay) was performed for cell migration properties. The combination of nanoconjugate CPI444 and vatalanib-treated cells shows smaller numbers of migrated cells compared to control. (D) The adhesive property of GBM cells was significantly reduced after the treatment with the GO-PEG conjugated combination of CPI444 and vatalanib. RAU%, Relative absorbance units in percentage. (E) Invadopodia causing dark gelatin degradation patches (indicated by white arrows) were detected by the gelatin degradation assay under different treatment conditions. **** $p < 0.0001$, *** $p < 0.001$, and ** $p < 0.01$.

factors and conditions. GBM U87 cells secrete particular growth factors that cause neo-angiogenesis in pre-existing capillaries (49). We analyzed the effect of CPI444 and vatalanib loaded GO-PEG on the angiogenic potential of GBM U87. The essential developmental molecules for tube formation are found in the tissue culture media (TCM) of GBM U87 cells. The TCM of treated and untreated GBM U87 cells was collected and provided to the primary endothelial cells for tube formation. The TCM of control cells revealed a rich and progressive vasculature and showed a larger number of branches and nodes compared to the treated cells (Figures 9A–C). Previous reports have shown that vatalanib exhibits anti-angiogenic properties in multiple cancers, including tumors (53, 54). Purinergic signaling has also been shown to help in tumor neovascularization by inducing the secretion of VEGF into the tumor microenvironment (55, 56). Therefore, a combinatorial treatment with GO-PEG mediated high cellularity proves to be

very effective in the inhibition of angiogenic signals from GBM U87 cells. The observed morphology also explains why VEGF2R was downregulated upon treatment with CPI444 + vatalanib@GO-PEG (Figure 7D).

So far, in this study, multiple assays have indicated that the loss of stemness properties leads to reduced proliferation capacity upon CPI444 + vatalanib@GO-PEG treatment. At the same time, GBM U87 cells were also not differentiated into any specialized cell types (Figures 7D, 9A–C). This indicates that the cells might be exhibiting arrested growth or undergoing programmed cell death. To understand this, the expression of apoptotic markers such as the proteolytic cleavage product of poly (ADP-Ribose) polymerase (PARP) and B-cell lymphoma 2 (Bcl2) was scored (Figures 9D–F). Here, upregulated cleaved PARP and downregulation of Bcl2 clearly demonstrate that combinatorial treatment with improved cellular uptake results in apoptosis of GBM U87 cells.

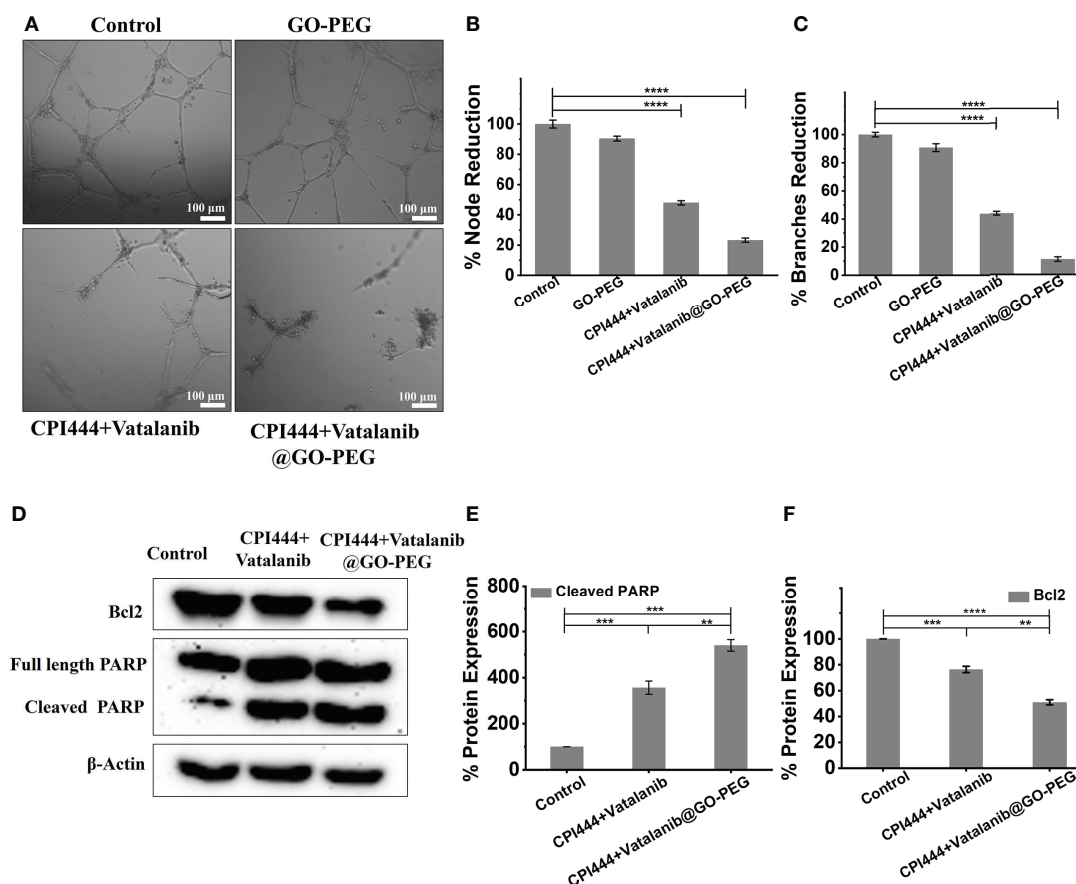


FIGURE 9

Treatment of CPI444 and vatalanib-loaded GO-PEG inhibits the angiogenic potential and causes apoptosis of GBM U87. (A–C) A tube formation assay was performed for angiogenesis analysis in GBM cells. GBM U87 cells showed a smaller number of nodes and branches compared to control cells. (D–F) Western blot analysis of Bcl2, intact PARP, cleaved PARP. β-actin was used as an internal control. The Western blot shown is a representative of three independent experiments. **** $p < 0.0001$, *** $p < 0.001$, and ** $p < 0.01$.

4 Conclusion

In this study, a nanocarrier GO-PEG was synthesized and characterized. PEGylation of graphene oxide resulted in a significant reduction in hydrodynamic size, and zeta potential, which facilitated a high cellular uptake of GO-PEG. Additionally, PEGylation of graphene oxide led to reduced cytotoxicity. This nanocarrier was used to deliver potential therapeutic drug molecules, CPI444 and vatalanib, to target GBM U87 cells derived from glioblastoma multiforme. These drugs were mainly selected to target divergent cellular mechanisms as GBM exhibits molecular and cellular heterogeneity to its advantage. This study clearly demonstrates that the stem cell properties of GBM U87 were severely affected by custom-designed nanoformulation. Additionally, the treatment with CPI444 and vatalanib *via* GO-PEG led to a drastic reduction in the metastatic ability of GBM U87 cells. The

current work has proven the importance of the novel formulation under study in the effective reduction of the angiogenic potential of GBM. Ultimately, this nanosized CPI444 and vatalanib caused elevated apoptosis, which will lead to a reduced tumor size. This nanoparticle-based combinatorial therapy approach enhances the efficacy of the existing therapeutic drugs by targeting the key molecular players at very low concentrations. This property will provide a huge advantage in tackling drug resistance exhibited by tumors and avoiding off-target effects due to overdosage.

Data availability statement

The original contributions presented in the study are included in the article/[Supplementary Material](#). Further inquiries can be directed to the corresponding authors.

Author contributions

BL conceived the concept and designed the chemical structures. PR designed the biological assays. SP performed the chemical synthesis, and characterization of nanoparticles. VM performed the biological assays. BL and PR interpreted the data. VM and SP made equal contributions. All authors listed have made a substantial, direct, and intellectual contribution to the work and approved it for publication.

Funding

BL and PR are thankful for the financial support received from the Shiv Nadar Foundation. PR is also supported by the Early Career Fellowship of the Wellcome Trust-DBT India Alliance (IA/E/16/1/503057).

Acknowledgments

VM and SP acknowledge the fellowship received from Shiv Nadar University. The authors thank Dr. Seema Sehrawat for the initial discussion. The authors would like to thank Dr. Sri

Krishna Jayadev Magani (SNU, Delhi-NCR) for his kind gift of PARP and Bcl2 antibodies.

Conflict of interest

The authors declare that the research was conducted in the absence of any commercial or financial relationships that could be construed as a potential conflict of interest.

Publisher's note

All claims expressed in this article are solely those of the authors and do not necessarily represent those of their affiliated organizations, or those of the publisher, the editors and the reviewers. Any product that may be evaluated in this article, or claim that may be made by its manufacturer, is not guaranteed or endorsed by the publisher.

Supplementary material

The Supplementary Material for this article can be found online at: <https://www.frontiersin.org/articles/10.3389/fonc.2022.953098/full#supplementary-material>

References

- Louis DN, Ohgaki H, Wiestler OD, Cavenee WK, Burger PC, Jouvet A, et al. The 2007 WHO classification of tumours of the central nervous system. *Acta Neuropathol* (2007) 114(2):97–109. doi: 10.1007/s00401-007-0243-4
- Pearson JR, Regad T. Targeting cellular pathways in glioblastoma multiforme. *Signal Transduct Target Ther* (2017) 2(1):1–11. doi: 10.1038/sigtrans.2017.40
- Lauko A, Lo A, Ahluwalia MS, Lathia JD. Cancer cell heterogeneity & plasticity in glioblastoma and brain tumors. *Semin Cancer Biol* (2022) 82:162–75. doi: 10.1016/j.semcancer.2021.02.014
- Gerstner ER, Eichler AF, Plotkin SR, Drappatz J, Doyle CL, Xu L, et al. Phase I trial with biomarker studies of vatalanib (PTK787) in patients with newly diagnosed glioblastoma treated with enzyme inducing anti-epileptic drugs and standard radiation and temozolomide. *J Neurooncol* (2011) 103(2):325–32. doi: 10.1007/s11060-010-0390-7
- Xu C, Wu X, Zhu J. VEGF promotes proliferation of human glioblastoma multiforme stem-like cells through VEGF receptor 2. *Sci World J* (2013). doi: 10.1155/2013/417413
- Gramatzki D, Roth P, Rushing E, Weller J, Andrasschke N, Hofer S, et al. Bevacizumab may improve quality of life, but not overall survival in glioblastoma: An epidemiological study. *Ann Oncol* (2018) 29(6):1431–6. doi: 10.1093/annonc/mdy106
- Shankar A, Borin TF, Iskander A, Varma NR, Achyut BR, Jain M, et al. Combination of vatalanib and a 20-HETE synthesis inhibitor results in decreased tumor growth in an animal model of human glioma. *Onco Targets Ther* (2016) 9:1205. doi: 10.2147/OTT.S93790
- Dragovich T, Laheru D, Dayyani F, Bolejack V, Smith L, Seng J, et al. Phase II trial of vatalanib in patients with advanced or metastatic pancreatic adenocarcinoma after first-line gemcitabine therapy (PCRT O4-001). *Cancer Chemother Pharmacol* (2014) 74(2):379–87. doi: 10.1007/s00280-014-2499-4
- Jost LM, Gschwind H-P, Jalava T, Wang Y, Guenther C, Souppart C, et al. Metabolism and disposition of vatalanib (PTK787/ZK-222584) in cancer patients. *Drug Metab Dispos* (2006) 34(11):1817–28. doi: 10.1124/dmd.106.009944
- Jeon SG, Lee H-J, Park H, Han K-M, Hoe H-S. The VEGF inhibitor vatalanib regulates AD pathology in 5xFAD mice. *Mol Brain* (2020) 13(1):131. doi: 10.1186/s13041-020-00673-7
- Goldbrunner RH, Bendszus M, Wood J, Kiderlen M, Sasaki M, Tonn JC. PTK787/ZK222584, an inhibitor of vascular endothelial growth factor receptor tyrosine kinases, decreases glioma growth and vascularization. *Neurosurgery* (2004) 55(2):426–32. doi: 10.1227/01.neu.0000129551.64651.74
- Jacobson KA, Gao Z-G. Adenosine receptors as therapeutic targets. *Nat Rev Drug Discovery* (2006) 5(3):247–64. doi: 10.1038/nrd1983
- Fredholm BB, IJzerman AP, Jacobson KA, Linden J, Müller CE. International union of basic and clinical pharmacology. LXXXI. nomenclature and classification of adenosine receptors—an update. *Pharmacol Rev* (2011) 63(1):1–34. doi: 10.1124/pr.110.003285
- Lecca D, Ceruti S, Fumagalli M, Abbracchio MP. Purinergic trophic signalling in glial cells: Functional effects and modulation of cell proliferation, differentiation, and death. *Purinergic Signal* (2012) 8(3):539–57. doi: 10.1007/s11302-012-9310-y
- Willingham SB, Hotson AN, Miller RA. Targeting the A2AR in cancer: early lessons from the clinic. *Curr Opin Pharmacol* (2020) 53:126–33. doi: 10.1016/j.coph.2020.08.003
- Ohta A, Sitkovsky M. Role of G-Protein-Coupled adenosine receptors in downregulation of inflammation and protection from tissue damage. *Nature* (2001) 414(6866):916–20. doi: 10.1038/414916a
- Ohta A, Gorelik E, Prasad SJ, Ronchese F, Lukashev D, Wong MK, et al. A2A adenosine receptor protects tumors from antitumor T cells. *Proc Natl Acad Sci* (2006) 103(35):13132–7. doi: 10.1073/pnas.0605251103
- Gillespie RJ, Cliffe IA, Dawson CE, Dourish CT, Gaur S, Jordan AM, et al. Antagonists of the human adenosine A2A receptor. part 3: Design and synthesis of pyrazolo [3, 4-d] pyrimidines, pyrrolo [2, 3-d] pyrimidines and 6-aryl purines. *Bioorg Med Chem Lett* (2008) 18(9):2924–9. doi: 10.1016/j.bmcl.2008.03.072

19. Fong L, Hotson A, Powderly JD, Szol M, Heist RS, Choueiri TK, et al. Adenosine 2A receptor blockade as an immunotherapy for treatment-refractory renal cell cancer. *Cancer Discovery* (2020) 10(1):40–53. doi: 10.1158/2159-8290.CD-19-0980
20. Willingham SB, Ho PY, Hotson A, Hill C, Piccione EC, Hsieh J, et al. A2AR antagonism with CPI-444 induces antitumor responses and augments efficacy to anti-PD-(L) 1 and anti-CTLA-4 in preclinical models. *Cancer Immunol Res* (2018) 6(10):1136–49. doi: 10.1158/2326-6066.CIR-18-0056
21. Available at: <https://www.sec.gov/Archives/edgar/data/1626971/000104746917001459/a2231221z10-k.htm> (Accessed 02 July 2022).
22. Torchilin VP. Multifunctional, stimuli-sensitive nanoparticulate systems for drug delivery. *Nat Rev Drug Discovery* (2014) 13(11):813–27. doi: 10.1038/nrd4333
23. Yadav N, Kumar N, Prasad P, Shirbhate S, Sehrawat S, Lochab B. Stable dispersions of covalently tethered polymer improved graphene oxide nanoconjugates as an effective vector for siRNA delivery. *ACS Appl Mat Interfaces* (2018) 10(17):14577–93. doi: 10.1021/acsami.8b03477
24. Liu Z, Robinson JT, Sun X, Dai H. PEGylated nanographene oxide for delivery of water-insoluble cancer drugs. *J Am Chem Soc* (2008) 130(33):10876–7. doi: 10.1021/ja803688x
25. Li Y, Zhang T, Liu Q, He J. PEG-derivatized dual-functional nanomicelles for improved cancer therapy. *Front Pharmacol* (2019) 10:808. doi: 10.3389/fphar.2019.00808
26. Tabish TA, Narayan RJ. Crossing the blood–brain barrier with graphene nanostructures. *Mat Today* (2021) 51:393–401. doi: 10.1016/j.mattod.2021.08.013
27. Syama S, Paul W, Sabareeswaran A, Mohanan PV. Raman spectroscopy for the detection of organ distribution and clearance of PEGylated reduced graphene oxide and biological consequences. *Biomaterials* (2017) 131:121–30. doi: 10.1016/j.biomaterials.2017.03.043
28. Liu G, Shen H, Mao J, Zhang L, Jiang Z, Sun T, et al. Transferrin modified graphene oxide for glioma-targeted drug delivery: *In vitro* and *in vivo* evaluations. *ACS Appl Mat Interfaces* (2013) 5(15):6909–14. doi: 10.1021/am402128s
29. Louis DN, Perry A, Wesseling P, Brat DJ, Cree IA, Figarella-Branger D, et al. The 2021 WHO classification of tumors of the central nervous system: A summary. *Neuro Oncol* (2021) 23(8):1231–51. doi: 10.1093/neuonc/noab106
30. Cançado L, Takai K, Enoki T, Endo M, Kim Y, Mizusaki H, et al. General equation for the determination of the crystallite size l_a of nanographite by raman spectroscopy. *Appl Phys Lett* (2006) 88(16):163106. doi: 10.1063/1.2196057
31. Diaz B. Invadopodia detection and gelatin degradation assay. *Bio-protocol* (2013) 3(24):e997. doi: 10.21769/BioProtoc.997
32. Kumar N, Prasad P, Jash E, Jayasundar S, Singh I, Alam N, et al. cAMP regulated EPAC1 supports microvascular density, angiogenic and metastatic properties in a model of triple negative breast cancer. *Carcinogenesis* (2018) 39(10):1245–53. doi: 10.1093/carcin/bgy090
33. Chua CK, Pumera M. Monothiolation and reduction of graphene oxide *via* one-pot synthesis: Hybrid catalyst for oxygen reduction. *ACS Nano* (2015) 9(4):4193–9. doi: 10.1021/acs.nano.5b00438
34. Fang M, Wang K, Lu H, Yang Y, Nutt S. Covalent polymer functionalization of graphene nanosheets and mechanical properties of composites. *J Mat Chem* (2009) 19(38):7098–105. doi: 10.1039/b908220d
35. Yadav N, Lochab B. A comparative study of graphene oxide: Hummers, Intermediate and Improved method. *FlatChem* (2019) 13:40–9. doi: 10.1016/j.flatc.2019.02.001
36. Marcano DC, Kosynkin DV, Berlin JM, Sinitskii A, Sun Z, Slesarev A, et al. Improved synthesis of graphene oxide. *ACS Nano* (2010) 4(8):4806–14. doi: 10.1021/nn1006368
37. Kabiri S, Tran DN, Azari S, Losic D. Graphene-diatom silica aerogels for efficient removal of mercury ions from water. *ACS Appl Mat Interfaces* (2015) 7(22):11815–23. doi: 10.1021/acsami.5b01159
38. Chen J, Li Y, Huang L, Li C, Shi G. High-yield preparation of graphene oxide from small graphite flakes *via* an improved Hummers method with a simple purification process. *Carbon* (2015) 81:826–34. doi: 10.1016/j.carbon.2014.10.033
39. Yu F, Zhu C, Xie Q, Wang Y. Adenosine A2A receptor antagonists for cancer immunotherapy: Miniperspective. *J Med Chem* (2020) 63(21):12196–212. doi: 10.1021/acs.jmedchem.0c00237
40. Merighi S, Battistello E, Giacomelli L, Varani K, Vincenzi F, Borea PA, et al. Targeting A3 and A2A adenosine receptors in the fight against cancer. *Expert Opin Ther Targets* (2019) 23(8):669–78. doi: 10.1080/14728222.2019.1630380
41. Wood JM, Bold G, Buchdunger E, Cozens R, Ferrari S, Frei J, et al. PTK787/ZK 222584, a novel and potent inhibitor of vascular endothelial growth factor receptor tyrosine kinases, impairs vascular endothelial growth factor-induced responses and tumor growth after oral administration. *Cancer Res* (2000) 60(8):2178–89.
42. Peruzynska M, Cendrowski K, Barylak M, Tkacz M, Piotrowska K, Kurzawski M, et al. Comparative *in vitro* study of single and four layer graphene oxide nanoflakes–cytotoxicity and cellular uptake. *Toxicol In Vitro* (2017) 41:205–13. doi: 10.1016/j.tiv.2017.03.005
43. Berridge MJ, Bootman MD, Roderick HL. Calcium signalling: Dynamics, homeostasis and remodelling. *Nat Rev Mol Cell Biol* (2003) 4(7):517–29. doi: 10.1038/nrm1155
44. Terrié E, Déliot N, Benzidane Y, Harnois T, Cousin L, Bois P, et al. Store-operated calcium channels control proliferation and self-renewal of cancer stem cells from glioblastoma. *Cancers (Basel)* (2021) 13(14):3428. doi: 10.3390/cancers13143428
45. Rosenberg SS, Spitzer NC. Calcium signaling in neuronal development. *Cold Spring Harb Perspect Biol* (2011) 3(10):a004259. doi: 10.1101/cshperspect.a004259
46. Maklad A, Sharma A, Azimi I. Calcium signaling in brain cancers: Roles and therapeutic targeting. *Cancers (Basel)* (2019) 11(2):145. doi: 10.3390/cancers11020145
47. Leclerc C, Haeich J, Aulestia FJ, Kilhoffer M-C, Miller AL, Neant I, et al. Calcium signaling orchestrates glioblastoma development: Facts and conjunctures. *Biochim Biophys Acta Mol Cell Res* (2016) 1863(6):1447–59. doi: 10.1016/j.bbamcr.2016.01.018
48. Tiburcio PD, Locke MC, Bhaskara S, Chandrasekharan MB, Huang LE. The neural stem-cell marker CD24 is specifically upregulated in idh-mutant glioma. *Transl Oncol* (2020) 13(10):100819. doi: 10.1016/j.tranon.2020.100819
49. Mishra VS, Kumar N, Raza M, Sehrawat S. Amalgamation of PI3K and EZH2 blockade synergistically regulates invasion and angiogenesis: Combination therapy for glioblastoma multiforme. *Oncotarget* (2020) 11(51):4754. doi: 10.18632/oncotarget.27842
50. Deng J, Gao G, Wang L, Wang T, Yu J, Zhao Z. CD24 expression as a marker for predicting clinical outcome in human gliomas. *J BioMed Biotechnol* (2012) 517172. doi: 10.1155/2012/517172
51. Tsai F-C, Kuo G-H, Chang S-W, Tsai P-J. Ca^{2+} signaling in cytoskeletal reorganization, cell migration, and cancer metastasis. *BioMed Res Int* (2015):409245. doi: 10.1155/2015/409245
52. Davis FM, Azimi I, Faville RA, Peters AA, Jalink K, Putney J, et al. Induction of epithelial–mesenchymal transition (EMT) in breast cancer cells is calcium signal dependent. *Oncogene* (2014) 33(18):2307–16. doi: 10.1038/ncr.2013.187
53. Scott EN, Meinhardt G, Jacques C, Laurent D, Thomas AL. Vatalanib: The clinical development of a tyrosine kinase inhibitor of angiogenesis in solid tumours. *Expert Opin Investig Drugs* (2007) 16(3):367–79. doi: 10.1517/13543784.16.3.367
54. Paesler J, Gehrke I, Razavi R, Gandhirajan RK, Filipovich A, Hertweck M, et al. Selective targeting of vascular endothelial growth factor (VEGF) receptor signaling with pazopanib and vatalanib induces apoptosis in chronic lymphocytic leukemia (CLL) cells *in vitro* inhibits growth of human CLL like tumor xenografts in mice. *Blood* (2009) 114(22):3451. doi: 10.1182/blood.V114.22.3451.3451
55. Montesinos MC, Desai A, Chen J-F, Yee H, Schwarzschild MA, Fink JS, et al. Adenosine promotes wound healing and mediates angiogenesis in response to tissue injury *via* occupancy of A2A receptors. *Am J Pathol* (2002) 160(6):2009–18. doi: 10.1016/S0002-9440(10)61151-0
56. Luttj G, Mathews MK, Merges C, McLeod D. Adenosine stimulates canine retinal microvascular endothelial cell migration and tube formation. *Curr Eye Res* (1998) 17(6):594–607. doi: 10.1080/02713689808951232



Diallyl Disulfide: A Bioactive Garlic Compound with Anticancer Potential

Saikat Mitra^{1†}, Rajib Das^{1†}, Talha Bin Emran^{2,3*}, Rafiuddin Khan Labib¹, Noor-E-Tabassum¹, Fahadul Islam³, Rohit Sharma⁴, Islamudin Ahmad⁵, Firzan Nainu⁶, Kumarappan Chidambaram⁷, Fahad A. Alhumaydhi⁸, Deepak Chandran⁹, Raffaele Capasso^{10*} and Polrat Wilairatana^{11*}

¹Department of Pharmacy, Faculty of Pharmacy, University of Dhaka, Dhaka, Bangladesh, ²Department of Pharmacy, BGC Trust University Bangladesh, Chittagong, Bangladesh, ³Department of Pharmacy, Faculty of Allied Health Sciences, Daffodil International University, Dhaka, Bangladesh, ⁴Department of Rasa Shastra and Bhaishajya Kalpana, Faculty of Ayurveda, Institute of Medical Sciences, Banaras Hindu University, Varanasi, India, ⁵Department of Pharmaceutical Sciences, Faculty of Pharmacy, Mulawarman University, Samarinda, Indonesia, ⁶Department of Pharmacy, Faculty of Pharmacy, Hasanuddin University, Makassar, Indonesia, ⁷Department of Pharmacology and Toxicology, College of Pharmacy, King Khalid University, Abha, Saudi Arabia, ⁸Department of Medical Laboratories, College of Applied Medical Sciences, Qassim University, Buraydah, Saudi Arabia, ⁹Department of Veterinary Sciences and Animal Husbandry, Amrita School of Agricultural Sciences, Amrita Vishwa Vidyapeetham University, Coimbatore, India, ¹⁰Department of Agricultural Sciences, University of Naples Federico II, Naples, Italy, ¹¹Department of Clinical Tropical Medicine, Faculty of Tropical Medicine, Mahidol University, Bangkok, Thailand

OPEN ACCESS

Edited by:

Sandeep Singh,
Central University of Punjab, India

Reviewed by:

Yosra Bouraoui,
Jendouba University, Tunisia
Marina Gorbunova,
Institute of Technical Chemistry (RAS),
Russia
Qi Su,
University of South China, China

*Correspondence:

Talha Bin Emran
talhabmb@bgctub.ac.bd
Raffaele Capasso
rafcapas@unina.it
Polrat Wilairatana
polrat.wil@mahidol.ac.th

[†]These authors have contributed
equally to this work

Specialty section:

This article was submitted to
Pharmacology of Anti-Cancer Drugs,
a section of the journal
Frontiers in Pharmacology

Received: 14 May 2022

Accepted: 21 June 2022

Published: 22 August 2022

Citation:

Mitra S, Das R, Emran TB, Labib RK,
Noor-E-Tabassum, Islam F,
Sharma R, Ahmad I, Nainu F,
Chidambaram K, Alhumaydhi FA,
Chandran D, Capasso R and
Wilairatana P (2022) Diallyl Disulfide: A
Bioactive Garlic Compound with
Anticancer Potential.
Front. Pharmacol. 13:943967.
doi: 10.3389/fphar.2022.943967

Cancer is a life-threatening disease caused by the uncontrolled division of cells, which culminates in a solid mass of cells known as a tumor or liquid cancer. It is the leading cause of mortality worldwide, and the number of cancer patients has been increasing at an alarming rate, with an estimated 20 million cases expected by 2030. Thus, the use of complementary or alternative therapeutic techniques that can help prevent cancer has been the subject of increased attention. Garlic, the most widely used plant medicinal product, exhibits a wide spectrum of biological activities, including antibacterial, hypolipidemic, antithrombotic, and anticancer effects. Diallyl disulfide (DADS) is a major organosulfur compound contained within garlic. Recently, several experimental studies have demonstrated that DADS exhibits anti-tumor activity against many types of tumor cells, including gynecological cancers (cervical cancer, ovarian cancer), hematological cancers (leukemia, lymphoma), lung cancer, neural cancer, skin cancer, prostate cancer, gastrointestinal tract and associated cancers (esophageal cancer, gastric cancer, colorectal cancer), hepatocellular cancer cell line, etc. The mechanisms behind the anticancer action of DADS include epithelial-mesenchymal transition (EMT), invasion, and migration. This article aims to review the available information regarding the anti-cancer potential of DADS, as well as summarize its mechanisms of action, bioavailability, and pharmacokinetics from published clinical and toxicity studies.

Keywords: oncology, garlic, diallyl disulfide, clinical, pre-clinical, Pharmacology, drug discovery

1 INTRODUCTION

Cancer is a severely detrimental health condition that is experienced by people across the world. The number of cancer-afflicted patients is rising rapidly and is estimated to be around 20 million by 2030 (Nussbaumer et al., 2011; Munari et al., 2014; Siegel et al., 2016; Society, 2016). Unbridled cellular growth leads to the modification of internal cellular or tissue materials as well as genetic instabilities,

converting normal, healthy cells into malignant ones (Feller et al., 2013; Rauf et al., 2021). These genetic instabilities include mutations in the oncogenes, tumor suppressors, DNA repairing genes, and genes involved in the metabolism of cell growth (Dixon and Kopras, 2004). Cancer has several internal (hormonal abnormalities, genetic mutations, and the immune system) and external (smoking, cigarettes, drinking polluted water, food, radiation, chemicals, heavy metals, air, and infectious agents) causes (Bigby, 1988; Zhou et al., 2017; Mitra et al., 2022a). Thus, the discovery and development of phytochemical compounds that can be used as promising drugs for carcinoma treatment purposes have become a strong priority for researchers (Mitra et al., 2022e; Rahman et al., 2022).

Current therapeutic strategies for cancer treatment include surgery, radiotherapy, and chemotherapy, among others. However, patients undergoing these cancer preventative therapies experience intense stress; potentially leading to damaging, long-term health issues (Haberkorn, 2007; Moding et al., 2013; Mitra et al., 2022d). Several studies have shown that many medicinal plant species can be used to prevent or cure cancer (Mitra et al., 2021, 2022c; Islam et al., 2022). Anticancer effects have been observed in many plant species, especially in plants that have been utilized in traditional herbal treatments used in developing countries (Greenwell and Rahman, 2015). It is estimated that dietary modifications could prevent nearly one-third of current cancer cases (Brennan et al., 2010; Rastegari and Rafieian-Kopaei, 2016; Rauf et al., 2022).

Garlic, the most widely used plant in medicinal products, has several pharmacological properties, such as antibacterial, hypolipidemic, antithrombotic, and anticancer effects (Lai et al., 2013; Mikaili et al., 2013). Garlic oil is soluble in both oil and water, and it has long been considered to be both a dietary supplement and an anticancer agent (Omar and Al-Wabel, 2010). Experimental animal studies have shown that specific sulfur-containing compounds can chemically suppress carcinogenesis in different organs (Kim et al., 2014). Diallyl disulfide (DADS), a compound composed of two allyl groups connected by two sulfur atoms, is a vital organosulfur compound found in garlic (De Greef et al., 2021; He et al., 2021; Song et al., 2021). DADS is produced during the decomposition of alliin, and there have been many detailed studies regarding its medicinal applications (Liang et al., 2015). DADS, diallyl tetrasulfide, and diallyl trisulfide are the key elements of distilled garlic oil. DADS is a yellow liquid that has a distinct garlic odor and is not soluble in water. Allicin is released when garlic or other plants belonging to the family Alliaceae are crushed; DADS is produced during the decomposition of alliin. DADS can easily be oxidized to allicin in the presence of peracetic acid or hydrogen peroxide. Similarly, allicin hydrolyses to produce diallyl trisulfide and DADS. When DADS reacts with liquid sulfur, it produces diallyl polysulfide mixtures that can create unbroken sulfur chains up to 22 atoms in length (Yi and Su, 2013).

An increasing number of studies have found that DADS exhibits anticancer activity against several kinds of tumor cells, including gastric cancer, breast cancer, and colon cancer cell lines (Altonsy et al., 2012; Tang et al., 2013; Xiao et al., 2014). Specifically, the underlying mechanism behind the anticancer

action of DADS involves inducing apoptosis, activating metabolizing enzymes that detoxify carcinogens, inhibiting the production of reactive oxygen species, suppressing DNA adduct formation, and regulating cell cycle arrest. DADS can also suppress the metastatic potential of tumors such as EMT, invasion, and migration (Tsubura et al., 2012).

The purpose of this review is to evaluate the existing information on the potential of the anticancer activities exhibited by DADS as well as its mechanism of action, while also summarizing toxicity and pharmacokinetic studies conducted on this substance.

2 IN VITRO AND IN VIVO PRECLINICAL STUDIES

2.1 Breast Cancer

DADS has been successfully shown to intrinsically induce the apoptosis pathway in breast cancer (Fulda and Debatin, 2006; Lei et al., 2008; Lee et al., 2011b; Williams et al., 2018). The apoptosis pathway is regulated by several complex molecules that affect the production of distinct antiapoptotic and proapoptotic proteins. The upregulation of activating caspase occurs during mitochondria-mediated apoptosis, which is regulated by the proteins of the Bcl-2 family. Proapoptotic molecules (Bax, Bim, and Bad) co-exist with a variety of antiapoptotic proteins in the Bcl-2 protein family but can improve the expression of antiapoptotic proteins. Bcl-2 proteins prevent the permeabilization of the outer mitochondrial membrane and suppress apoptosis (Elmore, 2007; Tait and Green, 2010; Elumalai et al., 2012; Marie Hardwick and Soane, 2013; Redza-Dutordoir and Averill-Bates, 2016). In comparison to DADS, DADS-SLN resulted in the increased expression of the proapoptotic proteins Bad, Bax, caspase-3, and caspase-9, while also reducing the expression of antiapoptotic proteins, including Bcl-2. This shows that DADS-SLN causes apoptosis *via* intrinsic signaling (Talluri et al., 2017).

The percentages of late and early apoptosis in the control samples were 0.8% and 0.7%, respectively; this was considerably lower than the 55.6% and 3.3% exhibited by DADS-SLN. These values were also considerably larger than that of the blank SLN (0.9% and 1.4%) and DADS (12.42% and 2.61%), indicating that DADS-SLN enhanced apoptosis after medicating for 24 h at a concentration of 8 μ M. The greater proportion of apoptotic cells in DADS-SLN compared to DADS suggests that the former has a much larger impact on apoptosis. Blank-SLNs appeared to have very little effect on the MCF-7 cells in terms of apoptosis; this minor cytotoxicity may be related to excipients. Thus, the nano-encapsulation of DADS might improve its anticancer impact, which is mostly associated with the increased induction of apoptosis (Talluri et al., 2017). In another trial, the late and early apoptosis cells in a control sample accounted for 0.9% and 0.6% of the cells, respectively. The study showed that DADS-RAGE-SLN improved the apoptotic activity of DADS in MDA-MB231 cells (Siddhartha et al., 2018).

Altonsy et al. (2012) found that DADS causes apoptosis in MCF-7 breast cancer cell lines by interfering with cell-cycle

development stages such that the sub-G₀ population increases and the synthesis of DNA are slowed significantly. In addition, DADS activates caspase-3 by inducing phosphatidylserine translocation from the inner to the outer leaflet of the plasma membrane. Additional research found that DADS regulates Bcl-w, Bcl-xL, Bcl-2, and Bax levels in cells in a dose-dependent manner, suggesting that the Bcl-2 proteins are involved in the apoptosis induced by DADS. Histone deacetylation inhibitors (HDACi) have been shown to reduce cancer cell growth and cause apoptosis. In the context of MCF-7 cells, DADS possesses HDACi characteristics because it prevents the loss of an acetyl group from the acetylated substrate and causes histone-4 (H4) hyperacetylation. Thus, the HDACi characteristics of DADS may be responsible for the activation of apoptosis in breast cancer cells (Altonsy et al., 2012). Another experiment found that miR-34a expression was upregulated in MDA-MB-231 cells that were treated with DADS. miR-34a suppressed breast cancer development both *in vitro* and *in vivo* while also enhancing the antitumor effectiveness of DADS. Specifically, miR-34a inhibits the expression of SRC, which results in the suppression of the Ras/SRC/ERK pathway. miR-34a can also be considered to be an effective agent for gene therapy procedures as it boosts the antitumor activity of DADS (Xiao et al., 2014).

DADS was used to pretreat (PreTx) MCF-10A cells in the presence of the carcinogen benzo(a)pyrene (BaP). MCF-10A cells were also co-treated (CoTx) with BaP and DADS for up to 24 h to evaluate the inhibitory influence of DADS on early carcinogenic events. The cells were monitored for any changes in the cell cycle, DNA damage, cell proliferation and viability, and the induction of peroxide formation. BaP tended to significantly increase cell proliferation at 6 h; DADS CoTx suppressed this phenomenon. Within 24 h, DADS prevented BaP-induced extracellular aqueous peroxide production; this behavior was independent of concentration or technique. Throughout DADS CoTx and PreTx, with notable suppression for every treatment sustaining after 6 h, DADS suppressed the single-strand break in DNA induced by BaP at all times. In normal cell lines, DADS was effective at inhibiting BaP-induced cell cycle transitions, cell proliferation, DNA damage, and the production of reactive oxygen species; thus, DADS may also suppress the environmentally-induced initiation of breast cancer (Nkrumah-Elie et al., 2012). The role of DADS, as well as the mechanisms behind its influence on breast cancer stem cells (BCSCs), were explored in a separate study. The findings showed that DADS reduced glucose metabolism and cell stemness in BCSCs. DADS also reduced the metastasis and the growth of BCSCs *in vivo* investigations by targeting the pyruvate kinase M2 (PKM2), CD44, and AMPK signaling pathways in BCSCs. An IHC analysis found that the expression levels of AMPK, CD44, and PKM2 were positively correlated in the tissues of 125 breast cancer patients. Furthermore, the positive expression of PKM2, AMPK, and CD44 was linked to poor overall survival and disease-free survival in patients (Xie et al., 2018). Furthermore, DADS caused the downregulation of MMP-9, the dysregulation of Bcl-2 family members, and the reversal of the epithelial-mesenchymal transition (EMT). Remarkably, DADS also suppressed the activation of the β -catenin signaling pathway,

which is associated with the regulation of the Bcl-2 family, EMT, and MMP-9 in TNBC cells. The effectiveness of the anticancer properties of DADS was confirmed in MDA-MB-231 xenograft mice, which was consistent with the *in vitro* findings. Treating these mice with DADS appreciably lowered tumor weight and volume while raising apoptosis; in addition, active β -catenin expression levels were reduced and the downstream molecules underwent dysregulation (**Table 1**) (Huang et al., 2015).

Bauer et al. (2014) demonstrated the anticancer properties by showing a prominent expression profile for the sustained release of IL-8, IL-6, plasminogen activator inhibitor-1, and TIMP1/2 in untreated/resting MDA-MB-231 cells using an initial chemokine/adipokine protein panel microarray. TNF- α (40 ng/ml) did not affect most of these molecules, except for a single large increase in CCL2 release (an approximately 1,300-fold upregulation). A sub-lethal dose of DADS (100 μ M) inhibited and reversed the release of TNF- α -induced CCL2 (Bauer et al., 2014).

2.2 Gastrointestinal Tract and Associated Cancers

2.2.1 Esophageal Cancer

EC is the sixth most frequently occurring cancer. It has a terrible prognosis worldwide and affects about 450,000 people. At one point, squamous cell carcinoma accounted for around 90% of EC cases, although epidemiology has seen a shift in various western nations (Epidemiologic differences in esophageal cancer between Asian and Western populations; Kamangar et al., 2009; Sadjadi et al., 2010; Yang et al., 2020). The occurrence of esophageal adenocarcinoma (EAC) has been gradually increasing over the last 30 years, and currently outnumbers squamous cell cases (Dabrowski et al., 1998; Comprehensive and Network, 2014). One study showed that DADS halted cancerous cells in the G2/M phase by modulating proteins that were related to the cell cycle; this modulation was linked to a decrease in the production of cyclin B1, cdc25c, cdc2, and p-cdc2. Furthermore, DADS regulated cellular apoptosis by upregulating the ratio of Bax to Bcl-2, activating caspase-3, and downregulating the MEK-ERK signaling pathway. The activation of the p53/p21 pathway involves the suppression of the G2/M phase, the induction of apoptosis, and the inhibition of cell differentiation. Hence, DADS controlled esophageal squamous cell carcinoma (ESCC) cells *via* many signaling pathways and was revealed to be a prospective anticancer therapy for ESCC (Yin et al., 2014b).

Feng et al. (2017) investigated the chemopreventive effectiveness of DADS against Barrett's esophagus (BE) as well as any potentially linked signaling pathways by treating BAR-T cells with deoxycholic acid (DCA) in the absence or presence of DADS. DADS was not observed to decrease cell viability for a given range of concentrations. Like PDTC, an NF- κ B inhibitor, DADS suppressed the ROS production induced by DCA, I κ B α phosphorylation, inflammation, and the production of p50 in the nucleus in a dose-dependent manner. By lowering the amount of Bcl-2, DADS also boosted the rate of cell apoptosis. DADS had a minimal cytotoxic effect on BAR-T cells. DADS exhibited an anti-inflammatory effect against BAR-T cells through the NF- κ B signaling pathway and ROS inhibition. Furthermore, DADS

TABLE 1 | Possible antineoplastic properties of DADS as well as their underlying mechanisms as established by *in vitro* research.

Cell lines	Duration and conc.	Anticancer properties	Mechanism of action	References
Breast cancer				
MCF-7	8 μ M (24 h)	Induced apoptosis	\uparrow caspase-3, \uparrow Bax, \uparrow caspase-9, \uparrow Bad, \downarrow Bcl-2	Talluri et al. (2017)
MDA-MB231	5 μ M (24 h)	Increased apoptosis	\uparrow caspase-9, \downarrow Bcl2 and surviving, \uparrow ROS	Siddhartha et al. (2018)
Breast cancer stem cells (BCSCs)		Inhibited cell proliferation	\downarrow glucose metabolism, \downarrow metastasis, \downarrow CD44, \downarrow PKM2, \downarrow AMPK	Xie et al. (2018)
MDA-MB-468, MDA-MB-231, and BT-549	50–400 μ M (48 h)	Induced apoptosis	\downarrow Bcl-2, \downarrow β -catenin signaling pathway, \downarrow MMP-9	Huang et al. (2015)
MCF7	0–100 μ M	Induced apoptosis	\uparrow sub-G0 population, \downarrow DNA synthesis, \uparrow phosphatidylserine translocation, \uparrow caspase-3, \uparrow Bax, \uparrow Bcl-xL, \uparrow Bcl-2, \uparrow Bcl-w, \downarrow Histone deacetylation (HDACi), \uparrow histone-4 (H4) Hyper-acetylation	Altonsy et al. (2012)
MDA-MB-231, MCF-10A	0–400 μ M (48 h)	Inhibited proliferation of cells	\uparrow miR-34a, \downarrow SRC/Ras/ERK pathway, \downarrow SRC	Xiao et al. (2014)
MDA-MB-231	50–1,200 μ M (24 h)	Inhibited cell growth	\downarrow TNF- α -induced release of CCL2 from triple-negative human breast tumor (MDA-MB-231) cells	Bauer et al. (2014)
MDA-MB-468	46.85–1,500.0 μ M (24, 48 h)	Inhibited cell growth	\uparrow caspase-3, \uparrow apoptosis, \uparrow NQO1, \uparrow SOD, \uparrow GSH	Sujatha et al. (2017)
MCF-7	100–400 μ M (24 h)	Inhibited invasion and metastasis of cells	\downarrow Vimentin, \downarrow MMP-9, \uparrow E-cadherin, \downarrow p38	Chen et al. (2016)
MDA-MB-231	100 μ M (24 h)	Inhibited cell growth	\uparrow NF- κ B mRNA, \downarrow p38, \downarrow MEK, \downarrow TNF- α invoked CCL2 production, \downarrow IKK ϵ , \downarrow MAPK/ERK, \downarrow NF- κ B pathway signaling	Bauer et al. (2015)
MDA-MB-231	40 μ M (24 h)	Inhibited cell proliferation	Not reported	Wei et al. (2017)
CMT-13	Less or equal 1,000 μ M (72 h)	Suppressed cell growth	\downarrow cell cycle G2/M phase	Tsubura et al. (2012)
MCF-7	7.62 mg	Induced apoptosis	\downarrow mitochondrial membrane potential, \uparrow mitochondrial depolarization, \uparrow Caspase-3, \uparrow procaspase-3	An et al. (2015)
MCF-10A	6, 60, and 600 μ M 24 h	Induced apoptosis	\downarrow BaP-induced G2/M arrest, \uparrow extracellular aqueous peroxide, \downarrow BaP-induced DNA single-strand breaks, \downarrow reactive oxygen species	Nkrumah-Elie et al. (2012)
Esophageal cancer				
ECA109, LQ2	20, 40, 60 μ g/ml (24 h)	Induced G2/M arrest and promoted apoptosis	\downarrow cyclin B1, \downarrow cdc2, \downarrow p-cdc2, \downarrow cdc25c, \uparrow p53, \uparrow p21	Yin et al. (2014b)
BAR-T	0–30 μ g/ml (24, 48, and 72 h)	Abolished apoptotic resistance	\downarrow NF- κ B, \downarrow ROS, \downarrow I κ B α phosphorylation, \downarrow p50, \downarrow Bcl-2	Feng et al. (2017)
ECA109	0, 20 and 40 μ g/ml (24 h)	Induced apoptosis	\downarrow PCNA, \downarrow RAF/MEK/ERK, \uparrow caspase-3, \uparrow p53, \uparrow Bax/Bcl-2 ratio	Yin et al. (2014a)
CE81T/VGH	50 μ M (24 h)	Caused DNA damage	\downarrow NAT1 mRNA, \downarrow protein levels of NAT	Yu et al. (2005)
Gastric cancer				
MGC803	30 mg/L (12, 24, 36 and 48 h)	Cell cycle arrest and apoptosis	\uparrow phospho-Chk1 protein, \uparrow phospho-ATR expression	Ling et al. (2014)
AGS	0, 50, 100, 200, and 400 μ M (48 h)	Induced apoptosis	\downarrow percentage of live AGS cells and sub-diploid DNA content, \downarrow Bcl-2, \uparrow Annexin V positive/PI negative area, \uparrow ROS production, \uparrow expressions of Fas, caspase-3, \uparrow Bax	Lee et al. (2011a)
OE19	\leq 10 μ g/ml (24-h)	Inhibited metastasis	\downarrow MMPs, \downarrow NF- κ B, and PI3K signaling pathways, \uparrow u-PA, \uparrow TIMPs	Yin et al. (2018)
AGS	100 mM (6 h)	Inhibited tumor cell motility and invasion	\downarrow MMP-2 and -9 mRNA and proteins, \uparrow TIMP-1 and -2 mRNA levels and proteins	Park et al. (2011)
BGC-823, MGC-803, MKN-28, HGC-27, SGC-7901, and AGS	100 μ M (48 h)	Suppressed proliferation and induced apoptosis	\uparrow miR-200b, \uparrow miR-22	Tang et al. (2013)
MGC803	30 mg/L (12, 24, and 48 h)	Inhibited cell migration and invasion	\downarrow p-LIMK1, \downarrow p-cofilin1, \downarrow Rac1-Pak1/Rock1-LIMK1 pathway, \downarrow EMT, \downarrow MMP-9, \uparrow TIMP-3	Bo et al. (2016)
MGC-803	20.30 and 40 mg/ml (24 h)	Halted cell migration and invasion	\uparrow ROR α , \uparrow nM23, \uparrow TIMP-3, \uparrow E-cadherin, \downarrow LIMK1, \downarrow uPAR, \downarrow CDK1 receptor, \downarrow ERK/Fra-1 pathway, \downarrow MMP-9, \downarrow vimentin	Su et al. (2015)
BGC823	15 mg/L (12, 24, 36, and 48 h)	Significantly reduced the proliferation of cells	\downarrow Cdc25C, \downarrow cyclin B1, \uparrow Chk1 phosphorylation, \uparrow phospho-ATR, \uparrow p21, \uparrow GADD45a, \uparrow p53	Ling et al. (2010), Bo et al. (2014)

(Continued on following page)

TABLE 1 | (Continued) Possible antineoplastic properties of DADS as well as their underlying mechanisms as established by *in vitro* research.

Cell lines	Duration and conc.	Anticancer properties	Mechanism of action	References
MGC803	30 mg/L (0.12, 24 and 48 h)	exerted anti-EMT and antitumor growth effects	↓TGF-β1, ↓Rac1, ↓β-catenin, ↓vimentin, ↑E-cadherin	Su et al. (2018)
MGC803	30 mg/L (0, 6, 12, or 24 h)	Arrested cell cycle and inhibited cell proliferation	↑Acetylated histones H3 and H4, ↑p21 ^{WAF1} protein expression	Su, (2012)
Colon cancer SW480	0–500 μM (1 h)	Induced apoptosis and cytotoxicity	↑[Ca ²⁺] concentration, ↑phospholipase C-independent Ca ²⁺ release from ER, ↑extracellular Ca ²⁺ influx	Chen et al. (2012)
HT-29	0, 30, 60, 120 and 240 μmol/L (12, 24 and 48 h)	Induced anti-proliferative and cytotoxic activity	↑expression of p21, ↑MM1, ↓YWHae, ↓RRM1	Lu et al. (2007)
HCT-116	50, 100, 200, and 400 μM (12.24 and 48 h)	Cell cycle arrest in the G2/M phase	↓ROS, ↓proliferation, ↑p53 expression, ↑cyclin B1	(Jo et al., 2008; Song et al., 2009)
Colo 205	25 μM (24-h and 48-h)	Elevated chemo-resistance	↑expression of drug resistant genes, ↑MRP3 gene expression	Lai et al. (2012)
Colo 205	10 and 25 μM	Inhibited migration and invasion	↓Ras, ↓PI3K, ↓p38, ↓MEKK3, ↓ERK1/2, ↓MKK7, ↓JNK1/2, ↓MMP-2, -7, and -9	Lai et al. (2013)
SW480	85ppm (24 h)	Attenuated proliferation and induced apoptosis	↓GSK-3β; ↓NF-κB	Saud et al. (2016)
HT29	ED ₅₀ 69 μm (16 h)	Induced redox potential oxidation and reduced cell proliferation	↓cell proliferation, ↓reduced GSH, ↑oxidized GSH	Odom et al. (2009)
COLO 205	25 μM (24 h)	Induced apoptosis	↓the mitochondrial membrane potential, ↓Bcl-2, ↓Bcl-xL, ↑Bak, ↑Bax, ↑cyclin B; ↑cdc25c-ser-216-9; ↑Wee1; ↑caspase-3, -8 and -9 activity, ↑Fas, ↑phospho-Ask1, ↑JNK, ↑p53, ↑cytochrome c	Yang et al. (2009)
HT-29 CT26	120 μM (12, 24 and 48 h) 100 μg/ml (1, 2, 4, and 8 h)	Suppressed cell growth Enhanced cytotoxicity	↑p21, ↑MM1, ↓YWHAE, ↓RRM1 ↑dual functioning ability, ↑drug release, ↑ease of penetration through mucous membranes, ↑ cell cycle arrest at sub-G1 phase	Huang et al. (2011) Saraf et al. (2021)
SW620, SW480, and HCT116	1.008 g/ml (24 h)	Inhibited migration and invasion	↓Rac1	Xia et al. (2019)
HCT116, DLD-1, HT29, and SW620	100 μl (24 h)	Initiated apoptosis	↓Bcl-2, ↑Bak, ↑Bax, ↑caspase-9	Kim et al. (2019)
SW480	45 mg/L (24 h)	Inhibited the migration and invasion	↓phosphorylation of ADF/cofilin, ↓LIMK1, ↓vimentin; ↓CD34; ↓Ki-67	Su et al. (2017)
Caco-2, HT-29	200 μM (6 h)	Increased histone acetylation and provided protective properties	↑p21 ^{WAF1/CIP1} expression, ↑histone H3 acetylation, ↑histone H4 hyperacetylation, ↓HDAC activity, ↓AM at the same	Druesne et al. (2004)
Caco-2, HT-29	200 μM (3 h and 6 h)	Increased histone acetylation and cell cycle arrest	↑CDKN1A promoter-associated histone acetylation, ↑p21 ^{CIP1} mRNA and protein levels	Druesne-Pecollo et al. (2008)
Cervical cancer HeLa	10 μM 24 h	Inhibition of cell viability	↑apoptosis, ↓p73, ↓radiation-induced G2/M phase arrest, ↑Tap73, ↑ΔNp73, ↑FASLG, ↑APAF1	Di et al. (2015)
HeLa	0–100 μM 24 h	Cell growth inhibition	↑sub-G1 phase (apoptosis), ↑G0/G1 cell cycle arrest, ↑dysfunction of mitochondria, ↑DNA damage, ↑cytochrome c, ↑pro-caspase-3 and -9, ↑AIF, ↑Endo G	Wu et al. (2011)
Caski	-	Inhibited cell proliferation	↑Intracellular ROS, ↑apoptosis, ↑cell cycle arrest in G0/G1 phase, ↓cyclin D1, ↓CDK4, ↑p21WAF1/CIP1, ↑p27KIP1, ↓E6, ↓E7	Ansari et al. (2020)
Ovarian cancer SK-OV-3 and OVCAR-3 ovarian	30 mg/L	Inhibited cell proliferation	↑p-Chk1, ↑p-CDC25C, ↑p-P53, ↑P21WAF1, ↑p-CDK1, ↓CDK1, ↓CyclinB1 protein, ↓PCNA, ↓Ki-67, ↓Survivin, ↑Cleaved-caspase3	Zhang et al. (2019b)
Leukemia K562 and NB4	0, 25, 50, 75, 100, 200, 300, and 500 μg/ml (24 and 48 h)	Induced apoptosis and autophagy	↓cell viability, ↓mTOR expression, ↑the percentage of cell apoptosis	Suangtamai and Tanyong, (2016)
HL-60	4, 8, 16, 32, 64 and 128 μM (72 h)	Inhibited proliferation, migration, invasion and arrested cells at G0/G1 stage	↑differentiation, ↑CD11b expression, ↓NBT, ↓DJ-1; ↓cofilin 1; ↓RhoGDI2; ↓calreticulin (CTR) and PCNA	Ling et al. (2017)
HL-60	500 μl (24, 48 and 72 h)	Inhibited migration and invasion	↓DJ-1, ↓p-Src, ↓p-Fak	Liu et al. (2018)

(Continued on following page)

TABLE 1 | (Continued) Possible antineoplastic properties of DADS as well as their underlying mechanisms as established by *in vitro* research.

Cell lines	Duration and conc.	Anticancer properties	Mechanism of action	References
HL-60	8 μ M (72 h)	Suppressed proliferation of cell	\uparrow CD11b and CD33 expression, \downarrow cofilin 1, \downarrow phosphorylated cofilin 1, \downarrow Rac1, \downarrow ROCK1, \downarrow LIMK1, \downarrow phosphorylation of LIMK1	Ling et al. (2020)
HL-60	5, 10, 15 mg / L (24 h)	Induced apoptosis	\uparrow Rac2 gene, \uparrow NADPH oxidase, \uparrow ROS, \uparrow JNK	Yi et al. (2010)
HL-60	1.25 mg/L (8 h)	Induced apoptosis	\downarrow cytoplasmic DJ-1 protein expression	Li et al. (2016)
	1.25 mg/L (8 h)		\uparrow nuclear DJ-1 protein expression	
	5 and 10 mg/L (4, 8 or 12 h)		\downarrow mitochondrial DJ-1 protein expression	
HL-60	1.25 mg/L (48 h)	Decreased proliferation, differentiation and invasion	\downarrow CRT	Yi et al. (2016)
HL-60	1.25 mg/L (48 h)	Reduced cell proliferation, invasion, and differentiation	\downarrow CRT, \downarrow CD33, \uparrow C/EBP α , \uparrow ROS	Sun et al. (2019)
HL-60	20 micro mol/L (12 h)	induced the G(2)/M arrest	\uparrow phospho-p38 MAPK, \uparrow phospho-Cdc25B, \uparrow phospho-Cdc2	Tan et al. (2004)
HL-60	1.25 μ g/ml (24 h)	Triggered apoptosis	\uparrow ROS, \uparrow PKC δ cleavage	Agassi et al. (2020)
HL-60	0.625, 1.250, and 2.500 μ g/ml (24, 48, and 72 h)	Inhibited the proliferation	\downarrow VEGF mRNA, \uparrow VEGF protein	Fan et al. (2006)
KF62	10, 20, 40, 80 mg/L (48 h)	Induced autophagy	\uparrow p-ERK, \uparrow LC3-II	Ye and Yin, (2017)
Lymphoma U937	50 μ M (24 h)	Induced apoptosis	\downarrow hTERT, \downarrow DNA-binding activity of c-Myc and Sp-1, \uparrow Mad1, \uparrow Mad/Max complex	Dasgupta and Sengupta Bandyopadhyay, (2015)
Lung cancer A549	0–80 μ M (24 h)	inhibited cell proliferation	\downarrow MMP-2/9, \uparrow E-cadherin, \downarrow N-cadherin, \downarrow Nrf2 signaling	Xu et al. (2021)
A549	7.5 μ M and 10 μ M 24 h	Decreased cell viability	\downarrow gelatinases, \uparrow E-cadherin, \uparrow cytokeratin-18, \downarrow N-cadherin and \downarrow vimentin	Das and Sinha, (2019)
Neural cancer SH-SY5Y, HeLa	50 μ M (3 h)	Caused early morphological changes	\uparrow SOD1, \uparrow ROS, \uparrow PP1-mediated Tau dephosphorylation	Aquilano et al. (2010)
SH-SY5Y	100 μ M (24 h)	Induced apoptosis	\uparrow [Ca ²⁺], \uparrow cytosolic Smac/Diablo, \uparrow caspase-9, \uparrow caspase-3, \uparrow Calpain, \uparrow SBDP, \downarrow NF- κ B, \downarrow ICAD	Karmakar et al. (2007)
SH-SY5Y	50 μ mol/L (24 h)	Caused nuclear damage, protein oxidation, and lipid peroxidation	\uparrow ROS, \uparrow NO	Aquilano et al. (2007)
CCF STTG1, SW1783, SW1088, CHLA-03-AA	15 and 150 μ g/ml (24 h)	Triggered apoptosis	\downarrow Akt/PKB	Choromanska et al. (2020)
T98G and U87MG	100 μ M (24 h)	Induced apoptosis	\uparrow ROS, \uparrow phosphorylation of p38 MAPK, \uparrow JNK1 pathway, \uparrow [Ca ²⁺], \uparrow calreticulin, \uparrow caspase-4, \uparrow caspase-9, \uparrow caspase-3, \uparrow Bax, \uparrow cytochrome, \uparrow Smac, \uparrow calpain, \downarrow Bcl-2, \downarrow BIRC proteins	Das et al. (2007)
Prostate cancer PC-3	10–50 μ M	Inhibited cell growth	\uparrow apoptosis, \uparrow IGF, \downarrow phosphorylation of Akt, \uparrow cyclin D1, \uparrow Bcl-2 molecule \uparrow Bad, \uparrow NF- κ B, \uparrow Bax	Arunkumar et al. (2012)
LNCaP	200, 400 μ M 24 h	Inhibited cell growth	\uparrow TER, \downarrow claudin, \downarrow (MMP)-2 and -9	Shin et al. (2010)
PC-3	50–1,000 μ M	Increased cytotoxicity	\downarrow thapsigargin, \uparrow apoptosis, \uparrow ROS, \uparrow [Ca ²⁺], ROS production	Chen et al. (2011)
DU145	200, 400 μ M 24 h	Inhibited cell growth	\uparrow Apoptosis, modulation of \uparrow Bcl-2, \downarrow IAP, \uparrow DR4, \uparrow FasL, \downarrow Bid proteins, \uparrow phosphorylation of MAPKs	Shin et al. (2012)
PC-3	20, 40 μ M 24 h	Decreased cell viability	\downarrow NF- κ B, \downarrow IKK α , \downarrow IKK β	Arunakaran et al. (2013)

inhibited the DCA-induced resistance of apoptosis *via* a mechanism that is NF- κ B/Bcl-2 dependent, suggesting that it could be a promising option for the chemical prevention and treatment of EAC and BE (Feng et al., 2017). Yin et al. (2014a) found that DADS dramatically decreased the viability of human esophageal cancer ECA109A cells while being considerably less toxic to normal liver cells. Annexin V-FITC/propidium iodide

(PI) staining identified the proapoptotic impact of DADS on ECA109 cells. Flow cytometry analysis revealed that DADS enhanced apoptosis in a dose-dependent manner and that the caspase-3 inhibitor Ac-DEVD-CHO could reduce the rate of apoptosis. In a xenograft trial conducted on nude mice, DADS therapy decreased the development of ECA109 tumors at concentrations of 20 mg/kg and 40 mg/kg with no apparent

adverse effects. By suppressing the proliferation of nuclear antigen (PCNA) cells, DADS reduced the proliferation of ECA109. In ECA109 xenograft tumors, DADS activated a mitochondria-dependent network with the executor of caspase-3, increased the ratio of Bax and Bcl-2, increased p53 levels, and downregulated the ERK/MEK/RAF pathway. These findings suggest that DADS is an efficient and reliable anti-cancer agent against esophageal carcinoma (**Table 1**) (Yin et al., 2014a).

2.2.2 Gastric Cancer

With over an estimated one million new cases diagnosed in 2020 and 769,000 predicted deaths, gastric cancer remains a serious health concern across the world and ranks fifth in terms of its incidence and fourth in terms of its lethality (UICC, 2020; Sung et al., 2021). Its etiology might be influenced by several factors, including genetics and the environment. Garlic consumption is a commonly prescribed means of preventing gastric cancer (Wang et al., 2012; Shamshirian et al., 2018). Ling et al. (2014) showed the anticancer properties of DADS that it induced the buildup of phosphorylated Chk1 and had a downregulating effect on the expression of cyclin B1 and CDC25C. The overexpression of Chk1 resulted in a significant increase in G2/M arrest induced by DADS, the inhibition of CDC25C expression, and an increase in DADS-mediated Chk1 phosphorylation. Chk1 suppression decreased DADS-associated G2/M arrest and prevented the DADS-induced suppression of cyclin B1 and CDC25C. In addition, Chk1 signaling *via* CDC25C/Chk1/ATR/cyclin B1 mediated the DADS-induced G2/M checkpoint responses (Ling et al., 2014). By triggering apoptosis and increasing ROS generation, DADS considerably reduced the growth of AGS human gastric adenocarcinoma cells. DADS also decreased the expression levels of Bcl-2 in AGS cells while also increasing the expression levels of Bax, Fas, and caspase-3 (Lee et al., 2011a). DADS hindered the metastasis of type II esophageal-gastric junction adenocarcinoma cells (OE19) by suppressing the Akt/PI3K and NF- κ B signaling pathways, downregulating uPA, MMP-9, and MMP-2 in the process (Yin et al., 2018). DADS inhibited cell proliferation by increasing tissue inhibitors of metalloproteinase (TIMP)-1 and TIMP2 mRNA levels and proteins while decreasing claudin proteins (claudin-3, claudin-4, and claudin-2), which are important components of tight junctions (TJs) (Park et al., 2011).

Tang et al. (2013) found that DADS inhibits cell proliferation and causes apoptosis *via* the Wnt-1 signaling pathway by upregulating miR-22 and miR-200b. Variations in the expression of miRNA were identified in DADS-treated MGC-803 cells, while the upregulation of miR-22 and miR-200b was also observed. Wnt-1 was also discovered to be a target of both miR-22 and miR-200b. miR-200b and miR-22 not only synergistically decreased gastric cancer development but also improved the antitumor effects of DADS both *in vitro* and *in vivo*. Thus, it was suggested that miR-22 and miR-200b could be used in possible gene therapy procedures to boost the antitumor effectiveness of DADS (Tang et al., 2013). By downregulating LIMK1, DADS prevented the epithelial-mesenchymal transition

(EMT), preventing gastric cancer invasion and development. The expression of LIMK1 is linked with the differentiation, clinical stage, invasion level, lymph node metastasis, and poor diagnosis of tumors, both *in vitro* and *in vivo* (Bo et al., 2016). To investigate the potential of DADS-regulated molecules, Su et al. (2015) compared the protein expression profiles of DADS-treated gastric cancer MGC-803 cells to untreated control cells. 23 proteins with statistically important variations in expression were found through proteomic approaches, comprised of 14 downregulated proteins and 9 upregulated proteins. Ling et al. (2010) demonstrated that there was an association between the cell cycle arrest of G2/M and the phosphorylated forms of Chk1 buildup, but not Chk2; this suggests that the G2/M cell cycle arrest was associated with the DADS-induced growth suppression of the BGC823 gastric cancer cell line in humans. Additionally, Chk1 signaling *via* the Cdc25C/Chk1/cyclin B1/ATR pathway mediates the DADS-induced G2/M checkpoint response; this process is independent of Chk2 (Ling et al., 2010). Bo et al. (2014) reported similar results; they found that Chk1, and not Chk2, was directly responsible for the arrest of G2/M, which is induced in the human gastric cancer BGC823 cells by DADS (**Table 1**). An *in vitro* trial conducted by Su (2012) found that DADS increased the acetylation of the H4 and H3 histones in human gastric cancer MGC803 cells in a time-dependent manner; this was supported by an increase in p21WAF1 protein levels increase and was consistent with the arrest of the G2/M phase cell cycle. DADS also exhibited dose-dependent antitumor effectiveness in an *in vivo* trial of MGC803-xenografted nude mice, resulting in the inhibition of tumor cell development and the arrest of the G2/M phase. Furthermore, the xenografted tumor cells exhibited distinct cell differentiation characteristics. These findings suggest that DADS, by causing the hyperacetylation of histones H4 and H3 while also boosting the expression of p21WAF1 in MGC803 cells, might trigger the arrest of the cell cycle and reduce cell proliferation, which may be responsible for its antitumor effects against gastric cancer (Su, 2012).

2.2.3 Colorectal Cancer

Well over 1.9 million new cases of colorectal cancer (CRC) are expected to be diagnosed in 2020, with an estimated 935,000 fatalities. CRC is the third most frequently-occurring cancer and has the second-highest mortality rate (1. Hyuna Sung et al., 2020; UICC, 2020). A lack of exercise or physical activity, obesity, as well as the consumption of alcohol, red meats, and tobacco are all known to contribute to the development of CRC. CRC fatalities can be reduced if it is detected and treated early. The use of garlic as a dietary supplement can help prevent and lower the risk of CRC (Fleischauer and Arab, 2001). DADS had a preliminary signaling impact on the SW480 colon cancer cell line by increasing Ca²⁺ mobilization (Chen et al., 2012). The DADS-induced apoptosis of colo205 cells was related to the elevated expression of transcription 1 (STAT1) signal activators and transducers (Lu et al., 2007). In HCT-116 cells, DADS triggered the arrest of the cell cycle in the G2/M phase, while also elevating the expression of p53 and cyclin B1 (Jo et al., 2008), as well as the production of ROS (Song et al., 2009). DADS

targeted drug-resistant genes in human colon cancer cells (colo205). The expression levels of the multidrug resistance-associated protein-3 (MRP-3) were increased by DADS. DADS elevated the expression of the MRP6 and MRP4 genes while also inhibiting the growth of colo205 cells by lowering the Ras, PI3K, MEKK3, MKK7, JNK1/2, p38, and ERK1/2 expression levels, which consequently suppressed MMP-9, MMP-2, NF- κ B, COX-2, and MMP-7 expressions levels (Lai et al., 2012; Lai et al., 2013).

DADS prevented colorectal tumorigenesis in mouse models through a process that involved the NF- κ B signaling pathway and the nuclear localization of NF- κ B, causing it to have a reduced activity while also inhibiting the activation of GSK-3 β (Saud et al., 2016). An *in vivo* study using human colon cancer colo205 cells transplanted into mice revealed that DADS decreased the tumor's weight and size (Lai et al., 2012). DADS dramatically decreased cell proliferation and triggered the arrest of the cell cycle in the G2/M phase in human colon cancer SW480 cells both *in vitro* and *in vivo*; this was most likely accomplished by downregulating cyclin B1, p53, and PCNA expression while upregulating p21WAF1 (Liao et al., 2007). Through the alteration of its intracellular redox environment, DADS suppressed the growth and arrest of the G2/M phase in human colon cancer HT-29 cells (Odom et al., 2009; Yang et al., 2009). The anti-proliferative properties of DADS against colon cancer HT-29 cells were linked to several genes that had varied expression patterns and that were engaged in different physiological systems (Huang et al., 2011). Colon-targeting DADS-loaded nanoparticles that had dual functionalities and a significant cytotoxic impact were successfully produced. In colon cancer therapy, ES100/PLGA-NPs might be a viable method of targeting water-insoluble bioactive phytochemicals with better safety measures and patient compliance. Furthermore, the polymeric mixture used can be precisely adjusted to create nano-carriers that can deliver dietary phytochemicals (Saraf et al., 2021).

DADS inhibited the expression levels and activity of Rac1 by inhibiting the PI3K/Akt pathway, preventing EMT as well as cell migration and invasion. The Rac1 knockdown improved the tumor prevention capabilities of DADS; in contrast, the overexpression of Rac1 counteracted its effects (Table 1) (Xia et al., 2019). In CRC cell lines, Kim et al. (2019) found that non-cytotoxic doses of DADS boosted tumor necrosis factor-related apoptosis-inducing ligand (TRAIL)-related cell death. In addition, the synergistic impact between TRAIL and DADS was confirmed *in vivo* using mice models. One of the mechanisms involved in these observations was the reduced production of the antiapoptotic protein Bcl-2; the synergistic effect of DADS and TRAIL was diminished in cells with overexpressed Bcl-2. This study revealed new insights into the involvement of DADS in the TRAIL-associated suppression of CRC development *via* Bcl-2 inhibition (Kim et al., 2019). The overexpression of LIMK1 considerably aids colon cancer cell invasion and migration. DADS reduced cancer cell invasion and migration by decreasing the phosphorylation of ADF/cofilin *via* the suppression of LIMK1 in colon cancer cells. The knockdown and overexpression of LIMK1 increased and decreased DADS-induced cell proliferation suppression, respectively; this was confirmed both *in vitro* and *in vivo*. Similar results were

observed in DADS-induced alterations to the expression of E-cadherin, Ki-67, CD34, and vimentin in xenografted tumors. These findings suggested that LIMK1 was a viable target molecule to enhance the anti-invasion and anti-migration effects of DADS on colon cancer cells (Su et al., 2017). By inhibiting histone hyperacetylation and HDAC while increasing the expression of cip1/p21waf1, DADS suppressed cell proliferation in HT-29 and Caco-2 cells. The cellular and molecular effects evoked by DADS are potentially connected to its impact on histone acetylation and thus contribute to its anti-carcinogenic capabilities in the colon (Druesne et al., 2004). In both short-term, solitary treatments as well as persistent, repetitive treatments, DADS caused rapid histone hyperacetylation in human tumor colon cell lines. Histone hyperacetylation is linked to anti-proliferative effects, including the arrest of the cell cycle in the G2/M phase and the increase of p21cip1 mRNA and protein expression levels (Druesne-Pecollo et al., 2008).

2.2.4 Hepatocellular Cancer

There were an estimated number of 906,000 new cases and 830,000 fatalities attributed to primary liver cancer in 2020. It is the most common form of cancer, has the highest mortality rate, and is the sixth most frequently diagnosed cancer worldwide (Anwanwan et al., 2020; Globocan, 2020; Sung et al., 2021). The two treatments available for liver cancer are immunotherapy and chemotherapy. However, new therapeutic approaches that incorporate natural ingredients may result in better prognoses. In particular, garlic has exhibited anticancer and preventative effects against liver cancer (Zhou et al., 2016). Through inhibition of I κ B α phosphorylation and NF- κ B translocation in CCL4-induced liver injury, DADS boosted the levels of phase II antioxidant enzymes while simultaneously decreasing the expression of inflammatory mediators. This suggests that DADS activated the Nrf2 pathway, which enhanced antioxidant defense, inhibited NF- κ B activation, and decreased inflammation (Lee et al., 2014). Another study found that DADS successfully reduced the acute hepatic damage caused by acetaminophen in rats. The beneficial impacts of DADS are due to its ability to regulate inflammatory reactions by suppressing NF- κ B activation and reducing oxidative stress-mediated JNK activation by inhibiting CYP2E1 or by increasing antioxidant enzyme activity (Table 1) (Ko et al., 2017). DADS suppressed the critical regulators of lipid peroxidation, inflammation, and metabolism, while also having appreciable effects on nonalcoholic steatohepatitis (NASH) induced by high-fat diets (HFD) or methionine and choline-deficient diets (MCD) (Zhang et al., 2019a). The administration of DADS reduced cyclophosphamide-induced hepatotoxicity in rats by simultaneously upregulating both anti-inflammatory and antioxidant activity, demonstrating its promising therapeutic utility against the adverse effects of cyclophosphamide (Hasan et al., 2020). The pre-treatment of epithelial cells in CdCl₂-treated rat liver with DADS compounds exhibited a protective effect against the toxicity of CD by modulating cytokine protein production, which resulted in improved viability (Odewumi et al., 2019).

Table 1 demonstrates the possible antineoplastic properties of DADS as well as their underlying mechanisms as established by *in vitro* research.

2.3 Gynecological Cancers

2.3.1 Cervical Cancer

Cervical cancer is the fourth most common cancer, with 342,000 fatalities and 604,000 new cases diagnosed in women globally in 2020. Middle and low-income nations accounted for over 90% of cases worldwide (Sung et al., 2021; Mitra et al., 2022b). Thus, therapeutic treatments that use natural products are urgently needed. Several experimental studies have shown that DADS is effective against cervical cancer. Di et al. (2015) investigated the molecular mechanisms associated with DADS using human cervical cancer cells. As radiotherapy is the most basic form of treatment, HeLa cells were treated with 10 μ M of DADS before being exposed to radiation, increasing their radiosensitivity and reducing cell viability. DADS pre-treatment reduced the radiation-induced arrest of the G2/M phase while also boosting radiation-induced apoptosis. In addition, coupled DADS and radiation treatment boosted the activation of apoptosis pathways as well as increased the Tap73 (proapoptotic) to Np73 (antiapoptotic) ratio and the levels of APAF1 and FASLG downstream proteins (Di et al., 2015). DADS had a substantial anti-proliferative impact on Caski cells, dose-dependently decreasing cell viability and increasing intracellular ROS production and apoptosis. Downregulating cyclin CDK4 and D1 and the overexpression of p27KIP1 and p21WAF1/CIP1 inhibitors of CDK enhanced the ability of DADS to arrest the G0/G1 cell cycle in Caski cells. DADS also downregulates the viral oncogenes E7 and E6 while restoring the functions of p53 (Ansari et al., 2020).

2.3.2 Ovarian Cancer

Ovarian cancer is the seventh most frequent disease in women across the globe and the 18th most prevalent cancer. In 2012, there were almost 239,000 new instances of ovarian cancer in women, which accounts for approximately 4% of all new cancer cases in women (2% of all cancer cases across both genders). Ovarian cancer is generally lethal. The age-standardized prevalence rate of this cancer ranges from less than 5 per 100,000 in Africa to more than 11 per 100,000 in Eastern and Central Europe (Sánchez et al., 2013). To mitigate the extreme prevalence of ovarian cancer, novel therapeutics must be considered. DADS has been used for decades to treat this disease. SK-OV-3 and OVCAR-3 cells were incubated with different concentrations of DADS to explore the influence of the DADS-induced arrest of the G2/M phase on the development and death of ovarian cancer cells as well as the molecular mechanisms that are involved in this process. The test was run on xenograft models *in vivo* which demonstrated that the inhibition rate of cell proliferation dramatically increased as the concentration of DADS increased. The suppression rates of the OVCAR-3 and SK-OV-3 cells were noticeably greater at 24 h than at 12 and 48 h, demonstrating remarkable time-dependency. Another test demonstrated that when OVCAR-3 and SK-OV-3 cells were medicated with DADS of various concentrations, the

rates of apoptosis increased as the concentration of DADS. Notably, the apoptosis rates of DADS treated OVCAR-3 and SK-OV-3 cells at 24 h were much greater than the rates at 12 and 48 h. The intraperitoneal injection of a solution containing DADS significantly reduced the volume of xenografted cancer cells in the ovaries of nude mice compared to the blank control groups. When 30 mg/L of DADS was administered to OVCAR-3 and SK-OV-3 cells for 24 h, the proportion of OVCAR-3 and SK-OV-3 cells in the G2 phase rose dramatically compared to the blank cells. Survivin, PCNA, and Ki-67, which are associated with cell apoptosis and proliferation, were all dramatically reduced while the levels of the protein cleaved-caspase3 significantly increased [54].

2.4 Hematological Cancers

2.4.1 Leukemia

The type of leukemia is determined by the type of malignant blood cell and the rate at which it proliferates (Van Den Heuvel-Eibrink, 2004). Leukemia is the most frequent cancer in patients older than 55 while also being the most prevalent illness in children younger than 15 years old (Deschler and Lübbert, 2008). In the cell lines of NB4 and K562 myeloid leukemia, autophagy and apoptosis could both be triggered by DADS *via* the mTOR pathway (Tan and Xiao-xia, 2011). After treatment with DADS at different concentrations for 24–48 h, it was found that DADS suppressed cell viability and increased the apoptosis rate in a time- and dose-dependent manner. The expression of mTOR was significantly reduced in cells that had been treated with DADS and mTOR inhibitors. Cells treated with 10 μ M of mTOR inhibitor and 100 g/ml of DADS exhibited high rates of autophagy and death (Suangtamai and Tanyong, 2016). DADS halted cells at the G0/G1 stage and reduced the proliferation, invasion, and migration of HL-60 cells. DADS also lowered the capacity of NBT, improved the expression of CD11b, slowed tumorigenesis, and promoted differentiation in xenografts *in vivo* (Table 2). The expression of Rho GDP dissociation inhibitor 2 (Rho GDI2), Dj-1, Calreticulin (CTR), PCNA, and cofilin 1 were all lowered by DADS (Ling et al., 2017). DADS suppressed DJ 1-mediated migration and invasion in leukemic cells by inhibiting the Src-Fak-Integrin signaling pathway; the Src inhibitor synergistically improved the anticancer effects of DADS (Liu et al., 2018). Due to the reduced ability of nitro-blue tetrazolium as well as elevated CD33 and CD11b expressions, 8 μ M of DADS inhibited cell migration, proliferation, and invasion, while also causing differentiation. DADS significantly decreased the generation of phosphorylated cofilin 1 in HL 60 leukemia cells. DADS also decreased the protein and mRNA expression of Rac1, LIM domain kinase 1 (LIMK1), and Rho-associated protein kinase 1 (ROCK1), as well as LIMK1 phosphorylation in HL 60 cells (Ling et al., 2020).

NADPH oxidase is another key ROS source that is enhanced by DADS. Rac2 activated the c-JNK pathway in DADS-induced apoptosis but did not activate the p38 pathway. NADPH oxidase, reactive oxygen species, and Rac2 played a role in the DADS-induced apoptosis of HL 60 human leukemia cells (Yi et al., 2010). The expression of DJ 1 proteins was significantly reduced in the cytoplasm when the HL 60 cells were exposed to 1.25 mg/L DADS

TABLE 2 | Potential antineoplastic effects of DADS and its underlying mechanisms based on *in vivo* studies.

Animal tumor models	Anticancer effects	Mechanisms	Dose (route)	Duration	References
Breast cancer Female athymic mice (breast)	Retarded the tumor growth	Not reported	Intraperitoneal injection (1 or 2 mg) 3 times a week	35 days	Tsubura et al. (2012)
Ehrlich ascites carcinoma (EAC) bearing female albino mice	Modulated apoptosis	↑Apoptosis, ↓Bcl-2, ↑p53, ↑deoxynucleotidyl transferase, ↓sialic acid	Intraperitoneally 100 mg/kg	2 weeks	Ahmed and Ahmed, (2015)
Esophageal cancer ECA109 injected nude mice	Induced apoptosis	↓PCNA, ↓RAF/MEK/ERK, ↑caspase-3, ↑p53, ↑Bax/Bcl-2 ratio	20 and 40 mg/kg (i.p.)	24 h	Yin et al. (2014a)
Gastric cancer Male Balb/c nude mice	Induced apoptosis	↑miR-22, ↑miR-200b	100 mg kg ⁻¹ (s.c.)	48 h	Tang et al. (2013)
MGC803 injected nude mice	Inhibited cell invasion	↓ p-cofilin1, ↓Rac1-Pak1/Rock1-LIMK1 pathway, ↓EMT, ↓p-LIMK1, ↓MMP-9, ↑TIMP-3	30 mg/L (s.c.)	12, 24, and 48 h	Bo et al. (2016)
MGC803 injected male athymic BALB/c nude mice	Exerted anti-EMT and antitumor growth effects	↓Ki-67, ↓CD34, ↓vimentin, ↑E-cadherin	30 mg/L (s.c.)	0, 12, 24 and 48 h	Su et al. (2018)
MGC803 -xenografted nude mice	Arrested cell cycle and inhibited cell proliferation	↑Acetylated histones H3 and H4, ↑p21 ^{WAF1} protein expression	50, 100, and 200 mg/kg (s.c.)	0, 6, 12, or 24 h	Su, (2012)
Colon cancer Colo 205 xenograft mice	Elevated chemo-resistance of human cancer cells	↑Mdr1, MRP1, MRP3, MRP4 and MRP6 gene expression	25 μM (s.c.)	24-h and 48-h	Lai et al. (2012)
FVB/N mice	Prevented colorectal tumorigenesis	↓prolonged inflammation and cellular transformation; ↓GSK-3β, ↓NF-κB	10 mg/kg (i.p.)	24 h	Saud et al. (2016)
SW480 injected nude mice	Inhibited proliferation and arrested cell cycle	↓PCNA, ↓p53, ↓cyclin B1, ↑p21WAF1	30 mg/kg (s.c.)	24 h	Liao et al. (2007)
SW620, SW480, and HCT116 injected nude mice	Inhibited migration and invasion	↓Rac1, ↓N-cadherin, ↓vimentin, ↓snail1, ↑E-cadherin	1.008 g/ml (i.v.)	24 h	Xia et al. (2019)
HCT116, DLD-1, HT29, and SW620 injected BALB/c nude mice	Initiated apoptosis	↓Bcl-2, ↑Bak, ↑Bax, ↑caspase-9	100 μL (s.c.)	24 h	Kim et al. (2019)
SW480 injected nude mice	Inhibited the migration and invasion	↓phosphorylation of ADF/cofilin, ↓LIMK1, ↓vimentin, ↓CD34, ↓Ki-67	45 mg/L (s.c.)	24 h	Su et al. (2017)
Caco-2, HT-29 injected rodents	Increased histone acetylation and provided protective properties	↑p21 ^{waf1/cip1} expression, ↑histone H3 acetylation, ↑histone H4 hyperacetylation, ↓HDAC activity, ↓AM at the same	200 μM (s.c.)	6 h	Druesne et al. (2004)
Caco-2, HT-29 injected colonocytes	Increased histone acetylation and cell cycle arrest	↑CDKN1A promoter-associated histone acetylation, ↑p21 ^{cip1} mRNA and protein levels	200 mg/kg (Intracaecal perfusion and gavage)	1 and 21 h	Druesne-Pecollo et al. (2008)
Hepatocellular cancer Thirty male Sprague-Dawley rats	Induced antioxidant defense mechanism and reduced inflammatory response	↓NF-κB translocation, ↓IκBα phosphorylation, ↑Bax, ↑cytochrome c, ↑caspase-3, ↑Nrf2 translocation, ↑phase II/ antioxidant enzyme activities	50 and 100 mg/kg/day (gavaged)	5 days	Lee et al. (2014)
Twenty four healthy male rats	Provided protective effects	↓hepatic CYP2E1 expression, ↓NF-κB activation, ↓serum AST and ALT levels, ↓MDA, ↓JNK activation, ↑GSH, ↑antioxidant enzymes activities	100 mg/kg/day (oral gavage)	5 days	Ko et al. (2017)
c57Bl/6J mice	Effectively attenuated hepatic steatosis, lipotoxicity, lipid peroxidation and inflammation	↓serum AST and ALT levels, ↓liver TG and TC contents, ↓ mRNA levels of SREBP-1 and ApoA-I, ↓SCD-1, ↓NF-κB, ↓TNF-α, ↓IL-6, ↓MDA, ↓SOD, ↑PPARα, ↑mRNA levels of CREBH and FGF21	20, 50, and 100 mg/kg (s.c.)	4 or 20 weeks	Zhang et al. (2019a)
CP feeded male adult albino rats	Reduced hepatotoxicity	↑ALT, ↑AST, ↑ALP, ↑total and direct bilirubin levels, ↑γ-GT, ↑HDL-C, ↓GPx, ↓serum cholesterol, ↓triglycerides, ↑CAT, ↓LDL-C, ↓VLDL-C levels, ↓MDA, ↓PCC, ↓NOX-4	200 mg/kg (oral)	10 days	Hasan et al. (2020)
CRL1439 treated rats	Triggered apoptosis	↓IGF-1R, ↓Fas/TNFRSF6/APO	150 μM (oral)	2 h	Odewumi et al. (2019)

Leukemia

(Continued on following page)

TABLE 2 | (Continued) Potential antineoplastic effects of DADS and its underlying mechanisms based on *in vivo* studies.

Animal tumor models	Anticancer effects	Mechanisms	Dose (route)	Duration	References
HL-60 injected mice	Inhibited proliferation, migration, invasion and arrested cells at G0/G1 stage	↑differentiation, ↑ CD11b expression, ↓NBT, ↓DJ-1, ↓ cofilin 1, ↓RhoGDI2, ↓CTR, ↓PCNA	21, 42 and 84 mg/kg (s.c.)	5 days	Ling et al. (2017)
HL-60 injected SCID mice	Reduced cell proliferation, invasion, and differentiation	↓CRT, ↓CD33, ↑C/EBPα, ↑ROS	21 or 42 mg/kg (s.c.)	21 days	Sun et al. (2019)
Skin cancer DMBA/TPA-treated mouse	Inhibited chemically induced papilloma genesis	↑CAT, ↑SOD, ↑GPx, ↑GR, ↑nuclear accumulation of Nrf2	4 μM (topical)	4 days	Shan et al. (2016)

over 8 h. However, the expression DJ 1 was greatly elevated in the nucleus fractions compared to the untreated controls. Following treatment with 5 mg/L and 10 mg/L of DADS, the expression levels of DJ 1 proteins were dramatically reduced in the mitochondria of the HL 60 cells. These findings revealed that exposing HL 60 cells to low dosages of DADS increases the translocation of the DJ one protein from the cytoplasm to the nucleus, suggesting that DJ one could be a cofactor binding protein or transcription factor in cell differentiation. The expression of DJ one in mitochondria may be connected to the induction of apoptosis in HL 60 cells that were exposed to moderate concentrations of DADS (Li et al., 2016). Calreticulin (CRT) played a significant role in human acute myeloid leukemia (AML) cell invasion and proliferation and is the subject of a significant amount of research. Yi et al. (Yi et al., 2016) found that CRT caused cell differentiation, proliferation, and invasion in DADS-treated HL 60 cells, as evidenced by the DADS-induced CRT downregulation across differentiated HL 60 cells. Following DADS-induced differentiation, CRT expression levels decreased while C/EBPα expression levels increased in the HL 60 cells. In severe combined immunodeficiency mice injected with HL 60 cells, DADS reduced tumor tissue growth *in vivo*, decreased levels of CRT, and increased C/EBPα. Furthermore, it was demonstrated that the DADS-mediated increased expression of C/EBPα and decreased expression of CRT expression resulted in an upregulation of reactive oxidant species. In an RNA immunoprecipitation experiment, CRT bound to C/EBPα mRNA, indicating that it controls C/EBPα mRNA degradation by conjugating with UG-rich elements in the 3' untranslated region (Sun et al., 2019). The DADS-induced arrest of the G2/M phase in HL-60 cells may be linked to the activation of p38 MAP kinase. Following the expression of phospho-Cdc2 and phospho-Cdc25B, DADS elevated the expression levels of phospho-p38 MAPK and activated the G2/M checkpoint when HL-60 cells were exposed to 20 μM/L of DADS over 12 h (Tan et al., 2004).

DADS dramatically inhibited the growth of HL-60 cells by suppressing the expression of VEGF mRNA and the generation of VEGF proteins in HL-60 cells, leading to anti-leukemic effects (Fan et al., 2006). As the concentration of DADS was increased, the number of K562 cells reduced significantly, and the form of some of the fixed K562 cells became irregular, resulting in a twisted membrane. The number of green spots in the stained cells increased as the concentration of DADS increased. The rate of

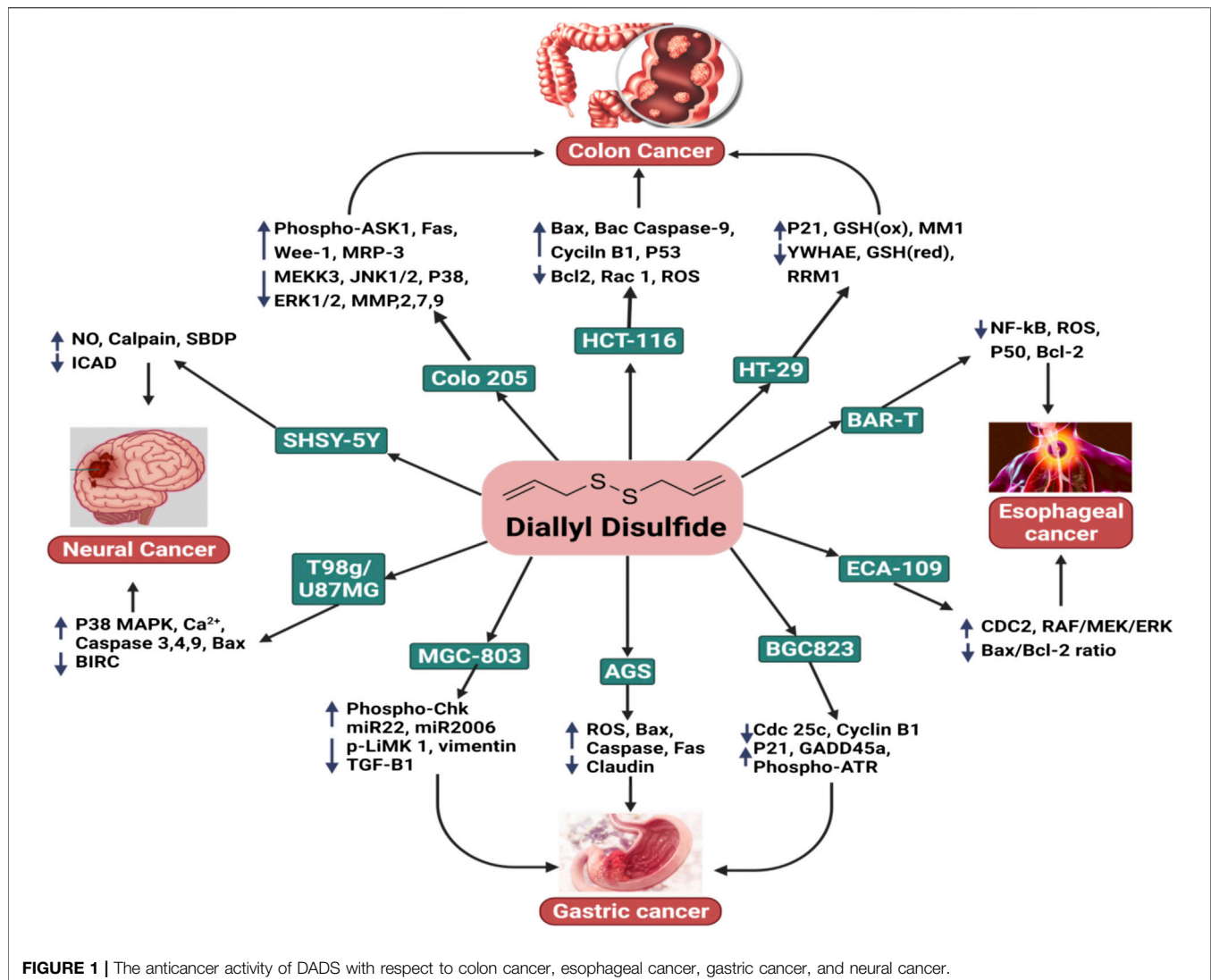
autophagy in K562 cells increased steadily after 48 h of DADS culture. The groups that had been exposed to 20, 40, and 80 mg/L of DADS exhibited greater autophagy rates compared to the group of blank control, of which the group that had been exposed to 40 mg/L of DADS exhibited the highest autophagy rate. There was no discernable variation in the expression of ERK protein between groups, but the expression of p-ERK and LC3-II proteins increased as the concentration of DADS increased; a substantial change in the expression of the proteins of the 40 mg/L DADS group was also observed. DADS activated the MEK-ERK signaling pathway through the phosphorylation of ERK, which induced autophagy in the K562 cells (Ye and Yin, 2017).

2.4.2 Lymphoma

Lymphomas refer to solid tumors found in the immune system. Hodgkin lymphomas account for 10% of all lymphomas. Lymphomas are relatively common and most clinicians will have encountered a lymphoma patient regardless of their specialty. Early diagnosis is critical since many lymphomas have excellent, and quite curative, therapies (Pinkerton, 2013). DADS inhibited the activity of telomerase through the transcriptional downregulation of hTERT, the catalytic subunit of telomerase, while keeping the expression of its RNA component unchanged. The suppression of the transcription factors Sp-1 and c-Myc by caspases and the cysteine protease, calpain, led to decreased DNA-binding efficiency at their relative binding sites on the hTERT promoter, culminating in apoptosis *via* the reduction of telomerase activity. Elevated Mad1 levels generated by DADS treatment may also lead to the creation of additional Max/Mad complexes that may interfere with the Max/Myc complex which binds the E-box of the hTERT promoter, thus transcriptionally decreasing the expression of hTERT (Table 2) (Dasgupta and Sengupta Bandyopadhyay, 2015).

2.5 Lung Cancer

Non-small cell lung cancer (NSCLC) is the single biggest reason for cancer-associated fatalities. Radiotherapy is still the primary treatment for NSCLC. However, ionizing radiation (IR) at low doses can cause invasion and migration (Xu et al., 2021). One study showed that IR significantly boosted A549 cell invasion and migration. A549 cells treated with 40 μM of DADS decreased the IR-induced invasion and migration while improving their radiosensitivity. Furthermore, IR-induced EMT was inhibited by 40 μM of DADS by suppressing the protein matrix, which



is related to metalloproteinase-9 (MMP-9) and metalloproteinase-2 (MMP-2) generation, as well as the reduction of the mesenchymal marker N-cadherin and the elevation of the epithelial marker E-cadherin in A549 cells. In addition to this, the expression of Nrf2 signaling was shown to be inhibited by DADS. The IR-induced invasion and migration were suppressed by DADS by inhibiting the activation of Nrf2 signaling in A549 cells (**Table 2**) (Xu et al., 2021).

The EMT is critical to the process of malignant transformations, and fibronectin (FN), a component of the extracellular matrix, can induce metastasis and invasion. Due to the reduced function of gelatinase, DADS hindered the FN-induced migration and invasion of A549 cells. In DADS-treated A549 cells, cytokeratin-18 and E-cadherin, which are epithelial indicators, were elevated, while vimentin and N-cadherin, which are the mesenchymal markers, as well as factors of transcription, such as twist, snail, and slug, were downregulated. DADS inhibited the FN-induced nuclear translocation of catenin and

glycogen synthase kinase-3 phosphorylation in A549 cells, as well as disorganized lymphoid enhancer factor/T-cell factor and homolog 2 activities (**Figure 1**) (Das and Sinha, 2019).

2.6 Neural Cancer

Neural cancers are a heterogeneous group of over 100 illnesses that cause considerable morbidity and mortality when combined. Glioblastoma multiform (GBM), the most common form of brain tumor, is almost always fatal, with a survival rate (5-year) of only 2%; current treatments only provide palliative relief. GBMs have a high degree of cellular heterogeneity, which may explain why patients' nodular or regional patterns frequently advance or recur (**Figure 1**) (Lathia et al., 2011).

Due to its extensive cytoskeletal modification and particularly lethal effect on growing neuroblastoma cells, Aquilano et al. (2010) emphasized the use of DADS in cancer therapy. As the phosphorylation of Tau is strongly associated with the functions of the neuronal cytoskeleton, their investigations found Tau to be

a novel target for the anti-cytoskeletal action of DADS and can be used to develop new ways of treating neuronal illnesses linked with Tau phosphatases and the impairment of hyperphosphorylation (Aquilano et al., 2010). DADS has been shown to suppress antiapoptotic factors while simultaneously inherently triggering a caspase cascade as well as activating calpain, resulting in the apoptosis of SH-SY5Y cells (Karmakar et al., 2007). DADS was also found to regulate nNOS, suggesting that nitric oxide plays a significant role in preventing the cytotoxicity caused by reactive oxygen species (Aquilano et al., 2007). DADS exhibited potential anti-glioma properties, especially with regard to their proliferation, while also inducing apoptosis in four distinct types of glioma cell lines that represented the different phases of the illness (Choromanska et al., 2020). DADS caused glioblastoma cells to die by forming ROS, increasing ER stress, lowering $\Delta\Psi_m$, and activating apoptosis-inducing cysteine proteases and stress kinases (Table 2) (Das et al., 2007).

2.7 Skin Cancer

Skin cancer is a lethal illness and a major public health issue that has resulted in significant economic and human losses across the world (Didona et al., 2018). A variety of internal and environmental variables can aggravate the pathophysiology of skin cancer and worsen the illness (Siegel et al., 2018). The importance of the early identification and diagnosis of skin cancer cannot be overstated. The mortality rate of skin cancer has decreased dramatically because of improved screening procedures, early detection and diagnosis, and innovative treatment modalities (Table 2) (Casari et al., 2018).

The topical application of DADS reduced the prevalence and development of skin cancer in mice models. Shan et al. (2016) revealed that DADS decreased the occurrence and development of skin tumors in mice models in a dose-dependent manner. This mechanism was associated with the upregulation of antioxidant enzyme activity, including catalase, SOD, and glutathione peroxidase, as well as the nuclear accumulation of Nrf2. DADS also enhanced the endogenous link between Nrf2 and p21 and was critical in helping Keap-1 prevent the degradation of Nrf2 (Figure 1) (Shan et al., 2016).

2.8 Prostate Cancer

Prostate cancer is the second most frequent cancer in males after skin cancer, and yet its treatments have the highest success rates. An *in vitro* experiment was used to study the impact of DADS on growth factor signaling molecules (like insulin) that are involved in the proliferation and survival of the human prostate cancer cells (Arunkumar et al., 2012). It was found that DADS reduces the rate of survival of androgen-independent prostate cancer cells by modulating the expression of the IGF system, resulting in the inhibition of Akt phosphorylation, and consequently inhibiting cell cycle survival and progression by reducing the expression of NF- κ B, cyclin D1, and antiapoptotic Bcl-2 molecules while enhancing the expression of proapoptotic signaling molecules (Bax and Bad) which trigger apoptosis (Arunkumar et al., 2012). Shin et al. (2010) investigated the anti-invasive potential of DADS in prostate cancer LNCaP cells; its mechanism involved the

tightening of TJs and inhibiting matrix metalloproteinase activities. DADS inhibited the expression of claudin proteins, the important components of TJs, which are crucial for the selectivity and regulation of paracellular transport. In addition, the administration of DADS suppressed the activity of MMP-9 and MMP-2 in LNCaP cells in a dose-dependent manner; this was also associated with a decrease in the expression of proteins and mRNA (Table 2) (Shin et al., 2010).

Chen et al. studied the impacts of DADS on Ca^{2+} viability and mobility in human prostate cancer PC3 cells. 500 μM of DADS caused apoptosis in a mechanism that was independent of Ca^{2+} . Annexin V/pi staining revealed that concentrations of both 10 and 500 μM of DADS induced apoptosis. DADS also boosted the formation of ROS. DADS caused an increase in Ca^{2+} in PC3 cells by inducing phospholipase C-independent Ca^{2+} release from the endoplasmic reticulum as well as the influx of Ca^{2+} via phospholipase A2 sensitive channels. In summary, DADS induced Ca^{2+} -independent apoptosis, Ca^{2+} -dependent cell death, and the generation of ROS (Figure 2) (Chen et al., 2011).

DADS significantly suppressed the development of human prostate cancer DU145 cells by inducing apoptosis. Apoptosis was accompanied by the modulation of Bcl-2 and the inhibitor of apoptosis proteins (IAP) family of proteins, the depolarization of the mitochondrial membrane potential (MMP, $\Delta\Psi_m$), and proteolytic activation of caspases. DADS boosted the expression of Fas ligand (FasL) and death receptor 4 (DR4) proteins while decreasing the number of intact Bid proteins. Furthermore, DADS stimulated the phosphorylation of mitogen-activated protein kinases (MAPKs) such as extracellular-signal regulating kinase (ERK), p38 MAPK, and c-Jun N-terminal kinase (JNK). SP600125, an inhibitor of JNK, greatly inhibited DADS-induced apoptosis, but p38, MAPK (SB203580), and ERK (PD98059) inhibitors did not produce the same effect. DADS-induced apoptosis was followed by the inactivation of phosphatidylinositol 3-kinase (PI3K)/Akt and the inhibition of PI3K. In addition, LY29004 dramatically boosted DADS-induced cell death (Shin et al., 2012).

The growth and progression of breast and prostate cancers have been associated with NF- κ B activation. DADS had an IC-50 value of 40 μM whereas MDA-MB-231 and MCF-7 cells had IC-50 values of 6 and 4 μM , respectively. PC3 cells were administered with DADS/quercetin, which significantly reduced the expression of NF- κ B, IKK α , and IKK β . This suggests that DADS or quercetin blocks the expression of nuclear factor kappa-B in androgen-independent prostate cancer cells (Arunakaran et al., 2013).

3 BIOAVAILABILITY AND PHARMACOKINETIC PROFILE OF DALLYL DISULFIDE

A comprehensive investigation of DADS pharmacokinetics profiles was conducted by orally administering a 200 mg/kg dose to rats. Allylmethyl sulfide (AMS), allylmercaptan (AM), allyl methyl sulfone, and allyl methyl sulfoxide were recognized as

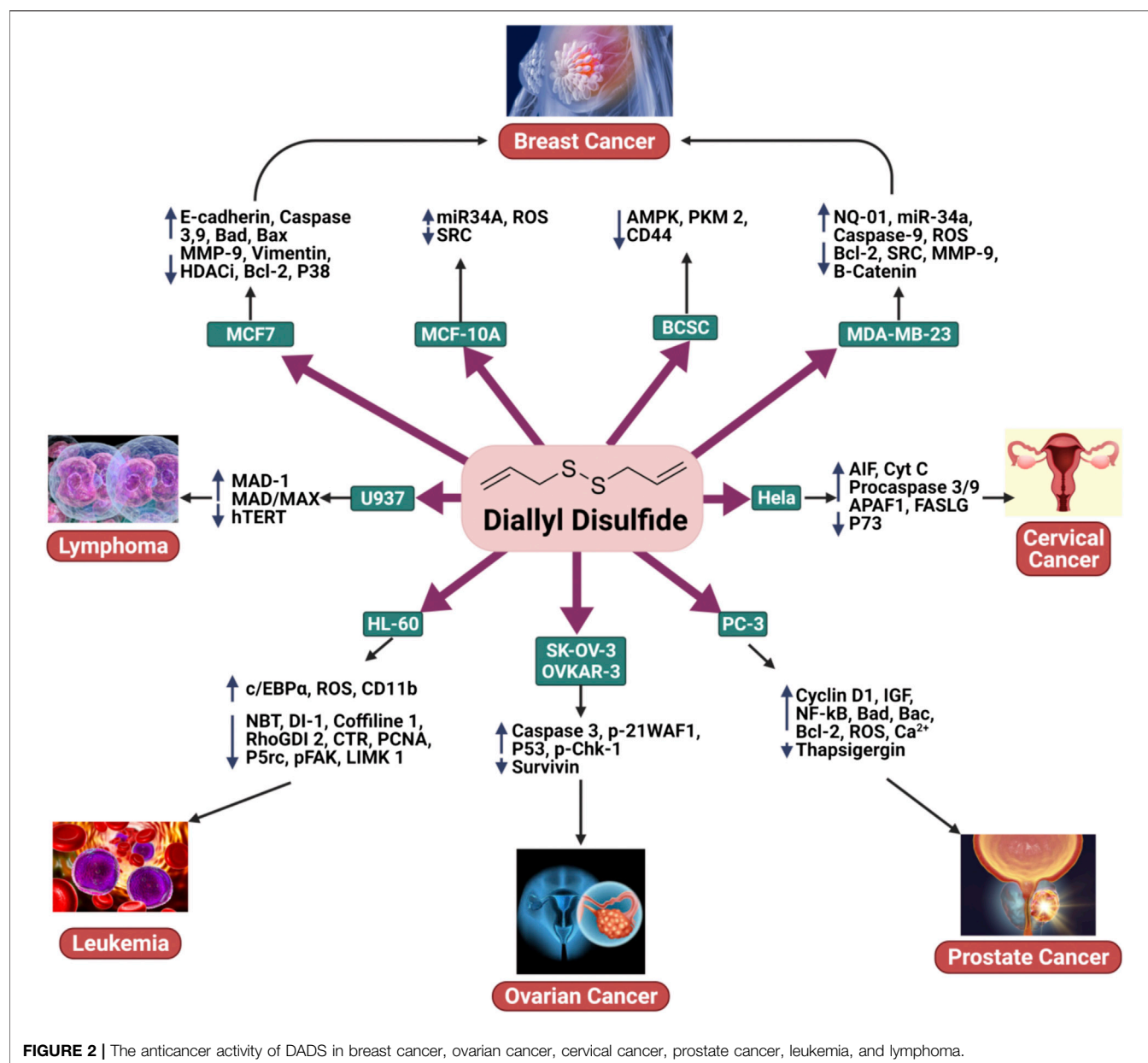


FIGURE 2 | The anticancer activity of DADS in breast cancer, ovarian cancer, cervical cancer, prostate cancer, leukemia, and lymphoma.

DADS metabolites in the plasma, stomach, urine, and liver of rats (Zhang et al., 2020). When the prepared garlic was consumed, the alliinase enzyme was activated, accelerating the transformation of alliin to allicin, an unstable metabolite. The decomposition of allicin leads to the formation of organic diallyl polysulfides such as diallyl sulfide (DAS) and DADS (Bradley et al., 2016; Yamaguchi and Kumagai, 2019; He et al., 2021). In the human body, DADS degrades quickly, metabolizing into different metabolites, such as diallyl thiosulphinate (DADSO), allylmercaptan (AM), allylmethyl sulfoxide (AMSO), allylmethyl sulfide (AMS), and allylmethyl sulfone (AMSO₂). The presence of DADS has been identified in the breath of human subjects following the consumption of garlic. DADS could not be identified in the urine of a volunteer after the oral intake of 1–3 g

of garlic powder; this was because DADS cannot easily reach μM -level concentrations *in vivo* (Alma et al., 2014; He et al., 2021). Similarly, allicin is rapidly removed from circulation after intravenous injections as it is converted into secondary metabolites such as DADS, 2-ethenyl-4H-1,3-dithiin, and E-ajoene (Jacob and Anwar, 2008; Ansary et al., 2020).

For enteric tablets, the allicin, which would eventually metabolized to DADS, various bioavailability were found ranging from 36% to 104%. This was reduced to 22%–57% when consumed with a high-protein meal. Nonenteric tablets gave high bioavailability (80%–111%), while garlic powder capsules gave 26%–109% bioavailability, whatever the meal type is Allicin rapidly disappears from circulation after iv injection, suggesting that it is transformed into secondary products. (Zhang et al., 2020).

Yamaguchi and Kumagai, (2019) found in their animal studies that alliin was absorbed primarily from the intestine *via* the amino acid transporter for cysteine. The split products of alliin appeared in the circulation 20 min after the administration of alliin by gastric intubation. These investigators concluded that splitting of alliin would take place in the intestinal cells by the action of an alliinase (or C-S-lyase)-like enzyme. The sulfides derived from alliin are known to be absorbed very fast from the intestine, which can be attributed to chemopreventive potential of this molecule (Ariga and Seki, 2006). The bioavailability of OSCs is high in animal subjects treated with aqueous garlic extracts (98% in liver, 103% in blood plasma, and 87% in kidneys for rats, mice, and dogs, respectively). It was estimated that 1 g of ingested garlic will biosynthesize 2.5 mg of alliin, 60 µg of SAC, 1,000 ± 100 µg of DATS, and 570 ± 40 µg of DADS (Gao et al., 2013).

The bioactivity of Allium is mainly attributed to the allyl derivatives that showed *in vivo* anticarcinogenic activity in various tissues. For instance, in garlic extracts, OSCs are mainly found in allyl and methyl forms (Thompson, 2014; Ramirez et al., 2017). These clearly demonstrates that the significant amount of these molecules can contribute to anticancer properties of DADS.

DADS was determined to have a half-life of less than 1 h in isolated rat livers. Four metabolites of DADS, AMS, AM, AMSO₂, and AMSO, were determined to have half-lives ($T_{1/2}$) of 6.78, 4.39, 8.64, and 7.16 h, respectively. AMS, AM, AMSO₂, and AMSO were found to have the peak concentrations (C_{max}) of 8, 8, 1,440, and 376 µM, respectively, suggesting that it is possible to achieve effective therapeutic concentrations of these active metabolites. DADS was shown to be quickly absorbed, with the peak concentrations observed 90 min after it was administered. After 2 h, 70% of the radioactivity was still detectable in the cytosol of liver cells, 80% of which was metabolized into sulfides while only 8% as remained as 3S-DADS. Within 2–3 h, DATS, AMDS, DADS, and DAS reached their maxima while the rate of increase of the other compounds was slower (Haina Wang, 2013).

The RBCs of humans convert the organic polysulfides that are derived from garlic into H₂S, an endogenous cardio-protective vascular cell-signaling molecule. Increasing numbers of sulfur-tethering atoms and substituents of allyl accelerate the production of H₂S from the organic polysulfides. Hydropolysulfide (RSnH) is a critical intermediate in the production of H₂S; RSnH is formed when polysulfides that are allyl-substituted undergo nucleophilic substitution at the α-carbon of the allyl substituent. Nucleophilic substitution takes place at the sulfur atom of the organic polysulfides, yielding H₂S and RSnH. H₂S is also released when the intact aorta rings process the garlic-derived organic polysulfides under physiologically relevant oxygen levels (Benavides et al., 2007).

The behavior of drug release in different pH environments, such as the intracellular lysosome (pH 4.5) and the cellular exterior (pH 7.4), was investigated. The profile of the regulated release of DADS from solid lipid nanoparticles (SNL) was examined. Under these conditions, a greater DADS release rate was observed at lower pHs. Due to the presence of the pair of sulfide groups, DADS acts as both an alkaline and a weak

acid and is more soluble at lower pHs. As a result, DADS encapsulated within SLN were more likely to be released at lower pH. Drug release in a more favorable acidic environment would result in a greater rate of release of DADS to the tumor cells; this is especially important in cell lines that are resistant, increasing the therapeutic potential of the delivery system (Talluri et al., 2017; Siddhartha et al., 2018).

4 CLINICAL STUDIES

According to the FDA's proof-based assessment procedure for scientific health appraisal, there is no clear evidence that links garlic to decreased risks of lung, breast, or gastric cancer. (Rivlin, 2009). Even though almost all experiments were observational, the number of investigations that were deemed to be scientifically relevant to this assessment was comparatively small. In addition, the number of subjects involved was relatively small, and no conclusive proof regarding a link between garlic consumption and esophageal, oral, colon, ovarian, prostate, renal, and laryngeal cell cancers has been recorded. Consequently, the relationship between cancer risk reduction and garlic remains unknown (Zuniga et al., 2019). Garlic appears to assist with a wide range of cancer symptoms, including those associated with pancreatic, lung, colon, gastric, colorectal, and breast cancers. In this context, a potential personalized diet with supplementary foods, including beneficial phytochemicals such as allyl sulfur compounds and alliin, could be a potential alleviative treatment. Patients in remission or undergoing therapy have been administered high dosages of alliin antioxidants (Table 3) (Ansary et al., 2020).

A 6-month eating plan that followed a Mediterranean-style diet was found to increase the intake of anti-inflammatory ingredients such as garlic among the survivors of breast cancer (Zuniga et al., 2019). Another experiment revealed that taking 200 mg capsules or 1 mg of garlic oil twice a day decreased progressive gastric lesions (You et al., 2006). Similar outcomes were observed when the same doses of garlic supplementations were administered over 7.3 years. In addition, long-term garlic intake, such as garlic pills or garlic mixed with vitamins reduced cancer risk (Ma et al., 2012), mortality rate (Li et al., 2019), and precancerous gastric lesions (Gail and You, 2006). A garlic treatment of two capsules twice a day for 7.3 years improved mild folate insufficiency and enhanced serum folate in individuals who were experiencing gastric lesions in rural Chinese communities (Wang et al., 2009). In addition, consuming 3.65 kg of garlic supplements per year for 2 years was linked to a lower incidence of colorectal adenoma, a precursor to colorectal cancer (CRC) (Table 3) (Jin et al., 2013; Gatt et al., 2015; Dreher, 2018; Wu et al., 2019). Several theories have been proposed to explain the chemopreventive benefits of garlic, including the suppression of the formation of DNA adducts, the inhibition of mutagenesis by limiting metabolism, the scavenging of free radicals, or the lowering of cell growth and tumor development (Jin et al., 2013; Charron et al., 2015). In another study, cancer patients were asked to follow either the remission support diet (RD; for the patients in remission) or the

TABLE 3 | Clinical studies on garlic constituents in cancer prevention and intervention.

Subjects	Types of study	Population of study	No. of patients	Intervention	Key findings	References
Breast cancer patient	Randomized intervention trial	United States	153	39.0%–69.5% garlic diet	Improved adherence to a Mediterranean style	Zuniga et al. (2019)
Individuals with gastric lesion	Factorial, double-blind, placebo-controlled trial	China	4,326	AGE 400 mg	Reduction of burden of gastric cancer in high risk areas	Gail and You, (2006)
Gastric cancer patient	Factorial, double-blind, placebo-controlled trial	China	3,411	4 capsules/day	Elevated concentration of serum folate	Wang et al. (2009)
Colorectal cancer patient	Comparison based study	Germany	57,560	One bulb/day	Condensed colorectal adenoma risk	Dreher, (2018)
Healthy adults	Case-control	China	966 men and 700 women	—	Condensed colorectal adenoma risk	Wu et al. (2019)
Lung cancer patient and healthy adults	Case-control	China	5,967	garlic compounds 33.4 g per week	Chemopreventive effect	Jin et al. (2013)
Hematological patients	Double-blind, placebo-controlled trial	Israel	95	900 mg/day	No significant effects in the entire cohort	Gatt et al. (2015)
Healthy adults	Randomized crossover feeding trial	United States	17	—	Activated genes correlated to apoptosis, immunity, and xenobiotic metabolism	Charron et al. (2015)

treatment support diet (TD; for the patients undergoing chemotherapy) over 3–9 weeks. The diets were low in fat and glucose and high in plant proteins; however, the TD group had an extra 0.5 protein servings. Additional quantities of tomato, rice bran, garlic, kale, pineapples, onion, blueberry, turmeric powder, and/or shiitake were included in daily meals based on clinical studies. The TD had a higher estimated daily consumption of quercetin, plant fat, allicin, onion, protein, and garlic than the RD. Both groups experienced an elevated consumption of vitamin A, C, and E, as well as a decreased consumption of the D-dimer relative to baseline diets. TD showed a greater impulse in cytotoxicity and increased albumin while RD showed reduced D-ROMS (Lee et al., 2015).

5 CONCLUSION AND FUTURE RECOMMENDATIONS

Garlic, a widely consumed spice of the genus *Allium*, has been found to contain various organosulfur components. DADS has received attention in cancer prevention research as a natural product with potent anticancer properties. This review aims to provide an inclusive evaluation of clinical and preclinical research on the chemopreventive and anticancer effects of DADS. Toxicity and pharmacokinetic investigations of DADS were also included. The potential of this phytochemical as an anti-cancer agent has been supported by many *in vitro* and *in vivo* investigations. Pharmacokinetic investigations revealed that this chemical has high bioavailability in a variety of tissues. Injections are the most common delivery method in animal experiments, but clinical experiments have focused on oral ingestion. Future animal studies should more efficiently mimic the conditions of clinical trials conditions to obtain a better understanding of the actual

anticancer effectiveness of DADS. The bulk of the literature discussed in this review focuses on preclinical investigations; however, it also covers clinical tests conducted on DADS and its biogenic precursors. These investigations proposed several mechanistic pathways for DADS' anticancer effects, such as invasion, migration, metastasis, cell cycle arrest, oxidative stress, and cell death. Many *in vitro* investigations have shown that DADS induces several distinct anticancer activities across a variety of cancer subtypes. More *in vivo* research is required to provide support for these mechanisms. Garlic was also used in several trials; however, this review recommends concentrating on DADS due to its potency. Pure DADS should be studied in more detail to completely understand its anticancer characteristics, especially since several investigations have proposed conflicting mechanisms. More *in vivo* studies must be conducted to elucidate the true mechanisms and the target biomolecules of DADS, while also identifying biomarkers that can measure the effectiveness of DADS in anticancer therapy. The literature suggests that DADS could be a promising agent for future natural chemotherapy and that it has significant potential as a safe and efficacious natural remedy to cancer.

AUTHOR CONTRIBUTIONS

SM, RD, TE, and PW conceptualized and designed the manuscript, participating in drafting the article and/or acquisition of data, and/or analysis and interpretation of data; RL, NE-T, FI, RS, IA, and FN prepared the figures and tables. TE, KC, FA, DC, RC, and PW wrote, edited and revised the manuscript critically. TE and PW revised the final written. All authors critically revised the manuscript concerning intellectual content and approved the final manuscript.

REFERENCES

- Agassi, S. F. T., Yeh, T. M., Chang, C. D., Hsu, J. L., and Shih, W. L. (2020). Potentiation of differentiation and apoptosis in a human promyelocytic leukemia cell line by garlic essential oil and its organosulfur compounds. *Anticancer Res.* 40, 6345–6354. doi:10.21873/anticancer.14655
- Ahmed, O., and Ahmed, R. (2015). Anti-proliferative and apoptotic efficacy of diallyl disulfide on Ehrlich ascites carcinoma. *Hepatology Res.* 1, 67. doi:10.4103/2394-5079.157602
- Alma, E., Eken, A., Ercil, H., Yelsel, K., and Daglioglu, N. (2014). The effect of garlic powder on human urinary cytokine excretion. *Urol. J.* 11, 1308–1315.
- Altonsy, M. O., Habib, T. N., and Andrews, S. C. (2012). Diallyl disulfide-induced apoptosis in a breast-cancer cell line (MCF-7) may be caused by inhibition of histone deacetylation. *Nutr. Cancer* 64, 1251–1260. doi:10.1080/01635581.2012.721156
- An, X., Zhang, X., Yao, H., Li, H., and Ren, J. (2015). Effects of diallyl disulfide in elephant garlic extract on breast cancer cell apoptosis in mitochondrial pathway. *J. Food Nutr. Res. (Newark)*. 3, 196–201. doi:10.12691/jfnr-3-3-11
- Ansari, I. A., Ahmad, A., Imran, M. A., Saeed, M., and Ahmad, I. (2020). Organosulphur compounds induce apoptosis and cell cycle arrest in cervical cancer cells via downregulation of HPV E6 and E7 oncogenes. *Anticancer Agents Med. Chem.* 21, 393–405. doi:10.2174/1871520620999200818154456
- Ansary, J., Forbes-Hernández, T. Y., Gil, E., Cianciosi, D., Zhang, J., Elempuru-Zabaleta, M., et al. (2020). Potential health benefit of garlic based on human intervention studies: A brief overview. *Antioxidants* 9, E619–E635. doi:10.3390/antiox9070619
- Anwanwan, D., Singh, S. K., Singh, S., Saikam, V., and Singh, R. (2020). Challenges in liver cancer and possible treatment approaches. *Biochim. Biophys. Acta. Rev. Cancer*, 1873, 188314. doi:10.1016/j.bbcan.2019.188314
- Aquilano, K., Filomeni, G., Baldelli, S., Piccirillo, S., De Martino, A., Rotilio, G., et al. (2007). Neuronal nitric oxide synthase protects neuroblastoma cells from oxidative stress mediated by garlic derivatives. *J. Neurochem.* 101, 1327–1337. doi:10.1111/j.1471-4159.2006.04431.x
- Aquilano, K., Vigilanza, P., Filomeni, G., Rotilio, G., and Ciriolo, M. R. (2010). Tau dephosphorylation and microfilaments disruption are upstream events of the anti-proliferative effects of DADS in SH-SY5Y cells. *J. Cell. Mol. Med.* 14, 564–577. doi:10.1111/j.1582-4934.2008.00588.x
- Ariga, T., and Seki, T. (2006). Antithrombotic and anticancer effects of garlic-derived sulfur compounds: A review. *BioFactors* 26, 93–103. doi:10.1002/biof.5520260201
- Arunakaran, J., Arunkumar, R., Elumalai, P., and Senthilkumar, K. (2013). Impact of quercetin, diallyl disulfide and nimbolide on the regulation of nuclear factor kappa B expression in prostate and breast cancer cell lines. *Nat. Prod. Chem. Res.* 1. doi:10.4172/2329-6836.1000115
- Arunkumar, R., Sharmila, G., Elumalai, P., Senthilkumar, K., Banudevi, S., Gunadharini, D. N., et al. (2012). Effect of diallyl disulfide on insulin-like growth factor signaling molecules involved in cell survival and proliferation of human prostate cancer cells *in vitro* and *in silico* approach through docking analysis. *Phytomedicine*. 19, 912–923. doi:10.1016/j.phymed.2012.04.009
- Bauer, D., Mazzio, E., Soliman, K. F., Taka, E., Oriaku, E., Womble, T., et al. (2014). Diallyl disulfide inhibits TNF α -induced CCL2 release by MDA-MB-231 cells. *Anticancer Res.* 34, 2763–2770.
- Bauer, D., Redmon, N., Mazzio, E., Taka, E., Reuben, J. S., Day, A., et al. (2015). Diallyl disulfide inhibits TNF α induced CCL2 release through MAPK/ERK and NF-Kappa-B signaling. *Cytokine* 75, 117–126. doi:10.1016/j.cyt.2014.12.007
- Benavides, G. A., Squadrito, G. L., Mills, R. W., Patel, H. D., Isbell, T. S., Patel, R. P., et al. (2007). Hydrogen sulfide mediates the vasoactivity of garlic. *Proc. Natl. Acad. Sci. U. S. A.* 104, 17977–17982. doi:10.1073/pnas.0705710104
- Bigby, J. (1988). Harrison's principles of internal medicine. *Arch. Dermatol.* 124, 287. doi:10.1001/archderm.1988.01670020093028
- Bo, S., Hui, H., Li, W., Hui, L., Hong, X., Lin, D., et al. (2014). Chk1, but not Chk2, is responsible for G2/M phase arrest induced by diallyl disulfide in human gastric cancer BGC823 cells. *Food Chem. Toxicol.* 68, 61–70. doi:10.1016/j.fct.2014.03.007
- Bo, S., Jian, S., Ying, S., Fang, L., Hong, X., Yan-Hua, M., et al. (2016). Diallyl disulfide suppresses epithelial-mesenchymal transition, invasion and proliferation by downregulation of LIMK1 in gastric cancer. *Oncotarget* 7, 10498–10512. doi:10.18632/oncotarget.7252
- Bradley, J. M., Organ, C. L., and Lefer, D. J. (2016). Garlic-derived organic polysulfides and myocardial protection. *J. Nutr.* 146, 403S–409S. doi:10.3945/jn.114.208066
- Brennan, S. F., Cantwell, M. M., Cardwell, C. R., Velentzis, L. S., and Woodside, J. V. (2010). Dietary patterns and breast cancer risk: A systematic review and meta-analysis. *Am. J. Clin. Nutr.* 91, 1294–1302. doi:10.3945/ajcn.2009.28796
- Casari, A., Chester, J., and Pellacani, G. (2018). Actinic keratosis and non-invasive diagnostic techniques: An update. *Biomedicine* 6, E8. doi:10.3390/biomedicine6010008
- Charron, C. S., Dawson, H. D., Albaugh, G. P., Solverson, P. M., Vinyard, B. T., Solano-Aguilar, G. I., et al. (2015). A single meal containing raw, crushed garlic influences expression of immunity- and cancer-related genes in whole blood of humans. *J. Nutr.* 145, 2448–2455. doi:10.3945/jn.115.215392
- Chen, C. Y., Huang, C. F., Tseng, Y. T., and Kuo, S. Y. (2012). Diallyl disulfide induces Ca²⁺ mobilization in human colon cancer cell line SW480. *Arch. Toxicol.* 86, 231–238. doi:10.1007/s00204-011-0748-4
- Chen, W. C., Hsu, S. S., Chou, C. T., Kuo, C. C., Huang, J. K., Fang, Y. C., et al. (2011). Effect of diallyl disulfide on Ca²⁺ movement and viability in PC3 human prostate cancer cells. *Toxicol. Vitro*. 25, 636–643. doi:10.1016/j.tiv.2010.12.015
- Chen, X. X., Liu, X. W., Zhou, Z. G., Chen, X. Y., Li, L. D., Xiong, T., et al. (2016). Diallyl disulfide inhibits invasion and metastasis of MCF-7 breast cancer cells *in vitro* by down-regulating p38 activity. *Nan Fang. Yi Ke Da Xue Xue Bao* 36, 814–818.
- Choromanska, A., Kulbacka, J., Saczko, J., and Surowiak, P. (2020). Effect of diallyl disulfide and garlic oil on different human astrocytoma cell lines. *Biomed. Rep.* 13, 32–36. doi:10.3892/br.2020.1339
- Comprehensive, N., and Network, C. (2014). *Esophageal and esophagogastric junction*.
- Dabrowski, A., Abramowicz, K., and Zinkiewicz, K. (1998). Epidemiology of esophageal cancer. *Pol. Merkur. Lek.* 5, 145–172. doi:10.1007/978-1-4684-2442-3_7
- Das, A., Banik, N. L., and Ray, S. K. (2007). Garlic compounds generate reactive oxygen species leading to activation of stress kinases and cysteine proteases for apoptosis in human glioblastoma T98G and U87MG cells. *Cancer* 110, 1083–1095. doi:10.1002/cncr.22888
- Das, B., and Sinha, D. (2019). Diallyl disulfide suppresses the canonical Wnt signaling pathway and reverses the fibronectin-induced epithelial mesenchymal transition of A549 lung cancer cells. *Food Funct.* 10, 191–202. doi:10.1039/c8fo00246k
- Dasgupta, P., and Sengupta Bandyopadhyay, S. (2015). Role of diallyl disulfide-mediated cleavage of c-Myc and Sp-1 in the regulation of telomerase activity in human lymphoma cell line U937. *Nutrition* 31, 1031–1037. doi:10.1016/j.nut.2015.02.016
- De Greef, D., Barton, E. M., Sandberg, E. N., Croley, C. R., Pumarol, J., Wong, T. L., et al. (2021). Anticancer potential of garlic and its bioactive constituents: A systematic and comprehensive review. *Semin. Cancer Biol.* 73, 219–264. doi:10.1016/j.semcancer.2020.11.020
- Deschler, B., and Lübbert, M. (2008). Acute myeloid leukemia: Epidemiology and etiology. *Acute Leuk.* 47–56. doi:10.1007/978-3-540-72304-2_3
- Di, C., Sun, C., Li, H., Si, J., Zhang, H., Han, L., et al. (2015). Diallyl disulfide enhances carbon ion beams-induced apoptotic cell death in cervical cancer cells through regulating Tap73/ Δ Np73. *Cell Cycle* 14, 3725–3733. doi:10.1080/15384101.2015.1104438
- Didona, D., Paolino, G., Bottoni, U., and Cantisani, C. (2018). Non melanoma skin cancer pathogenesis overview. *Biomedicine* 6. doi:10.3390/biomedicine6010006
- Dixon, K., and Kopras, E. (2004). Genetic alterations and DNA repair in human carcinogenesis. *Semin. Cancer Biol.* 14, 441–448. doi:10.1016/j.semcancer.2004.06.007
- Dreher, M. L. (2018). Dietary patterns, whole plant foods, nutrients and phytochemicals in colorectal cancer prevention and management. *Diet. Patterns Whole Plant Foods Aging Dis.*, 521–555. doi:10.1007/978-3-319-59180-3_19
- Druesen, N., Pagniez, A., Mayeur, C., Thomas, M., Cherbuy, C., Duée, P. H., et al. (2004). Diallyl disulfide (DADS) increases histone acetylation and p21waf1/cip1 expression in human colon tumor cell lines. *Carcinogenesis* 25, 1227–1236. doi:10.1093/carcin/bgh123

- Druesne-Pecollo, N., Chaumontet, C., and Latino-Martel, P. (2008). Diallyl disulfide increases histone acetylation in colon cells *in vitro* and *in vivo*. *Nutr. Rev.* 66, S39–S41. doi:10.1111/j.1753-4887.2008.00066.x
- Elmore, S. (2007). Apoptosis: A review of programmed cell death. *Toxicol. Pathol.* 35, 495–516. doi:10.1080/01926230701320337
- Elumalai, P., Gunadharini, D. N., Senthilkumar, K., Banudevi, S., Arunkumar, R., Benson, C. S., et al. (2012). Induction of apoptosis in human breast cancer cells by nimbolide through extrinsic and intrinsic pathway. *Toxicol. Lett.* 215, 131–142. doi:10.1016/j.toxlet.2012.10.008
- Fan, Z. L., Qi, Z. H., and Xie, Y. (2006). Effect of diallyl disulfide on the expression and secretion of VEGF in HL-60 cells. *Zhonghua Xue Ye Xue Za Zhi* 27, 626–629.
- Feller, L. L., Khammissa, R. R. A. G., Kramer, B. B., and Lemmer, J. J. (2013). Oral squamous cell carcinoma in relation to field precancerisation: Pathobiology. *Cancer Cell Int.* 13, 31. doi:10.1186/1475-2867-13-31
- Feng, C., Luo, Y., Nian, Y., Liu, D., Yin, X., Wu, J., et al. (2017). Diallyl disulfide suppresses the inflammation and apoptosis resistance induced by DCA through ROS and the NF- κ B signaling pathway in human Barrett's epithelial cells. *Inflammation* 40, 818–831. doi:10.1007/s10753-017-0526-4
- Fleischauer, A. T., and Arab, L. (2001). Garlic and cancer: A critical review of the epidemiologic literature. *J. Nutr.* 131, 1032S–1040S. doi:10.1093/jn/131.3.1032s
- Fulda, S., and Debatin, K. M. (2006). Extrinsic versus intrinsic apoptosis pathways in anticancer chemotherapy. *Oncogene* 25, 4798–4811. doi:10.1038/sj.onc.1209608
- Gail, M. H., and You, W. C. (2006). A factorial trial including garlic supplements assesses effect in reducing precancerous gastric lesions. *J. Nutr.* 136, 813S–815S. doi:10.1093/jn/136.3.813s
- Gao, S., Basu, S., Yang, G., Deb, A., and Hu, M. (2013). Oral bioavailability challenges of natural products used in cancer chemoprevention. *Prog. Chem.* 25, 1553–1574.
- Gatt, M. E., Strahilevitz, J., Sharon, N., Lavie, D., Goldschmidt, N., Kalish, Y., et al. (2015). A randomized controlled study to determine the efficacy of garlic compounds in patients with hematological malignancies at risk for chemotherapy-related febrile neutropenia. *Integr. Cancer Ther.* 14, 428–435. doi:10.1177/1534735415588928
- Globocan, M. (2020). *New Global Cancer*, 1.
- Greenwell, M., and Rahman, P. K. S. M. (2015). Medicinal plants: Their use in anticancer treatment. *Int. J. Pharm. Sci. Res.* 6, 4103–4112. doi:10.13040/IJPSR.0975-8232.6(10).4103-12
- Haberkorn, U. (2007). What is cancer? *Adv. Nucl. Oncol.* 2007, 1–16. doi:10.3109/9781420091380-2
- Haina Wang, X. J. (2013). Drug metabolism and pharmacokinetics of organosulfur compounds from garlic. *J. Drug Metab. Toxicol.* 04. doi:10.4172/2157-7609.1000159
- Hasan, H. F., Abdel-Hamid, G. R., and Ebrahim, S. I. (2020). Antioxidant and anti-inflammatory effects of diallyl disulfide on hepatotoxicity induced by cyclophosphamide in rats. *Nat. Prod. Commun.* 15, 1934578X2096908. doi:10.1177/1934578X20969083
- He, H., Ma, Y., Huang, H., Huang, C., Chen, Z., Chen, D., et al. (2021). A comprehensive understanding about the pharmacological effect of diallyl disulfide other than its anti-carcinogenic activities. *Eur. J. Pharmacol.* 893, 173803. doi:10.1016/j.ejphar.2020.173803
- Huang, J., Yang, B., Xiang, T., Peng, W., Qiu, Z., Wan, J., et al. (2015). Diallyl disulfide inhibits growth and metastatic potential of human triple-negative breast cancer cells through inactivation of the β -catenin signaling pathway. *Mol. Nutr. Food Res.* 59, 1063–1075. doi:10.1002/mnfr.201400668
- Huang, Y. S., Xie, N., Su, Q., Su, J., Huang, C., and Liao, Q. J. (2011). Diallyl disulfide inhibits the proliferation of HT-29 human colon cancer cells by inducing differentially expressed genes. *Mol. Med. Rep.* 4, 553–559. doi:10.3892/mmr.2011.453
- Islam, M. R., Islam, F., Nafady, M. H., Akter, M., Mitra, S., Das, R., et al. (2022). Natural small molecules in breast cancer treatment: Understandings from a therapeutic viewpoint. *Molecules* 27, 2165. doi:10.3390/molecules27072165
- Jacob, C., and Anwar, A. (2008). The chemistry behind redox regulation with a focus on sulphur redox systems. *Physiol. Plant.* 133, 469–480. doi:10.1111/j.1399-3054.2008.01080.x
- Jin, Z. Y., Wu, M., Han, R. Q., Zhang, X. F., Wang, X. S., Liu, A. M., et al. (2013). Raw garlic consumption as a protective factor for lung cancer, a population-based case-control study in a Chinese population. *Cancer Prev. Res.* 6, 711–718. doi:10.1158/1940-6207.CAPR-13-0015
- Jo, H. J., Song, J. D., Kim, K. M., Cho, Y. H., Kim, K. H., and Park, Y. C. (2008). Diallyl disulfide induces reversible G2/M phase arrest on a p53-independent mechanism in human colon cancer HCT-116 cells. *Oncol. Rep.* 19, 275–280. doi:10.3892/or.19.1.275
- Kamangar, F., Chow, W. H., Abnet, C., and Dawsey, M. (2009). Environmental causes of esophageal cancer. *Gastroenterol. Clin. North Am.* 38, 27–57. doi:10.1016/j.gtc.2009.01.004
- Karmakar, S., Banik, N. L., Patel, S. J., and Ray, S. K. (2007). Garlic compounds induced calpain and intrinsic caspase cascade for apoptosis in human malignant neuroblastoma SH-SY5Y cells. *Apoptosis* 12, 671–684. doi:10.1007/s10495-006-0024-x
- Kim, H. J., Kang, S., Kim, D. Y., You, S., Park, D., Oh, S. C., et al. (2019). Diallyl disulfide (DADS) boosts TRAIL-Mediated apoptosis in colorectal cancer cells by inhibiting Bcl-2. *Food Chem. Toxicol.* 125, 354–360. doi:10.1016/j.fct.2019.01.023
- Kim, S. H., Lee, I. C., Baek, H. S., Shin, I. S., Moon, C., Bae, C. S., et al. (2014). Mechanism for the protective effect of diallyl disulfide against cyclophosphamide acute urotoxicity in rats. *Food Chem. Toxicol.* 64, 110–118. doi:10.1016/j.fct.2013.11.023
- Ko, J. W., Park, S. H., Shin, N. R., Shin, J. Y., Kim, J. W., Shin, I. S., et al. (2017). Protective effect and mechanism of action of diallyl disulfide against acetaminophen-induced acute hepatotoxicity. *Food Chem. Toxicol.* 109, 28–37. doi:10.1016/j.fct.2017.08.029
- Lai, K. C., Hsu, S. C., Kuo, C. L., Yang, J. S., Ma, C. Y., Lu, H. F., et al. (2013). Diallyl sulfide, diallyl disulfide, and diallyl trisulfide inhibit migration and invasion in human colon cancer colo 205 cells through the inhibition of matrix metalloproteinase-2, -7, and -9 expressions. *Environ. Toxicol.* 28, 479–488. doi:10.1002/tox.20737
- Lai, K. C., Kuo, C. L., Ho, H. C., Yang, J. S., Ma, C. Y., Lu, H. F., et al. (2012). Diallyl sulfide, diallyl disulfide and diallyl trisulfide affect drug resistant gene expression in colo 205 human colon cancer cells *in vitro* and *in vivo*. *Phytomedicine* 19, 625–630. doi:10.1016/j.phymed.2012.02.004
- Lathia, J. D., Heddleston, J. M., Venere, M., and Rich, J. N. (2011). Deadly teamwork: Neural cancer stem cells and the tumor microenvironment. *Cell Stem Cell* 8, 482–485. doi:10.1016/j.stem.2011.04.013
- Lee, G. Y., Lee, J. J., and Lee, S. M. (2015). Antioxidant and anticoagulant status were improved by personalized dietary intervention based on biochemical and clinical parameters in cancer patients. *Nutr. Cancer* 67, 1083–1092. doi:10.1080/01635581.2015.1073754
- Lee, I. C., Kim, S. H., Baek, H. S., Moon, C., Kang, S. S., Kim, S. H., et al. (2014). The involvement of Nrf2 in the protective effects of diallyl disulfide on carbon tetrachloride-induced hepatic oxidative damage and inflammatory response in rats. *Food Chem. Toxicol.* 63, 174–185. doi:10.1016/j.fct.2013.11.006
- Lee, J. E., Lee, R. A., Kim, K. H., and Lee, J. H. (2011a). Induction of apoptosis with diallyl disulfide in AGS gastric cancer cell line. *J. Korean Surg. Soc.* 81, 85–95. doi:10.4174/jkss.2011.81.2.85
- Lee, S. T., Li, Z., Wu, Z., Aau, M., Guan, P., Karuturi, R. K. M., et al. (2011b). Context-specific regulation of NF- κ B target gene expression by EZH2 in breast cancers. *Mol. Cell* 43, 798–810. doi:10.1016/j.molcel.2011.08.011
- Lei, H., Hemminki, K., Johansson, R., Altieri, A., Enquist, K., Henriksson, R., et al. (2008). PAI-1 -675 4G/5G polymorphism as a prognostic biomarker in breast cancer. *Breast Cancer Res. Treat.* 109, 165–175. doi:10.1007/s10549-007-9635-3
- Li, Q., Tang, Y., Qin, J., Yi, L., Yang, Y., Wang, J., et al. (2016). Subcellular localization of DJ-1 in human HL-60 leukemia cells in response to diallyl disulfide treatment. *Mol. Med. Rep.* 14, 4666–4672. doi:10.3892/mmr.2016.5831
- Li, W. Q., Zhang, J. Y., Ma, J. L., Li, Z. X., Zhang, L., Zhang, Y., et al. (2019). Effects of *Helicobacter pylori* treatment and vitamin and garlic supplementation on gastric cancer incidence and mortality: Follow-up of a randomized intervention trial. *BMJ* 366, 15016. doi:10.1136/bmj.15016
- Liang, D., Wu, H., Wong, M. W., and Huang, D. (2015). Diallyl trisulfide is a fast H₂S donor, but diallyl disulfide is a slow one: The reaction pathways and intermediates of glutathione with polysulfides. *Org. Lett.* 17, 4196–4199. doi:10.1021/acs.orglett.5b01962
- Liao, Q. J., Su, J., Zhou, X. T., Tang, H. L., Song, Y., and Su, Q. (2007). Inhibitory effect of diallyl disulfide on proliferation of human colon cancer cell line SW480 in nude mice. *Ai Zheng* 26, 828–832.

- Ling, H., He, J., Tan, H., Yi, L., Liu, F., Ji, X., et al. (2017). Identification of potential targets for differentiation in human leukemia cells induced by diallyl disulfide. *Int. J. Oncol.* 50, 697–707. doi:10.3892/ijo.2017.3839
- Ling, H., Ji, X., Lei, Y., Jia, Y., Liu, F., Xia, H., et al. (2020). Diallyl disulfide induces downregulation and inactivation of cofilin 1 differentiation via the Rac1/ROCK1/LIMK1 pathway in leukemia cells. *Int. J. Oncol.* 56, 772–782. doi:10.3892/ijo.2020.4968
- Ling, H., Lu, L. F., He, J., Xiao, G. H., Jiang, H., and Su, Q. (2014). Diallyl disulfide selectively causes checkpoint kinase-1 mediated G2/M arrest in human MGC803 gastric cancer cell line. *Oncol. Rep.* 32, 2274–2282. doi:10.3892/or.2014.3417
- Ling, H., Wen, L., Ji, X. X., Tang, Y. L., He, J., Tan, H., et al. (2010). Growth inhibitory effect and Chk1-dependent signaling involved in G 2/M arrest on human gastric cancer cells induced by diallyl disulfide. *Braz. J. Med. Biol. Res.* 43, 271–278. doi:10.1590/S0100-879X2010007500004
- Liu, R., Yang, Y. N., Yi, L., Qing, J., Li, Q. Y., Wang, W. S., et al. (2018). Diallyl disulfide effect on the invasion and migration ability of HL-60 cells with a high expression of DJ-1 in the nucleus through the suppression of the src signaling pathway. *Oncol. Lett.* 15, 6377–6385. doi:10.3892/ol.2018.8139
- Lu, H. F., Yang, J. S., Lin, Y. T., Tan, T. W., Ip, S. W., Li, Y. C., et al. (2007). Diallyl disulfide induced signal transducer and activator of transcription 1 expression in human colon cancer colo 205 cells using differential display RT-PCR. *Cancer Genomics Proteomics* 4, 93–97.
- Ma, J. L., Zhang, L., Brown, L. M., Li, J. Y., Shen, L., Pan, K. F., et al. (2012). Fifteen-year effects of helicobacter pylori, garlic, and vitamin treatments on gastric cancer incidence and mortality. *J. Natl. Cancer Inst.* 104, 488–492. doi:10.1093/jnci/djs003
- Marie Hardwick, J., and Soane, L. (2013). Multiple functions of BCL-2 family proteins. *Cold Spring Harb. Perspect. Biol.* 5, a008722. doi:10.1101/cshperspect.a008722
- Mikaili, P., Maadirad, S., Moloudizargari, M., Aghajanshakeri, S., and Sarahroodi, S. (2013). Therapeutic uses and pharmacological properties of garlic, shallot, and their biologically active compounds. *Iran. J. Basic Med. Sci.* 16, 1031–1048. doi:10.22038/ijbms.2013.1865
- Mitra, S., Chakraborty, A. J., Tareq, A. M., Emran, T. B., Nainu, F., Khushro, A., et al. (2022a). Impact of heavy metals on the environment and human health: Novel therapeutic insights to counter the toxicity. *J. King Saud Univ. - Sci.* 34, 101865. doi:10.1016/j.jksus.2022.101865
- Mitra, S., Lami, M. S., Ghosh, A., Das, R., Tallei, T. E., Fatimawali, et al. (2022b). Hormonal therapy for gynecological cancers: How far has science progressed toward clinical applications? *Cancers (Basel)* 14, 759. doi:10.3390/cancers14030759
- Mitra, S., Lami, M. S., Uddin, T. M., Das, R., Islam, F., Anjum, J., et al. (2022c). Prospective multifunctional roles and pharmacological potential of dietary flavonoid narirutin. *Biomed. Pharmacother.* 150, 112932. doi:10.1016/j.biopha.2022.112932
- Mitra, S., Rauf, A., Tareq, A. M., Jahan, S., Emran, T. B., Shahriar, T. G., et al. (2021). Potential health benefits of carotenoid lutein: An updated review. *Food Chem. Toxicol.* 154, 112328. doi:10.1016/j.fct.2021.112328
- Mitra, S., Sarker, J., Mojumder, A., Shabbir, T. B., Das, R., Emran, T. B., et al. (2022d). Genome editing and cancer: How far has research moved forward on CRISPR/Cas9? *Biomed. Pharmacother.* 150, 113011. doi:10.1016/j.biopha.2022.113011
- Mitra, S., Tareq, A. M., Das, R., Emran, T. B., Nainu, F., Chakraborty, A. J., et al. (2022e). Polyphenols: A first evidence in the synergism and bioactivities. *Food Rev. Int.* 1–23. doi:10.1080/87559129.2022.2026376
- Moding, E. J., Kastan, M. B., and Kirsch, D. G. (2013). Strategies for optimizing the response of cancer and normal tissues to radiation. *Nat. Rev. Drug Discov.* 12, 526–542. doi:10.1038/nrd4003
- Munari, C. C., De Oliveira, P. F., Campos, J. C. L., Martins, S. D. P. L., Da Costa, J. C., Bastos, J. K., et al. (2014). Antiproliferative activity of Solanum lycocarpum alkaloid extract and their constituents, solamargine and solasonine, in tumor cell lines. *J. Nat. Med.* 68, 236–241. doi:10.1007/s11418-013-0757-0
- Nkrumah-Elie, Y. M., Reuben, J. S., Hudson, A. M., Taka, E., Badisa, R., Ardley, T., et al. (2012). The attenuation of early benzo(a)pyrene-induced carcinogenic insults by diallyl disulfide (DADS) in MCF-10A cells. *Nutr. Cancer* 64, 1112–1121. doi:10.1080/01635581.2012.712738
- Nussbaumer, S., Bonnabry, P., Veuthey, J. L., and Fleury-Souverain, S. (2011). Analysis of anticancer drugs: A review. *Talanta* 85, 2265–2289. doi:10.1016/j.talanta.2011.08.034
- Odewumi, C., Latinwo, L. M., Badisa, V. L., Smith, S., Cobb Abdullah, A., Kent First, M., et al. (2019). Modulation of cadmium induced apoptotic, cancer and inflammation related cytokines by diallyl disulfide in rat liver cells. *Ann. Toxicol.* 1. doi:10.36959/736/633
- Odom, R. Y., Dansby, M. Y., Rollins-Hairston, A. M., Jackson, K. M., and Kirlin, W. G. (2009). Phytochemical induction of cell cycle arrest by glutathione oxidation and reversal by N-acetylcysteine in human colon carcinoma cells. *Nutr. Cancer* 61, 332–339. doi:10.1080/01635580802549982
- Omar, S. H., and Al-Wabel, N. A. (2010). Organosulfur compounds and possible mechanism of garlic in cancer. *Saudi Pharm. J.* 18, 51–58. doi:10.1016/j.jsps.2009.12.007
- Park, H. S., Kim, G. Y., Choi, I. W., Kim, N. D., Hwang, H. J., Choi, Y. W., et al. (2011). Inhibition of matrix metalloproteinase activities and tightening of tight junctions by diallyl disulfide in AGS human gastric carcinoma cells. *J. Food Sci.* 76, T105–T111. doi:10.1111/j.1750-3841.2011.02114.x
- Pinkerton, R. (2013). “Non-Hodgkin lymphoma,” in *Evidence-based pediatri. Oncol.* Third Ed., 88–104. doi:10.1002/9781118625309.ch10
- Rahman, M. M., Islam, F., Afsana Mim, S., Khan, M. S., Islam, M. R., Haque, M. A., et al. (2022). Multifunctional therapeutic approach of nanomedicines against inflammation in cancer and aging. *J. Nanomater.*, 1–19. doi:10.1155/2022/4217529
- Ramirez, D. A., Locatelli, D. A., González, R. E., Cavagnaro, P. F., and Camargo, A. B. (2017). Analytical methods for bioactive sulfur compounds in Allium: An integrated review and future directions. *J. Food Compos. Anal.* 61, 4–19. doi:10.1016/j.jfca.2016.09.012
- Rastegari, F., and Rafeian-Kopaei, M. (2016). Antioxidant supplements and cancer. *Immunopathol. Persa* 2.
- Rauf, A., Abu-Izneid, T., Khalil, A. A., Imran, M., Shah, Z. A., Bin Emran, T., et al. (2021). Berberine as a potential anticancer agent: A comprehensive review. *Molecules* 26, 7368. doi:10.3390/molecules26237368
- Rauf, A., Shariati, M. A., Imran, M., Bashir, K., Khan, S. A., Mitra, S., et al. (2022). Comprehensive review on naringenin and naringin polyphenols as a potent anticancer agent. *Environ. Sci. Pollut. Res. Int.* 29, 31025–31041. doi:10.1007/s11356-022-18754-6
- Redza-Dutordoir, M., and Averill-Bates, D. A. (2016). Activation of apoptosis signalling pathways by reactive oxygen species. *Biochim. Biophys. Acta* 1863, 2977–2992. doi:10.1016/j.bbamcr.2016.09.012
- Rivlin, R. S. (2009). Can garlic reduce risk of cancer? *Am. J. Clin. Nutr.* 89, 17–18. doi:10.3945/ajcn.2008.27181
- Sadjadi, A., Marjani, H., Semnani, S., and Nasseri-Moghaddam, S. (2010). Esophageal cancer in Iran: A review. *Middle East J. Cancer* 1, 5–14.
- Sánchez, A. R., Fernández, B. C., Raposo, C. G., and Castellanos, P. C. (2013). Ovarian cancer. *Med. - Programa Form. Médica Contin. Acreditado* 11, 1641–1648. doi:10.1016/S0304-5412(13)70518-3
- Saraf, A., Dubey, N., Dubey, N., and Sharma, M. (2021). Enhancement of cytotoxicity of diallyl disulfide toward colon cancer by Eudragit S100/PLGA nanoparticles. *J. Drug Deliv. Sci. Technol.* 64, 102580. doi:10.1016/j.jddst.2021.102580
- Saud, S. M., Li, W., Gray, Z., Matter, M. S., Colburn, N. H., Young, M. R., et al. (2016). Diallyl disulfide (DADS), a constituent of garlic, inactivates NF-κB and prevents colitis-induced colorectal cancer by inhibiting GSK-3β. *Cancer Prev. Res.* 9, 607–615. doi:10.1158/1940-6207.CAPR-16-0044
- Shamshirian, A., Alizadeh-Navaei, R., Shamshirian, A., Hedayatizadeh-Omran, A., Ghadimi, R., and Janbabai, G. (2018). Effect of garlic in gastric cancer prognosis: a systematic review and meta-analysis. *WCRJ* 5 (4), e1184.
- Shan, Y., Wei, Z., Tao, L., Wang, S., Zhang, F., Shen, C., et al. (2016). Prophylaxis of diallyl disulfide on skin carcinogenic model via p21-dependent Nrf2 stabilization. *Sci. Rep.* 6, 35676. doi:10.1038/srep35676
- Shin, D. Y., Kim, G. Y., Kim, J. I., Yoon, M. K., Kwon, T. K., Lee, S. J., et al. (2010). Anti-invasive activity of diallyl disulfide through tightening of tight junctions and inhibition of matrix metalloproteinase activities in LNCaP prostate cancer cells. *Toxicol. Vitro* 24, 1569–1576. doi:10.1016/j.tiv.2010.06.014
- Shin, D. Y., Kim, G. Y., Lee, J. H., Choi, B. T., Yoo, Y. H., and Choi, Y. H. (2012). Apoptosis induction of human prostate carcinoma DU145 cells by diallyl

- disulfide via modulation of JNK and PI3K/AKT signaling pathways. *Int. J. Mol. Sci.* 13, 14158–14171. doi:10.3390/ijms131114158
- Siddhartha, V. T., Pindiprolu, S. K. S., Chintamaneni, P. K., Tummala, S., and Nandha Kumar, S. (2018). RAGE receptor targeted bioconjugate lipid nanoparticles of diallyl disulfide for improved apoptotic activity in triple negative breast cancer: *In vitro* studies. *Artif. Cells Nanomed. Biotechnol.* 46, 387–397. doi:10.1080/21691401.2017.1313267
- Siegel, R. L., Miller, K. D., and Jemal, A. (2016). Cancer statistics, 2016. *Ca. Cancer J. Clin.* 66, 7–30. doi:10.3322/caac.21332
- Siegel, R. L., Miller, K. D., and Jemal, A. (2018). Cancer statistics, 2018. *Ca. Cancer J. Clin.* 68, 7–30. doi:10.3322/caac.21442
- Society, A. C. (2016). *Cancer Facts & Figures 2016*, 1–9. *Cancer Facts Fig.*
- Song, J. D., Lee, S. K., Kim, K. M., Park, S. E., Park, S. J., Kim, K. H., et al. (2009). Molecular mechanism of diallyl disulfide in cell cycle arrest and apoptosis in HCT-116 colon cancer cells. *J. Biochem. Mol. Toxicol.* 23, 71–79. doi:10.1002/jbt.20266
- Song, X., Yue, Z., Nie, L., Zhao, P., Zhu, K., and Wang, Q. (2021). Biological functions of diallyl disulfide, a garlic-derived natural organic sulfur compound. *Evid. Based. Complement. Altern. Med.* 2021, 5103626. doi:10.1155/2021/5103626
- Su, B. (2012). Diallyl disulfide increases histone acetylation and P21WAF1 expression in human gastric cancer cells *in vivo* and *in vitro*. *Biochem. Pharmacol.* 01. doi:10.4172/2167-0501.1000106
- Su, B., Jian, S. U., Zeng, Y., Ding, E., Liu, F., Tan, T., et al. (2018). Diallyl disulfide inhibits TGF- β 1-induced upregulation of Rac1 and β -catenin in epithelial-mesenchymal transition and tumor growth of gastric cancer. *Oncol. Rep.* 39, 2797–2806. doi:10.3892/or.2018.6345
- Su, B., Su, J., He, H., Wu, Y., Xia, H., Zeng, X., et al. (2015). Identification of potential targets for diallyl disulfide in human gastric cancer MGC-803 cells using proteomics approaches. *Oncol. Rep.* 33, 2484–2494. doi:10.3892/or.2015.3859
- Su, J., Zhou, Y., Pan, Z., Shi, L., Yang, J., Liao, A., et al. (2017). Downregulation of LIMK1-ADF/cofilin by DADS inhibits the migration and invasion of colon cancer. *Sci. Rep.* 7, 45624. doi:10.1038/srep45624
- Suangtarnmai, T., and Tanyong, D. I. (2016). Diallyl disulfide induces apoptosis and autophagy via mTOR pathway in myeloid leukemic cell line. *Tumour Biol.* 37, 10993–10999. doi:10.1007/s13277-016-4989-y
- Sujatha, P., Anantharaju, P. G., Veeresh, P. M., Dey, S., Bovilla, V. R., and Madhunapantula, S. V. (2017). Diallyl disulfide (DADS) retards the growth of breast cancer cells *in vitro* and *in vivo* through apoptosis induction. *Biomed. Pharmacol. J.* 10, 1619–1630. doi:10.13005/bpj/1273
- Sun, J., Mu, H., Yu, J., Li, L., Yan, H., Li, G., et al. (2019). Diallyl disulfide down-regulates calreticulin and promotes C/EBP α expression in differentiation of human leukaemia cells. *J. Cell. Mol. Med.* 23, 194–204. doi:10.1111/jcmm.13904
- Sung, H., Ferlay, J., Siegel, R. L., Laversanne, M., Soerjomataram, I., Jemal, A., et al. (2021). Global cancer statistics 2020: GLOBOCAN estimates of incidence and mortality worldwide for 36 cancers in 185 countries. *Ca. Cancer J. Clin.* 71, 209–249. doi:10.3322/caac.21660
- Sung, H., Ferlay, J., and Siegel, R. L., (2020). GLOBOCAN estimates of incidence and mortality worldwide for 36 cancers in 185 countries. *Glob. Cancer Stat.* 71. doi:10.3322/caac.21660
- Tait, S. W. G., and Green, D. R. (2010). Mitochondria and cell death: Outer membrane permeabilization and beyond. *Nat. Rev. Mol. Cell Biol.* 11, 621–632. doi:10.1038/nrm2952
- Talluri, S. V., Kuppusamy, G., Karri, V. V. S. R., Yamjala, K., Wadhwani, A., Madhunapantula, S. R. V., et al. (2017). Application of quality-by-design approach to optimize diallyl disulfide-loaded solid lipid nanoparticles. *Artif. Cells Nanomed. Biotechnol.* 45, 474–488. doi:10.3109/21691401.2016.1173046
- Tan, H., and Xiao-xia, W. J. (2011). *Growth inhibition and apoptosis of K562 cells induced by diallyl disulfide*. South China, Hengyang, Hunan 421001, China: Inst. Cancer Res.
- Tan, L., Zhang, M., Xia, L., Mei, H. Z., Zhi, Y., Li, J., et al. (2004). The initiation of G2/M checkpoint by diallyl disulfide requires the activation of p38 MAP kinase in HL-60 cells. *Zhonghua Xue Ye Xue Za Zhi* 25, 273–276.
- Tang, H., Kong, Y., Guo, J., Tang, Y., Xie, X., Yang, L., et al. (2013). Diallyl disulfide suppresses proliferation and induces apoptosis in human gastric cancer through Wnt-1 signaling pathway by up-regulation of miR-200b and miR-22. *Cancer Lett.* 340, 72–81. doi:10.1016/j.canlet.2013.06.027
- Thompson, A. K. (2014). Health-promoting properties of fruit and vegetables. *Fruit. Veg.*, 557–572. doi:10.1002/9781118653975.ch14
- Tsubura, A., Lai, Y.-C., Kuwata, M., Uehara, N., and Yoshizawa, K. (2012). Anticancer effects of garlic and garlic-derived compounds for breast cancer control. *Anticancer. Agents Med. Chem.* 11, 249–253. doi:10.2174/187152011795347441
- UICC (2020). *Globocan 2020: New global cancer data*, 5. New York, USA: Website.
- Van Den Heuvel-Eibrink, M. (2004). “Acute myeloid leukaemia,” in *Paediatr. Oncol.* Third Ed., 203–229. doi:10.1201/b13276-14
- Wang, X., Jiao, F., Wang, Q. W., Wang, J., Yang, K., Hu, R. R., et al. (2012). Aged black garlic extract induces inhibition of gastric cancer cell growth *in vitro* and *in vivo*. *Mol. Med. Rep.* 5, 66–72. doi:10.3892/mmr.2011.588
- Wang, Y., Zhang, L., Mosleh, R., Ma, J., Pan, K., Zhou, T., et al. (2009). Long-term garlic or micronutrient supplementation, but not anti-Helicobacter pylori therapy, increases serum folate or glutathione without affecting serum vitamin B-12 or homocysteine in a rural Chinese population. *J. Nutr.* 139, 106–112. doi:10.3945/jn.108.091389
- Wei, Z., Shan, Y., Tao, L., Liu, Y., Zhu, Z., Liu, Z., et al. (2017). Diallyl trisulfides, a natural histone deacetylase inhibitor, attenuate HIF-1 α synthesis, and decreases breast cancer metastasis. *Mol. Carcinog.* 56, 2317–2331. doi:10.1002/mc.22686
- Williams, M. M., Lee, L., Werfel, T., Joly, M. M. M., Hicks, D. J., Rahman, B., et al. (2018). Intrinsic apoptotic pathway activation increases response to anti-estrogens in luminal breast cancers. *Cell Death Dis.* 9, 21. doi:10.1038/s41419-017-0072-x
- Wu, P. P., Chung, H. W., Liu, K. C., Wu, R. S. C., Yang, J. S., Tang, N. Y., et al. (2011). Diallyl sulfide induces cell cycle arrest and apoptosis in HeLa human cervical cancer cells through the p53, caspase- and mitochondria-dependent pathways. *Int. J. Oncol.* 38, 1605–1613. doi:10.3892/ijo.2011.973
- Wu, X., Shi, J., Fang, W., Xia, G., Guo, X., Zhang, L., Yun, L., et al. (2019). Allium vegetables are associated with reduced risk of colorectal cancer: A hospital-based matched case-control study in China. *Asia. Pac. J. Clin. Oncol.* 15, e132–e141. doi:10.1111/ajco.13133
- Xia, L., Lin, J., Su, J., Oyang, L., Wang, H., Tan, S., et al. (2019). Diallyl disulfide inhibits colon cancer metastasis by suppressing Rac1-mediated epithelial-mesenchymal transition. *Oncotargets Ther.* 12, 5713–5728. doi:10.2147/OTT.S208738
- Xiao, X., Chen, B., Liu, X., Liu, P., Zheng, G., Ye, F., et al. (2014). Diallyl disulfide suppresses SRC/Ras/ERK signaling-mediated proliferation and metastasis in human breast cancer by up-regulating miR-34a. *PLoS One* 9, e112720. doi:10.1371/journal.pone.0112720
- Xie, X., Huang, X., Tang, H., Ye, F., Yang, L., Guo, X., et al. (2018). Diallyl disulfide inhibits breast cancer stem cell progression and glucose metabolism by targeting CD44/PKM2/AMPK signaling. *Curr. Cancer Drug Targets* 18, 592–599. doi:10.2174/1568009617666171024165657
- Xu, S., Huang, H., Tang, D., Xing, M., Zhao, Q., Li, J., et al. (2021). Diallyl disulfide attenuates ionizing radiation-induced migration and invasion by suppressing Nrf2 signaling in non-small-cell lung cancer. *Dose. Response.* 19, 15593258211033114. doi:10.1177/15593258211033114
- Yamaguchi, Y., and Kumagai, H. (2019). Characteristics, biosynthesis, decomposition, metabolism and functions of the garlic odour precursor, S-allyl-L-cysteine sulfoxide (Review). *Exp. Ther. Med.* doi:10.3892/etm.2019.8385
- Yang, J., Liu, X., Cao, S., Dong, X., Rao, S., and Cai, K. (2020). Understanding esophageal cancer: The challenges and opportunities for the next decade. *Front. Oncol.* 10, 1727. doi:10.3389/fonc.2020.01727
- Yang, J. S., Chen, G. W., Hsia, T. C., Ho, H. C., Ho, C. C., Lin, M. W., et al. (2009). Diallyl disulfide induces apoptosis in human colon cancer cell line (COLO 205) through the induction of reactive oxygen species, endoplasmic reticulum stress, caspases cascade and mitochondrial-dependent pathways. *Food Chem. Toxicol.* 47, 171–179. doi:10.1016/j.fct.2008.10.032
- Ye, X., and Yin, X. (2017). Effect of MEK-ERK signaling pathway on diallyl disulfide-induced autophagy in human leukemia K562 cells. *J. Leuk. Lymphoma* 26, 665–669. doi:10.3760/cma.j.issn.1009-9921.2017.11.007
- Yi, L., Ji, X. X., Tan, H., Lin, M., Tang, Y., Wen, L., et al. (2010). Role of Ras-related C3 botulinum toxin substrate 2 (Rac2), NADPH oxidase and reactive oxygen species in diallyl disulfide-induced apoptosis of human leukaemia HL-60 cells. *Clin. Exp. Pharmacol. Physiol.* 37, 1147–1153. doi:10.1111/j.1440-1681.2010.05444.x

- Yi, L., Shan, J., Chen, X., Li, G., Li, L., Tan, H., et al. (2016). Involvement of calreticulin in cell proliferation, invasion and differentiation in diallyl disulfide-treated HL-60 cells. *Oncol. Lett.* 12, 1861–1867. doi:10.3892/ol.2016.4850
- Yi, L., and Su, Q. (2013). Molecular mechanisms for the anti-cancer effects of diallyl disulfide. *Food Chem. Toxicol.* 57, 362–370. doi:10.1016/j.fct.2013.04.001
- Yin, X., Feng, C., Han, L., Ma, Y., Jiao, Y., Wang, J., et al. (2018). Diallyl disulfide inhibits the metastasis of type II esophageal-gastric junction adenocarcinoma cells via NF- κ B and PI3K/AKT signaling pathways *in vitro*. *Oncol. Rep.* 39, 784–794. doi:10.3892/or.2017.6113
- Yin, X., Zhang, J., Li, X., Liu, D., Feng, C., Liang, R., et al. (2014a). DADS suppresses human esophageal xenograft tumors through RAF/MEK/ERK and mitochondria-dependent pathways. *Int. J. Mol. Sci.* 15, 12422–12441. doi:10.3390/ijms150712422
- Yin, X., Zhang, R., Feng, C., Zhang, J., Liu, D., Xu, K., et al. (2014b). Diallyl disulfide induces G2/M arrest and promotes apoptosis through the p53/p21 and MEK-ERK pathways in human esophageal squamous cell carcinoma. *Oncol. Rep.* 32, 1748–1756. doi:10.3892/or.2014.3361
- You, W. C., Brown, L. M., Zhang, L., Li, J. Y., Jin, M. L., Chang, Y. S., et al. (2006). Randomized double-blind factorial trial of three treatments to reduce the prevalence of precancerous gastric lesions. *J. Natl. Cancer Inst.* 98, 974–983. doi:10.1093/jnci/djj264
- Yu, F. S., Yu, C. S., Lin, J. P., Chen, S. C., Lai, W. W., and Chung, J. G. (2005). Diallyl disulfide inhibits N-acetyltransferase activity and gene expression in human esophagus epidermoid carcinoma CE 81T/VGH cells. *Food Chem. Toxicol.* 43, 1029–1036. doi:10.1016/j.fct.2005.02.009
- Zhang, N., Wang, Y., Zhang, J., Liu, B., Li, G., Xin, S., et al. (2019a). Diallyl disulfide attenuates non-alcoholic steatohepatitis by suppressing key regulators of lipid metabolism, lipid peroxidation and inflammation in mice. *Mol. Med. Rep.* 20, 1363–1372. doi:10.3892/mmr.2019.10316
- Zhang, R., Shi, H., Ren, F., Liu, Z., and Ji, P. (2019b). Effects of diallyl disulfide on the proliferation and apoptosis of epithelial ovarian cancer cells by inducing G2/M arrest. *Zhongguo Yi Xue Ke Xue Yuan Xue Bao.* 41, 43–52. doi:10.3881/j.issn.1000-503X.10494
- Zhang, Y., Liu, X., Ruan, J., Zhuang, X., Zhang, X., and Li, Z. (2020). Phytochemicals of garlic: Promising candidates for cancer therapy. *Biomed. Pharmacother.* 123, 109730. doi:10.1016/j.biopha.2019.109730
- Zhou, Y., Li, Y., Zhou, T., Zheng, J., Li, S., and Li, H. B. (2016). Dietary natural products for prevention and treatment of liver cancer. *Nutrients* 8, 156. doi:10.3390/nu8030156
- Zhou, Z., Tang, M., Liu, Y., Zhang, Z., Lu, R., and Lu, J. (2017). Apigenin inhibits cell proliferation, migration, and invasion by targeting Akt in the A549 human lung cancer cell line. *Anticancer. Drugs* 28, 446–456. doi:10.1097/CAD.0000000000000479
- Zuniga, K. E., Parma, D. L., Muñoz, E., Spaniol, M., Wargovich, M., and Ramirez, A. G. (2019). Dietary intervention among breast cancer survivors increased adherence to a mediterranean-style, anti-inflammatory dietary pattern: The rx for better breast health randomized controlled trial. *Breast Cancer Res. Treat.* 173, 145–154. doi:10.1007/s10549-018-4982-9

Conflict of Interest: The authors declare that the research was conducted in the absence of any commercial or financial relationships that could be construed as a potential conflict of interest.

Publisher's Note: All claims expressed in this article are solely those of the authors and do not necessarily represent those of their affiliated organizations, or those of the publisher, the editors and the reviewers. Any product that may be evaluated in this article, or claim that may be made by its manufacturer, is not guaranteed or endorsed by the publisher.

Copyright © 2022 Mitra, Das, Emran, Labib, Noor-E-Tabassum, Islam, Sharma, Ahmad, Nainu, Chidambaram, Alhumaydhi, Chandran, Capasso and Wilairatana. This is an open-access article distributed under the terms of the Creative Commons Attribution License (CC BY). The use, distribution or reproduction in other forums is permitted, provided the original author(s) and the copyright owner(s) are credited and that the original publication in this journal is cited, in accordance with accepted academic practice. No use, distribution or reproduction is permitted which does not comply with these terms.



OPEN ACCESS

EDITED BY

Rajkumar S. Kalra,
Okinawa Institute of Science and
Technology Graduate University, Japan

REVIEWED BY

Wenliang Zhang,
The University of Hong Kong, China
Desi Shang,
Harbin Medical University, China
Ling Wang,
South China University of Technology,
China

*CORRESPONDENCE

Ruiqing Zheng,
rqzheng@csu.edu.cn
Xue Xu,
xuexu007@wust.edu.cn
Hongcai Shang,
shanghongcai@foxmail.com

[†]These authors have contributed equally
to this work

SPECIALTY SECTION

This article was submitted to
Pharmacology of Anti-Cancer Drugs,
a section of the journal
Frontiers in Pharmacology

RECEIVED 17 March 2022

ACCEPTED 19 July 2022

PUBLISHED 29 August 2022

CITATION

Wei X, Yang J, Li S, Li B, Chen M, Lu Y,
Wu X, Cheng Z, Zhang X, Chen Z,
Wang C, Wang E, Zheng R, Xu X and
Shang H (2022), TAIGET: A small-
molecule target identification and
annotation web server.
Front. Pharmacol. 13:898519.
doi: 10.3389/fphar.2022.898519

COPYRIGHT

© 2022 Wei, Yang, Li, Li, Chen, Lu, Wu,
Cheng, Zhang, Chen, Wang, Wang,
Zheng, Xu and Shang. This is an open-
access article distributed under the
terms of the [Creative Commons
Attribution License \(CC BY\)](https://creativecommons.org/licenses/by/4.0/). The use,
distribution or reproduction in other
forums is permitted, provided the
original author(s) and the copyright
owner(s) are credited and that the
original publication in this journal is
cited, in accordance with accepted
academic practice. No use, distribution
or reproduction is permitted which does
not comply with these terms.

TAIGET: A small-molecule target identification and annotation web server

Xuxu Wei^{1,2†}, Jiarui Yang^{3†}, Simin Li¹, Boyuan Li¹,
Mengzhen Chen¹, Yukang Lu¹, Xiang Wu¹, Zeyu Cheng¹,
Xiaoyu Zhang², Zhao Chen², Chunxia Wang², Edwin Wang⁴,
Ruiqing Zheng^{3*}, Xue Xu^{1*} and Hongcai Shang^{2*}

¹Key Laboratory of Occupational Hazard Identification and Control, Wuhan University of Science and Technology, Wuhan, China, ²Key Laboratory of Chinese Internal Medicine of MOE, Dongzhimen Hospital, Beijing University of Chinese Medicine, Beijing, China, ³School of Computer Science and Engineering, Central South University, Changsha, China, ⁴Cumming School of Medicine, University of Calgary, Calgary, AB, Canada

Background: Accurate target identification of small molecules and downstream target annotation are important in pharmaceutical research and drug development.

Methods: We present TAIGET, a friendly and easy to operate graphical web interface, which consists of a docking module based on AutoDock Vina and LeDock, a target screen module based on a Bayesian–Gaussian mixture model (BGMM), and a target annotation module derived from >14,000 cancer-related literature works.

Results: TAIGET produces binding poses by selecting ≤ 5 proteins at a time from the UniProt ID–PDB network and submitting ≤ 3 ligands at a time with the SMILES format. Once the identification process of binding poses is complete, TAIGET then screens potential targets based on the BGMM. In addition, three medical experts and 10 medical students curated associations among drugs, genes, gene regulation, cancer outcome phenotype, 2,170 cancer cell types, and 73 cancer types from the PubMed literature, with the aim to construct a target annotation module. A target-related PPI network can be visualized by an interactive interface.

Conclusion: This online tool significantly lowers the entry barrier of virtual identification of targets for users who are not experts in the technical aspects of virtual drug discovery. The web server is available free of charge at <http://www.taiget.cn/>.

KEYWORDS

target prediction, web server, target annotation, cancer, botanical drug

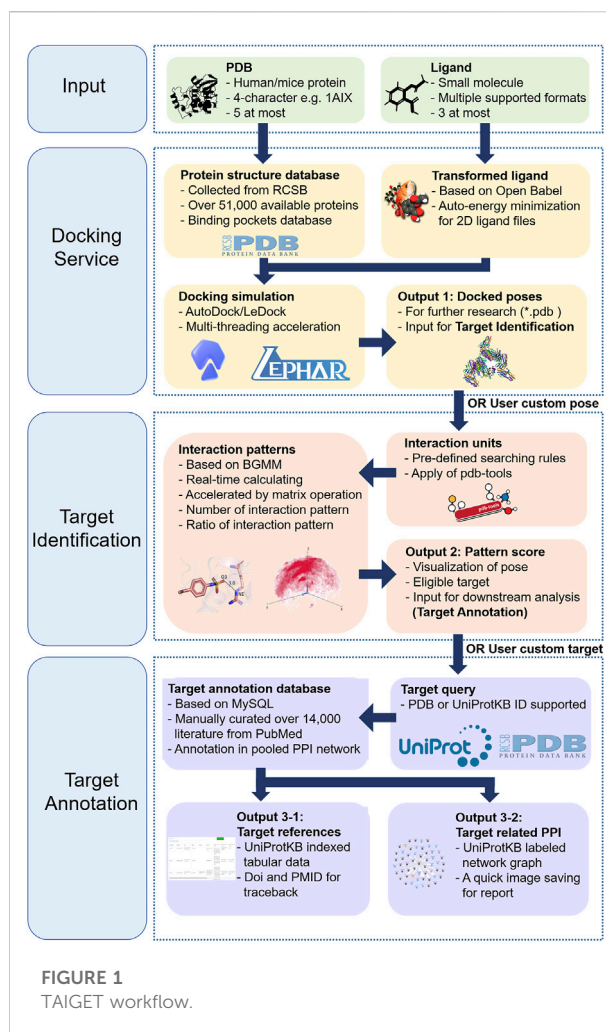
Key points

- TAIGET is a graphical web interface to identify potential targets of small molecules, which consists of a docking module, a target screen module, and a target annotation module.
- The target annotation module is constructed by text mining and manually curating >14,000 cancer-related literature works, which involves 73 cancer types and 2,170 cell types.
- TAIGET supports docking service in a mini-batch mode.

Instruction

A drug discovery process starts with identification of targets and clarification of mechanism of action of drugs, with the hope to win the battle of disease treatment (Vamathevan et al., 2019). Approaches for target identification in drug discovery include virtual and experimental screening. As one of the most widely used structure-based virtual screening approaches, molecular docking allows identifying the most likely target of a query ligand. There are many popular docking procedures, such as AutoDock, LeDock, Glide, GOLD, and DOCK (Lapillo et al., 2019; Shahid et al., 2021). To reduce scoring bias, Lee and Kim, (2020) constructed a web server for target prediction, by ranking scoring algorithms of GOLD, AutoDock Vina, and LeDock. To assist identification of putative targets for herbal ingredients, Zhang et al. (2019) used a reverse docking approach to predict ligand–target interactions. When Ma and Zou, (2021) developed an inverse docking procedure using the DOCK algorithm to support docking ligands against an ensemble of multiple protein structures.

However, the advantages of docking are balanced by a serious deficit: docking creates many false-positive events (Lyu et al., 2019). This is caused by relatively rough search algorithms, for example, Monte Carlo algorithm generates a random initial configuration of ligand in the active site consisting of a random conformation, translation, and rotation; tabu search algorithm made a number of small random changes to the current configuration of ligand and ranked them (Sulimov et al., 2019). To avoid the false-positive events, we previously developed a target filter algorithm based on a Bayesian–Gaussian mixture model (BGMM) (Wei et al., 2022). We clustered the interaction pairs between ligand atoms and protein fragments extracted from the crystal structures of ligand-binding proteins in the PDB (released from January 1995 to April 2021) and found that the potential targets should meet with ≥ 600 significant interaction pairs, and meanwhile, ≥ 0.8 ratio of them to all the interaction pairs (Wei et al., 2022). The advantage of our method was that we not only considered the major bonds between the ligand and protein, such as hydrogen bonds, salt bridges, hydrophobic contacts, halogen bonds, and pi-stacking (Shaikh et al., 2021), but also summarized all the atomic contacts between



the ligand and protein by defining an atomic contact between one ligand atom and the first atom of the protein fragment with an interatomic distance ≤ 5 Å. We proposed that the diverse characteristics of atomic contacts could accurately screen the targets of small molecules.

In addition, target annotation is important for researchers to identify functional elements of targets and to get an insight into target-related proteins/genes and their functions (Xu et al., 2022; Zhang et al., 2022). There are two main ways to annotate targets. One is based on literature curation or experimental results. Several popular databases provided information about protein/gene interactions collected from literature or experimental results, for example, IntAct molecular interaction database, BioGRID, and Molecular INTeraction (MINT) database (Licata et al., 2012; Orchard et al., 2014; Chatr-Aryamontri et al., 2015). The protein interaction network analysis (PINA) platform integrated protein–protein interactions (PPIs) with RNA-seq transcriptomes and mass spectrometry-based proteomes (Du et al., 2021). Another method is based on

machine learning or deep learning. Sun et al. applied stacked autoencoder (SAE) to study sequence-based PPI prediction with an average accuracy of 97.19% (Hashemifar et al., 2018). Chen et al. presented a residual recurrent convolutional neural network in the Siamese architecture for PPI prediction. Zeng et al. (2020) developed an end-to-end deep learning framework with combined local contextual and global sequence features to predict PPI. The aforementioned studies raised the following three questions: 1) Different drugs have different effects on protein/gene regulation, so whether some PPIs could be broken by specific drugs? 2) Are PPIs different in different cell lines? 3) Are PPIs different in different diseases?

In this study, we developed TAIGET, a web server integrating target identification and annotation (Figure 1). We provide here the description of docking service, target screen, target annotation, and PPI analysis. User guide and examples of how to use TAIGET are further provided online.

Implementation

We first collected 176,773 PDB files (January 1995–April 2021) from the Protein Data Bank (PDB). Only *Homo sapiens*/mouse protein–ligand binding files were maintained. After filtering of the PDB files based on our previous work (Wei et al., 2022), hydrogen atoms in proteins were removed by pdb-tools (Rodrigues et al., 2018) and were added again by Reduce. Size and position of binding pockets were calculated based on 3D-coordinates of ligands in the PDB files. A UniProt ID-PDB database was then constructed, consisting of 3D structures of 51,362 proteins named by four-character PDB IDs. The corresponding UniProt IDs of proteins were also involved in the UniProt ID-PDB database. Thus, users could provide UniProt IDs or four-character PDB IDs as protein inputs.

The details about the BGMM-based target filter algorithm could be found in our previous work (Wei et al., 2022). Briefly, protein–ligand binding structures in the PDB files were split into interaction pairs of ligand atoms and protein fragments (covalently linked three heavy atoms) with an interatomic distance of ≤ 5 Å. The interaction pairs were grouped into ligand atoms with the same SYBYL atom type surrounding the same protein fragment, which were further clustered via the BGMM. Gaussian distributions with ≥ 20 ligand atoms were identified as significant interaction patterns. Finally, the number of significant docked interaction pairs and the ratio of them to all the docked interaction pairs were defined as two important criteria to screen potential targets after docking.

To validate the importance of the aforementioned two features, we constructed a dataset involving 314 representative ligand–protein complexes from the PDB database in the previous work. Docking was conducted on the ligand and the corresponding protein involved in the 314 complex structures.

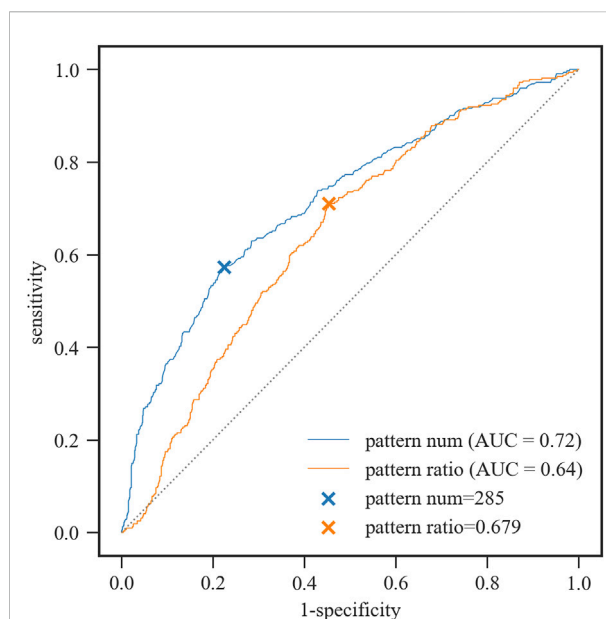


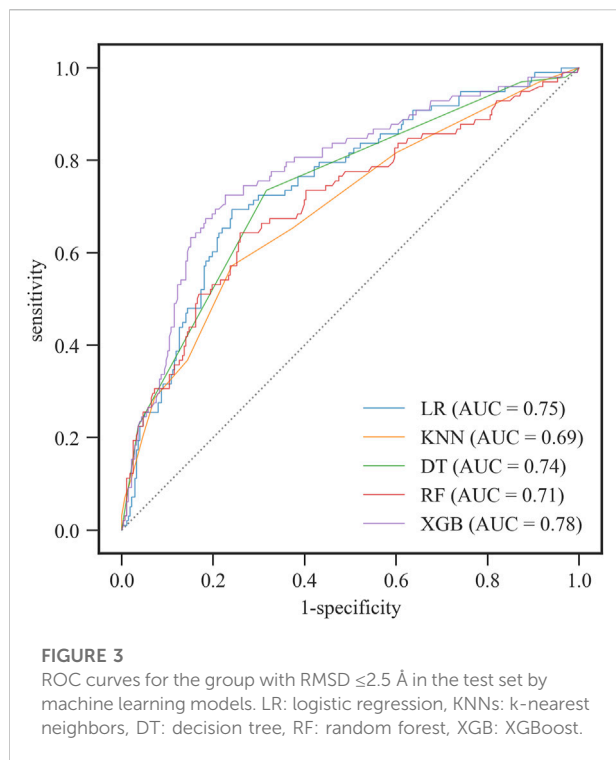
FIGURE 2

ROC curves for the group with RMSD ≤ 2.5 Å by the pattern number and pattern ratio, respectively. Pattern num: the number of significant docked interaction pairs. Pattern ratio: the ratio of significant docked interaction pairs to all the docked interaction pairs.

For each docking case, root-mean square deviation (RMSD) was used to estimate structural similarity between the ligand poses and their corresponding crystal structure, respectively, and the ligand poses with the highest and lowest RMSD values were maintained. The process produced 1,252 binding poses. We further classified the binding poses into two groups with a threshold of RMSD of 2.5 Å. We proposed that the significant interaction patterns were reliable if the aforementioned two features were significantly higher in the group with RMSD ≤ 2.5 Å than in the group with RMSD > 2.5 Å.

Here, we used ROC analysis of the two features to evaluate the classification accuracy. The Youden Index (YI) was used to obtain the optimal cut-off point (Figure 2). When the number of significant docked interaction pairs was equal to 285, the sensitivity at the maximal Youden Index was 0.573 for the group with RMSD ≤ 2.5 Å, while the specificity was 0.776. When the ratio of significant docked interaction pairs to all the docked interaction pairs was equal to 0.679, the sensitivity at the maximal Youden Index was 0.71 for the group with RMSD ≤ 2.5 Å, while the specificity was 0.547.

Because the number of significant docked interaction pairs and the ratio of them to all the docked interaction pairs were two independent and non-linear correlated features, we further constructed machine learning models by using the two features to predict probability of the binding pose with RMSD ≤ 2.5 Å. We randomly divided the 1,252 binding poses



into a training set ($n = 876$) and a test set ($n = 376$). Among logistic regression (LR), k-nearest neighbors (KNNs), decision tree (DT), random forest (RF), and XGBoost, XGBoost yielded the best AUC of 0.78 (Figure 3). As shown in Table 1, XGBoost in the test set showed 77% accuracy and 95% specificity. Thus, we used XGBoost as the classification model in TAIGET to predict the probability of obtaining a true-positive target.

For target annotation, 55,299 cancer-related literature works ranging from 1995 to 2021 was first filtered by searching (cancer [Title/Abstract]) AND (viability [Title/Abstract]) OR (apoptosis [Title/Abstract]) OR (invasion [Title/Abstract]) OR (migration [Title/Abstract]) AND (drug [Title/Abstract]) in PubMed. Titles, abstracts, PMID, article types, and other related categories of the literature were downloaded. After removing reviews, meta-analyses, and clinical assays, information on PMID, species, drugs, genes, regulation, cancer cell lines, cancer subtypes, and cancer outcome was extracted from 14,394 literature studies.

TABLE 1 Model performance on the test set.

	AUC	Accuracy	Sensitivity	Specificity	PPV	NPV
LR	0.75	0.75	0.11	0.97	0.58	0.76
KNN	0.74	0.78	0.3	0.95	0.67	0.79
DT	0.74	0.77	0.22	0.96	0.69	0.78
RF	0.71	0.76	0.32	0.91	0.55	0.79
XGB	0.78	0.77	0.24	0.95	0.63	0.78

LR, logistic regression; KNNs, k-nearest neighbors; DT, decision tree; RF, random forest; XGB, XGBoost; PPV, positive predictive value; NPV, negative predictive value.

Three medical experts and 10 medical students then manually curated all the literature, especially in the following situations: 1) regularization for cell lines in the abstracts could not distinguish drug response in a specific cell line from many cell lines, for example, lanatoside C had an anti-proliferation effect on different human cancer cell lines (MKN-45, SGC-7901, HN4; MCF-7, and HepG2). MKN-45 cells treated with lanatoside C showed upregulation of cleaved caspase-9 and cleaved PARP and downregulation of Bcl-xl. Medical experts and students replaced “cancer cell lines (MKN-45, SGC-7901, HN4; MCF-7, and HepG2)” with “MKN-45 cell line.” 2) Regularization for cell lines in the abstracts could not distinguish the name of a specific cell line from the names of many cell lines, for example, breast cancer and melanoma cell lines were checked for the response to PTX by cytotoxic assay. Medical experts and students replaced “breast cancer and melanoma cell lines” with “breast cancer cell line” and “melanoma cell line.” Furthermore, gene information was standardized by protein ID in UniProt and protein-coding genes in GENCODE (Frankish et al., 2021), while cell line information was standardized by cancer cell lines in CCLE (Nusinow et al., 2020).

In addition, PPIs in AFFINOMICS and cancer and cardiac datasets in BioGRID (<https://thebiogrid.org/>) and IntAct (<https://www.ebi.ac.uk/intact/>) were combined, with the aim to construct target-related networks.

The TAIGET web server integrated, for the first time, a docking service module, a target screen module, and a target annotation module in a single GUI environment. Users have two ways to submit a protein or ligand: 1) selecting a PDB ID or a UniProt ID as a protein and 2) submitting a SMILES molecular formula or a ligand file prepared by users. Also, the users have two ways to run a job: 1) providing an input and sequentially running the job from step 1 to step 3 and 2) selecting a specific step among the three steps and providing the corresponding input to run a sub-job.

The following parameters are available in the “STEP1: Docking Service” module:

- Input files: Users can provide protein by entering four-character PDB IDs or selecting UniProt IDs from our UniProt ID-PDB database. Users can provide ≤ 5 proteins at a time. In addition, users can provide ligands by entering

SMILES molecular formulas or uploading ligand files in one of the following formats, that is, *.pdb, *.pdbqt, *.smi, *.sdf, and *.mol2. The SMILES molecular formulas of ligands can be transformed to 3D structures by Open Babel (O'Boyle et al., 2011) involved in TAIGET. Users can provide ≤ 3 ligands at a time.

- Docking service: users can select AutoDock Vina (Trott and Olson, 2010) or LeDock (Wang et al., 2016) to run docking. AutoDock Vina and LeDock are the two popular academic docking tools with relatively high accuracy. However, although AutoDock Vina achieves a large docking success rate, the correlation between estimated and experimental binding free energy is low ($R < 0.5$) (Nguyen et al., 2020). The weakness of LeDock is its inability to calculate accurate binding energies. During the docking process in TAIGET, a progress bar will be shown.
- Data download: when the docking is complete, users can download protein–ligand binding poses or click the “Go to step 2” button.
- Run time: ~ 10 s is required for each pair of protein and ligand.

The following parameters are available in the “STEP2: Target Screen” module:

- Input files: if users click the “Go to step 2” button, TAIGET starts the target screen immediately. Users can also provide a protein–ligand binding pose created by themselves in this step.
- Target screen: when the job running is finished, a table, portraying protein–ligand poses, PDB names, ligand names, interaction patterns, interaction pattern ratios, and probability will be shown.
- An interactive image: when users click a specific row of the table, a 3D protein–ligand binding structure will be shown on the left window. Users can rotate the image by the mouse.
- Data download: users can download the target-related matrix and the 3D image.
- Run time: ~ 30 s is required for the identification of interaction pairs and the pattern calculation for each protein–ligand pose.

The following parameters are available in the “STEP 3: Target Annotation” module:

- Input files: users can submit a UniProt ID that they are interested in. After clicking the “Find Target” button, a new window appears to show the four-character PDB IDs related to the UniProt ID. Users can also submit a four-character PDB ID in the step.
- Target annotation: if the four-character PDB ID or UniProt ID can be found in our standardized and curated

associations among drugs, genes, gene regulation, cancer outcome, cancer cell lines, and cancer types, a new table will be created to show the associations.

- A PPI network: after clicking the “Target-related PPI” button, the screened targets can be projected to the PPI network constructed by AFFINOMICS and cancer and cardiac datasets in BioGRID and IntAct. Users can visualize and drag the nodes in the target-related PPI network using the mouse. Node colors represent the number of literature, and the darker the color, the larger the number of target-related literature. By placing the mouse on one node, users can observe the node-related representative literature.
- Image download: TAIGET supports export of a high-quality picture of the PPI network, with the aim to facilitate academic research or education.

Results and discussion

TAIGET consists of a docking service module, a target screen module, and a target annotation module, with the aim to facilitate traditional experiment researchers to identify potential targets. Compared with DrugComb (Zheng et al., 2021) that collected drugs, drug concentration, cell lines, drug response from drug combination screening studies, and monotherapy drug screening datasets, we text-mined and manually curated $>14,000$ PubMed literature works to construct associations among drugs, genes, gene regulation, cancer outcome, and cancer types for target annotation. Finally, 7,553 associations among drugs (6,109 types), genes (3,063 types), gene regulation, cancer outcome, cancer cell lines (2,170 types), and cancer types (73 types) were extracted from the literature. As we known, there is no active web server constructing such a simplified and comprehensive pipeline for target identification. In TAIGET, we only allow users to input ≤ 5 proteins at a time for docking because of the limitation of computing power. If users have more requirements, they could contact the authors by e-mails.

Input files for TAIGET

For docking, users can input PDB IDs or UniProt IDs. For example, one user attempts to study the interactions of the serine/threonine kinase BRAF, a promising therapeutic target for lung cancer, with gefitinib, a tyrosine kinase inhibitor used as first-line therapy to treat non-small cell lung cancer. By providing UniProt ID P15056 of BRAF as the protein input, a new window will be created, showing 76 BRAF-related PDB files. Here, the user selects 1UWH as the protein structure, and meanwhile, provides the SMILE format of gefitinib

TABLE 2 Browser compatibility: TAIGET works in all major browsers and operating systems.

OS	Version	Chrome	Firefox	Microsoft Edge	Safari
Linux	Ubuntu 20.04.3 LTS	N/a	95.0	N/a	N/a
MacOS	OS X 10.11.6	95.0.4638.54	Not tested	N/a	11.1.2
Windows	10	96.0.4664.93	95.0	96.0.1054.53	N/a

COC1=C(C=C2C(=C1)N=CN=C2NC3=CC(=C(C=C3)F)Cl)OCCCN4CCOCC4 as the ligand input.

For the target screen, the user can input protein–ligand files created by oneself. TAIGET will identify interaction pairs and calculate interaction patterns for each interaction pair.

For target annotation, the user can enter a four-character PDB ID or a UniProt ID. For example, when the user provides 1UWH as an input, a new window will be created to show UniProt ID P15056. By clicking the UniProt ID with the mouse, a new table will be created, showing all the BRAF-related literature.

Output files for TAIGET

In the docking step, a user can download ≤ 5 docked protein–ligand poses at a time or directly go to the next step. Here, we select AutoDock Vina for the docking of BRAF with gefitinib, which produces two poses.

In the target screen step, a table related to BRAF–gefitinib binding information will be created. The user can download the target-related information by clicking the “Download Results” button.

In the target annotation step, the user can get associations among drugs, genes, gene regulation, cancer outcome, cancer cell lines, and cancer types. Here, the user can provide 1UWH as an input to find three cancer-related literature works in a new table. For example, when the PubMed literature with doi of 10.2119/molmed.2011.00164 is identified, the user has access to the BRAF-related information, that is, sorafenib resulted in cell apoptosis of marrow stromal cells, nurse-like cells, and CLL cells by upregulation of BRAF and several related genes.

Supported browsers and systems by TAIGET

The web server has been tested on all major browsers and operating systems (Table 2).

Conclusion

TAIGET combines docking and a BGMM-based target filter model to identify potential targets of small molecules, which is

friendly to non-expert users via a GUI. More importantly, TAIGET involves a target annotation database, which contains curated associations among drugs, genes, gene regulation, cancer outcome, cancer cell lines, and cancer types derived from >14,000 PubMed literature works. This greatly favors experts and non-experts to explore target function and regulation in specific cancer cell lines.

Data availability statement

The original contributions presented in the study are included in the article/Supplementary Material; further inquiries can be directed to the corresponding authors.

Author contributions

XW, JY, and MC analyzed and interpreted the target annotation data from PubMed literatures, and constructed the TAIGET web server. ZC, BL, SL, YL, XW, CW, XZ, and ZC participated in the web server construction and manually curated the literatures data. EW, RZ, XX, and HS contributed the main idea of the project, and XX was a major contributor in writing the manuscript. All authors read and approved the final manuscript.

Funding

This study received funding from the National Natural Science Foundation of China (no. 82104695) and the Science and Technology Research Project of Education Department of Hubei Province (No. Q20211109).

Acknowledgments

We thank the High-Performance Computing Center of Wuhan University of Science and Technology, for providing access to the computing resources used in this research. We thank Qiguang Zheng and Prof. Xuezhong Zhou at Beijing Jiaotong University who provided a private text marking system to help us for literatures mining. We thank Xu Li, Man Mo, Jianlun Li, Ying Wang, and

Yougang Wang at School of Medicine, Wuhan University of Science and Technology, who participated in literatures curation.

Conflict of interest

The authors declare that the research was conducted in the absence of any commercial or financial relationships that could be construed as a potential conflict of interest.

References

- Chatr-Aryamontri, A., Breitkreutz, B. J., Oughtred, R., Boucher, L., Heinicke, S., Chen, D., et al. (2015). The BioGRID interaction database: 2015 update. *Nucleic Acids Res.* 43, D470–D478. doi:10.1093/nar/gku1204
- Du, Y., Cai, M., Xing, X., Ji, J., Yang, E., and Wu, J. (2021). PINA 3.0: mining cancer interactome. *Nucleic Acids Res.* 49, D1351–D1357. doi:10.1093/nar/gkaa1075
- Frankish, A., Diekhans, M., Jungreis, I., Lagarde, J., Loveland, J. E., Mudge, J. M., et al. (2021). Gencode 2021. *Nucleic Acids Res.* 49, D916–D923. doi:10.1093/nar/gkaa1087
- Hashemifar, S., Neyshabur, B., Khan, A. A., and Xu, J. (2018). Predicting protein-protein interactions through sequence-based deep learning. *Bioinformatics* 34, i802–i810. doi:10.1093/bioinformatics/bty573
- Lapillo, M., Tuccinardi, T., Martinelli, A., Macchia, M., Giordano, A., and Poli, G. (2019). Extensive reliability evaluation of docking-based target-fishing strategies. *Int. J. Mol. Sci.* 20, E1023. doi:10.3390/ijms20051023
- Lee, A., and Kim, D. (2020). CRDS: Consensus reverse docking system for target fishing. *Bioinformatics* 36, 959–960. doi:10.1093/bioinformatics/btz656
- Licata, L., Briganti, L., Peluso, D., Perfetto, L., Iannuccelli, M., Galeota, E., et al. (2012). MINT, the molecular interaction database: 2012 update. *Nucleic Acids Res.* 40, D857–D861. doi:10.1093/nar/gkr930
- Lyu, J., Wang, S., Balius, T. E., Singh, I., Levit, A., Moroz, Y. S., et al. (2019). Ultra-large library docking for discovering new chemotypes. *Nature* 566, 224–229. doi:10.1038/s41586-019-0917-9
- Ma, Z., and Zou, X. (2021). MDock: A suite for molecular inverse docking and target prediction. *Methods Mol. Biol.* 2266, 313–322. doi:10.1007/978-1-0716-1209-5_18
- Nguyen, N. T., Nguyen, T. H., Pham, T. N. H., Huy, N. T., Bay, M. V., Pham, M. Q., et al. (2020). Autodock vina adopts more accurate binding poses but Autodock4 forms better binding affinity. *J. Chem. Inf. Model.* 60, 204–211. doi:10.1021/acs.jcim.9b00778
- Nusinow, D. P., Szpyt, J., Ghandi, M., Rose, C. M., McDonald, E. R., 3rd, Kalocsay, M., et al. (2020). Quantitative proteomics of the cancer cell line encyclopedia. *Cell* 180, 387–402. e16. doi:10.1016/j.cell.2019.12.023
- O'Boyle, N. M., Banck, M., James, C. A., Morley, C., Vandermeersch, T., and Hutchison, G. R. (2011). Open Babel: An open chemical toolbox. *J. Cheminform.* 3, 33. doi:10.1186/1758-2946-3-33
- Orchard, S., Ammari, M., Aranda, B., Breuza, L., Briganti, L., Broackes-Carter, F., et al. (2014). The MINTAct project--IntAct as a common curation platform for 11 molecular interaction databases. *Nucleic Acids Res.* 42, D358–D363. doi:10.1093/nar/gkt1115
- Rodrigues, J., Teixeira, J. M. C., Trellet, M., and Bonvin, A. (2018). pdb-tools: a Swiss army knife for molecular structures. *F1000Res.* 7, 1961. doi:10.12688/f1000research.17456.1
- Shahid, M., Azfaralariff, A., Law, D., Najm, A. A., Sanusi, S. A., Lim, S. J., et al. (2021). Comprehensive computational target fishing approach to identify Xanthorrhizol putative targets. *Sci. Rep.* 11, 1594. doi:10.1038/s41598-021-81026-9
- Shaikh, F., Tai, H. K., Desai, N., and Siu, S. W. I. (2021). LigTMap: ligand and structure-based target identification and activity prediction for small molecular compounds. *J. Cheminform.* 13, 44. doi:10.1186/s13321-021-00523-1
- Sulimov, V. B., Kutov, D. C., and Sulimov, A. V. (2019). Advances in docking. *Curr. Med. Chem.* 26, 7555–7580. doi:10.2174/0929867325666180904115000
- Trott, O., and Olson, A. J. (2010). AutoDock vina: improving the speed and accuracy of docking with a new scoring function, efficient optimization, and multithreading. *J. Comput. Chem.* 31, 455–461. doi:10.1002/jcc.21334
- Vamathevan, J., Clark, D., Czodrowski, P., Dunham, I., Ferran, E., Lee, G., et al. (2019). Applications of machine learning in drug discovery and development. *Nat. Rev. Drug Discov.* 18, 463–477. doi:10.1038/s41573-019-0024-5
- Wang, Z., Sun, H., Yao, X., Li, D., Xu, L., Li, Y., et al. (2016). Comprehensive evaluation of ten docking programs on a diverse set of protein-ligand complexes: the prediction accuracy of sampling power and scoring power. *Phys. Chem. Chem. Phys.* 18, 12964–12975. doi:10.1039/c6cp01555g
- Wei, X., Wu, X., Cheng, Z., Wu, Q., Cao, C., Xu, X., et al. (2022). Botanical drugs: a new strategy for structure-based target prediction. *Brief. Bioinform.* 23, bbab425. doi:10.1093/bib/bbab425
- Xu, M., Bai, X., Ai, B., Zhang, G., Song, C., Zhao, J., et al. (2022). TF-marker: a comprehensive manually curated database for transcription factors and related markers in specific cell and tissue types in human. *Nucleic Acids Res.* 50, D402–D412. doi:10.1093/nar/gkab1114
- Zeng, M., Zhang, F., Wu, F. X., Li, Y., Wang, J., and Li, M. (2020). Protein-protein interaction site prediction through combining local and global features with deep neural networks. *Bioinformatics* 36, 1114–1120. doi:10.1093/bioinformatics/btz699
- Zhang, H., Pan, J., Wu, X., Zuo, A. R., Wei, Y., and Ji, Z. L. (2019). Large-scale target identification of herbal medicine using a reverse docking approach. *ACS Omega* 4, 9710–9719. doi:10.1021/acsomega.9b00020
- Zhang, Y., Song, C., Zhang, Y., Wang, Y., Feng, C., Chen, J., et al. (2022). TcoFBase: a comprehensive database for decoding the regulatory transcription co-factors in human and mouse. *Nucleic Acids Res.* 50, D391–D401. doi:10.1093/nar/gkab950
- Zheng, S., Aldahdooh, J., Shadbahr, T., Wang, Y., Aldahdooh, D., Bao, J., et al. (2021). DrugComb update: a more comprehensive drug sensitivity data repository and analysis portal. *Nucleic Acids Res.* 49, W174–W184. doi:10.1093/nar/gkab438

Publisher's note

All claims expressed in this article are solely those of the authors and do not necessarily represent those of their affiliated organizations, or those of the publisher, the editors, and the reviewers. Any product that may be evaluated in this article, or claim that may be made by its manufacturer, is not guaranteed or endorsed by the publisher.



OPEN ACCESS

EDITED BY
Sandeep Singh,
Central University of Punjab, India

REVIEWED BY
Indrani Manna,
University of Calcutta, India
Saurabh Srivastav,
Rice University, United States

*CORRESPONDENCE
Abdur Rauf,
abdurrauf@uoswabi.edu.pk
Bonglee Kim,
bongleekim@khu.ac.kr

SPECIALTY SECTION
This article was submitted to
Pharmacology of Anti-Cancer Drugs,
a section of the journal
Frontiers in Pharmacology

RECEIVED 22 May 2022
ACCEPTED 15 August 2022
PUBLISHED 08 September 2022

CITATION
Rahman MM, Sarker MT,
Alam Tumpa MA, Yamin M, Islam T,
Park MN, Islam MR, Rauf A, Sharma R,
Cavalu S and Kim B (2022), Exploring the
recent trends in perturbing the cellular
signaling pathways in cancer by
natural products.
Front. Pharmacol. 13:950109.
doi: 10.3389/fphar.2022.950109

COPYRIGHT
© 2022 Rahman, Sarker, Alam Tumpa,
Yamin, Islam, Park, Islam, Rauf, Sharma,
Cavalu and Kim. This is an open-access
article distributed under the terms of the
[Creative Commons Attribution License](https://creativecommons.org/licenses/by/4.0/)
(CC BY). The use, distribution or
reproduction in other forums is
permitted, provided the original
author(s) and the copyright owner(s) are
credited and that the original
publication in this journal is cited, in
accordance with accepted academic
practice. No use, distribution or
reproduction is permitted which does
not comply with these terms.

Exploring the recent trends in perturbing the cellular signaling pathways in cancer by natural products

Md. Mominur Rahman¹, Md. Taslim Sarker¹,
Mst. Afroza Alam Tumpa¹, Md. Yamin¹, Tamanna Islam¹,
Moon Nyee Park², Md. Rezaul Islam¹, Abdur Rauf^{3*},
Rohit Sharma⁴, Simona Cavalu⁵ and Bonglee Kim^{2*}

¹Department of Pharmacy, Faculty of Allied Health Sciences, Daffodil International University, Dhaka, Bangladesh, ²Department of Pathology, College of Korean Medicine, Kyung Hee University, Seoul, South Korea, ³Department of Chemistry, University of Swabi, Swabi, Anbar, Pakistan, ⁴Department of Rasa Shastra and Bhaishajya Kalpana, Faculty of Ayurveda, Institute of Medical Sciences, Banaras Hindu University, Varanasi, Uttar Pradesh, India, ⁵Faculty of Medicine and Pharmacy, University of Oradea, Oradea, Romania

Cancer is commonly thought to be the product of irregular cell division. According to the World Health Organization (WHO), cancer is the major cause of death globally. Nature offers an abundant supply of bioactive compounds with high therapeutic efficacy. Anticancer effects have been studied in a variety of phytochemicals found in nature. When Food and Drug Administration (FDA)-approved anticancer drugs are combined with natural compounds, the effectiveness improves. Several agents have already progressed to clinical trials based on these promising results of natural compounds against various cancer forms. Natural compounds prevent cancer cell proliferation, development, and metastasis by inducing cell cycle arrest, activating intrinsic and extrinsic apoptosis pathways, generating reactive oxygen species (ROS), and down-regulating activated signaling pathways. These natural chemicals are known to affect numerous important cellular signaling pathways, such as NF- κ B, MAPK, Wnt, Notch, Akt, p53, AR, ER, and many others, to cause cell death signals and induce apoptosis in pre-cancerous or cancer cells without harming normal cells. As a result, non-toxic "natural drugs" taken from nature's bounty could be effective for the prevention of tumor progression and/or therapy of human malignancies, either alone or in combination with conventional treatments. Natural compounds have also been shown in preclinical studies to improve the sensitivity of resistant cancers to currently available chemotherapy agents. To summarize, preclinical and clinical findings against cancer indicate that natural-sourced compounds have promising anticancer efficacy. The vital purpose of these studies is to target cellular signaling pathways in cancer by natural compounds.

KEYWORDS

cancer, natural compounds, therapeutic efficacy, reactive oxygen species, metastasis

Introduction

Cellular signaling is a complicated signaling network that governs and organizes cells' key biological processes. Signaling cascades are three-dimensional protein pathways that interact with one another in a specific cell site (Shaw and Filbert, 2009). Cancer cells regularly exhibit changes in several cellular signaling pathways as a result of the complex transmission of cell signaling. This could explain why specific inhibitors that target a single pathway have so often failed to treat cancer. In cancer cells, the cell cycle and apoptosis regulatory systems almost always fail, resulting in uncontrolled cell proliferation and tumor formation [1]. NF- κ B, Akt, MAPK, Wnt, Notch, p53, AR, and ER, among others, have been discovered as cellular signaling pathways that influence cell growth and death. All of these signaling pathways are damaged in cancer cells, which promotes the growth of cancer cells and inhibits apoptosis (Karin et al., 2002; Martin, 2003; Sebolt-Leopold and Herrera, 2004; Stiewe, 2007; Klaus and Birchmeier, 2008). As a result, in order to effectively eradicate cancer cells, it is important to create a technology that can concurrently target many biological signaling pathways (Sarkar et al., 2009).

Chronological diseases that severely endanger human life are cancers. Many treatments have been developed for cancer care, involving surgery, radiotherapy, targeted therapy, and chemotherapy. The occurrence pace of malignancy has been steady in women. It has decreased marginally in men over the past decade (2006–2015) due to all these therapies, and the cancer mortality rate (2007–2016) has also decreased (Siegel et al., 2019). In 2018, cancer caused an expected 9.6 million deaths, and cancer is predicted to be the primary source of death worldwide in the 21st century (Bray et al., 2018; Rahman et al., 2022a; Rahman et al., 2022b). Chemoprevention is a somewhat expensive option for treating cancer. The idea is gaining popularity because it is more affordable and efficient. Chemoprevention involves the administration of one or more naturally occurring and synthetic agents. It can prevent, slow down, or reverse the initiation and progression of the disease (Haddad and Shin, 2009). Berenblum pioneered chemoprevention in the 1920s, and Sporn's work in the 1970s brought it back into the mainstream of cancer research (Amin et al., 2009).

Consequently, in addition to cancer treatment, malignancy counteraction stays an inventive region of anticancer science. Because of increased studies, the components of variant signal transduction pathways in malignant growth and the effects of these pathways on apoptosis, tumorigenesis, and metastasis have been progressively exposed (Lezhnina et al., 2014). Traditional cancer treatment strategies, however, are only successful for certain malignant tumors (Sun, 2015). Unscheduled and unregulated cell proliferation characterizes it in the cell spectrum. Cancer incidence in developed nations has been tumor forms associated with viral, genetic mutations, and

bacterial infection have prevailed (Jemal et al., 2010). Metastasis, heterogeneity, recurrence, resistance to radiotherapy and chemotherapy, and shirking of immunological surveillance are the key reasons cancer treatment has failed (Batlle and Clevers, 2017). In its growth and the progression of the disease, cancer has a high occurrence and a long dormancy time. Several risk factors for cancer development are identified, including geographic region, age, and race (Wiat, 2007). The revelation of various biomarkers related to antibiotic development, and even as epidermal growth factor receptor (EGFR), cyclo-oxygenase-2 (COX-2), and Ras, as well as the invention of Novel tailored inhibitors for such biomarkers, has opened up new avenues for chemoprevention (Arber et al., 2009; Toshiya et al., 2012). Numerous targeted medicines have since been found, including the COX-2 inhibitors celecoxib and rofecoxib, the EGFR inhibitors erlotinib and gefitinib, and farnesyltransferase inhibitors (Deng et al., 2019; Forouzanfar and Mousavi, 2020).

Macro autophagy, or autophagy for short, is a highly conserved stress repercussion and degradation process. Stresses such as hunger trigger autophagy, which results in double-membrane autophagosomes capturing intracellular proteins and organelles (Deng et al., 2019). Cargos (protein clusters and malfunctioning mitochondria) will be carried to lysosomes for breakdown, allowing biomolecules to be recycled and lifespan to be maintained (Nawaz et al., 2020). Autophagy governs several cellular activities, including attribute monitoring and the destruction of defective proteins and organelles, in addition to its functions in energy homeostasis (Singh et al., 2017a). As a result, defective autophagy can play a role in developing various diseases, notably cancer, neurological sickness, and immune disorders (Dikic and Elazar, 2018; Wang et al., 2019; Rahman et al., 2021a; Rahman et al., 2021b; Rahman et al., 2021c; Islam et al., 2021; Rauf et al., 2021; Bhattacharya et al., 2022; Rahman et al., 2022c; Rahman et al., 2022d). Several bits of research point to a relationship between nutrition and cancer therapy efficacy. Appropriate utilization of phytochemicals arising from dietary and medicinal herbs has been shown to lower cancer fatality by influencing the stimulation of numerous oncogenic molecules (Singletary and Milner, 2008; Hsieh et al., 2015).

Natural cancer chemoprevention, particularly phytochemicals, vitamins, and minerals has emerged as a viable and practical way to reduce cancer's impact and is gaining traction as a safe and cost-effective substitute to anticancer therapy. Contrary to pharmaceutical medications, which are mono-target molecules, herbal remedies have multitarget compounds that can control the initiation and spread of cancer (Deeb et al., 2007; Shu et al., 2010; Khan et al., 2015). Herbal substances exhibit several anti-cancer properties, particularly anti-inflammatory, anti-mutagenic, anti-oxidative, and apoptosis-inducing properties, which may aid in preventing cancer growth in its initial phase

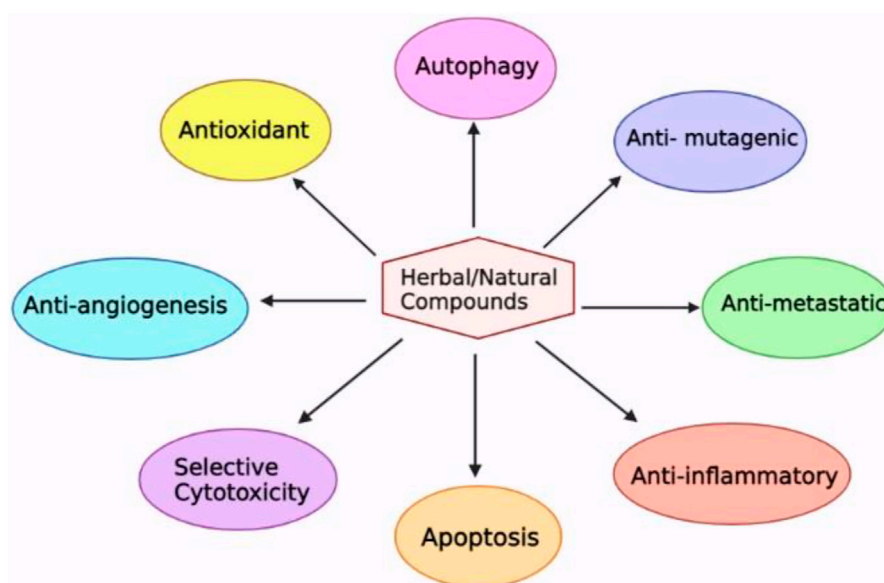


FIGURE 1

Aspects of herbal substances that contribute to their chemotherapeutic action (Laskar et al., 2020).

(Figure 1). By suppressing the cell cycle, inducing apoptosis, controlling the metabolism of carcinogens and the expression of oncogenes, restricting cell adhesion, multiplication, and migratory, and blocking signaling pathways that are crucial for cancer development, dietary ingestion of a sufficient amount of these herbal supplements may aid in the preventive measures and treatment of cancer (Huang et al., 2009). A total of 136 anticancer medications were introduced for usage between 1981 and 2014, and about 83 percent of them were either herbal substances or their derivatives (Amaral et al., 2019).

In various studies in both *in vitro* and *in vivo* settings, the prevention of cancer by natural compounds, particularly phytochemicals, minerals, and vitamins, has shown encouraging outcomes against different malignancies (Manson, 2003). Raw materials have a rich and long tradition when it comes to producing bioactive chemicals. As a significant novel source with a wide variety of pharmaceutical promise, herbal medicines are used to cure human diseases, involving nearly all forms of cancer (Christen and Cuendet, 2012; Rahman et al., 2022e; Rahman et al., 2022f). The inclusion at epigenetic, genomic, molecular, and cellular levels of several factors influencing the developmental stages of cancer opens up immense opportunities to disrupt and reverse the onset and development of the disorders. It offers various targets for scientists and researchers to avoid cancer growth through physiological and pharmacological mechanisms (Cragg and Newman, 2005; Chopra et al., 2022; Rahman et al., 2022g; Rahman et al., 2022h; Rahman et al., 2022i; Rahman et al.,

2022j; Rahman et al., 2022k; Rauf et al., 2022). This article will focus on advances in understanding the signaling pathways of cancer by natural compounds. According to recent findings from an increasing number of studies on these natural products, these natural compounds exhibit their pleiotropic effects on cancer cells by targeting numerous cellular signaling pathways, such as NF- κ B, MAPK, Wnt, Akt, Notch, p53, AR, and ER pathways. This suggests that these natural compounds might be useful alone or in combination with conventional therapeutic agents for the prevention and/or treatment of tumor development. This article summarizes the functions of many of these signaling pathways. It also reflects the various natural-sourced compounds and their associated mode of action in various cancer lines with chemical structure. The newly found anticancer drug (dostarlimab) and its mode of action are also briefly discussed in this article. This article is unique due to the brief overview of numerous cancers signaling pathways, natural compounds and their modes of action, and recently identified anticancer medicines with modes of action. Overall, this article on using natural resources as sources for the development of novel anticancer drugs abundantly supports the idea that natural resources remain very attractive for the discovery and manufacture of cutting-edge medical devices for the treatment of cancer patients. Phytoconstituents separation of novel compounds and their molecular and cellular analysis in *in vitro* cancer cells must come first in order to develop new drugs with improved pharmacological features regarding efficacy to target tumor cells and safety to spare adverse effects towards normal tissues.

Cancer management signaling pathways

Cancer is the driving reason for death in developed countries, with a dynamic mechanism of improvement in pathophysiology. It causes cells to avoid homeostatic controls. Creating an effective therapeutic strategy that tackles all fanatical cancer components (Sever and Brugge, 2015). Many therapeutic strategies are currently being developed for the prevention and treatment of cancer. A small number of rectal cancer patients recently witnessed a sort of scientific miracle: after receiving an experimental medication, their cancer just disappeared. Patients took the medication dostarlimab for 6 months as part of a relatively limited trial run by specialists at the Memorial Sloan Kettering Cancer Center in New York. Every single one of their malignancies vanished as a result of the experiment. There is plenty to learn about the treatment's mechanism of action since this trial group consisted of only 18 individuals (Guardian, 2022). GlaxoSmithKline, a pharmaceutical manufacturer, manufactured dostarlimab. The medicine cost \$11,000 per dose and was administered to the individuals every three to 6 months. The medicine is referred to as a checkpoint suppressor. Cancer cells create a barrier around themselves to thwart T-cells from the body's immune system from destroying them. This medication removes that barrier. Cancer cells are more susceptible to being eliminated by the immune system when the shield is absent. Over a follow-up term, which lasted an average of about a year, none of the individuals had a return of their disease or required additional therapy. None of the patients encountered the more severe side effects that are frequently associated with rectal cancer therapies, such as infertility, neuropathy, or sexual dysfunction, despite some of them having rashes, dermatitis, exhaustion, pruritis, or nausea (Cercek et al., 2022). The dostarlimab injection inhibits the activity of a specific protein in cancer cells, which is how it works. This aids in slowing the growth of tumors and aids the immune system's defense against cancer cells (Adnal, 2022). The initiation of unregulated cellular proliferation and disease metastasis cancer can be separated in multiple pathological stages of a natural cell's mutation into cancer cells due to deregulation of different unique pathways. The nuclear factor kappa B (NF- κ B) has been shown in the action stage of cancer where normal cells are transformed into cancer cells, improvements in immunological and cellular pathways, and relaxation (Lin et al., 2010; Vinay et al., 2015). NF- κ B is an inducer of inflammation. The cellular connections between inflammation and carcinogenesis are explored, and there is mounting evidence that NF- κ B (Nuclear factor kappa B) plays a critical role in the correlation between them. The regulation of innate and adaptive immune responses that are present in inflammatory states and the integration of various stress stimuli depends on transcription factors (NF- κ B) (Karin et al., 2006). It was only reasonable to anticipate a connection between

NF- κ B and cancer, as was initially proposed several years ago, given the understanding that inflammatory diseases are frequently related to or cause cancer (KarinM et al., 2002). Since then, a rapid accumulation of experimental data has revealed precise pathways by which NF- κ B affects cancer to start, develop, and progress. The emergence of RelA/p65 cloning and sequencing immediately exposed its kindred to c-Rel and its malignant variant v-Rel, which led to the emergence of a potential link between NF- κ B and cancer. Oncogenic mutations that confer transformative action on RelA, c-Rel, or other NF- κ B proteins, on the other hand, were discovered to be uncommon and mostly restricted to lymphoid malignancies (Gilmore, 2003).

If inflammation and infection promote tumor growth, they must do so via altering signal transduction pathways that affect cells engaged in either cancer monitoring or malignant transformation. Unless they contain their oncogenes, poisons, or growth regulators, infectious organisms often affect the recipient by activating pattern recognition receptors (PRRs), such as components of the Toll-like receptor (TLR) family (Medzhitov, 2001). As a result of the activation of multiple signaling pathways by PRR and TLR activation, many transcription factors are targeted, which regulate genes expressing cytokines, chemokines, and enzymes that drive innate and adaptive immune responses (Karin et al., 2006). The inflammatory response is propagated and amplified by a number of these genetic variants that stimulate certain receptors; it is one aspect of the broader innate immune response. While activating multiple important signaling pathways, activation of TLRs and receptors for proinflammatory cytokines, including as TNF- α and interleukin (IL)-1, plays a crucial role in inflammation and innate immunity (Li and Verma, 2002). Uncontrolled cell multiplication is responsible for the dissatisfaction of the autophagy and apoptotic pathway. They assume that the second stage of cancer is an important aspect of sustaining stable cell endurance and eradicating mutant cells (Hassan et al., 2014; Nagelkerke et al., 2015). The metabolic pathway continues to change as a consequence of the increased energy requirements of cancer cells. Every location where RAS protein activity occurs, which is required for the signaling pathway of RAS proteins to function, represents a new stage of cancer (Galluzzi et al., 2013; Bahrami et al., 2018). Lopsided angiogenesis pathways regulate the mechanism for cancer attack and metastasis of new organs in the high-level phase of cancer (Zhao and Adjei, 2015). Table 1 describes the clinical goals of the different processes involved in cancer treatment and their therapeutic action mechanisms.

Signaling pathway

It explains various chemical reactions, such as cell division or cell death, a process in which a community of molecules in a cell

TABLE 1 Targets of common pathways implicated in cancer treatment with clinical action strategies (Singh and Shukla, 2018).

Pathway	Targets	Activity	Targeting mechanisms	References
Immune Pathway	Regulatory T cells (Tregs)	Reduce the immune system's reaction.	Reducing Tregs have a suppressive effect.	Byrne et al. (2011)
	Tumor Necrosis Factor Receptor (TNFR)	T-cell activation and immune responses may be manipulated.	TNFR contact inhibition.	Du et al. (2017)
	II NK cells and M2 macrophages	Growth of a tumor	Release of cytokines is inhibited.	Singh et al. (2017b)
Metabolic pathway	HK1 and HK2	Phosphorylation of ATP	Silencing of HK2 and HK1.	Singh et al. (2015); Gupta et al. (2017)
	3BP	ATP supply is being reduced.	Increasing the supply of 3BP.	Shoshan, (2012)
	GAPDH	For energy, break down glucose.	GAPDH levels are reduced.	Birsoy et al. (2013)
Apoptosis pathway	SRTFs	This protein transcribes Bcl-2 and Bcl-xL genes.	SRTF activation is inhibited.	Green and Evan, (2002)
	HDACs	Bcl-2 and Bcl-xL must be activated.	Changing the expression of HDACs.	DAMASKOS et al. (2017)
RAS pathway	Nucleotide exchange	RAS signaling activation	Nucleotide exchange is inhibited.	Huang et al. (2015)
	GRB2	RAS signaling activation	preventing the interaction of GRB2 receptors.	Ahmed et al. (2015)
	SHC	Mediate between GRB2 and the receptor.	SHC auto-phosphorylation is reduced.	Niemitz, (2013)
NF- κ B pathway	IKK kinase complex	NF- κ B activation requires this part.	IKK expression is reduced.	Strickson et al. (2013)
	Proteasome	This protein aids in the development of NF- κ B.	Proteasome inhibition.	Kubiczkova et al. (2014)

collaborate to regulate a cell process. When a chemical, growth factor, or hormone, interacts with a particular protein receptor on or within the membrane, a cell gets signals from its surroundings. It activates another molecule after the first molecule on the route receives a call. Until the very last molecule is stimulated and the cell work is completed, this step is replicated through the whole signaling cascade. Abnormal signaling pathway activation can contribute to illnesses such as cancer. By targeting particular molecules involved in these pathways, drugs are being produced. Such medicines can help to prevent cancer cells from rising (National Cancer Institute, 2022).

Notch signaling

The Notch signaling pathway has been around for a long time. It has remained relatively unchanged during evolution that many organisms play a significant role in the growth of the embryo and the baby after birth. The pathway has several pleiotropic implications, affecting critical organ growth processes and adult stem cell self-renewal control, resulting in tissue homeostasis (Kopan and Ilagan, 2009). This pathway, however, is vulnerable to irregular signaling due to its multifunctional structure and has been related to a host of human diseases, including developmental syndromes and cancer. Notch signals are a well-organized, multi-tiered, closely controlled cascade of cell/tissue signaling occurrences.

For its maturation, activation, and execution, it requires different components. Four receptors, known as Notch-1 to Notch-4, and five DSL (Delta/Serrate/Lag-2) ligands, known as Jagged-1 and Jagged-2 (Jag-1 and Jag-2) and Delta-like-1, Delta-like-3, and Delta-like-4, are in the Notch signaling family (Dll-1, Dll-3, and Dll-4) (Angulo et al., 2017). Transmembrane proteins, ligands, receptors, and pathway activation happens when an adjacent cell ligand communicates with the receptor (Ehebauer et al., 2006). The encounter causes conformational modifications in the ligand-receptor complex, which reveal a notch receptor site to proteolytic divide through the tumor necrosis factor- α converting enzyme (TACE/ADAM17/CD156q) and metalloprotease part, or ADAM (Figure 2). This cleavage results in the membrane-attached notch extracellular truncation (NEXT) fragment, a vital regulatory step in notch activation and signaling, which is located in the negative regulatory area of the notch receptor extracellular domain (Okajima and Matsuda, 2006; Sato et al., 2007).

Notch signaling is uncommon in many cancers, and tissue and cell history-based may play complex oncogenic or tumor-suppressive roles in multiple tumors (xi et al., 2020). Notch receptor mutations cause gain-of-function (for example, in malignant hematological disorders (Arruga et al., 2018; Sorrentino et al., 2019)) or loss-of-function (for example, cancer of the bladder (Goriki et al., 2018) and carcinomas of squamous cells (Zhang et al., 2016)). They are a fundamental cause of dysregulation of Notch signaling. The mechanisms that control Notch signaling by four Notch receptors, as well as their

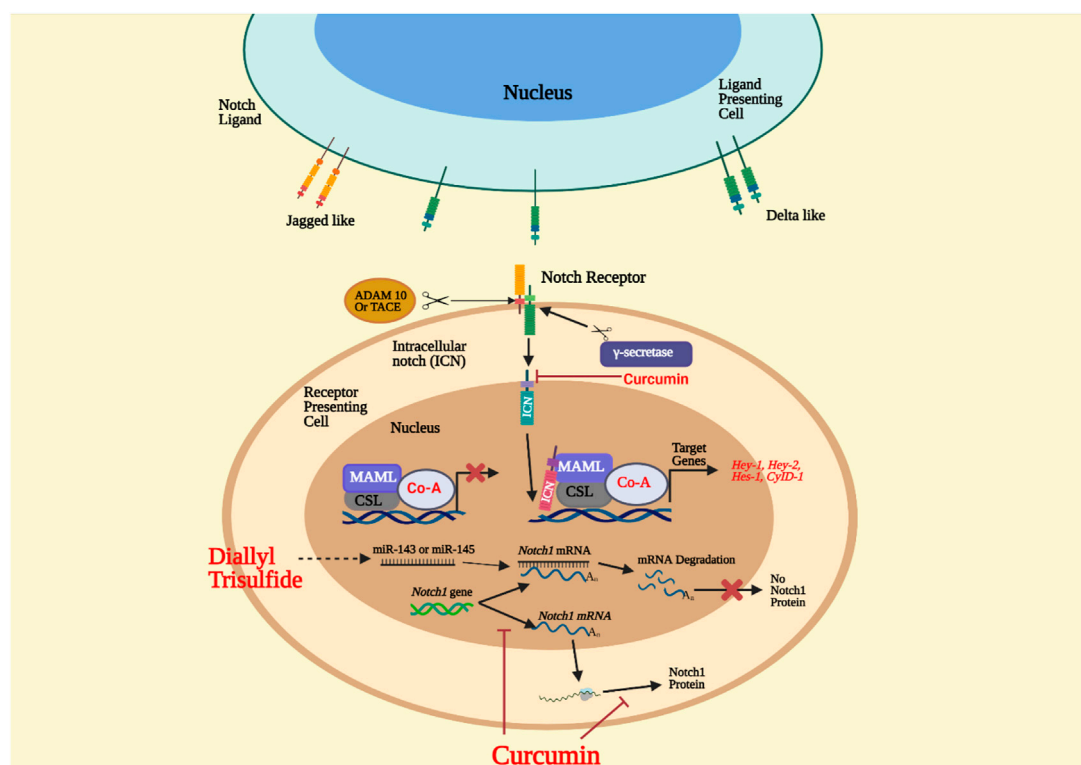


FIGURE 2

Notch signaling pathway. The ligand on the receiving cell connects the cell that acts as a presenter for the notch receptor. ADAM metalloprotease and γ -secretase split the Notch extracellular truncated (NEXT) domain, forming the notch intracellular domain (NICD). NICD is introduced into the nucleus and is a complex of transcription factors CSL 9 CBF1/hairless/lack 1 and transcriptional coactivator of mastermind-like proteins (MAML). The complex would then activate the target gene's transcription. Treatment with diallyl trisulfide (DATS) boosts the expression of tumor suppressor microRNAs miR-143 and miR-145. When microRNAs bind to Notch1 mRNA, the mRNA is degraded, but the Notch1 protein is not translated. Curcumin inhibits Notch1 transcription and expression and the nucleus' Hes-1, Hey-1, and Hey-2 genes (Angulo et al., 2017).

distinct functions in the progression, occurrence, and recurrence of cancer, to date have been well known, indicating that Notch receptor-based therapeutic approaches may be helpful (xi et al., 2020).

It is generally acknowledged that Notch signaling is crucial for maintaining the harmony between cell proliferation, survival, apoptosis, and diversification, which has an influence on the growth and operation of numerous organs. As a result, Notch malfunction inhibits distinction and eventually leads undifferentiated cells onto malignant transformation (Jubb et al., 2010; Wang et al., 2010; Espinoza and Miele, 2013). In fact, a number of information indicate that modifications in Notch signaling may be connected to a variety of human cancers. Furthermore, Notch receptors and ligands have been identified to serve as prognostic indicators in human cancers (Wang et al., 2009; Moretti and Brou, 2013). It is really remarkable that Notch signaling may play either an anti-proliferative or an oncogenic role in the development of tumors, depending on the situation. A limited fraction of tumor forms, including human hepatocellular carcinoma, medullary thyroid, small cell lung cancer, skin cancer,

and cervical cancer, have revealed that notch signaling is anti-proliferative (Anusewicz et al., 2021; Christopoulos et al., 2021; Zhou et al., 2022).

WNT/ β -catenin signaling

Organogenesis, cell proliferation, cell fate determination, and stem cell renewal are regulated by the Wnt signaling pathway, which is strongly conserved (Angulo et al., 2017). Wnt signaling is traditionally classified as either β -catenin-dependent (canonical, Wnt/ β -catenin pathway) or β -catenin-independent (noncanonical, Wnt/planar cell polarity [PCP] and calcium pathway) (Grumolato et al., 2010; Katoh, 2017). Skin, breast, and colon cancers may be caused by changes and dysregulation in the Wnt pathway (Angulo et al., 2017). Wnt signaling regulates gene transcription and cell-to-cell adhesion, and β -catenin is a critical player in this process. Degradation and phosphorylation ensure that the protein's amount remains stable—amino acid substitutions occurring as a result of β -catenin mutations,

TABLE 2 Impact of natural compounds affecting significant stem pathways cell signaling (Angulo et al., 2017).

Major paths for signaling	Components	Objective	Effect	References
Notch	Curcumin	The notch-1 and downstream genes Hes-1, Hey-1, and Hey-2 mRNA speed downregulate transcriptions and translations.	Causes apoptosis by increasing reactive species of oxygen.	Tu et al. (2012)
	Diallyl trisulfide	Intracellular domain targets Notch-1	Decreases downstream gene expression of Notch. Enhances expression of microRNAs (miR143 and miR-145) possible tumor suppressants and reduces tumor support for miR-21 MicroRNA.	Tutelyan and Lashneva, (2013)
WNT/ β -catenin	Resveratrol	histone H2AX; β -catenin	Apoptosis in ROS cells triggers telomere instability and DNA disruption by lowering -catenin mRNA and protein expression and c-Myc Histone H2AX phosphorylation.	Angulo et al. (2017)
Hedgehog	Cyclopamine	SMO-binding	Signal transduction to GLIS is prevented.	Kumar and Fuchs, (2015)
PI3/AKT	Sulforaphane	AKT and ERK	It suppresses phosphorylation of ERK and AKT and induces apoptosis by arresting cells in the G2/M process.	Aggarwal et al. (2007)

resulting in the protein's improper phosphorylation Table 2. The ubiquitin ligase E3 does not accept the phosphorylated protein properly. As a result of the dysregulation of the Wnt pathway, β catenin accumulates without being destroyed and then translocates to the nucleus, stimulating oncogene transcription (Zou et al., 2015), *c-Myc*, *cyclin D1*, and *survivin* (an apoptosis inhibitor) are examples of expressed downstream genes. Wnt glycoproteins tie to the Frizzled receptor family of extracellular, transmembrane proteins. The signal then stimulates the cytoplasmic protein Disheveled (Dsh/DV1). Wnt then divides into three signaling pathways: canonical and noncanonical Wnt/ Ca^{2+} , noncanonical planar cell polarity (Komiya and Habas, 2008).

Hedgehog signaling

The signaling pathway of Hedgehog (Hh), also called the Hedgehog-Gli (Hh-Gli), Hedgehog-Patched (Hh-Ptch), or Hedgehog-Patched-Smoothed (Hh-Ptch-Smo), is an evolutionarily conserved signaling pathway that transmits signals from the cell membrane to the nucleus (Table 2). Invertebrates and vertebrates both use the Hh signaling pathway to help them usually evolve (Varjosalo and Taipale, 2008). In the human body, the Hh pathway is inactive mainly or only moderately active. It can be triggered if necessary, such as in the cure of the wound (Le et al., 2008). It also promotes the growth of somatic stem cells and pluripotent stem cells required to reconstruct tissue such as skin, mammary, erythropoietic, neural, and pulmonary stem cells, and epithelial cells in internal organ systems. As a result, Hh signaling is needed for lung epithelial regeneration, exocrine pancreas cell regeneration, and prostate epithelial regeneration (Skoda et al., 2018). The

Hh signaling pathway is only found in primary cilia (PC), which are microtubule-based organelles that protrude from the cell surface and receive chemical, mechanical, and thermal signals (Plotnikova et al., 2008). The PC contains all Hh signal transduction pathway components (Michaud and Yoder, 2006). Natural substances including Cyclopamine, Nitidine Chloride, Sulforaphane, and Genistein may be able to kill CSCs by specifically targeting the Hedgehog pathway components and inactivating the signaling cascade (Figure 3) (Cross and Bury, 2004; Varjosalo and Taipale, 2008; Rodova et al., 2012).

Hh signaling has been implicated in multiple stages of carcinogenesis in various tumors, according to several reports. The activation of the signaling pathway is seen in the early stages of pancreatic and esophageal cancers and metastatic tumors (Ma et al., 2006; Bailey et al., 2009). Regulation of the Hh signaling pathway is connected to tissue invasion and increasing metastatic risk in other cancers, such as prostate cancer and gastric cancer. Inhibition of the Hh signaling pathway inhibits tumor cell proliferation in prostate and gastric cancers, according to those studies (Karhadkar et al., 2004; Sheng et al., 2004).

PI3K-AKT-mTOR pathway

Many cellular stimuli activate PI3K/Akt/mTOR, which controls essential cellular functions like translation, transcription, proliferation, development, and survival. Disrupted activation of the PI3K/Akt pathway has been linked to various human cancers, making it essential for producing new antitumor drugs (Porta and Figlin, 2009). Several studies have suggested that PI3K plays a part in cancer cell survival at different levels (Asati et al., 2016). The loss or downregulation of PTEN, an

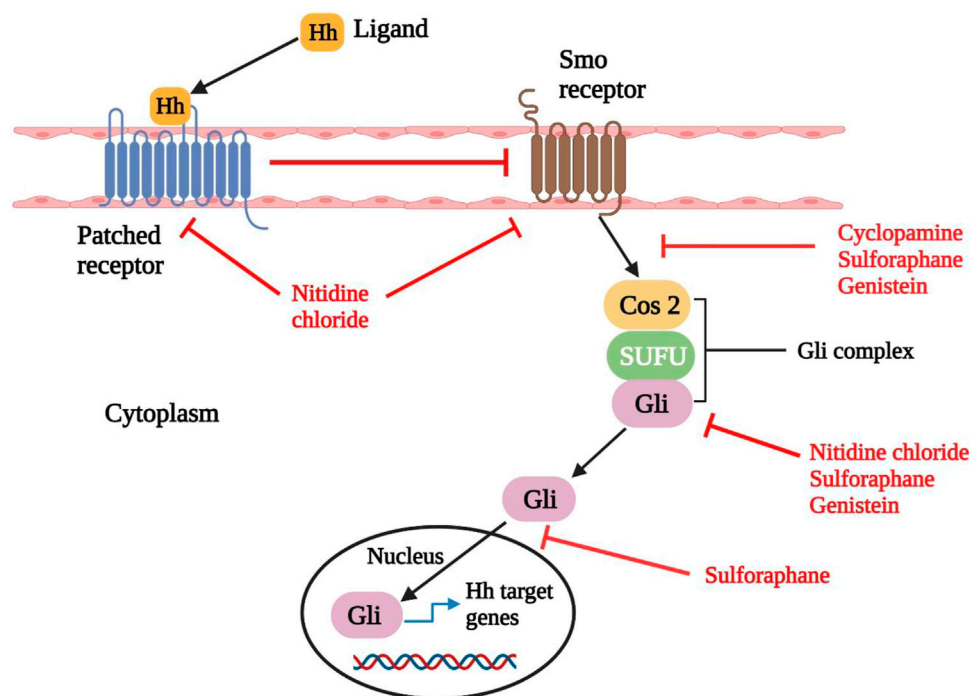


FIGURE 3

Hedgehog signaling and its interference in natural compounds. Upon binding of Hedgehog ligand (Hh) to Patched receptor, Smo is activated (Patched generally inactivates Smo when it is not engaged with ligand). Then Smo brings about the translocation of Gli protein into the nucleus, subsequently causes the transcription of downstream genes. Compounds such as cyclopamine and genistein decrease the expression of Smo. Whereas nitidine chloride downregulates the expression of both Smo and Patched receptors. On the other hand, sulforaphane, nitidine chloride and genistein decrease the expression of Gli protein. Sulforaphane also reduces the expression of Smo, Gli and inhibits the nuclear translocation of Gli. Smo: Smoothened; Cos 2: Costal-2; SUFU: Suppressor of fused homolog; Hh: Hedgehog ligand (Skoda et al., 2018; Das et al., 2019).

essential tumor suppressor protein that encodes phosphatidylinositol-3,4,5-triphosphate (PIP3) 3'-phosphatase, has been shown to stimulate the PI3K pathway (Li et al., 1997; Sansal and Sellers, 2004). Akt is phosphorylated at T308 and S473, while the binding of specific cytokines stimulates PI3K to their receptors. Phosphorylation of Akt facilitates the downregulation of some downstream substrates, such as Bad and GSK-3b, which may contribute to cancerous transformation (Chang et al., 2003). One of the essential functions of Akt during cancer cell proliferation is the aggregation of the cyclin D1 protein, which is mainly regulated by the loss of kinase activity of GSK-3b due to Akt phosphorylation (Diehl et al., 1998). The activation of the PI3K/Akt/mTOR signaling pathway has been linked to the pathogenesis of multiple cancers. It indicated that targeting individual components of this pathway, such as PI3K, phosphoinositide-dependent kinase-1 (PDK-1), Akt, and mTOR (mammalian Target of Rapamycin), may be a possible cancer therapy technique (Asati et al., 2016). According to new research, Ras appears to play an essential role in activating the PI3K/Akt pathway and controls a variety of downstream substrates (Sasaki and Firtel, 2005).

Ras-Raf-MEK-ERK pathways

The Ras/Raf/MEK/ERK pathway is also essential for cell survival at various stages of cancer. In around 30 percent of human cancer, Ras system mutations lead to the expression of Ras proteins that are constitutively active (Stirewalt et al., 2001). Upstream activation by the epidermal growth factor receptor (EGFR) and Ras small guanosine triphosphatases promotes cell proliferation, survival, and metastasis (GTPases) (Roberts and Der, 2007). Phosphorylation positively regulates the activities of ERK 1/2, which include Serine/Threonine Kinases, which MEK1 and MEK2 mediate (Chang et al., 2003). The Ras/Raf/MEK/ERK signaling pathway's phosphorylated ERK (pERK) is a well-known downstream portion. It translocates to the nucleus after being phosphorylated, causing changes in gene expression and regulating various transcription factors such as the Ets family transcription factors (Elk-1) (Roberts and Der, 2007). The Ras/Raf/MEK/ERK signaling cascades are also crucial in regulating gene expression and preventing apoptosis by transmitting signals from growth factor receptors (McCubrey et al., 2007). Since tumors frequently have abnormal expression, they may be candidates for slight molecule inhibition (Ripple et al., 2013).

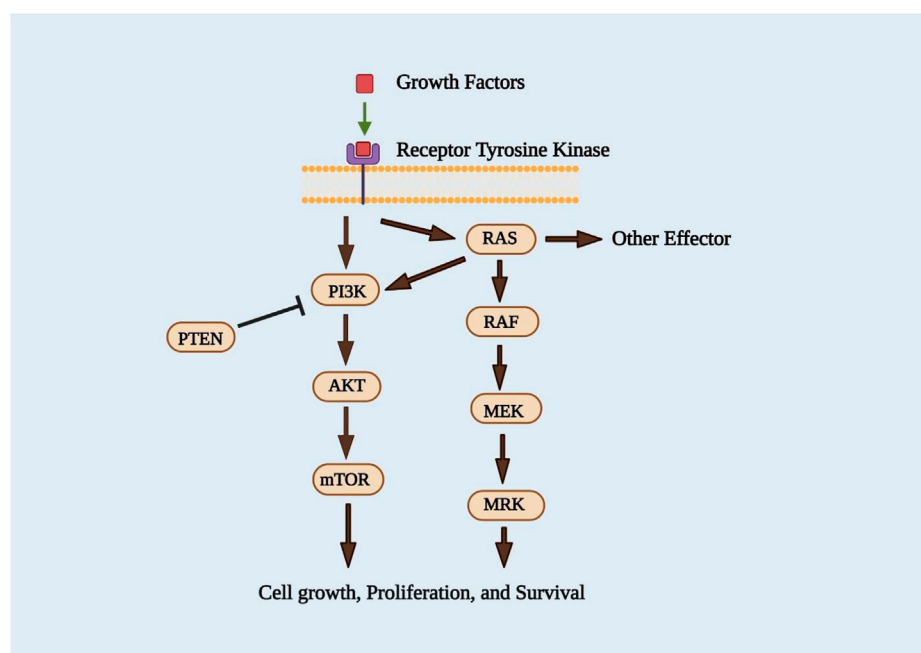


FIGURE 4
PI3K/Akt/mTOR and Ras/Raf/MEK/ERK signaling pathways (Asati et al., 2016).

In recent years, two critical methods for identifying Ras inhibitors have been systematically pursued. Various inhibitors for Ras downstream effector signaling have been developed in the first approach, with hard work focusing on the ERK/MAPK pathway. The second strategy aimed to prevent Ras membrane interaction by blocking post-translational modifications (Roberts and Der, 2007). The development of inhibitors of the PI3K/AKT/mTOR and Ras/MEK/ERK pathways (Figure 4), which are known to be the critical transducers of oncogenic signals in tumor progression, has been crucial (Jokinen et al., 2012).

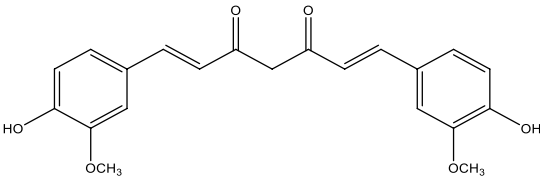
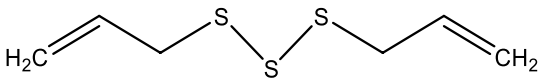
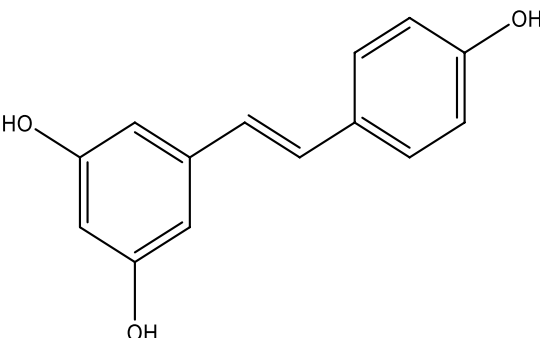
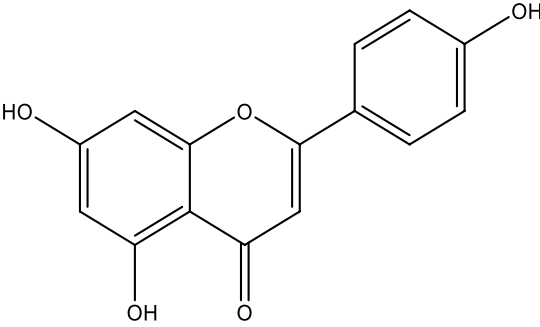
Role of natural compounds in cancer prevention

Plants provide a vast pool of natural ingredients, displaying significant structural diversity, and offer a wide range of new and exciting chemical species, as well as a long tradition of use in the treatment of several diseases (Table 3). According to a survey, 80% of the world's population already uses plant-derived drugs to meet their healthcare needs (Fulda, 2010). It is also been recorded that natural products, their derivatives, or analogs account for 50% of all medications in clinical use, with plant-derived active ingredients accounting for 74% of the most effective drugs (Mandal and Jaganathan, 2009; Hsu et al., 2010). In modern medicine, more than 3,000 plant species have been long-established to be used to treat cancer (Millimouno et al.,

2014). Taxol, irinotecan, vincristine, vinblastine, eribulin, topotecan, trabectedin, and cytarabine are a few examples (Atanasov et al., 2015; ÁK, 2016). The prevention and treatment of cancer with one or more natural substances continue to attract significant interest. Combination treatment entails the use of two or more agents at the same time. Because of the disease's many targets nature, monotherapy has poor success in treating most adult malignancies. It has limited value in prevention due to the diverse paths through which cancer might arise (AS and WF, 1975). Tissue toxicity frequently restricts the usage of a single agent. Other than dosage, natural substances are more likely than pharmacologic treatments to be connected with hazardous consequences, such as adulteration, substitution, contamination, and lack of standardization (JH, 1990). Multiple chemotherapeutic drugs and, more recently, chemotherapy with targeted biologic therapy have been used in cancer treatment as combinations (Bartlett and Chu, 2012).

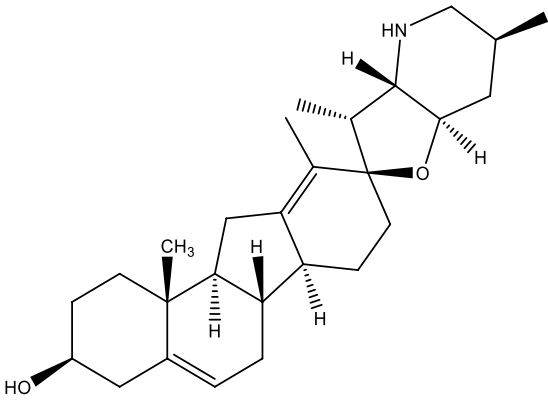
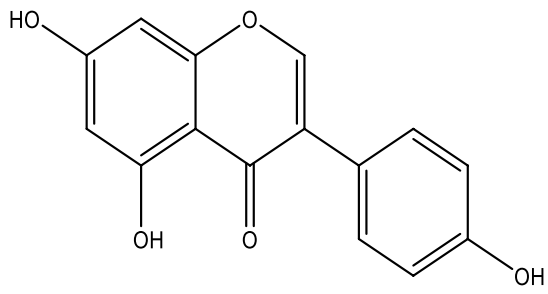
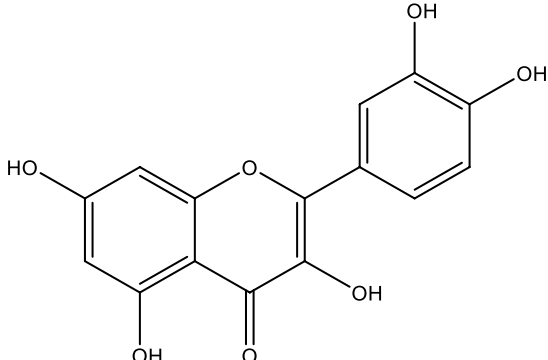
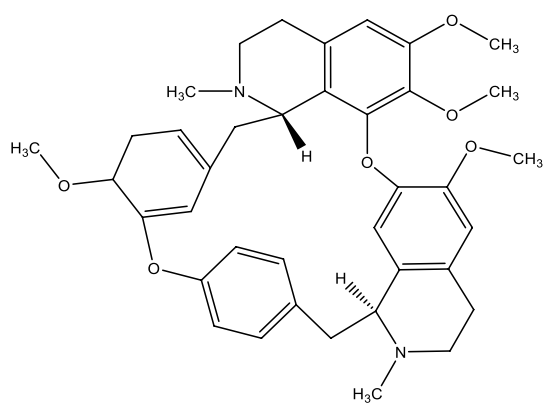
Although a single chemical extracted from nature may not be ideally efficient in preventing or treating cancer, combination therapy utilizing lower dosages with no or decreased toxicity may be beneficial (Bode and Dong, 2009). If possible, use a combination of medicines that targets distinct disease pathways and mechanisms. When possible, combination therapy should use medications that do not cross-resistance and have overlapping side effects. When feasible, tailored treatment should be utilized to match specific molecular

TABLE 3 Mode of action and chemical structure of natural compounds.

Natural compounds	Chemical structure	Mode of action	Cancer Lines	References
Curcumin		Stopping tumor cell invasion and proliferation by inhibiting a number of biological signaling pathways, hence inducing apoptosis.	Colorectal, breast, pancreatic, prostate, brain cancer	Kunnumakkara et al. (2017); Tomeh et al. (2019)
Diallyl trisulfide		Controls a number of processes that are characteristic of cancer, including the cell cycle, apoptosis, angiogenesis, invasion, and metastasis. Arrest cancer cells at several cell cycle stages, with the G2/M arrest receiving the most attention.	Colorectal, lung, myeloma, prostate cancer	Puccinelli and Stan. (2017a); Bansal et al. (2018)
Resveratrol		Since it blocks the monooxygenase cytochrome P450 isoenzyme CYP1 A1, the enzyme responsible for the liver's metabolism of xenobiotics, it acts as a blocking agent by preventing the development of procarcinogen into carcinogen.	Lymphoid, cervix, breast, skin, stomach, prostate, colon, pancreas, thyroid carcinoma cell cancer	Chun et al. (1999); Diaz-Gerevini et al. (2016); Varoni et al. (2016); Ko et al. (2017)
Apigenin		Activate cell apoptosis and autophagy, cause cell cycle arrest, inhibit cell migration and invasion, and stimulate an immunological response to control a variety of human malignancies both <i>in vitro</i> and <i>in vivo</i> .	Colorectal, lung, prostate, breast, ovarian, melanoma, Glioblastoma, Pancreatic, cervical cancer	Yan et al. (2017a)
Cyclopamine		Blocked the hedgehog signaling pathway (Hh).	Prostate, pancreas, breast cancer	Chai et al. (2013); Aphios (2022)

(Continued on following page)

TABLE 3 (Continued) Mode of action and chemical structure of natural compounds.

Natural compounds	Chemical structure	Mode of action	Cancer Lines	References
				
Genistein		Activates the transcription factor CCAAT/enhancer-binding protein homologous protein (CHOP) to cause apoptosis by increasing the production of the glucose-regulated protein 78 (GRP78), which in turn boosts the activity of protein kinase R-like ER kinase (PERK).	Breast, lung, and colon cancer	Tuli et al. (2019)
Quercetin		Caspase activation and apoptotic cell death are the end results of activating p53, which causes the overexpression of Bax and the downregulation of Bcl-2 in tumor cells. Quercetin alters mesangial cells' apoptosis by preventing the activation of the JNK and other ERK pathways.	Breast, colorectal, stomach, head, melanoma, ovarian, lung, leukemia and neck cancer	Khan et al., (2016); Hashemzaei et al. (2017)
Tetrandrine		Induce apoptosis in a dose-dependent manner leading cancer prevention.	Breast, liver, leukemia, colon, pancreatic cancer	Shang et al. (2021); Aphios (2022)

changes (Nikanjam et al., 2017). Maximizing response rates while minimizing standard tissue damage is achieved by targeting several routes or the same pathway through a different method (Gravitz, 2011). Tumor resistance can be overcome better with combination therapy than with monotherapy, as most adult malignancies display substantial genetic variability (Piccart, 2015).

Chemo preventive agents and anticancer compounds

Chemoprevention has become a successful and proactive medical approach to minimizing cancer incidence as a method of cancer control. The development of the disease may be avoided entirely or slowed down by using a nontoxic naturally derived item (Amin et al., 2009). Cancer therapy with economically obtainable manufactured chemotherapeutic agents is restricted due to extreme side effects (Surh and Chun, 2007). Phytochemicals obtained from some kind of food items which are known as chemopreventive agents such as Curcumin, Diallyl trisulfide, Resveratrol, Apigenin, Cyclopamine, Genistein, Quercetin, Tetrandrine, Silibinin, Thymoquinone. When opposed to their synthetic counterparts, natural goods are typically thought to be harmless and free from serious adverse consequences at therapeutic doses, which drives up demand for them dramatically (Pradhan et al., 2020). Phytochemicals obtained from natural sources could be a mix of other compounds. This mixture of other compounds is hard to separate or isolate from target compound. These may interfere with the effectivity of the target compound. The technology of isolating and purifying bioactive or target compounds from plants has recently undergone new advancement. This cutting-edge method allows for a parallel between the creation and accessibility of numerous sophisticated bioassays on the one hand, and the provision of exact techniques for isolation, separation, and purification on the other. Finding a suitable approach that can screen the source material for bioactivity, such as antioxidant, antibacterial, or cytotoxicity, while combining simplicity, specificity, and speed is the aim while looking for bioactive or target compounds (Altemimi et al., 2017). It has been shown that these agents prevent the propagation of carcinogenesis, inhibit the signaling pathways of the development factor, trigger apoptosis, inhibit the activation of NF- κ B, AP-1, and JAK/STAT pathways, inhibit angiogenesis, and inhibit cyclooxygenase-2 (Table 3) (Dorai and Aggarwal, 2004).

Curcumin

It is also known as Diferuloylmethane. It is a light-yellow dye that is part of the polyphenol class. It is obtained from the

turmeric rhizomes (*Curcuma longa* L.) (Plants of the World Online KS, 2022). It is a type of condiment used chiefly for food conservation and well-being in Asian countries. Additionally, utilized as a beauty product and in some pharmaceutical preparations (Rajasekaran, 2011). The compound had been extracted for the first time two centuries earlier, and it was used to treat many systemic conditions such as respiratory, dermatological, and gastrointestinal disorders. Because of its wide variety of functional attributes, Curcumin has been capable of performing many of these activities, “including antioxidant, antiviral, antibacterial, antifungal, anti-inflammatory, and anticancer” characteristics (Aggarwal et al., 2007).

Curcumin is likely to have a suppressing impact on cancer development by many processes including inhibiting carcinogenic activation and cancer-causing agent detoxification, preventing oxidative DNA damage, and reducing inflammation (Surh and Chun, 2007). Curcumin has been proven beneficial in all three stages of carcinogenesis (initiation, promotion, and progression). Plenty of its potential impact is obtained because of inhibiting transcription factor NF- κ B and subsequent suppression of the pro-inflammatory pathways (Thangapazham et al., 2006). It has the good prophylactic and curative ability for many cancers, “including cancer of leukemia, cancer of the gastrointestinal tract, lymphoma cancer, head and neck cancer, lung cancer, genitourinary cancer, breast cancer, ovarian cancer, and skin cancer” (Anand et al., 2008).

Curcumin restrained development and facilitated autophagy and apoptosis (Fu et al., 2018). Mechanistic research has shown that Curcumin can enhance p53 and p21, thereby enabling the signaling pathway for p53. Curcumin has also been shown to denature the PI3K signaling pathway. These findings established Curcumin’s role in inhibiting GC progression, suggesting that it could be used as a GC treatment. By inhibiting the expression of MMP-2/9/9, Curcumin has regulated the invasiveness of oral squamous cell carcinoma (Lee et al., 2015). It also prevented the EMT process by overexpressing p53 function in oral squamous cell carcinoma (OSCC) cells. Curcumin could be used for OSCC medicinal services as an adjunctive method (Li et al., 2015). A higher therapeutic technique for treating human cervical cancer could be Curcumin combined with paclitaxel I (Wang et al., 2019).

Diallyl trisulfide

Food items including fruits, vegetables, and condiments have been used to both prevent and treat a variety of ailments, such as infections, irritability, and wounds. In recent times, it has been shown that bioactive compounds obtained from all of these foods have anti-microbial, anti-inflammatory, and anticancer effects. Plant species of the *Allium* genus, like garlic and onions, are

renowned for their therapeutic quality for a long time (Block, 1985; Petrovska and Cekovska, 2010). Studies have found that organosulfur compounds (OSCs) are the principal bioactive agents responsible for positive effects. Diallyl trisulfide (DATS), a bioactive OSC contained in garlic, can be used to attenuate disease conditions like cancer, infection, and metabolic processes (Mikaili et al., 2013). Cell-cycle deregulation mechanisms are an initiatory cancer production event that allows the unrestrained progression of the cell cycle and rapid growth of the tumor. Few numbers of researching have shown that DATS mediates G2/M-stage cell cycle arrest. DATS induced cell cycle arrest by increasing reactive oxygen species (ROS) (Hosono et al., 2005; Xiao et al., 2005; Antosiewicz et al., 2006). The DATS increase apoptosis which is an effective anti-cancer treatment intended to slow tumor growth. Evidence is mounting that DATS causes cancer cells to respond to cell death signals like oxidative stress, DNA damage, and cellular damage. Results across a variety of cancer cell types have shown that DATS therapy activates the intrinsic apoptotic pathway. Numerous studies have demonstrated increased activation of the apoptosis-regulating protein c-Jun N-terminal kinase (JNK) following DATS incubation. Recent investigations have shown that DATS therapy can inhibit the proteins related to invasion and migration. Following DATS treatment, levels of Tissue Inhibitors of Metalloproteinases (TIMP) -1 and -2, known Matrix Metalloproteinases (MMPs) inhibitors, increased, resulting in improved tight connection formation between bladder cancer cells. The progression of breast and prostate cancers is known to be significantly influenced by estrogen and androgen hormone signaling, respectively. Estrogen sensitivity and HER-2 expression are significant determinants of patient outcome in breast cancer. Studies with breast cancer cell lines that varied in their sensitivity to estrogen and HER-2 status revealed reduced cell viability after DATS therapy (Puccinelli and Stan, 2017b).

Resveratrol

It is also named as 3,5,4'-trihydroxytrans-stilbene. Resveratrol is a naturally appearing phytoalexin and phenol derived from various plants in response to wounds and microbes. Other sources like mulberry, raspberry, blueberry, raisin, and peanut (Ferrucci et al., 2016). Initially, it was separated from the roots of the white hellebore. This phenol is a practical component of the root from *Polygonum cuspidatum* (Dandawate et al., 2013). Resveratrol has antioxidant, anti-inflammatory, and antiproliferative effects on many cancer cells. It efficiently breaks down the enzyme and non-enzyme-generated superoxide, hydroxyl, and peroxynitrite fundamentals and provides defense against DNA damage caused by these ROS (Leonard et al., 2003; Lee and Lee, 2006; Gagliano et al., 2010).

Resveratrol, relying on its striking restrictive impact on cellular events linked to cancer initiation, promotion, and progression, is a viable contender for cancer chemoprevention (Zhu, 2011). It promotes antitumor activity by controlling multiple cell-signaling molecules, including drug therapy transporters, proteins for cell survival, cell proliferative proteins, and signals to members of the NF- κ B and STAT3 (Gupta et al., 2011). In order to effectively lead the multiple cycles of cancer from start and promotion to progression, resveratrol alters the several signal-transduction pathways that control cell growth and division, inflammation, metastasis, apoptosis, and angiogenesis. It has been discovered that resveratrol can stop processes connected to the development of cancers. For instance, resveratrol therapy reduced the production of free radicals in human leukemia HL-60 cells that were generated by 12-O-tetradecanoylphorbol-13-acetate (TPA) (Sharma et al., 1994). Studies conducted *in vitro* have demonstrated that resveratrol has an anti-proliferative impact through inducing apoptosis. Resveratrol affects the proportions of cyclins and cyclin-dependent kinases (CDKs), which inhibits the cell cycle at the G0/G1 phase. For instance, a connection has been discovered between cell cycle arrest in the G0/G1 phase inside several cancer cells and resveratrol's suppression of cyclin D1/CDK4 (Gatouillat et al., 2010). Additionally, it has been demonstrated that resveratrol raises cyclin A and cyclin E levels, causing cell cycle arrest in the G2/M and S phases (Filippi-Chiela et al., 2011). Similar research has shown that resveratrol stops cell cycles and activates a mechanism that is dependent on p53 (Hsieh et al., 2011). Tumor metastasis is caused by a number of processes that are involved in the progression of the tumor. The deletion or mutation of many genes promotes the growth of malignant cancers. Proteolytic enzymes like matrix metalloproteinases are used by cancer cells to invade and spread by destroying the extracellular matrix (ECM) and basement membrane (MMPs). MMP-2 and MMP-9 are two of these enzymes that are overexpressed and regulate cell invasion and metastasis in a range of malignant cancers (Nelson et al., 2000). Resveratrol may decrease the expression of angiogenesis indicators like VEGF, EGFR, and FGF-2 as well as MMPs, particularly MMP-9 (Trapp et al., 2010; Ko et al., 2017).

Apigenin

It is also known as 4',5,7-trihydroxyflavone. Apigenin is a naturally appearing glycoside that belongs to the class of flavone. Various vegetables and fruits produce the compound, including onions, tea, wheat sprouts, and oranges (Tutelyan and Lashneva, 2013). It has characteristics as being anti-oxidant, anti-inflammatory, anti-growth, anti-mutagenic, anti-carcinogenic, and anti-progression (Patel et al., 2007). Previous researches have shown that apigenin prevents tumor proliferation,

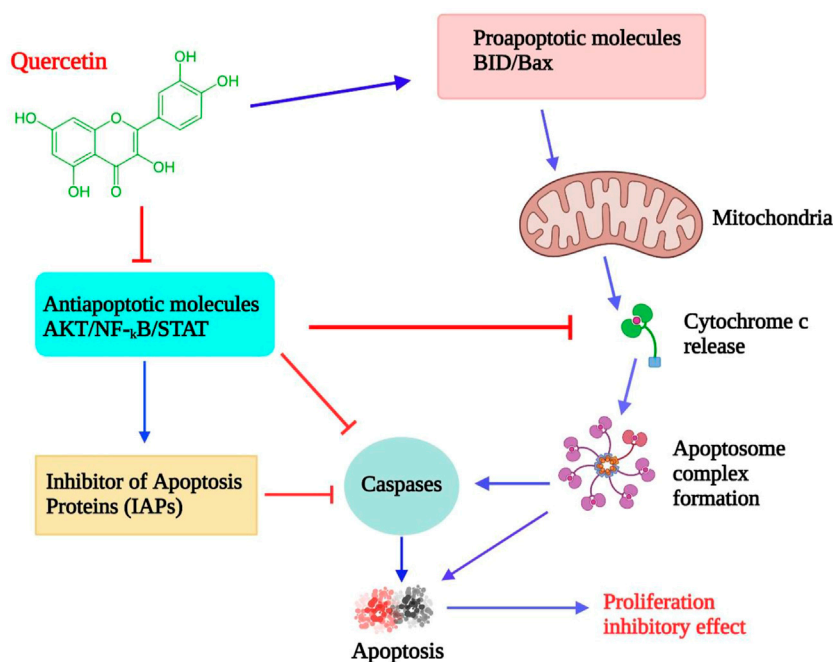


FIGURE 5

Effects of quercetin on lymphoma cells: proposed model. By inhibiting antiapoptotic signaling molecules and inducing proapoptotic proteins, which activate mitochondrial-mediated caspase activation and apoptosis, quercetin reduces cell proliferation (GULATI et al., 2006; Srivastava et al., 2016).

invasion, and tumor development in prostate cancer cells (Shukla et al., 2015). Dimethyl benzantracene-induced skin tumors are suppressed by topical use of apigenin (Wei et al., 1990). It also decreased the prevalence of UV-induced cancer and improved tumor-free survival studies (Birt et al., 1997). Apigenin encourages metal chelation, searches for free radicals, and boosts phase II detoxifying enzymes in cell culture and *in vivo* malignant tumors (Elliott et al., 2000). In the PC-3 tumor model, therapy with apigenin ended in 32 percent and 51 percent suppression of tumor growth (Wei et al., 1990). Studies conducted *in vitro* have demonstrated that resveratrol has an anti-proliferative impact through inducing apoptosis (Liu et al., 2015). Apigenin's anti-cancer properties and minimal toxicity have recently attracted a lot of attention. Apigenin has been shown to inhibit a number of human malignancies both *in vitro* and *in vivo* by a variety of biological mechanisms, including inducing cell apoptosis and autophagy, cell cycle arrest, inhibiting cell migration and invasion, and eliciting an immunological response (Yan et al., 2017b).

Cyclopamine

Cyclopamine is a steroidal alkaloid that can counteract cancers including prostate, gastrointestinal, breast, and

osteosarcoma cancer (Qualtrough et al., 2004; Warzecha et al., 2012; Lü et al., 2014; Zhu et al., 2015). It was separated from the plant corn lily (*Veratrum californicum*) in the late '60s (Lee et al., 2014). Cyclopamine binds to the receptor smoothly, inhibiting additional signal transduction to the GLI5 destination gene (Warzecha et al., 2012). Apart from having a significant role in the development of an embryo, improper initiation of the sonic hedgehog signaling pathway in different cells has been related to nevoid basal cell cancers and many cancers, including basal cell cancers medulloblastoma, and rhabdomyosarcoma (Chen et al., 2002; Heretsch et al., 2010). Nevoid basal cell cancer has been identified as a hereditary condition with several basal cell carcinomas, malignant and benign tumors, and malformations (Bale and Yu, 2001). In a way, the Shh (Sonic hedgehog) signaling pathway's disruption could effectively cure cancer because it can prevent the development of tumors without some typical side effects of conventional carcinogenic therapy. It has been demonstrated that cyclopamine can prevent tumor development. Numerous cancers, including prostate cancer, pancreatic cancer, ovarian cancer, gastrointestinal cancer, lung cancer, and basal cell carcinoma, are linked to aberrant Hedgehog (Hh) signaling. One of the most actively researched targets for cancer therapy is the Hh signaling system, and several drugs that block Hh signaling are currently undergoing clinical trials to treat a variety

of malignancies. More people die from lung cancer than from the next three most frequent malignancies combined (colon, breast, and prostate). Understanding the role of Hh signaling in development and cancer has benefited greatly from the discovery of the first drug to suppress Hh signaling, cyclopamine (Alam et al., 2016).

Genistein

Also known as 4',5,7-Trihydroxyisoflavone. It is a phytoestrogen in soybeans and tofu, soy milk, and soy sauce and is an effective therapeutic agent for cancer (Fotsis et al., 1995; Li et al., 2010). Genistein therapy was found to prevent the development of several cancerous cells by enhancing apoptosis, triggering delayed cell cycles, and regulating intracellular signaling pathways (Li et al., 2010). The potency of intakes of genistein for breast, prostate, and colorectal cancers has been shown in epidemiological reports (Hwang et al., 2009). Modern research has shown that genistein disrupted EGF-induced proliferation by modulation of the PI3K/Akt routes in cancerous colon cells (Qi et al., 2011). Genistein is attributed to cell cycle blockage and cell death in breast cancer cell lines (Magee and Rowland, 2004). It can induce the death of breast cancer cells through the accumulation of intrinsic copper ions and reactive oxygen species (ROS) (Ullah et al., 2011). Genistein is a potent anti-angiogenic compound that can suppress VEGF-induced endothelial cell activation by reducing the function of protein tyrosine kinase (PTK) and the activation of MAPK (Yu et al., 2012). Anti-proliferative activities of genistein obtain from reduced insulin-like growth factor receptor (IGFR) phosphorylation and IGF signaling, which suppresses cell development (Lee et al., 2012). When genistein is used in combination with chemotherapeutic substances, “including letrozole, resveratrol, vitamin-D, paclitaxel, erlotinib, doxorubicin, and cetuximab,” it may be of greatest benefit (Park et al., 2010). Genistein induces ER stress by upregulating the expression of the protein glucose-regulated protein 78 (GRP78). The transcription factor CCAAT/enhancer-binding protein homologous protein (CHOP), which induces apoptosis, is then triggered by the activation of PERK (Tuli et al., 2019). By influencing the nuclear translocation of phosphorylated ERK molecules, genistein reduced the activity and proliferation of cells. ERK regulates cell growth, differentiation, and proliferation, whereas p38 is more closely associated with stress and inflammatory responses (Irrera et al., 2017).

Quercetin

Quercetin is a naturally occurring bioflavonoid found in a wide assortment of foods, along with apples, grapes, berries,

broccoli, onions, tea, tomatoes, nuts, barks, and leaves (Kelly, 2011). As a lipophilic substance, quercetin can pass through cell membranes and start a number of intracellular signaling pathways. The ability of quercetin to serve as both an antioxidant and a peroxidant is one of its distinctive properties (Wätjen et al., 2005). It appears to happen as O-glycosides, and the most common sugar residue is D-glucose. About 170 glycosides of quercetin were identified (Yang et al., 2001). It has several medicinal properties, “including anti-oxidant, anti-bacterial, anti-inflammatory, and anticancer” (Rafiq et al., 2015). It is an effective agent of chemoprevention due to its cardinal effect on the distinctive characteristics of carcinoma and its impact on the signaling pathways associated with tumors (Russo et al., 2012). It exhibits various activities, including modulation of the cell cycle, interacting with type II estrogen receptors, and inhibiting tyrosine kinase (Lamson and Brignall, 2000). When quercetin is administered intravenously, it blocked lymphocyte tyrosine kinase in people with cancer and is the first inhibitory agent of tyrosine kinase tested in a clinical phase I trial (Ferry et al., 1996). It appears that quercetin may have anti-proliferative, anti-tumor, and apoptosis-inducing properties (Figure 5) (Wätjen et al., 2005; Ezzati et al., 2020).

Excessive reactive oxygen species (ROS) generated oxidative strain carries a significant factor in cancer growth. ROS serves itself as a “redox messenger” to promote the growing phases of cells at lower physiological volumes. Residual ROS could damage DNA under oxidative strain. Quercetin can prevent ROS-mediated hepatocarcinogenesis by increased activation of enzymatic and non-enzymatic anti-oxidant defense mechanisms. So, like an antioxidant, quercetin can scour ROS and lower the threat of DNA disruption and cancer development. Due to its overall antioxidant Capacity and higher reducing ability, quercetin inhibits ROS production and active nitrogen molecules in severe monocytic leukemia cells (Waris and Ahsan, 2006; Vásquez-Garzón et al., 2009; Circu, 2010; Zhang et al., 2011). In chemotherapeutic procedures, apoptosis plays an important role. Quercetin can excite apoptosis pathways both intrinsically and extrinsically (Chien et al., 2009).

Tetrandrine

It is a bis-benzylisoquinoline (BBI) alkaloid, separated from the root of *Stephania tetrandra* (Yang et al., 2021). Tetrandrine has different beneficial effects such anti-rheumatic, anti-inflammatory, immunomodulatory, and anti-hypertensive (Yu-Jen, 2002). Collected data shows that tetrandrine has a resistant effect on several cancers, including leukemia, primary hepatic cancer, colorectal cancer, lung cancer, glioblastoma, and nasopharyngeal cancer (Lai et al., 1998; Lee et al., 2002; Kuo and Lin, 2003; Meng et al., 2004; Ng et al., 2006; Sun et al., 2007; Chen et al., 2009; Cho et al., 2009; Wu et al., 2010). Remedial actions of tetrandrine on many cancerous cells have been documented,

including inhibition of growth, anti-inflammatory, modulation of the cell cycle, apoptosis stimulation, angiogenesis prevention, and the abstraction of multidrug sensitivity (Yu-Jen, 2002). Pharmacologically, a few numbers of signaling pathways or essential conditions for example, “mitogen-activated protein kinases (MAPKs), Wnt/ β -catenin, PI3K/Akt, and p53,” have been documented to participate in the cancer prevention process by tetrandrine (Meng et al., 2004; NOMURA et al., 2007; Wu et al., 2010). By influencing Wnt/ β -Catenin, Tetrandrine could prevent the development of the human colorectal cancer cells (He et al., 2011). Tetrandrine has also been seen to incite cytotoxicity and apoptosis of human nasopharyngeal cancerous cells through stimulating ROS-mediated mitochondrial and endoplasmic reticulum (ER) stress pathways and Akt/FOXO3-activation (Chaudhary and Vishwanatha, 2014; Zhang et al., 2015; Lin et al., 2016). Tetrandrine suppressed endometrial cancer cells in a time- and dose-dependent way, the research showed. Tetrandrine caused endometrial cancer cells to undergo apoptosis in a dose-dependent manner, according to flow cytometric analyses (Shang et al., 2021).

Targeting kinase activity by instinctive agents in chemoprevention

Natural substances obtained from several resources can help to activate a range of biological pathways that can protect from cancer (Balunas and Kinghorn, 2005; Cragg and Newman, 2005). The catalyzation of protein phosphorylation by protein kinases is essential for controlling cellular activity. Protein kinases are manifested in different cellular components such as on the cell's exterior, cytoplasm (e.g. Cyclin-based protein kinases), and intracellular regions (e.g. nucleus). Undesirable protein phosphorylation is involved in various disease pathways, including cancer. The construction of multi-targeted and much more efficient PTK blockers gives potential prospects for cancer treatment (Marston, 2011). So, we focused on the evaluation of two agents which are used as significant substances to prevent tumor development/Epstein Barr virus-related cancer.

Grifolin, a potential agent for kinase inhibitor, controls cancer development by targeting ERK1/2 and DAPK1

Grifolin, an active farnesyl phenolic agent, is a secondary plant metabolite derived from the mushroom *Albatrellus confluens*. This also derives from the eatable *Boletus pseudocalopus* mushroom (Song et al., 2009). It has been proven to trigger apoptosis or cell cycle arrest in several

tumor cell lines by targeting ERK or upregulation of DAPK1 via p53 (Ye et al., 2007; Luo et al., 2011). The ERK-1/2 pathway plays some crucial roles in modulating many biological functions, including cell proliferation, division, cell cycle transformation, and longevity. The majority of evidence indicates that ERK1/2 pathway activity leads to tumorigenesis or cancer development and increases cell death (Ishikawa and Kitamura, 1999). ERK modulates several transcription factors such as Elk1, c-Jun, c-Myc, and c-Fos. These variables restrict genetic expression, which is essential for cell cycle propagation, specifically cyclin D1 and p21 (MacCorkle and Tan, 2005). Analyzing the impacts of grifolin on the function of G1-related protein shows that the down-regulation of cyclin D1, CDK4, cyclin E, and the phosphorylation of grifolin-inducing pRB are correlated with the cell cycle blockage. Grifolin resists the multiplication of CNE1 cells by the G1 phase blockage, mediated by G1-protein regulation. Grifolin mainly has an impact on CNE1 cells involving the ERK1/2 route. At high enough doses, the ERK1/2 route could be inhibited (Ye et al., 2005). DAPK1 is a positive moderator which is apoptotic-positive (Pelled et al., 2002). It operates as a tumor suppressor because of its capability to sensitize cells to multiple apoptotic signals, “including those produced by mortal receptors, cytokines, matrix removal, and oncogenic hyperproliferation,” which are envisaged as a cell occurs tumorigenesis. DAPK1 mRNA and protein function has been up-regulated with grifolin in NPC cells in a dose-dependent way. Up-regulation of DAPK1 by grifolin can be an essential process to cause an apoptotic response in the tumor cells. Grifolin can retrieve the pro-apoptotic role of DAPK1 through the p53 route because of the higher occurrence of DAPK1 activity loss in various tumor forms (Luo et al., 2015).

Neoalbaconol, a potent antagonist of PDK1, causes many cell deaths through the PI3K/AKT pathway

It is a new tiny-molecular compound derived from mushroom *Albatrellus confluens*, which can aim at 3-phosphoinositide-dependent protein kinase 1 (PDK1) and suppress its phosphoinositide-3 kinase (PI3-K)/Akt-hexokinase 2 (HK2) routes, which contributed to energy abolition. By locating PDK1, Neoalbaconol decreases glucose and ATP production, triggered autophagy, and induced apoptotic and necroptotic death of cancerous cells by a separate route. The probability that increased activity of Akt counteracts the energy shortage caused by Neoalbaconol, confirms the significance of the PDK1-Akt energy route in NA-induced cell death (Deng et al., 2013). The metabolic energy reconfiguration of cancerous cells is among the essential aspects. The oncogenic PI3K/AKT/mTOR route plays a significant role in reconfiguring metabolic processes in cancerous cells. PDK1 is an Akt/mTOR signaling

controller, that stimulates some protein kinases belonging to the AGC kinase group, such as A, G, and C (Toker and Newton, 2000; Vivanco and Sawyers, 2002). PDK1 phosphorylates function at Ser308 in response to different cell stimulation, contributing to the Akt activation and controlling energy synthesis, cellular proliferation, cell cycle progress, and migratory. Depending on essential activities of PDK1 in tumor cells, analysts lately demonstrated that PDK1 acts as an appropriate therapeutic tool for anticancer and established multiple PDK1 blockers, including AR-12 and GSK233447, for the killing of cancerous cells (Peifer and Alessi, 2008).

So, restructuring cellular energy metabolic processes by locating the PDK1/PI3K/Akt signal pathway, NA is concerned with NA-mediated apoptotic and necroptotic cell destruction. These observations demonstrate that NA is an appropriate choice as a key anticancer agent to inhibit tumor cell development.

Molecular targets for natural chemopreventive agents

In the study of cells and animal models, natural products, such as alkaloids, sesquiterpenes lactones, diterpenoids, flavonoids, and polyphenolics, have been widely studied and discovered to exhibit a considerable range of chemopreventive qualities against several forms of cancer. Many other preventives peruse are underway. The pathways of cell signaling, triggered by natural anticancer chemical substances, are various and specific to individual functions for insistence. Besides that, depending on the cell categories, the same substance stimulates multiple signaling pathways (Millimouno et al., 2014).

p53 Family members

In regulating the genomic integrity, cell cycle, apoptosis, deoxyribonucleic acid repair and response to variations of tumor protein p53 gene and TP53 gene, genotoxic stresses, regarded as the protector of the genome, play an indispensable role (Heinrich et al., 1998; Budram-Mahadeo et al., 2002; Bode and Dong, 2004). Regulation of p53 signaling may suppress the growth and spread of cancer and induce apoptosis of cells (Gong et al., 2017; Su et al., 2017). In GC cells, the signaling pathways which rely on p53 are essential elements to stress cellular responses. Fourcelline in parthenolide, NCI-H1299 lung carcinoma, RKO colon carcinoma, HCT116, and HL60 myeloblastoma activated the substantial decrease in the apoptotic cell frequency in the p53-proficient UV-irradiated row (Guzman et al., 2007; Szoltysek et al., 2008). Parthenolide stimulated p53 and other tumor-suppressor proteins controlled by double mouse minute 2 homolog (MDM2) (Gopal et al., 2009). In PC-3 cells, alanto-lactone causes p53-independent apoptosis in carcinoma of the prostate (Rasul et al., 2013).

Nuclear factor-Kappa B

A prominent transcription factor is the NF- κ B (pro-oncogenic nuclear factor-Kappa B) composed of strongly correlated proteins that form dimers and interact with the κ B B site within target gene promoters. It can enhance target gene transcription by recruiting coactivators and corepressors (Aggarwal, 2004). Genes that, after a viral infection, are used to delegate the replication of (a viral gene) through the presence of a gene at another locus are associated with angiogenesis, cell proliferation, apoptosis, metastasis, tumor cell invasion; the NF- κ B pathway takes part in an influential role in carcinogenesis (Orlowski and Baldwin, 2002). The NF- κ B transcription factor family comprises five types, are- NF- κ B1 (p50), NF- κ B2 (p52), c-Rel, RelB, and RelA (p65), which express the N-terminal Rel homology domain essential for ankyrin repeat deoxyribonucleic acid (DNA) binding and homodimerization and heterodimerization, encompassing the NF- κ B1 nuclear position series (Aggarwal, 2004; Baud and Karin, 2009).

Nuclear factor-related factor 2 is a possible molecular source that compounds found in nature for cancer prevention. By inducing the procurement of Nrf2, some limited natural substances have been identified as possible contenders for chemoprevention. And that is in the nucleus, which actively participates in the transcriptional activation of phase II detoxification enzymes. In the Choi-CK and SCK cells, low parthenolide thresholds resulted in the induction of Nrf2-dependent HO-1, followed by a decrease in its apoptogenic activity. Furthermore, with the protein kinase C- α inhibitor Ro317549 (Ro), parthenolide-mediated apoptosis inhibits activation and nuclear translocation of nuclear factor erythroid 2-related factor 2(Nrf2), resulting in HO-1 expression blockage (Millimouno et al., 2014).

Activator protein 1

Cellular proliferation, modification, and death have been described in the transcription factor. The target genes and molecular pathways modulating these mechanisms have previously been investigated using mice and cells missing AP-1 components. Appropriately, c-growth-promoting Jun's function is negotiated by tumor suppressor incarceration and up-regulation in positive cell cycle regulators (Shaulian and Karin, 2002). Other naturally occurring chemopreventive substances have also been shown to decrease AP-1 synthesis and amplify AP-1 target genes, which is ultimately connected with their chemopreventive potential. These substances include resveratrol, green tea, and curcumin. Activator protein 1 (AP-1) transcriptional activity is regulated by green tea polyphenols in a variety of cell types, which is crucial for their function as development inhibitors. A cell employs transcriptional activity

to monitor the translation of DNA to RNA and hence organize gene activity (Amin et al., 2009).

Signal transducers and activators of transcription pathway

STAT (Signal Transducers and Activators of Transcription) is a unique signal transduction pathway to the nucleus discovered in connection with IFN through the analysis of transcriptional regulation. Several procedures, such as development, immune system feature, multiplicity, differentiation, survival, and EMT (epithelial to mesenchymal transformation), have been involved (Sano et al., 1999; Silver and Montell, 2001). Utilization of different tyrosine kinases leads to STAT protein phosphorylation, nuclear localization, dimerization, linking to and significant transcription of specific DNA components. So many other cancers, namely lymphoma, myeloma, leukemia, and several solid tumors, have been documented to require constitutive STAT3 and STAT5 activation (Rubin Grandis et al., 1998; Sano et al., 1999). Natural substances have been involved in modulating STAT function in tumor cells over the last couple of years. STAT1 dephosphorylation managed to prevent wedelolactone by specifically inhibiting T-cell protein tyrosine phosphatase, an essential enzyme in T-cells for STAT1 tyrosine phosphatase, and STAT1 dephosphorylation inhibited wedelolactone by specifically inhibiting T-cell protein tyrosine phosphatase, which is vital for STAT1 tyrosine phosphatase (Liu et al., 2012; Chen et al., 2013). Parthenolide ($C_{15}H_{20}O_3$) shows significant transcriptional repression of proapoptotic genes activated by STAT inhibition, and alantolactone prevents the formation of STAT3 in HepG2 (Liver Hepatocellular Carcinoma) cells (Legendre et al., 2003; Nakshatri et al., 2004; Khan et al., 2013). In addition to validating STAT as a new goal for chemotherapy of cancer, these combined findings including both *in vivo* studies and *in vitro* have also provided the basis for the production of natural component STAT inhibitors (Millimouno et al., 2014).

Growth factors and their receptors

Factors that foster growth are proteins that associate with the cell surface receptors and documented to influence various cellular mechanisms, with the most important influence of causing apoptosis, proliferation of cells, cytoskeleton rearrangement (Klippel et al., 1996; Kauffmann-Zeh et al., 1997). In carcinogenesis, many growth factors signaling molecules are involved. One of them is a platelet growth factor, endothelial growth factor, the transformation of growth factor, FGF, colony-stimulating factor and insulin-like growth factor (Han et al., 2007). Numerous downstream signals, such as PI3K-Akt and Ras-MAPK, are also involved as a significant

intracellular pathway outcome of growth factor receptor stimulation. The critical impact of these signaling pathways is that many natural chemopreventive and chemotherapeutic compounds relate to reduced prognosis and tumor growth, which are becoming aims. Biological agents, specifically the drug selected, quickly induce Akt phosphorylation after activation, which could be used as an active inhibitor of cancer cells (Millimouno et al., 2014).

Immunoprevention

A re-emergence of concern in cancer immunosurveillance and an expansion of this concept into one termed cancer immunoediting especially have been seen over the past 15 years. The immune system provides protection to the body in the development of primary non-viral cancers and sculpts the immunogenicity of tumors, accompanied by clear observational evidence from murine tumor models and interesting comparative results from human cancer experiments (Dunn et al., 2004). Numerous different natural agents, essential to their prophylactic chemical ability, have modulated specific host factors. Stimulating IL-12-dependent deoxyribonucleic acid (DNA) maintenance, encouraging tumor cell apoptosis, causing cytotoxic ($CD8^+$) T cells, and suppressing angiogenic factors have been shown to inhibit UV-induced skin cancer. Epigallocatechin-3-gallate (EGCG) has improved DNA vaccination-affected $CD8^+$ T cell-mediated antitumor immunity (Amin et al., 2009). 4,7, 4'-trihydroxyisoflavone (Isoflavone genistein) is an elevated phytoestrogen that has been associated with soy products connected with a low prevalence of breast and prostate cancer. The conceivable immune system outcomes of genistein were monitored in adult female B6C3F1 mice. Gavage or genistein is administered to mouse groups for 28 days (Guo et al., 2001). In a murine xenograft model, VEGF luteolin inhibited vascular-induced angiogenesis and *in vivo* tumor development. A range of research has already shown that the purpose of chemical prevention of Curcumin is angiogenesis (Amin et al., 2009).

Safety and effectiveness of chemopreventive agents

While the field of cancer chemoprevention is emerging beyond its pioneering phase, widespread acceptance and use have not yet been established. Many agents described above have been identified through studies *in vitro*, animals, and in humans that can inhibit the growth of cancer and other mutation illnesses. These agents should also meet specific requirements, including 1) low price, as defined by standard costing and the target population, 2) pragmatism of use, as determined by accessibility, storage environments,

and route of administration, 3) efficacy, and 4) safety (Kelloff et al., 2004; Ferguson et al., 2004; D'Agostini et al., 2005). The Latin word *primum non-nocere* serves as a reminder that the most important condition for a medical treatment is that it not cause harm to healthy people. Accordingly, the essential need for pharmacological agents employed in the treatment of people living with cancer is their efficacy, even though this kind of treatment is expensive and inconvenient and associated with severe harmful effects (De Flora and Ferguson, 2005). However, certain chemopreventive drugs, which have been demonstrated to be effective but are also toxic, have been described. The effects of chemotherapeutic agents in cancer development are based on *in vitro* studies and animal studies, which typically use higher dosage levels than what is consumed by humans, and it might be challenging to adopt these results directly to humans. Many chemopreventive agents can have side effects, including mutagenicity, carcinogenicity, and other toxic effects (Kelloff et al., 2000; MB S and SuhN., 2000). Therefore, It is thus necessary to develop definite preventative recommendations for distinct types of malignancies that should be carefully designed, considering ethnic differences, efficacy, and safety of chemopreventive medicines in mind (Lee and Park, 2003).

Conclusion and future perspective

Cancer is perhaps the deadliest disease in the Universe, and it has a massive impact on society, with one out of every three people in the world who have some kind of cancer. Although several existing drugs are ineffective in providing complete cancer protection, it is critical to be developed new treatment methods to treat or slow cancer progression. Bioactive compounds have a wide range of chemical configurations and are likely to be useful in cancer therapy. Anticancer properties vary depending on the variable. Along with their poor aqueous solubility and fast digestion, flavonoids may enhance the performance of stomach, lung, esophageal, colon, and endometrial cancers with limited extreme harmful effects. Alkaloids have a great deal of difficulty meeting their intended destination due to their low bioavailability and poor aqueous solubility. Natural compounds will serve as a stepping stone for reducing the public health effects of primary cancers in the future, thanks to the integration of chemoprevention and chemotherapy drug production. These compounds like chemotherapeutic and immunomodulators are linked to several different targets. Signaling pathways are connected to complex chemical configurations, and this connection is crucial for drug production to continue.

According to data from *in vivo* human and animal research as well as *in vitro* tests, natural products (natural agents) such as

curcumin, isoflavones, resveratrol, I3C, DIM, EGCG, and lycopene have inhibitory action on carcinogenesis and cancer progression. Many cells signaling pathways are thought to be involved in these effects, including the NF- κ B, Wnt, Notch, Akt, MAPK, p53, AR, and ER pathways, among others. Cancer cells constantly exhibit changes in a variety of cellular signaling pathways as a result of the complex interactions between cell signaling networks. As a result, managing cancer cell behavior like cell growth inhibition and death requires medicines that can target numerous cells signaling pathways, and many of these natural products are now regarded to be great examples of natural agents that can target multiple pathways. As a result, we believe that these non-toxic chemicals derived from nature's bounty could be useful in the prevention and/or treatment of most human cancers, either alone or in combination with established therapies (chemotherapy and radiotherapy). Further in-depth mechanistic research *in vitro*, as well as appropriate and relevant animal model studies *in vivo*, as well as unique clinical trials, are required in the future to fully comprehend the significance of these and other natural products in human health and disease.

Author contributions

All authors listed have made a substantial, direct, and intellectual contribution to the work and approved it for publication.

Funding

This research was supported by Basic Science Research Program through the National Research Foundation of Korea (NRF) funded by the Ministry of Education (NRF-2020R1I1A2066868), the National Research Foundation of Korea (NRF) grant funded by the Korea government (MSIT) (No. 2020R1A5A2019413), a grant of the Korea Health Technology R&D Project through the Korea Health Industry Development Institute (KHIDI), funded by the Ministry of Health and Welfare, Republic of Korea (grant number : HF20C0116), and a grant of the Korea Health Technology R&D Project through the Korea Health Industry Development Institute (KHIDI), funded by the Ministry of Health and Welfare, Republic of Korea (grant number : HF20C0038).

Conflict of interest

The authors declare that the research was conducted in the absence of any commercial or financial relationships that could be construed as a potential conflict of interest.

Publisher's note

All claims expressed in this article are solely those of the authors and do not necessarily represent those of their affiliated

References

- Adnal, Madhuri (2022). Explained: What is Dostarlimab, an antibody drug used in rectal cancer trial? *oneindia news* <https://www.oneindia.com/india/explained-what-is-dostarlimab-an-antibody-drug-used-in-rectal-cancer-trial-3417889.html> (Accessed July 14, 2022).
- Aggarwal, B. B. (2004). Nuclear factor-kappaB: The enemy within. *Cancer Cell* 6, 203–208. doi:10.1016/j.ccr.2004.09.003
- Aggarwal, B. B., Sundaram, C., Malani, N., and Ichikawa, H. (2007). Curcumin: The Indian solid gold. *Adv. Exp. Med. Biol.* 595, 1–75. doi:10.1007/978-0-387-46401-5_1
- Ahmed, Z., Timsah, Z., Suen, K. M., Cook, N. P., Lee, G. R., Lin, C. C., et al. (2015). Grb2 monomer-dimer equilibrium determines normal versus oncogenic function. *Nat. Commun.* 6, 1–11. doi:10.1038/ncomms8354
- ÅK (2016). *The origin of FDA approved natural product new chemical entities*. University of Iceland.
- Alam, M. M., Sohoni, S., Kalainayakan, S. P., Garrossian, M., and Zhang, L. (2016). Cyclopamine tartrate, an inhibitor of Hedgehog signaling, strongly interferes with mitochondrial function and suppresses aerobic respiration in lung cancer cells. *BMC Cancer* 16, 150–210. doi:10.1186/s12885-016-2200-x
- Altamimi, A., Lakhssassi, N., Baharlouei, A., Watson, D. G., and Lightfoot, D. A. (2017). Phytochemicals: Extraction, isolation, and identification of bioactive compounds from plant extracts. *Plants*, E42. doi:10.3390/PLANTS6040042
- Amaral, R. G., dos Santos, S. A., Andrade, L. N., Severino, P., and Carvalho, A. A. (2019). Natural products as treatment against cancer: A historical and current vision. *Clin. Oncol.* 4, 1562.
- Amin, A. R. M. R., Kucuk, O., Khuri, F. R., and Shin, D. M. (2009). Perspectives for cancer prevention with natural compounds. *J. Clin. Oncol.* 27, 2712–2725. doi:10.1200/JCO.2008.20.6235
- Anand, P., Sundaram, C., Jhurani, S., Kunnumakkara, A. B., and Aggarwal, B. B. (2008). Curcumin and cancer: An “old-age” disease with an “age-old” solution. *Cancer Lett.* 267, 133–164. doi:10.1016/j.canlet.2008.03.025
- Angulo, P., Kaushik, G., Subramaniam, D., Dandawate, P., Neville, K., Chastain, K., et al. (2017). Natural compounds targeting major cell signaling pathways: A novel paradigm for osteosarcoma therapy. *J. Hematol. Oncol.* 10, 10. doi:10.1186/s13045-016-0373-z
- Antosiewicz, J., Herman-Antosiewicz, A., Marynowski, S. W., and Singh, S. V. (2006). c-Jun NH2-terminal kinase signaling axis regulates diallyl trisulfide-induced generation of reactive oxygen species and cell cycle arrest in human prostate cancer cells. *Cancer Res.* 66, 5379–5386. doi:10.1158/0008-5472.CAN-06-0356
- Anusewicz, D., Orzechowska, M., and Bednarek, A. K. (2021). Notch signaling pathway in cancer—review with bioinformatic analysis. *Cancers (Basel)* 13, 768. doi:10.3390/CANCERS13040768
- Aphios (2022). *Cyclopamine*. Woburn, MA: Aphios. Available at: <https://aphios.com/products/research-chemicals-apis/cyclopamine/> (Accessed June 30, 2022).
- Arber, N., Eagle, C. J., Spicak, J., Rác, I., Dite, P., Hajer, J., et al. (2009). Celecoxib for the prevention of colorectal adenomatous polyps. *N. Engl. J. Med.* 355, 885–895. doi:10.1056/NEJMOA061652
- Arruga, F., Vaisitti, T., and Deaglio, S. (2018). The NOTCH pathway and its mutations in mature B cell malignancies. *Front. Oncol.* 8, 550. doi:10.3389/fonc.2018.00550
- As, K., and Wf, S. (1975). Risk factors in breast cancer. *Prog. Clin. Cancer* 6, 99–114.
- Asati, V., Mahapatra, D. K., and Bharti, S. K. (2016). PI3K/Akt/mTOR and Ras/Raf/MEK/ERK signaling pathways inhibitors as anticancer agents: Structural and pharmacological perspectives. *Eur. J. Med. Chem.* 109, 314–341. doi:10.1016/j.ejmech.2016.01.012
- Atanasov, A. A. G., Waltenberger, B., Pferschy-Wenzig, E. M., Linder, T., Wawrosch, C., Uhrin, P., et al. (2015). *Discovery and resupply of pharmacologically active plant-derived natural products: A review*, 33. doi:10.1016/J.BIOTECHADV.2015.08.001
- Bahrami, A., Hassanian, S. M., ShahidSales, S., Farjami, Z., Hasanzadeh, M., Anvari, K., et al. (2018). Targeting RAS signaling pathway as a potential therapeutic target in the treatment of colorectal cancer. *J. Cell. Physiol.* 233, 2058–2066. doi:10.1002/jcp.25890
- Bailey, J. M., Mohr, A. M., and Hollingsworth, M. A. (2009). Sonic hedgehog paracrine signaling regulates metastasis and lymphangiogenesis in pancreatic cancer. *Oncogene* 28, 3513–3525. doi:10.1038/ncr.2009.220
- Bale, A. E., and Yu, K. P. (2001). The hedgehog pathway and basal cell carcinomas. *Hum. Mol. Genet.* 10, 757–762. doi:10.1093/hmg/10.7.757
- Balunas, M. J., and Kinghorn, A. D. (2005). Drug discovery from medicinal plants. *Life Sci.* 78, 431–441. doi:10.1016/j.lfs.2005.09.012
- Bansal, M., Singh, N., Pal, S., Dev, I., and Ansari, K. M. (2018). Chemopreventive role of dietary phytochemicals in colorectal cancer. *Adv. Mol. Toxicol.* 12, 69–121. doi:10.1016/B978-0-444-64199-1.00004-X
- Bartlett, D. L., and Chu, E. (2012). Can metastatic colorectal cancer Be cured? - ProQuest. *Oncology* 26, 266–275.
- Battle, E., and Clevers, H. (2017). Cancer stem cells revisited. *Nat. Med.* 23, 1124–1134. doi:10.1038/nm.4409
- Baud, V., and Karin, M. (2009). Is NF-κB a good target for cancer therapy? Hopes and pitfalls. *Nat. Rev. Drug Discov.* 8, 33–40. doi:10.1038/nrd2781
- Bhattacharya, T., Soares, G. A. B. E., Chopra, H., Rahman, M. M., Hasan, Z., Swain, S. S., et al. (2022). Applications of phyto-nanotechnology for the treatment of neurodegenerative disorders. *Materials* 15 (15), 804804. doi:10.3390/MA15030804
- Birsoy, K., Wang, T., Possemato, R., Yilmaz, O. H., Koch, C. E., Chen, W. W., et al. (2013). MCT1-mediated transport of a toxic molecule is an effective strategy for targeting glycolytic tumors. *Nat. Genet.* 45, 104–108. doi:10.1038/ng.2471
- Birt, D. F., Mitchell, D., Gold, B., Pour, P., and Pinch, H. C. (1997). Inhibition of ultraviolet light induced skin carcinogenesis in SKH-1 mice by apigenin, a plant flavonoid. *Anticancer Res.* 17, 85–91.
- Block, Eric (1985). The chemistry of garlic and onions. *Sci. Am.* 252, 114–118. doi:10.1038/scientificamerican0385-114
- Bode, A. M., and Dong, Z. (2009). Epigallocatechin 3-gallate and green tea catechins: United they work, divided they fail. *Cancer Prev. Res.* 2, 514–517. doi:10.1158/1940-6207.CAPR-09-0083
- Bode, A. M., and Dong, Z. (2004). Post-translational modification of p53 in tumorigenesis. *Nat. Rev. Cancer* 4, 793–805. doi:10.1038/nrc1455
- Bray, F., Ferlay, J., Soerjomataram, I., Siegel, R. L., Torre, L. A., and Jemal, A. (2018). Global cancer statistics 2018: GLOBOCAN estimates of incidence and mortality worldwide for 36 cancers in 185 countries. *Ca. Cancer J. Clin.* 68, 394–424. doi:10.3322/caac.21492
- Budram-Mahadeo, V., Morris, P. J., and Latchman, D. S. (2002). The Brn-3a transcription factor inhibits the pro-apoptotic effect of p53 and enhances cell cycle arrest by differentially regulating the activity of the p53 target genes encoding Bax and p21CIP1/Waf1. *Oncogene* 21, 6123–6131. doi:10.1038/sj.onc.1205842
- Byrne, W. L., Mills, K. H. G., Lederer, J. A., and O'Sullivan, G. C. (2011). Targeting regulatory T cells in cancer. *Cancer Res.* 71, 6915–6920. doi:10.1158/0008-5472.CAN-11-1156
- Cercek, A., Lumish, M., Sinopoli, J., Weiss, J., Shia, J., Lamendola-Essel, M., et al. (2022). PD-1 blockade in mismatch repair-deficient, locally advanced rectal cancer. *N. Engl. J. Med.* 386, 2363–2376. doi:10.1056/NEJMoa2201445
- Chai, F., Zhou, J., Chen, C., Xie, S., Chen, X., Su, P., et al. (2013). The Hedgehog inhibitor cyclopamine antagonizes chemoresistance of breast cancer cells. *Onco. Targets. Ther.* 6, 1643–1647. doi:10.2147/OTT.S51914
- Chang, F., Lee, J. T., Navolanic, P. M., Steelman, L. S., Shelton, J. G., Blalock, W. L., et al. (2003). Involvement of PI3K/Akt pathway in cell cycle progression, apoptosis, and neoplastic transformation: A target for cancer chemotherapy. *Leukemia* 17, 590–603. doi:10.1038/sj.leu.2402824
- Chaudhary, P., and Vishwanatha, J. K. (2014). C-Jun NH2-terminal kinase-induced proteasomal degradation of c-FLIP/L and Bcl2 sensitize prostate cancer

- cells to Fas- and mitochondria-mediated apoptosis by tetrandrine. *Biochem. Pharmacol.* 91, 457–473. doi:10.1016/j.bcp.2014.08.014
- Chen, J. K., Taipale, J., Cooper, M. K., and Beachy, P. A. (2002). Inhibition of Hedgehog signaling by direct binding of cyclopamine to Smoothened. *Genes. Dev.* 16, 2743–2748. doi:10.1101/gad.1025302
- Chen, Y., Chen, J. C., and Tseng, S. H. (2009). Tetrandrine suppresses tumor growth and angiogenesis of gliomas in rats. *Int. J. Cancer* 124, 2260–2269. doi:10.1002/ijc.24208
- Chen, Z., Sun, X., Shen, S., Zhang, H., Ma, X., Liu, J., et al. (2013). Wedelolactone, a naturally occurring coumestan, enhances interferon- γ signaling through inhibiting STAT1 protein dephosphorylation. *J. Biol. Chem.* 288, 14417–14427. doi:10.1074/jbc.M112.442970
- Chien, S. Y., Wu, Y. C., Chung, J. G., Yang, J. S., Lu, H. F., Tsou, M. F., et al. (2009). Quercetin-induced apoptosis acts through mitochondrial- and caspase-3-dependent pathways in human breast cancer MDA-MB-231 cells. *Hum. Exp. Toxicol.* 28, 493–503. doi:10.1177/0960327109107002
- Cho, H. S., Chang, S. H., Chung, Y. S., Shin, J. Y., Park, S. J., Lee, E. S., et al. (2009). Synergistic effect of ERK inhibition on tetrandrine-induced apoptosis in A549 human lung carcinoma cells. *J. Vet. Sci.* 10, 23–28. doi:10.4142/jvs.2009.10.1.23
- Chopra, H., Bibi, S., Singh, I., Hasan, M. M., Khan, M. S., Yousafi, Q., et al. (2022). Green metallic nanoparticles: Biosynthesis to applications. *Front. Bioeng. Biotechnol.* 0, 874742. doi:10.3389/fbioe.2022.874742
- Christen, P., and Cuendet, M. (2012). Plants as a source of therapeutic and health products. *Chim. (Aarau)* 66, 320–323. doi:10.2533/chimia.2012.320
- Christopoulos, P. F., Gjolberg, T. T., Krüger, S., Haraldsen, G., Andersen, J. T., and Sundisæter, E. (2021). Targeting the notch signaling pathway in chronic inflammatory diseases. *Front. Immunol.* 12, 1194. doi:10.3389/fimmu.2021.668207
- Chun, Y. J., Kim, M. Y., and Guengerich, F. P. (1999). Resveratrol is a selective human cytochrome P450 1A1 inhibitor. *Biochem. Biophys. Res. Commun.* 262, 20–24. doi:10.1006/BBRC.1999.1152
- Circu, M. L. (2010). Reactive oxygen species, cellular redox systems, and apoptosis. *Free Radic. Biol. Med.* 48, 749–762. doi:10.1016/j.freeradbiomed.2009.12.022
- Cragg, G. M., and Newman, D. J. (2005). Plants as a source of anti-cancer agents. *J. Ethnopharmacol.* 100, 72–79. doi:10.1016/j.jep.2005.05.011
- Cross, S. S., and Bury, J. P. (2004). The Hedgehog signalling pathways in human pathology. *Curr. Diagn. Pathol.* 10, 157–168. doi:10.1016/j.cdip.2003.11.005
- D'Agostini, F., Izzotti, A., Balansky, R. M., Bennicelli, C., and De Flora, S. (2005). Modulation of apoptosis by cancer chemopreventive agents. *Mutat. Res.* 591, 173–186. doi:10.1016/J.MRFMMM.2005.03.034
- Damaskos, C., Valsami, S., Kontos, M., Spartalis, E., Kalampokas, T., Kalampokas, E., et al. (2017). Histone deacetylase inhibitors: An attractive therapeutic strategy against breast cancer. *Anticancer Res.* 37, 35–46. doi:10.21873/anticancer.11286
- Dandawate, P., Padhye, S., Ahmad, A., and Sarkar, F. H. (2013). Novel strategies targeting cancer stem cells through phytochemicals and their analogs. *Drug Deliv. Transl. Res.* 3, 165–182. doi:10.1007/s13346-012-0079-x
- Das, P. K., Zahan, T., Abdur Rakib, M., Khanam, J. A., Pillai, S., and Islam, F. (2019). Natural compounds targeting cancer stem cells: A promising resource for chemotherapy. *Anticancer. Agents Med. Chem.* 19, 1796–1808. doi:10.2174/1871520619666190704111714
- De Flora, S., and Ferguson, L. R. (2005). Overview of mechanisms of cancer chemopreventive agents. *Mutat. Res.* 591, 8–15. doi:10.1016/J.MRFMMM.2005.02.029
- Deeb, K. K., Trump, D. L., and Johnson, C. S. (2007). Vitamin D signalling pathways in cancer: Potential for anticancer therapeutics. *Nat. Rev. Cancer* 7 (7), 684–700. doi:10.1038/nrc2196
- Deng, Q., Yu, X., Xiao, L., Hu, Z., Luo, X., Tao, Y., et al. (2013). Neolbaconol induces energy depletion and multiple cell death in cancer cells by targeting PDK1-PI3-K/Akt signaling pathway. *Cell. Death Dis.* 4, e804. doi:10.1038/cddis.2013.324
- Deng, S., Shanmugam, M. K., Kumar, A. P., Yap, C. T., Sethi, G., and Bishayee, A. (2019). Targeting autophagy using natural compounds for cancer prevention and therapy. *Cancer* 125, 1228–1246. doi:10.1002/CNCR.31978
- Diaz-Gerevini, G. T., Repossi, G., Dain, A., Tarres, M. C., Das, U. N., and Eynard, A. R. (2016). Beneficial action of resveratrol: How and why? *Nutrition* 32, 174–178. doi:10.1016/J.NUT.2015.08.017
- Diehl, J. A., Cheng, M., Roussel, M. F., and Sherr, C. J. (1998). Glycogen synthase kinase-3 β regulates cyclin D1 proteolysis and subcellular localization. *Genes. Dev.* 12, 3499–3511. doi:10.1101/gad.12.22.3499
- Dikic, I., and Elazar, Z. (2018). Mechanism and medical implications of mammalian autophagy. *Nat. Rev. Mol. Cell. Biol.* 19619, 349–364. doi:10.1038/s41580-018-0003-4
- Dorai, T., and Aggarwal, B. B. (2004). Role of chemopreventive agents in cancer therapy. *Cancer Lett.* 215, 129–140. doi:10.1016/j.canlet.2004.07.013
- Du, W., Yang, M., Turner, A., Xu, C., Ferris, R., Huang, J., et al. (2017). TIM-3 as a target for cancer immunotherapy and mechanisms of action. *Int. J. Mol. Sci.* 18, 645. doi:10.3390/ijms18030645
- Dunn, G. P., Old, L. J., and Schreiber, R. D. (2004). The immunobiology of cancer immunosurveillance and immunoediting. *Immunity* 21, 137–148. doi:10.1016/j.immuni.2004.07.017
- Ehebauer, M., Hayward, P., and Martinez-Arias, A. (2006). Notch signaling pathway. *Sci. STKE*, cm7. cm7–cm7. doi:10.1126/stke.3642006cm7
- Elliott, Middleton, Jr., Kandaswami, Chithan, and Theoharides, Theoharis C. (2000). The effects of plant flavonoids on mammalian cells: implications for inflammation, heart disease, and cancer | pharmacological reviews. *Pharmacol. Rev.* 52, 673–751.
- Espinoza, I., and Miele, L. (2013). Notch inhibitors for cancer treatment. *Pharmacol. Ther.* 139, 95–110. doi:10.1016/J.PHARMTHERA.2013.02.003
- Ezzati, M., Yousefi, B., Velaei, K., and Safa, A. (2020). A review on anti-cancer properties of Quercetin in breast cancer. *Life Sci.* 248, 117463. doi:10.1016/J.LFS.2020.117463
- Ferguson, L. R., Philpott, M., and Karunasinghe, N. (2004). Dietary cancer and prevention using antimutagens. *Toxicology* 198, 147–159. doi:10.1016/J.TOX.2004.01.035
- Ferrucci, V., Boffa, I., De Masi, G., and Zollo, M. (2016). Natural compounds for pediatric cancer treatment. *Naunyn. Schmiedeb. Arch. Pharmacol.* 389, 131–149. doi:10.1007/s00210-015-1191-5
- Ferry, D. R., Smith, A., Malkhandi, J., Fyfe, D. W., deTakats, P. G., Anderson, D., et al. (1996). Phase I clinical trial of the flavonoid quercetin: Pharmacokinetics and evidence for *in vivo* tyrosine kinase inhibition. *Clin. Cancer Res.* 2, 659–668.
- Filippi-Chiela, E. C., Villodre, E. S., Zamin, L. L., and Lenz, G. (2011). Autophagy interplay with apoptosis and cell cycle regulation in the growth inhibiting effect of resveratrol in glioma cells. *PLoS One* 6, e20849. doi:10.1371/JOURNAL.PONE.0020849
- Forouzanfar, F., and Mousavi, S. H. (2020). Targeting autophagic pathways by plant natural compounds in cancer treatment. *Curr. Drug Targets* 21, 1237–1249. doi:10.2174/1389450121666200504072635
- Fotsis, T., Pepper, M., Adlercreutz, H., Hase, T., Montesano, R., and Schweigerer, L. (1995). Genistein, a dietary ingested isoflavonoid, inhibits cell proliferation and *in vitro* angiogenesis. *J. Nutr.* 125, 790S–797S–797S. doi:10.1093/jn/125.suppl_3.790S
- Fu, H., Wang, C., Yang, D., Wei, Z., Xu, J., Hu, Z., et al. (2018). Curcumin regulates proliferation, autophagy, and apoptosis in gastric cancer cells by affecting PI3K and P53 signaling. *J. Cell. Physiol.* 233, 4634–4642. doi:10.1002/jcp.26190
- Fulda, S. (2010). Evasion of apoptosis as a cellular stress response in cancer. *Int. J. Cell. Biol.* 370835. doi:10.1155/2010/370835
- Gagliano, N., Aldini, G., Colombo, G., Rossi, R., Colombo, R., Gioia, M., et al. (2010). The potential of resveratrol against human gliomas. *Anticancer. Drugs* 21, 140–150. doi:10.1097/CAD.0b013e32833498f1
- Galluzzi, L., Kepp, O., Heiden, M. G. V., and Kroemer, G. (2013). Metabolic targets for cancer therapy. *Nat. Rev. Drug Discov.* 12, 829–846. doi:10.1038/nrd4145
- Gatouillat, G., Balasse, E., Joseph-Pietras, D., Morjani, H., and Madoulet, C. (2010). Resveratrol induces cell-cycle disruption and apoptosis in chemoresistant B16 melanoma. *J. Cell. Biochem.* 110, 893–902. doi:10.1002/JCB.22601
- Gilmore, T. D. (2003). The Re1/NF-kappa B/I kappa B signal transduction pathway and cancer. *Cancer Treat. Res.* 115, 241–265.
- Gong, H., Yu, C., Gang, H., Zhang, Y., Qing, Y., Wang, Y., et al. (2017). P53/microRNA-374b/AKT1 regulates colorectal cancer cell apoptosis in response to DNA damage. *Int. J. Oncol.* 50, 1785–1791. doi:10.3892/ijo.2017.3922
- Gopal, Y. N. V., Chanchorn, E., and Van Dyke, M. W. (2009). Parthenolide promotes the ubiquitination of MDM2 and activates p53 cellular functions. *Mol. Cancer Ther.* 8, 552–562. doi:10.1158/1535-7163.MCT-08-0661
- Goriki, A., Seiler, R., Wyatt, A. W., Contreras-Sanz, A., Bhat, A., Matsubara, A., et al. (2018). Unravelling disparate roles of NOTCH in bladder cancer. *Nat. Rev. Urol.* 15, 345–357. doi:10.1038/s41585-018-0005-1
- Gravitz, L. (2011). Chemoprevention: First line of defence. *Nature*, 471S5–S7. doi:10.1038/471s5a
- Green, D. R., and Evan, G. I. (2002). A matter of life and death. *Cancer Cell.* 1, 19–30. doi:10.1016/S1535-6108(02)00024-7

- Grumolato, L., Liu, G., Mong, P., Mudbhary, R., Biswas, R., Arroyave, R., et al. (2010). Canonical and noncanonical Wnts use a common mechanism to activate completely unrelated coreceptors. *Genes. Dev.* 24, 2517–2530. doi:10.1101/gad.1957710
- Guardian, T. (2022). *Rectal cancer: Researchers hail 'breakthrough' experimental treatment*. London: Royal. Available at: <https://www.theguardian.com/science/2022/jun/08/rectal-cancer-research-breakthrough-experimental-treatment-remission> (Accessed July 1, 2022).
- Gulati, N., Laudet, B., Zohrabian, V. M., Murali, R., and Jhanwar-Uniyal, M. (2006). The antiproliferative effect of quercetin in cancer cells is mediated via inhibition of the PI3K-Akt/PKB pathway. *Anticancer Res.* 26, 1177–1181.
- Guo, T. L., McCay, J. A., Zhang, L. X., Brown, R. D., You, L., Karrow, N. A., et al. (2001). Genistein modulates immune responses and increases host resistance to B16F10 tumor in adult female B6C3F1 mice. *J. Nutr.* 131, 3251–3258. doi:10.1093/jn/131.12.3251
- Gupta, S., Roy, A., and Dwarakanath, B. S. (2017). Metabolic cooperation and competition in the tumor microenvironment: Implications for therapy. *Front. Oncol.* 7, 68. doi:10.3389/fonc.2017.00068
- Gupta, S. C., Kannappan, R., Reuter, S., Kim, J. H., and Aggarwal, B. B. (2011). Chemosensitization of tumors by resveratrol. *Ann. N. Y. Acad. Sci.* 1215, 150–160. doi:10.1111/j.1749-6632.2010.05852.x
- Guzman, M. L., Rossi, R. M., Neelakantan, S., Li, X., Corbett, C. A., Hassane, D. C., et al. (2007). An orally bioavailable parthenolide analog selectively eradicates acute myelogenous leukemia stem and progenitor cells. *Blood* 110, 4427–4435. doi:10.1182/blood-2007-05-090621
- Haddad, R. I., and Shin, D. M. (2009). Recent advances in head and neck cancer. *N. Engl. J. Med.* 359, 1143–1154. doi:10.1056/NEJMRA0707975
- Han, Z., Hong, L., Han, Y., Wu, K., Han, S., Shen, H., et al. (2007). Phospho Akt mediates multidrug resistance of gastric cancer cells through regulation of P-gp, Bcl-2 and Bax. *J. Exp. Clin. Cancer Res.* 26, 261–268.
- Hashemzaei, M., Far, A. D., Yari, A., Heravi, R. E., Tabrizian, K., Taghdisi, S. M., et al. (2017). Anticancer and apoptosis-inducing effects of quercetin *in vitro* and *in vivo*. *Oncol. Rep.* 38, 819–828. doi:10.3892/OR.2017.5766
- Hassan, M., Watari, H., Abualmaaty, A., Ohba, Y., and Sakuragi, N. (2014). Apoptosis and molecular targeting therapy in cancer. *Biomed. Res. Int.*, 150845. doi:10.1155/2014/150845
- He, B. C., Gao, J. L., Zhang, B. Q., Luo, Q., Shi, Q., Kim, S. H., et al. (2011). Tetrandrine inhibits Wnt/ β -catenin signaling and suppresses tumor growth of human colorectal cancer. *Mol. Pharmacol.* 79, 211–219. doi:10.1124/mol.110.068668
- Heinrich, M., Robles, M., West, J. E., Ortiz De Montellano, B. R., and Rodriguez, E. (1998). Ethnopharmacology of Mexican asteraceae (compositae). *Annu. Rev. Pharmacol. Toxicol.* 38, 539–565. doi:10.1146/annurev.pharmtox.38.1.539
- Heretsch, P., Tzagkaroulaki, L., and Giannis, A. (2010). Cyclopamine and hedgehog signaling: Chemistry, biology, medical perspectives. *Angew. Chem. Int. Ed. Engl.* 49, 3418–3427. doi:10.1002/anie.200906967
- Hosono, T., Fukao, T., Ogihara, J., Ito, Y., Shiba, H., Seki, T., et al. (2005). Diallyl trisulfide suppresses the proliferation and induces apoptosis of human colon cancer cells through oxidative modification of β -tubulin. *J. Biol. Chem.* 280, 41487–41493. doi:10.1074/jbc.M507127200
- Hsieh, T. C., Wong, C., John Bennett, D., and Wu, J. M. (2011). Regulation of p53 and cell proliferation by resveratrol and its derivatives in breast cancer cells: An *in silico* and biochemical approach targeting integrin $\alpha\beta$ 3. *Int. J. Cancer* 129, 2732–2743. doi:10.1002/IJC.25930
- Hsieh, Y. S., Yang, S. F., Sethi, G., and Hu, D. N. (2015). Natural bioactives in cancer treatment and prevention. *Biomed. Res. Int.*, 182835. doi:10.1155/2015/182835
- Hsu, C. L., Yu, Y. S., and Yen, G. C. (2010). Anticancer effects of *Alpinia pricei* Hayata roots. *J. Agric. Food Chem.* 58, 2201–2208. doi:10.1021/jf9038056
- Huang, O., Wu, D., Xie, F., Lin, L., Wang, X., Jiang, M., et al. (2015). Targeting rho guanine nucleotide exchange factor ARHGEF5/TIM with auto-inhibitory peptides in human breast cancer. *Amino Acids* 47, 1239–1246. doi:10.1007/s00726-015-1950-0
- Huang, W. Y., Cai, Y. Z., and Zhang, Y. (2009). Natural phenolic compounds from medicinal herbs and dietary plants: Potential use for cancer prevention. *Nutr. Cancer* 62, 1–20. doi:10.1080/01635580903191585
- Hwang, Y. W., Kim, S. Y., Jee, S. H., Kim, Y. N., and Nam, C. M. (2009). Soy food consumption and risk of prostate cancer: A meta-analysis of observational studies. *Nutr. Cancer* 61, 598–606. doi:10.1080/01635580902825639
- Irrera, N., Pizzino, G., D'Anna, R., Vaccaro, M., Arcoraci, V., Squadrito, F., et al. (2017). Dietary management of skin health: The role of genistein. *Nutrients* 9, E622. doi:10.3390/NU9060622
- Ishikawa, Y., and Kitamura, M. (1999). Dual potential of extracellular signal-regulated kinase for the control of cell survival. *Biochem. Biophys. Res. Commun.* 264, 696–701. doi:10.1006/bbrc.1999.1542
- Islam, F., Bibi, S., Meem, A. F. K., Islam, M. M., Rahaman, M. S., Bepary, S., et al. (2021). Natural bioactive molecules: An alternative approach to the treatment and control of COVID-19. *Int. J. Mol. Sci.* 22, 12638. doi:10.3390/IJMS222312638
- Jemal, A., Siegel, R., Xu, J., and Ward Cancer Statistics, E. (2010). Cancer statistics, 2010. *Ca. Cancer J. Clin.* 60, 277–300. doi:10.3322/caac.20073
- Jh, K. (1990). Winning the battle, losing the war? Another editorial about rheumatoid arthritis. *J. Rheumatol.* 17, 1118–1122.
- Jokinen, E., Laurila, N., and Koivunen, J. P. (2012). Alternative dosing of dual PI3K and MEK inhibition in cancer therapy. *BMC Cancer* 12, 612. doi:10.1186/1471-2407-12-612
- Jubb, A. M., Soilleux, E. J., Turley, H., Steers, G., Parker, A., Low, I., et al. (2010). Expression of vascular notch ligand delta-like 4 and inflammatory markers in breast cancer. *Am. J. Pathol.* 176, 2019–2028. doi:10.2353/AJPATH.2010.090908
- Karhadkar, S. S., Bova, G. S., Abdallah, N., Dhara, S., Gardner, D., Maitra, A., et al. (2004). Hedgehog signalling in prostate regeneration, neoplasia and metastasis. *Nature* 431, 707–712. doi:10.1038/nature02962
- Karin, M., Cao, Y., Greten, F. R., and Li, Z. W. (2002). NF- κ B in cancer: From innocent bystander to major culprit. *Nat. Rev. Cancer* 2, 301–310. doi:10.1038/nrc780
- Karin, M., Lawrence, T., and Nizet, V. (2006). Innate immunity gone awry: Linking microbial infections to chronic inflammation and cancer. *Cell* 124, 823–835. doi:10.1016/j.CELL.2006.02.016
- Karin, M., Greten, F. R., and Li, Z. W. (2002). NF- κ B in cancer: From innocent bystander to major culprit. *Nat. Rev. Cancer* 2, 301–310. doi:10.1038/nrc780
- Katoh, M. (2017). Canonical and non-canonical WNT signaling in cancer stem cells and their niches: Cellular heterogeneity, omics reprogramming, targeted therapy and tumor plasticity (Review). *Int. J. Oncol.* 51, 1357–1369. doi:10.3892/ijo.2017.4129
- Kauffmann-Zeh, A., Rodriguez-Vician, P., Ulrich, E., Gilbert, C., Coffey, P., Downward, J., et al. (1997). Suppression of c-Myc-induced apoptosis by Ras signalling through PI(3)K and PKB. *Nature* 385, 544–548. doi:10.1038/385544a0
- Kelloff, G., Hawk, E. T., and Sigman, C. C. (2004). *Cancer chemoprevention*.
- Kelloff, G. J., Crowell, J. A., Steele, V. E., Lubet, R. A., Malone, W. A., Boone, C. W., et al. (2000). Progress in cancer chemoprevention: Development of diet-derived chemopreventive agents. *J. Nutr.* 130, 467S–471S–471S. doi:10.1093/JN/130.2.467S
- Kelly, G. S. (2011). Quercetin. Monograph. *Quercetin. Altern. Med. Rev.* 16, 172–194.
- Khan, F., Niaz, K., Maqbool, F., Hassan, F. I., Abdollahi, M., Nagulapalli Venkata, K. C., et al. (2016). Molecular targets underlying the anticancer effects of quercetin: An update. *Nutrients* 8, 529. doi:10.3390/NU8090529
- Khan, M., Li, T., Ahmad Khan, M. K., Rasul, A., Nawaz, F., Sun, M., et al. (2013). Alantolactone induces apoptosis in HepG2 cells through GSH depletion, inhibition of STAT3 activation, and mitochondrial dysfunction. *Biomed. Res. Int.*, 719858. doi:10.1155/2013/719858
- Khan, M., Maryam, A., Qazi, J. I., and Ma, T. (2015). Targeting apoptosis and multiple signaling pathways with icaride II in cancer cells. *Int. J. Biol. Sci.* 11, 1100–1112. doi:10.7150/IJBS.11595
- Klaus, A., and Birchmeier, W. (2008). Wnt signalling and its impact on development and cancer. *Nat. Rev. Cancer* 8, 387–398. doi:10.1038/nrc2389
- Klippel, A., Reinhard, C., Kavanaugh, W. M., Apell, G., Escobedo, M. A., and Williams, L. T. (1996). Membrane localization of phosphatidylinositol 3-kinase is sufficient to activate multiple signal-transducing kinase pathways. *Mol. Cell. Biol.* 16, 4117–4127. doi:10.1128/mcb.16.8.4117
- Ko, J. H., Sethi, G., Um, J. Y., Shanmugam, M. K., Arfuso, F., Kumar, A. P., et al. (2017). The role of resveratrol in cancer therapy. *Int. J. Mol. Sci.* 18, E2589. doi:10.3390/IJMS18122589
- Komiya, Y., and Habas, R. (2008). Wnt signal transduction pathways. *Organogenesis* 4, 68–75. doi:10.4161/org.4.2.5851
- Kopan, R., and Ilagan, M. X. G. (2009). The canonical notch signaling pathway: Unfolding the activation mechanism. *Cell* 137, 216–233. doi:10.1016/j.cell.2009.03.045
- Kubiczkova, L., Pour, L., Sedlarikova, L., Hajek, R., and Sevcikova, S. (2014). Proteasome inhibitors - molecular basis and current perspectives in multiple myeloma. *J. Cell. Mol. Med.* 18, 947–961. doi:10.1111/jcmm.12279

- Kumar, R., and Fuchs, B. (2015). Hedgehog signaling inhibitors as anti-cancer agents in osteosarcoma. *Cancers (Basel)* 7, 784–794. doi:10.3390/cancers7020784
- Kunnumakkara, A. B., Bordoloi, D., Padmavathi, G., Monisha, J., Roy, N. K., Prasad, S., et al. (2017). Curcumin, the golden nutraceutical: Multitargeting for multiple chronic diseases. *Br. J. Pharmacol.* 174, 1325–1348. doi:10.1111/BPH.13621
- Kuo, P. L., and Lin, C. C. (2003). Tetrandrine-induced cell cycle arrest and apoptosis in Hep G2 cells. *Life Sci.* 73, 243–252. doi:10.1016/S0024-3205(03)00266-2
- Lai, Y. L., Chen, Y. J., Wu, T. Y., Wang, S. Y., Chang, K. H., Chung, C. H., et al. (1998). Induction of apoptosis in human leukemic U937 cells by tetrandrine. *Anticancer. Drugs* 9, 77–81. doi:10.1097/00001813-199801000-00009
- Lamson, D. W., and Brignall, M. S. (2000). Antioxidants and cancer, part 3: Quercetin. *Altern. Med. Rev.* 5, 196–208.
- Laskar, Y. B., Lourebam, R. M., and Mazumder, P. B. (2020). “Herbal remedies for breast cancer prevention and treatment,” in *Medicinal plants-use in prevention and treatment of diseases* (London: IntechOpen).
- Le, H., Kleinerman, R., Lerman, O. Z., Brown, D., Galiano, R., Gurtner, G. C., et al. (2008). Hedgehog signaling is essential for normal wound healing. *Wound Repair Regen.* 16, 768–773. doi:10.1111/j.1524-475X.2008.00430.x
- Lee, A. Y. L., Fan, C. C., Chen, Y. A., Cheng, C. W., Sung, Y. J., Hsu, C. P., et al. (2015). Curcumin inhibits invasiveness and epithelial-mesenchymal transition in oral squamous cell carcinoma through reducing matrix metalloproteinase 2, 9 and modulating p53-E-cadherin pathway. *Integr. Cancer Ther.* 14, 484–490. doi:10.1177/1534735415588930
- Lee, B. M., and Park, K. K. (2003). Beneficial and adverse effects of chemopreventive agents. *Mutat. Res.* 523–524, 265–278. doi:10.1016/S0027-5107(02)00342-1
- Lee, J., Ju, J., Park, S., Hong, S. J., and Yoon, S. (2012). Inhibition of IGF-1 signaling by genistein: Modulation of E-cadherin expression and downregulation of β -catenin signaling in hormone refractory PC-3 prostate cancer cells. *Nutr. Cancer* 64, 153–162. doi:10.1080/01635581.2012.630161
- Lee, J. H., Kang, G. H., Kim, K. C., Kim, K. M., Park, D. Il, Choi, B. T., et al. (2002). Tetrandrine-induced cell cycle arrest and apoptosis in A549 human lung carcinoma cells. *Int. J. Oncol.* 21, 1239–1244. doi:10.3892/ijo.21.6.1239
- Lee, K. W., and Lee, H. J. (2006). The roles of polyphenols in cancer chemoprevention. *BioFactors* 26, 105–121. doi:10.1002/biof.5520260202
- Lee, S. T., Welch, K. D., Panter, K. E., Gardner, D. R., Garrossian, M., and Chang, C. W. T. (2014). Cyclopamine: From cyclops lambs to cancer treatment. *J. Agric. Food Chem.* 62, 7355–7362. doi:10.1021/jf5005622
- Legendre, F., Dudhia, J., Pujol, J. P., and Bogdanowicz, P. (2003). JAK/STAT but not ERK1/ERK2 pathway mediates interleukin (IL)-6/soluble IL-6R down-regulation of type II collagen, aggrecan core, and link protein transcription in articular chondrocytes. Association with a down-regulation of Sox9 expression. *J. Biol. Chem.* 278, 2903–2912. doi:10.1074/jbc.M110773200
- Leonard, S. S., Xia, C., Jiang, B. H., Stinefelt, B., Klandorf, H., Harris, G. K., et al. (2003). Resveratrol scavenges reactive oxygen species and effects radical-induced cellular responses. *Biochem. Biophys. Res. Commun.* 309, 1017–1026. doi:10.1016/j.bbrc.2003.08.105
- Lezhnina, K., Kovalchuk, O., Zhavoronkov, A. A., Korzinkin, M. B., Zabolotneva, A. A., Shegay, P. V., et al. (2014). Novel robust biomarkers for human bladder cancer based on activation of intracellular signaling pathways. *Oncotarget* 5, 9022–9032. doi:10.18632/oncotarget.2493
- Li, J., Yen, C., Liaw, D., Podsypanina, K., Bose, S., Wang, S. I., et al. (1997). PTEN, a putative protein tyrosine phosphatase gene mutated in human brain, breast, and prostate cancer. *Science* 275, 1943. doi:10.1126/science.275.5308.1943
- Li, Q., and Verma, I. M. (2002). NF- κ B regulation in the immune system. *Nat. Rev. Immunol.* 2, 725–734. doi:10.1038/nri910
- Li, W., Frame, L. T., Hirsch, S., and Cobos, E. (2010). Genistein and hematological malignancies. *Cancer Lett.* 296, 1–8. doi:10.1016/j.canlet.2010.05.002
- Li, W., Wang, Y., Song, Y., Xu, L., Zhao, J., and Fang, B. (2015). A preliminary study of the effect of curcumin on the expression of p53 protein in a human multiple myeloma cell line. *Oncol. Lett.* 9, 1719–1724. doi:10.3892/ol.2015.2946
- Lin, Y., Bai, L., Chen, W., and Xu, S. (2010). The NF- κ B activation pathways, emerging molecular targets for cancer prevention and therapy. *Expert Opin. Ther. Targets* 14, 45–55. doi:10.1517/14728220903431069
- Lin, Y. J., Peng, S. F., Lin, M. L., Kuo, C. L., Lu, K. W., Liao, C. L., et al. (2016). Tetrandrine induces apoptosis of human nasopharyngeal carcinoma npc-Tw 076 cells through reactive oxygen species accompanied by an endoplasmic reticulum stress signaling pathway. *Molecules* 21, 1353. doi:10.3390/molecules21101353
- Liu, S. H., Wang, K. Bin, Lan, K. H., Lee, W. J., Pan, H. C., Wu, S. M., et al. (2012). Calpain/SHP-1 interaction by honokiol dampening peritoneal dissemination of gastric cancer in nu/nu mice. *PLoS One* 7, e43711. doi:10.1371/journal.pone.0043711
- Liu, X., Li, L., Lv, L., Chen, D., Shen, L., and Xie, Z. (2015). Apigenin inhibits the proliferation and invasion of osteosarcoma cells by suppressing the Wnt/ β -catenin signaling pathway. *Oncol. Rep.* 34, 1035–1041. doi:10.3892/or.2015.4022
- Lü, Z. Y., Lü, L. D., and Liang-Hong, M. A. (2014). Effects of cyclopamine on the proliferation and apoptosis of LNCaP cells and expression of the PCA3 gene in human prostate cancer. *Zhonghua Nan Ke Xue* 20, 213–217.
- Luo, X., Yu, X., Liu, S., Deng, Q., Liu, X., Peng, S., et al. (2015). The role of targeting kinase activity by natural products in cancer chemoprevention and chemotherapy (Review). *Oncol. Rep.* 34, 547–554. doi:10.3892/or.2015.4029
- Luo, X. J., Li, L. L., Deng, Q. P., Yu, X. F., Yang, L. F., Luo, F. J., et al. (2011). Grifolin, a potent antitumor natural product upregulates death-associated protein kinase 1 DAPK1 via p53 in nasopharyngeal carcinoma cells. *Eur. J. Cancer* 47, 316–325. doi:10.1016/j.ejca.2010.09.021
- Ma, X., Sheng, T., Zhang, Y., Zhang, X., He, J., Huang, S., et al. (2006). Hedgehog signaling is activated in subsets of esophageal cancers. *Int. J. Cancer* 118, 139–148. doi:10.1002/ijc.21295
- MacCorkle, R. A., and Tan, T. H. (2005). Mitogen-activated protein kinases in cell-cycle control. *Cell. biochem. Biophys.* 43, 451–461. doi:10.1385/CBB:43:3:451
- Magee, P. J., and Rowland, I. R. (2004). Phyto-oestrogens, their mechanism of action: Current evidence for a role in breast and prostate cancer. *Br. J. Nutr.* 91, 513–531. doi:10.1079/bjn20031075
- Mandal, M., and Jaganathan, S. K. (2009). Antiproliferative effects of honey and of its polyphenols: A review. *J. Biomed. Biotechnol.* 830616. doi:10.1155/2009/830616
- Manson, M. M. (2003). Cancer prevention - the potential for diet to modulate molecular signalling. *Trends Mol. Med.* 9, 11–18. doi:10.1016/S1471-4914(02)00002-3
- Marston, A. (2011). Natural products as a source of protein kinase Activators and inhibitors. *Curr. Top. Med. Chem.* 11, 1333–1339. doi:10.2174/156802611795589575
- Martin, G. S. (2003). Cell signaling and cancer. *Cancer Cell.* 4, 167–174. doi:10.1016/S1535-6108(03)00216-2
- Mb, S. N. S., and SuhN. (2000). Chemoprevention of cancer. *Carcinogenesis* 21, 525–530. doi:10.1093/CARCIN/21.3.525
- McCubrey, J. A., Steelman, L. S., Chappell, W. H., Abrams, S. L., Wong, E. W. T., Chang, F., et al. (2007). Roles of the Raf/MEK/ERK pathway in cell growth, malignant transformation and drug resistance. *Biochim. Biophys. Acta* 1773, 1263–1284. doi:10.1016/j.bbamcr.2006.10.001
- Medzhitov, R. (2001). Toll-like receptors and innate immunity. *Nat. Rev. Immunol.* 1, 135–145. doi:10.1038/35100529
- Meng, L. H., Zhang, H., Hayward, L., Takemura, H., Shao, R. G., and Pommier, Y. (2004). Tetrandrine induces early G1 arrest in human colon carcinoma cells by down-regulating the activity and inducing the degradation of G1-S-specific cyclin-dependent kinases and by inducing p53 and p21Cip1. *Cancer Res.* 64, 9086–9092. doi:10.1158/0008-5472.CAN-04-0313
- Michaud, E. J., and Yoder, B. K. (2006). The primary cilium in cell signaling and cancer. *Cancer Res.* 66, 6463–6467. doi:10.1158/0008-5472.CAN-06-0462
- Mikaili, P., Maadirad, S., Moloudizargari, M., Aghajanshakeri, S., and Sarahroodi, S. (2013). Therapeutic uses and pharmacological properties of garlic, shallot, and their biologically active compounds. *Iran. J. Basic Med. Sci.* 16, 1031–1048. doi:10.22038/ijbms.2013.1865
- Millimouno, F. M., Dong, J., Yang, L., Li, J., and Li, X. (2014). Targeting apoptosis pathways in cancer and perspectives with natural compounds from mother nature. *Cancer Prev. Res.* 7, 1081–1107. doi:10.1158/1940-6207.CAPR-14-0136
- Moretti, J., and Brou, C. (2013). Ubiquitinations in the notch signaling pathway. *Int. J. Mol. Sci.* 14, 6359–6381. doi:10.3390/IJMS14036359
- Nagelkerke, A., Bussink, J., Geurts-Moespot, A., Sweep, F. C. G. J., and Span, P. N. (2015). Therapeutic targeting of autophagy in cancer. Part II: Pharmacological modulation of treatment-induced autophagy. *Semin. Cancer Biol.* 31, 99–105. doi:10.1016/j.semcancer.2014.06.001
- Nakshatri, H., Rice, S. E., and Bhat-Nakshatri, P. (2004). Antitumor agent parthenolide reverses resistance of breast cancer cells to tumor necrosis factor-related apoptosis-inducing ligand through sustained activation of c-Jun N-terminal kinase. *Oncogene* 23, 7330–7344. doi:10.1038/sj.onc.1207995

- National Cancer Institute (2022). *Definition of signaling pathway - NCI dictionary of cancer terms*. Maryland: Natl Cancer Inst.
- Nawaz, J., Rasul, A., Shah, M. A., Hussain, G., Riaz, A., Sarfraz, I., et al. (2020). Cardamonin: A new player to fight cancer via multiple cancer signaling pathways. *Life Sci.* 250, 117591. doi:10.1016/j.lfs.2020.117591
- Nelson, A. R., Fingleton, B., Rothenberg, M. L., and Matrisian, L. M. (2000). Matrix metalloproteinases: Biologic activity and clinical implications. *J. Clin. Oncol.* 18, 1135–1149. doi:10.1200/jco.2000.18.5.1135
- Ng, L. T., Chiang, L. C., Lin, Y. T., and Lin, C. C. (2006). Antiproliferative and apoptotic effects of tetrandrine on different human hepatoma cell lines. *Am. J. Chin. Med.* 34, 125–135. doi:10.1142/S0192415X06003692
- Niemitz, E. (2013). Ras pathway activation in breast cancer. *Nat. Genet.* 45, 1273. doi:10.1038/ng.2817
- Nikanjam, M., Liu, S., Yang, J., and Kurzrock, R. (2017). Dosing three-drug combinations that include targeted anti-cancer agents: Analysis of 37,763 patients. *Oncologist* 22, 576. doi:10.1634/THEONCOLOGIST.2016-0357
- Nomura, M., Yamazaki, R., Takaya, M., Kikuchi, M., Takahashi-Nishioka, T., Akiyama, K., et al. (2007). Inhibition of tetrandrine on epidermal growth factor-induced cell transformation and its signal transduction. *Anticancer Res.* 27, 3187–3193.
- Okajima, T., and Matsuda, T. (2006). Roles of O-fucosyltransferase 1 and O-linked fucose in notch receptor function. *Methods Enzymol.* 417, 111–126. doi:10.1016/S0076-6879(06)17009-3
- Orlowski, R. Z., and Baldwin, A. S. (2002). NF-kappaB as a therapeutic target in cancer. *Trends Mol. Med.* 8, 385–389. doi:10.1016/S1471-4914(02)02375-4
- Park, S. J., Kim, M. J., Kim, Y. K., Kim, S. M., Park, J. Y., and Myoung, H. (2010). Combined cetuximab and genistein treatment shows additive anti-cancer effect on oral squamous cell carcinoma. *Cancer Lett.* 292, 54–63. doi:10.1016/j.canlet.2009.11.004
- Patel, D., Shukla, S., and Gupta, S. (2007). Apigenin and cancer chemoprevention: Progress, potential and promise (Review). *Int. J. Oncol.* 30, 233–245. doi:10.3892/ijo.30.1.233
- Peifer, C., and Alessi, D. R. (2008). Small-molecule inhibitors of PDK1. *ChemMedChem* 3, 1810–1838. doi:10.1002/cmdc.200800195
- Pelled, D., Raveh, T., Riebeling, C., Fridkin, M., Berissi, H., Futerman, A. H., et al. (2002). Death-associated protein (DAP) kinase plays a central role in ceramide-induced apoptosis in cultured hippocampal neurons. *J. Biol. Chem.* 277, 1957–1961. doi:10.1074/jbc.M104677200
- Petrovska, B., and Cekovska, S. (2010). Extracts from the history and medical properties of garlic. *Pharmacogn. Rev.* 4, 106–110. doi:10.4103/0973-7847.65321
- Piccart, M. (2015). Clinical management of breast cancer heterogeneity. *Nat. Rev. Clin. Oncol.* 12, 381–394. doi:10.1038/NRCLINONC.2015.73
- Plants of the World Online KS (2022). *Curcuma longa* L. Royal Botanic Gardens, Kew: Kew Sci. <https://powo.science.kew.org/taxon/urn:lsid:ipni.org:names:796451-1> (Accessed July 14, 2022).
- Plotnikova, O. V., Golemis, E. A., and Pugacheva, E. N. (2008). Cell cycle-dependent cellinogenesis and cancer. *Cancer Res.* 68, 2058–2061. doi:10.1158/0008-5472.CAN-07-5838
- Porta, C., and Figlin, R. A. (2009). Phosphatidylinositol-3-Kinase/Akt signaling pathway and kidney cancer, and the therapeutic potential of phosphatidylinositol-3-kinase/akt inhibitors. *J. Urol.* 182, 2569–2577. doi:10.1016/j.juro.2009.08.085
- Pradhan, D., Biswasroy, P., Sahu, A., Sahu, D. K., Ghosh, G., and Rath, G. (2020). Recent advances in herbal nanomedicines for cancer treatment. *Curr. Mol. Pharmacol.* 14, 292–305. doi:10.2174/1874467213666200525010624
- Puccinelli, M. T., and Stan, S. D. (2017). Dietary bioactive diallyl trisulfide in cancer prevention and treatment. *Int. J. Mol. Sci.* 18, 1645. doi:10.3390/IJMS18081645
- Puccinelli, M. T., and Stan, S. D. (2017). Dietary bioactive diallyl trisulfide in cancer prevention and treatment. *Int. J. Mol. Sci.* E1645. doi:10.3390/IJMS18081645
- Qi, W., Weber, C. R., Wasland, K., and Savkovic, S. D. (2011). Genistein inhibits proliferation of colon cancer cells by attenuating a negative effect of epidermal growth factor on tumor suppressor FOXO3 activity. *BMC Cancer* 11, 219. doi:10.1186/1471-2407-11-219
- Qualtrough, D., Buda, A., Gaffield, W., Williams, A. C., and Paraskeva, C. (2004). Hedgehog signalling in colorectal tumour cells: Induction of apoptosis with cyclopamine treatment. *Int. J. Cancer* 110, 831–837. doi:10.1002/ijc.20227
- Rafiq, R. A., Quadri, A., Nazir, L. A., Peerzada, K., Ganai, B. A., and Tasduq, S. A. (2015). A potent inhibitor of phosphoinositide 3-kinase (PI3K) and mitogen activated protein (MAP) kinase signalling, Quercetin (3,3',4',5,7-pentahydroxyflavone) promotes cell death in Ultraviolet (UV)-B-irradiated B16F10 melanoma cells. *PLoS One* 10, e0131253. doi:10.1371/journal.pone.0131253
- Rahman, M. M., Islam, R., Shohag, S., Hossain, E., Shah, M., Khan, Shuvo S., et al. (2022). Multifaceted role of natural sources for COVID-19 pandemic as marine drugs. *Environ. Sci. Pollut. Res. Int.* 2022 (1), 46527–46550. doi:10.1007/S11356-022-20328-5
- Rahman, M. M., Behl, T., Islam, M. R., Alam, M. N., Islam, M. M., Albarrati, A., et al. (2022). Emerging management approach for the adverse events of immunotherapy of cancer. *Molecules* 27, 3798. doi:10.3390/MOLECULES27123798
- Rahman, M. M., Bibi, S., Rahaman, M. S., Rahman, F., Islam, F., Khan, M. S., et al. (2022). Natural therapeutics and nutraceuticals for lung diseases: Traditional significance, phytochemistry, and pharmacology. *Biomed. Pharmacother.* 150, 113041. doi:10.1016/j.biopha.2022.113041
- Rahman, M. M., Dhar, P. S., Sumaia, S., Anika, F., Ahmed, L., Islam, M. R., et al. (2022). Exploring the plant-derived bioactive substances as antidiabetic agent: An extensive review. *Biomed. Pharmacother.* 152, 113217. doi:10.1016/j.biopha.2022.113217
- Rahman, M. M., Ferdous, K. S., Ahmed, M., Islam, M. T., Khan, M. R., Perveen, A., et al. (2021). Hutchinson-gilford progeria syndrome: An overview of the molecular mechanism, pathophysiology and therapeutic approach. *Curr. Gene Ther.* 21, 216–229. doi:10.2174/1566523221666210303100805
- Rahman, M. M., Islam, F., -Or-Rashid, M. H., Mamun, A. Al, Rahaman, M. S., Islam, M. M., et al. (2022). The gut microbiota (microbiome) in cardiovascular disease and its therapeutic regulation. *Front. Cell. Infect. Microbiol.* 0, 903570. doi:10.3389/fcimb.2022.903570
- Rahman, M. M., Islam, F., Afsana Mim, S., Khan, M. S., Islam, M. R., Haque, M. A., et al. (2022). Multifunctional therapeutic approach of nanomedicines against inflammation in cancer and aging. *J. Nanomater.* 1–19. doi:10.1155/2022/4217529
- Rahman, M. M., Islam, F., Parvez, A., Azad, M. A. K., Ashraf, G. M., Ullah, M. F., et al. (2022). Citrus limon L. (lemon) seed extract shows neuro-modulatory activity in an *in vivo* thiopental-sodium sleep model by reducing the sleep onset and enhancing the sleep duration. *J. Integr. Neurosci.* 21, 42. doi:10.31083/J.JIN2101042/1757-448X-21-1-042/FIG1
- Rahman, M. M., Islam, M. R., Akash, S., Harun-Or-Rashid, M., Ray, T. K., Rahaman, M. S., et al. (2022). Recent advancements of nanoparticles application in cancer and neurodegenerative disorders: At a glance. *Biomed. Pharmacother.* 153, 113305. doi:10.1016/j.biopha.2022.113305
- Rahman, M. M., Islam, M. R., Islam, M. T., Harun-Or-rashid, M., Islam, M., Abdullah, S., et al. (2022). Stem cell transplantation therapy and neurological disorders: Current status and future perspectives. *Biol. (Basel)* 11, 147. doi:10.3390/BIOLOGY11010147
- Rahman, M. M., Islam, M. R., Shohag, S., Ahasan, M. T., Sarkar, N., Khan, H., et al. (2022). Microbiome in cancer: Role in carcinogenesis and impact in therapeutic strategies. *Biomed. Pharmacother.* 149, 112898. doi:10.1016/j.biopha.2022.112898
- Rahman, M. M., Rahaman, M. S., Islam, M. R., Hossain, M. E., Mithi, F. M., Ahmed, M., et al. (2021). Multifunctional therapeutic potential of phytocomplexes and natural extracts for antimicrobial properties. *Antibiotics* 1010, 10761076. doi:10.3390/ANTIBIOTICS10091076
- Rahman, M. M., Rahaman, M. S., Islam, M. R., Rahman, F., Mithi, F. M., Alqahtani, T., et al. (2021). Role of phenolic compounds in human disease: Current knowledge and future prospects. *Molecules* 27, 233. doi:10.3390/MOLECULES27010233
- Rahman, M. M., Tumpa, M. A. A., Zehravi, M., Sarker, M. T., Yamin, M., Islam, M. R., et al. (2022K). An overview of antimicrobial stewardship optimization: The use of antibiotics in humans and animals to prevent resistance. *Antibiotics* 1111, 667667. doi:10.3390/ANTIBIOTICS11050667
- Rajasekaran, S. A. (2011). Therapeutic potential of curcumin in gastrointestinal diseases. *World J. Gastrointest. Pathophysiol.* 2, 1. doi:10.4291/wjg.v2.i1.1
- Rasul, A., Khan, M., Ali, M., Li, J., and Li, X. (2013). Targeting apoptosis pathways in cancer with alantolactone and isosalantolactone. *ScientificWorldJournal*, 248532. doi:10.1155/2013/248532
- Rauf, A., Abu-Izneid, T., Khalil, A. A., Imran, M., Shah, Z. A., Bin Emran, T., et al. (2021). Berberine as a potential anticancer agent: A comprehensive review. *Molecules* 2626, 73687368. doi:10.3390/MOLECULES26237368
- Rauf, A., Badoni, H., Abu-Izneid, T., Olatunde, A., Rahman, M. M., Painuli, S., et al. (2022). Neuroinflammatory markers: Key indicators in the pathology of neurodegenerative diseases. *Molecules* 27, 3194. doi:10.3390/MOLECULES27103194
- Ripple, M. O., Kim, N., and Springett, R. (2013). Acute mitochondrial inhibition by mitogen-activated protein kinase/extracellular signal-regulated kinase kinase

- (MEK) 1/2 inhibitors regulates proliferation. *J. Biol. Chem.* 288, 2933–2940. doi:10.1074/jbc.M112.430082
- Roberts, P. J., and Der, C. J. (2007). Targeting the Raf-MEK-ERK mitogen-activated protein kinase cascade for the treatment of cancer. *Oncogene* 26, 3291–3310. doi:10.1038/sj.onc.1210422
- Rodova, M., Fu, J., Watkins, D. N., Srivastava, R. K., and Shankar, S. (2012). Sonic hedgehog signaling inhibition provides opportunities for targeted therapy by sulforaphane in regulating pancreatic cancer stem cell self-renewal. *PLoS One* 7, e46083. doi:10.1371/JOURNAL.PONE.0046083
- Rubin Grandis, J., Drenning, S. D., Chakraborty, A., Zhou, M. Y., Zeng, Q., Pitt, A. S., et al. (1998). Requirement of Stat3 but not Stat1 activation for epidermal growth factor receptor-mediated cell growth *in vitro*. *J. Clin. Invest.* 102, 1385–1392. doi:10.1172/jci3785
- Russo, M., Spagnuolo, C., Tedesco, I., Bilotto, S., and Russo, G. L. (2012). The flavonoid quercetin in disease prevention and therapy: Facts and fancies. *Biochem. Pharmacol.* 83, 6–15. doi:10.1016/j.bcp.2011.08.010
- Sano, S., Itami, S., Takeda, K., Tarutani, M., Yamaguchi, Y., Miura, H., et al. (1999). Keratinocyte-specific ablation of Stat3 exhibits impaired skin remodeling, but does not affect skin morphogenesis. *EMBO J.* 18, 4657–4668. doi:10.1093/emboj/18.17.4657
- Sansal, I., and Sellers, W. R. (2004). The biology and clinical relevance of the PTEN tumor suppressor pathway. *J. Clin. Oncol.* 22, 2954–2963. doi:10.1200/JCO.2004.02.141
- Sarkar, F. H., Li, Y., Wang, Z., and Kong, D. (2009). Cellular signaling perturbation by natural products. *Cell. Signal.* 21, 1541–1547. doi:10.1016/j.CELLSIG.2009.03.009
- Sasaki, A. T., and Firtel, R. A. (2005). Finding the way: Directional sensing and cell polarization through Ras signalling. *Novartis Found. Symp.* 269, 73–87. doi:10.1002/047001766x.ch8
- Sato, T., Diehl, T. S., Narayanan, S., Funamoto, S., Ihara, Y., De Strooper, B., et al. (2007). Active γ -secretase complexes contain only one of each component. *J. Biol. Chem.* 282, 33985–33993. doi:10.1074/jbc.M705248200
- Sebolt-Leopold, J. S., and Herrera, R. (2004). Targeting the mitogen-activated protein kinase cascade to treat cancer. *Nat. Rev. Cancer* 4, 937–947. doi:10.1038/nrc1503
- Sever, R., and Brugge, J. S. (2015). Signal transduction in cancer. *Cold Spring Harb. Perspect. Med.* 5, a006098. doi:10.1101/cshperspect.a006098
- Shang, W., Zhang, J., Song, H., Zhu, S., Zhang, A., Hua, Y., et al. (2021). Mechanism of tetrandrine against endometrial cancer based on network pharmacology. *Drug Des. devel. Ther.* 15, 2907–2919. doi:10.2147/DDDT.S307670
- Sharma, S., Stutzman, J. D., Kelloff, G. J., and Steele, V. E. (1994). Screening of potential chemopreventive agents using biochemical markers of carcinogenesis. *Cancer Res.* 54, 5848–5855.
- Shaulian, E., and Karin, M. (2002). AP-1 as a regulator of cell life and death. *Nat. Cell. Biol.* 4, E131–E136. doi:10.1038/ncb0502-e131
- Shaw, A. S., and Filbert, E. L. (2009). Scaffold proteins and immune-cell signalling. *Nat. Rev. Immunol.* 9, 47–56. doi:10.1038/nri2473
- Sheng, T., Li, C., Zhang, X., Chi, S., He, N., Chen, K., et al. (2004). Activation of the hedgehog pathway in advanced prostate cancer. *Mol. Cancer* 3, 29. doi:10.1186/1476-4598-3-29
- Shoshan, M. C. (2012). 3-bromopyruvate: Targets and outcomes. *J. Bioenerg. Biomembr.* 44, 7–15. doi:10.1007/s10863-012-9419-2
- Shu, L., Cheung, K.-L., Khor, T. O., Chen, C., and Kong, A.-N. (2010). Phytochemicals: Cancer chemoprevention and suppression of tumor onset and metastasis. *Cancer Metastasis Rev.* 29, 483–502. doi:10.1007/S10555-010-9239-Y
- Shukla, S., Kanwal, R., Shankar, E., Datt, M., Chance, M. R., Fu, P., et al. (2015). Apigenin blocks IKK α activation and suppresses prostate cancer progression. *Oncotarget* 6, 31216–31232. doi:10.18632/oncotarget.5157
- Siegel, R. L., Miller, K. D., and Jemal, A. (2019). Cancer statistics, 2019. *Ca. Cancer J. Clin.* 69, 7–34. doi:10.3322/caac.21551
- Silver, D. L., and Montell, D. J. (2001). Paracrine signaling through the JAK/STAT pathway activates invasive behavior of ovarian epithelial cells in drosophila. *Cell* 107, 831–841. doi:10.1016/S0092-8674(01)00607-9
- Singh, A. V., Raymond, M., Pace, F., Certo, A., Zuidema, J. M., McKay, C. A., et al. (2015). Astrocytes increase ATP exocytosis mediated calcium signaling in response to microgroove structures. *Sci. Rep.* 5, 7847–7848. doi:10.1038/srep07847
- Singh, S., Mehta, N., Lilan, J., Budhthok, M. B., Chao, F., and Yong, L. (2017). Initiative action of tumor-associated macrophage during tumor metastasis. *Biochim. Open* 4, 8–18. doi:10.1016/j.biopen.2016.11.002
- Singh, S., and Shukla, R. (2018). Key signaling pathways engaged in cancer management: Current update. *Curr. Cancer Ther. Rev.* 16, 36–48. doi:10.2174/1573394714666180904122412
- Singh, S. S., Vats, S., Chia, A. Y.-Q., Tan, T. Z., Deng, S., Ong, M. S., et al. (2017). Dual role of autophagy in hallmarks of cancer. *Oncogene* 37, 1142–1158. doi:10.1038/s41388-017-0046-6
- Singletary, K., and Milner, J. (2008). Diet, autophagy, and cancer: A review. *Cancer Epidemiol. Biomarkers Prev.* 17, 1596–1610. doi:10.1158/1055-9965.EPI-07-2917
- Skoda, A. M., Simovic, D., Karin, V., Kardum, V., Vranic, S., and Serman, L. (2018). The role of the hedgehog signaling pathway in cancer: A comprehensive review. *Bosn. J. Basic Med. Sci.* 18, 8–20. doi:10.17305/bjbm.2018.2756
- Song, J., Manir, M. M., and Moon, S. S. (2009). Cytotoxic grifolin derivatives isolated from the wild mushroom *Boletus pseudocalopus* (Basidiomycetes). *Chem. Biodivers.* 6, 1435–1442. doi:10.1002/cbdv.200800217
- Sorrentino, C., Cuneo, A., and Roti, G. (2019). Therapeutic targeting of notch signaling pathway in hematological malignancies. *Mediterr. J. Hematol. Infect. Dis.* 11, 2019037. doi:10.4084/MJHID.2019.037
- Srivastava, S., Somasagara, R. R., Hegde, M., Nishana, M., Tadi, S. K., Srivastava, M., et al. (2016). Quercetin, a natural flavonoid interacts with DNA, arrests cell cycle and causes tumor regression by activating mitochondrial pathway of apoptosis. *Sci. Rep.* 6, 1–3. doi:10.1038/srep24049
- Stiewe, T. (2007). The p53 family in differentiation and tumorigenesis. *Nat. Rev. Cancer* 7, 165–168. doi:10.1038/nrc2072
- Stirewalt, D. L., Kopecky, K. J., Meshinchi, S., Appelbaum, F. R., Slovak, M. L., Willman, C. L., et al. (2001). FLT3, RAS, and TP53 mutations in elderly patients with acute myeloid leukemia. *Blood* 97, 3589–3595. doi:10.1182/blood.V97.11.3589
- Strickson, S., Campbell, D. G., Emmerich, C. H., Knebel, A., Plater, L., Ritorto, M. S., et al. (2013). The anti-inflammatory drug BAY 11-7082 suppresses the MyD88-dependent signalling network by targeting the ubiquitin system. *Biochem. J.* 451, 427–437. doi:10.1042/BJ20121651
- Su, P., Wang, F., Qi, B., Wang, T., and Zhang, S. (2017). P53 regulation-association long non-coding RNA (LncRNA PRAL) inhibits cell proliferation by regulation of P53 in human lung cancer. *Med. Sci. Monit.* 23, 1751–1758. doi:10.12659/MSM.900205
- Sun, X., Xu, R., Deng, Y., Cheng, H., Ma, J., Ji, J., et al. (2007). Effects of tetrandrine on apoptosis and radiosensitivity of nasopharyngeal carcinoma cell line CNE. *Acta Biochim. Biophys. Sin.* 39, 869–878. doi:10.1111/j.1745-7270.2007.00349.x
- Sun, Y. (2015). Translational horizons in the tumor microenvironment: Harnessing breakthroughs and targeting cures. *Med. Res. Rev.* 35, 408–436. doi:10.1002/med.21338.med
- Surh, Y. J., and Chun, K. S. (2007). Cancer chemopreventive effects of curcumin. *Adv. Exp. Med. Biol.* 595, 149–172. doi:10.1007/978-0-387-46401-5_5
- Szoltyssek, K., Pietranek, K., Kalinowska-Herok, M., Pietrowska, M., Kimmel, M., and Widlak, P. (2008). TNF α -induced activation of NF κ B protects against UV-induced apoptosis specifically in p53-proficient cells. *Acta Biochim. Pol.* 55, 741–748. doi:10.18388/abp.2008_3035
- Thangapazham, R. L., Sharma, A., and Maheshwari, R. K. (2006). Multiple molecular targets in cancer chemoprevention by curcumin. *AAPS J.* 8, E443–E449. doi:10.1208/aapsj080352
- Toker, A., and Newton, A. C. (2000). Cellular signaling: Pivoting around PDK-1. *Cell* 103, 185–188. doi:10.1016/S0092-8674(00)00110-0
- Tomeh, M. A., Hadianamrei, R., and Zhao, X. (2019). A review of curcumin and its derivatives as anticancer agents. *Int. J. Mol. Sci.* 20, E1033. doi:10.3390/IJMS20051033
- Toshiya, K., Testuya, T., Akira, H., and Takuji, T. (2012). Cancer chemoprevention through the induction of apoptosis by natural compounds. *J. Biophys. Chem.* 03, 156–173. doi:10.4236/JBPC.2012.32018
- Trapp, V., Parmakhtiar, B., Papazian, V., Willmott, L., and Fruehauf, J. P. (2010). Anti-angiogenic effects of resveratrol mediated by decreased VEGF and increased TSP1 expression in melanoma-endothelial cell co-culture. *Angiogenesis* 13, 305–315. doi:10.1007/s10456-010-9187-8
- Tu, B., Du, L., Fan, Q. M., Tang, Z., and Tang, T. T. (2012). STAT3 activation by IL-6 from mesenchymal stem cells promotes the proliferation and metastasis of osteosarcoma. *Cancer Lett.* 325, 80–88. doi:10.1016/j.canlet.2012.06.006
- Tuli, B., S., Tuorkey, M. J., Thakral, F., Sak, K., Kumar, M., Sharma, A. K., et al. (2019). Molecular mechanisms of action of genistein in cancer: Recent advances. *Front. Pharmacol.* 10, 1336. doi:10.3389/fphar.2019.01336

- Tutelyan, V. A., and Lashneva, N. V. (2013). Biologically active substances of plant origin. Flavonols and flavones: Prevalence, dietary sources and consumption. *Vopr. Pitani.* 82, 4–22.
- Ullah, M. F., Ahmad, A., Zubair, H., Khan, H. Y., Wang, Z., Sarkar, F. H., et al. (2011). Soy isoflavone genistein induces cell death in breast cancer cells through mobilization of endogenous copper ions and generation of reactive oxygen species. *Mol. Nutr. Food Res.* 55, 553–559. doi:10.1002/mnfr.201000329
- Varjosalo, M., and Taipale, J. (2008). Hedgehog: Functions and mechanisms. *Genes. Dev.* 22, 2454–2472. doi:10.1101/gad.1693608
- Varoni, E. M., Lo Faro, A. F., Sharifi-Rad, J., and Iriti, M. (2016). Anticancer molecular mechanisms of resveratrol. *Front. Nutr.* 3, 8. doi:10.3389/fnut.2016.00008
- Vásquez-Garzón, V., Arellanes-Robledo, J., García-Román, R., Aparicio-Rautista, D., and Villa-Treviño, S. (2009). Inhibition of reactive oxygen species and pre-neoplastic lesions by quercetin through an antioxidant defense mechanism. *Free Radic. Res.* 43, 128–137. doi:10.1080/10715760802626535
- Vinay, D. S., Ryan, E. P., Pawelec, G., Talib, W. H., Stagg, J., Elkord, E., et al. (2015). Immune evasion in cancer: Mechanistic basis and therapeutic strategies. *Semin. Cancer Biol.* 35, S185–S198. doi:10.1016/j.semcancer.2015.03.004
- Vivanco, I., and Sawyers, C. L. (2002). The phosphatidylinositol 3-kinase-AKT pathway in human cancer. *Nat. Rev. Cancer* 2, 489–501. doi:10.1038/nrc839
- Wang, M., Jiang, S., Zhou, L., Yu, F., Ding, H., Li, P., et al. (2019). Potential mechanisms of action of curcumin for cancer prevention: Focus on cellular signaling pathways and miRNAs. *Int. J. Biol. Sci.* 15, 1200–1214. doi:10.7150/ijbs.3710
- Wang, Z., Li, Y., Ahmad, A., Azmi, A. S., Banerjee, S., Kong, D., et al. (2010). Targeting Notch signaling pathway to overcome drug resistance for cancer therapy. *Biochim. Biophys. Acta* 1806, 258–267. doi:10.1016/j.BBcan.2010.06.001
- Wang, Z., Li, Y., Banerjee, S., and Sarkar, F. H. (2009). Emerging role of Notch in stem cells and cancer. *Cancer Lett.* 279, 8–12. doi:10.1016/j.CANLET.2008.09.030
- Waris, G., and Ahsan, H. (2006). Reactive oxygen species: Role in the development of cancer and various chronic conditions. *J. Carcinog.* 5, 14. doi:10.1186/1477-3163-5-14
- Warzecha, J., Dinges, D., Kaszap, B., Henrich, D., Marzi, I., and Seebach, C. (2012). Effect of the Hedgehog-inhibitor cyclopamine on mice with osteosarcoma pulmonary metastases. *Int. J. Mol. Med.* 29, 423–427. doi:10.3892/ijmm.2011.851
- Wätjen, W., Michels, G., Steffan, B., Niering, P., Chovolou, Y., Kampkötter, A., et al. (2005). Low concentrations of flavonoids are protective in rat H4IIE cells whereas high concentrations cause DNA damage and apoptosis. *J. Nutr.* 135, 525–531. doi:10.1093/JN/135.3.525
- Wei, H., Tye, L., Bresnick, E., and Birt, D. F. (1990). Inhibitory effect of apigenin, a plant flavonoid, on epidermal ornithine decarboxylase and skin tumor promotion in mice. *Cancer Res.* 50, 499–502.
- Wiert, C. (2007). Goniiothalamus species: A source of drugs for the treatment of cancers and bacterial infections? *Evid. Based. Complement. Altern. Med.* 4, 299–311. doi:10.1093/ecam/nem009
- Wu, J. M., Chen, Y., Chen, J. C., Lin, T. Y., and Tseng, S. H. (2010). Tetrandrine induces apoptosis and growth suppression of colon cancer cells in mice. *Cancer Lett.* 287, 187–195. doi:10.1016/j.canlet.2009.06.009
- xi, Xiu M., Liumeng, Y., and hai, Kuang B. (2020). The oncogenic role of Jagged1/Notch signaling in cancer. *Biomed. Pharmacother.* 129, 110416. doi:10.1016/j.biopha.2020.110416
- Xiao, D., Herman-Antosiewicz, A., Antosiewicz, J., Xiao, H., Brisson, M., Lazo, J. S., et al. (2005). Diallyl trisulfide-induced G2-M phase cell cycle arrest in human prostate cancer cells is caused by reactive oxygen species-dependent destruction and hyperphosphorylation of Cdc25C. *Oncogene* 24, 6256–6268. doi:10.1038/sj.onc.1208759
- Yan, X., Qi, M., Li, P., Zhan, Y., and Shao, H. (2017). Apigenin in cancer therapy: Anti-cancer effects and mechanisms of action. *Cell. Biosci.* 7, 50–16. doi:10.1186/S13578-017-0179-X
- Yan, X., Qi, M., Li, P., Zhan, Y., and Shao, H. (2017). Apigenin in cancer therapy: Anti-cancer effects and mechanisms of action. *Cell. Biosci.* 7, 50. doi:10.1186/S13578-017-0179-X
- Yang, C. S., Landau, J. M., Huang, M. T., and Newmark, H. L. (2001). Inhibition of carcinogenesis by dietary polyphenolic compounds. *Annu. Rev. Nutr.* 21, 381–406. doi:10.1146/annurev.nutr.21.1.381
- Yang, L. J., Yang, Z. D., Li, Z. J., Yang, S. H., and Shu, Z. M. (2021). Steptetrandrine A-D, bisbenzylisoquinoline alkaloids from *Stephania tetrandra*. *Nat. Prod. Res.* 1–12. doi:10.1080/14786419.2021.1961135
- Ye, M., Liu, J. K., Lu, Z. X., Zhao, Y., Liu, S. F., Li, L. L., et al. (2005). Grifolin, a potential antitumor natural product from the mushroom *Albatrellus confluens*, inhibits tumor cell growth by inducing apoptosis *in vitro*. *FEBS Lett.* 579, 3437–3443. doi:10.1016/j.febslet.2005.05.013
- Ye, M., Luo, X., Li, L., Shi, Y., Tan, M., Weng, X., et al. (2007). Grifolin, a potential antitumor natural product from the mushroom *Albatrellus confluens*, induces cell-cycle arrest in G1 phase via the ERK1/2 pathway. *Cancer Lett.* 258, 199–207. doi:10.1016/j.canlet.2007.09.001
- Yu, X., Zhu, J., Mi, M., Chen, W., Pan, Q., and Wei, M. (2012). Anti-angiogenic genistein inhibits VEGF-induced endothelial cell activation by decreasing PTK activity and MAPK activation. *Med. Oncol.* 29, 349–357. doi:10.1007/s12032-010-9770-2
- Yu-Jen, C. (2002). Potential role of tetrandrine in cancer therapy. *Acta Pharmacol. Sin.* 23, 1102–1106.
- Zhang, M., Biswas, S., Qin, X., Gong, W., Deng, W., and Yu, H. (2016). Does Notch play a tumor suppressor role across diverse squamous cell carcinomas? *Cancer Med.* 5, 2048–2060. doi:10.1002/cam4.731
- Zhang, M., Swarts, S. G., Yin, L., Liu, C., Tian, Y., Cao, Y., et al. (2011). Antioxidant properties of quercetin. *Adv. Exp. Med. Biol.* 701, 283–289. doi:10.1007/978-1-4419-7756-4_38
- Zhang, Y. X., Liu, X. M., Wang, J., Li, J., Liu, Y., Zhang, H., et al. (2015). Inhibition of AKT/FoxO3a signaling induced puma expression in response to p53-independent cytotoxic effects of H1: A derivative of tetrandrine. *Cancer Biol. Ther.* 16, 965–975. doi:10.1080/15384047.2015.1040950
- Zhao, Y., and Adjei, A. A. (2015). Targeting angiogenesis in cancer therapy: Moving beyond vascular endothelial growth factor. *Oncologist* 20, 660–673. doi:10.1634/theoncologist.2014-0465
- Zhou, B., Lin, W., Long, Y., Yang, Y., Zhang, H., Wu, K., et al. (2022). Notch signaling pathway: Architecture, disease, and therapeutics. *Signal Transduct. Target. Ther.* 7, 95–33. doi:10.1038/s41392-022-00934-y
- Zhu, D. M., Xue, W. L., Tao, W., and Li, J. C. (2015). Effects of cyclopamine on the biological characteristics of human breast cancer MCF-7 cell line and its mechanism. *Eur. J. Gynaecol. Oncol.* 36, 469–472. doi:10.12892/ejgo2670.2015
- Zhu, H.-L. (2011). Resveratrol and its analogues: Promising antitumor agents. *Anticancer. Agents Med. Chem.* 11, 479–490. doi:10.2174/187152011795677427
- Zou, Y., Yang, J., and Jiang, D. (2015). Resveratrol inhibits canonical Wnt signaling in human MG-63 osteosarcoma cells. *Mol. Med. Rep.* 12, 7221–7226. doi:10.3892/mmr.2015.4338



OPEN ACCESS

EDITED BY
Sandeep Singh,
Central University of Punjab, India

REVIEWED BY
Nicolas Andre,
Aix Marseille Université, France
Rajkumar S. Kalra,
Okinawa Institute of Science and
Technology Graduate University,
Japan

*CORRESPONDENCE
Alaa Embaby
a.embaby@nki.nl

[†]These authors have contributed
equally to this work and share
first authorship

SPECIALTY SECTION
This article was submitted to
Pharmacology of Anti-Cancer Drugs,
a section of the journal
Frontiers in Oncology

RECEIVED 10 May 2022
ACCEPTED 30 August 2022
PUBLISHED 15 September 2022

CITATION
Embaby A, van Merendonk L,
Steeghs N, Beijnen J and Huitema A
(2022) Beta-adrenergic receptor
blockade in angiosarcoma: Which
beta-blocker to choose?
Front. Oncol. 12:940582.
doi: 10.3389/fonc.2022.940582

COPYRIGHT
© 2022 Embaby, van Merendonk,
Steeghs, Beijnen and Huitema. This is an
open-access article distributed under
the terms of the [Creative Commons
Attribution License \(CC BY\)](https://creativecommons.org/licenses/by/4.0/). The use,
distribution or reproduction in other
forums is permitted, provided the
original author(s) and the copyright
owner(s) are credited and that the
original publication in this journal is
cited, in accordance with accepted
academic practice. No use,
distribution or reproduction is
permitted which does not comply with
these terms.

Beta-adrenergic receptor blockade in angiosarcoma: Which beta-blocker to choose?

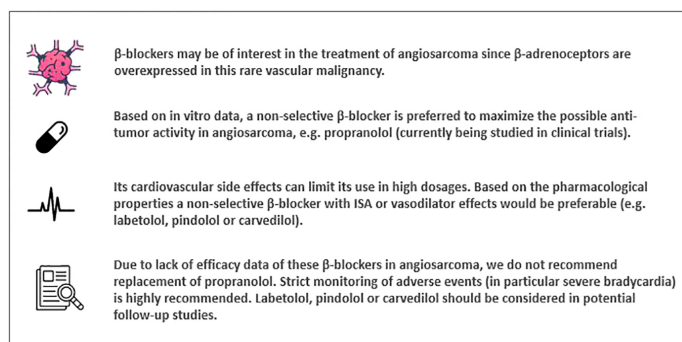
Alaa Embaby^{1*†}, Lisanne van Merendonk^{2†}, Neeltje Steeghs¹,
Jos Beijnen² and Alwin Huitema^{2,3,4}

¹Department of Medical Oncology and Clinical Pharmacology, The Netherlands Cancer Institute-Antoni van Leeuwenhoek, Amsterdam, Netherlands, ²Department of Pharmacy and Pharmacology, The Netherlands Cancer Institute-Antoni van Leeuwenhoek, Amsterdam, Netherlands, ³Department of Pharmacology, Princess Máxima Center for Pediatric Oncology, Utrecht, Netherlands, ⁴Department of Clinical Pharmacy, University Medical Center Utrecht, Utrecht University, Utrecht, Netherlands

Beta-blockers are currently studied to improve therapeutic options for patients with angiosarcoma. However, most of these patients have no cardiovascular co-morbidity and it is therefore crucial to discuss the most optimal pharmacological properties of beta-blockers for this population. To maximize the possible effectiveness in angiosarcoma, the use of a non-selective beta-blocker is preferred based on *in vitro* data. To minimize the risk of cardiovascular adverse events a beta-blocker should ideally have intrinsic sympathomimetic activity or vasodilator effects, e.g. labetalol, pindolol or carvedilol. However, except for one case of carvedilol, only efficacy data of propranolol is available. In potential follow-up studies labetalol, pindolol or carvedilol can be considered to reduce the risk of cardiovascular adverse events.

KEYWORDS

beta-blockade, angiosarcoma, drug repurposing, pharmacological characteristics, propranolol



GRAPHICAL ABSTRACT

Introduction

Beta (β)-blockers or β -adrenoceptor antagonists were first introduced in the early 1960s for the treatment of angina pectoris (1). The use of β -blockers in ischemic cardiac disease is based on the reduction of the catecholaminergic stimulation of the heart in order to improve the exercise capacity of the cardiac muscle by slowing heart rate and lowering the oxygen consumption. The anti-hypertensive and anti-arrhythmic effects of this drug class have led to its extensive use in the treatment of hypertension and cardiac arrhythmias. Other (off-label) indications for the use of β -blockers are migraine, the treatment of essential tremor, prophylaxis of esophageal variceal hemorrhage caused by portal hypertension, control of anxiety symptoms (exam anxiety and stage fright) and thyrotoxicosis.

The expression of β -adrenergic receptors has been investigated previously in both benign and malignant vascular tumors (2, 3). The registered indication of propranolol, a non-selective β -blocker, has now been extended to the treatment of infantile hemangioma requiring systemic therapy (4, 5). Since β -adrenoceptors are also overexpressed in some cancer types, such as soft tissue sarcomas, propranolol might be a drug of interest in these rare malignancies. Hence, propranolol obtained the orphan designation by the European Commission for the treatment of soft tissue sarcomas (6, 7). Furthermore, the effect of β -receptor blockade with propranolol on angiosarcoma is currently being studied in two clinical trials: The PropAngio trial (NCT04518124, study start date December 2019, status ongoing) and the PROPAN trial (NCT02732678, study start date May 2016, status unknown) (8–10). The aim of the PropAngio trial is to prospectively assess the anti-proliferative effect of neoadjuvant propranolol as monotherapy in primary, recurrent and metastatic angiosarcoma. In the PROPAN trial, propranolol is given in combination with cyclophosphamide in locally advanced or metastatic angiosarcoma (10). The usual daily dose range of propranolol for hypertension is 160 to 320 mg (5). In the PropAngio trial, propranolol is given orally in a dose-escalation schedule (40–80 mg twice daily in the first two weeks, thereafter 80 mg three times a day) until initiation of standard therapy (chemotherapy and/or surgery or radiation). Since the anti-proliferative effect of propranolol on angiosarcoma cells has been shown to be dose dependent, evaluating the effect of dose escalation in this trial is necessary (3). However, these patients have no cardiovascular comorbidity or other indications for β -receptor blockade, making them more at risk for treatment related cardiovascular adverse events, mainly bradycardia and hypotension. These known side effects of propranolol can limit its use in high dosages in this patient population. Ideally, one should adapt a β -blocker with proven efficacy in angiosarcoma and which is characterized by minimal cardiovascular side effects. Here, we

discuss the pharmacological properties of the diverse β -blockers and consider the usage of propranolol in angiosarcoma.

Pharmacological properties

β -blockers can be distinguished based on their pharmacological properties by selectivity, intrinsic sympathomimetic activity (ISA), vasodilator activity and lipophilicity (Table 1). These pharmacological properties can be of use to define treatment and to predict adverse events. Intrinsic sympathomimetic activity or partial agonist activity of β -blockers is caused by inhibition of β -receptors in the presence of agonists, such as catecholamines, and stimulation of β -receptors in rest when these agonists are absent (11). This results in less bradycardia or peripheral vasoconstriction (12). Consequently, β -blockers with ISA can be of use in patients in whom strong decline of heart rate is unwanted. A comparison between pindolol and propranolol confirms this clinical benefit of β -blockers with ISA in patients with angina pectoris (13). Of the non-selective β -blockers with a vasodilator effect, there is some evidence that carvedilol causes less bradycardia compared to other β -blockers (14). Lipophilic β -blockers can more easily cross the blood-brain barrier increasing theoretically the incidence of central nervous system adverse events (12). However, studies were unable to associate lipophilicity to the incidence of adverse events (18).

β_1 -receptors are primarily located in the heart and most adverse effects of β -blockers are a result of antagonism of β_1 -receptors (notably bradycardia), whereas inhibition of β_2 -receptors, located on vascular and bronchial smooth muscle, can lead to adverse events like constriction of airways or peripheral vasculature (11, 15, 16). Therefore, cardioselective β -blockers are better tolerated and are preferred in patients with respiratory disease (15).

Differences in pharmacological properties can theoretically lead to varying adverse events. However, in head-to-head trials, the incidence of adverse events could not be clearly differentiated among most β -blockers (18, 19). Some studies report a difference in adverse events e.g.; carvedilol showed a higher rate of dizziness compared to metoprolol and propranolol was associated with a higher overall rate of adverse events compared to pindolol (13, 17). However, no β -blocker can be distinguished with highest incidence of adverse events (19).

Use of β -blockers in angiosarcoma

Overexpression of β_1 -, β_2 - and β_3 -adrenoceptors in angiosarcoma cells has been demonstrated in several preclinical studies (2, 3). This finding suggests that, as in

TABLE 1 Properties of β -blockers divided into selectivity, intrinsic sympathomimetic activity and vasodilator activity (11–17).

	Group	Examples	Mechanism	Clinical impact
Selectivity (11, 12, 15, 16)	Selective β -blockers or cardioselective β -blockers	Acebutolol, atenolol, bisoprolol, celiprolol, esmolol, metoprolol, nebivolol	Higher affinity for β_1 compared to β_2 . Selectivity can be lost at higher dosage	Less pulmonaric and metabolic adverse events**
	Non-selective β -blockers	Carvedilol, labetalol, pindolol, propranolol, sotalol	No selectivity for β_1 or β_2	N.A.
	β -blockers with ISA	Acebutolol, celiprolol, labetalol, pindolol*	At a low sympathetic tone stimulation of β -receptors	At rest less decrease in heart rate and cardiac output
Intrinsic sympathomimetic activity (ISA) (11–13, 16)	β -blockers without ISA	Atenolol, bisoprolol, carvedilol, esmolol, metoprolol, nebivolol, propranolol, sotalol	No stimulation of β -receptors	N.A.
	Vasodilator activity	Carvedilol, labetalol, nebivolol	Carvedilol + labetalol: α_1 -receptor antagonismNebivolol: Nitric oxide (NO) release	Reduced peripheral vascular resistance
Vasodilator activity (11, 12, 14, 16, 17)	No vasodilator activity	Acebutolol, atenolol, bisoprolol, celiprolol, esmolol, metoprolol, pindolol, propranolol, sotalol	N.A.	N.A.
	Lipophilic	Acebutolol, bisoprolol, carvedilol, metoprolol, nebivolol, pindolol, propranolol	Passage of blood-brain barrier	Possible more central adverse events ***
Lipophilicity (12, 15, 16)	Hydrophilic	Atenolol, celiprolol, esmolol, labetalol, sotalol	Less passage of blood brain barrier	N.A.

*Most ISA compared to other β -blockers.

** β -blockers increase LDL and triglyceride levels and reduce HDL levels (more pronounced effect in non-selective β -blockers without ISA).

***e.g. sleep disturbances, psychosis, depression, hallucination.

infantile hemangioma, β -blockers may also be of use in the treatment of this aggressive vascular tumor. Several mechanisms behind this anticancer effect have been suggested. Direct effects of β -blockers on tumor cells due to antagonism of β -receptors could lead to less proliferation, migration and differentiation of tumor cells (20). In addition, β -blockers can also influence tumor angiogenesis by downregulation of VEGF (2, 21–23). Furthermore, β -receptors play a role in immunostimulation and β -blockers can have effects on several immune cells (in both the adaptive and innate immune system) and on the tumor microenvironment (20, 22, 23). Several preclinical studies describe the synergy between β -blockers and chemotherapy resulting in less drug-resistance (3, 6, 21–24). Affecting the tumor microenvironment and immune system could also increase sensibility to immune checkpoint inhibitors by increasing T-cell infiltration and decreasing suppression of CD8+ cytotoxic T-cells (20, 25). Additionally the used isomer of β -blockers can be of importance. Studies on the isomers of propranolol suggest that the use of the R-isomer, which has no significant activity against the β -receptor, could lead to less side effects while maintaining efficacy. This supports a mechanism of action independent of β -blockade (24, 26). Using *in vitro* angiosarcoma models, it was found that the anti-proliferative effect of non-selective β -blockers was superior to cardioselective β -blockers (esmolol and atenolol) (27).

The anti-tumor activity of propranolol (as single agent and in combination with chemotherapy) in different types of angiosarcoma has been described in several case reports and case series (23, 28–35). Table 2 shows the characteristics and

results of these reports. Pasquier et al. reported the results of an unpowered pilot study in 7 patients with metastatic angiosarcoma in which propranolol was administered in combination with metronomic vinblastine-based chemotherapy. A response rate of 100% was observed (16). One single arm prospective clinical trial studied the efficacy of beta-blockade with propranolol or carvedilol in metastatic angiosarcoma (27). A total of 9 patients received either propranolol 20–100 mg per day (n=8) or carvedilol 6.25 mg per day (n=1) in combination with standard treatment protocols according to physicians choice. An improvement of the median progression-free survival (PFS) and overall survival (OS) was observed compared with historical controls (PFS 9 months vs. 3–6 months, OS 36 months vs. 12 months) (27).

Discussion

The aim of this perspective was to give an overview of the efficacy and safety of different β -blockers in angiosarcoma in order to recommend the use of the most appropriate β -blocker in this patient population. In accordance with the summarized preclinical and clinical data, we hypothesize that use of a non-selective β -blocker is preferred to maximize the possible effectiveness in angiosarcoma. Propranolol has been reported to be effective as monotherapy and in combination with chemotherapy in diverse cases of angiosarcoma. This is possibly the result of a synergistic effect of this non-selective β -blocker with chemotherapy by decreasing drug-resistance of tumor cells. β -blockade is also expected to enhance the

TABLE 2 Case reports and case series of propranolol in angiosarcoma.

Report reference	Patient characteristics	Treatment given	Efficacy/best response	Toxicity
Luczynska et al. (28)	Female, 45 years, primary bilateral angiosarcoma of the breast	Doxorubicin + cyclophosphamide + propranolol 10 mg TID followed by surgery	Partial response (PR)	Not reported
Fiste et al. (29)	Male, 33 years, metastatic cardiac angiosarcoma	Paclitaxel (150 mg/m ²) + propranolol 40 mg TID	Progression-free survival (PFS) of 8 months	Manageable toxicity; not specified
Daguze et al. 2017 (30)	Male, 49 years, nose angiosarcoma	Cyclophosphamide 200 mg QD (1 out of 2 weeks) + propranolol 120 mg daily	Complete remission after 2 months	Good tolerance; not specified
Daguze et al. 2016 (31)	Male, 73 years, metastatic angiosarcoma of the scalp	Cyclophosphamide 200 mg QD (1 out of 2 weeks) + propranolol 120 mg daily	PR of visceral metastasis and CR of cutaneous lesions (minimal duration of response 7 months)	No severe toxicity
Banavali et al. (32)	Female, 69 years, metastatic angiosarcoma of left arm	Celecoxib 200 mg BID + etoposide 50 mg (for 3 months) + cyclophosphamide 50 mg daily during 15-21 days of a 28-day cycle + propranolol 40 mg BID	Complete response (CR). Relapse after 20 months from start of treatment.	No grade 3 or 4 toxicities
Pramanik et al. (33)	Female, 37 years, metastatic angiosarcoma of the breast	Oral thalidomide 200 mg daily + celecoxib 400 mg BID + intermittent etoposide 50 mg daily + intermittent cyclophosphamide 100 mg daily + propranolol 40 mg BID	SD	Neutropenia due to chemotherapy
Galvan et al. (34)	Female, 61 years, metastatic cardiac angiosarcoma	Propranolol monotherapy 40 mg/kg	On 12-month evaluation PET/CT regression of lesions and resolution of pericard effusion	Not reported
Chow et al. (35)	Male, 60+ years, angiosarcoma of the scalp	Neoadjuvant propranolol monotherapy 40 mg BID – 40 mg TID Followed by weekly paclitaxel (10 cycles) + daily propranolol. Thereafter combined with radiotherapy	Clinical improvement of lesion and decrease of proliferative index (also observed during propranolol monotherapy)	No adverse events observed (monotherapy)
Pasquier et al. (23)	7 patients (2 female, 5 male, age 20-72 years) with metastatic angiosarcoma	Metronomic vinblastine 6mg/m ² + methotrexate 35 mg/m ² + propranolol 40 mg BID. After 12 months intermittent cyclophosphamide + etoposide 50 mg daily + propranolol	100% response rate (very good partial response in n=3 and complete response in n=1).	Grade II fatigue in all patients

immunomodulatory effects combinations of checkpoint inhibitors due to their positive effects on T-cells. However, propranolol is known to cause (cardiovascular) side effects by β -receptor antagonism, repurposing the R-isomer of propranolol could be a strategy to decrease side effects.

Given the abovementioned pharmacological features of β -blockers, one should ideally adopt a non-selective β -blocker with ISA to lower the risk of potential severe cardiovascular events such as bradycardia in patients with angiosarcoma. β -blockers that fulfill these criteria are labetalol and pindolol. As mentioned earlier, carvedilol has no ISA, but is known to cause less bradycardia because of its mainly vasodilator effects and may, therefore, be a suitable drug. To our knowledge, these agents have never been studied in angiosarcoma (except of carvedilol which is described in one case). Therefore, we do not recommend replacement of propranolol with another β -adrenoceptor antagonist in angiosarcoma due to lack of efficacy data. Hence, strict monitoring of adverse events and in particular (severe) bradycardia is highly recommended. The use of non-selective β -blockers with ISA should be considered in potential follow-up studies.

Data availability statement

The original contributions presented in the study are included in the article/supplementary material. Further inquiries can be directed to the corresponding author.

Author contributions

Conception and design: AE, LM, AH, and NS; Literature search and collection of data: AE and LM; Data interpretation: AE and LM; Manuscript writing: All authors. All authors contributed to the article and approved the submitted version.

Conflict of interest

The authors declare that the research was conducted in the absence of any commercial or financial relationships that could be construed as a potential conflict of interest.

Publisher's note

All claims expressed in this article are solely those of the authors and do not necessarily represent those of their affiliated

organizations, or those of the publisher, the editors and the reviewers. Any product that may be evaluated in this article, or claim that may be made by its manufacturer, is not guaranteed or endorsed by the publisher.

References

- Baker JG, Hill SJ, Summers RJ. Evolution of β -blockers: from anti-anginal drugs to ligand-directed signalling. *Trends Pharmacol Sci* (2011) 32(4):227–34. doi: 10.1016/j.tips.2011.02.010
- Chisholm KM, Chang KW, Truong MT, Kwok S, West RB, Heerema-Mckenney AE. β -adrenergic receptor expression in vascular tumors. *Modern Pathol* (2012) 25(11):1446–51. doi: 10.1038/modpathol.2012.108
- Stiles JM, Amaya C, Rains S, Diaz D, Pham R, Battiste J, et al. Targeting of beta adrenergic receptors results in therapeutic efficacy against models of hemangioendothelioma and angiosarcoma. *PLoS One* (2013) 8(3):e60021. doi: 10.1371/journal.pone.0060021
- Léauté-Labrèze C, Hoeger P, Mazereeuw-Hautier J, Guibaud L, Baselga E, Posiunas G, et al. A randomized, controlled trial of oral propranolol in infantile hemangioma. *N Engl J Med* (2015) 372(8):735–46. doi: 10.1056/NEJMoa1404710
- Propranolol 10mg tablets BP - summary of product characteristics. Available at: <https://www.medicines.org.uk/emc/product/5888/smpc#MACHINEOPS>.
- Porcelli L, Garofoli M, di Fonte R, Fucci L, Volpicella M, Strippoli S, et al. The β -adrenergic receptor antagonist propranolol offsets resistance mechanisms to chemotherapeutics in diverse sarcoma subtypes: a pilot study. *Sci Rep* (2020) 10(1):10465. doi: 10.1038/s41598-020-67342-6
- Medicines Agency EPublic summary of opinion on orphan designation propranolol for the treatment of soft tissue sarcoma. Available at: www.ema.europa.eu/contact.
- Heinhuis KM, Ijzerman NS, Koenen AM, van der Graaf WTA, Haas RL, Beijnen JH, et al. PropAngio study protocol: a neoadjuvant trial on the efficacy of propranolol monotherapy in cutaneous angiosarcoma—a proof of principle study. *BMJ Open* (2020) 10(9). doi: 10.1136/bmjopen-2020-039449
- Propranolol in angiosarcoma. Available at: <https://clinicaltrials.gov/ct2/show/NCT04518124?term=propranolol&cond=Angiosarcoma&draw=2&rank=1>.
- Dose-finding of propranolol in combination with metronomic fixed oral cyclophosphamide based on bivariate efficacy-tolerability outcome in patients with locally advanced or metastatic angiosarcoma: A collaborative and innovative phase I-II sequential trial by the French sarcoma group (GSF/GETO). Available at: <https://clinicaltrials.gov/ct2/show/study/NCT02732678>.
- Oliver E, Mayor FJR, D'Ocon P. Beta-blockers: Historical perspective and mechanisms of action. *Rev espanola cardiologia (English ed)* (2019) 72(10):853–62. doi: 10.1016/j.recesp.2019.02.023
- Poirier L, Tobe SW. Contemporary use of β -blockers: clinical relevance of subclassification. *Can J Cardiol* (2014) 30(5 Suppl):S9–15. doi: 10.1016/j.cjca.2013.12.001
- Frishman W, Kostis J, Strom J, Hossler M, Elkayam U, Goldner S, et al. Clinical pharmacology of the new beta-adrenergic blocking drugs. part 6. a comparison of pindolol and propranolol in treatment of patients with angina pectoris. the role of intrinsic sympathomimetic activity. *Am Heart J* (1979) 98(4):526–35. doi: 10.1016/0002-8703(79)90261-8
- Pedersen ME, Cockcroft JR. The vasodilatory beta-blockers. *Curr Hypertens Rep* (2007) 9(4):269–77. doi: 10.1007/s11906-007-0050-2
- Farzam K, Jan A. Beta Blockers. In: StatPearls [Internet]. Treasure Island (FL): StatPearls Publishing (2022).
- Borchard U. Pharmacological properties of β -adrenoceptor blocking drugs. *J Clin Bas Cardiol* (1998) 1(1):5–9.
- Metra M, Giubbini R, Nodari S, Boldi E, Modena MG, Cas LD. Differential effects of beta-blockers in patients with heart failure: A prospective, randomized, double-blind comparison of the long-term effects of metoprolol versus carvedilol. *Circulation* (2000) 102(5):546–51. doi: 10.1161/01.CIR.102.5.546
- Ko DT, Hebert PR, Coffey CS, Sedrakyan A, Curtis JP, Krumholz HM. Beta-blocker therapy and symptoms of depression, fatigue, and sexual dysfunction. *JAMA* (2002) 288(3):351–7. doi: 10.1001/jama.288.3.351
- Helfand M, Peterson K, Christensen V, Dana T, Thakurata S. *Drug class review: Beta adrenergic blockers*. Oregon Health and Science University (2009) p. 1–616.
- Wagner MJ, Cranmer LD, Loggers ET, Pollack SM. Propranolol for the treatment of vascular sarcomas. *J Exp Pharmacol* (2018) 10:51. doi: 10.2147/JEP.S146211
- Pasquier E, Ciccolini J, Carre M, Giacometti S, Fanciullino R, Pouchy C, et al. Propranolol potentiates the anti-angiogenic effects and anti-tumor efficacy of chemotherapy agents: implication in breast cancer treatment. *Oncotarget* (2011) 2(10):797–809. doi: 10.18632/oncotarget.343
- Pantziarka P, Bouche G, Sukhatme V, Meheus L, Rooman I, Sukhatme VP. Repurposing drugs in oncology (ReDO) - propranolol as an anti-cancer agent. *ecancermedicinescience* (2016) 12:10. doi: 10.3332/ecancer.2016.680
- Pasquier E, André N, Street J, Chougule A, Rekhi B, Ghosh J, et al. Effective management of advanced angiosarcoma by the synergistic combination of propranolol and vinblastine-based metronomic chemotherapy: A bench to bedside study. *EBioMedicine* (2016) 6:87–95. doi: 10.1016/j.ebiom.2016.02.026
- Saha J, Kim JH, Amaya CN, Witcher C, Khammanivong A, Korpela DM, et al. Propranolol sensitizes vascular sarcoma cells to doxorubicin by altering lysosomal drug sequestration and drug efflux. *Front Oncol* (2021) 1:10. doi: 10.3389/fonc.2020.614288
- Fjæstad KY, Rømer AMA, Goitea V, Johansen AZ, Thorseth ML, Carretta M, et al. Blockade of beta-adrenergic receptors reduces cancer growth and enhances the response to anti-CTLA4 therapy by modulating the tumor microenvironment. *Oncogene* (2022) 41(9):1364–75. doi: 10.1038/s41388-021-02170-0
- Sasaki M, North PE, Elsej J, Bublej J, Rao S, Jung Y, et al. Propranolol exhibits activity against hemangiomas independent of beta blockade. *NPJ Precis Oncol* (2019) 3(1):27. doi: 10.1038/s41698-019-0099-9
- Amaya CN, Perkins M, Belmont A, Herrera C, Nasrazadani A, Vargas A, et al. Non-selective beta blockers inhibit angiosarcoma cell viability and increase progression free- and overall-survival in patients diagnosed with metastatic angiosarcoma. *Oncoscience* (2018) 5(3–4):109–19. doi: 10.18632/oncoscience.413
- Luczynska E, Rudnicki W, Kargol J, Szpor J, Hodorowicz-Zaniewska D, Wysocki PJ, et al. Primary bilateral angiosarcoma of the breast treated with neoadjuvant chemotherapy combined with propranolol. *Breast J* (2021) 27(10):781–6. doi: 10.1111/tbj.14272
- Fiste O, Dimos A, Kardara VE, Ballasis K, Karampeazis A. Propranolol and weekly paclitaxel in the treatment of metastatic heart angiosarcoma. *Cureus* (2020) 12(12). doi: 10.7759/cureus.12262
- Daguzé J, Saint-Jean M, Dréno B. Large Nose angiosarcoma treated effectively with oral cyclophosphamide combined with propranolol. *J Eur Acad Dermatol Venereol* (2018) 32(2):e52–4. doi: 10.1111/jdv.14528
- Daguzé J, Saint-Jean M, Peuvrel L, Cassagnau E, Quéréux G, Khammari A, et al. Visceral metastatic angiosarcoma treated effectively with oral cyclophosphamide combined with propranolol. *JAAD Case Rep* (2016) 2(6):497–9. doi: 10.1016/j.jdc.2016.10.005
- Banavali S, Pasquier E, Andre N. Targeted therapy with propranolol and metronomic chemotherapy combination: sustained complete response of a relapsing metastatic angiosarcoma. *Ecancermedicinescience* (2015) 8:9. doi: 10.3332/ecancer.2015.499
- Pramanik R, Gogia A, Malik PS, Gogi R. Metastatic primary angiosarcoma of the breast: Can we tame it the metronomic way. *Indian J Med Paediatr Oncol* (2017) 38(2):228–31. doi: 10.4103/ijmpo.ijmpo_156_16
- Galván DC, Ayyappan AP, Bryan BA. Regression of primary cardiac angiosarcoma and metastatic nodules following propranolol as a single agent treatment. *Oncoscience* (2018) 5(9–10):264–8. doi: 10.18632/oncoscience.472
- Chow W, Amaya CN, Rains S, Chow M, Dickerson EB, Bryan BA. Growth attenuation of cutaneous angiosarcoma with propranolol-mediated β -blockade. *JAMA Dermatol* (2015) 151(11):1226–9. doi: 10.1001/jamadermatol.2015.2554



OPEN ACCESS

EDITED BY

Sandeep Singh,
Central University of Punjab, India

REVIEWED BY

Venkatesh Katari,
University of Toledo, United States
Santosh Karnewar,
University of Virginia, United States
Eduardo Martínez-León,
Genetics and Metabolism (INIGEM),
Argentina

*CORRESPONDENCE

Feng Tan,
tanfengsong@163.com
Jian Lin,
linjian3222@126.com
Hansong Sheng,
shenghansong@126.com

[†]These authors have contributed equally
to this work

SPECIALTY SECTION

This article was submitted to
Pharmacology of Anti-Cancer Drugs,
a section of the journal
Frontiers in Pharmacology

RECEIVED 26 April 2022

ACCEPTED 20 September 2022

PUBLISHED 07 October 2022

CITATION

Fang H, Wang L, Yu L, Shen F, Yang Z,
Yang Y, Li S, Dai H, Tan F, Lin J and
Sheng H (2022), Effects of metformin on
Sonic hedgehog subgroup
medulloblastoma progression: In vitro
and in vivo studies.
Front. Pharmacol. 13:928853.
doi: 10.3389/fphar.2022.928853

COPYRIGHT

© 2022 Fang, Wang, Yu, Shen, Yang,
Yang, Li, Dai, Tan, Lin and Sheng. This is
an open-access article distributed
under the terms of the [Creative
Commons Attribution License \(CC BY\)](#).
The use, distribution or reproduction in
other forums is permitted, provided the
original author(s) and the copyright
owner(s) are credited and that the
original publication in this journal is
cited, in accordance with accepted
academic practice. No use, distribution
or reproduction is permitted which does
not comply with these terms.

Effects of metformin on Sonic hedgehog subgroup medulloblastoma progression: *In vitro* and *in vivo* studies

Huangyi Fang^{1,2}, Lingfei Wang², Lisheng Yu¹, Fang Shen³,
Zelin Yang¹, Yue Yang¹, Shize Li¹, Haipeng Dai², Feng Tan^{4*†},
Jian Lin^{1*†} and Hansong Sheng^{1*†}

¹Department of Neurosurgery, The Second Affiliated Hospital of Wenzhou Medical University, Wenzhou, China, ²The Second School of Medicine, Wenzhou Medical University, Wenzhou, China, ³Department of Surgery, Box Hill Hospital Eastern Health, VIC, Australia, ⁴School of Basic Medical Sciences, Wenzhou Medical University, Wenzhou, China

Metformin is a first-line drug for type 2 diabetes, and its anticancer effects have also been widely studied in recent years. The Sonic hedgehog (Shh) signaling pathway is involved in the initiation and progression of medulloblastoma. In order to develop a new treatment strategy for medulloblastoma (MB), this study investigated the inhibitory effect of metformin on MB and the underlying mechanism of metformin on the Shh signaling pathway. The effect of metformin on proliferation was evaluated by the cell counting kit-8 (CCK-8) test and colony formation experiment. The effect of metformin on metastasis was assessed by the scratch-wound assay and transwell invasion assay. Cell cycle and apoptosis were evaluated by flow cytometry, and the associated proteins were examined by western blotting. The mRNA and protein expression levels related to the Shh pathway were measured by quantitative PCR, western blotting, and immunofluorescence staining. The xenograft murine model was carried out to evaluate the anticancer effect of metformin on medulloblastoma *in vivo*. Metformin inhibited proliferation and metastasis of the Shh subgroup MB cell line, and the inhibitory effect on proliferation was related to apoptosis and the block of the cell cycle at the G0/G1 phase. Animal experiments showed that metformin inhibits medulloblastoma growth *in vivo*. Moreover, metformin decreased mRNA and protein expression levels of the Shh pathway, and this effect was reversed by the AMP-activated protein kinase (AMPK) siRNA. Furthermore, the pro-apoptotic and cell cycle arrest effects of metformin on Daoy cells could be reversed by the Shh pathway activators. Our findings demonstrated that metformin could inhibit medulloblastoma progression *in vitro* and *in vivo*, and this effect was associated with AMPK-mediated inhibition of the Shh signaling pathway *in vitro* studies.

KEYWORDS

medulloblastoma, metformin, Sonic hedgehog signaling pathway, AMPK, anticancer

Introduction

MB is the most common malignant brain tumor in children, accounting for about 20% of all brain tumors in children under 15 years of age (Patel et al., 2014). MB has the characteristics of high malignancy, rapid growth, easy metastasis, and easy recurrence, and the 5-year survival rate is only 50%–75% (Northcott et al., 2019). The comprehensive treatment of MB patients with surgery, radiotherapy, and chemotherapy is effective for most patients with medulloblastoma. Still, most survivors endure the adverse effects of radiotherapy and chemotherapy for a long time, including developmental, neurological, and endocrine misalignment (Yeole et al., 2021).

With the development of molecular diagnostics, MB has been divided into four subgroups (Wnt, Shh, Group 3, and Group 4) (Chatterjee et al., 2022). The Shh subtype accounts for about 30%, which is more common in infants and adults and has a poor prognosis. In most cases, the Shh subgroup involves somatic mutations in one or more genes of the Shh pathway (such as Ptc, Sufu, or Smo, etc.), leading to abnormal activation of the pathway and further leading to the occurrence of MB (Amayiri et al., 2021), (Skowron et al., 2021)).

Metformin is an oral hypoglycemic drug for treating type 2 diabetes, which mainly acts through AMPK (de Maraño et al., 2022). Previous clinical observational studies have found that taking metformin can significantly reduce the incidence and mortality of various cancers, including gastric cancer, thyroid cancer, and prostate cancer (Kim et al., 2014; Heckman-Stoddard et al., 2017; Park et al., 2018). In the study of prostate cancer and breast cancer, it was also found that activation of AMPK mediates the anticancer effects of metformin (Fan et al., 2015; Chen et al., 2021). In recent years, studies have found that AMPK has a direct and indirect regulatory impact on the Shh pathway. In this study, we selected the Daoy and ONS-76 cell lines (Shh pathway-activated medulloblastoma) as the research object (Azatyan et al., 2021). We examined the inhibitory effect of metformin on MB and identified its association with the AMPK/Shh signaling pathway.

Methods

Chemicals

Metformin was ordered from Sigma-Aldrich (St. Louis, MO, United States). Fetal calf serum (FBS), RPMI 1640 medium, and 0.25% Trypsin-EDTA were purchased from Gibco (Grand Island, NY, United States). Smoothed Agonist SAG was purchased from Abcam (Cambridge, MA, United States). The small interfering RNA (siRNA) specific to AMPK (sc-45312) and normal control (sc-37007) came from Santa Cruz (CA, United States). The CCK-8 was purchased from Dojindo

Chemical Research Institute (Tokyo, Japan). 0.5% crystal violet was ordered from Sigma-Aldrich (St. Louis, MO, United States). The primary antibody of Caspase-3 (AF6311), Cleaved-caspase-3 (Asp175) (AF7022), Bax (AF0120), Bcl-2 (AF6139), Cyclin B1 (AF6168), Cyclin D1 (AF0931), Cdk4 (DF6102), Shh (DF7747), Ptc (AF5202), Smo (DF5152), Sufu (DF7687), Gli-1 (DF7523), AMPK alpha (AF6423), Phospho-AMPK alpha (Thr172) (AF3423), and β -actin (AF7018) for western blot was obtained from Affinity Biosciences (Cincinnati, OH, United States). All primary antibodies were used at a ratio of 1:1,000 in western blot assays.

Cell culture

The Daoy and ONS-76 cell lines were obtained from American Type Culture Collection (ATCC, Manassas, VA, United States). The Daoy and ONS-76 cells were maintained in RPMI 1640 medium supplemented with 10% FBS and 1% penicillin–streptomycin (HyClone, Logan, UT, United States). The cells were maintained at 37°C with 5% CO₂ under the condition of a humidified atmosphere.

RNA interference

To transfect Daoy cells, the AMPK α 1 siRNA or control siRNA was used with Lipofectamine 3,000 Transfection Reagent (Invitrogen, Carlsbad, CA, United States), according to the manufacturer's protocol. The cells were treated in a serum-free medium for 48 h after transfection, then used in the following experiments.

Cell proliferation analysis

The CCK-8 assay was performed to detect cell proliferation according to the instructions of the kit. The Daoy and ONS-76 cells were seeded into a 96-well plate at a density of 8×10^3 cells/well and treated separately with different concentrations of metformin and SAG (100 nm) after cell attachment. Subsequently, 10 μ L CCK-8 and 100 μ L fresh RPMI 1640 medium solution were added to each well and incubated for 1 h. The absorbance at 450 nm was measured with a microplate reader (Thermo Fisher Scientific, Waltham, MA, United States). For the colony formation experiment, Daoy and ONS-76 cells were trypsinized, and 500 viable cells were seeded into 6-well plates. After 24 h, the cells were treated with metformin at a concentration of 0, 1, 3, and 9 mm. After 7 days, the cells were fixed and dyed with 0.5% crystal violet staining (Sigma-Aldrich, St. Louis, MO, United States). Finally, the number of visible colonies was counted.

Scratch assay

A scratch was made on the top center of cells using a sterile plastic 200- μ L micropipette tip. And the medium was replaced with a serum-free medium. Cell migration at 0, 12, 24, and 48 h after scratching was recorded with a microscope. We used Adobe Photoshop (Adobe Systems, San Jose, CA, United States) to measure the scratch with to calculate the migration rate.

Cell invasion assay

Daoy cells were seeded into the 6.5 mm Matrigel-coated (BD Biosciences, San Jose, CA, United States) Transwell inserts (Corning Costar Corp, Cambridge, MA, United States) at a density of 3×10^5 cells per insert. RPMI 1640 medium with 20% FBS and pure RPMI 1640 medium without FBS were respectively placed in the lower and upper chambers. Following 24 h of treatment with different concentrations of metformin, the cells in the lower chamber were fixed with 4% paraformaldehyde and stained with 0.5% crystal violet. Then the cell images were captured and counted at $\times 200$ magnification using a Nikon Eclipse E 400 microscope (Nikon, Fukuoka, Japan). Finally, we used ImageJ (National Institutes of Health, Bethesda, MD, United States) to measure the cell number.

Apoptosis analysis

Daoy cells were seeded into a 6-well plate (1×10^6 cells/well) and treated separately with different metformin concentrations and SAG (100 nm) for 24 h. The cells were trypsinized, then washed with phosphate-buffered saline (PBS). We used the Annexin V-fluorescein isothiocyanate (FITC) kit (Beyotime Institute of Biotechnology) to quantify apoptosis, according to the instructions. The cells were resuspended in a binding buffer and stained with Annexin V-FITC/propidium iodide (PI). Cell apoptosis was examined by flow cytometry (Thermo Fisher Scientific, Waltham, MA, United States). Data analysis was analyzed using the FlowJo software (Tree Star Inc, Ashland, OR).

Cell cycle analysis

Daoy cells were seeded into a 6-well plate (1×10^6 cells/well) and treated separately with different metformin concentrations and SAG (100 nm) for 24 h. The cells were trypsinized, then washed with PBS. The cells were centrifuged and fixed with ice-cold 70% ethanol at 4°C overnight. The cells were incubated with RNase (Dojindo, Kumamoto, Japan) and PI in an incubator at 37°C for 30 min (min) on the second day. The cell cycle distribution was examined by flow cytometry (Thermo Fisher Scientific, Waltham, MA, United States). Data analysis was analyzed using the FlowJo software.

Quantitative PCR

Daoy cells were seeded into a 6-well plate (1×10^6 cells/well) and treated with different metformin concentrations for 24 h. Total cellular RNA was extracted with TRIzol reagent (Invitrogen) according to the manufacturer's instructions. The total RNA extracted was then reverse-transcribed into cDNA with the PrimeScript RT Master Mix. The primers specific for each molecule were designed to generate the PCR products. The following primers were used: Shh-Forward: 5'-CGCACGGGGACAGCTCGGAAGT-3'; Shh-Reverse: 5'-CTGCGCGGCCCTCGTAGTGC-3'; Smo-Forward: 5'-TTACCTTCAGCTGCCACTTCTACG-3'; Smo-Reverse: 5'-GCCTTGGCAATCATCTTGCTCTTC-3'; Ptc-Forward: 5'-TCT GCAGCAACTATACGAGC-3'; Ptc-Reverse: 5'-GAACAGCTCGACC GTCATCA-3'; Gli-1-Forward: 5'-GGACAACCGCCATCCAGACT-3'; Gli-1-Reverse: 5'-GCCAGGGACACCTCCATCTC-3'; GAPDH-Forward: 5'-TCACCATCTTCCCAGGAGCGAG-3'; GAPDH-Reverse: 5'-TGTCGCTGTTGAAGTCAGAG-3'. The samples were examined with a PCR array (Takara, Japan). Data were analyzed by the $2^{-\Delta\Delta CT}$ method.

Western blot analysis

The cells are properly treated and placed on ice before adding RIPA buffer containing protease inhibitor cocktail (ratio, 100:1) (Roche Diagnostics Corp. Indianapolis, IN, United States). The protein concentration was examined by the BCA method (ab102536; Abcam), separated by 8%–12% sodium dodecyl sulfate–polyacrylamide gel electrophoresis, then transferred to a polyvinylidene difluoride membrane (Abcam, Cambridge, MA, United States). Subsequently, the membrane was blocked with 5% non-fat milk in Tris-buffered saline containing Tween-20 (TBST) for 90 min at room temperature. Then the membrane was washed with TBST and incubated at 4°C overnight with the primary antibody in a ratio of 1:1,000. The next day, the membrane was washed with TBST and followed by incubation with horseradish peroxidase-coupling secondary antibody (goat anti-rabbit) at room temperature for 2 h. At last, the membrane was washed with TBST and detected with BeyoECL Plus developer (Beyotime, Shanghai, China) using the Bio-Rad Molecular Imager FX.

Immunofluorescence staining

Daoy cells were treated separately with metformin (3 mm) and SAG (100 nm) for 24 h, fixed in 4% paraformaldehyde for 15 min at room temperature and then permeabilized with 0.2% Triton X-100 for 20 min. After blocking for 30 min in 10% goat serum, the cells were incubated with the primary antibodies Gli-1 (1:200 dilution) overnight at 4°C. Then, the cells were washed

three times with PBS and incubated with AlexaFluor 488 (goat anti-rabbit IgG, Abcam, Cambridge, UK, 1:1,000 dilution) for 1 h at room temperature. Finally, the cells were stained with Dapi (1 µg/ml) for 10 min and imaged using an inverted IX71 microscope system (Olympus, Tokyo, Japan). The mean intensity was measured by ImageJ software.

Tumor xenografts in nude mice

Daoy cells (5×10^6) were resuspended in PBS and injected subcutaneously into 6-week-old BALB/c nude mice (Shanghai Laboratory Animal Center, Shanghai, China). About 10 days later, the mice were randomly assigned to two groups (control group and metformin group). The mice in the control group were orally administrated with 300 µL PBS daily, while the mice in the metformin group were orally administrated with 300 µL metformin (200 mg/kg) daily. The mice were measured for body weight and tumor volume every 3 days. The tumor volumes were measured using a vernier caliper and calculated as $0.5 \times \text{length} \times \text{width}^2$. After 24 days of treatment, the tumors were removed from the mice, weighed, and photographed. All mouse studies were carried out according to the institutional guidelines for the use of animals, and all procedures were approved by the Ethics Committee of the Second Affiliated Hospital of Wenzhou Medical University.

Statistical analysis

Statistical results were analyzed with GraphPad Prism 8.00 (GraphPad Software, Version X; La Jolla, CA, United States). All experimental data were shown as mean \pm standard deviation. Data were statistically analyzed by Student's t-test, one-way analysis of variance (ANOVA), or two-way ANOVA. $p < 0.5$ was considered statistically significant.

Results

Metformin inhibited the growth, migration, and invasion of the Shh subgroup MB cell line

To examine the anticancer effect of metformin in Shh subgroup MB, cell viability was detected by the CCK-8 assay. After treating Daoy cells with metformin (0, 1, 3, and 9 mm) for 12 h, 24 h, 48 h, and 72 h, we found the cell viability decreased with the increase in metformin concentration and treatment time (Figure 1A). The results of the colony formation experiment showed that the number and size of the colonies decreased with the increase in metformin concentration (Figures 1B and C). Similar results were obtained in ONS-76 cells (Supplementary

Figure S1). Scratch-wound assay (for migration) and transwell invasion assay (for invasion) were used to investigate the effect of metformin on the Daoy cell migration and invasion. Compared with the control group, the cellular migration and invasive capacity decreased with the increased metformin concentration and prolonged treatment time (Figures 2A–D).

Metformin promoted apoptosis of the Shh subgroup MB cell line

To determine the apoptosis effect of metformin on Daoy cells, cell apoptosis was detected by flow cytometry. After treating Daoy cells with metformin (0, 1, 3, and 9 mm) for 24 h, the percentage of apoptotic Daoy cells elevated with the increase of metformin concentration (Figures 3A and B). In western blot, metformin inhibited the expression level of Bcl-2 and promoted the levels of Bax and Cleaved-caspase-3 in Daoy cells but had no significant effect on Caspase-3 (Figures 3C and D). These results indicated that metformin induced the apoptosis of Daoy cells.

Metformin arrested cell cycle of the Shh subgroup MB cell line

To investigate the effect of metformin on the Daoy cell cycle, the cell cycle was detected by flow cytometry. After treating Daoy cells with metformin (0, 1, 3, and 9 mm) for 24 h, the percentage of cells in the G0/G1 phase was increased, and the rate of cells in the S and G2/M phase was decreased (Figures 4A and B). In addition, the expression of key G1-phase proteins Cyclin D1, CDK4, and the mitosis-related protein Cyclin B1 decreased (Figures 4C and D). These results indicated that metformin arrested the cell cycle of Daoy cells in the G0/G1 phase.

Metformin suppressed the Shh signaling pathway through AMPK in the Shh subgroup MB cell line

To determine the effects of metformin on Shh signaling and whether this effect is exerted by activating AMPK. After treating Daoy cells with metformin (0, 1, 3, and 9 mm) for 24 h, the mRNA and protein levels of Shh, Smo, Ptc, and Gli-1 decreased in a dose-dependent manner following treatment with metformin (Figures 5A–C). To verify the role of AMPK in regulating the expressions of Shh signaling pathway proteins, we treated Daoy cells with AMPK siRNA for 24 h and then treated them with metformin (3 mm) for another 24 h. The results showed that metformin upregulated the phosphorylation level of AMPK (Thr172) (p-AMPK). In addition, the effect of metformin on reducing Gli-1 expression

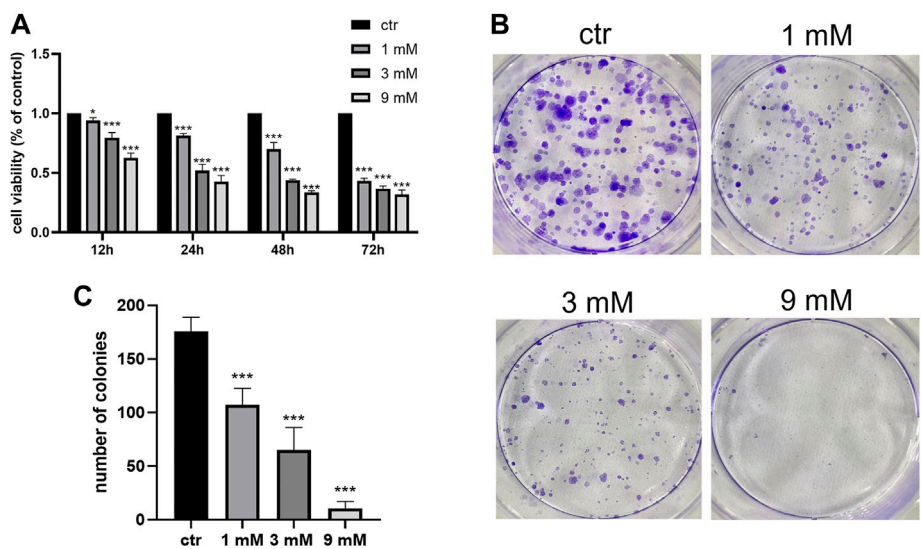


FIGURE 1
Metformin inhibited the proliferation of Daoy cells. **(A)** CCK-8 assay was used to investigate the effects of metformin treatment on cell viability ($n = 6$). **(B,C)** Colony formation assay was used to detected the effects of metformin treatment on clone ability of cells ($n = 3$). Data are presented as the mean \pm SD, t-tests were used to determine the significance. * $p < 0.05$; *** $p < 0.001$ compared with the control group.

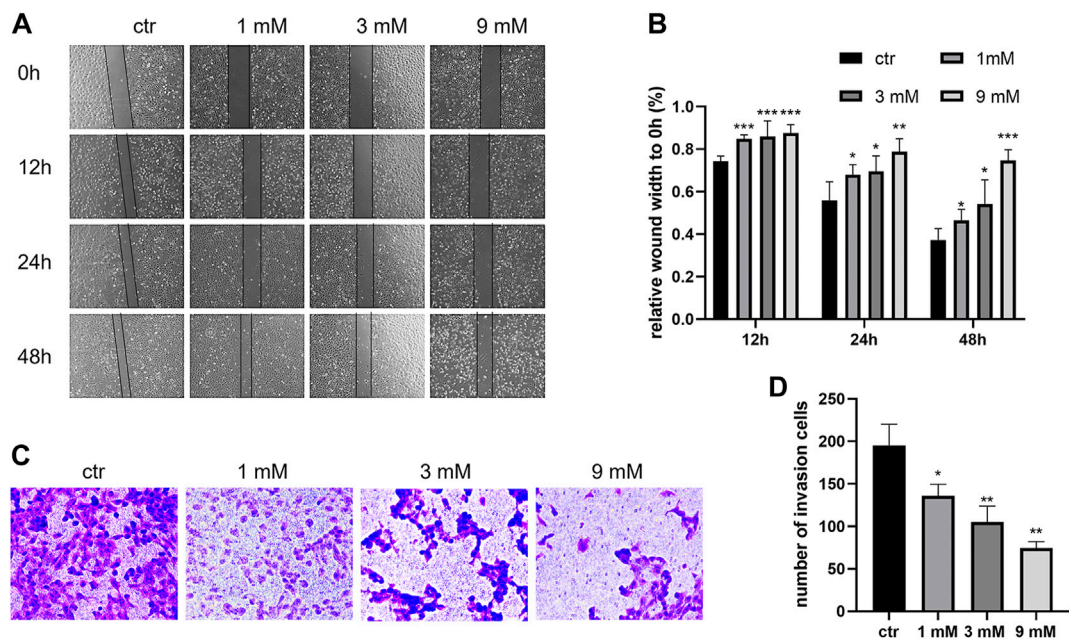


FIGURE 2
Metformin suppressed the migration and invasion of Daoy cells. **(A,B)** Scratch assay was used to assess the migration ability of Daoy cells after metformin treatment ($n = 4$). **(C,D)** Transwell assay was used to assess the invasion ability of Daoy cells after 24 h of metformin treatment ($n = 3$). Data are presented as the mean \pm SD, t-tests were used to determine the significance. * $p < 0.05$; ** $p < 0.01$; *** $p < 0.001$ compared with the control group.

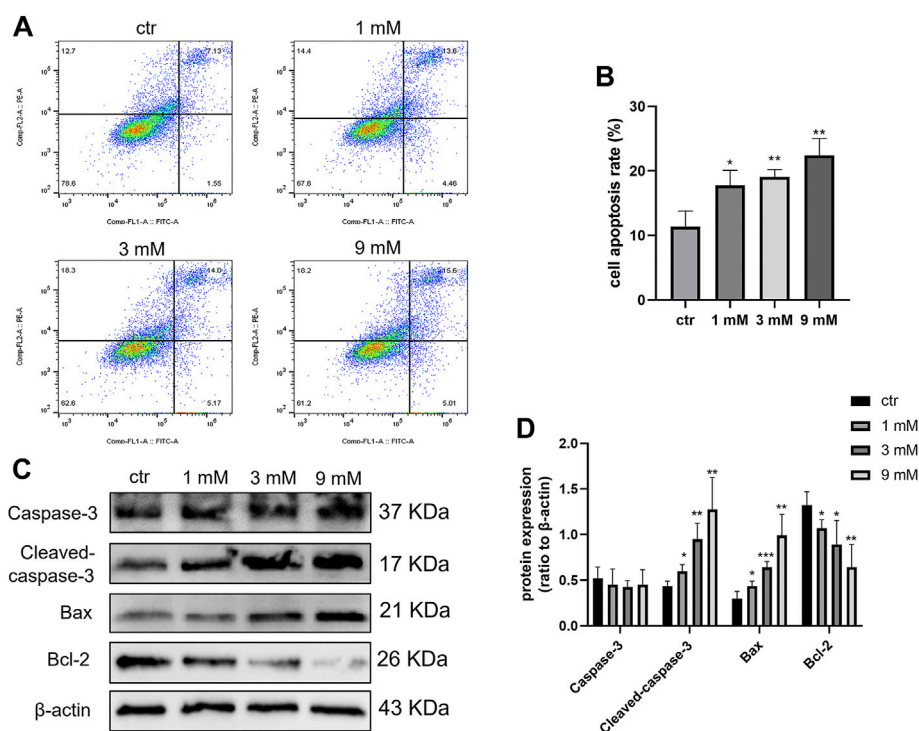


FIGURE 3

Cell apoptosis was induced by metformin treatment on Daoy cells. (A,B) Flow cytometry was used to analyze apoptosis on Daoy cells after 24 h of metformin treatment ($n = 3$). Annexin V-FITC-positive cells (Q2 + Q4) were considered as apoptotic. (C,D) Apoptosis-associated proteins were analyzed using western blot analysis. The relative Bcl-2, Bax, Caspase-3, and Cleaved-caspase-3 were normalized to that of β -actin ($n = 4$). Data are presented as the mean \pm SD, t-tests were used to determine the significance. * $p < 0.05$; ** $p < 0.01$; *** $p < 0.001$ compared with the control group.

could be reversed by AMPK siRNA (Figure 5D). These results indicated that the molecular mechanism by which metformin suppressed Shh signaling pathway might involve the activation of AMPK.

The antitumor effect of metformin on MB partly depended on the Shh pathway

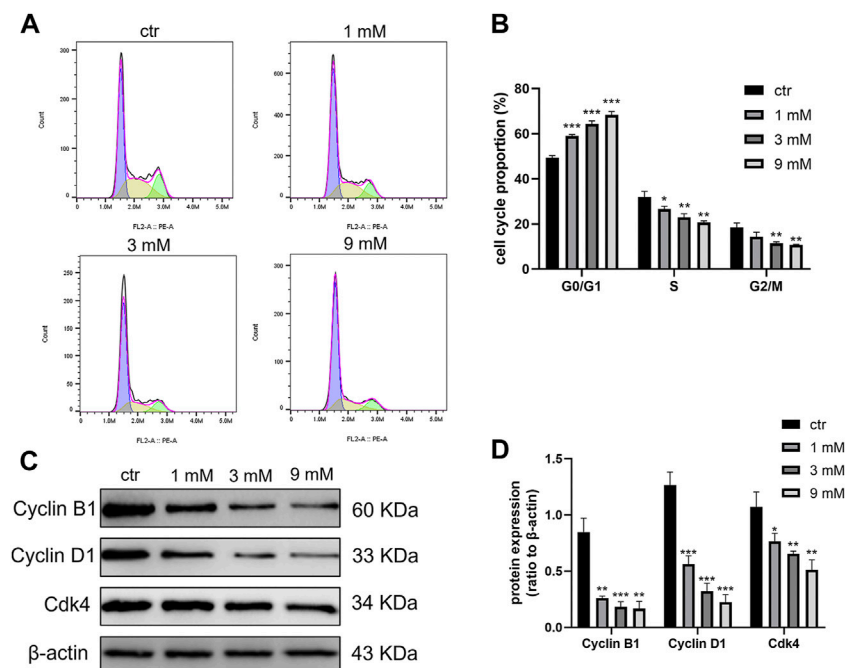
To explore whether the Shh pathway mediates the antitumor effect of metformin on medulloblastoma, after the treatment of Daoy cells with SAG (100 nm) and metformin (3 mM), we found that the SAG can attenuate the inhibitory effect of metformin on Gli-1 (Figures 6A and B). In the detection of cell proliferation viability, SAG also reduced the inhibitory effect of metformin on cell viability (Figure 6C). This effect may be related to apoptosis and cell cycle arrest. We found that SAG can reduce the pro-apoptotic and cell cycle arrest effects of metformin on Daoy cells (Figures 6D–G). These results suggested that the Shh signaling pathway mediated the anti-proliferation effect of metformin on the Daoy cells by participating in apoptosis and cell cycle (Figure 7).

Metformin resisted Shh subgroup MB growth *in vivo*

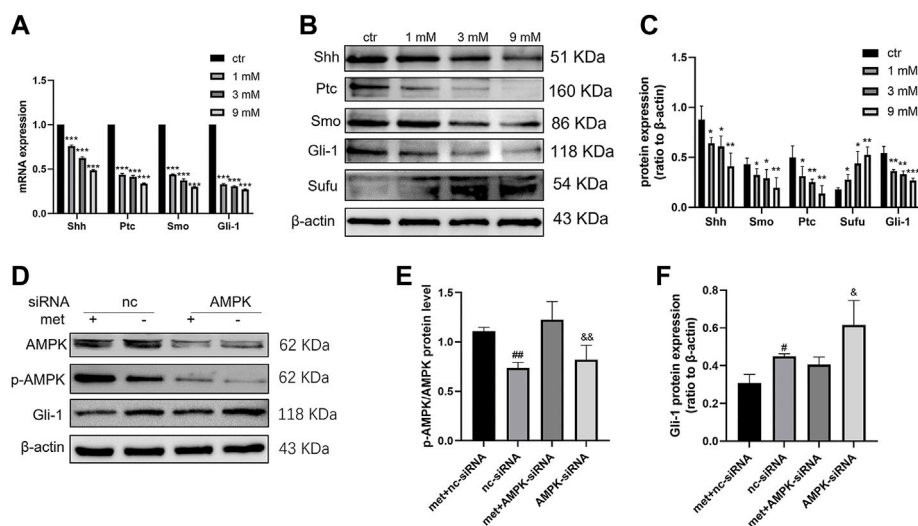
We conducted animal experiments to explore the anticancer effect of metformin on Shh subgroup MB *in vivo*. Oral administration of 300 μ L metformin (200 mg/kg) or an equivalent volume of PBS was adopted after the subcutaneous formation of the tumor using Daoy cells. After treatment for 24 days, the mice in the metformin group demonstrated reduced tumor volumes and reduction in excised tumor weights when compared to the mice in the control group (Figures 8A–D). During the experiment, there was no significant difference in body weight between the two groups of mice (Figure 8E).

Discussion

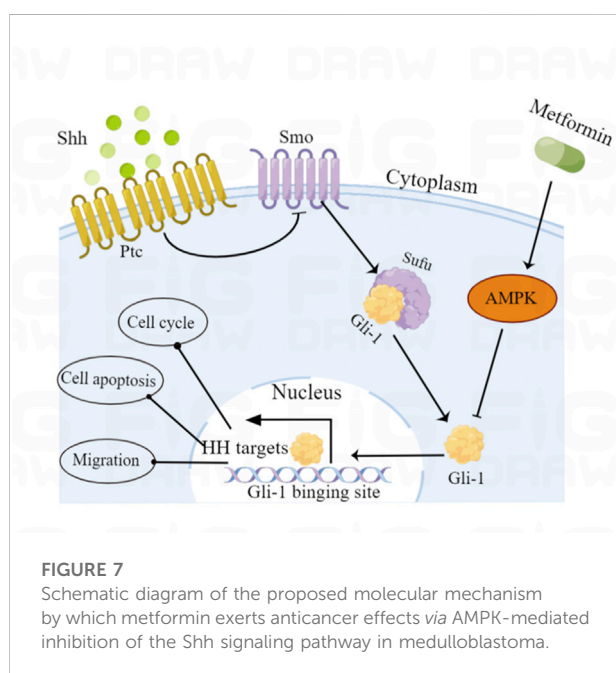
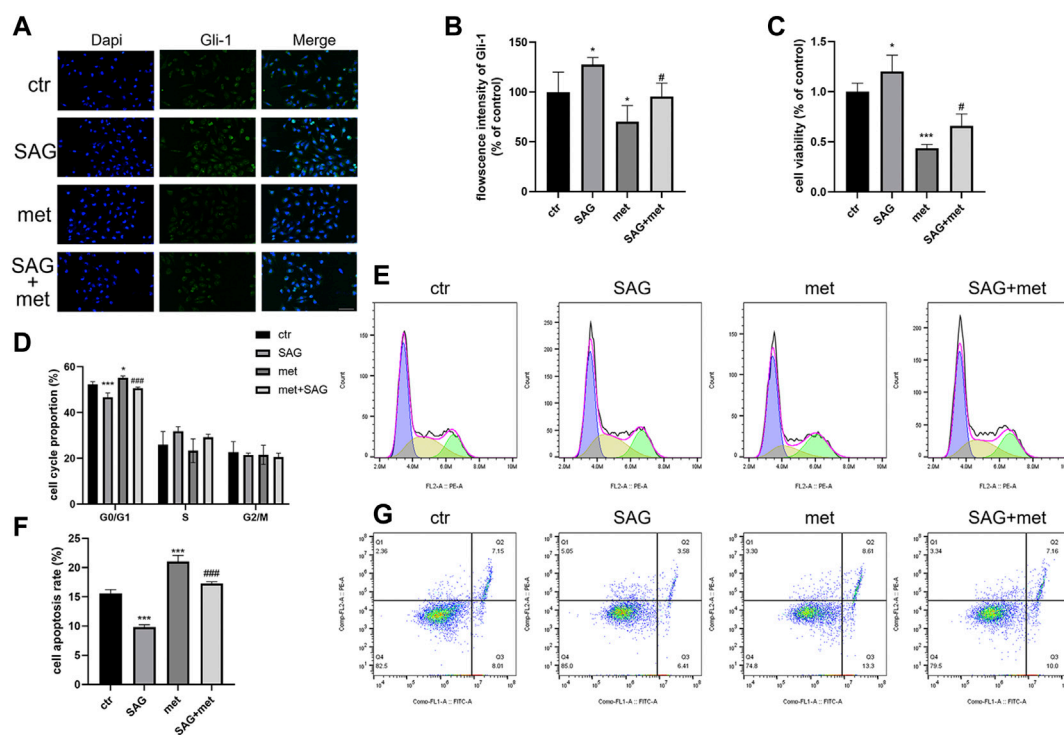
Most Shh subgroup MBs contain germline or somatic mutations in Shh signaling pathway-related genes, resulting in the activation of Shh signaling and promoting tumor progression (Cotter and Hawkins, 2022). Commonly mutated or deleted genes included Ptc (43%) and Sufu (10%); in addition, Smo

**FIGURE 4**

Cell cycle was blocked at the G0/G1 phase by metformin treatment on Daoy cells. **(A,B)** Flow cytometry was used to detect cell cycle distribution on Daoy cells after 24 h of metformin treatment ($n = 3$). **(C,D)** The proteins associated with the cell cycle were analyzed using western blot analysis. The relative Cyclin B1, Cyclin D1, and Cdk4 levels were normalized to that of β -actin ($n = 4$). Data are presented as the mean \pm SD, t-tests were used to determine the significance. * $p < 0.05$; ** $p < 0.01$; *** $p < 0.001$ compared with the control group.

**FIGURE 5**

Metformin inhibited the expression of the Shh signaling pathway in Daoy cells. **(A)** The mRNA levels of Shh, Smo, Ptc, and Gli-1 were analyzed using quantitative PCR after 24 h of metformin treatment; GAPDH served as a control ($n = 3$, t-tests were used to determine the significance). **(B,C)** The protein levels of Shh, Smo, Ptc, Sufu, and Gli-1 were analyzed using western blot analysis after metformin treatment, β -actin served as a control ($n = 4$, t-tests were used to determine the significance). **(D–F)** The protein levels of AMPK, p-AMPK (Thr172), and Gli-1 were analyzed by western blot after AMPK siRNA and metformin (3 mM) treatment for 24 h, β -actin served as a control ($n = 3$, one-way ANOVA multiple comparisons were used to determine the significance). Data are presented as the mean \pm SD. * $p < 0.05$; ** $p < 0.01$; *** $p < 0.001$ compared with the control group. # $p < 0.05$; ## $p < 0.01$ compared with the met + nc-siRNA group. $P < 0.05$; and $p < 0.01$ compared with the met + AMPK-siRNA group.



(9%) mutations, Gli-1/2 (9%), and N-myc (7%) amplifications were sometimes observed (Northcott et al., 2017). Early studies on Smo antagonists showed a good inhibitory effect on the Shh pathway. Unfortunately, drug resistance occurs due to mutations in SMO and its downstream genes (Yauch et al., 2009; Ocasio et al., 2019). Therefore, multi-target combination therapy may be a necessary means to effectively control the disease. Metformin is a biguanide semi-synthetic oral hypoglycemic drug, mainly used for the treatment of type 2 diabetes. In 2005, Evans JM et al. first found that metformin reduces the incidence of tumors in patients with type 2 diabetes, and a series of related basic and clinical studies have been carried out since then (Evans et al., 2005; Higurashi et al., 2016; Munoz et al., 2021). In the present study, we found that metformin exhibited anticancer activity in MB by inhibiting cell proliferation, migration, and invasion in a dose- and time-dependent manner *in vitro*. Moreover, metformin also showed an inhibitory effect on MB growth *in vivo* experiments. Among them, metformin inhibited cell proliferation by regulating cell cycle and apoptosis. Crucially, we found that metformin inhibited Shh signaling pathway in MB, and AMPK mediated part of this effect.

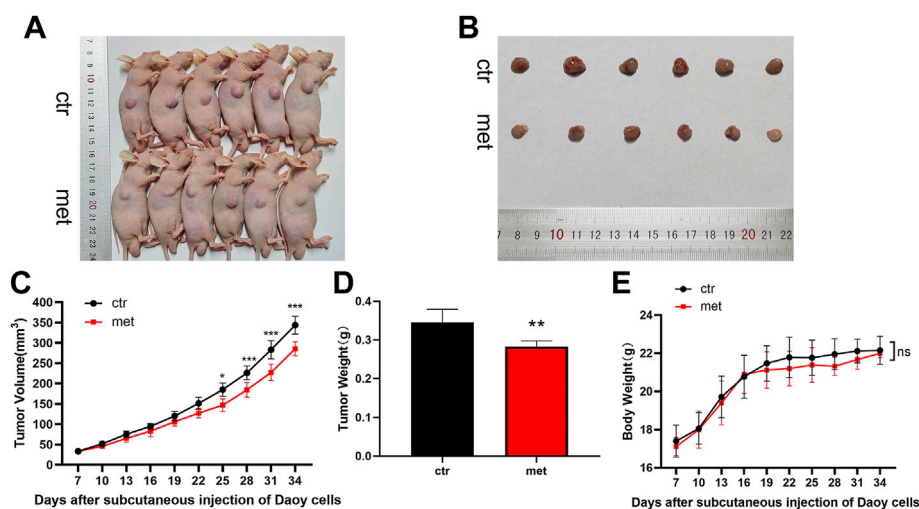


FIGURE 8

Metformin resisted Shh subgroup MB growth *in vivo*. (A) Photo of the nude mice bearing subcutaneous xenograft tumor. (B) Photo of tumors removed from mice after 24 days of metformin (200 mg/kg) or PBS treatment. (C) Tumor volume was recorded every 3 days (D) The weight of the excised tumor tissue. (E) Body weight of mice was recorded every 3 days ($n = 6$). Data are presented as the mean \pm SD, two-way ANOVA multiple comparisons were used to determine the significance. * $p < 0.05$; ** $p < 0.01$; *** $p < 0.001$ compared with the control group.

As a programmed cell death, apoptosis plays a key role in cancer therapy. Caspase-3 is an important protease in the process of apoptosis, and its activated form is involved in DNA repair and cell proliferation (Sergeeva et al., 2017). Previous studies have shown that metformin has a dual effect on apoptosis in different diseases, both promoting and inhibiting apoptosis. In studies related to cardiomyopathy, metformin inhibits apoptosis by reducing the expression of Cleaved-caspase-3, thereby attenuating hyperhomocysteinemia-induced cardiac hypertrophy and cardiac fibrosis (Zhao et al., 2021). However, metformin can reduce mitochondrial oxidative phosphorylation and intracellular ATP content, activate AMPK, and increase apoptosis in breast cancer cells (Haugrud et al., 2014). In related studies of the Shh signaling pathway, Ptc can activate caspase-mediated apoptosis when the Shh signaling pathway is inhibited (Brennan et al., 2012; Sigafos et al., 2021). This study shows that metformin induces apoptosis in Daoy cells. The results showed that Daoy cells treated with metformin showed a significant downregulation of the anti-apoptotic protein Bcl-2, while the pro-apoptotic protein Bax and Cleaved-caspase-3 increased. The results also showed that the mRNA and protein expression levels of the Shh pathway were significantly decreased in metformin-treated Daoy cells in a dose-dependent manner. To further investigate the correlation between the apoptotic effect of metformin and its inhibitory effect on the Shh signaling pathway, we treated cells with SAG (a specific activator of the Shh signaling pathway). We observed that SAG could reverse part of the apoptosis-promoting effects of metformin. These findings support a significant role in the

inhibition of the Shh signaling pathway in metformin-induced apoptosis in Daoy cells.

Disorders of cell cycle regulation exist in the occurrence and development of most malignant tumors. Previous studies have shown that G0/G1 cell cycle arrest is a mechanism of metformin's antitumor effect, which has been demonstrated in lung and kidney cancer cells (Jin et al., 2017; Xie et al., 2017). Regulation of the cell cycle is dependent on the action of a series of Cyclin-Cdk-CD inhibitors (Knudsen et al., 2022). These special complexes regulate each phase of the cell cycle. Cyclin D1/Cdk1-4 are vital proteins regulating the G1/S transition, while Cyclin B1 initiates mitosis by promoting the cell G2/M transition (Khan et al., 2022). The dysregulated expression of the cell cycle-related proteins plays an important role in the growth, differentiation, apoptosis, and metastasis of various tumor cells (Montalto and De Amicis, 2020). Western blot results of this study showed that Daoy cells treated with metformin showed a significant downregulation of the decreased Cyclin D1, Cdk4, and Cyclin B1 expression. This is consistent with our observation in flow cytometry that the cell cycle was arrested in the G0/G1 phase. The Shh pathway also plays an important role in regulating the cell cycle. Gli-1 can promote the transcription of Cyclin D1, and Ptc can phosphorylate Cyclin B1 to promote cell proliferation (Barnes et al., 2001; Sigafos et al., 2021). In our study, SAG was able to partially reverse the cycle arrest effect of metformin on Daoy cells. These results suggested that the Shh signaling pathway is involved in metformin-mediated cell cycle arrest in Daoy cells.

Tumor invasion and metastasis are closely related to epithelial to mesenchymal transition (EMT). The occurrence

of EMT results in the weakening of tight junctions between epithelial cells and the loss of epithelial cell polarity, thereby enhancing the motility of epithelial cells (Jinesh and Brohl, 2022). The Shh signaling pathway also played a role in promoting the occurrence of EMT. In pancreatic cancer studies, it was found that the Shh signaling pathway promotes the process of EMT by affecting the components of various signaling pathways, including TGF β , Ras, Wnt, PI3K/AKT, Integrin, and S100A4 (Xu et al., 2012). The study of gastric cancer also found that the increase in tumor lung metastasis was related to the activation of EMT by the Shh signaling pathway (Yoo et al., 2011). This is consistent with our observation that metformin inhibited the migration and invasion of Daoy cells, and inhibition of the Shh signaling pathway may mediate this effect by reducing EMT activity.

AMPK is the most important downstream effector of metformin and has been found to mediate the anticancer effects of metformin in multiple tumor cell lines (Chen et al., 2021; Lu et al., 2021). However, the relationship between AMPK and the Shh pathway is not clear, some studies pointed out that activated AMPK inhibits SHH signaling by phosphorylating Gli-1 and degrading it (Li et al., 2015). In addition, AMPK has indirect regulatory effects on the Shh pathway mediated by mTOR, FoxO1, and GSK3 β (Asha et al., 2020) (Sun et al., 2016). In the present study, we found that metformin reduced the expression levels of the Shh signaling pathway and increased the ratio of p-AMPK/AMPK in Daoy cells. Gli-1 is an important downstream effector of the Shh pathway, and its expression level was partially reversed by AMPK siRNA under the inhibitory effect of metformin. Moreover, with the reduction of Gli-1 expression, the expression of upstream molecules in the pathway was also suppressed. Interestingly, the expression of the pathway negative regulator Sufu was upregulated, which may be related to the NEK2A-mediated indirect inhibition of Sufu degradation by Gli-1. These results suggest that AMPK is involved in regulating the non-canonical Shh pathway in Daoy cells by metformin.

Our study showed that metformin inhibited the proliferation, migration, and invasion of Shh subtype MB and promoted apoptosis and cell cycle arrest. The AMPK/Shh signaling pathway mediates part of this tumor suppressor effect. However, the concentration of metformin in cell culture (1–9 mM) is much higher than the plasma drug concentration (5–25 μ M) of patients (Dowling et al., 2016). In order to explore the rationality of metformin as an anticancer drug, we established a medulloblastoma xenograft mouse model and administered it metformin orally at 200 mg/kg/day. According to the Reagan–Shaw formula (Reagan-Shaw et al., 2008), the human equivalent of the murine dose of 200 mg/kg is 973 mg in an average-sized human (60 kg), while the standard human therapeutic concentration of metformin is 1,000–2,500 mg/day. Satisfyingly, this dose of metformin effectively inhibited medulloblastoma growth and had no significant effect on growth in mice. These results suggest that metformin may be a potential chemotherapeutic agent for Shh-type medulloblastoma.

Nevertheless, the anticancer activity of such doses in mice and the possibility of achieving comparable levels in humans by rationally increasing the dose suggest a reassessment of metformin dosing regimens in anticancer treatment to optimize plasma drug levels and delivery to the tumor. In future studies, we need to fully characterize the mechanism of action of metformin at effective antitumor concentrations and evaluate its efficacy as a viable anticancer therapy.

Data availability statement

The original contributions presented in the study are included in the article/Supplementary Material; further inquiries can be directed to the corresponding authors.

Ethics statement

The animal study was reviewed and approved by the Ethics Committee of the Second Affiliated Hospital of Wenzhou Medical University.

Author contributions

HF, FT, JL, and HS conceived the study. HF, LW, LY, and HS designed the study. HF, LW, HS, HD, and ZY performed experiments. YY, LY, and SL analyzed the data. HF and FT drafted the manuscript. HF, JL, and HS revised the manuscript. All authors read and approved the manuscript.

Funding

This work was supported by the Wenzhou Municipal Science & Technology Bureau (Nos. Y2020419 and ZY2021007), Science Technology Department of Zhejiang Province (No. IGF22H160060) and Health Science and Technology Plan of Zhejiang Province (Nos. 2021KY794 and 2023KY147).

Conflict of interest

The authors declare that the research was conducted in the absence of any commercial or financial relationships that could be construed as a potential conflict of interest.

Publisher's note

All claims expressed in this article are solely those of the authors and do not necessarily represent those of their

affiliated organizations, or those of the publisher, the editors, and the reviewers. Any product that may be evaluated in this article, or claim that may be made by its manufacturer, is not guaranteed or endorsed by the publisher.

References

- Amayiri, N., Swaidan, M., Ibrahim, A., Hirmas, N., Musharbash, A., Bouffet, E., et al. (2021). Molecular subgroup is the strongest predictor of medulloblastoma outcome in a resource-limited country. *JCO Glob. Oncol.* 7, 1442–1453. doi:10.1200/GO.21.00127
- Asha, K., Balfe, N., and Sharma-Walia, N. (2020). Concurrent control of the kaposi's sarcoma-associated herpesvirus life cycle through chromatin modulation and host hedgehog signaling: A new prospect for the therapeutic potential of lipoxin A4. *J. Virol.* 94 (9), e021777-19. doi:10.1128/JVI.02177-19
- Azaty, A., Zhang, S., Darabi, A., Siesjö, P., Wang, T., and Zaphiropoulos, P. (2021). Circular RNAs in hedgehog signaling activation and hedgehog-mediated medulloblastoma tumors. *Cancers* 13 (20), 5138. doi:10.3390/cancers13205138
- Barnes, E., Kong, M., Ollendorff, V., and Donoghue, D. (2001). Patched1 interacts with cyclin B1 to regulate cell cycle progression. *EMBO J.* 20 (9), 2214–2223. doi:10.1093/emboj/20.9.2214
- Brennan, D., Chen, X., Cheng, L., Mahoney, M., and Riobo, N. (2012). Noncanonical hedgehog signaling. *Vitam. Horm.* 88, 55–72. doi:10.1016/B978-0-12-394622-5.00003-1
- Chatterjee, A., Maitre, M., Dasgupta, A., Sridhar, E., and Gupta, T. (2022). Multidisciplinary management of medulloblastoma: Consensus, challenges, and controversies. *Methods Mol. Biol.* 2423, 215–235. doi:10.1007/978-1-0716-1952-0_19
- Chen, C., Wang, H., Geng, X., Zhang, D., Zhu, Z., Zhang, G., et al. (2021). Metformin exerts anti-AR-negative prostate cancer activity via AMPK/autophagy signaling pathway. *Cancer Cell Int.* 21 (1), 404. doi:10.1186/s12935-021-02043-2
- Cotter, J., and Hawkins, C. (2022). Medulloblastoma: WHO 2021 and beyond. *Pediatr. Dev. Pathol.* 25 (1), 23–33. doi:10.1177/10935266211018931
- de Marañón, A., Díaz-Pozo, P., Canet, F., Díaz-Morales, N., Abad-Jiménez, Z., López-Domènech, S., et al. (2022). Metformin modulates mitochondrial function and mitophagy in peripheral blood mononuclear cells from type 2 diabetic patients. *Redox Biol.* 53, 102342. doi:10.1016/j.redox.2022.102342
- Dowling, R., Lam, S., Bassi, C., Mouaz, S., Aman, A., Kiyota, T., et al. (2016). Metformin pharmacokinetics in mouse tumors: Implications for human therapy. *Cell Metab.* 23 (4), 567–568. doi:10.1016/j.cmet.2016.03.006
- Evans, J., Donnelly, L., Emslie-Smith, A., Alessi, D., and Morris, A. (2005). Metformin and reduced risk of cancer in diabetic patients. *BMJ Clin. Res. ed* 330 (7503), 1304–1305. doi:10.1136/bmj.38415.708634.F7
- Fan, C., Wang, Y., Liu, Z., Sun, Y., Wang, X., Wei, G., et al. (2015). Metformin exerts anticancer effects through the inhibition of the Sonic hedgehog signaling pathway in breast cancer. *Int. J. Mol. Med.* 36 (1), 204–214. doi:10.3892/ijmm.2015.2217
- Haugrud, A., Zhuang, Y., Coppock, J., and Miskimins, W. (2014). Dichloroacetate enhances apoptotic cell death via oxidative damage and attenuates lactate production in metformin-treated breast cancer cells. *Breast Cancer Res. Treat.* 147 (3), 539–550. doi:10.1007/s10549-014-3128-y
- Heckman-Stoddard, B., DeCensi, A., Sahasrabudde, V., and Ford, L. (2017). Repurposing metformin for the prevention of cancer and cancer recurrence. *Diabetologia* 60 (9), 1639–1647. doi:10.1007/s00125-017-4372-6
- Higurashi, T., Hosono, K., Takahashi, H., Komiya, Y., Umezawa, S., Sakai, E., et al. (2016). Metformin for chemoprevention of metachronous colorectal adenoma or polyps in post-polypectomy patients without diabetes: A multicentre double-blind, placebo-controlled, randomised phase 3 trial. *Lancet. Oncol.* 17 (4), 475–483. doi:10.1016/S1470-2045(15)00565-3
- Jin, D., Kim, Y., Lee, B., Han, J., Kim, H., Shim, Y., et al. (2017). Metformin induces cell cycle arrest at the G1 phase through E2F8 suppression in lung cancer cells. *Oncotarget* 8 (60), 101509–101519. doi:10.18632/oncotarget.21552
- Jinesh, G., and Brohl, A. (2022). Classical epithelial-mesenchymal transition (EMT) and alternative cell death process-driven blebbistatin metastatic-witch (BMW) pathways to cancer metastasis. *Signal Transduct. Target. Ther.* 7 (1), 296. doi:10.1038/s41392-022-01132-6
- Khan, H., Alam, W., Alsharif, K., Aschner, M., Pervez, S., and Saso, L. (2022). Alkaloids and colon cancer: Molecular mechanisms and therapeutic implications for cell cycle arrest. *Mol. (Basel, Switz.)* 27 (3), 920. doi:10.3390/molecules27030920
- Kim, Y., Kim, S., Cho, S., Park, J., Choi, I., Lee, Y., et al. (2014). Long-term metformin use reduces gastric cancer risk in type 2 diabetics without insulin treatment: A nationwide cohort study. *Aliment. Pharmacol. Ther.* 39 (8), 854–863. doi:10.1111/apt.12660
- Knudsen, E., Kumarasamy, V., Nambiar, R., Pearson, J., Vail, P., Rosenheck, H., et al. (2022). CDK/cyclin dependencies define extreme cancer cell-cycle heterogeneity and collateral vulnerabilities. *Cell Rep.* 38 (9), 110448. doi:10.1016/j.celrep.2022.110448
- Li, Y., Luo, J., Mosley, Y., Hedrick, V., Paul, L., Chang, J., et al. (2015). AMP-activated protein kinase directly phosphorylates and destabilizes hedgehog pathway transcription factor GLI1 in medulloblastoma. *Cell Rep.* 12 (4), 599–609. doi:10.1016/j.celrep.2015.06.054
- Lu, T., Li, M., Zhao, M., Huang, Y., Bi, G., Liang, J., et al. (2021). Metformin inhibits human non-small cell lung cancer by regulating AMPK-CEBPB-PDL1 signaling pathway. *Cancer Immunol. Immunother.* 71 (4), 1733–1746. doi:10.1007/s00262-021-03116-x
- Montalto, F., and De Amicis, F. (2020). Cyclin D1 in cancer: A molecular connection for cell cycle control, adhesion and invasion in tumor and stroma. *Cells* 9 (12), E2648. doi:10.3390/cells9122648
- Munoz, L., Huang, L., Bommireddy, R., Sharma, R., Monterroza, L., Guin, R., et al. (2021). Metformin reduces PD-L1 on tumor cells and enhances the anti-tumor immune response generated by vaccine immunotherapy. *J. Immunother. Cancer* 9 (11), e002614. doi:10.1136/jitc-2021-002614
- Northcott, P., Buchhalter, I., Morrissy, A., Hovestadt, V., Weischenfeldt, J., Ehrenberger, T., et al. (2017). The whole-genome landscape of medulloblastoma subtypes. *Nature* 547 (7663), 311–317. doi:10.1038/nature22973
- Northcott, P., Robinson, G., Kratz, C., Mabbott, D., Pomeroy, S., Clifford, S., et al. (2019). Medulloblastoma. *Nat. Rev. Dis. Prim.* 5 (1), 11. doi:10.1038/s41572-019-0063-6
- Ocasio, J., Babcock, B., Malawsky, D., Weir, S., Loo, L., Simon, J., et al. (2019). scRNA-seq in medulloblastoma shows cellular heterogeneity and lineage expansion support resistance to SHH inhibitor therapy. *Nat. Commun.* 10 (1), 5829. doi:10.1038/s41467-019-13657-6
- Park, S., Willingham, M., Qi, J., and Cheng, S. (2018). Metformin and JQ1 synergistically inhibit obesity-activated thyroid cancer. *Endocr. Relat. Cancer* 25 (10), 865–877. doi:10.1530/ERC-18-0071
- Patel, S., Bhatnagar, A., Wear, C., Osiro, S., Gabriel, A., Kimball, D., et al. (2014). Are pediatric brain tumors on the rise in the USA? Significant incidence and survival findings from the SEER database analysis. *Childs Nerv. Syst.* 30 (1), 147–154. doi:10.1007/s00381-013-2307-1
- Reagan-Shaw, S., Nihal, M., and Ahmad, N. (2008). Dose translation from animal to human studies revisited. *FASEB J. official Publ. Fed. Am. Soc. Exp. Biol.* 22 (3), 659–661. doi:10.1096/fj.07-9574LSF
- Sergeeva, T., Shirmanova, M., Zlobovskaya, O., Gavrina, A., Dudenkova, V., Lukina, M., et al. (2017). Relationship between intracellular pH, metabolic co-factors and caspase-3 activation in cancer cells during apoptosis. *Biochim.*

Supplementary material

The Supplementary Material for this article can be found online at: <https://www.frontiersin.org/articles/10.3389/fphar.2022.928853/full#supplementary-material>

Biophys. Acta. Mol. Cell Res. 1864 (3), 604–611. doi:10.1016/j.bbamcr.2016.12.022

Sigafoos, A., Paradise, B., and Fernandez-Zapico, M. (2021). Hedgehog/GLI signaling pathway: Transduction, regulation, and implications for disease. *Cancers* 13 (14), 3410. doi:10.3390/cancers13143410

Skowron, P., Farooq, H., Cavalli, F., Morrissy, A., Ly, M., Hendrikse, L., et al. (2021). The transcriptional landscape of Shh medulloblastoma. *Nat. Commun.* 12 (1), 1749. doi:10.1038/s41467-021-21883-0

Sun, Y., Tao, C., Huang, X., He, H., Shi, H., Zhang, Q., et al. (2016). Metformin induces apoptosis of human hepatocellular carcinoma HepG2 cells by activating an AMPK/p53/miR-23a/FOX A1 pathway. *Onco. Targets. Ther.* 9, 2845–2853. doi:10.2147/OTT.S99770

Xie, W., Wang, L., Sheng, H., Qiu, J., Zhang, D., Zhang, L., et al. (2017). Metformin induces growth inhibition and cell cycle arrest by upregulating MicroRNA34a in renal cancer cells. *Med. Sci. Monit.* 23, 29–37. doi:10.12659/msm.898710

Xu, X., Zhou, Y., Xie, C., Wei, S., Gan, H., He, S., et al. (2012). Genome-wide screening reveals an EMT molecular network mediated by Sonic hedgehog-Gli1

signaling in pancreatic cancer cells. *PLoS one* 7 (8), e43119. doi:10.1371/journal.pone.0043119

Yauch, R., Dijkgraaf, G., Alicke, B., Januario, T., Ahn, C., Holcomb, T., et al. (2009). Smoothened mutation confers resistance to a Hedgehog pathway inhibitor in medulloblastoma. *Sci. (New York, NY)* 326 (5952), 572–574. doi:10.1126/science.1179386

Yeole, U., Hegde, S., Gothwal, M., Prabhuraj, A., Somanna, S., Thennarasu, K., et al. (2021). What happens after therapy? Quality of life and neurocognitive functions of children with malignant posterior fossa tumors after adjuvant therapy. *Neurol. India* 69 (5), 1293–1301. doi:10.4103/0028-3886.329599

Yoo, Y., Kang, M., Lee, H., Kim, B., Park, J., Kim, H., et al. (2011). Sonic hedgehog pathway promotes metastasis and lymphangiogenesis via activation of Akt, EMT, and MMP-9 pathway in gastric cancer. *Cancer Res.* 71 (22), 7061–7070. doi:10.1158/0008-5472.CAN-11-1338

Zhao, Q., Song, W., Huang, J., Wang, D., and Xu, C. (2021). Metformin decreased myocardial fibrosis and apoptosis in hyperhomocysteinemia -induced cardiac hypertrophy. *Curr. Res. Transl. Med.* 69 (1), 103270. doi:10.1016/j.retram.2020.103270

Frontiers in Oncology

Advances knowledge of carcinogenesis and tumor progression for better treatment and management

The third most-cited oncology journal, which highlights research in carcinogenesis and tumor progression, bridging the gap between basic research and applications to improve diagnosis, therapeutics and management strategies.

Discover the latest Research Topics

[See more →](#)

Frontiers

Avenue du Tribunal-Fédéral 34
1005 Lausanne, Switzerland
frontiersin.org

Contact us

+41 (0)21 510 17 00
frontiersin.org/about/contact

